# Characteristics of Environmental Data Layers for Use in Species Distribution Modelling in the Eastern Canadian Arctic and Sub-Arctic Regions

L. Beazley, J. Guijarro, C. Lirette, Z. Wang, E. Kenchington

Ocean and Ecosystem Sciences Division
Maritimes Region
Fisheries and Oceans Canada

Bedford Institute of Oceanography
PO Box 1006
Dartmouth, Nova Scotia
Canada B2Y 4A2

2018

**Canadian Technical Report of**
**Fisheries and Aquatic Sciences 3248**

Fisheries and Oceans Canada    Pêches et Océans Canada

Canada

## Canadian Technical Report of Fisheries and Aquatic Sciences

Technical reports contain scientific and technical information that contributes to existing knowledge but which is not normally appropriate for primary literature. Technical reports are directed primarily toward a worldwide audience and have an international distribution. No restriction is placed on subject matter and the series reflects the broad interests and policies of Fisheries and Oceans Canada, namely, fisheries and aquatic sciences.

Technical reports may be cited as full publications. The correct citation appears above the abstract of each report. Each report is abstracted in the data base *Aquatic Sciences and Fisheries Abstracts*.

Technical reports are produced regionally but are numbered nationally. Requests for individual reports will be filled by the issuing establishment listed on the front cover and title page.

Numbers 1-456 in this series were issued as Technical Reports of the Fisheries Research Board of Canada. Numbers 457-714 were issued as Department of the Environment, Fisheries and Marine Service, Research and Development Directorate Technical Reports. Numbers 715-924 were issued as Department of Fisheries and Environment, Fisheries and Marine Service Technical Reports. The current series name was changed with report number 925.

## Rapport technique canadien des sciences halieutiques et aquatiques

Les rapports techniques contiennent des renseignements scientifiques et techniques qui constituent une contribution aux connaissances actuelles, mais qui ne sont pas normalement appropriés pour la publication dans un journal scientifique. Les rapports techniques sont destinés essentiellement à un public international et ils sont distribués à cet échelon. II n'y a aucune restriction quant au sujet; de fait, la série reflète la vaste gamme des intérêts et des politiques de Pêches et Océans Canada, c'est-à-dire les sciences halieutiques et aquatiques.

Les rapports techniques peuvent être cités comme des publications à part entière. Le titre exact figure au-dessus du résumé de chaque rapport. Les rapports techniques sont résumés dans la base de données *Résumés des sciences aquatiques et halieutiques.*

Les rapports techniques sont produits à l'échelon régional, mais numérotés à l'échelon national. Les demandes de rapports seront satisfaites par l'établissement auteur dont le nom figure sur la couverture et la page du titre.

Les numéros 1 à 456 de cette série ont été publiés à titre de Rapports techniques de l'Office des recherches sur les pêcheries du Canada. Les numéros 457 à 714 sont parus à titre de Rapports techniques de la Direction générale de la recherche et du développement, Service des pêches et de la mer, ministère de l'Environnement. Les numéros 715 à 924 ont été publiés à titre de Rapports techniques du Service des pêches et de la mer, ministère des Pêches et de l'Environnement. Le nom actuel de la série a été établi lors de la parution du numéro 925.

Canadian Technical Report of

Fisheries and Aquatic Sciences 3248

2018

# Characteristics of Environmental Data Layers for Use in Species Distribution Modelling in the Eastern Canadian Arctic and Sub-Arctic Regions

by

L. Beazley, J. Guijarro, C. Lirette, Z. Wang, E. Kenchington

Ocean and Ecosystem Sciences Division

Maritimes Region

Fisheries and Oceans Canada

Bedford Institute of Oceanography

P.O. Box 1006

Dartmouth, N.S.

Canada B2Y 4A2

Cat. No. Fs97-6/3248E-PDF   ISBN 978-0-660-24509-6   ISSN 1488-5379

Correct citation for this publication:

Beazley, L., Guijarro, J., Lirette, C., Wang, Z., and Kenchington, E. 2018. Characteristics of Environmental Data Layers for Use in Species Distribution Modelling in the Eastern Canadian Arctic and Sub-Arctic Regions. Can. Tech. Rep. Fish. Aquat. Sci. 3248: vii + 488p.

## TABLE OF CONTENTS

# ABSTRACT

Beazley, L., Guijarro, J., Lirette, C., Wang, Z., and Kenchington, E. 2018. Characteristics of Environmental Data Layers for Use in Species Distribution Modelling in the Eastern Canadian Arctic and Sub-Arctic Regions. Can. Tech. Rep. Fish. Aquat. Sci. 3248: vii + 488p.

Species distribution modelling (SDM) is a tool that utilizes the relationship between a species and its environment in known (sampled) locations to predict the species' distribution in unsampled areas. Environmental data are typically collected at different spatial and temporal scales and often require spatial interpolation between data points to provide a continuous surface required by the modelling application. Here we provide detailed information on 111 environmental data layers collected over different spatial scales and temporal resolutions and interpolated using a geospatial method to provide continuous data surfaces for the Eastern Canadian Arctic and Sub-Arctic. Variables were obtained from a broad range of physical and biological data sources and spatially interpolated using ordinary kriging. For each environmental variable we show the distributional properties of the raw data prior to spatial interpolation, model performance indicators and assessment of model performance, and finally, maps of the prediction standard error and interpolation prediction surfaces. These layers have been archived in a common (raster) format at the Bedford Institute of Oceanography to facilitate future use. A subset of these variables has already been used in a conservation management application to identify deep-water coral and sponge Significant Benthic Areas in the Eastern Canadian Arctic.

# RÉSUMÉ

Beazley, L., Guijarro, J., Lirette, C., Wang, Z., et Kenchington, E. 2018. Characteristics of Environmental Data Layers for Use in Species Distribution Modelling in the Eastern Canadian Arctic and Sub-Arctic Regions. Rapp. tech. can. sci. halieut. Sci. 3248: vii + 488p.

La modélisation de la répartition des espèces (MRE) est un outil qui utilise la relation entre une espèce et son environnement dans des emplacements connus (échantillonnés) pour prédire la répartition de l'espèce dans les zones non échantillonnées. Les données environnementales sont habituellement recueillies à différentes échelles spatiales et temporelles et nécessitent souvent une interpolation spatiale entre les points de données pour produire la surface continue requise pour les besoins de l'application de modélisation. Dans ce document, nous donnons des renseignements détaillés sur les 111 couches de données environnementales qui ont été recueillies au fil des différentes échelles spatiales et résolutions temporelles et qui ont été interpolées au moyen d'une méthode géospatiale pour produire des surfaces de données continues pour l'est de l'Arctique canadien et les régions subarctiques. Des variables ont été obtenues à partir d'une vaste gamme de sources de données physiques et biologiques interpolées sur le plan spatial à l'aide du krigeage ordinaire. Pour chaque variable environnementale, nous montrons les propriétés de répartition des données brutes avant l'interpolation spatiale, les modèles d'indicateurs de performance et une évaluation du rendement des modèles. Enfin, nous présentons l'erreur type et les surfaces de prédiction interpolées. Ces couches de données ont été archivées dans un format commun (trame) à l'Institut océanographique de Bedford afin de simplifier leur utilisation future. Un sous-ensemble de ces variables a déjà été utilisé dans une application de gestion de conservation pour déterminer les zones benthiques importantes de coraux et d'éponges d'eau profonde dans l'est de l'Arctique canadien.

# INTRODUCTION

The physical environment of the Arctic Ocean is dynamic and characterized by strong seasonality and large inter-annual fluctuations. Air and ocean temperature, and perennial sea ice extent and duration are rapidly changing in this region (Boé et al., 2009; Peterson and Pettipas, 2013). Although the consequences of a changing climate on marine benthic communities remains largely undocumented (although see Wassmann et al. (2011) for a review of responses in Arctic benthos), the narrow environmental envelope of many polar benthic species (Peck et al., 2004) suggests they are highly susceptible to changes in their physical environment. For instance, small changes in the timing of sea ice break out in the summer months has shown to cause complete regime shifts in coastal benthic communities, from invertebrate to algae-dominated states (Clark et al., 2013). Further understanding of the parameters that control the distribution of these fauna will help determine their susceptibility to the projected rapid and eminent environmental change in this region.

Species distribution modelling (SDM) is a tool that utilizes the relationship between a species and its environment in known (sampled) locations to predict the species' distribution in unsampled areas. In the Arctic Ocean, SDMs have been recently applied to predict species' distribution under different climatic scenarios (see Gogina and Zettler, 2010; Gogina et al., 2010). In these applications it is essential to have continuous surfaces of environmental data and climate proxies in order to predict spatial distribution in unsampled areas and/or under different environmental scenarios. Environmental data are typically collected at different spatial and temporal resolutions, and often require spatial interpolation in order to provide continuous surfaces that can be used for predictive modelling at all spatial scales. There are over 60 spatial interpolation methods to choose from, including geospatial interpolators (e.g. kriging), non-geostatistical interpolators (e.g. inverse distance weighting, natural neighbours, nearest neighbours), and methods that combine both (Li and Heap, 2008).

Here we provide detailed information on 111 environmental data layers collected over different spatial scales and temporal resolutions and interpolated using ordinary kriging to provide continuous data surfaces for the Eastern Canadian Arctic and Sub-Arctic regions. The study extent for which these data layers were constructed included a combination of three Fisheries and Oceans Canada (DFO) Biogeographic Zones: the Hudson Bay Complex, Eastern Arctic, and the Newfoundland-Labrador (NL) Shelves. For each environmental variable we show the distributional properties of the raw data prior to spatial interpolation, model performance indicators and assessment of model performance, and finally, maps of the prediction standard error and interpolation prediction surfaces. These layers have been archived in a common (raster) format at the Bedford Institute of Oceanography to facilitate future use. Our intention is that these variables are used in species distribution modelling or other ecosystem-based management applications. A subset of these variables have already been used in random forest and generalized additive models to predict the probability of occurrence and biomass distribution of deep-water corals and sponges (see Beazley et al., 2016b), the results of which have been recently used in a conservation management application to identify deep-water coral and sponge Significant Benthic Areas (DFO, 2017; Kenchington et al., 2016) under DFO's Policy for Managing the Impacts of Fishing on Sensitive Benthic Areas.

# MATERIALS AND METHODS

## Study Area

Three Fisheries and Oceans Canada (DFO) Biogeographic Zones were used as the basis for construction of the spatial extent of the environmental layers described in this report (see Figure 1): The Hudson Bay Complex and Eastern Arctic Biogeographic Zones in the Arctic Ocean and the NL-Labrador Shelves Biogeographic Zone in the Atlantic Ocean (see DFO (2009)). The Hudson Bay Complex includes Hudson Strait, Foxe Basin, James Bay, and Hudson Bay, while the Eastern Arctic includes Lancaster Sound and the Baffin Bay-Davis Strait areas. The latter extends to the Barrow Strait in the North, and ends just northwest of the Gulf of Boothia in the west. The NL-Labrador Shelves zone was included as far south as the Strait of Belle Isle between Labrador and Newfoundland. All three zones were extended beyond the Exclusive Economic Zone (EEZ) to Greenland in order to fully encompass the circulation patterns and oceanographic characteristics that govern Baffin Bay and Davis Strait. Given the rugged coastline in these regions, a 20-km buffer was applied to all land values to ensure their exclusion.

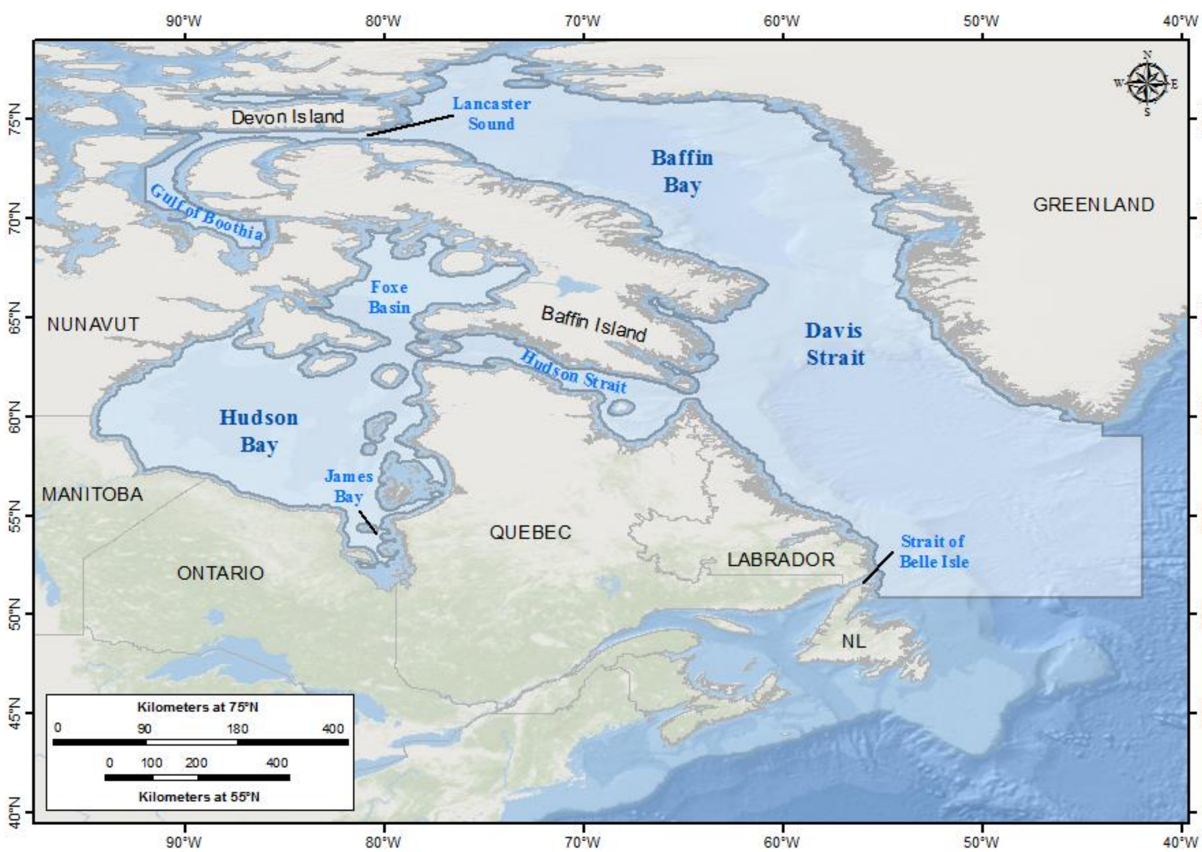


**Figure 1.** Extent of the boundary used to construct the interpolated surfaces of environmental variables in this report.

## Data Sources

### Global Ocean Reanalyses and Simulations (GLORYS)

Data for surface and bottom temperature, salinity, current speed, and mixed layer depth were extracted from the Global Ocean Reanalyses and Simulations (GLORYS2V1). GLORYS2V1 is a numerical ocean general circulation model reanalysis product with ¼º horizontal resolution (approximately ~25 km in the study extent (Figure 2) that aims to provide the mean and time-varying state of the oceanic states with a focus on capturing variation of meso-scale eddies (http://www.mercator-ocean.fr/eng/science/GLORYS). Details of this model can be found in Beazley et al. (2016a). For each point location, data were extracted for each month between January, 1993 and December, 2011.

For each environmental variable, two different sets of statistics were created from the GLORYS2V1 monthly data. First, the absolute minima, maxima, and range were calculated for each variable by taking the minimum and maximum values across all months and years at each point location. Range was calculated as the difference between the maximum and minimum values at each location, across all months and years. In this report these variables are denoted as ‘Minimum’, ‘Maximum’, or ‘Range’ (e.g. Bottom Current Maximum). These ‘absolute’ variables are likely reflective of anomalous events over the entire 19-year time period. The second dataset was created by calculating the average minima, maxima, and range by taking the minimum and maximum values at each location across all months within a year, and averaging

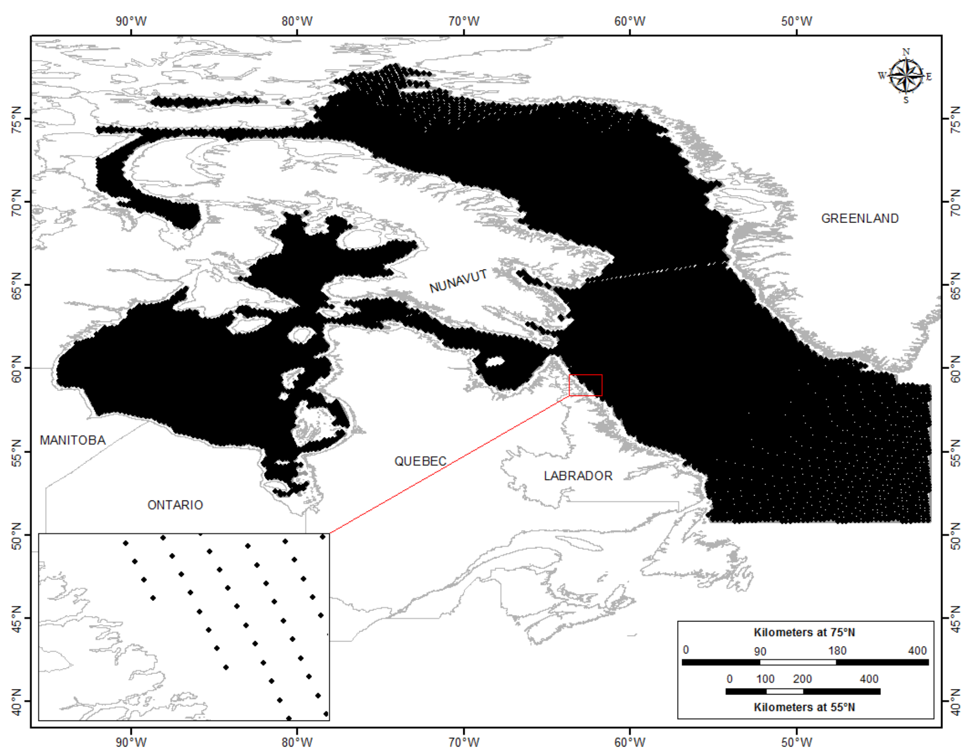


**Figure 2.** Distribution of point data extracted from the GLORYS2V1 model from 1993 to 2011 for the Eastern Canadian Arctic and Sub-Arctic. Point data have a native resolution of ¼º.

across years. These variables are denoted as ‘Average Minimum’, ‘Average Maximum’, or ‘Average Range’ throughout the report, and are likely more representative of long-term oceanographic climate in the region. Finally, the mean of each variable was calculated by averaging the values at each location across all months and years, and is denoted as the ‘Mean’ in this report. Zeroes in the current and shear data, which were falsely generated from a model topography issue, were removed prior to calculating the different statistics.

For some of the ‘bottom’ variables there is a gap in data that spans across Hudson Bay, Hudson Strait, and Davis Strait between ~60˚N to ~65˚N. In order to span the entire eastern Arctic and north Northwest Atlantic, two datasets were processed and combined, resulting in a gap in data approximately 1 km wide. Interpolation of the data filled in this gap. However, this line is evident in the standard error plots for some variables, but is not apparent in the final interpolated surfaces.

*Caveat for GLORYS variables*

Bottom temperature values derived from the GLORYS model (i.e. raw values prior to ordinary kriging) were abnormally low in some shallow, coastal portions of the study area, particularly in Hudson Bay. This is likely caused by the data assimilation scheme of the model. The unrealistically low values of bottom temperature (e.g. Bottom Temperature Minimum values of ~ -12˚C) cannot be interpreted by any physical means and are not representative of the actual values in those areas. These extreme values are found almost entirely in Hudson Bay, and therefore caution should be taken when using these layers for that area. Future releases of the GLORYS product hopes to resolve this issue.

**Sea Surface Chlorophyll *a***

Sea surface chlorophyll *a* (mg $m^{-3}$) data were derived from the Sea-viewing Wide Field-of-view Sensor (SeaWIFS) database. SeaWiFS data is primarily used to determine concentrations of chlorophyll in the oceanic water column. The ocean optical data from SeaWiFS can also be used to determine light attenuation in the oceanic water column, which provides information on suspended sediment concentrations and other parameters. Ocean color distribution can be used to investigate the forces influencing trophic productivity in the world's oceans.

Monthly SeaWIFS (Level 3 SMI) data from 2001 to 2010 were downloaded from NASA’s OceanColor Group (http://oceandata.sci.gsfc.nasa.gov/) using Duke University's Marine Geospatial Ecology Tools (Roberts et al., 2010) in ArcGIS (ESRI, 2011). Composite images were displayed in raster format with a spatial resolution of 9 km. The native resolution of the point data for SeaWIFS chlorophyll *a* data are shown in Figure 3.

Annual and seasonal averages were computed for the SeaWIFS dataset. Due to ice coverage in the winter months, sea surface chlorophyll *a* data were extracted for only two seasons: Spring (days of year 91 – 181) and Summer (days 182 – 273). These seasonal delimitations capture the peak of the spring and late summer phytoplankton blooms in most areas of the Arctic.

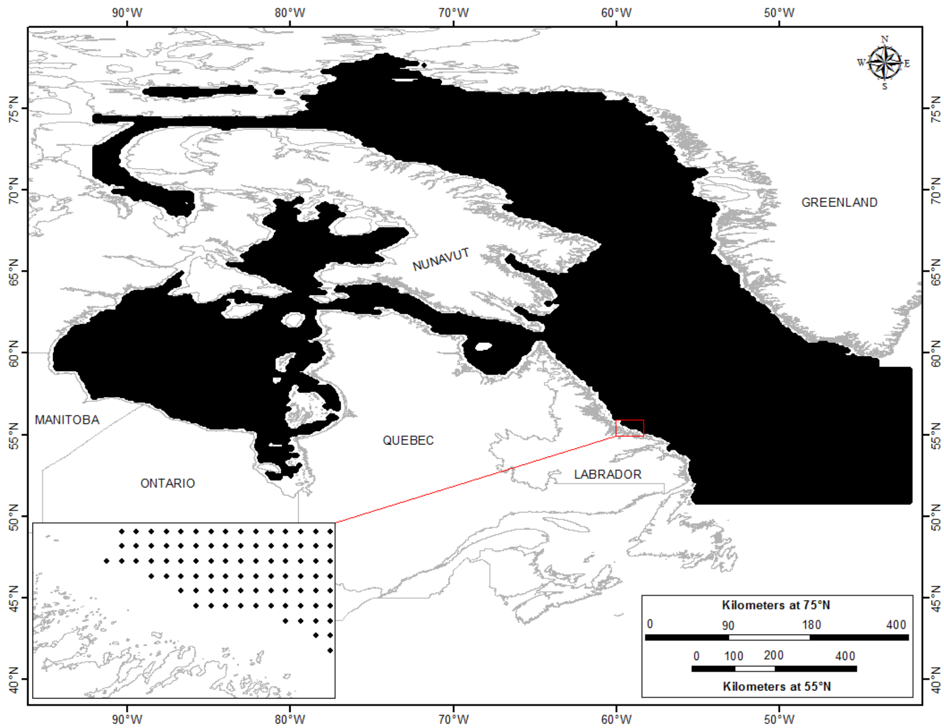


**Figure 3.** Distribution of sea surface chlorophyll *a* (SeaWIFS) point data (Spring, Summer and Annual) for the Eastern Canadian Arctic Region and Sub-Arctic, from 2001 to 2010. Point data have a native resolution of 9 km.

## Primary Production

Primary production was calculated following the method of Platt et al. (2008) using software developed by the Remote Sensing Unit of the Bedford Institute of Oceanography (RSU-BIO) and the Department of Oceanography at Dalhousie University. The calculation of primary production requires input from multiple sources. Monthly mean surface chlorophyll *a* and photosynthetically active radiation (PAR) was obtained from NASA's SeaWiFS Level 3, 9-km global coverage (reprocessing R2010.0; Feldman and McClain, 2012). Sea surface temperature (SST) was obtained from NOAA PathFinder version 5.2 data and was reprocessed from its native resolution of 4000 $m^2$ pixel-1 to match the spatial and temporal resolution of chlorophyll data. Monthly images of total cloud fraction data used in the model were obtained in November 2014 from MYD08_M3, a monthly aggregation of MYD35, collection 51 (ftp://ladsweb.nascom.nasa.gov/allData/51/MYD08_M3/). The *in situ* parameters, such as photosynthetic performance, chlorophyll *a*, sea surface temperature, and water depth originate from ship-based observations made by DFO's Atlantic Zone Monitoring Program (AZMP; http://www.bio.gc.ca/science/monitoring-monitorage/azmp-pmza-en.php). Reliability of the resulting primary production data is therefore unknown for areas outside the AZMP region. The model described in Platt et al. (2008) results in pixel-by-pixel depth-integrated net primary production (mg C $m^{-2}$ $day^{-1}$) calculated for the 15 day of each month from September 2006 to September 2010. Like the GLORYS2V1-derived variables, monthly values for primary production allowed for the calculation of both 'absolute' and 'average' minima, maxima, and range quantifications. However, for some months and years no data were available (see Table 1), therefore only spring (April – June), summer (July – September) and annual layers were created. For the creation of these variables, we ensured that each point location across the study extent had at least two months of data in each of the five years contributing to the quantifications. Summer and annual surfaces showed nearly full coverage across the Arctic Region, whereas portions of the Hudson Bay Complex, Baffin Basin and Davis Strait are not covered in the spring as these are locations with less than one month of data contributing across the 5-year data period (Figure 4).

The timing of sea ice formation and melting has a significant impact on the distribution of photosynthetically active radiation (PAR) (Fritsen et al., 2011). Primary production values for high latitude winter are not available for times and locations when ice covers the surface or the daylight period is very short. As much of Hudson Bay and the northern Eastern Arctic are ice covered in the spring months, the coverage of primary production in these areas is poor. Sea surface chlorophyll *a* may, however, be available from satellite passes that occur near local noon. Because the resolution of the passive microwave sensors used to determine seasonal ice coverage (25 km) is much lower than the resolution (1 km) of ocean colour sensors, chlorophyll values are sometimes available for times and locations where production cannot be determined by remote sensing.

**Table 1.** Contributing months to each of the five years of data for the primary production dataset. The √ indicates that data exists for this month. Note that even though data exists for a particular month, each point location across the full study extent may not have observation data.

| Season | Month | 2006 | 2007 | 2008 | 2009 | 2010 | Total number of years |
|---|---|---|---|---|---|---|---|
| | January | √ | √ | | √ | √ | 4 |
| | February | √ | √ | | √ | √ | 4 |
| | March | √ | √ | | √ | √ | 4 |
| Spring | April | √ | √ | √ | √ | √ | 5 |
| | May | √ | √ | √ | | √ | 4 |
| | June | √ | √ | √ | √ | √ | 5 |
| Summer | July | √ | √ | | √ | √ | 4 |
| | August | √ | √ | √ | √ | √ | 5 |
| | September | √ | √ | √ | | √ | 4 |
| | October | √ | √ | √ | | √ | 4 |
| | November | √ | | √ | √ | √ | 4 |
| | December | | | √ | √ | √ | 3 |

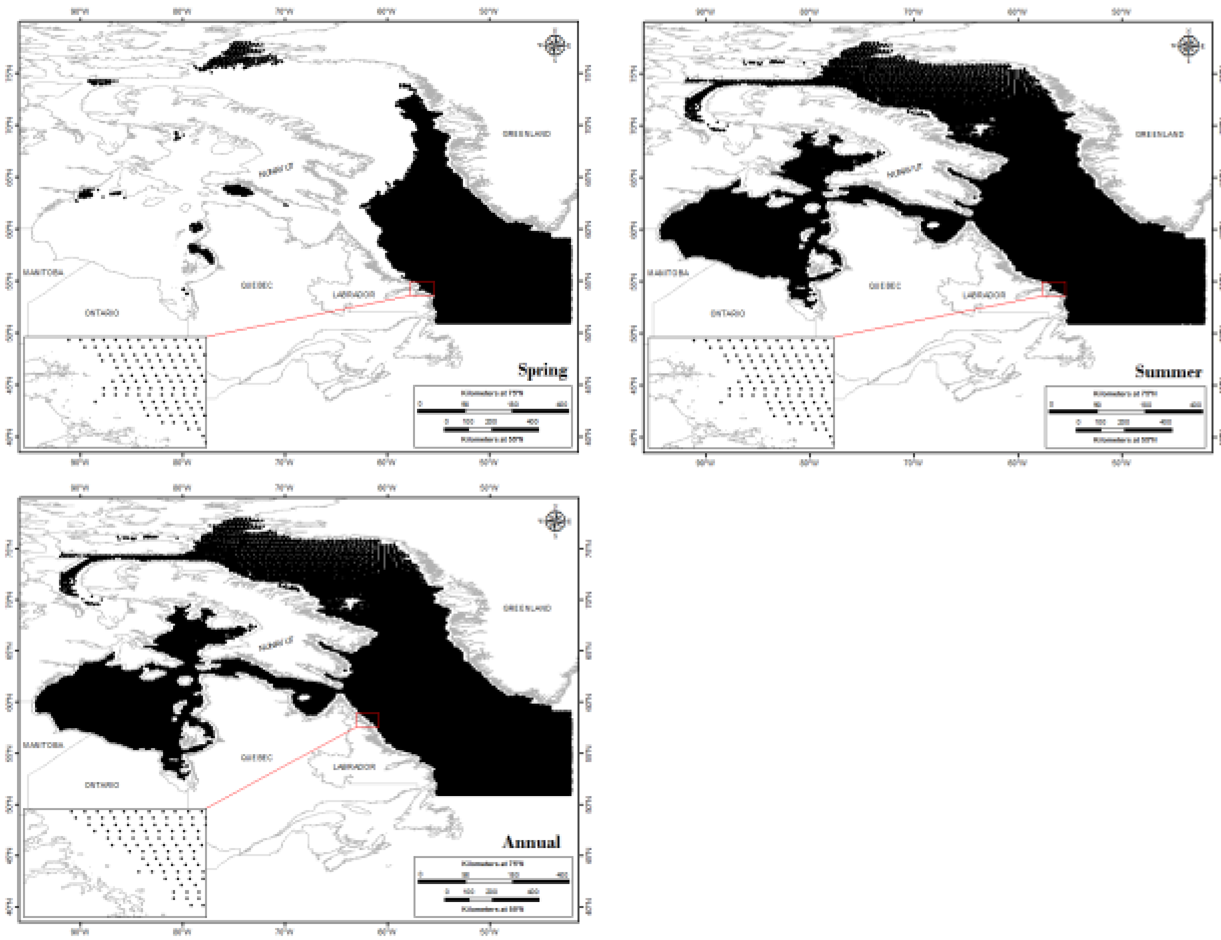


**Figure 4.** Distribution of Spring, Summer, and Annual primary production point data from 2006 to 2010 for the Eastern Canadian Arctic and Sub-Arctic. Point data have a native resolution of 9 km.

*Caveat for Sea Surface Chlorophyll* a *and Primary Production variables*

Ocean-colour satellite sensors degrade over time. As oceans are dark, most light reaching a satellite sensor is contributed by atmospheric scattering. Careful calibration and validation are needed to ensure measurements are accurate after atmospheric contributions are accounted for. Degradation is typically smooth in NASA's SeaWiFS sensor, making it possible to extrapolate calibrations forward in time. However in 2017, unexpected changes over time in the calibration of MODIS Aqua and VIIRS sensors were detected. These patterns were discovered after the ocean colour variables described in this report (chlorophyll a and primary production using MODIS Aqua) were generated, and also apply to previously-generated reports on the environmental variables for DFO's Maritimes, Gulf of St. Lawrence, Newfoundland and Labrador Regions (see Beazley et al., 2016, 2017; Guijarro et al., 2016).

These errors were shown to influence monthly mean surface chlorophyll a and photosynthetically active radiation (PAR) values in the Eastern Canadian Arctic, particularly when examining trends over time. Although general patterns in sea surface chlorophyll a and primary production were not shown to vary after these updates, we caution the user of these variables when examining trends over time and of over-interpretation of the empirical values of primary production and chlorophyll a. It is recommended that users compare trends for data from three or more sensors to guard against unexpected calibration changes.

**Sea Ice Cover**

The sea ice data used in this report are from the Hadley Centre Sea Ice and Sea Surface Temperature Data Set (HadISST; **http://www.metoffice.gov.uk/hadobs/hadisst/**). HadISST was developed at the Met Office Hadley Centre for Climate Prediction and Research, and is a 1° x 1° spatially infilled dataset with monthly data from 1871 to present. HadISST combines data from historical ice charts from shipping, expeditions and other activities, passive microwave satellite retrievals (primarily the NASA Goddard NASA Team data set), and NCEP operational ice analyses. The sea ice fields are made more homogeneous by compensating satellite microwave-based sea ice concentrations for the impact of surface melt effects on retrievals in the Arctic and for algorithm deficiencies in the Antarctic and by making the historical *in situ* concentrations consistent with the satellite data.

Seasonal sea ice was extracted from 1993 to 2010. Ice concentration is stored as double number from 0 to 1 and represents the percentage of ice cover (0 – 100%). Seasons were delimited by the following 'day of year' ranges: days 1 – 90 (Winter), 91 – 181 (Spring), and 274 – 365 (Fall). The native resolution of the point data for each season are 1˚ and is shown in Figure 5.

For each seasonal sea ice data, two different sets of statistics were created from the Hadley Centre Sea Ice and Sea Surface Temperature Data Set (HadISST) monthly data. First, the absolute minima, maxima, and range were calculated for each variable by taking the minimum and maximum values across all months and years at each point location. Range was calculated as the difference between the maximum and minimum values at each location, across all months and year. In this report these variables are denoted as 'Minimum', 'Maximum', or 'Range' (e.g. Sea Ice Cover Maximum). These 'absolute' variables are likely reflective of anomalous events over the entire 18 year time period. The second dataset was created by calculating the average minima, maxima, and range by taking the minimum and maximum values at each location across all months within a year, and averaging across years. These variables are denoted as 'Average Minimum', 'Average Maximum', or 'Average Range' throughout the report. Finally, the mean of each variable was calculated by averaging the values at each location across all months and years, and is denoted as the 'Mean' in this report.

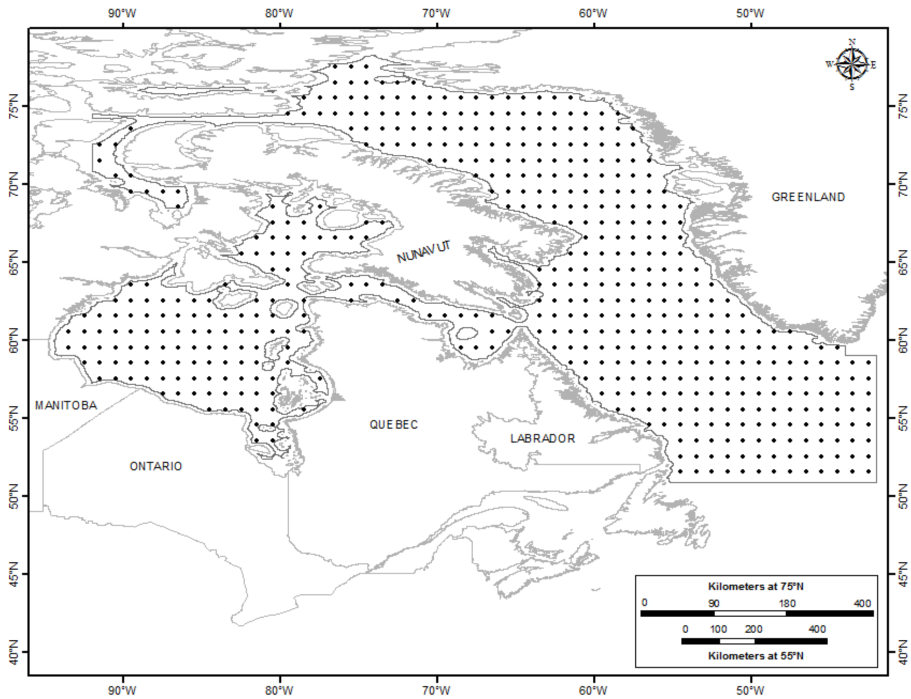


**Figure 5.** Distribution of Winter, Spring, and Fall sea ice point data from 1993 to 2010 for the Eastern Canadian Arctic and Sub-Arctic. Point data have a native resolution of 1˚, which is equivalent to approximately 111 km in this region.

### Nutrients

The distribution of surface silicate, phosphate, nitrate, and dissolved oxygen data for the Eastern Canadian Arctic and Sub-Arctic was examined from the World Ocean Database 2013 (https://www.nodc.noaa.gov/OC5/WOD13/; Boyer et al., 2013). The data were queried from the Ocean Station Data (OSD) dataset from the period of 2006 to 2011. The OSD dataset groups together bottle (Nansen and Niskin) and bucket data, plankton data, and low resolution CTD and expendable CTD (XCTD). Only data collected within the top 10 metres of water and with the highest quality control flag ('Accepted') were called. Data coverage of these variables was very sparse within the study region, making spatial interpolation of the data not possible. Nutrient variables were therefore not included in this report.

## Spatial Interpolation Methods

### Data Exploration and Model Fitting (extracted from Beazley et al. 2016a)

Kriging is a family of geostatistical estimators used to interpolate spatial data. It is a generalized least-square regression technique that allows for spatial prediction in unsampled locations by accounting for the spatial dependence between observed data (Goovaerts, 2000). Spatial dependence is captured by constructing an empirical semivariogram that shows the average semivariance between points by the distance between them. A semivariogram model is then fit to the points forming the empirical semivariogram, and predictions are generated for unmeasured locations based on a weighted average of neighbouring data and their spatial arrangement (Johnston et al., 2001).

Within the kriging family a number of different methods exist including but not limited to, ordinary kriging, universal kriging, and simple kriging. For this report, we chose ordinary kriging as the method of spatial interpolation as it assumes that the mean is unknown prior to modelling and approximately constant (stationary) only in the local neighbourhood of each estimation point and not over the entire data domain (Li and Heap, 2008; Krivoruchko, 2011). Thus ordinary kriging with a local search neighbourhood already accounts for trends in the data (Li and Heap, 2008). When compared against the Inverse Distance Weighting (IDW) interpolation method, ordinary kriging produced better overall mean prediction and root-mean-square errors and smoother prediction surfaces for the same variables interpolated in the Gulf Region (see Beazley et al., 2016a).

Ordinary kriging as a geostatistical interpolator does not require the data to follow a normal distribution (Krivoruchko, 2011). However, the generation of quantile and probability maps using ordinary kriging does require the data to meet this assumption (Krivoruchko, 2011). Transformation of highly skewed data prior to ordinary kriging may result in improved estimates and prediction errors, particularly if the dataset is small and contains outliers (Kravchenko and Bullock, 1999). If a variable shows positive skewness, the confidence limits on the variogram are wider than normal resulting in higher variance (Robinson and Metternicht, 2006; Yamamoto, 2007). Thus, data are often transformed prior to spatial interpolation in order to improve the calculation of statistics and weighted averages (Yamamoto, 2007). Transformation of the data results in estimates on a different scale than the original data, and so it is necessary to back-transform the kriging estimates to their original scale prior to creating the interpolation surface. However, for logarithmic transformation, back-transformation through exponentiation results in exaggerated interpolation-related errors, with extreme errors being the worst affected (Goovaerts, 1997; Robinson and Metternicht, 2006). In the Maritimes Region, variables that had been back-transformed within the Geostatistical Analyst package had poorer prediction errors when compared to variables that were log-transformed outside the ArcMap forum (and thus, were not back-transformed in ArcMap). Therefore, to avoid biased prediction errors, we chose not to transform our data prior to spatial interpolation.

Prior to interpolation we assessed the distributional properties of all variables by examining histograms and summary statistics generated in the 'Explore Data' option in ArcMap's Geostatistical Analyst package. These were reviewed to detect anomalous data points and to visually assess departures from a normal distribution (skewness, kurtosis) in advance of conducting geostatistics. Data distributions were described in terms of their skew (right, or positive, and left, or negative), and kurtosis. Kurtosis is a measure of the 'tailedness' of the distribution, where values equal to 3 are considered mesokurtic (zero tailedness), values < 3 platykurtic (thin-tailed), and values > 3 are leptokurtic (heavy-tailed) (DeCarlo, 1997). Normal Q-Q plots were then constructed to compare the distribution of the data against a standard normal (Gaussian) distribution. The data values are ordered and cumulative distribution values are calculated as (i– 0.5)/n for the $i^{th}$ ordered value out of n total values. If the data values are normally distributed they will form a perfect line at 45° to the origin. Data values that fell above and below the reference line were mapped to identify any spatial trend in the departure from normality.

Ordinary kriging models were created using all default settings in the Geostatistical Analyst wizard. Default settings are a stable semivariogram model type and a circular search neighbourhood with 4 sectors that capture a minimum of 2 and a maximum of 5 neighbours. The optimization function was set for each model, which determines the optimal partial sill, nugget, lag size, and number of lags based on the model range.

**Assessment of Model Performance (extracted from Beazley et al. 2016a)**

Model performance was examined by performing cross-validation, a process where each data point is removed in turn from the model and predicted by the remaining data points. Geostatistical Analyst provides several graphical summaries of the cross validation results, including a scatterplot of the measured versus predicted values (called the Prediction plot), a scatterplot of the residuals of the measured values versus the predicted values (Error plot), a standardized error plot, which shows measured values subtracted from the predicted values and divided by the estimated kriging standard errors, and finally a Q-Q plot, which shows the quantiles of the difference between the predicted and measured values and the corresponding quantiles from a standard normal distribution to assess the normality of the error distributions. Of these, we show only the Prediction plot in the report, although all plots were visually assessed. In the Prediction plot, a horizontal relationship indicates that the model has no information content. With autocorrelation and a good geostatistical model, the relationship between the measured and predicted values should be 1:1.

Also provided by cross validation are five prediction error statistics used for performance evaluation (see Table 2). The overall mean error represents the difference between the measured and predicted values, and should be near zero if the prediction errors are unbiased (i.e., centred on the measured values). However, this value depends on the scale and units of the data, therefore it is better to assess the standardized prediction errors, which are given as prediction errors divided by their prediction standard errors. The mean (Standardized Mean) of these should also be near zero. If the Average Standard Error is close to the Root-Mean-Square Prediction Error, variability in the predictions has been correctly assessed. The Standardized Root-Mean-Square error should be close to one. If the Average Standard Error is greater than the Root-Mean-Square Prediction Error, or if the Standardized Root-Mean-Square Prediction Error is less than one, then the variability of predictions has been overestimated. If the Average Standard Error is less than the Root-Mean-Square Prediction Error or if the Standardized Root-Mean-Square Prediction Error is greater than one, then the variability of predictions has been underestimated. In summary, a good geostatistical model has an Overall Mean Error and Standardized Mean near zero, a small Root-Mean-Square Prediction Error that is approximately equal to the Average Standard Error, an Average Standard Error approximately equal to the Root-Mean-Square Prediction Error, and a Standardized Root-Mean-Square Prediction Error close to one (Johnston et al., 2001). These five prediction error statistics are provided for each variable and are assessed against the rules in Table 2 to provide an overall assessment of model performance.

Finally, model performance was assessed through visual examination of a standard error map. A standard error map quantifies the uncertainty of the prediction and is calculated by taking the square root of the kriging variances. If the data comes from a normal distribution, the true value will be within ± 2 times the prediction standard errors about 95% of the time (Johnston et al. 2001). These maps were used to determine whether there was any spatial pattern in the error distribution.

**Table 2.** Prediction error statistics rules used to assess performance of ordinary kriging models.

| Prediction error | Rule |
|---|---|
| Overall Mean Error | Close to 0 |
| Root-Mean-Square Prediction Error | Close to 0 and approximately equal to the average standard error |
| Standardized Mean | Close to 0 |
| Standardized Root-Mean-Square Prediction Error | Close to 1 |
| Average Standard Error | Approximately equal to the root mean square prediction error |

During the assessment of model performance, we noted that data with a poor underlying distribution did not always result in poor cross validation statistics during the interpolation process. For instance, ordinary kriging on some variables displaying a bimodal distribution (e.g., Bottom Temperature Mean in Beazley et al. 2016a) produced a good fit between measured and predicted values and good to excellent cross validation statistics, suggesting the ordinary kriging is robust to non-normality. Similarly, a model displaying a good fit between measured and predicted values often showed poor cross validation statistics, particularly a higher-than-expected Standardized Root-Mean-Square Prediction Error, indicating that variability in the predictions has been underestimated.

## Caveat for Spatial Interpolation Using Ordinary Kriging

We noted that ordinary kriging of some GLORYS, sea surface chlorophyll *a*, and all sea ice cover variables resulted in negative values in the prediction surfaces. This is in addition to some of the small negative values produced by the GLORYS model itself (see Beazley et al., 2016a for description). Note that for the sea ice variables, ordinary kriging resulted in values outside the limits of the data (less than 0% and greater than 100%).

This issue has been previously described by Deutsch (1996) and Ly et al. (2011), who found that negative weights were generated by ordinary kriging models when outlying data points occurred close to the location being estimated. Ly et al. (2011) suggested two methods for dealing with this issue: 1) apply an *a posteriori* correction as outlined in Deutsch (1996), or 2) to replace all negative interpolated values with zero (or 1, in the case of the sea ice cover variables). In trials to determine the impact of these negative values in species distribution models in DFO's Newfoundland and Labrador Region (see Guijarro et al., 2016), these negative values were replaced with zero, the data remodelled, and the predictions were compared to those models containing the negative values. There was little difference in both the predictions and performance in these different models, suggesting a negligible impact of the negative values on species distribution modelling applications.

The location of these erroneous values in the prediction surface of each variable are shown in Appendix I.

## Recommended Use of Environmental Predictor Variables

At the end of this report we provide a recommendation on the use of these 111 environmental variables in species distribution modelling applications. Variables that provided poor results following spatial interpolation and therefore have limitations to their use are highlighted.

# RESULTS

## Temperature

Both surface and bottom temperatures have biological relevance to benthic invertebrates. In marine sponges, temperature influences various physiological activities, including rates of growth (Barthel, 1986), and pumping and filtration (Riigård et al., 1993). Temperature is also a cue for gametogenesis and larval release (Ettinger-Epstein et al., 2007). Surface water temperature can influence primary and secondary production and hence benthic food supply. Temperature, along with salinity, can be used to indicate water mass structure.

### Bottom Temperature Mean

This variable displayed a skewed, multimodal and platykurtic distribution prior to interpolation with multiple peaks (Table 3, Figure 6). The data were greater than predicted by a normal distribution at the lowest and upper mid-range values, and lower than predicted at the highest and lower mid-range values. These areas of under- and over-prediction showed spatial pattern over the region (Figure 7).

The semivariogram showed moderate autocorrelation present in the data (Figure 8). The kriged model showed an excellent fit between measured and predicted values (Figure 8). Good performance of the model was indicated by the cross-validation results (Table 4). The error map showed low error in Hudson Bay, and moderate error in Baffin Bay and Davis Strait, with higher error along the edges of the study area (Figure 9). The kriged surface is presented in Figure 10.

Table 3. Distributional properties of Bottom Temperature Mean (°C).

| **Property** | **Value** |
|---|---:|
| Number of Observations | 16376 |
| Minimum | -2.685 |
| Maximum | 4.725 |
| Mean | 0.357 |
| Median | 0.105 |
| Standard Deviation | 1.871 |
| Skewness | 0.282 |
| Kurtosis | 1.696 |

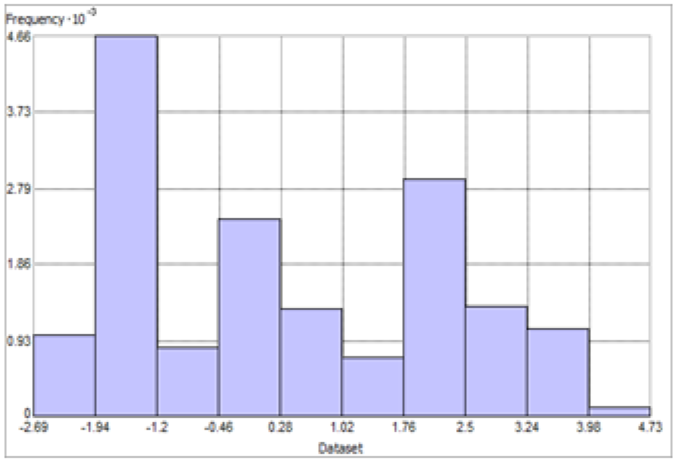


Figure 6. Distribution of Bottom Temperature Mean (°C). Histogram was illustrated using 10 bins. Y axis is shown at $10^{-3}$.

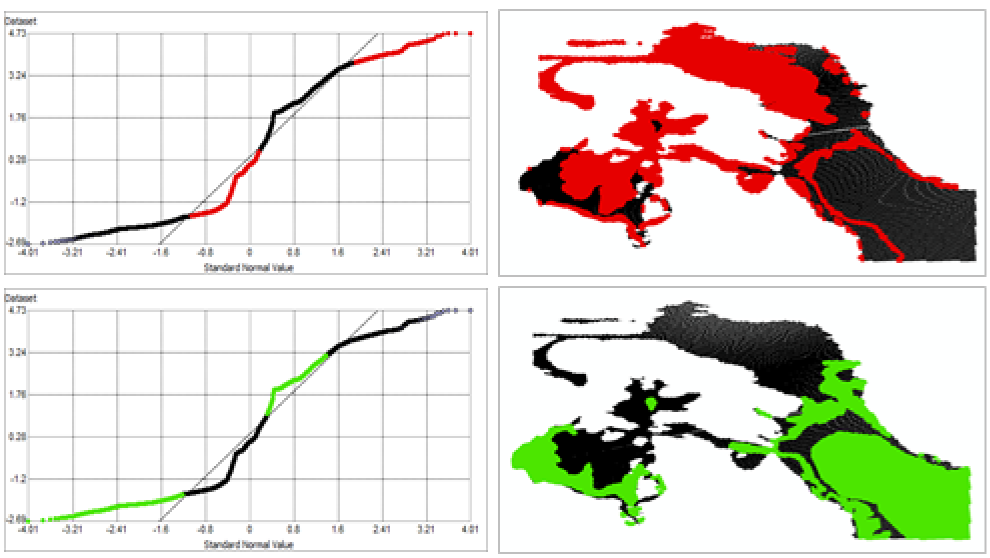


Figure 7. Normal Q-Q plot for data values of Bottom Temperature Mean (°C). Points falling under (top right panel) and over (bottom right panel) the reference line are mapped.

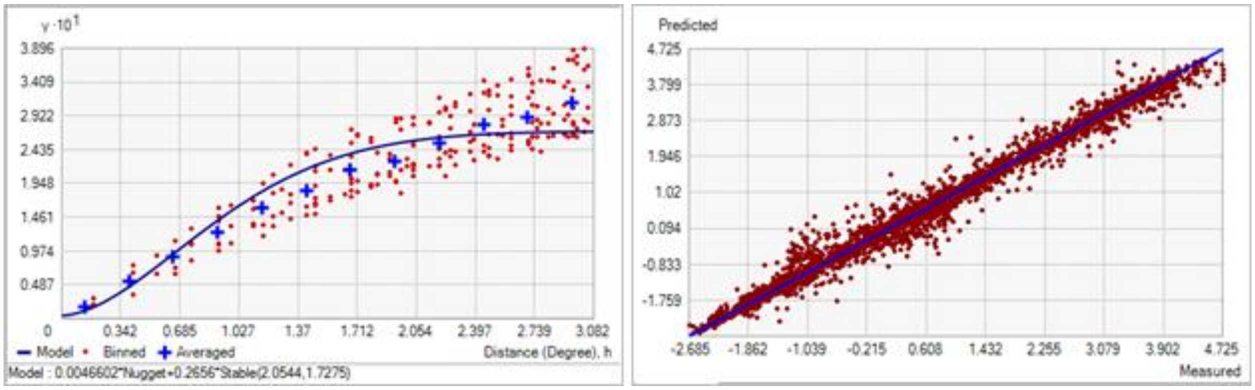

Figure 8. Left panel: Semivariogram of Bottom Temperature Mean (°C). Binned values are shown as red dots; average points are shown as blue crosses; the model fit to the averaged values is shown as a blue line. Lag size: 0.257 degrees; number of lags: 12; Parameter: 1.728; Range: 2.054 degrees; Partial Sill: 0.266. Right panel: Scatterplot of predicted values versus observed values for the model of Bottom Temperature Mean (°C).

Table 4. Results of cross-validation of the kriged model for Bottom Temperature Mean (°C).

| **Prediction Error** | **Value** |
|---|---:|
| Number of Observations | 16376 |
| Overall Mean Error | $4.920 \times 10^{-4}$ |
| Root Mean Square Prediction Error | 0.110 |
| Standardized Mean | $4.033 \times 10^{-3}$ |
| Standardized Root Mean Square Prediction Error | 1.097 |
| Average Standard Error | 0.095 |

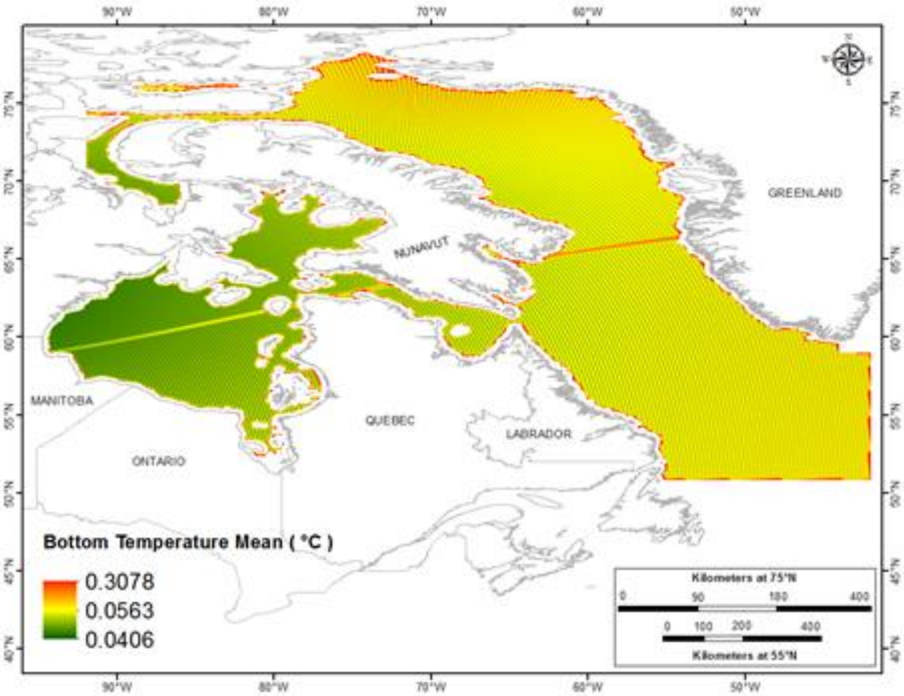


Figure 9. Prediction standard error surface of Bottom Temperature Mean (˚C).

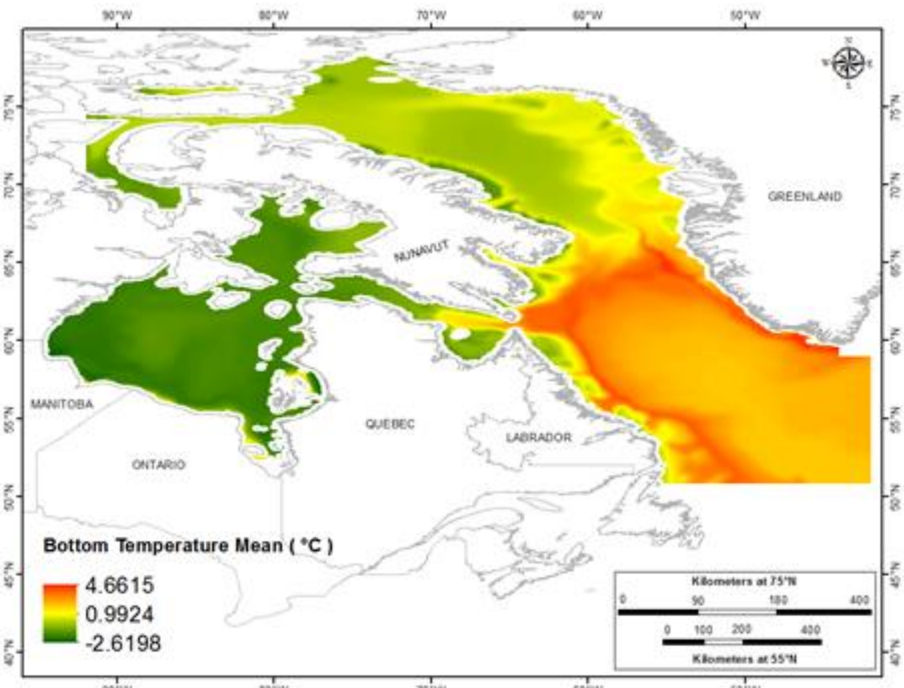


Figure 10. Interpolated prediction surface of Bottom Temperature Mean (˚C).

**Bottom Temperature Minimum**

This variable displayed a left-skewed, leptokurtic distribution prior to interpolation (Table 5, Figure 11). The data were lower than predicted by a normal distribution at both tails, while mid-values followed the reference line (Figure 12). These areas of under- and over-prediction showed spatial pattern over the region (Figure 12).

The semivariogram showed moderate autocorrelation present in the data (Figure 13). The kriged model showed an excellent fit between measured and predicted values (Figure 13). Good performance of the model was indicated by the cross-validation results (Table 6). The error map showed low error in Hudson Bay, and moderate error in Baffin Bay and Davis Strait, with higher error along the edges of the study extent and in the most northern areas (Figure 14). The kriged surface is presented in Figure 15. The extreme minimum values (~ -12˚C) are located along the coast in Hudson Bay and are not considered realistic. Therefore, caution should be taken when interpreting this variable in that region.

Table 5. Distributional properties of Bottom Temperature Minimum (°C).

| **Property** | **Value** |
|---|---:|
| Number of Observations | 16376 |
| Minimum | -12.801 |
| Maximum | 3.197 |
| Mean | -0.698 |
| Median | -0.425 |
| Standard Deviation | 2.284 |
| Skewness | -0.619 |
| Kurtosis | 3.754 |

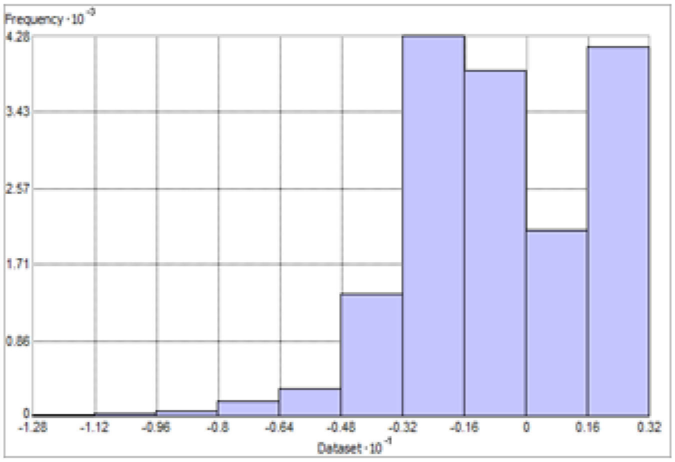


Figure 11. Distribution of Bottom Temperature Minimum (°C). Histogram was illustrated using 10 bins. X axis is shown at $10^{-1}$; Y axis is shown at $10^{-3}$.

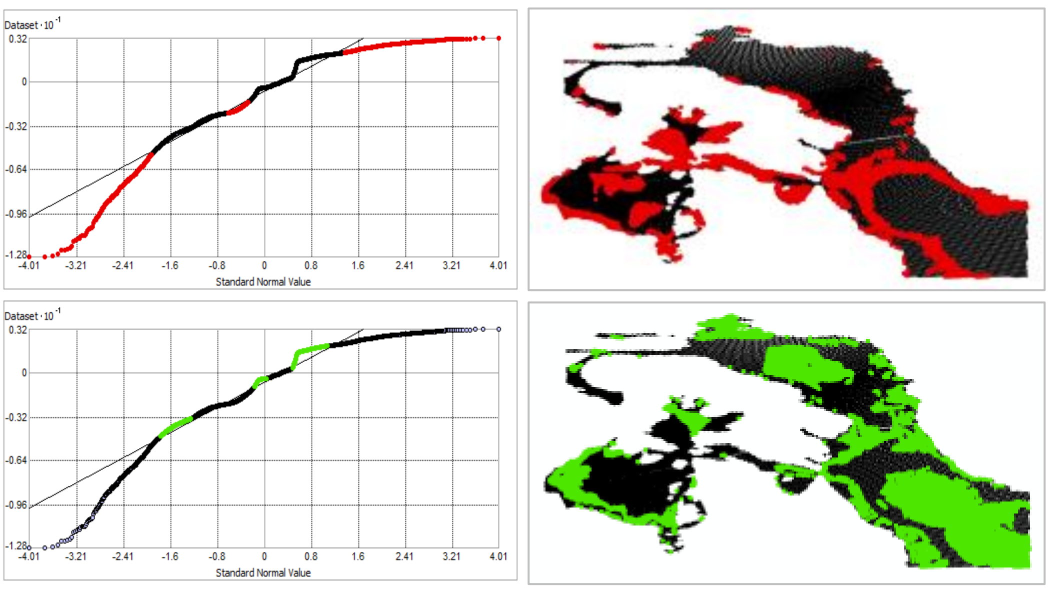


Figure 12. Normal Q-Q plot for data values of Bottom Temperature Minimum (°C). Points falling under (top right panel) and over (bottom right panel) the reference line are mapped.

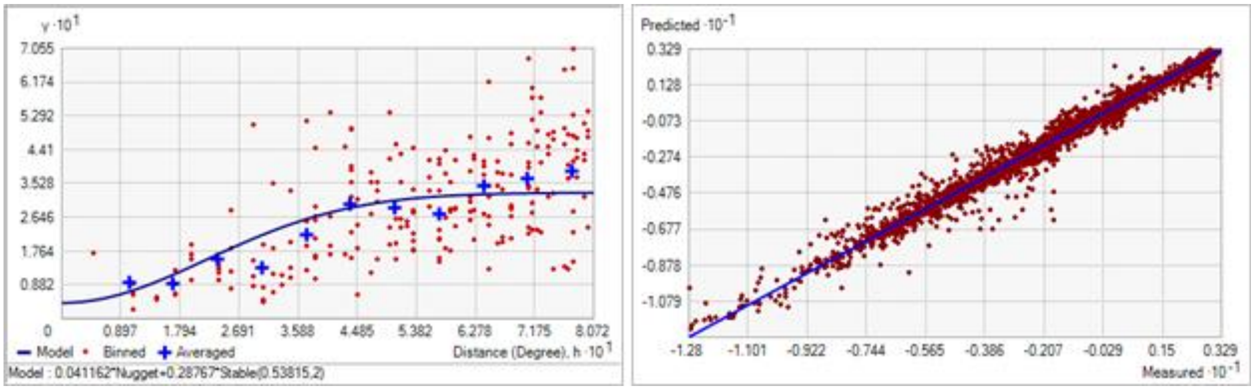

Figure 13. Left panel: Semivariogram of Bottom Temperature Minimum (°C). Binned values are shown as red dots; average points are shown as blue crosses; the model fit to the averaged values is shown as a blue line. Lag size: 0.067 degrees; number of lags: 12; Parameter: 2; Range: 0.538 degrees; Partial Sill: 0.288. Right panel: Scatterplot of predicted values versus observed values for the model of Bottom Temperature Minimum (°C).

Table 6. Results of cross-validation of the kriged model for Bottom Temperature Minimum (°C).

| **Prediction Error** | **Value** |
|---|---:|
| Number of Observations | 16376 |
| Overall Mean Error | $6.586 \times 10^{-4}$ |
| Root Mean Square Prediction Error | 0.205 |
| Standardized Mean | $1.302 \times 10^{-3}$ |
| Standardized Root Mean Square Prediction Error | 0.693 |
| Average Standard Error | 0.282 |

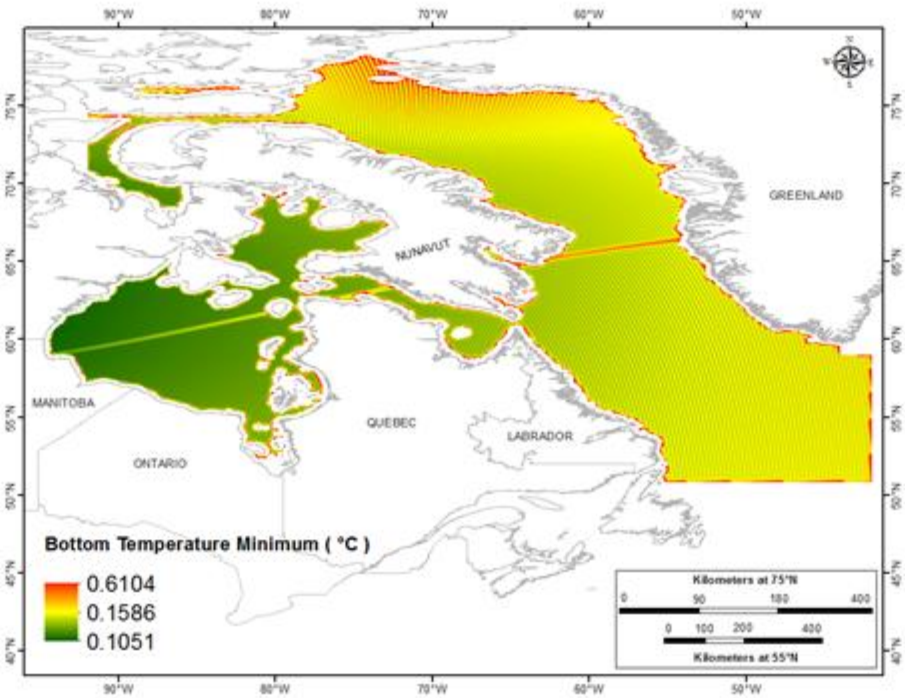


Figure 14. Prediction standard error surface of Bottom Temperature Minimum (˚C).

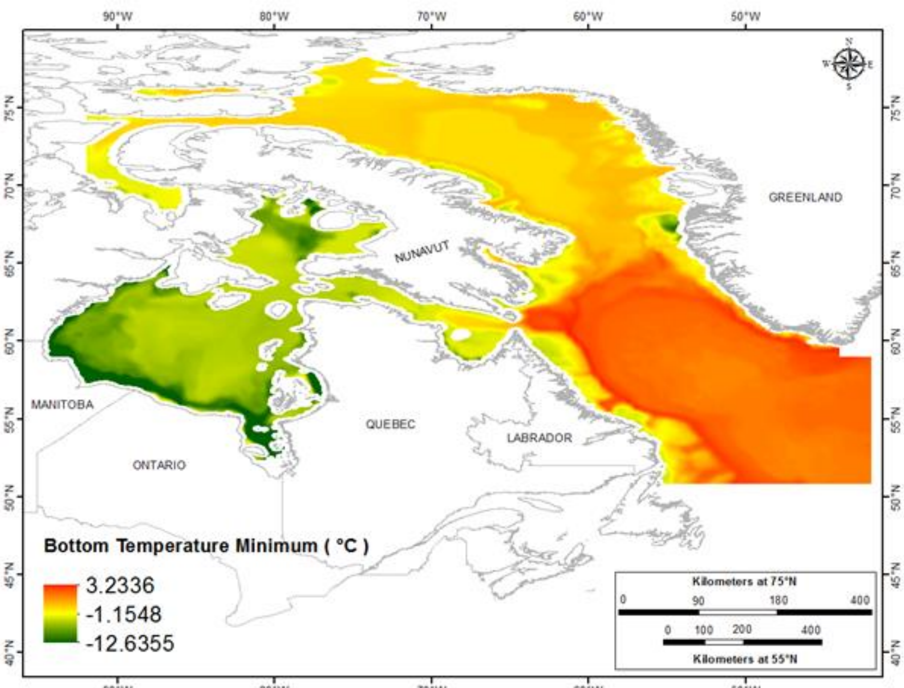


Figure 15. Interpolated prediction surface of Bottom Temperature Minimum (˚C).

### Bottom Temperature Maximum

This variable displayed a right-skewed, platykurtic distribution prior to interpolation (Table 7, Figure 16). The data were higher than predicted by a normal distribution at both tails, while mid-values followed the reference line but with some deviation (Figure 17). These areas of under- and over-prediction showed spatial pattern over the region (Figure 17).

The semivariogram showed moderate autocorrelation present in the data (Figure 18). The kriged model showed an excellent fit between measured and predicted values (Figure 18). Good performance of the model was indicated by the cross-validation results (Table 8). The error map showed low error in Hudson Bay, and moderate error in Baffin Bay and Davis Strait, with higher error along the edges of the study extent and in the most northern areas (Figure 19). The kriged surface is presented in Figure 20.

Table 7. Distributional properties of Bottom Temperature Maximum (°C).

| **Property** | **Value** |
|---|---:|
| Number of Observations | 16376 |
| Minimum | -1.390 |
| Maximum | 11.190 |
| Mean | 1.460 |
| Median | 1.120 |
| Standard Deviation | 2.067 |
| Skewness | 0.515 |
| Kurtosis | 2.482 |

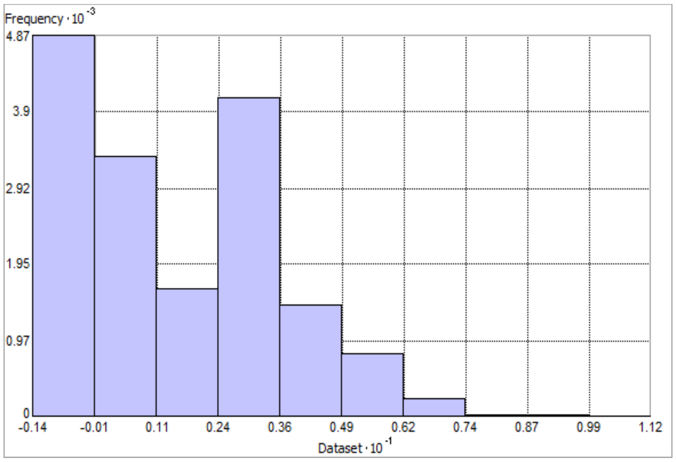


Figure 16. Distribution of Bottom Temperature Maximum (°C). Histogram was illustrated using 10 bins. X axis is shown at $10^{-1}$; Y axis is shown at $10^{-3}$.

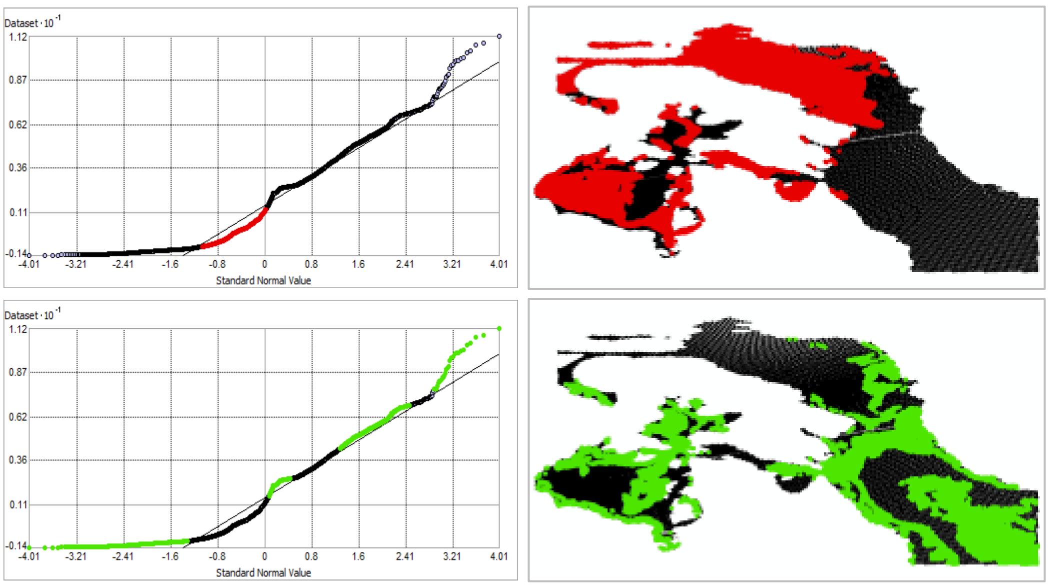


Figure 17. Normal Q-Q plot for data values of Bottom Temperature Maximum (°C). Points falling under (top right panel) and over (bottom right panel) the reference line are mapped.

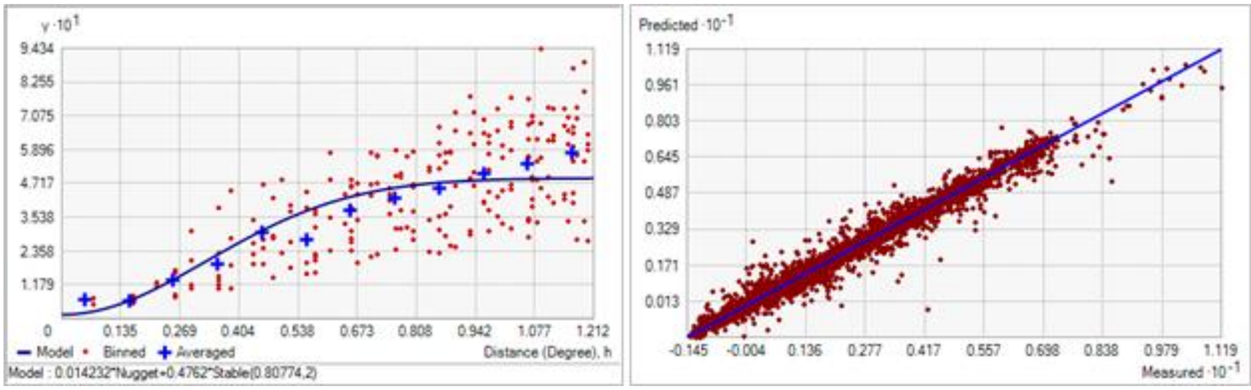


Figure 18. Left panel: Semivariogram of Bottom Temperature Maximum (°C). Binned values are shown as red dots; average points are shown as blue crosses; the model fit to the averaged values is shown as a blue line. Lag size: 0.101 degrees; number of lags: 12; Parameter: 2; Range: 0.808 degrees; Partial Sill: 0.476. Right panel: Scatterplot of predicted values versus observed values for the model of Bottom Temperature Maximum (°C).

Table 8. Results of cross-validation of the kriged model for Bottom Temperature Maximum (°C).

| **Prediction Error** | **Value** |
|---|---:|
| Number of Observations | 16376 |
| Overall Mean Error | -4.441 x $10^{-4}$ |
| Root Mean Square Prediction Error | 0.191 |
| Standardized Mean | 1.159 x $10^{-3}$ |
| Standardized Root Mean Square Prediction Error | 1.127 |
| Average Standard Error | 0.155 |

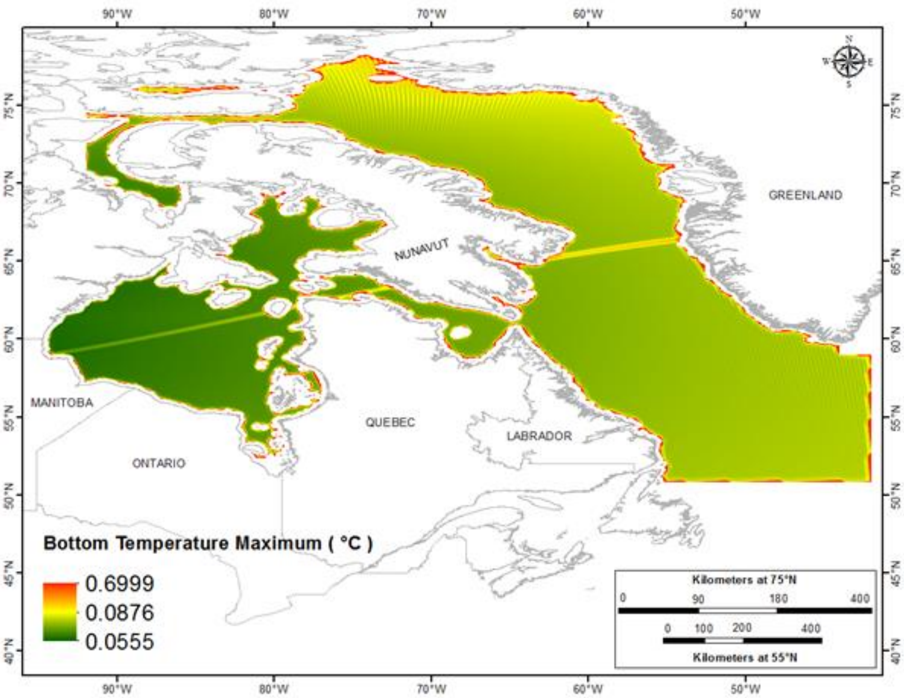


Figure 19. Prediction standard error surface of Bottom Temperature Maximum (˚C).

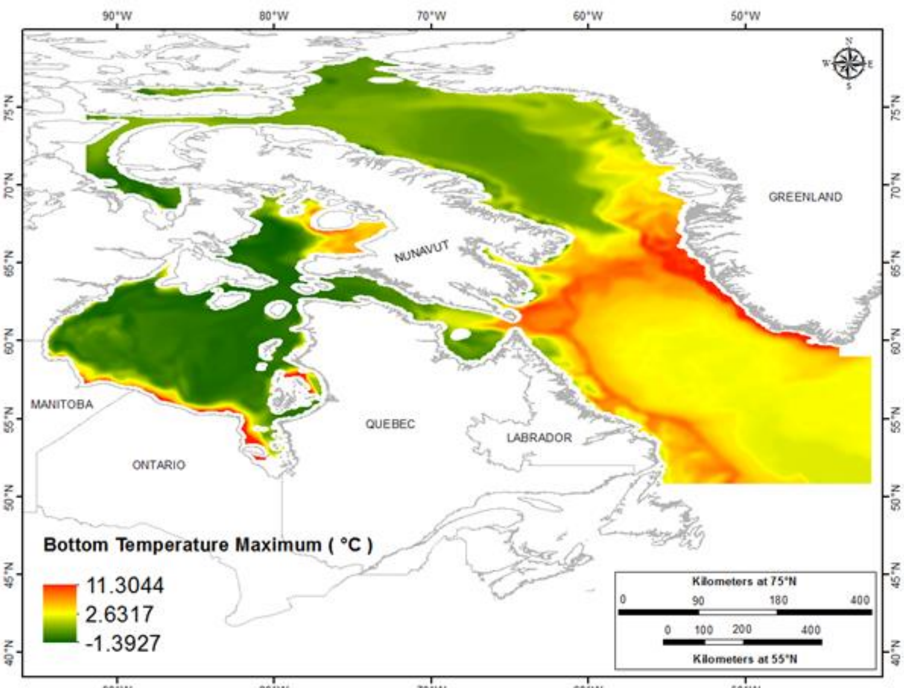


Figure 20. Interpolated prediction surface of Bottom Temperature Maximum (˚C).

## Bottom Temperature Range

This variable displayed a right-skewed, leptokurtic distribution prior to interpolation (Table 9, Figure 21). The data were higher than predicted by a normal distribution at both tails, while mid-values were lower than the reference line (Figure 22). These areas of under- and over-prediction showed spatial pattern over the region (Figure 22).

The semivariogram showed moderate autocorrelation present in the data (Figure 23). The kriged model showed an excellent fit between measured and predicted values (Figure 23). Fair performance of the model was indicated by the cross-validation results (Table 10), with overestimation of the variability of the predictions as indicated by the Standardized Root-Mean-Square Error less than 1. The error map showed lower error in Hudson Bay compared to Baffin Bay and Davis Strait, with higher error along the edges of the study extent and in the most northern areas (Figure 24). The kriged surface is presented in Figure 25.

Table 9. Distributional properties of Bottom Temperature Range (°C).

| Property | Value |
|---|---:|
| Number of Observations | 16376 |
| Minimum | 0.096 |
| Maximum | 17.281 |
| Mean | 2.157 |
| Median | 1.384 |
| Standard Deviation | 2.060 |
| Skewness | 2.374 |
| Kurtosis | 10.431 |

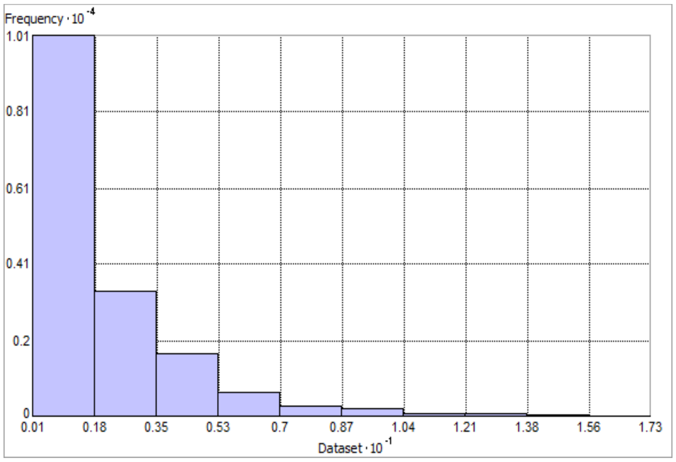


Figure 21. Distribution of Bottom Temperature Range (°C). Histogram was illustrated using 10 bins. X axis is shown at $10^{-1}$; Y axis is shown at $10^{-4}$.

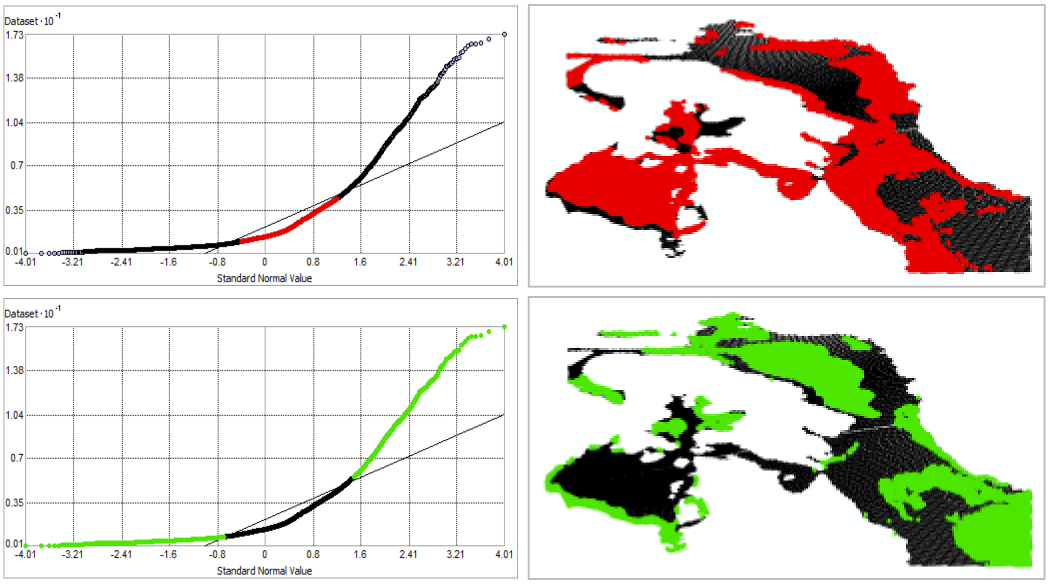


Figure 22. Normal Q-Q plot for data values of Bottom Temperature Range (°C). Points falling under (top right panel) and over (bottom right panel) the reference line are mapped.

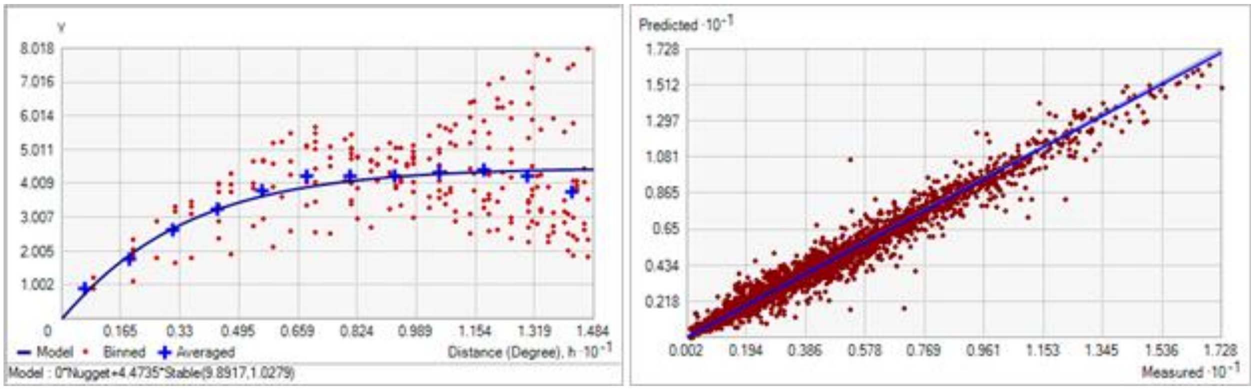


Figure 23. Left panel: Semivariogram of Bottom Temperature Range (°C). Binned values are shown as red dots; average points are shown as blue crosses; the model fit to the averaged values is shown as a blue line. Lag size: 1.236 degrees; number of lags: 12; Parameter: 1.028; Range: 9.892 degrees; Partial Sill: 4.474. Right panel: Scatterplot of predicted values versus observed values for the model of Bottom Temperature Range (°C).

Table 10. Results of cross-validation of the kriged model for Bottom Temperature Range (°C).

| **Prediction Error** | **Value** |
|---|---:|
| Number of Observations | 16376 |
| Overall Mean Error | $-1.416 \times 10^{-3}$ |
| Root Mean Square Prediction Error | 0.256 |
| Standardized Mean | $-1.107 \times 10^{-3}$ |
| Standardized Root Mean Square Prediction Error | 0.628 |
| Average Standard Error | 0.397 |

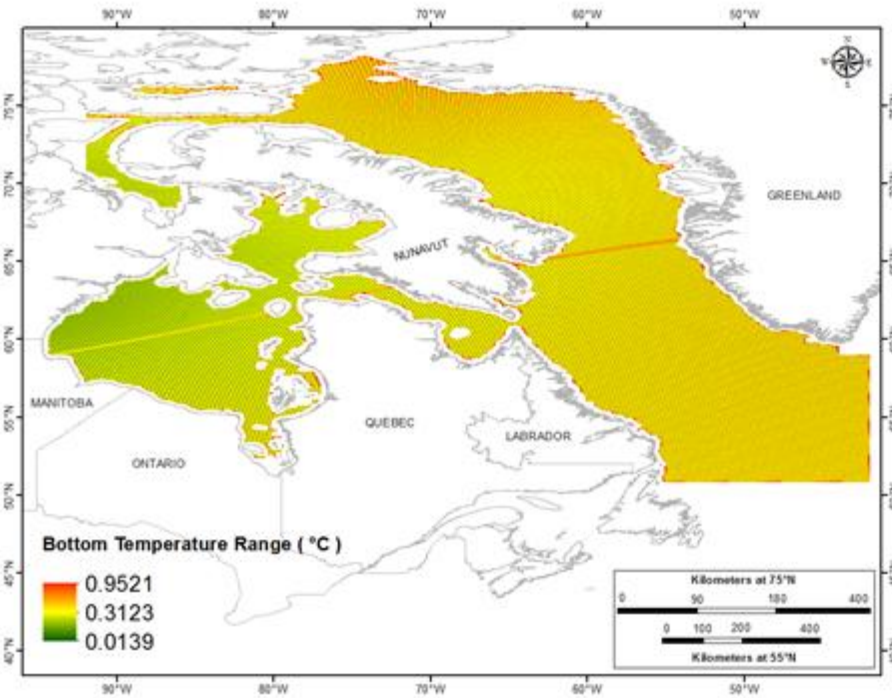


Figure 24. Prediction standard error surface of Bottom Temperature Range (˚C).

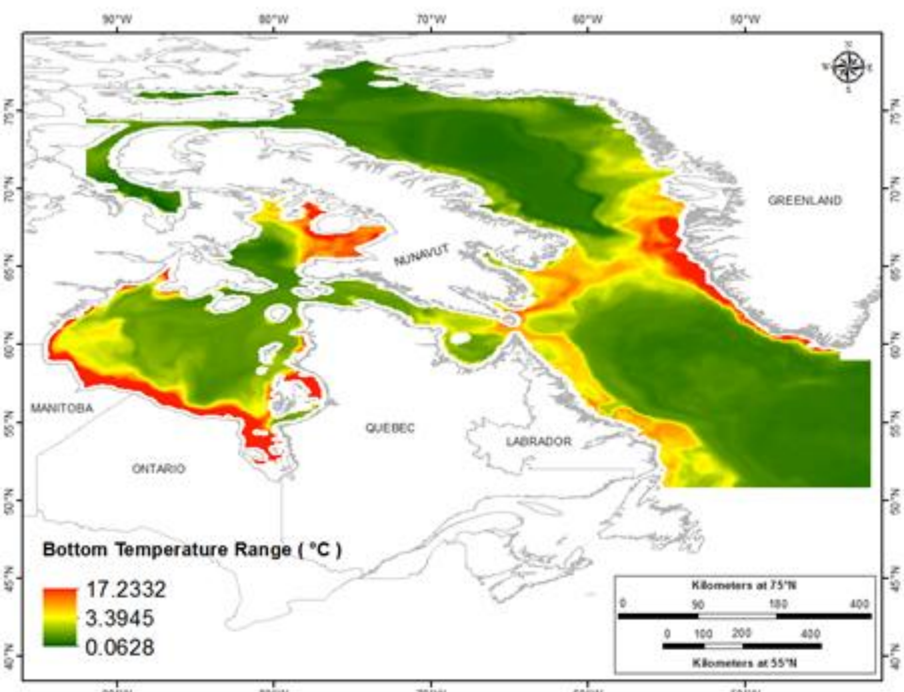


Figure 25. Interpolated prediction surface of Bottom Temperature Range (˚C).

## Bottom Temperature Average Minimum

This variable displayed a left-skewed, platykurtic distribution prior to interpolation (Table 11, Figure 26). The data were lower than predicted by a normal distribution at both tails, while mid-values followed the reference line but with some deviation (Figure 27). These areas of under- and over-prediction showed spatial pattern over the region (Figure 27).

The semivariogram showed moderate autocorrelation present in the data (Figure 28). The kriged model showed an excellent fit between measured and predicted values (Figure 28). Fair performance of the model was indicated by the cross-validation results (Table 12). The error map showed lower error in Hudson Bay compared to Baffin Bay and Davis Strait, with higher error along the edges of the study extent and in the most northern areas (Figure 29). The kriged surface is presented in Figure 30.

Table 11. Distributional properties of Bottom Temperature Average Minimum (°C).

| **Property** | **Value** |
|---|---:|
| Number of Observations | 16376 |
| Minimum | -8.911 |
| Maximum | 3.919 |
| Mean | -0.047 |
| Median | -0.062 |
| Standard Deviation | 2.025 |
| Skewness | -0.162 |
| Kurtosis | 2.450 |

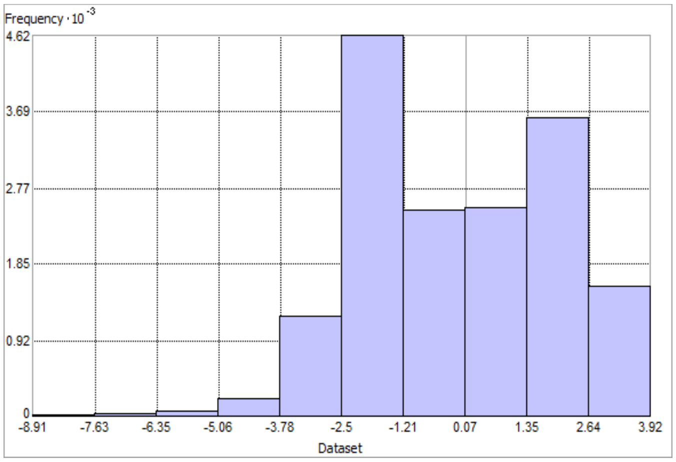


Figure 26. Distribution of Bottom Temperature Average Minimum (°C). Histogram was illustrated using 10 bins. Y axis is shown at $10^{-3}$.

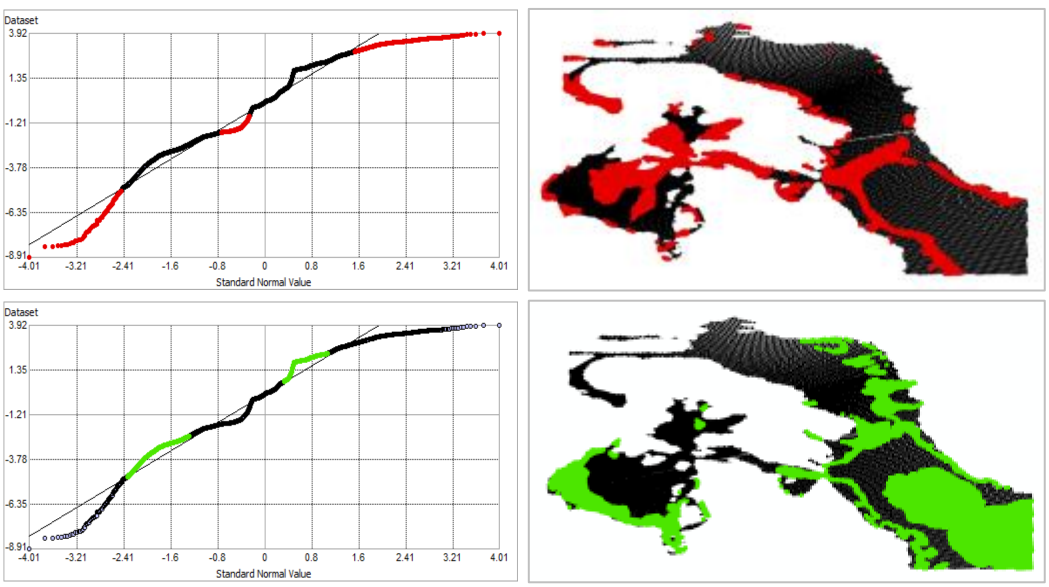


Figure 27. Normal Q-Q plot for data values of Bottom Temperature Average Minimum (°C). Points falling under (top right panel) and over (bottom right panel) the reference line are mapped.

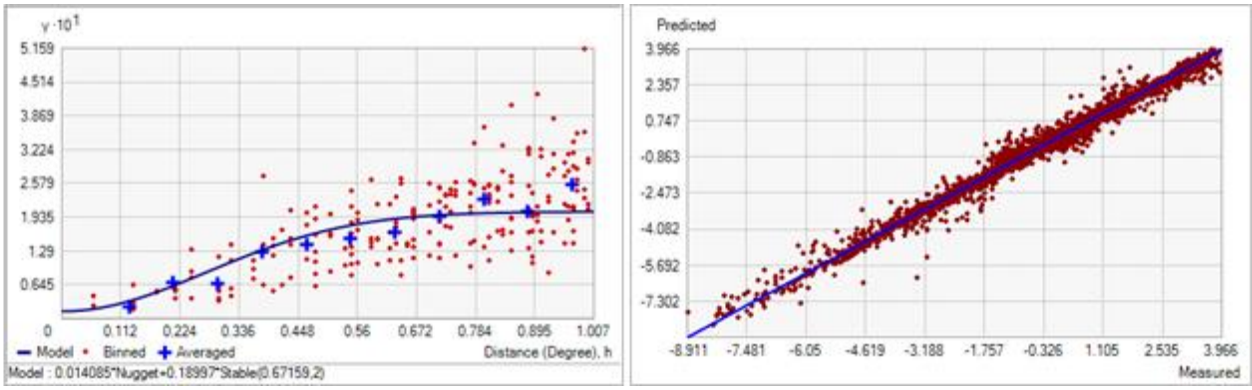


Figure 28. Left panel: Semivariogram of Bottom Temperature Average Minimum (°C). Binned values are shown as red dots; average points are shown as blue crosses; the model fit to the averaged values is shown as a blue line. Lag size: 0.084 degrees; number of lags: 12; Parameter: 2; Range: 0.672 degrees; Partial Sill: 0.190. Right panel: Scatterplot of predicted values versus observed values for the model of Bottom Temperature Average Minimum (°C).

Table 12. Results of cross-validation of the kriged model for Bottom Temperature Average Minimum (°C).

| **Prediction Error** | **Value** |
|---|---:|
| Number of Observations | 16376 |
| Overall Mean Error | $1.200 \times 10^{-3}$ |
| Root Mean Square Prediction Error | 0.136 |
| Standardized Mean | $4.622 \times 10^{-3}$ |
| Standardized Root Mean Square Prediction Error | 0.812 |
| Average Standard Error | 0.157 |

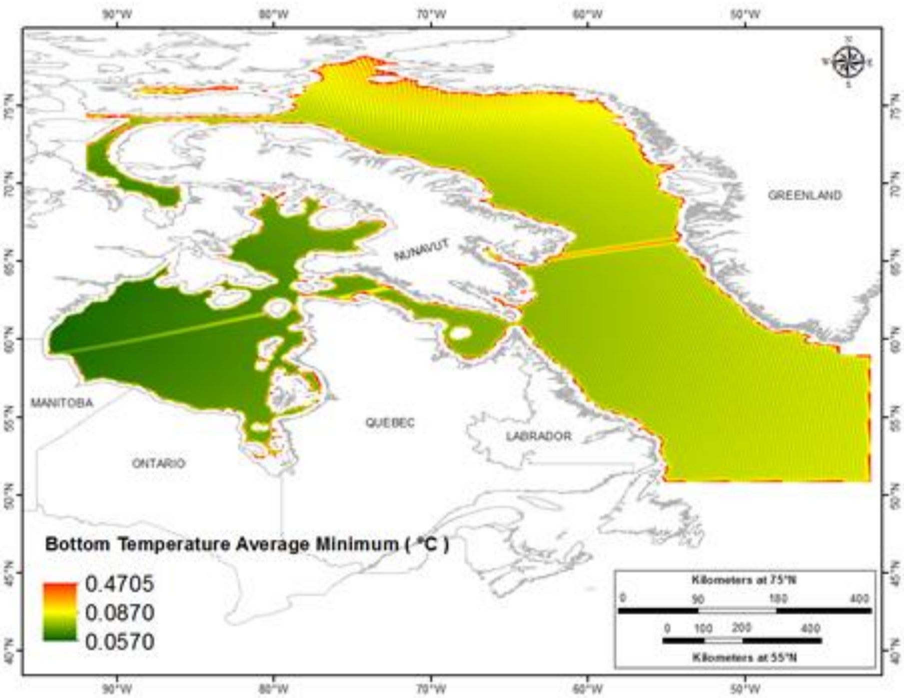


Figure 29. Prediction standard error surface of Bottom Temperature Average Minimum (˚C).

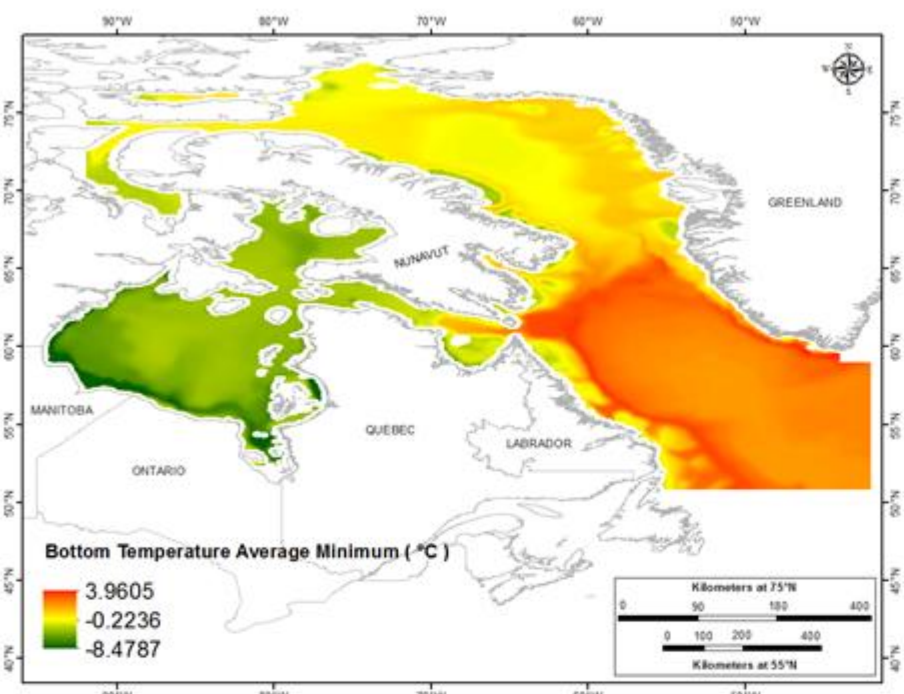


Figure 30. Interpolated prediction surface of Bottom Temperature Average Minimum (˚C).

**Bottom Temperature Average Maximum**

This variable displayed a bimodal, platykurtic distribution prior to interpolation (Table 13, Figure 31). The data were greater than predicted by a normal distribution at the lowest and upper mid-range values, and lower than predicted at the highest and lower mid-range values. These areas of under- and over-prediction showed no spatial pattern over the region (Figure 32).

The semivariogram showed moderate autocorrelation present in the data (Figure 33). The kriged model showed a good fit between measured and predicted values (Figure 33). Fair performance of the model was indicated by the cross-validation results (Table 14). The error map showed lower error in Hudson Bay compared to Baffin Bay and Davis Strait, with higher error along the edges of the study extent and in the most northern areas (Figure 34). The kriged surface is presented in Figure 35.

Table 13. Distributional properties of Bottom Temperature Average Maximum (°C).

| **Property** | **Value** |
|---|---:|
| Number of Observations | 16376 |
| Minimum | -1.704 |
| Maximum | 8.064 |
| Mean | 0.768 |
| Median | 0.289 |
| Standard Deviation | 1.927 |
| Skewness | 0.406 |
| Kurtosis | 2.037 |

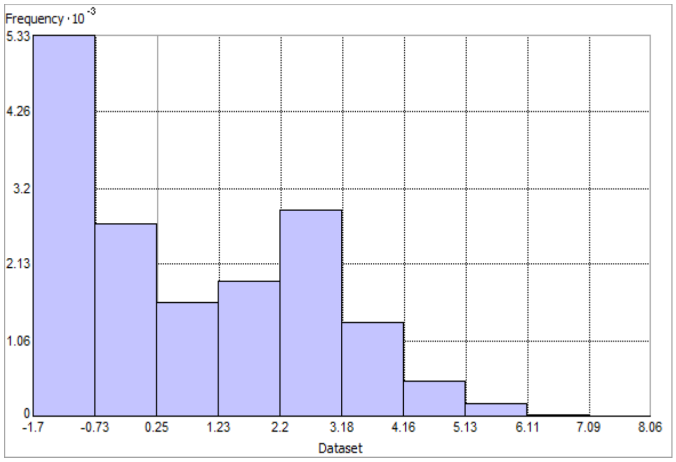


Figure 31. Distribution of Bottom Temperature Average Maximum (°C). Histogram was illustrated using 10 bins. Y axis is shown at $10^{-3}$.

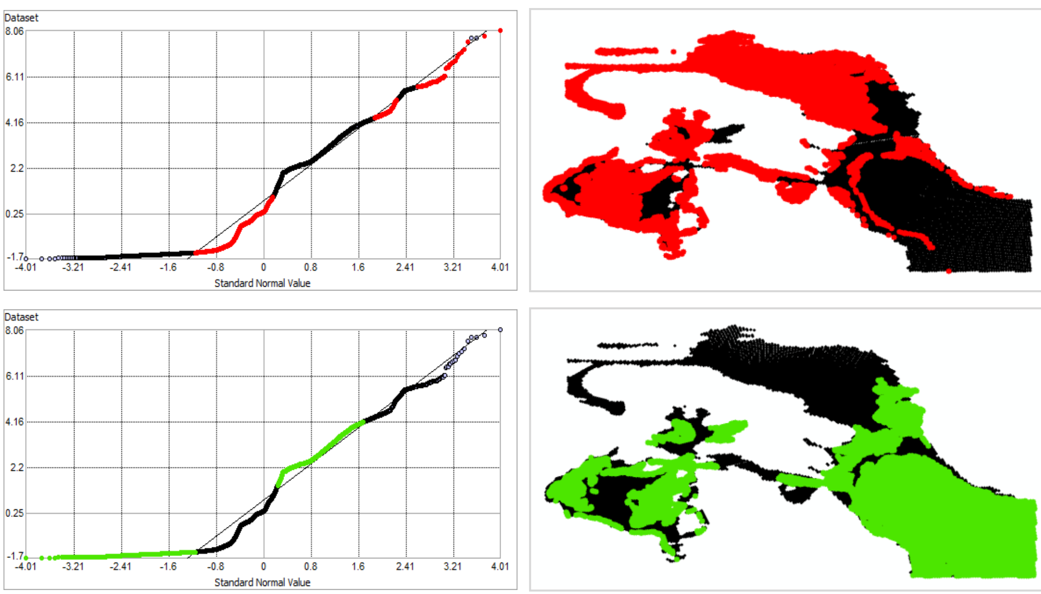


Figure 32. Normal Q-Q plot for data values of Bottom Temperature Average Maximum (°C). Points falling under (top right panel) and over (bottom right panel) the reference line are mapped.

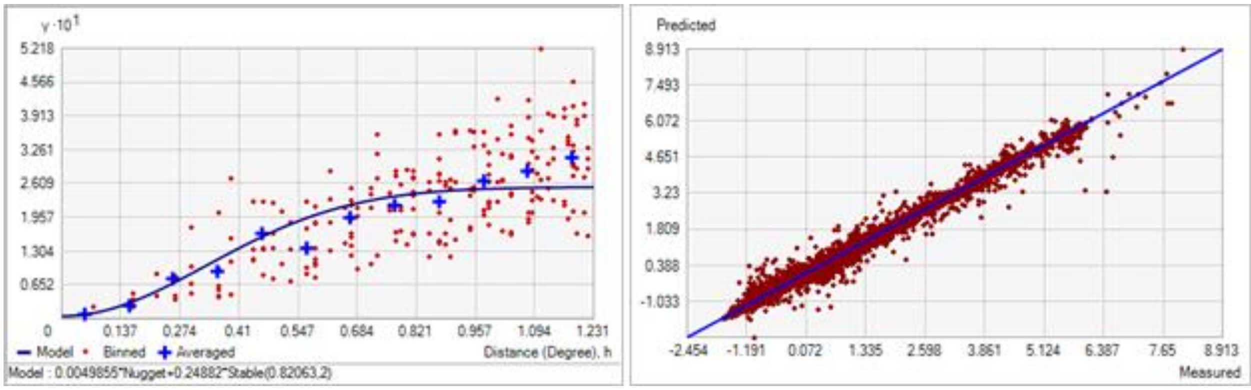

Figure 33. Left panel: Semivariogram of Bottom Temperature Average Maximum (°C). Binned values are shown as red dots; average points are shown as blue crosses; the model fit to the averaged values is shown as a blue line. Lag size: 0.103 degrees; number of lags: 12; Parameter: 2; Range: 0.821 degrees; Partial Sill: 0.249. Right panel: Scatterplot of predicted values versus observed values for the model of Bottom Temperature Average Maximum (°C).

Table 14. Results of cross-validation of the kriged model for Bottom Temperature Average Maximum (°C).

| **Prediction Error** | **Value** |
|---|---:|
| Number of Observations | 16376 |
| Overall Mean Error | $-2.334 \times 10^{-4}$ |
| Root Mean Square Prediction Error | 0.131 |
| Standardized Mean | $1.346 \times 10^{-3}$ |
| Standardized Root Mean Square Prediction Error | 1.253 |
| Average Standard Error | 0.094 |

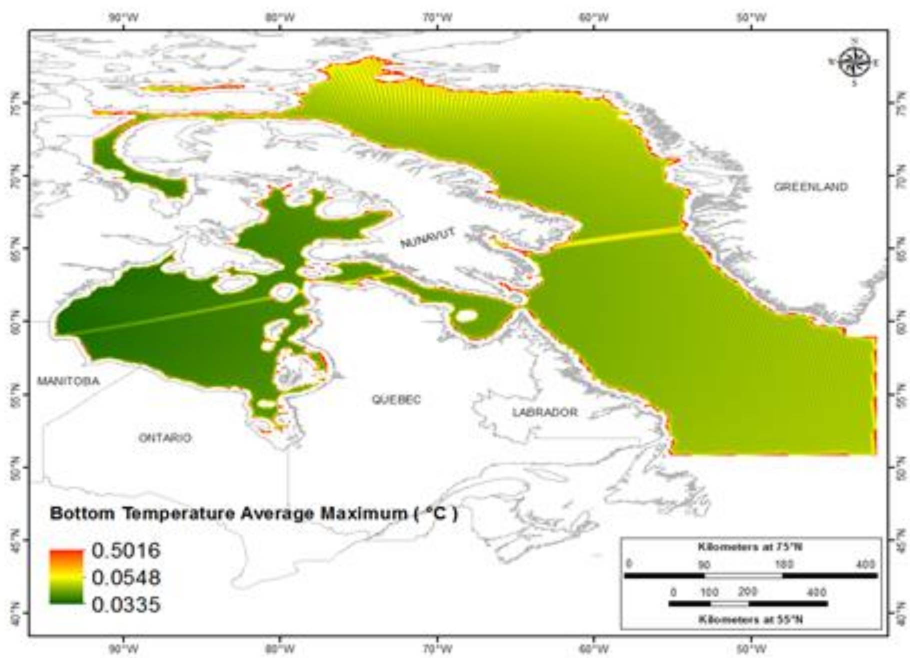


Figure 34. Prediction standard error surface of Bottom Temperature Average Maximum (˚C).

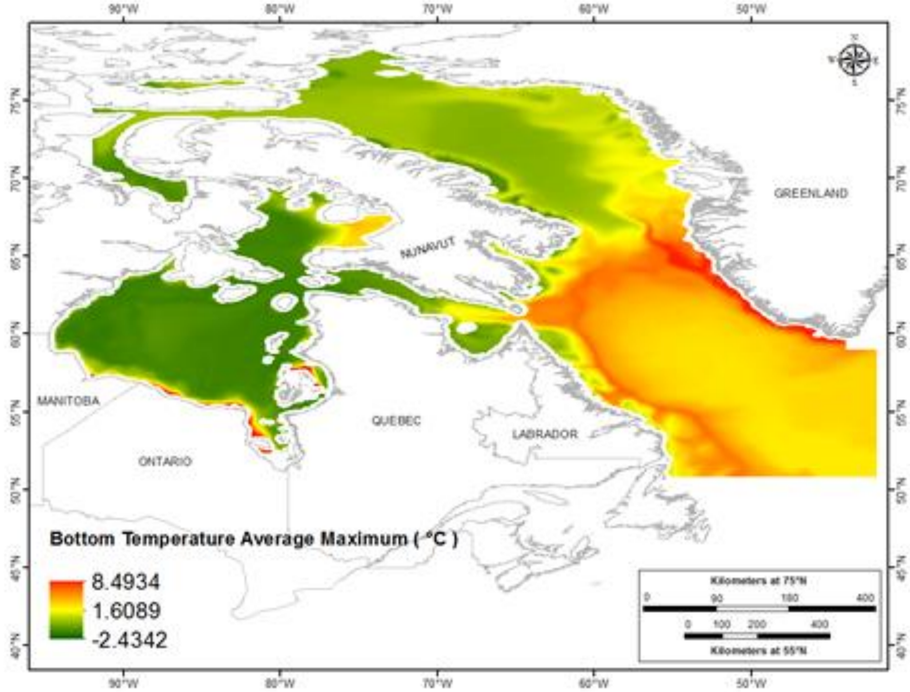


Figure 35. Interpolated prediction surface of Bottom Temperature Average Maximum (˚C).

### Bottom Temperature Average Range

This variable displayed a right-skewed, leptokurtic distribution prior to interpolation (Table 15, Figure 36). The data were higher than predicted by a normal distribution at both tails, while mid-values were lower than the reference line (Figure 37). These areas of under- and over-prediction showed spatial pattern over the region (Figure 37).

The semivariogram showed moderate autocorrelation present in the data (Figure 38). The kriged model showed a good fit between measured and predicted values (Figure 38). Fair performance of the model was indicated by the cross-validation results (Table 16). The error map showed lower error in Hudson Bay compared to Baffin Bay and Davis Strait, with higher error along the edges of the study extent and in the most northern areas (Figure 39). The kriged surface is presented in Figure 40.

Table 15. Distributional properties of Bottom Temperature Average Range (°C).

| **Property** | **Value** |
|---|---:|
| Number of Observations | 16376 |
| Minimum | 0.017 |
| Maximum | 9.603 |
| Mean | 0.816 |
| Median | 0.384 |
| Standard Deviation | 1.121 |
| Skewness | 3.140 |
| Kurtosis | 15.228 |

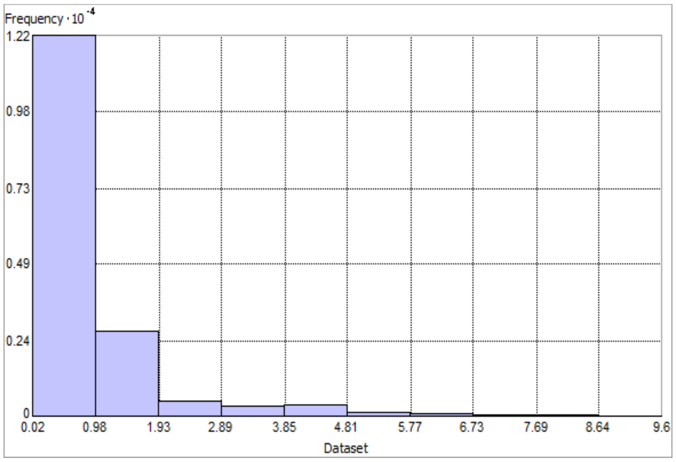


Figure 36. Distribution of Bottom Temperature Average Range (°C). Histogram was illustrated using 10 bins. Y axis is shown at $10^{-4}$.

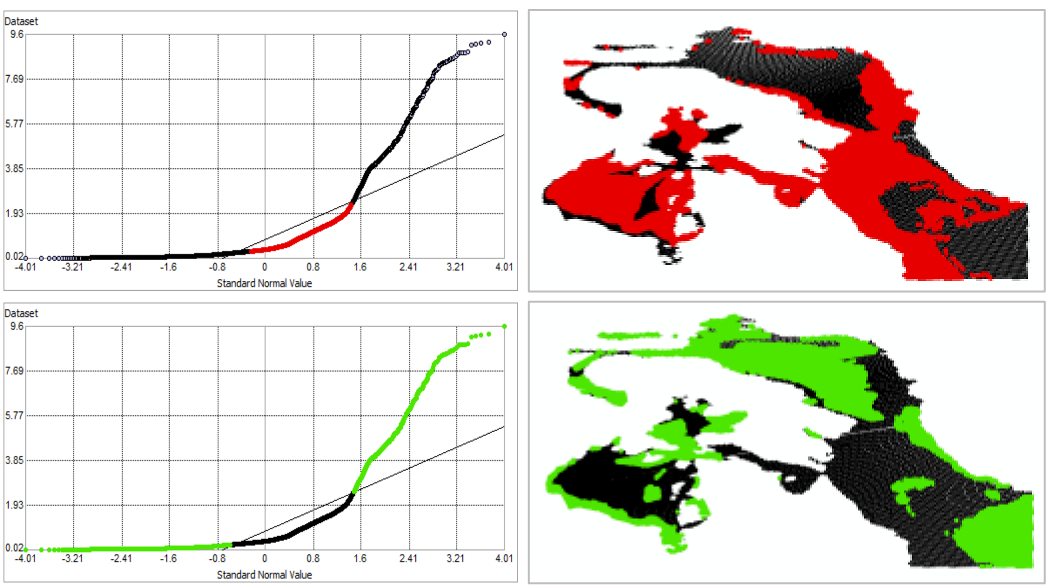


Figure 37. Normal Q-Q plot for data values of Bottom Temperature Average Range (°C). Points falling under (top right panel) and over (bottom right panel) the reference line are mapped.

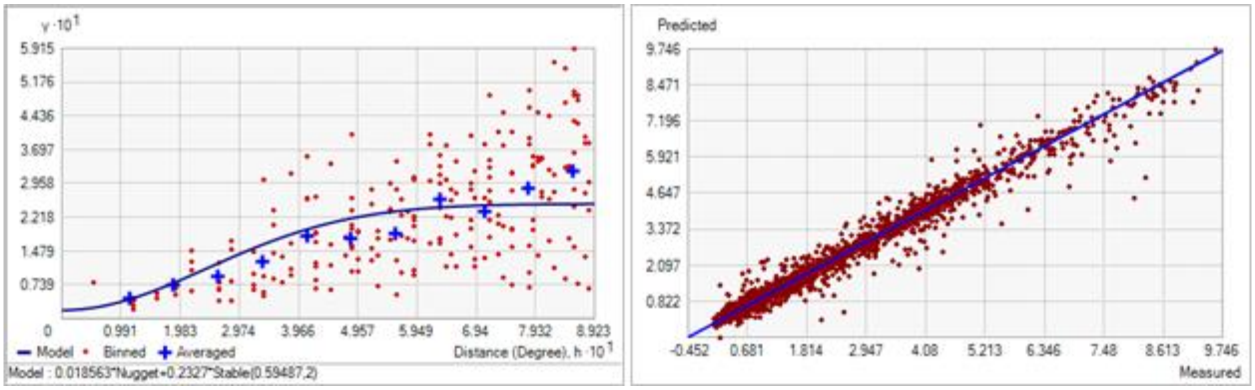

Figure 38. Left panel: Semivariogram of Bottom Temperature Average Range (°C). Binned values are shown as red dots; average points are shown as blue crosses; the model fit to the averaged values is shown as a blue line. Lag size: 0.074 degrees; number of lags: 12; Parameter: 2; Range: 0.595 degrees; Partial Sill: 0.233. Right panel: Scatterplot of predicted values versus observed values for the model of Bottom Temperature Average Range (°C).

Table 16. Results of cross-validation of the kriged model for Bottom Temperature Average Range (°C).

| Prediction Error | Value |
|---|---:|
| Number of Observations | 16376 |
| Overall Mean Error | $-1.858 \times 10^{-3}$ |
| Root Mean Square Prediction Error | 0.127 |
| Standardized Mean | $-4.619 \times 10^{-3}$ |
| Standardized Root Mean Square Prediction Error | 0.603 |
| Average Standard Error | 0.191 |

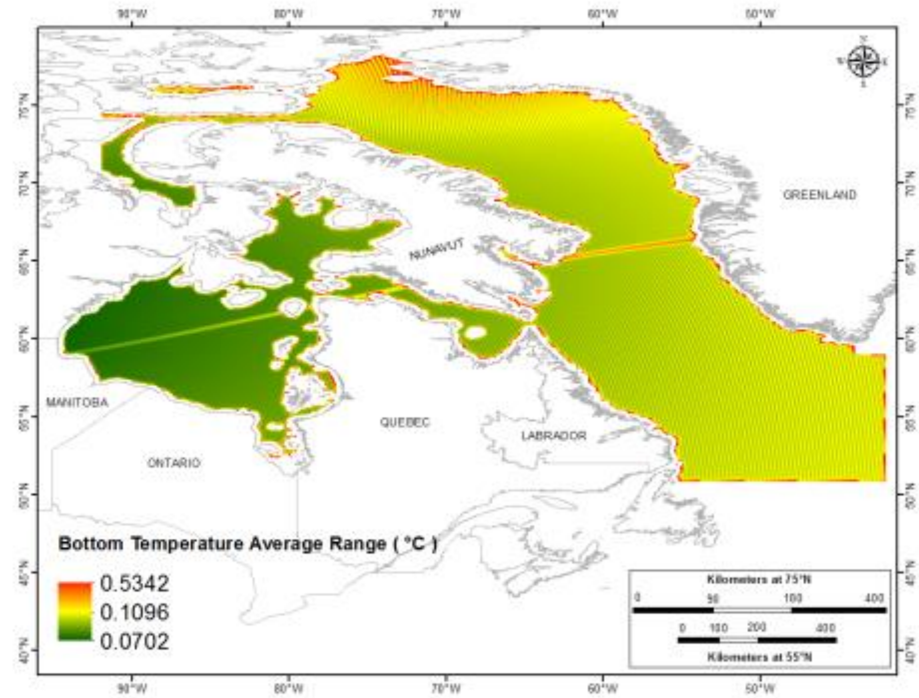

Figure 39. Prediction standard error surface of Bottom Temperature Average Range (˚C).

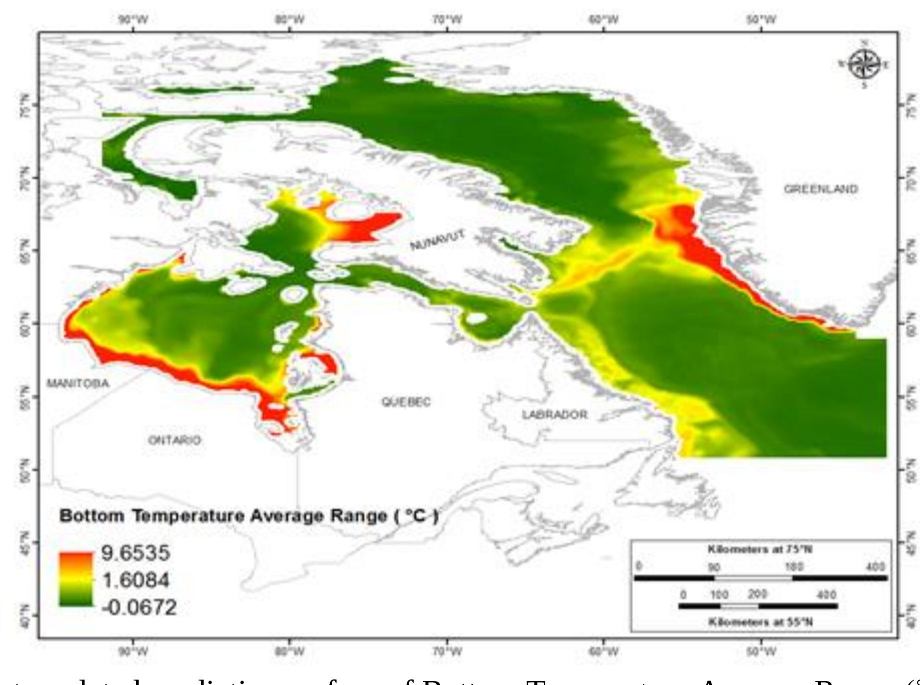

Figure 40. Interpolated prediction surface of Bottom Temperature Average Range (˚C).

### Surface Temperature Mean

This variable displayed a right-skewed, leptokurtic distribution prior to interpolation (Table 17, Figure 41). The data were higher than predicted by a normal distribution at both tails, while mid-values were lower than the reference line (Figure 42). These areas of under- and over-prediction showed spatial pattern over the region (Figure 42).

The semivariogram showed moderate autocorrelation present in the data (Figure 43). The kriged model showed an excellent fit between measured and predicted values (Figure 43). Good performance of the model was indicated by the cross-validation results (Table 18). The error map showed lower error in Hudson Bay compared to Baffin Bay and Davis Strait, with higher error along the edges of the study extent and in the most northern areas (Figure 44). The kriged surface is presented in Figure 45.

Table 17. Distributional properties of Surface Temperature Mean (°C).

| Property | Value |
|---|---:|
| Number of Observations | 16491 |
| Minimum | -1.572 |
| Maximum | 11.244 |
| Mean | 1.487 |
| Median | 0.709 |
| Standard Deviation | 2.426 |
| Skewness | 1.224 |
| Kurtosis | 3.833 |

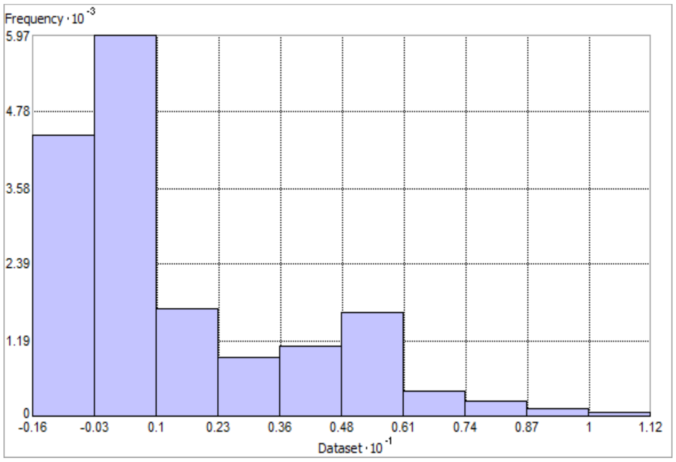


Figure 41. Distribution of Surface Temperature Mean (°C). Histogram was illustrated using 10 bins. X axis is shown at $10^{-1}$ Y axis is shown at $10^{-3}$.

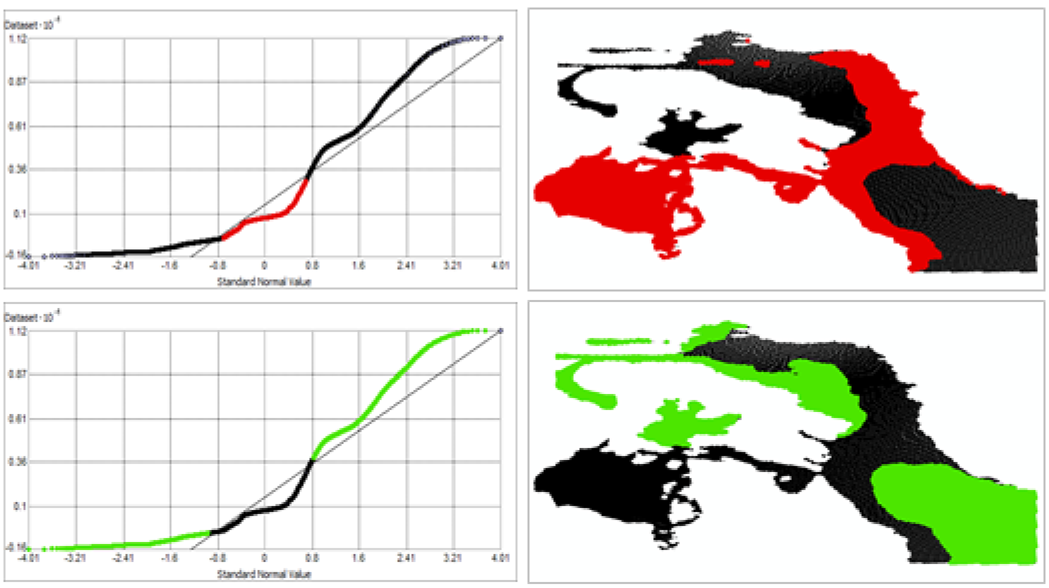

Figure 42. Normal Q-Q plot for data values of Surface Temperature Mean (°C). Points falling under (top right panel) and over (bottom right panel) the reference line are mapped.

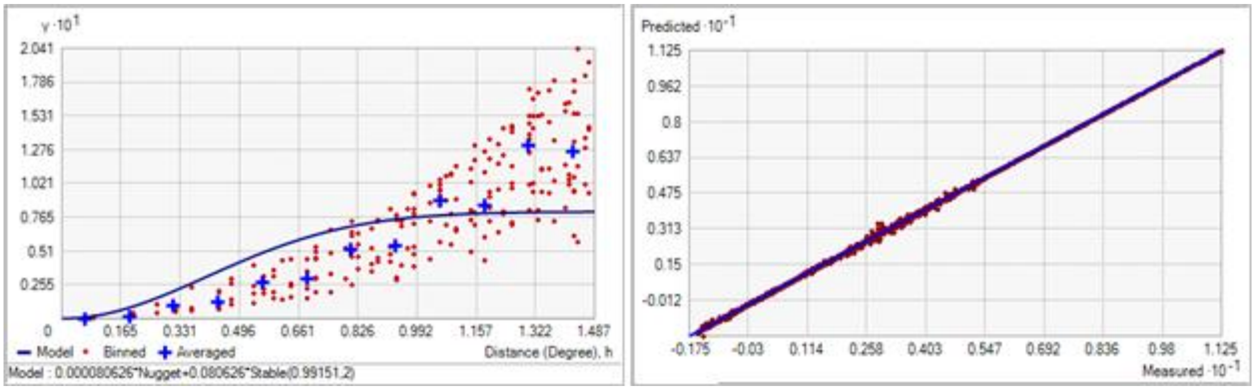

Figure 43. Left panel: Semivariogram of Surface Temperature Mean (°C). Binned values are shown as red dots; average points are shown as blue crosses; the model fit to the averaged values is shown as a blue line. Lag size: 0.124 degrees; number of lags: 12; Parameter: 2; Range: 0.992 degrees; Partial Sill: 0.081. Right panel: Scatterplot of predicted values versus observed values for the model of Surface Temperature Mean (°C).

Table 18. Results of cross-validation of the kriged model for Surface Temperature Mean (°C).

| **Prediction Error** | **Value** |
|---|---:|
| Number of Observations | 16491 |
| Overall Mean Error | $3.558 \times 10^{-5}$ |
| Root Mean Square Prediction Error | 0.017 |
| Standardized Mean | $1.592 \times 10^{-3}$ |
| Standardized Root Mean Square Prediction Error | 1.104 |
| Average Standard Error | 0.015 |

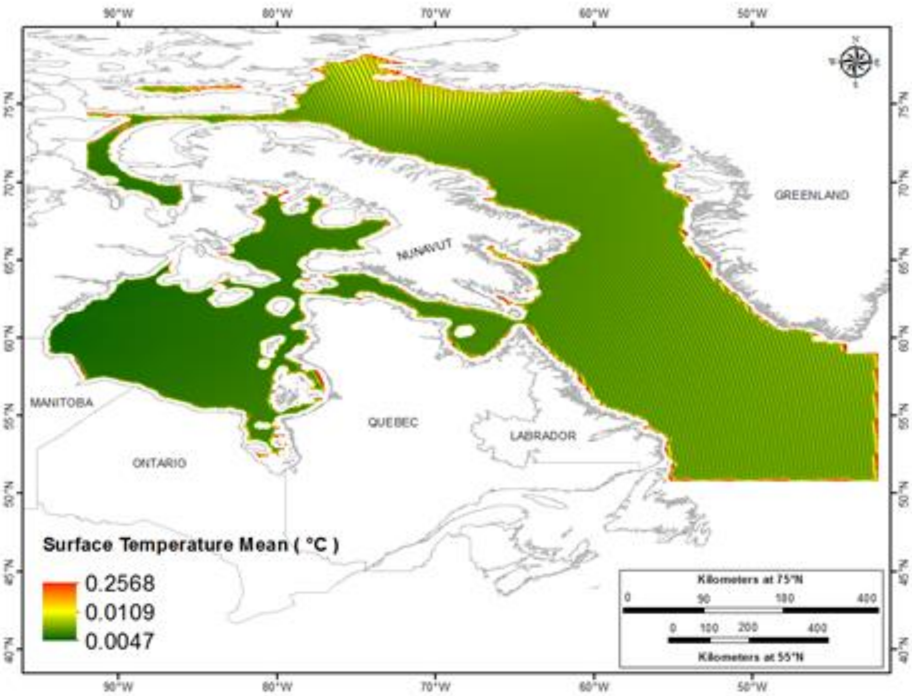


Figure 44. Prediction standard error surface of Surface Temperature Mean (˚C).

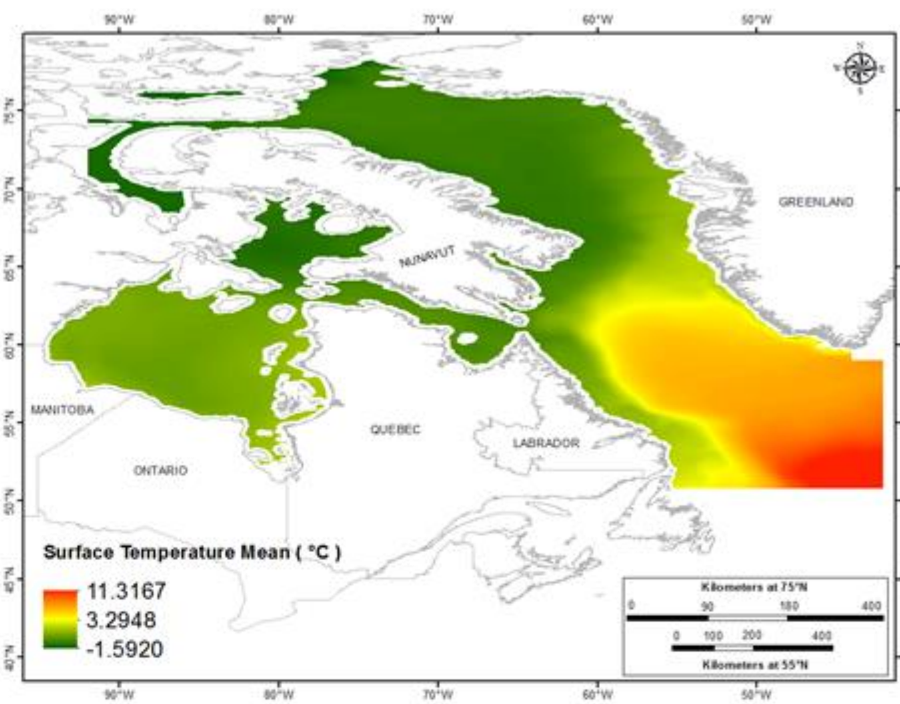


Figure 45. Interpolated prediction surface of Surface Temperature Mean (˚C).

## Surface Temperature Minimum

This variable displayed a right-skewed, leptokurtic distribution prior to interpolation (Table 19, Figure 46). The data were higher than predicted by a normal distribution at both tails, while mid-values were lower than the reference line (Figure 47). These areas of under- and over-prediction showed spatial pattern over the region (Figure 47).

The semivariogram showed moderate autocorrelation present in the data (Figure 48). The kriged model showed an excellent fit between measured and predicted values (Figure 48). Poor performance of the model was indicated by the cross-validation results (Table 20), with underestimation of the variability of the predictions as indicated by the Standardized Root-Mean-Square Error greater than 1. The error map showed lower error in Hudson Bay compared to Baffin Bay and Davis Strait, with higher error along the edges of the study extent and in the most northern areas (Figure 49). The kriged surface is presented in Figure 50.

Table 19. Distributional properties of Surface Temperature Minimum (°C).

| **Property** | **Value** |
|---|---:|
| Number of Observations | 16491 |
| Minimum | -2.553 |
| Maximum | 6.802 |
| Mean | -1.171 |
| Median | -1.817 |
| Standard Deviation | 1.440 |
| Skewness | 2.182 |
| Kurtosis | 7.136 |

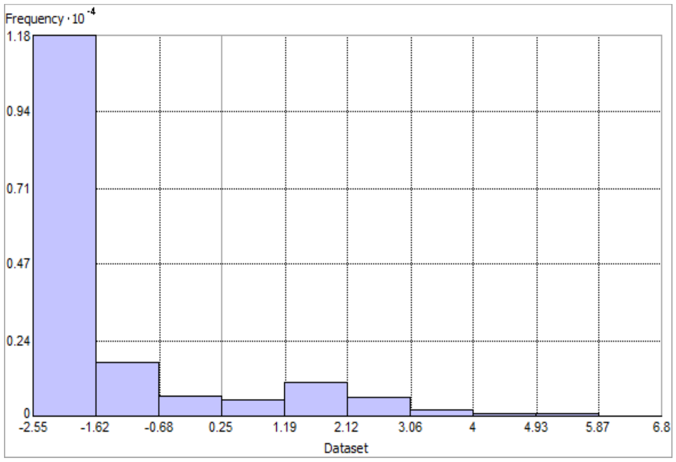

Figure 46. Distribution of Surface Temperature Minimum (°C). Histogram was illustrated using 10 bins. Y axis is shown at $10^{-4}$.

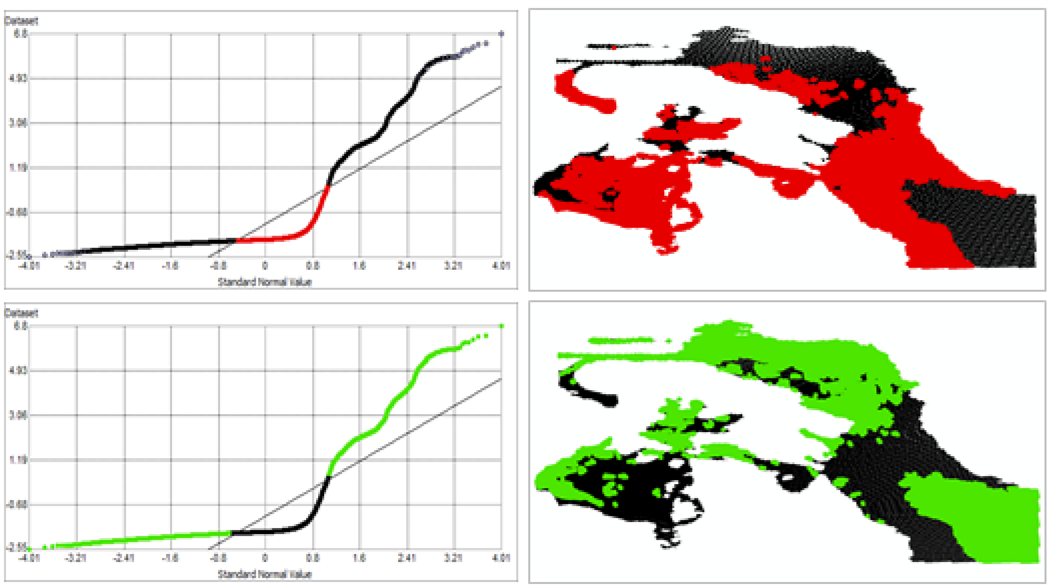

Figure 47. Normal Q-Q plot for data values of Surface Temperature Minimum (°C). Points falling under (top right panel) and over (bottom right panel) the reference line are mapped.

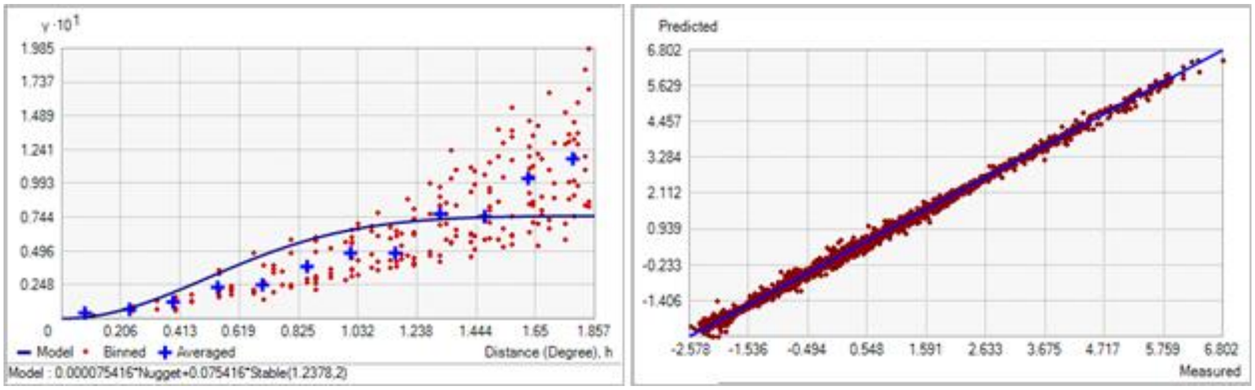

Figure 48. Left panel: Semivariogram of Surface Temperature Minimum (°C). Binned values are shown as red dots; average points are shown as blue crosses; the model fit to the averaged values is shown as a blue line. Lag size: 0.155 degrees; number of lags: 12; Parameter: 2; Range: 1.238 degrees; Partial Sill: 0.075. Right panel: Scatterplot of predicted values versus observed values for the model of Surface Temperature Minimum (°C).

Table 20. Results of cross-validation of the kriged model for Surface Temperature Minimum (°C).

| **Prediction Error** | **Value** |
|---|---:|
| Number of Observations | 16491 |
| Overall Mean Error | $1.100 \times 10^{-4}$ |
| Root Mean Square Prediction Error | 0.049 |
| Standardized Mean | $3.782 \times 10^{-3}$ |
| Standardized Root Mean Square Prediction Error | 4.097 |
| Average Standard Error | 0.012 |

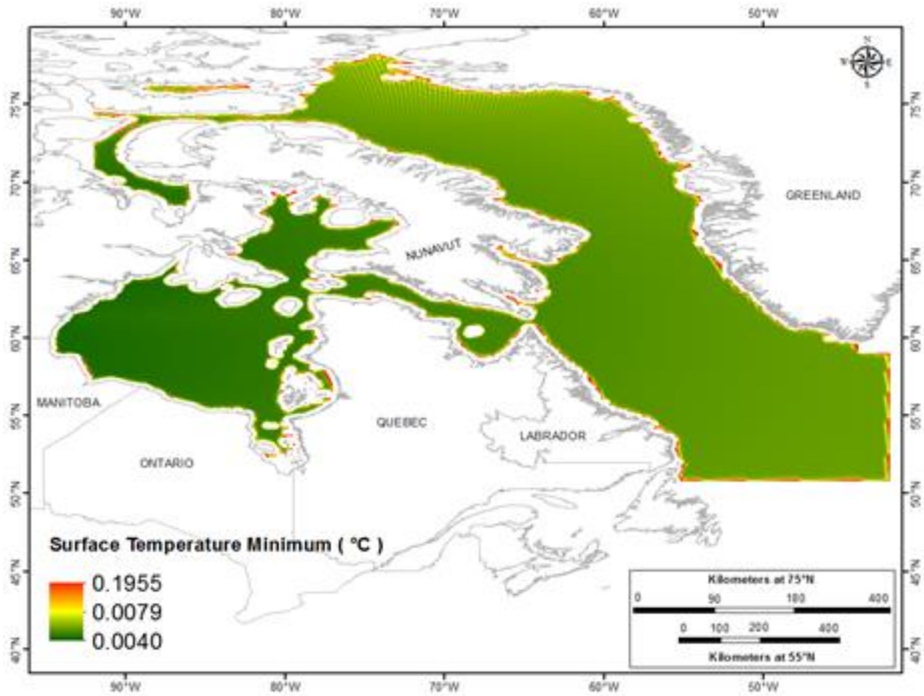


Figure 49. Prediction standard error surface of Surface Temperature Minimum (˚C).

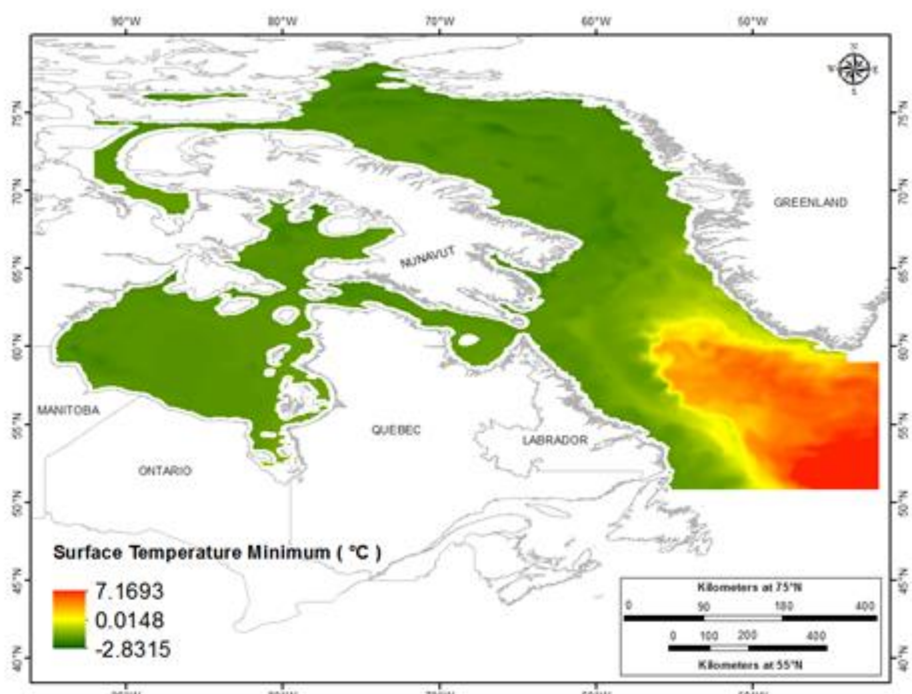


Figure 50. Interpolated prediction surface of Surface Temperature Minimum (˚C).

**Surface Temperature Maximum**

This variable displayed a left-skewed, platykurtic distribution prior to interpolation (Table 21, Figure 51). The data were greater than predicted by a normal distribution at the lowest and upper mid-range values, and lower than predicted at the highest and lower mid-range values (Figure 52). These areas of under- and over-prediction showed spatial pattern over the region (Figure 52).

The semivariogram showed weak autocorrelation present in the data (Figure 53). The kriged model showed an excellent fit between measured and predicted values (Figure 53). Good performance of the model was indicated by the cross-validation results (Table 22). The error map showed lower error in Hudson Bay compared to Baffin Bay and Davis Strait, with higher error along the edges of the study extent and in the most northern areas (Figure 54). The kriged surface is presented in Figure 55.

Table 21. Distributional properties of Surface Temperature Maximum (°C).

| **Property** | **Value** |
|---|---:|
| Number of Observations | 16491 |
| Minimum | 1.142 |
| Maximum | 17.658 |
| Mean | 8.385 |
| Median | 8.897 |
| Standard Deviation | 2.675 |
| Skewness | -0.166 |
| Kurtosis | 2.877 |

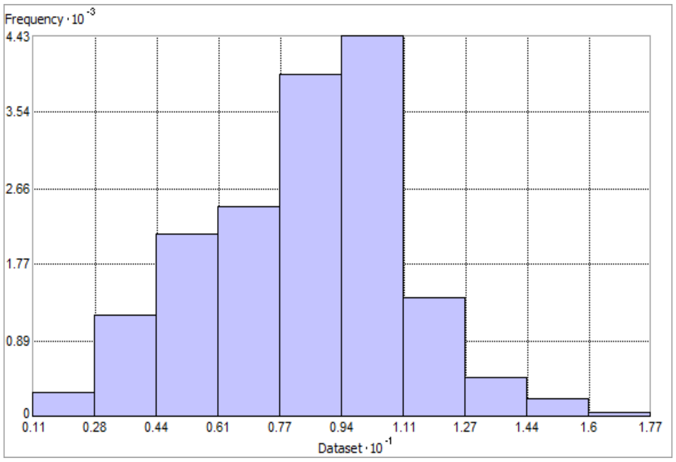

Figure 51. Distribution of Surface Temperature Maximum (°C). Histogram was illustrated using 10 bins. X axis is shown at $10^{-1}$ Y axis is shown at $10^{-3}$.

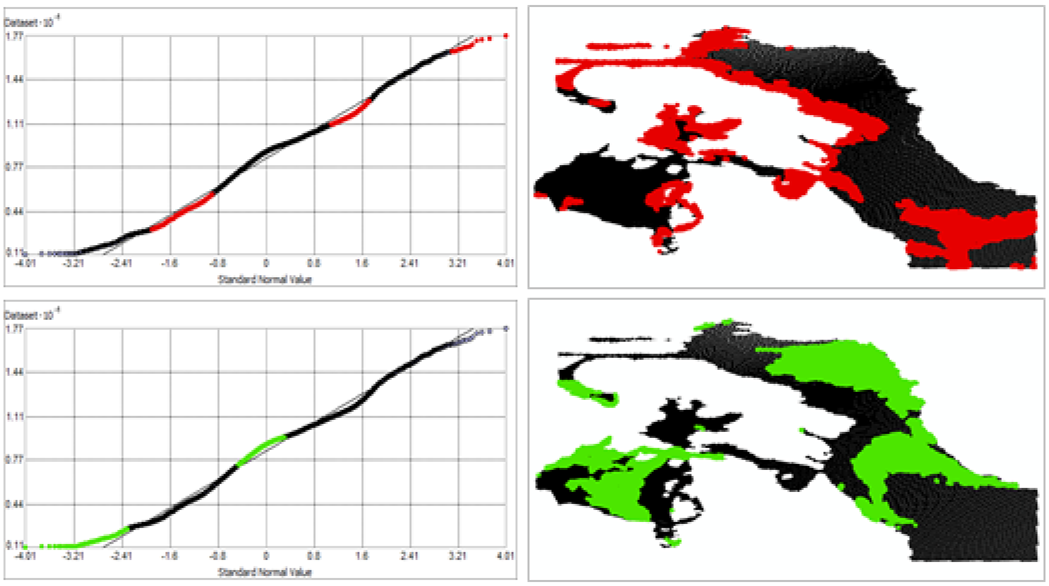
Figure 52. Normal Q-Q plot for data values of Surface Temperature Maximum (°C). Points falling under (top right panel) and over (bottom right panel) the reference line are mapped.

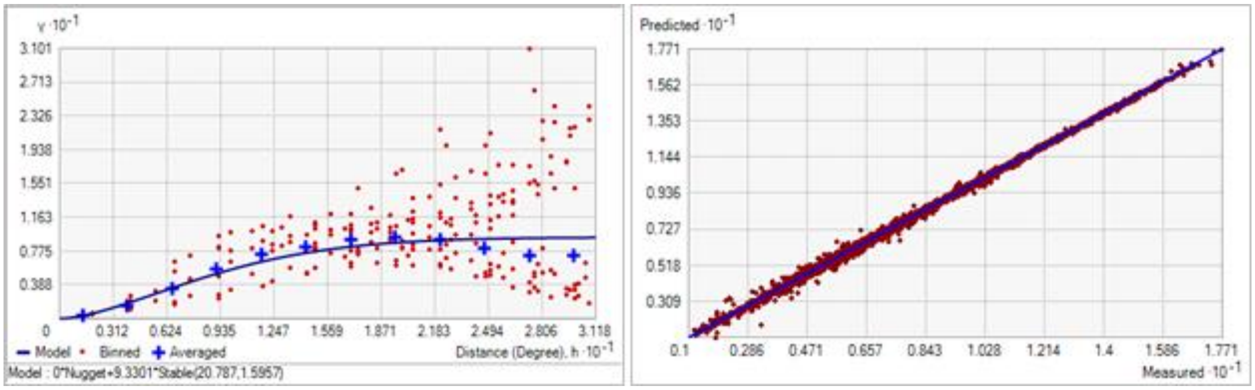

Figure 53. Left panel: Semivariogram of Surface Temperature Maximum (°C). Binned values are shown as red dots; average points are shown as blue crosses; the model fit to the averaged values is shown as a blue line. Lag size: 2.598 degrees; number of lags: 12; Parameter: 1.596; Range: 20.787 degrees; Partial Sill: 9.330. Right panel: Scatterplot of predicted values versus observed values for the model of Surface Temperature Maximum (°C).

Table 22. Results of cross-validation of the kriged model for Surface Temperature Maximum (°C).

| **Prediction Error** | **Value** |
|---|---:|
| Number of Observations | 16491 |
| Overall Mean Error | $1.580 \times 10^{-4}$ |
| Root Mean Square Prediction Error | 0.077 |
| Standardized Mean | $1.220 \times 10^{-3}$ |
| Standardized Root Mean Square Prediction Error | 1.077 |
| Average Standard Error | 0.066 |

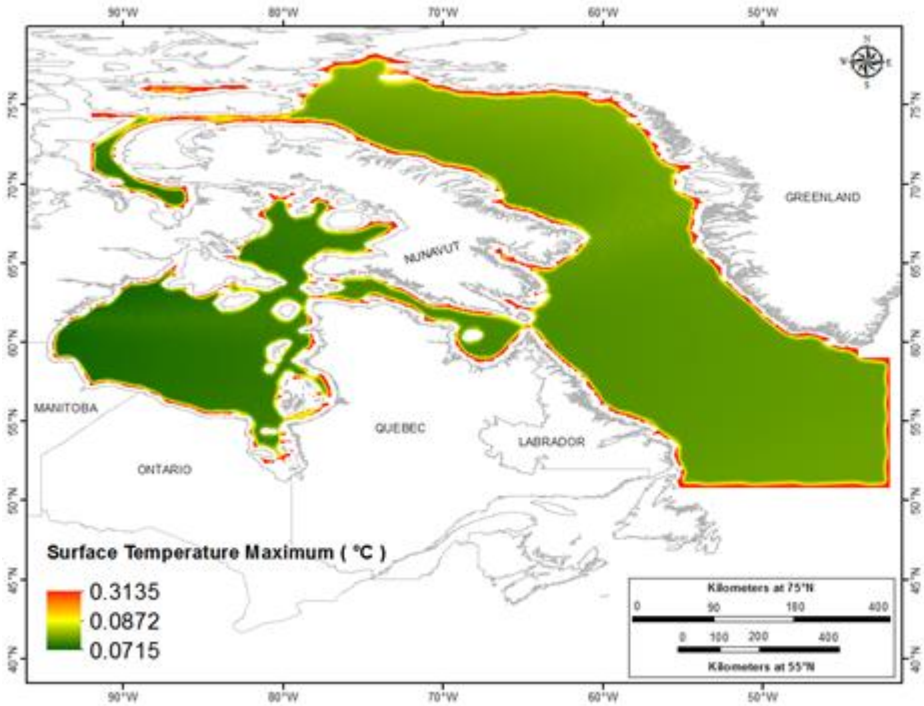


Figure 54. Prediction standard error surface of Surface Temperature Maximum (˚C).

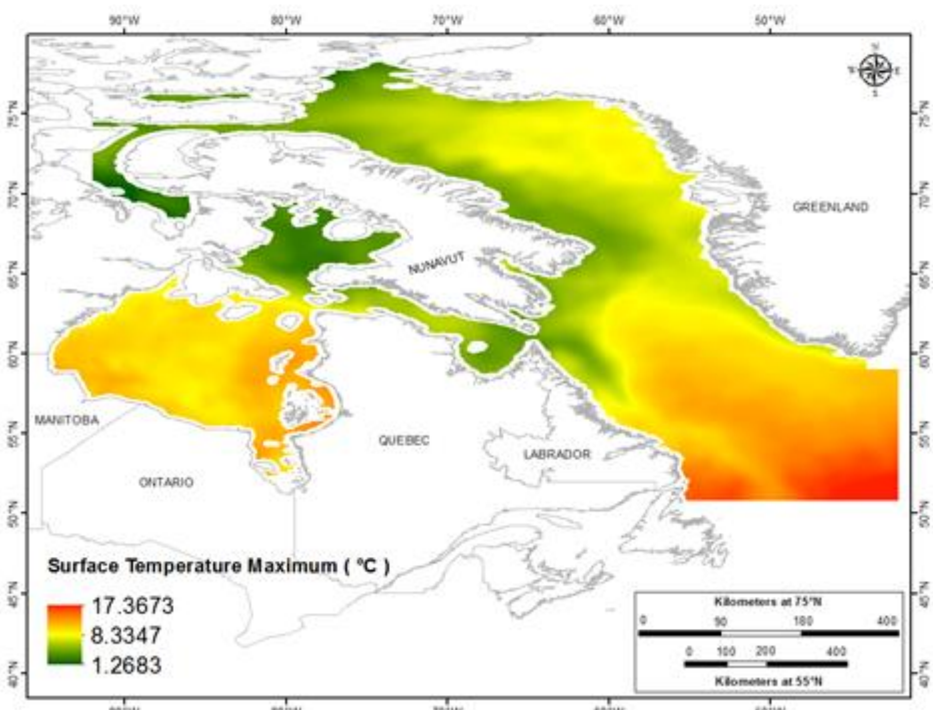


Figure 55. Interpolated prediction surface of Surface Temperature Maximum (˚C).

**Surface Temperature Range**

This variable displayed a left-skewed, platykurtic distribution prior to interpolation (Table 23, Figure 56). The data were greater than predicted by a normal distribution at the lowest and upper mid-range values, and lower than predicted at the highest and lower mid-range values (Figure 57). These areas of under- and over-prediction showed spatial pattern over the region (Figure 57).

The semivariogram showed weak autocorrelation present in the data (Figure 58). The kriged model showed an excellent fit between measured and predicted values (Figure 58). Good performance of the model was indicated by the cross-validation results (Table 24). The error map showed lower error in Hudson Bay compared to Baffin Bay and Davis Strait, with higher error along the edges of the study extent and in the most northern areas (Figure 59). The kriged surface is presented in Figure 60.

Table 23. Distributional properties of Surface Temperature Range (°C).

| **Property** | **Value** |
|---|---:|
| Number of Observations | 16491 |
| Minimum | 2.848 |
| Maximum | 16.114 |
| Mean | 9.556 |
| Median | 9.830 |
| Standard Deviation | 2.180 |
| Skewness | -0.390 |
| Kurtosis | 2.842 |

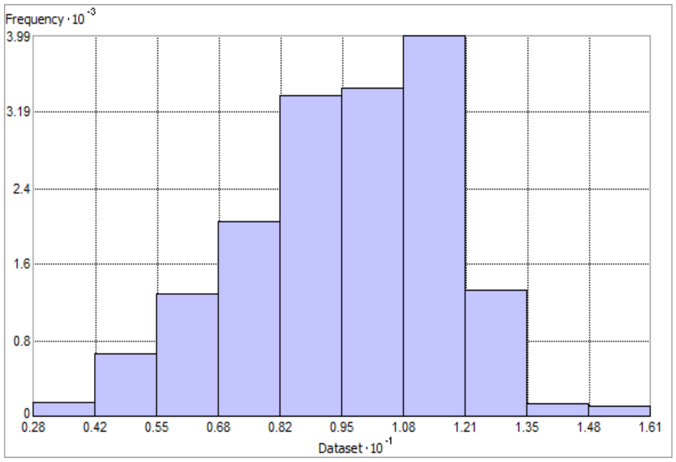


Figure 56. Distribution of Surface Temperature Range (°C). Histogram was illustrated using 10 bins. X axis is shown at $10^{-1}$ Y axis is shown at $10^{-3}$.

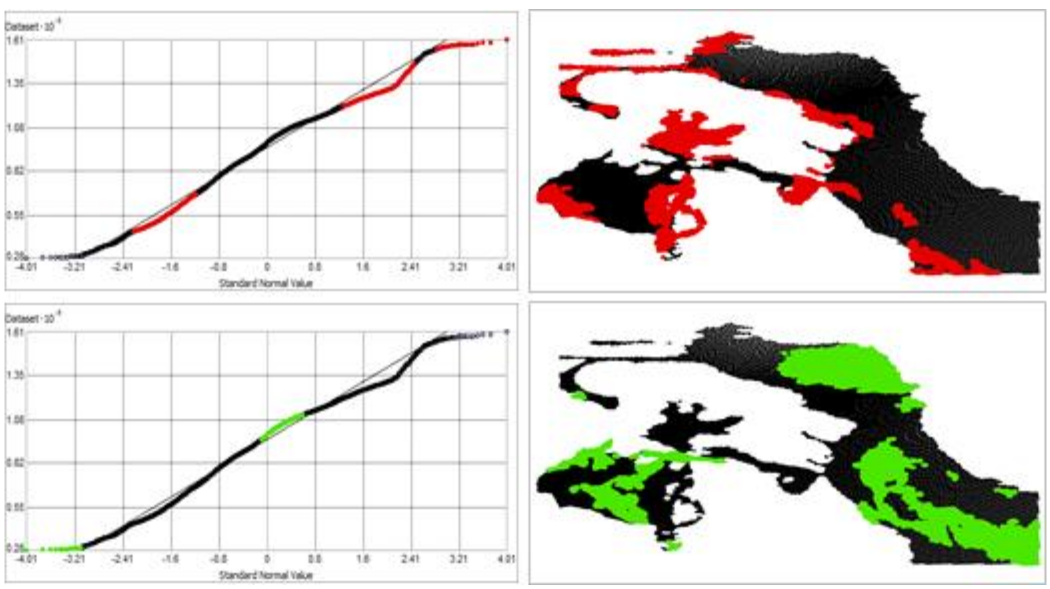

Figure 57. Normal Q-Q plot for data values of Surface Temperature Range (°C). Points falling under (top right panel) and over (bottom right panel) the reference line are mapped.

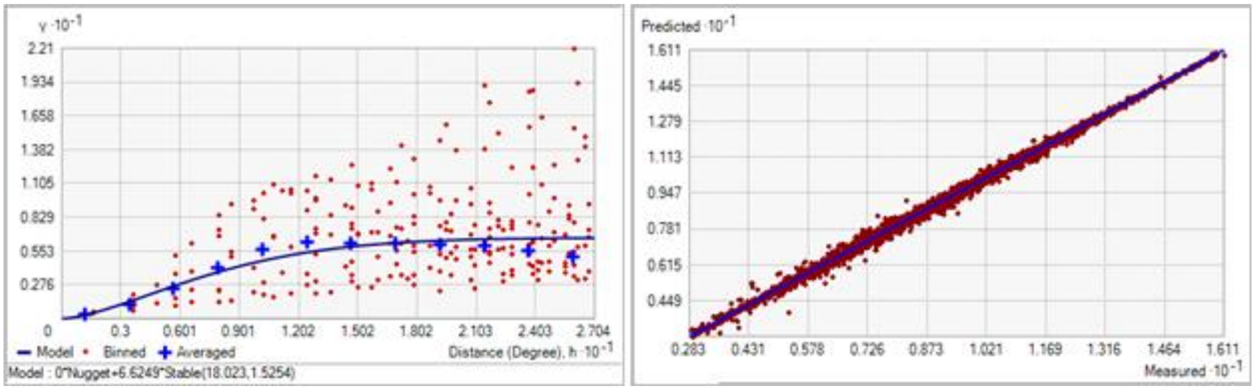

Figure 58. Left panel: Semivariogram of Surface Temperature Range (°C). Binned values are shown as red dots; average points are shown as blue crosses; the model fit to the averaged values is shown as a blue line. Lag size: 2.252 degrees; number of lags: 12; Parameter: 1.525; Range: 18.023 degrees; Partial Sill: 6.625. Right panel: Scatterplot of predicted values versus observed values for the model of Surface Temperature Range (°C).

Table 24. Results of cross-validation of the kriged model for Surface Temperature Range (°C).

| **Prediction Error** | **Value** |
|---|---:|
| Number of Observations | 16491 |
| Overall Mean Error | $1.635 \times 10^{-4}$ |
| Root Mean Square Prediction Error | 0.089 |
| Standardized Mean | $1.015 \times 10^{-3}$ |
| Standardized Root Mean Square Prediction Error | 1.048 |
| Average Standard Error | 0.080 |

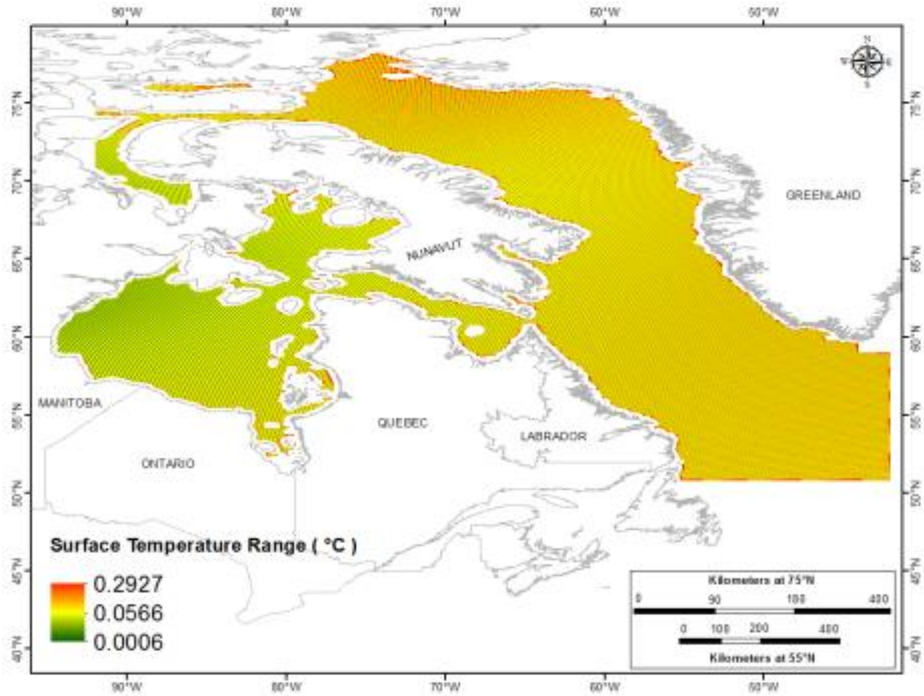


Figure 59. Prediction standard error surface of Surface Temperature Range (˚C).

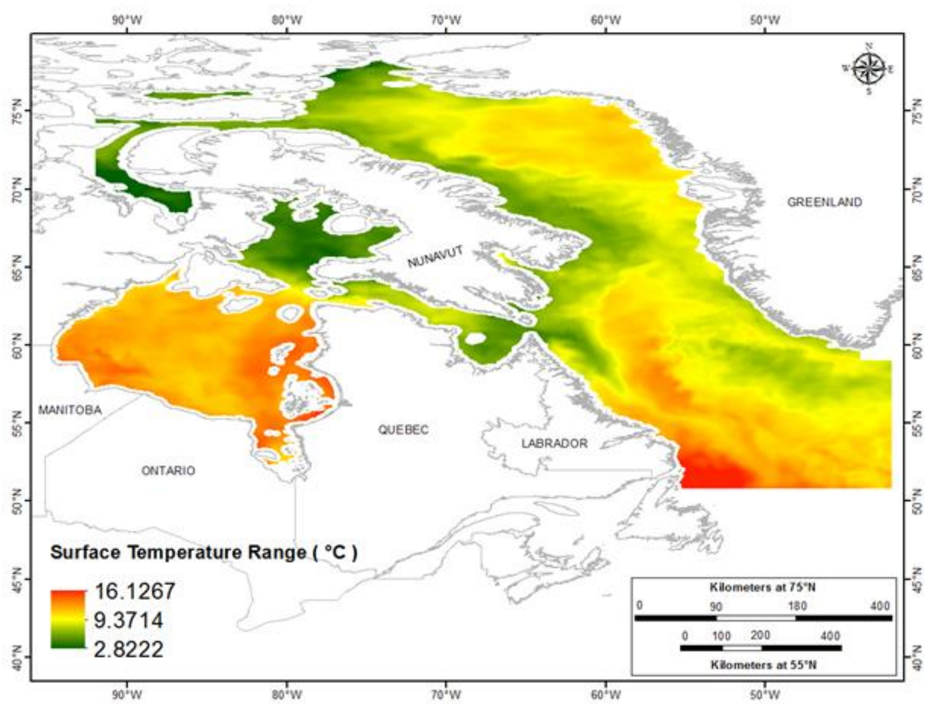


Figure 60. Interpolated prediction surface of Surface Temperature Range (˚C).

**Surface Temperature Average Minimum**

This variable displayed a right-skewed, leptokurtic distribution prior to interpolation (Table 25, Figure 61). The data were higher than predicted by a normal distribution at both tails, while mid-values were lower than the reference line (Figure 62). These areas of under- and over-prediction showed spatial pattern over the region (Figure 62).

The semivariogram showed moderate autocorrelation present in the data (Figure 63). The kriged model showed an excellent fit between measured and predicted values (Figure 63). Good performance of the model was indicated by the cross-validation results (Table 26). The error map showed lower error in Hudson Bay compared to Baffin Bay and Davis Strait, with higher error along the edges of the study extent and in the most northern areas (Figure 64). The kriged surface is presented in Figure 65.

Table 25. Distributional properties of Surface Temperature Average Minimum (°C).

| **Property** | **Value** |
|---|---:|
| Number of Observations | 16491 |
| Minimum | -1.977 |
| Maximum | 8.123 |
| Mean | -0.631 |
| Median | -1.755 |
| Standard Deviation | 1.990 |
| Skewness | 1.592 |
| Kurtosis | 4.432 |

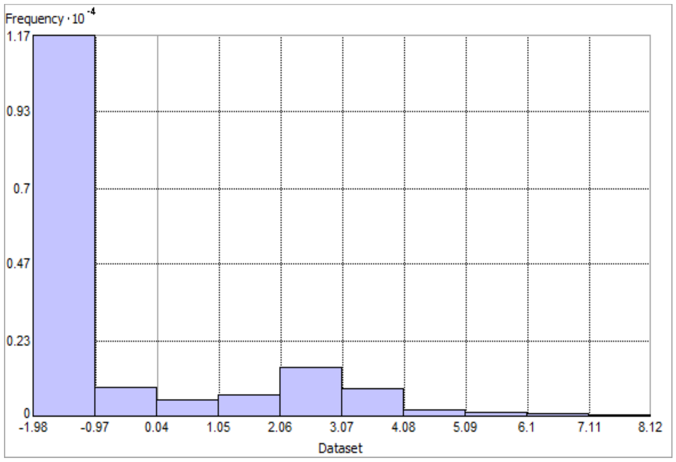


Figure 61. Distribution of Surface Temperature Average Minimum (°C). Histogram was illustrated using 10 bins. Y axis is shown at $10^{-4}$.

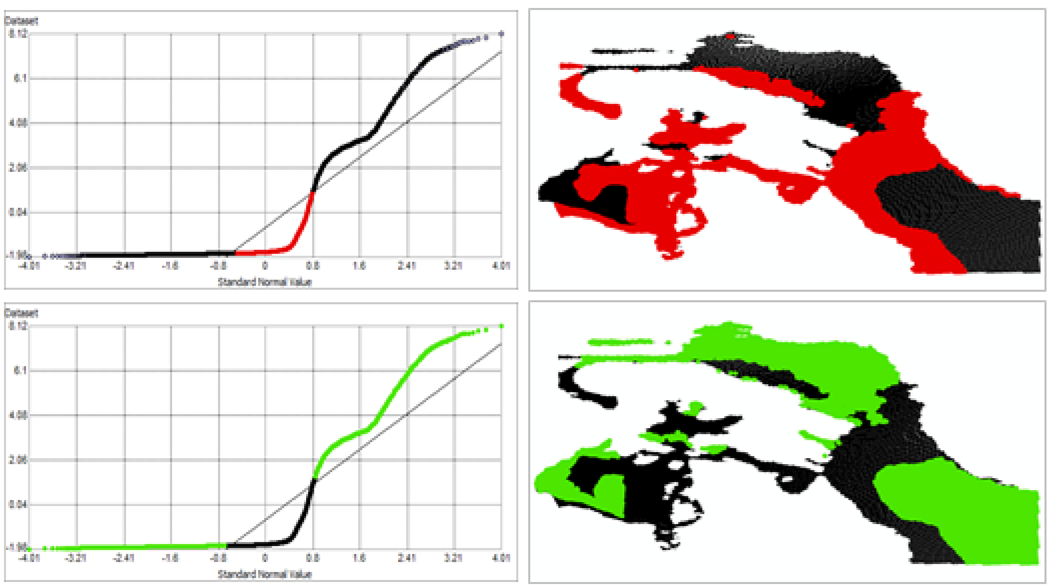


Figure 62. Normal Q-Q plot for data values of Surface Temperature Average Minimum (°C). Points falling under (top right panel) and over (bottom right panel) the reference line are mapped.

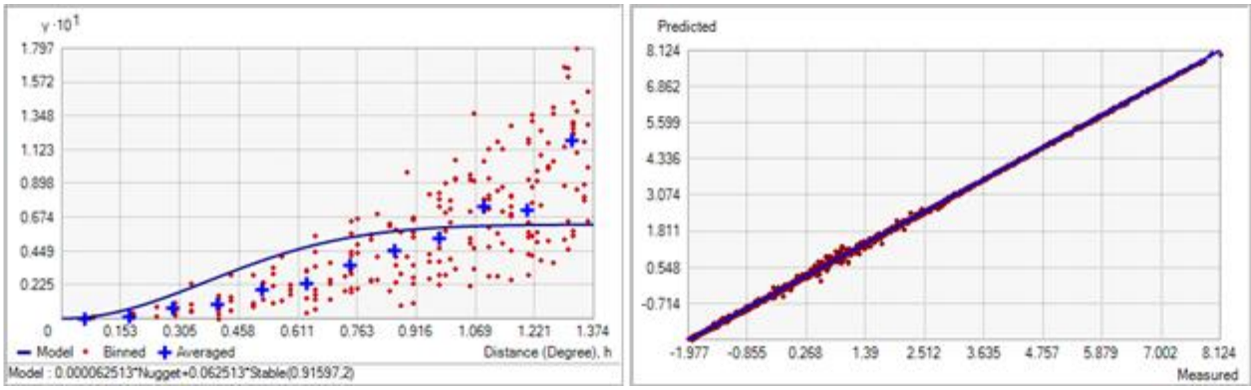

Figure 63. Left panel: Semivariogram of Surface Temperature Average Minimum (°C). Binned values are shown as red dots; average points are shown as blue crosses; the model fit to the averaged values is shown as a blue line. Lag size: 0.114 degrees; number of lags: 12; Parameter: 2; Range: 0.916degrees; Partial Sill: 0.062. Right panel: Scatterplot of predicted values versus observed values for the model of Surface Temperature Average Minimum (°C).

Table 26. Results of cross-validation of the kriged model for Surface Temperature Average Minimum (°C).

| **Prediction Error** | **Value** |
|---|---:|
| Number of Observations | 16491 |
| Overall Mean Error | $9.031 \times 10^{-5}$ |
| Root Mean Square Prediction Error | 0.018 |
| Standardized Mean | $2.685 \times 10^{-3}$ |
| Standardized Root Mean Square Prediction Error | 1.331 |
| Average Standard Error | 0.014 |

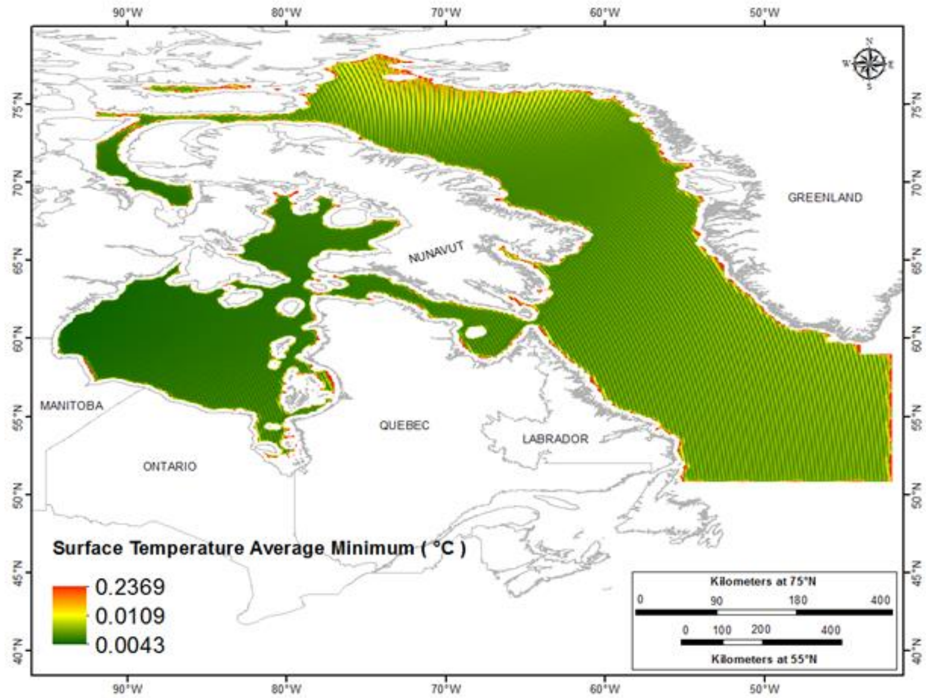


Figure 64. Prediction standard error surface of Surface Temperature Average Minimum (˚C).

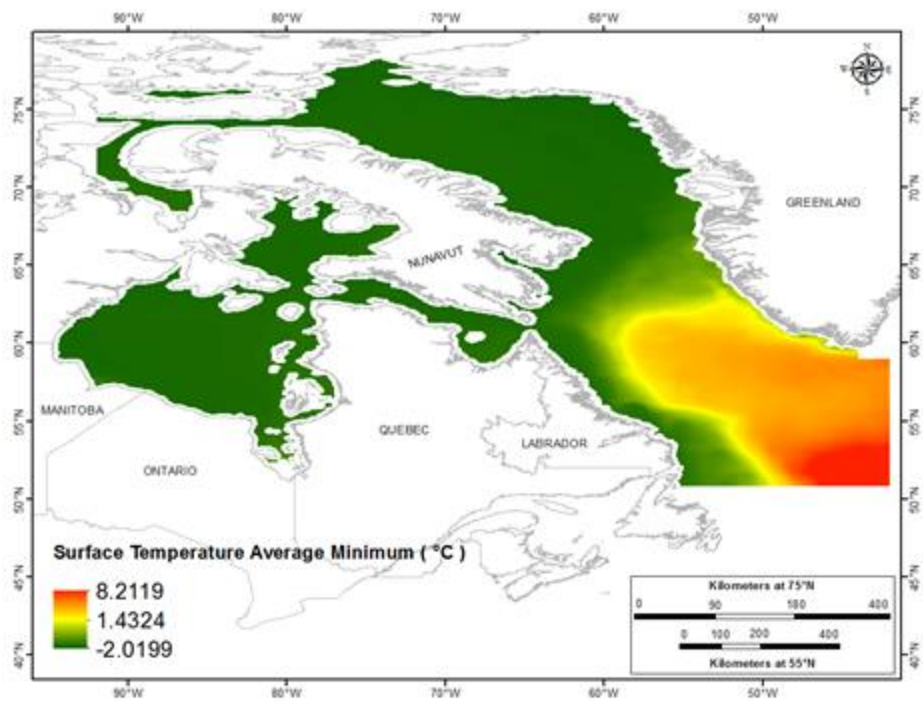


Figure 65. Interpolated prediction surface of Surface Temperature Average Minimum (˚C).

**Surface Temperature Average Maximum**

This variable displayed a bimodal, platykurtic distribution prior to interpolation (Table 27, Figure 66). The data were greater than predicted by a normal distribution at the lowest and upper mid-range values, and lower than predicted at the highest and lower mid-range values (Figure 67). These areas of under- and over-prediction showed spatial pattern over the region.

The semivariogram showed very weak autocorrelation present in the data (Figure 68). The kriged model showed an excellent fit between measured and predicted values (Figure 68). Poor performance of the model was indicated by the cross-validation results (Table 28), and variability in the predictions was overestimated as indicated by the Standardized Root-Mean-Square Error below 1. The error map showed lower error in Hudson Bay compared to Baffin Bay and Davis Strait, with higher error along the edges of the study extent and in the most northern areas (Figure 69). The kriged surface is presented in Figure 70.

Table 27. Distributional properties of Surface Temperature Average Maximum (°C).

| **Property** | **Value** |
|---|---:|
| Number of Observations | 16491 |
| Minimum | -0.589 |
| Maximum | 15.296 |
| Mean | 6.106 |
| Median | 6.814 |
| Standard Deviation | 2.881 |
| Skewness | 0.042 |
| Kurtosis | 2.557 |

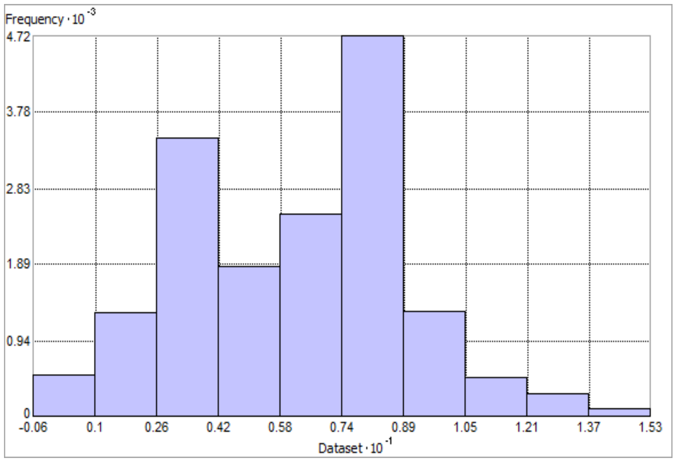


Figure 66. Distribution of Surface Temperature Average Maximum (°C). Histogram was illustrated using 10 bins. X axis is shown at $10^{-1}$; Y axis is shown at $10^{-3}$.

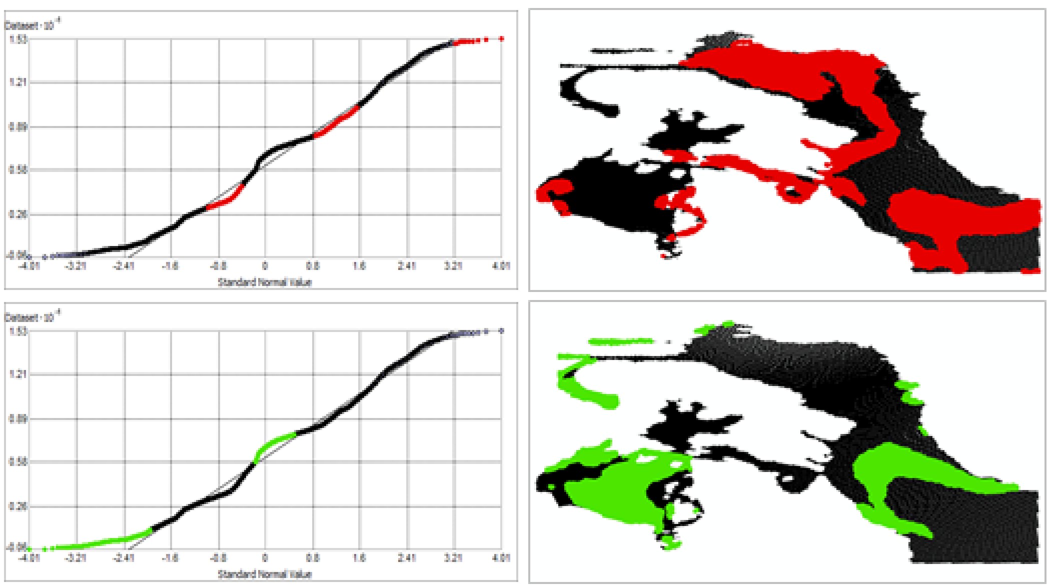

Figure 67. Normal Q-Q plot for data values of Surface Temperature Average Maximum (°C). Points falling under (top right panel) and over (bottom right panel) the reference line are mapped.

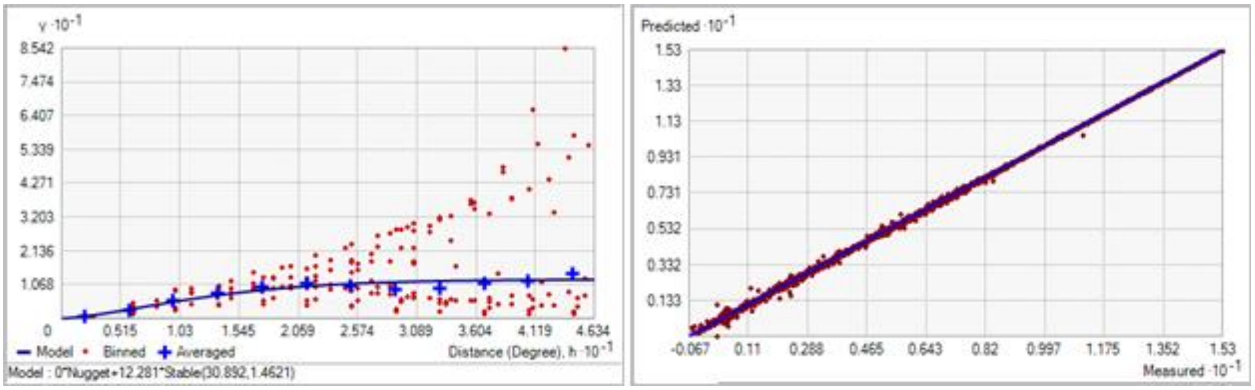

Figure 68. Left panel: Semivariogram of Surface Temperature Average Maximum (°C). Binned values are shown as red dots; average points are shown as blue crosses; the model fit to the averaged values is shown as a blue line. Lag size: 3.862 degrees; number of lags: 12; Parameter: 1.462; Range: 30.892 degrees; Partial Sill: 12.281. Right panel: Scatterplot of predicted values versus observed values for the model of Surface Temperature Average Maximum (°C).

Table 28. Results of cross-validation of the kriged model for Surface Temperature Average Maximum (°C).

| **Prediction Error** | **Value** |
|---|---:|
| Number of Observations | 16491 |
| Overall Mean Error | $9.011 \times 10^{-5}$ |
| Root Mean Square Prediction Error | 0.037 |
| Standardized Mean | $3.020 \times 10^{-4}$ |
| Standardized Root Mean Square Prediction Error | 0.346 |
| Average Standard Error | 0.090 |

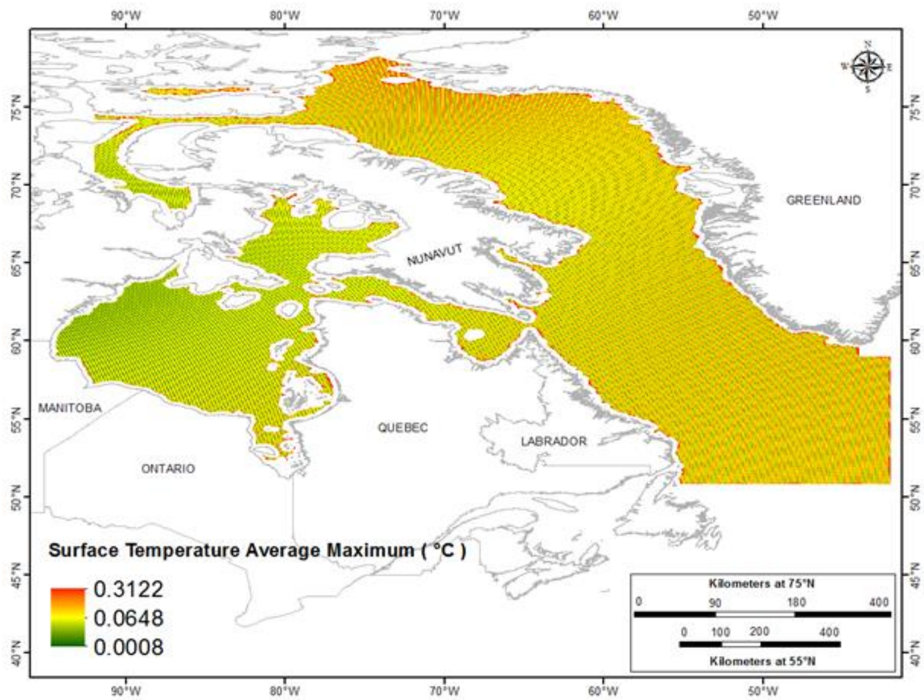


Figure 69. Prediction standard error surface of Surface Temperature Average Maximum (˚C).

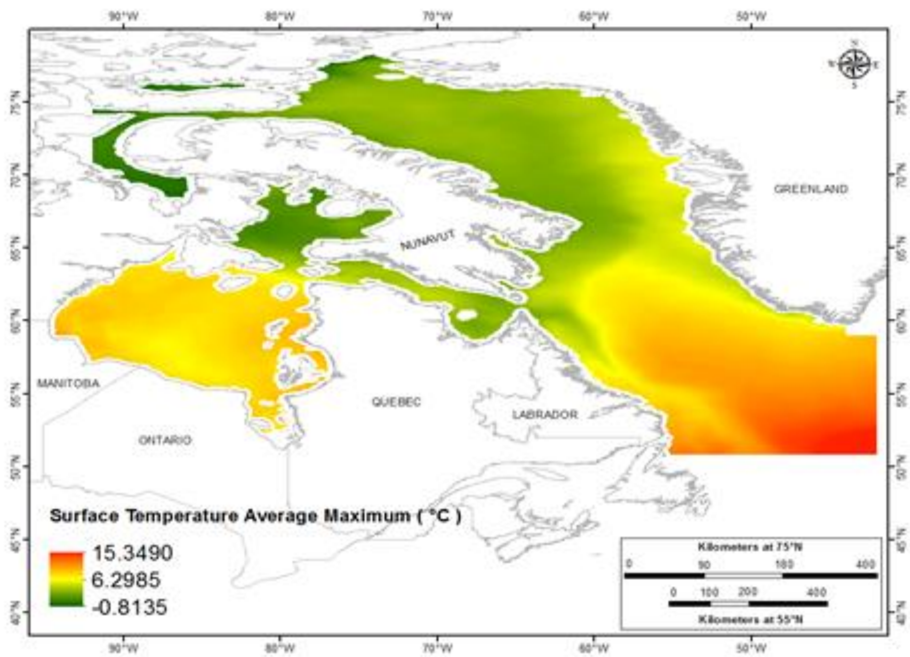


Figure 70. Interpolated prediction surface of Surface Temperature Average Maximum (˚C).

## Surface Temperature Average Range

This variable displayed a bimodal, platykurtic distribution prior to interpolation (Table 29, Figure 71). The data were greater than predicted by a normal distribution at the lowest and upper mid-range values, and lower than predicted at the highest and lower mid-range values (Figure 72). These areas of under- and over-prediction showed spatial pattern over the region.

The semivariogram showed weak autocorrelation present in the data (Figure 73). The kriged model showed an excellent fit between measured and predicted values (Figure 73). Poor performance of the model was indicated by the cross-validation results (Table 30), and variability in the predictions was overestimated as indicated by the Standardized Root-Mean-Square Error below 1. The error map showed lower error in Hudson Bay compared to Baffin Bay and Davis Strait, with higher error along the edges of the study extent and in the most northern areas (Figure 74). The kriged surface is presented in Figure 75.

Table 29. Distributional properties of Surface Temperature Average Range (°C).

| **Property** | **Value** |
|---|---:|
| Number of Observations | 16491 |
| Minimum | 1.170 |
| Maximum | 12.709 |
| Mean | 6.737 |
| Median | 6.420 |
| Standard Deviation | 2.189 |
| Skewness | $6.280 \times 10^{-4}$ |
| Kurtosis | 2.091 |

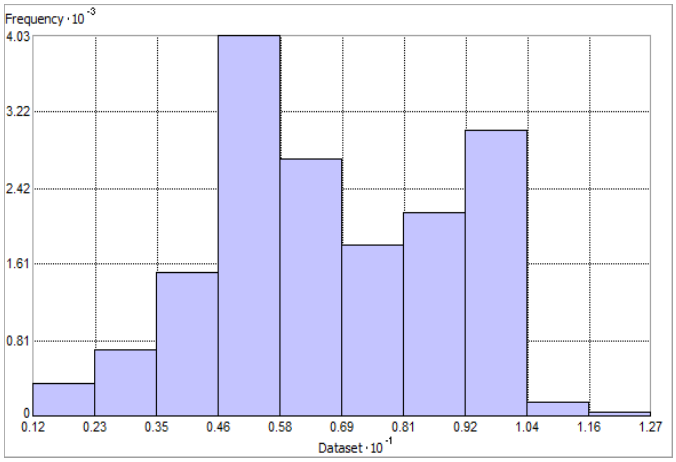


Figure 71. Distribution of Surface Temperature Average Range (°C). Histogram was illustrated using 10 bins. X axis is shown at $10^{-1}$; Y axis is shown at $10^{-3}$.

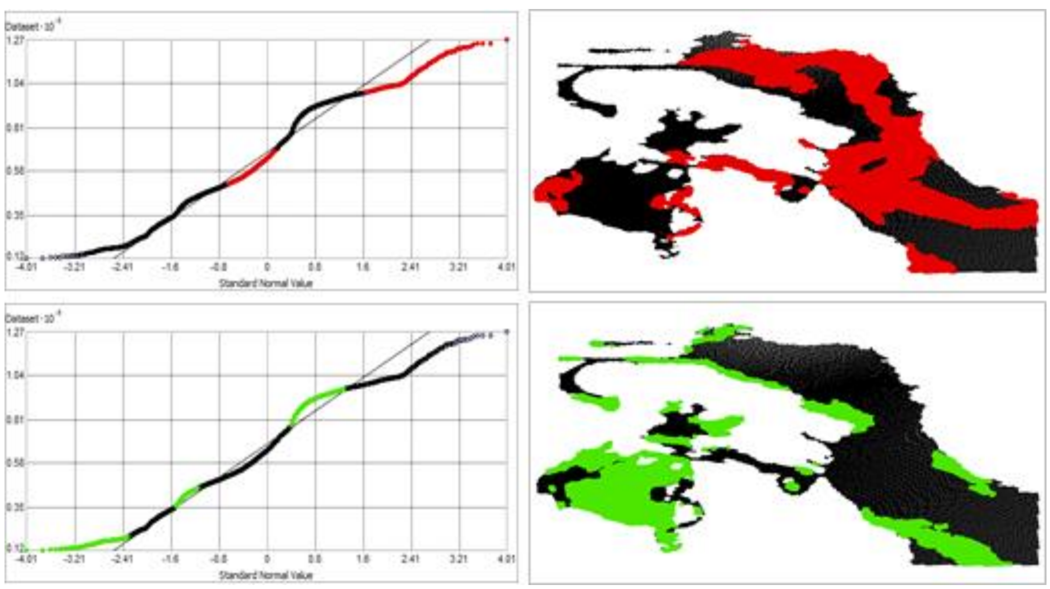

Figure 72. Normal Q-Q plot for data values of Surface Temperature Average Range (°C). Points falling under (top right panel) and over (bottom right panel) the reference line are mapped.

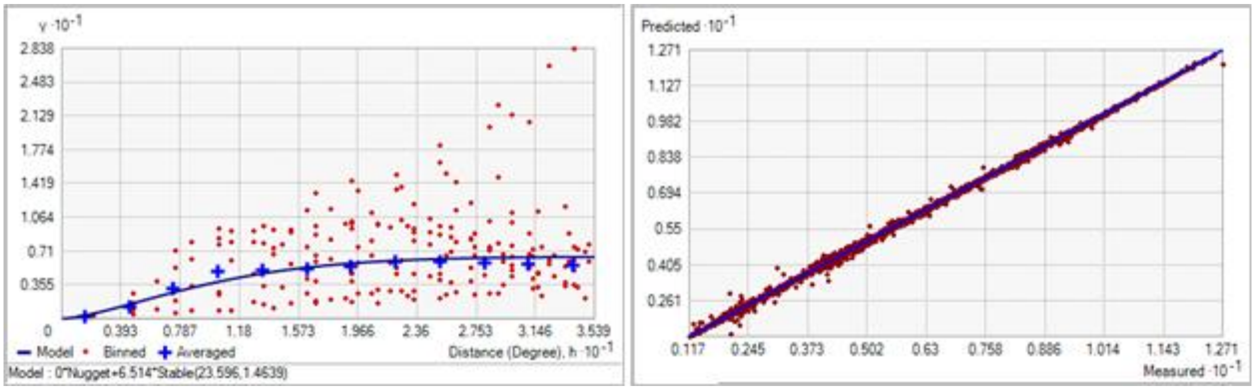

Figure 73. Left panel: Semivariogram of Surface Temperature Average Range (°C). Binned values are shown as red dots; average points are shown as blue crosses; the model fit to the averaged values is shown as a blue line. Lag size: 2.950 degrees; number of lags: 12; Parameter: 1.464; Range: 23.596 degrees; Partial Sill: 6.514. Right panel: Scatterplot of predicted values versus observed values for the model of Surface Temperature Average Range (°C).

Table 30. Results of cross-validation of the kriged model for Surface Temperature Average Range (°C).

| **Prediction Error** | **Value** |
|---|---:|
| Number of Observations | 16491 |
| Overall Mean Error | $7.177 \times 10^{-5}$ |
| Root Mean Square Prediction Error | 0.038 |
| Standardized Mean | $2.440 \times 10^{-4}$ |
| Standardized Root Mean Square Prediction Error | 0.416 |
| Average Standard Error | 0.079 |

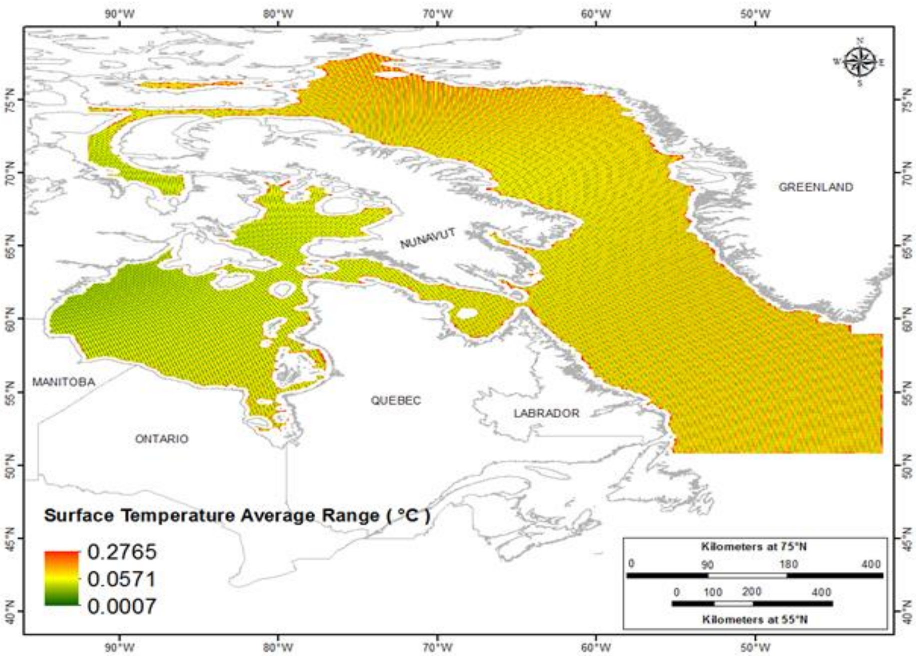


Figure 74. Prediction standard error surface of Surface Temperature Average Range (˚C).

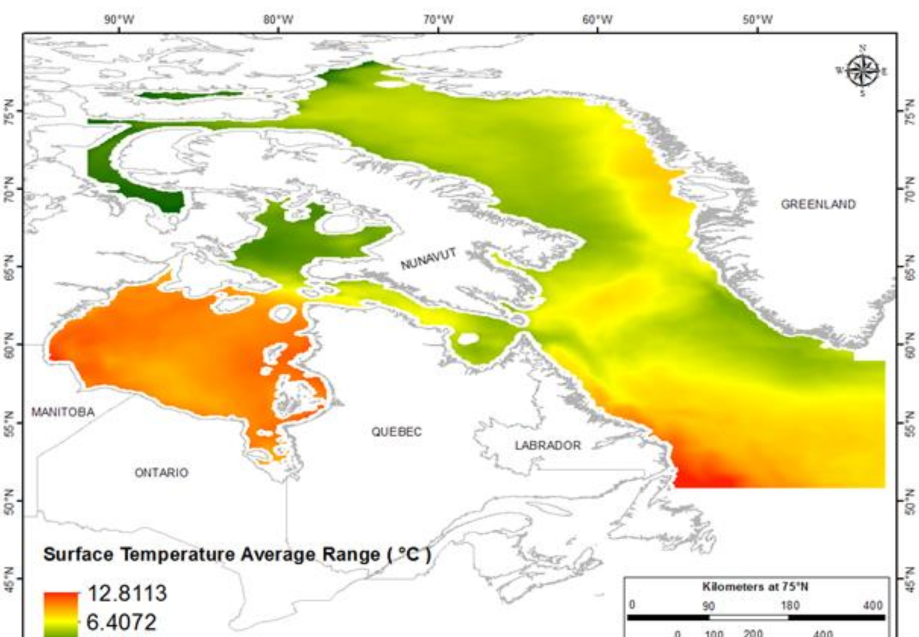


Figure 75. Interpolated prediction surface of Surface Temperature Average Range (˚C).

## Salinity

Salinity influences osmoregulation (control of osmosis and diffusion) in marine organisms. In marine molluscs, one of the most common reactions to changes in salinity is a decrease in respiration rate (Berger and Pharazova, 1997). Salinity is particularly important in shallow and estuarine environments where freshwater input can be substantial. An example of an area with significant freshwater input is Hudson Bay, where mean bottom salinity was as low as 16. Near-bottom salinity was shown to be an important driver of megafaunal species richness and abundance of megafauna associated with deep-water sponge communities in the northwest Atlantic (Beazley et al., 2013) and elsewhere (Papiol et al., 2012). Variations in salinity may also reflect changes in water mass structure which may also influence megafaunal boundaries (Flach et al., 1998; Howell et al., 2002; Arantes et al., 2009).

### Bottom Salinity Mean

This variable displayed a left-skewed, leptokurtic distribution prior to interpolation (Table 31, Figure 76). The data were lower than predicted by a normal distribution at both tails, while mid-values were slightly higher than the reference line (Figure 77). These areas of under- and over-prediction showed spatial pattern over the region (Figure 77).

The semivariogram showed moderate autocorrelation present in the data (Figure 78). The kriged model showed a good fit between measured and predicted values (Figure 78). Good performance of the model was indicated by the cross-validation results (Table 32). The error map showed lower error in Hudson Bay compared to Baffin Bay and Davis Strait, with higher error along the edges of the study extent and in the most northern areas (Figure 79). The kriged surface is presented in Figure 80.

Table 31. Distributional properties of Bottom Salinity Mean.

| **Property** | **Value** |
|---|---:|
| Number of Observations | 16376 |
| Minimum | 16.052 |
| Maximum | 34.953 |
| Mean | 34.062 |
| Median | 34.393 |
| Standard Deviation | 0.941 |
| Skewness | -3.157 |
| Kurtosis | 33.622 |

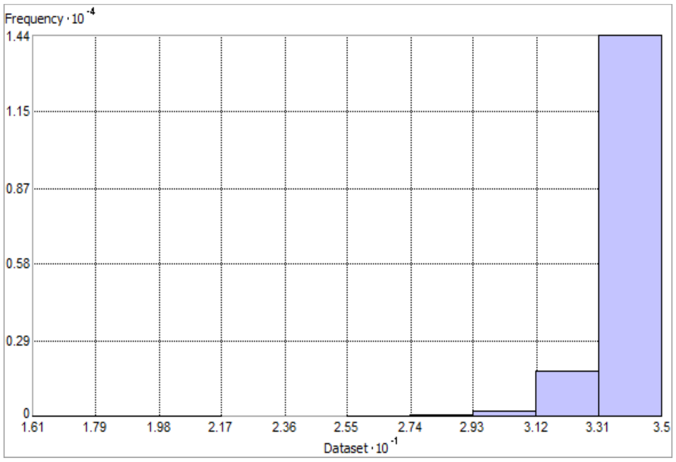

Figure 76. Distribution of Bottom Salinity Mean. Histogram was illustrated using 10 bins. X axis is shown at $10^{-1}$; Y axis is shown at $10^{-4}$.

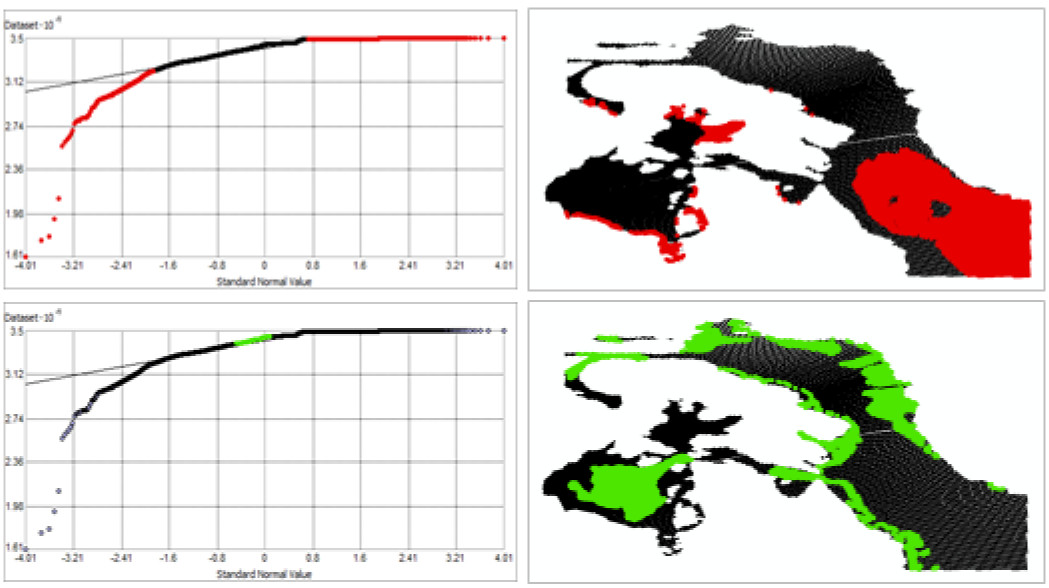
Figure 77. Normal Q-Q plot for data values of Bottom Salinity Mean. Points falling under (top right panel) and over (bottom right panel) the reference line are mapped.

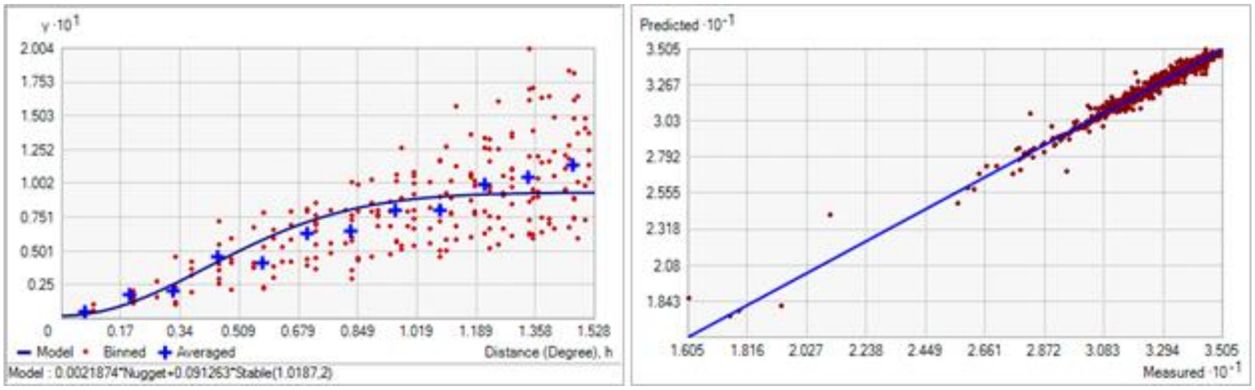

Figure 78. Left panel: Semivariogram of Bottom Salinity Mean. Binned values are shown as red dots; average points are shown as blue crosses; the model fit to the averaged values is shown as a blue line. Lag size: 0.127 degrees; number of lags: 12; Parameter: 2; Range: 1.019 degrees; Partial Sill: 0.091. Right panel: Scatterplot of predicted values versus observed values for the model of Bottom Salinity Mean.

Table 32. Results of cross-validation of the kriged model for Bottom Salinity Mean.

| **Prediction Error** | **Value** |
|---|---|
| Number of Observations | 16376 |
| Overall Mean Error | $6.095 \times 10^{-4}$ |
| Root Mean Square Prediction Error | 0.084 |
| Standardized Mean | $-2.505 \times 10^{-5}$ |
| Standardized Root Mean Square Prediction Error | 1.292 |
| Average Standard Error | 0.057 |

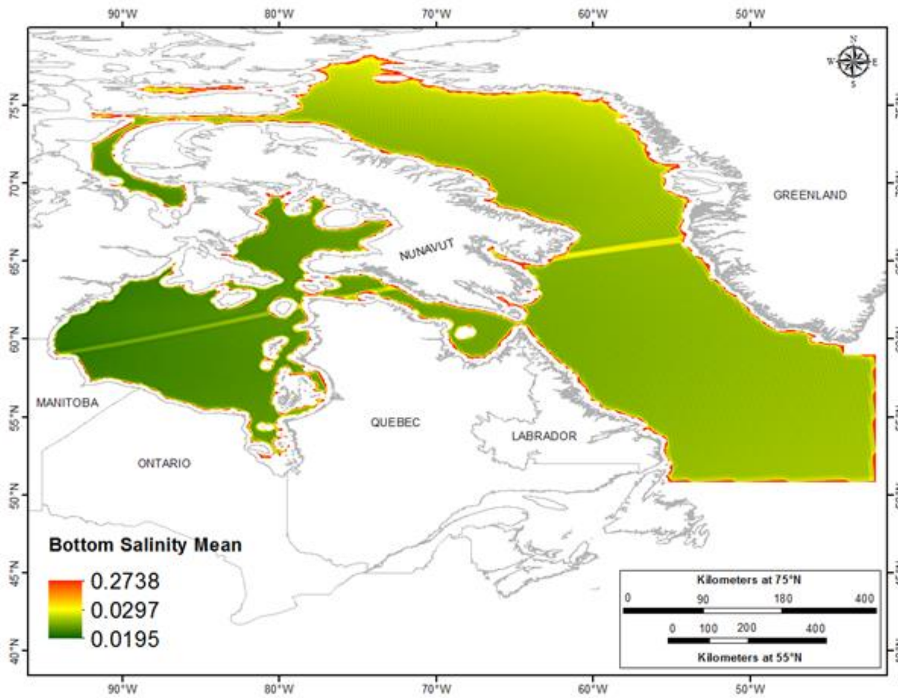


Figure 79. Prediction standard error surface of Bottom Salinity Mean.

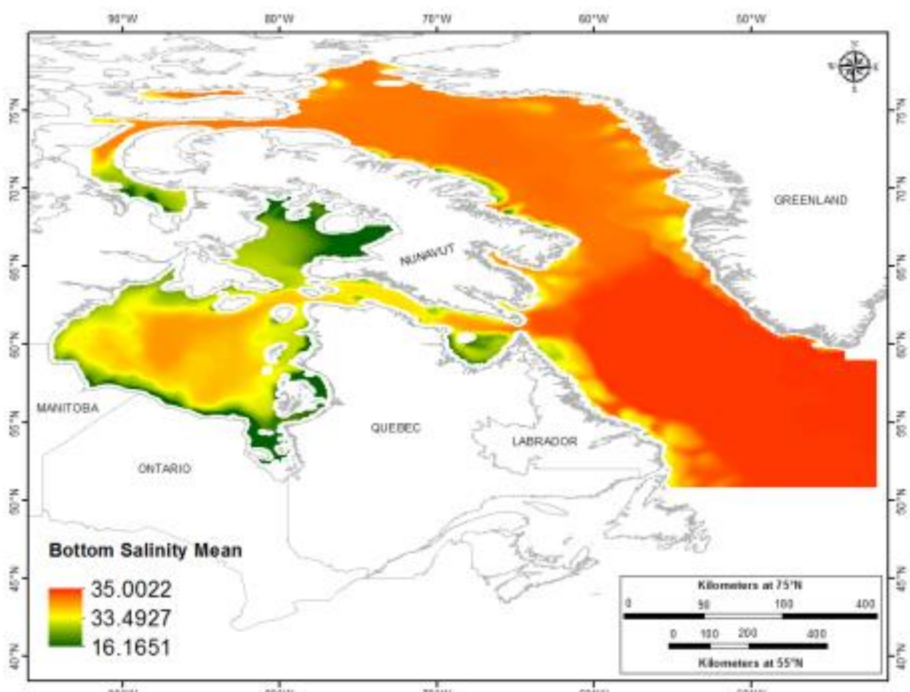


Figure 80. Interpolated prediction surface of Bottom Salinity Mean.

**Bottom Salinity Minimum**

This variable displayed a left-skewed, leptokurtic distribution prior to interpolation (Table 33, Figure 81). The data were lower than predicted by a normal distribution at both tails, while mid-values were slightly higher than the reference line (Figure 82). These areas of under- and over-prediction showed spatial pattern over the region (Figure 82).

The semivariogram showed moderate autocorrelation present in the data (Figure 83). The kriged model showed a good fit between measured and predicted values (Figure 83). Good performance of the model was indicated by the cross-validation results (Table 34). The error map showed lower error in Hudson Bay compared to Baffin Bay and Davis Strait, with higher error along the edges of the study extent and in the most northern areas (Figure 84). The kriged surface is presented in Figure 85.

Table 33. Distributional properties of Bottom Salinity Minimum.

| **Property** | **Value** |
|---|---:|
| Number of Observations | 16376 |
| Minimum | 12.067 |
| Maximum | 34.904 |
| Mean | 33.712 |
| Median | 34.146 |
| Standard Deviation | 1.317 |
| Skewness | -2.954 |
| Kurtosis | 23.370 |

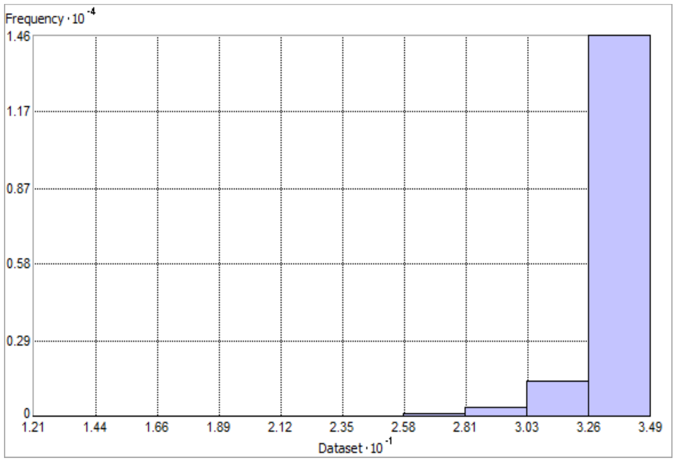


Figure 81. Distribution of Bottom Salinity Minimum. Histogram was illustrated using 10 bins. X axis is shown at $10^{-1}$; Y axis is shown at $10^{-4}$.

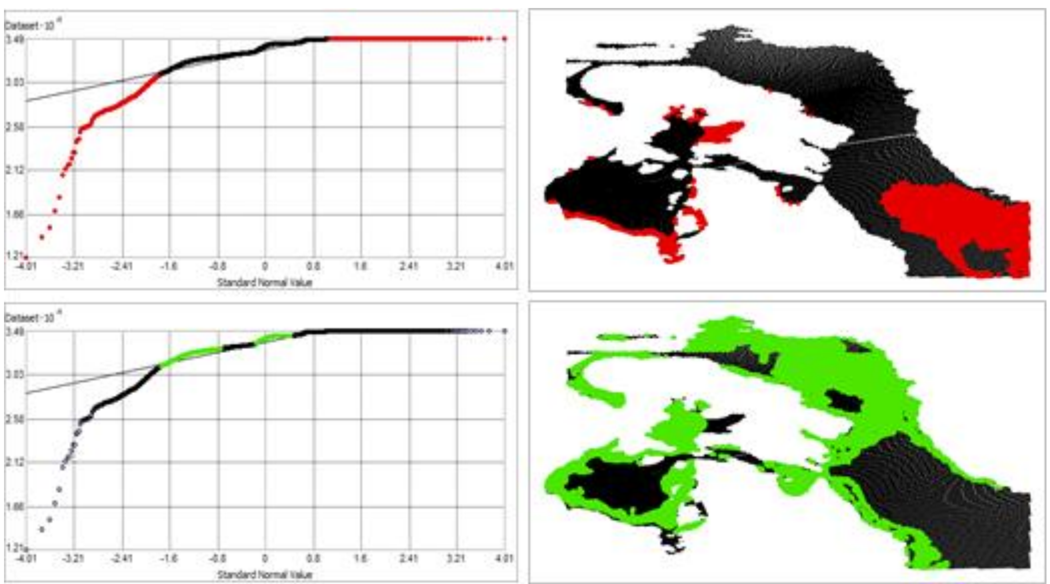

Figure 82. Normal Q-Q plot for data values of Bottom Salinity Minimum. Points falling under (top right panel) and over (bottom right panel) the reference line are mapped.

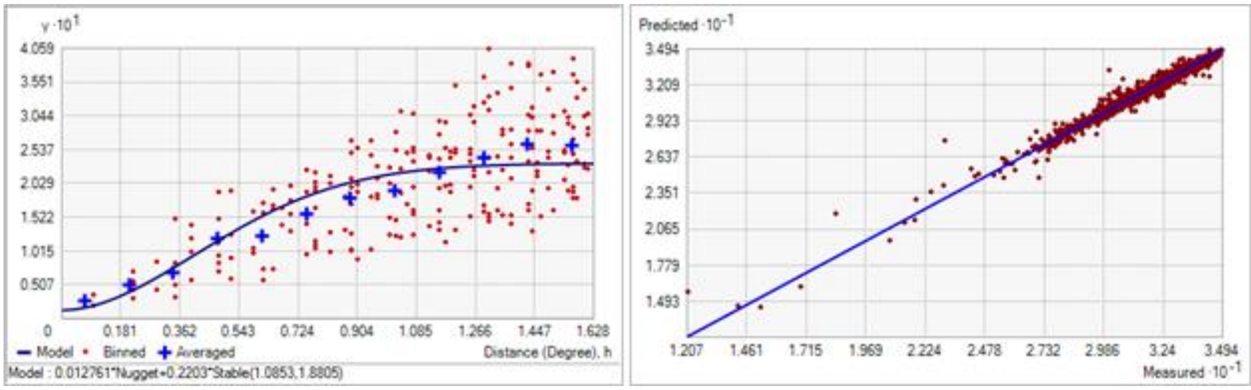

Figure 83. Left panel: Semivariogram of Bottom Salinity Minimum. Binned values are shown as red dots; average points are shown as blue crosses; the model fit to the averaged values is shown as a blue line. Lag size: 0.127 degrees; number of lags: 12; Parameter: 2; Range: 1.019 degrees; Partial Sill: 0.091. Right panel: Scatterplot of predicted values versus observed values for the model of Bottom Salinity Minimum.

Table 34. Results of cross-validation of the kriged model for Bottom Salinity Minimum.

| **Prediction Error** | **Value** |
|---|---:|
| Number of Observations | 16376 |
| Overall Mean Error | $2.571 \times 10^{-4}$ |
| Root Mean Square Prediction Error | 0.125 |
| Standardized Mean | $-5.435 \times 10^{-3}$ |
| Standardized Root Mean Square Prediction Error | 0.793 |
| Average Standard Error | 0.143 |

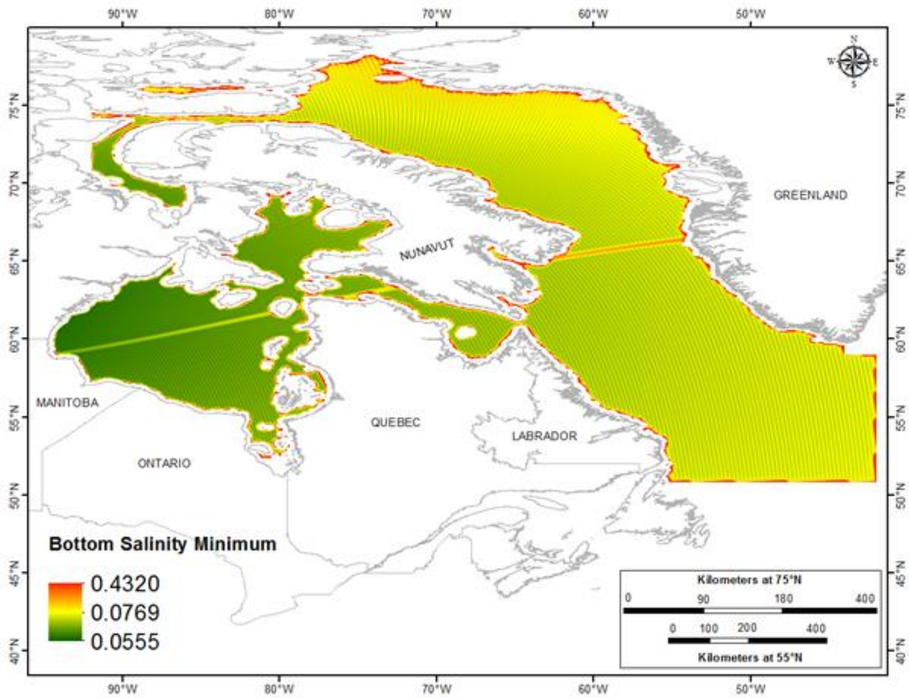

Figure 84. Prediction standard error surface of Bottom Salinity Minimum.

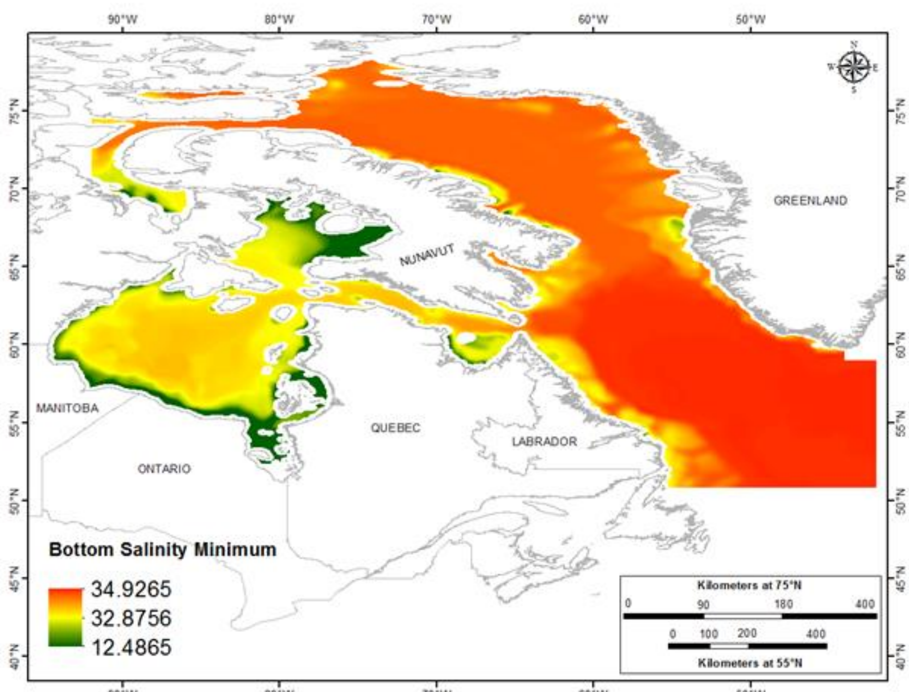

Figure 85. Interpolated prediction surface of Bottom Salinity Minimum.

**Bottom Salinity Maximum**

This variable displayed a left-skewed, leptokurtic distribution prior to interpolation (Table 35, Figure 86). The data were lower than predicted by a normal distribution at both tails, while mid-values were slightly higher than the reference line (Figure 87). These areas of under- and over-prediction showed spatial pattern over the region (Figure 87).

The semivariogram showed moderate autocorrelation present in the data (Figure 88). The kriged model showed a good fit between measured and predicted values (Figure 88). Fair performance of the model was indicated by the cross-validation results (Table 36). The error map showed lower error in Hudson Bay compared to Baffin Bay and Davis Strait, with higher error along the edges of the study extent and in the most northern areas (Figure 89). The kriged surface is presented in Figure 90.

Table 35. Distributional properties of Bottom Salinity Maximum.

| **Property** | **Value** |
|---|---:|
| Number of Observations | 16376 |
| Minimum | 25.560 |
| Maximum | 35.289 |
| Mean | 34.379 |
| Median | 34.542 |
| Standard Deviation | 0.652 |
| Skewness | -1.899 |
| Kurtosis | 10.966 |

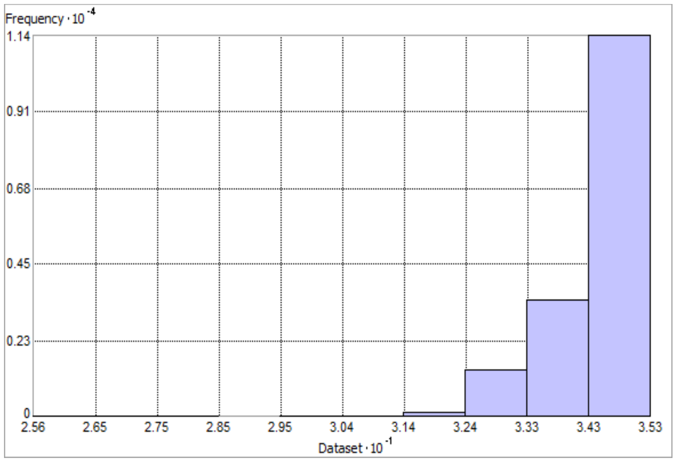


Figure 86. Distribution of Bottom Salinity Maximum. Histogram was illustrated using 10 bins. X axis is shown at $10^{-1}$; Y axis is shown at $10^{-4}$.

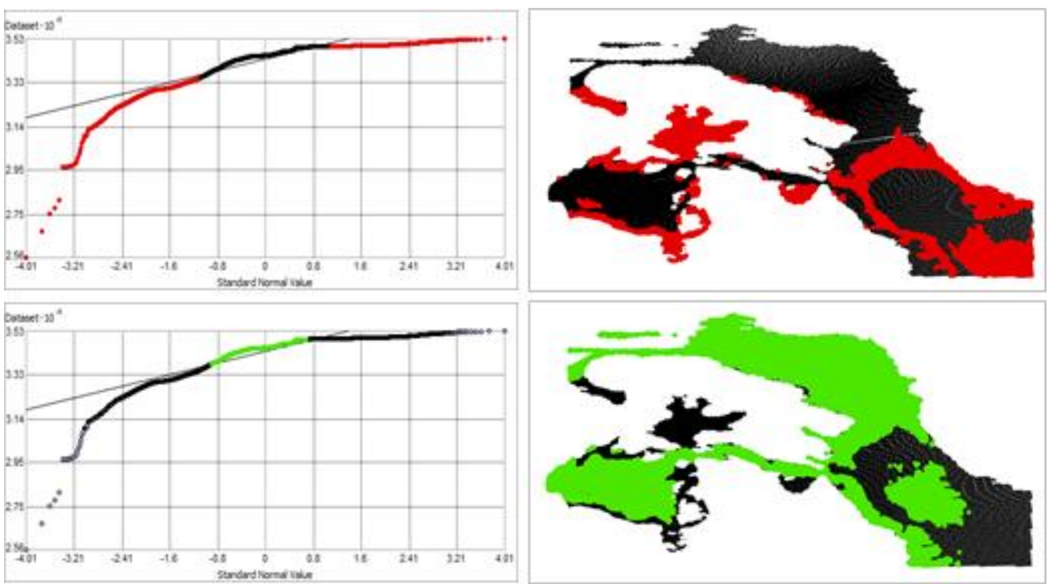

Figure 87. Normal Q-Q plot for data values of Bottom Salinity Minimum. Points falling under (top right panel) and over (bottom right panel) the reference line are mapped.

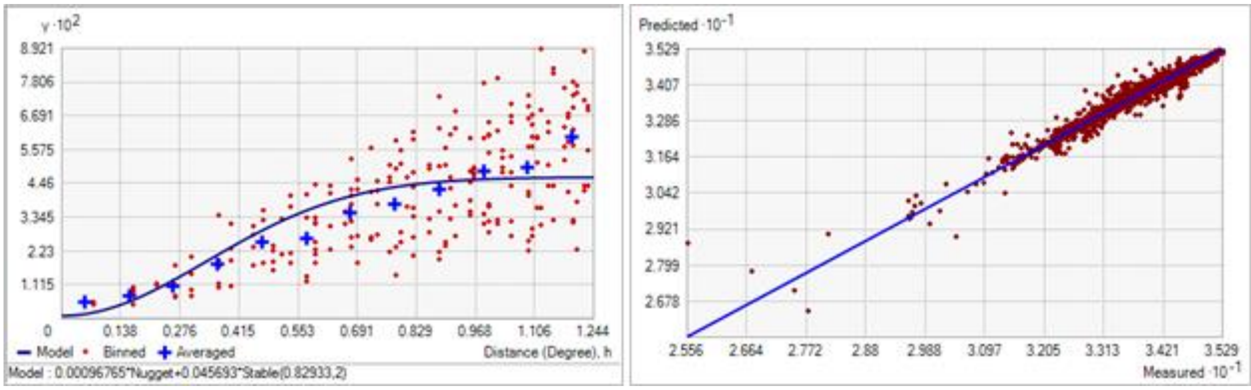


Figure 88. Left panel: Semivariogram of Bottom Salinity Maximum. Binned values are shown as red dots; average points are shown as blue crosses; the model fit to the averaged values is shown as a blue line. Lag size: 0.104 degrees; number of lags: 12; Parameter: 2; Range: 0.829 degrees; Partial Sill: 0.046. Right panel: Scatterplot of predicted values versus observed values for the model of Bottom Salinity Maximum.

Table 36. Results of cross-validation of the kriged model for Bottom Salinity Maximum.

| **Prediction Error** | **Value** |
|---|---:|
| Number of Observations | 16376 |
| Overall Mean Error | $7.806 \times 10^{-4}$ |
| Root Mean Square Prediction Error | 0.073 |
| Standardized Mean | $9.001 \times 10^{-3}$ |
| Standardized Root Mean Square Prediction Error | 1.520 |
| Average Standard Error | 0.041 |

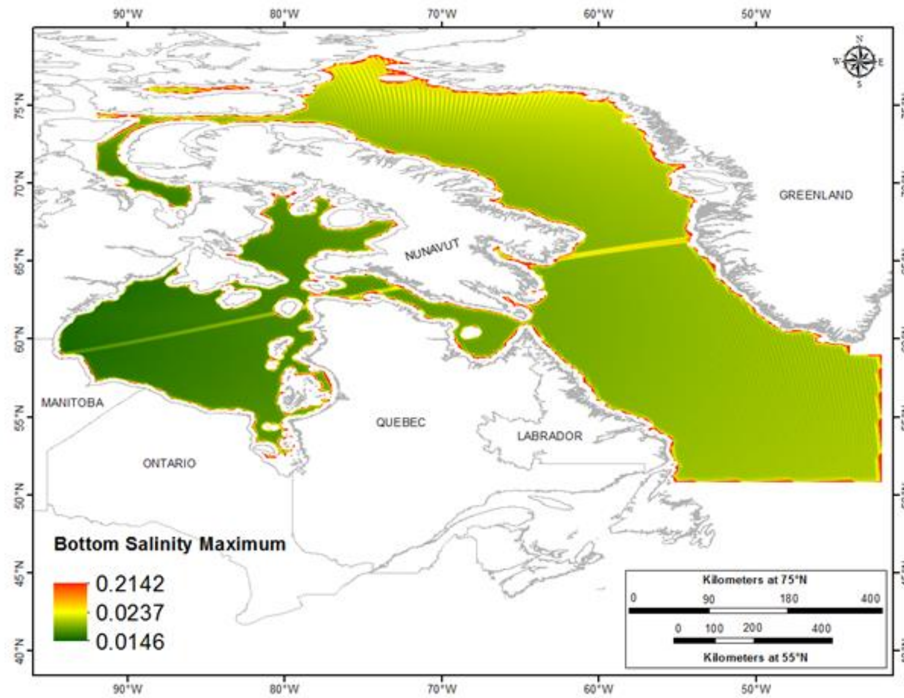


Figure 89. Prediction standard error surface of Bottom Salinity Maximum.

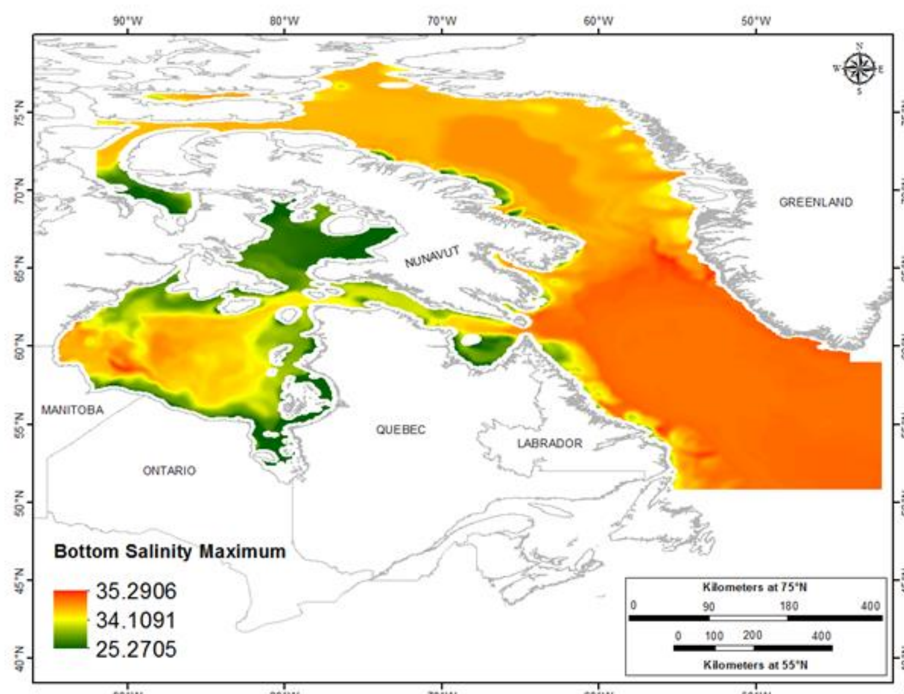


Figure 90. Interpolated prediction surface of Bottom Salinity Maximum.

**Bottom Salinity Range**

This variable displayed a right-skewed, leptokurtic distribution prior to interpolation (Table 37, Figure 91). The data were higher than predicted by a normal distribution at both tails, while mid-values were slightly lower than the reference line (Figure 92). These areas of under- and over-prediction showed spatial pattern over the region (Figure 92).

The semivariogram showed moderate autocorrelation present in the data (Figure 93). The kriged model showed a good fit between measured and predicted values (Figure 93). Good performance of the model was indicated by the cross-validation results (Table 38). The error map showed lower error in Hudson Bay compared to Baffin Bay and Davis Strait, with higher error along the edges of the study extent and in the most northern areas (Figure 94). The kriged surface is presented in Figure 95.

Table 37. Distributional properties of Bottom Salinity Range.

| **Property** | **Value** |
|---|---:|
| Number of Observations | 16376 |
| Minimum | 0.024 |
| Maximum | 13.524 |
| Mean | 0.667 |
| Median | 0.407 |
| Standard Deviation | 0.823 |
| Skewness | 3.902 |
| Kurtosis | 33.678 |

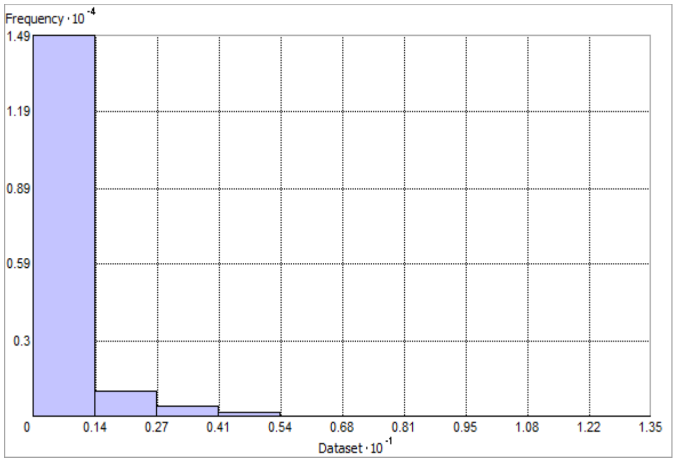

Figure 91. Distribution of Bottom Salinity Range. Histogram was illustrated using 10 bins. X axis is shown at $10^{-1}$; Y axis is shown at $10^{-4}$.

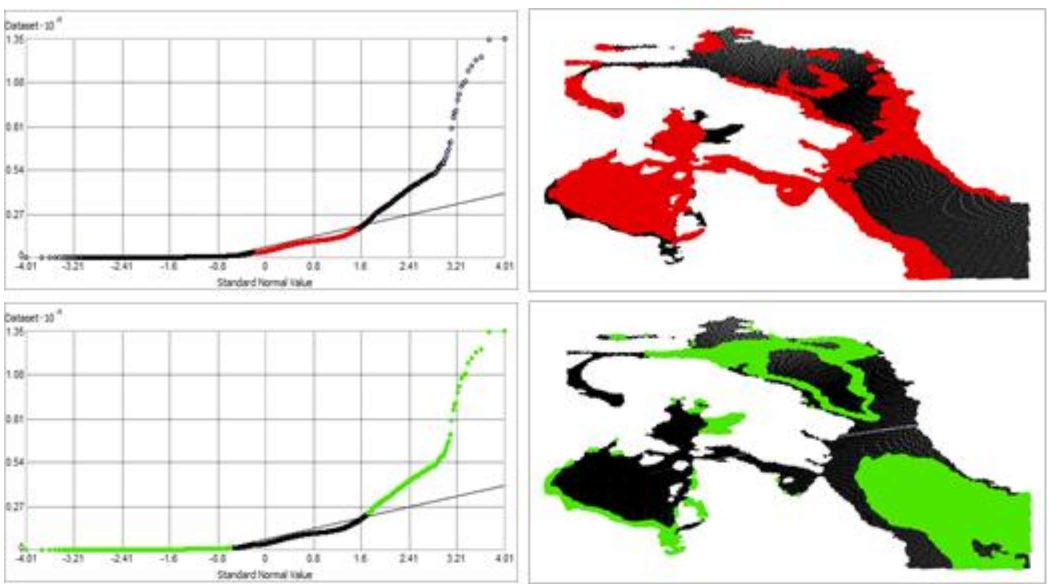
Figure 92. Normal Q-Q plot for data values of Bottom Salinity Range. Points falling under (top right panel) and over (bottom right panel) the reference line are mapped.

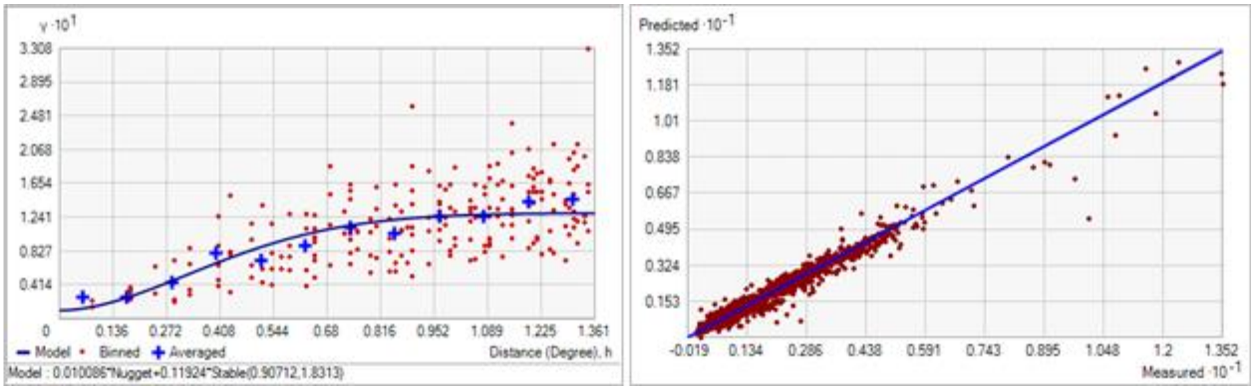

Figure 93. Left panel: Semivariogram of Bottom Salinity Range. Binned values are shown as red dots; average points are shown as blue crosses; the model fit to the averaged values is shown as a blue line. Lag size: 0.113 degrees; number of lags: 12; Parameter: 1.831; Range: 0.907 degrees; Partial Sill: 0.119. Right panel: Scatterplot of predicted values versus observed values for the model of Bottom Salinity Range.

Table 38. Results of cross-validation of the kriged model for Bottom Salinity Range.

| **Prediction Error** | **Value** |
|---|---:|
| Number of Observations | 16376 |
| Overall Mean Error | $-6.084 \times 10^{-4}$ |
| Root Mean Square Prediction Error | 0.102 |
| Standardized Mean | $1.376 \times 10^{-3}$ |
| Standardized Root Mean Square Prediction Error | 0.703 |
| Average Standard Error | 0.133 |

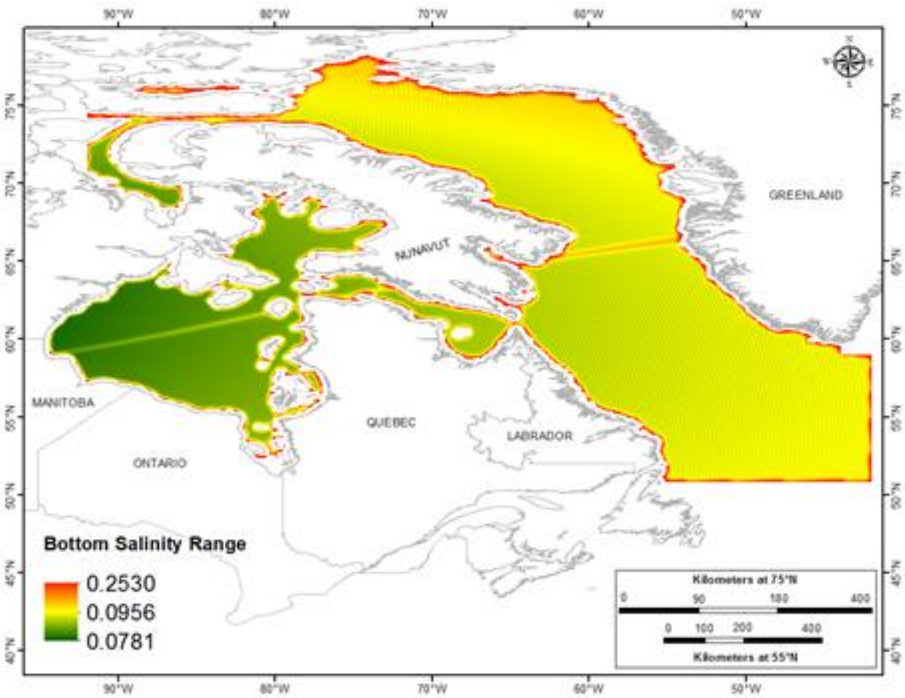


Figure 94. Prediction standard error surface of Bottom Salinity Range.

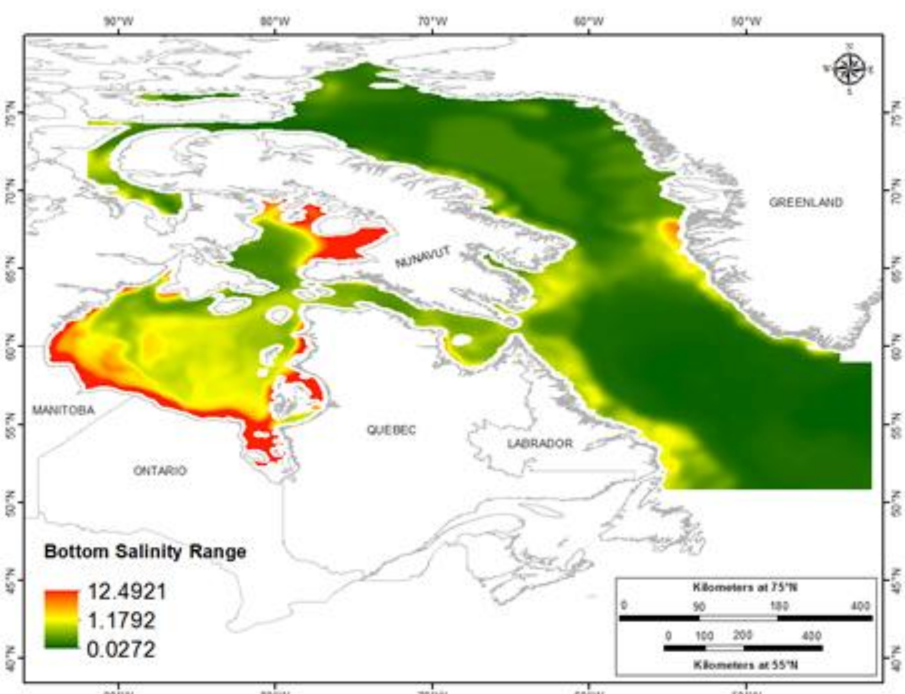


Figure 95. Interpolated prediction surface of Bottom Salinity Range.

**Bottom Salinity Average Minimum**

This variable displayed a left-skewed, leptokurtic distribution prior to interpolation (Table 39, Figure 96). The data were lower than predicted by a normal distribution at both tails, while mid-values were slightly higher than the reference line (Figure 97). These areas of under- and over-prediction showed spatial pattern over the region (Figure 97).

The semivariogram showed moderate autocorrelation present in the data (Figure 98). The kriged model showed a good fit between measured and predicted values (Figure 98). Good performance of the model was indicated by the cross-validation results (Table 40). The error map showed lower error in Hudson Bay compared to Baffin Bay and Davis Strait, with higher error along the edges of the study extent and in the most northern areas (Figure 99). The kriged surface is presented in Figure 100.

Table 39. Distributional properties of Bottom Salinity Average Minimum.

| **Property** | **Value** |
|---|---:|
| Number of Observations | 16376 |
| Minimum | 13.046 |
| Maximum | 34.915 |
| Mean | 33.929 |
| Median | 34.323 |
| Standard Deviation | 1.135 |
| Skewness | -3.330 |
| Kurtosis | 30.884 |

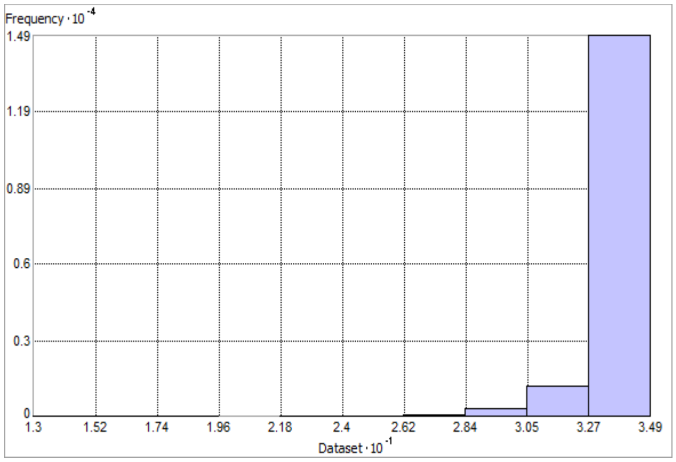


Figure 96. Distribution of Bottom Salinity Average Minimum. Histogram was illustrated using 10 bins. X axis is shown at $10^{-1}$; Y axis is shown at $10^{-4}$.

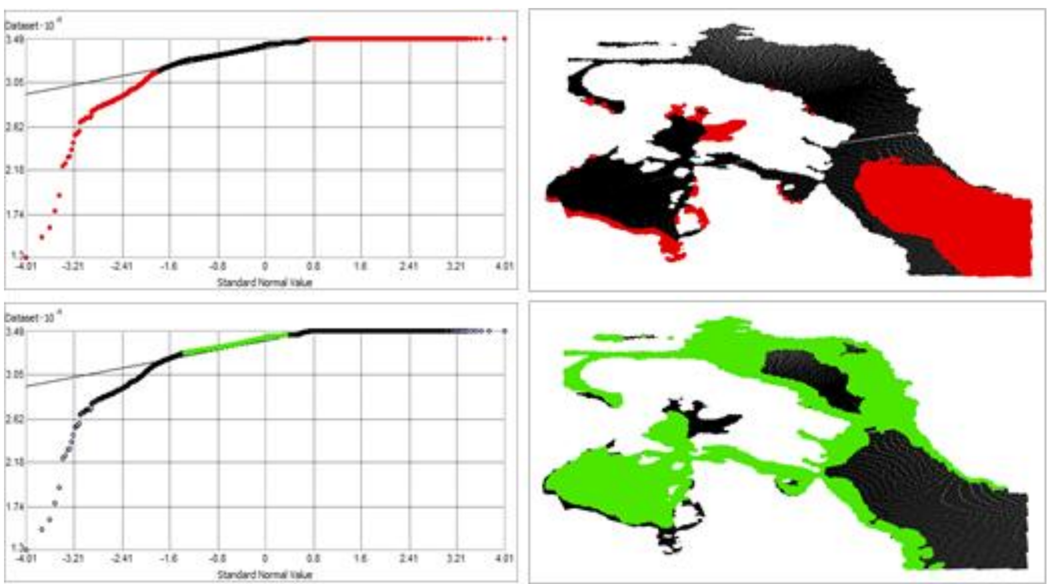

Figure 97. Normal Q-Q plot for data values of Bottom Salinity Average Minimum. Points falling under (top right panel) and over (bottom right panel) the reference line are mapped.

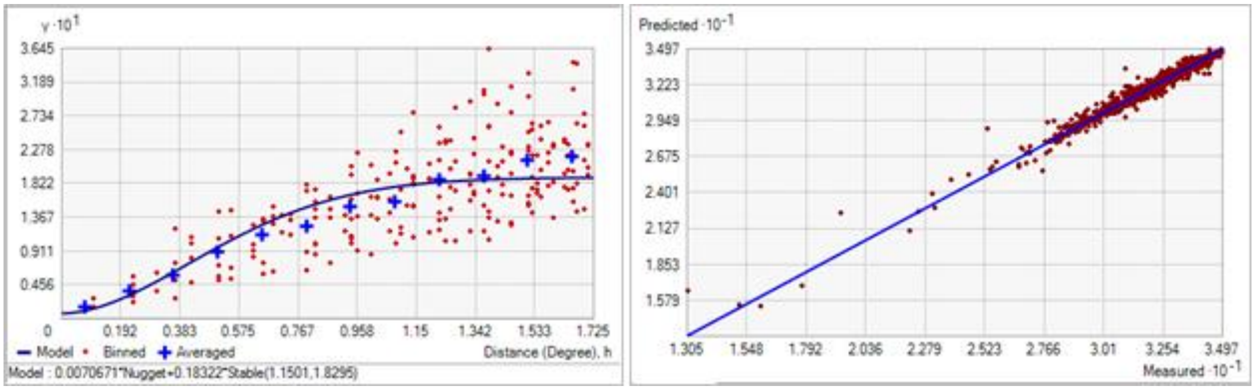

Figure 98. Left panel: Semivariogram of Bottom Salinity Average Minimum. Binned values are shown as red dots; average points are shown as blue crosses; the model fit to the averaged values is shown as a blue line. Lag size: 0.144 degrees; number of lags: 12; Parameter: 1.829; Range: 1.150 degrees; Partial Sill: 0.183. Right panel: Scatterplot of predicted values versus observed values for the model of Bottom Salinity Average Minimum.

Table 40. Results of cross-validation of the kriged model for Bottom Salinity Average Minimum.

| **Prediction Error** | **Value** |
|---|---:|
| Number of Observations | 16376 |
| Overall Mean Error | $6.730 \times 10^{-4}$ |
| Root Mean Square Prediction Error | 0.105 |
| Standardized Mean | $-2.376 \times 10^{-3}$ |
| Standardized Root Mean Square Prediction Error | 0.816 |
| Average Standard Error | 0.114 |

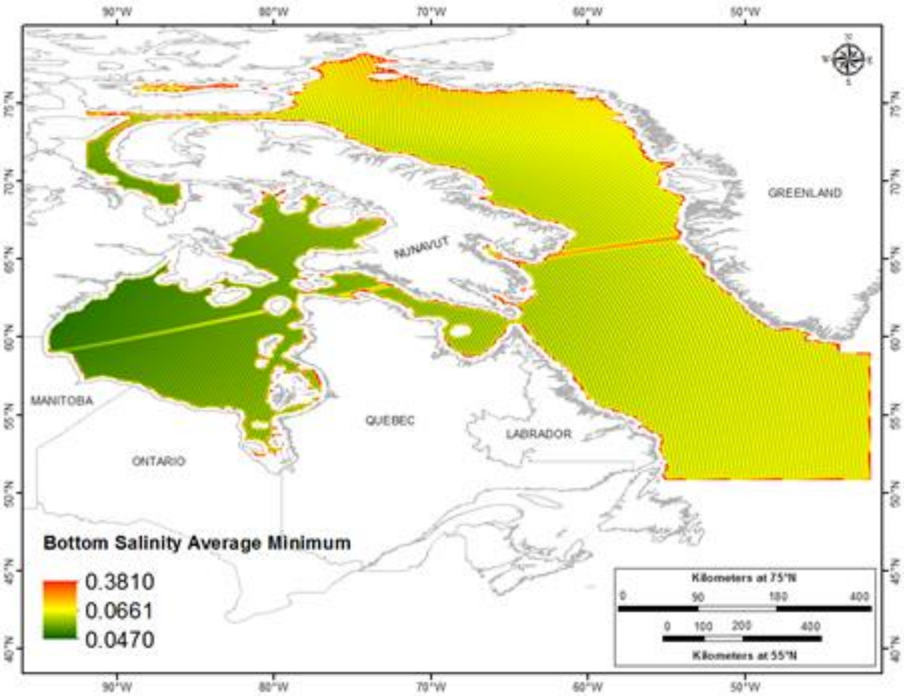


Figure 99. Prediction standard error surface of Bottom Salinity Average Minimum.

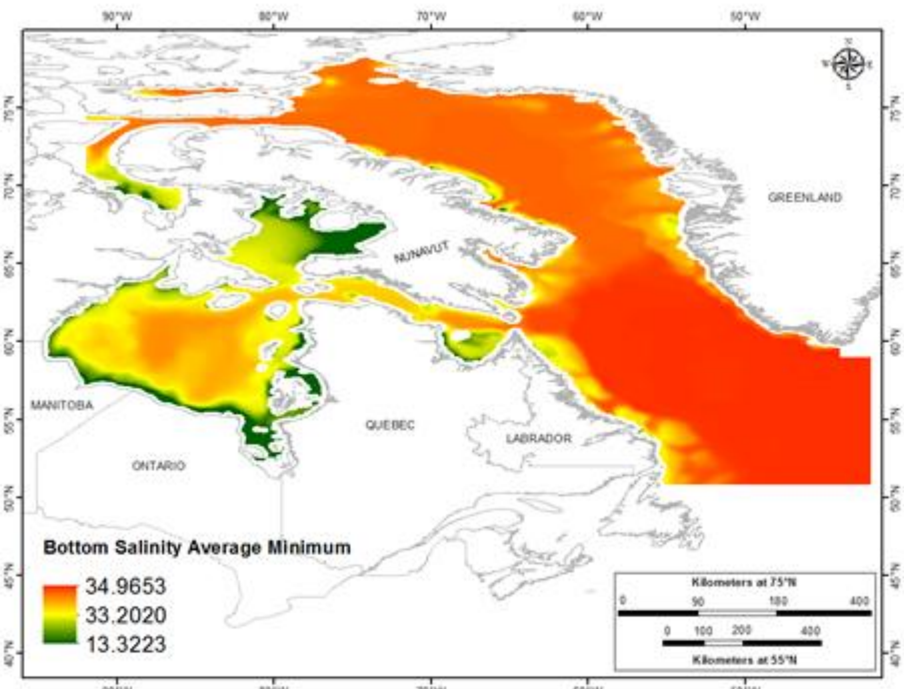


Figure 100. Interpolated prediction surface of Bottom Salinity Average Minimum.

## Bottom Salinity Average Maximum

This variable displayed a left-skewed, leptokurtic distribution prior to interpolation (Table 41, Figure 101). The data were lower than predicted by a normal distribution at both tails, while mid-values were slightly higher than the reference line (Figure 102). These areas of under- and over-prediction showed spatial pattern over the region (Figure 102).

The semivariogram showed moderate autocorrelation present in the data (Figure 103). The kriged model showed a good fit between measured and predicted values (Figure 103). Fair performance of the model was indicated by the cross-validation results (Table 42). The error map showed lower error in Hudson Bay compared to Baffin Bay and Davis Strait, with higher error along the edges of the study extent and in the most northern areas (Figure 104). The kriged surface is presented in Figure 105.

Table 41. Distributional properties of Bottom Salinity Average Maximum.

| **Property** | **Value** |
|---|---:|
| Number of Observations | 16376 |
| Minimum | 18.949 |
| Maximum | 35.064 |
| Mean | 34.181 |
| Median | 34.452 |
| Standard Deviation | 0.808 |
| Skewness | -2.785 |
| Kurtosis | 29.417 |

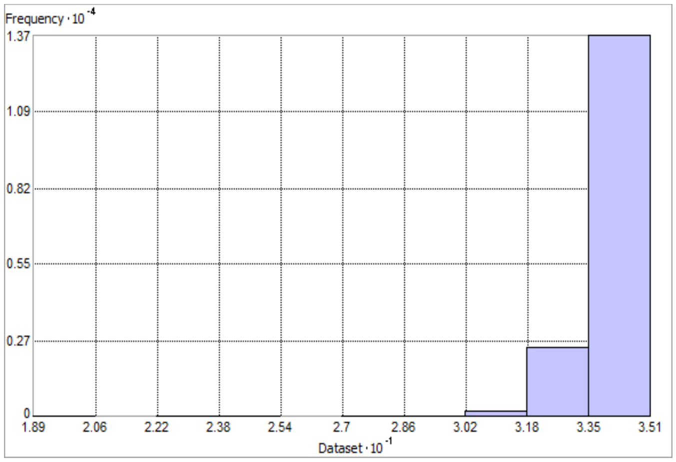


Figure 101. Distribution of Bottom Salinity Average Maximum. Histogram was illustrated using 10 bins. X axis is shown at $10^{-1}$; Y axis is shown at $10^{-4}$.

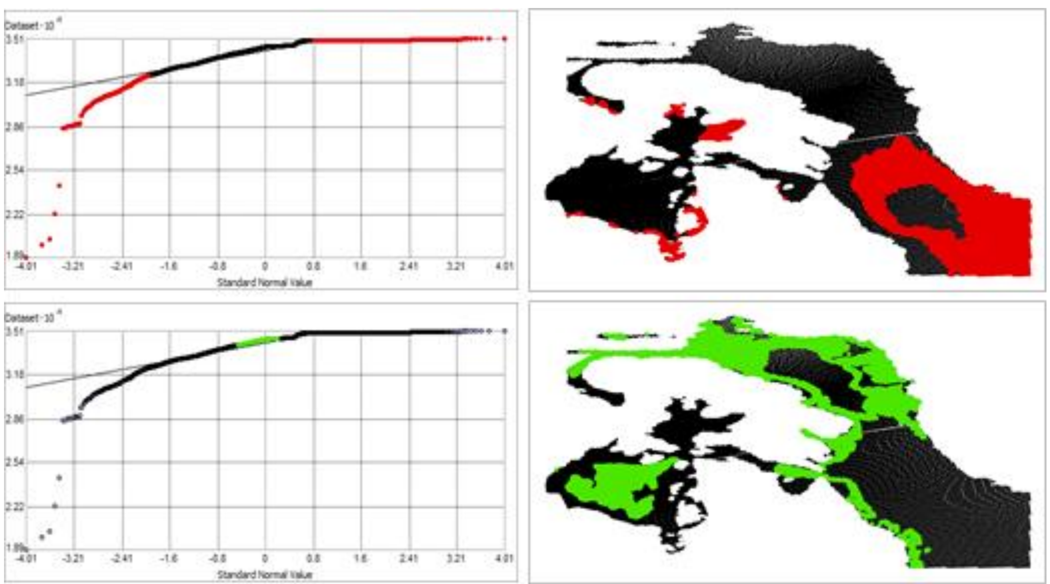

Figure 102. Normal Q-Q plot for data values of Bottom Salinity Average Maximum. Points falling under (top right panel) and over (bottom right panel) the reference line are mapped.

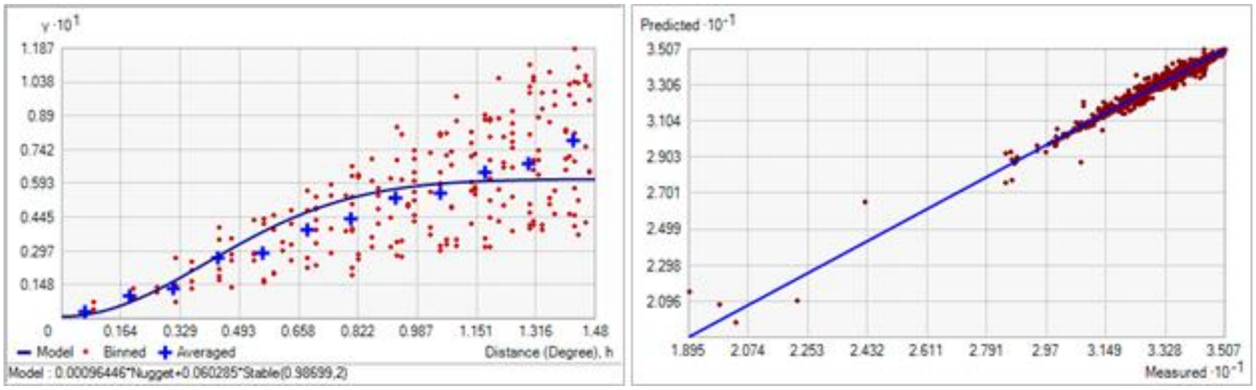

Figure 103. Left panel: Semivariogram of Bottom Salinity Average Maximum. Binned values are shown as red dots; average points are shown as blue crosses; the model fit to the averaged values is shown as a blue line. Lag size: 0.123 degrees; number of lags: 12; Parameter: 2; Range: 0.987 degrees; Partial Sill: 0.060. Right panel: Scatterplot of predicted values versus observed values for the model of Bottom Salinity Average Maximum.

Table 42. Results of cross-validation of the kriged model for Bottom Salinity Average Maximum.

| **Prediction Error** | **Value** |
|---|---:|
| Number of Observations | 16376 |
| Overall Mean Error | $7.139 \times 10^{-4}$ |
| Root Mean Square Prediction Error | 0.072 |
| Standardized Mean | $6.331 \times 10^{-3}$ |
| Standardized Root Mean Square Prediction Error | 1.616 |
| Average Standard Error | 0.039 |

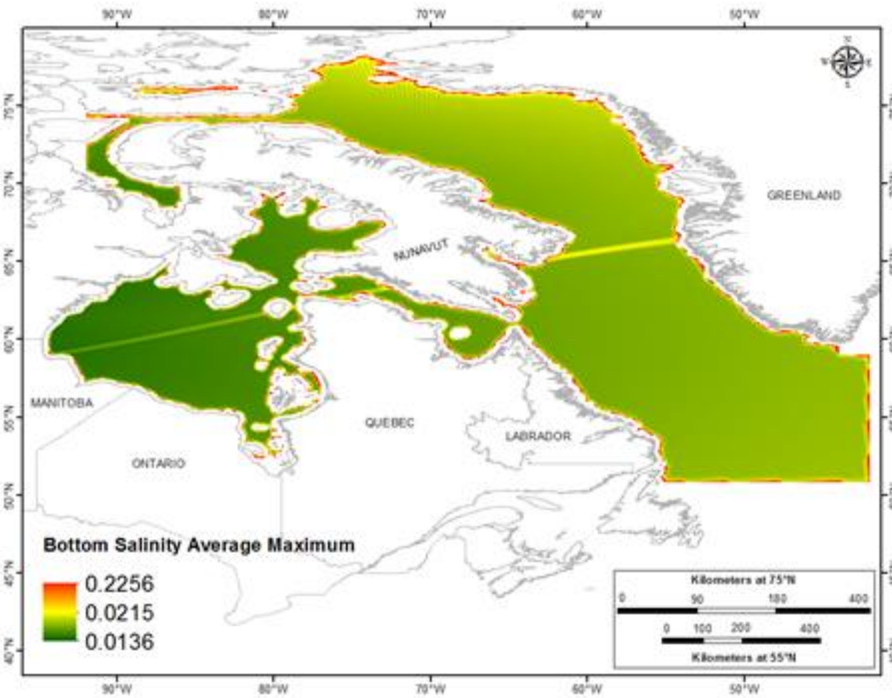


Figure 104. Prediction standard error surface of Bottom Salinity Average Maximum.

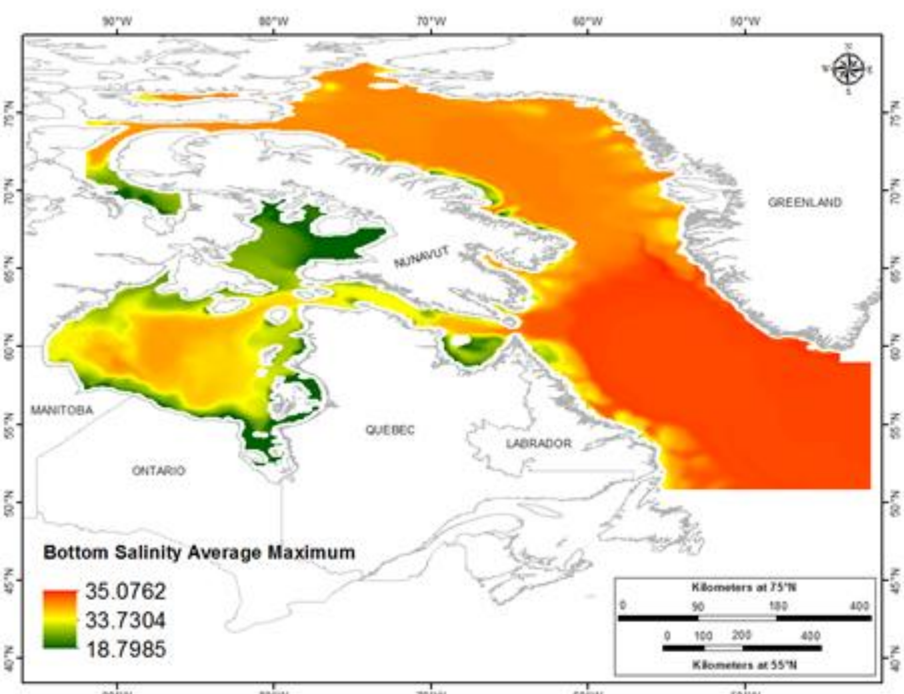


Figure 105. Interpolated prediction surface of Bottom Salinity Average Maximum.

**Bottom Salinity Average Range**

This variable displayed a right-skewed, leptokurtic distribution prior to interpolation (Table 43, Figure 106). The data were lower than predicted by a normal distribution at both tails, while mid-values were slightly higher than the reference line (Figure 107). These areas of under- and over-prediction showed spatial pattern over the region (Figure 107).

The semivariogram showed moderate autocorrelation present in the data (Figure 108). The kriged model showed a good fit between measured and predicted values (Figure 108). Fair performance of the model was indicated by the cross-validation results (Table 44). The error map showed lower error in Hudson Bay compared to Baffin Bay and Davis Strait, with higher error along the edges of the study extent and in the most northern areas (Figure 109). The kriged surface is presented in Figure 110.

Table 43. Distributional properties of Bottom Salinity Average Range.

| **Property** | **Value** |
|---|---:|
| Number of Observations | 16376 |
| Minimum | $6.262 \times 10^{-3}$ |
| Maximum | 7.910 |
| Mean | 0.252 |
| Median | 0.121 |
| Standard Deviation | 0.427 |
| Skewness | 5.357 |
| Kurtosis | 53.308 |

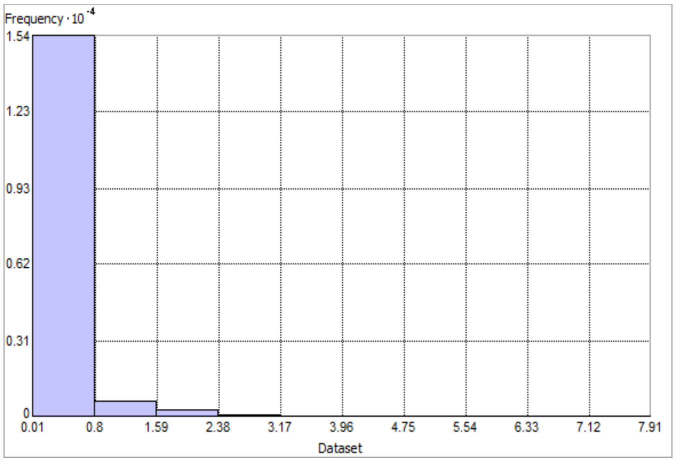

Figure 106. Distribution of Bottom Salinity Average Range. Histogram was illustrated using 10 bins. Y axis is shown at $10^{-4}$.

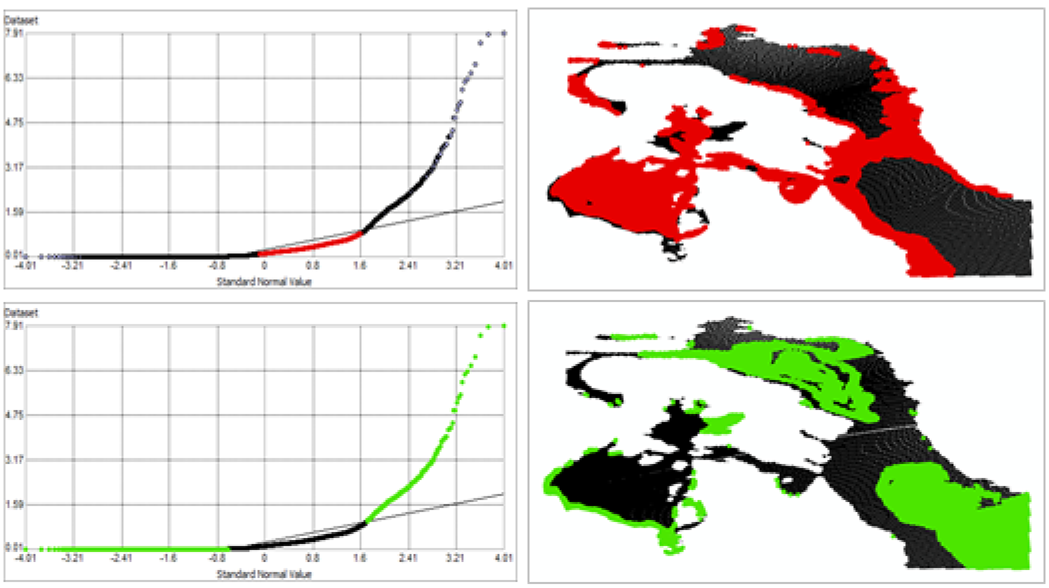

Figure 107. Normal Q-Q plot for data values of Bottom Salinity Average Range. Points falling under (top right panel) and over (bottom right panel) the reference line are mapped.

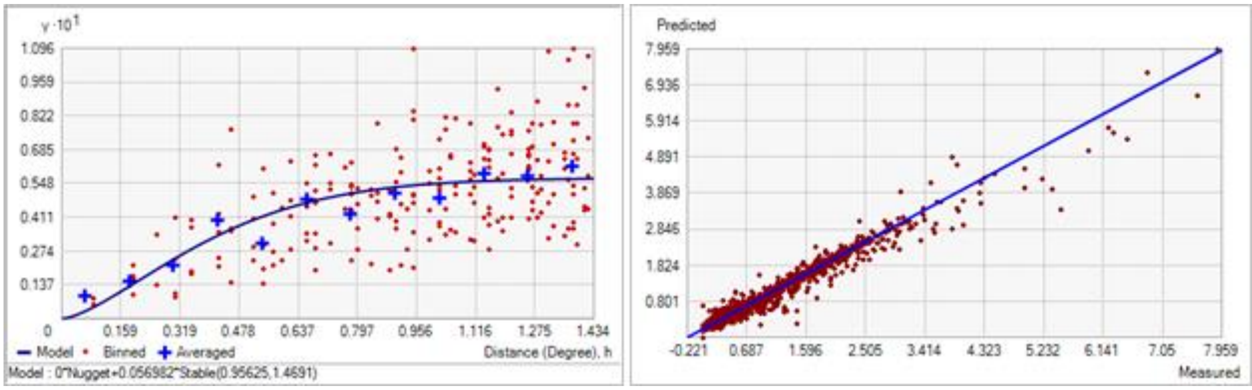

Figure 108. Left panel: Semivariogram of Bottom Salinity Average Range. Binned values are shown as red dots; average points are shown as blue crosses; the model fit to the averaged values is shown as a blue line. Lag size: 0.120 degrees; number of lags: 12; Parameter: 1.469; Range: 0.956 degrees; Partial Sill: 0.057. Right panel: Scatterplot of predicted values versus observed values for the model of Bottom Salinity Average Range.

Table 44. Results of cross-validation of the kriged model for Bottom Salinity Average Range.

| **Prediction Error** | **Value** |
|---|---|
| Number of Observations | 16376 |
| Overall Mean Error | $-1.333 \times 10^{-3}$ |
| Root Mean Square Prediction Error | 0.059 |
| Standardized Mean | $-7.820 \times 10^{-3}$ |
| Standardized Root Mean Square Prediction Error | 0.653 |
| Average Standard Error | 0.083 |

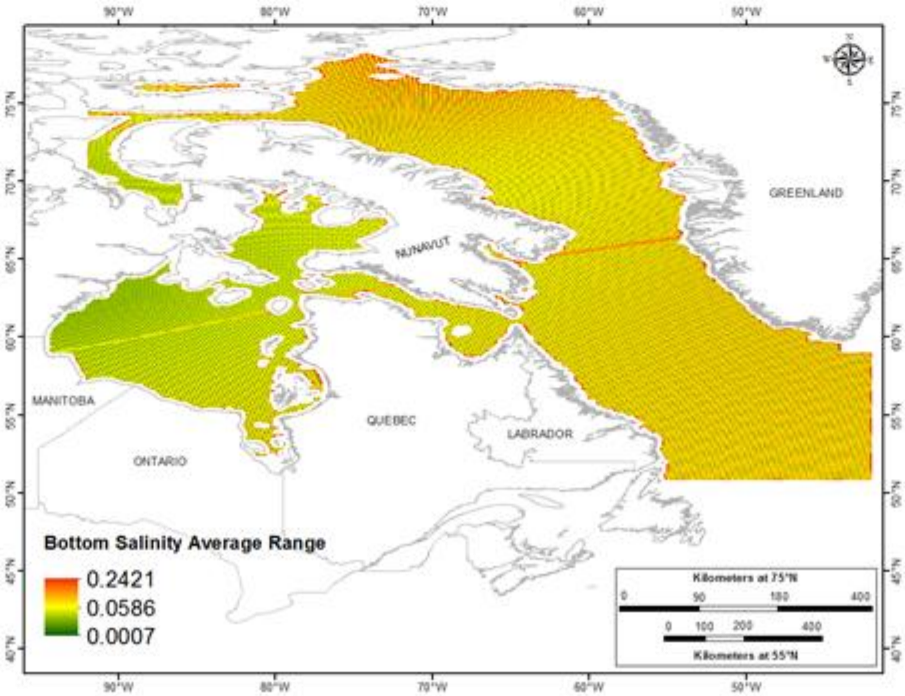


Figure 109. Prediction standard error surface of Bottom Salinity Average Range.

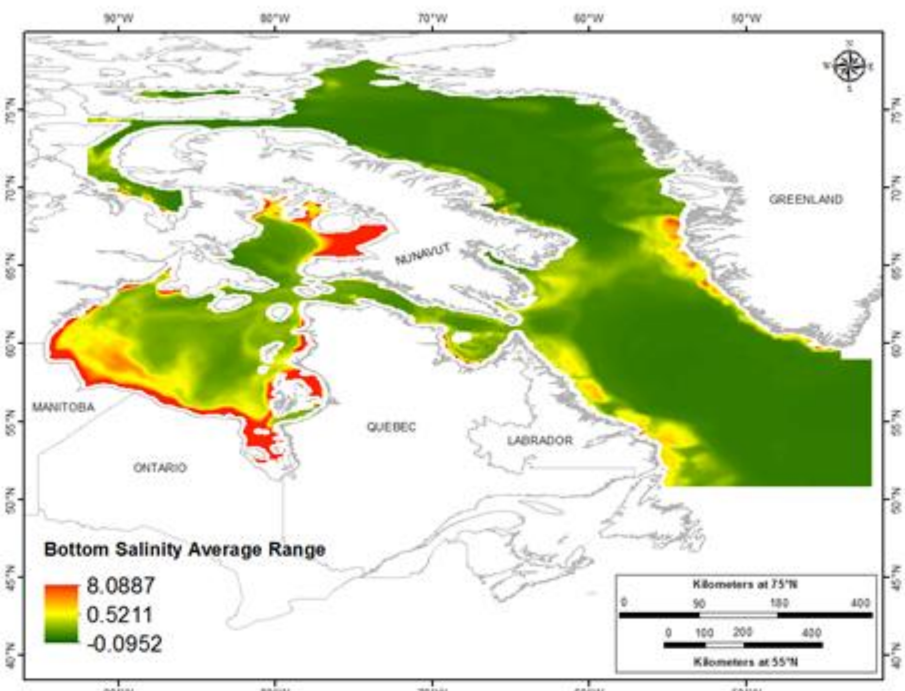


Figure 110. Interpolated prediction surface of Bottom Salinity Average Range.

## Surface Salinity Mean

This variable displayed a left-skewed, leptokurtic distribution prior to interpolation (Table 45, Figure 111). The data were lower than predicted by a normal distribution at both tails, while mid-values were slightly higher than the reference line (Figure 112). These areas of under- and over-prediction showed spatial pattern over the region (Figure 112).

The semivariogram showed moderate autocorrelation present in the data (Figure 113). The kriged model showed a very good fit between measured and predicted values (Figure 113). Good performance of the model was indicated by the cross-validation results (Table 46). The error map showed lower error in Hudson Bay compared to Baffin Bay and Davis Strait, with higher error along the edges of the study extent and in the most northern areas (Figure 114). The kriged surface is presented in Figure 115.

Table 45. Distributional properties of Surface Salinity Mean.

| **Property** | **Value** |
|---|---:|
| Number of Observations | 16491 |
| Minimum | 14.316 |
| Maximum | 34.891 |
| Mean | 32.255 |
| Median | 32.247 |
| Standard Deviation | 1.678 |
| Skewness | -1.202 |
| Kurtosis | 8.377 |

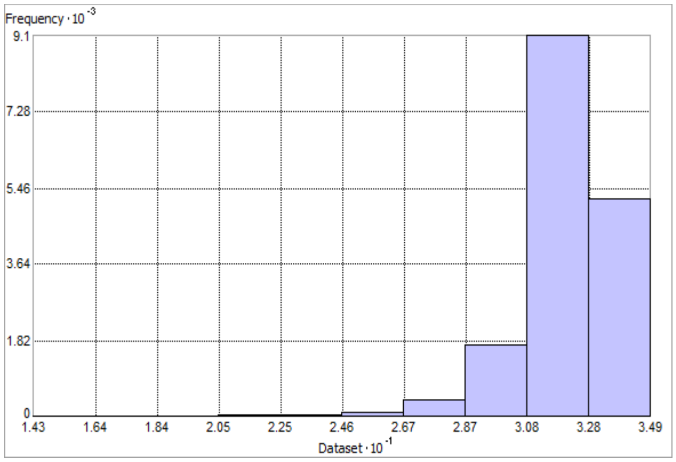


Figure 111. Distribution of Surface Salinity Mean. Histogram was illustrated using 10 bins. X axis is shown at $10^{-1}$; Y axis is shown at $10^{-3}$.

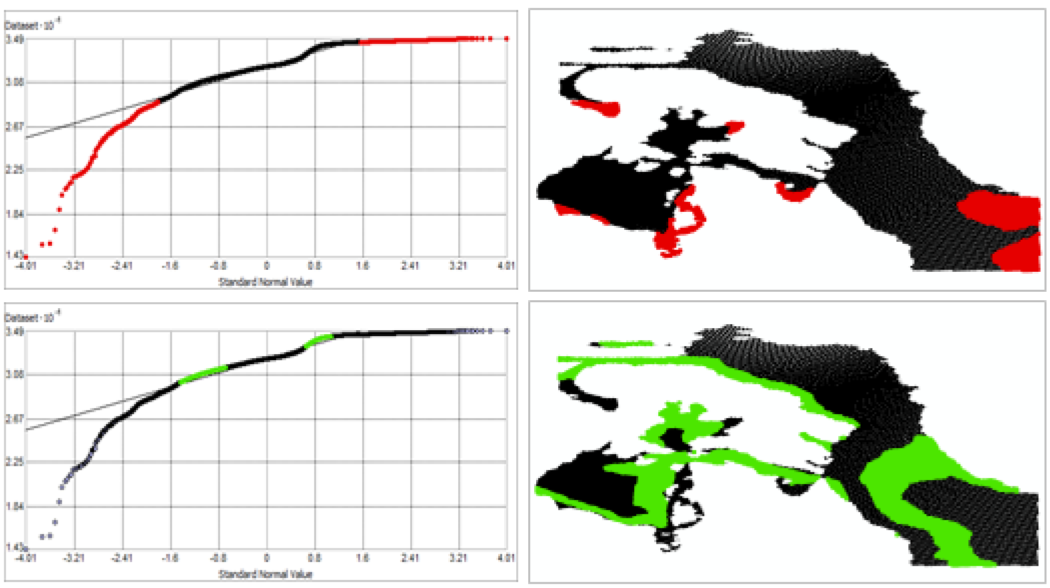

Figure 112. Normal Q-Q plot for data values of Surface Salinity Mean. Points falling under (top right panel) and over (bottom right panel) the reference line are mapped.

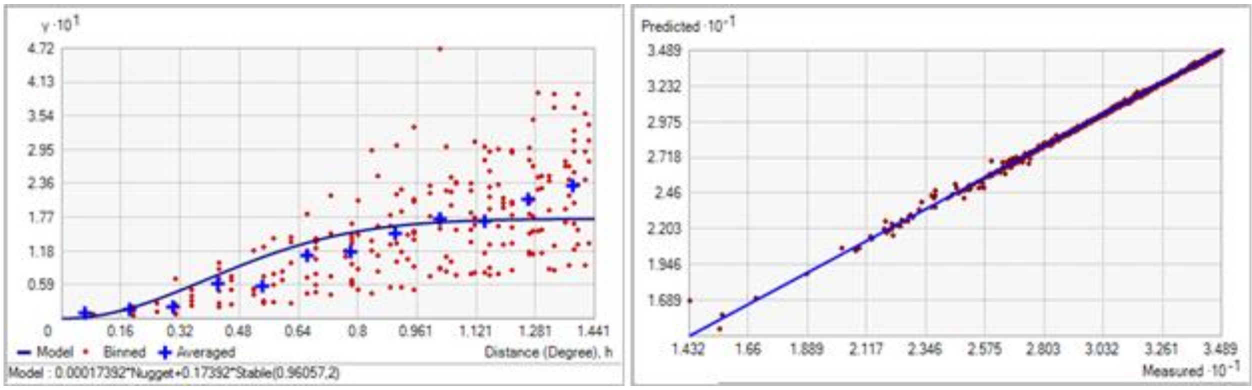


Figure 113. Left panel: Semivariogram of Surface Salinity Mean. Binned values are shown as red dots; average points are shown as blue crosses; the model fit to the averaged values is shown as a blue line. Lag size: 0.120 degrees; number of lags: 12; Parameter: 2; Range: 0.961 degrees; Partial Sill: 0.174. Right panel: Scatterplot of predicted values versus observed values for the model of Surface Salinity Mean.

Table 46. Results of cross-validation of the kriged model for Surface Salinity Mean.

| **Prediction Error** | **Value** |
|---|---:|
| Number of Observations | 16491 |
| Overall Mean Error | $8.044 \times 10^{-4}$ |
| Root Mean Square Prediction Error | 0.035 |
| Standardized Mean | 0.018 |
| Standardized Root Mean Square Prediction Error | 1.103 |
| Average Standard Error | 0.022 |

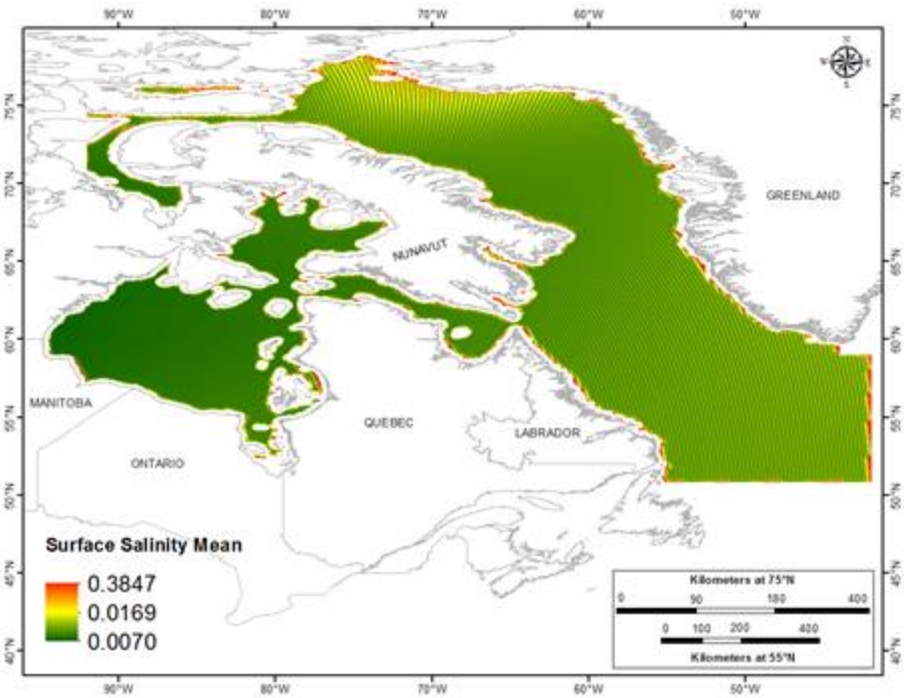


Figure 114. Prediction standard error surface of Surface Salinity Mean.

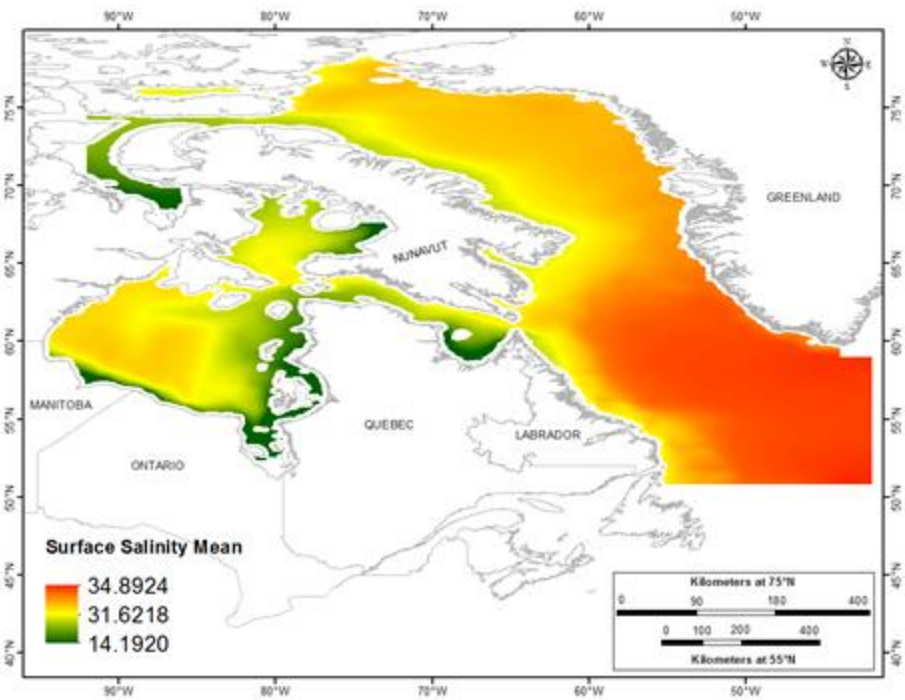


Figure 115. Interpolated prediction surface of Surface Salinity Mean.

**Surface Salinity Minimum**

This variable displayed a left-skewed, leptokurtic distribution prior to interpolation (Table 47, Figure 116). The data were lower than predicted by a normal distribution at both tails, while mid-values were slightly higher than the reference line (Figure 117). These areas of under- and over-prediction showed little spatial pattern over the region (Figure 117).

The semivariogram showed moderate autocorrelation present in the data (Figure 118). The kriged model showed a very good fit between measured and predicted values (Figure 118). Fair performance of the model was indicated by the cross-validation results (Table 48). Variability in the predictions was underestimated, as indicated by the Standardized Root-Mean-Square Error greater than 1. The error map showed lower error in Hudson Bay compared to Baffin Bay and Davis Strait, with higher error along the edges of the study extent and in the most northern areas (Figure 119). The kriged surface is presented in Figure 120.

Table 47. Distributional properties of Surface Salinity Minimum.

| **Property** | **Value** |
|---|---:|
| Number of Observations | 16491 |
| Minimum | 9.305 |
| Maximum | 34.230 |
| Mean | 29.570 |
| Median | 29.246 |
| Standard Deviation | 2.746 |
| Skewness | -0.561 |
| Kurtosis | 4.730 |

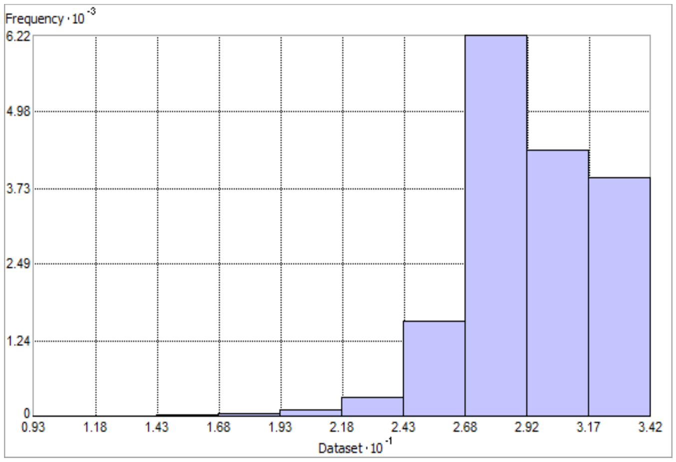


Figure 116. Distribution of Surface Salinity Minimum. Histogram was illustrated using 10 bins. X axis is shown at $10^{-1}$; Y axis is shown at $10^{-3}$.

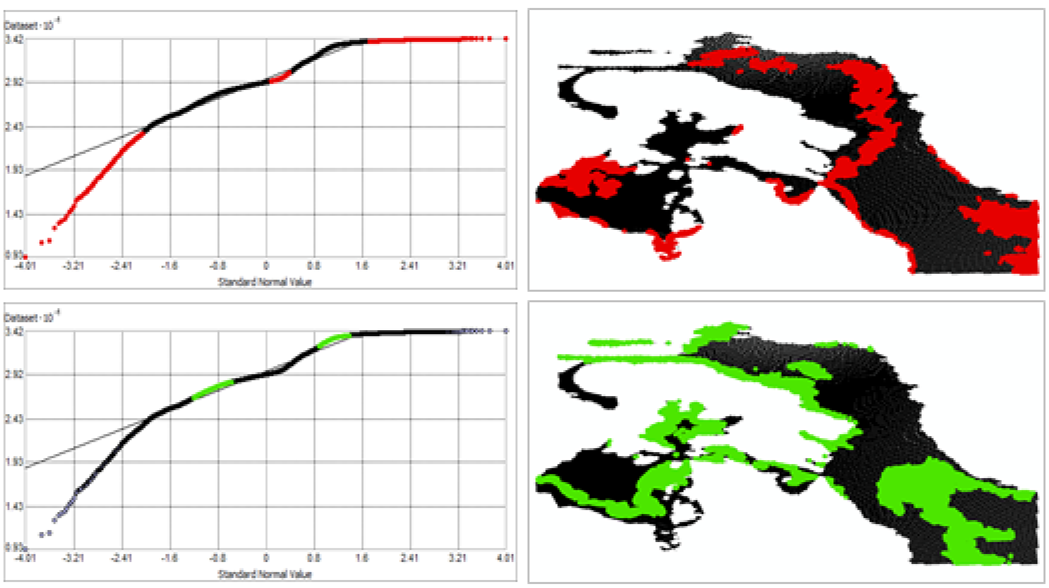


Figure 117. Normal Q-Q plot for data values of Surface Salinity Minimum. Points falling under (top right panel) and over (bottom right panel) the reference line are mapped.

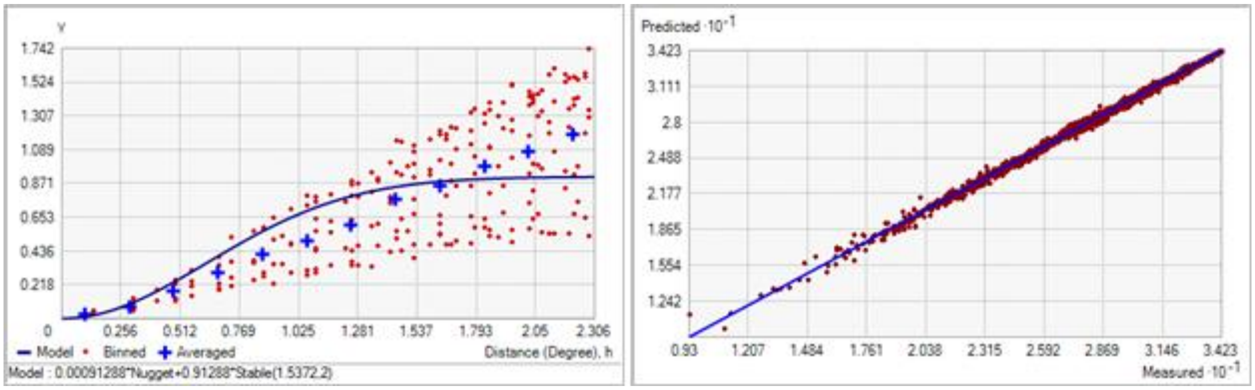


Figure 118. Left panel: Semivariogram of Surface Salinity Minimum. Binned values are shown as red dots; average points are shown as blue crosses; the model fit to the averaged values is shown as a blue line. Lag size: 0.192 degrees; number of lags: 12; Parameter: 2; Range: 1.537 degrees; Partial Sill: 0.913. Right panel: Scatterplot of predicted values versus observed values for the model of Surface Salinity Minimum.

Table 48. Results of cross-validation of the kriged model for Surface Salinity Minimum.

| **Prediction Error** | **Value** |
|---|---|
| Number of Observations | 16491 |
| Overall Mean Error | $8.114 \times 10^{-4}$ |
| Root Mean Square Prediction Error | 0.094 |
| Standardized Mean | $8.928 \times 10^{-3}$ |
| Standardized Root Mean Square Prediction Error | 2.409 |
| Average Standard Error | 0.038 |

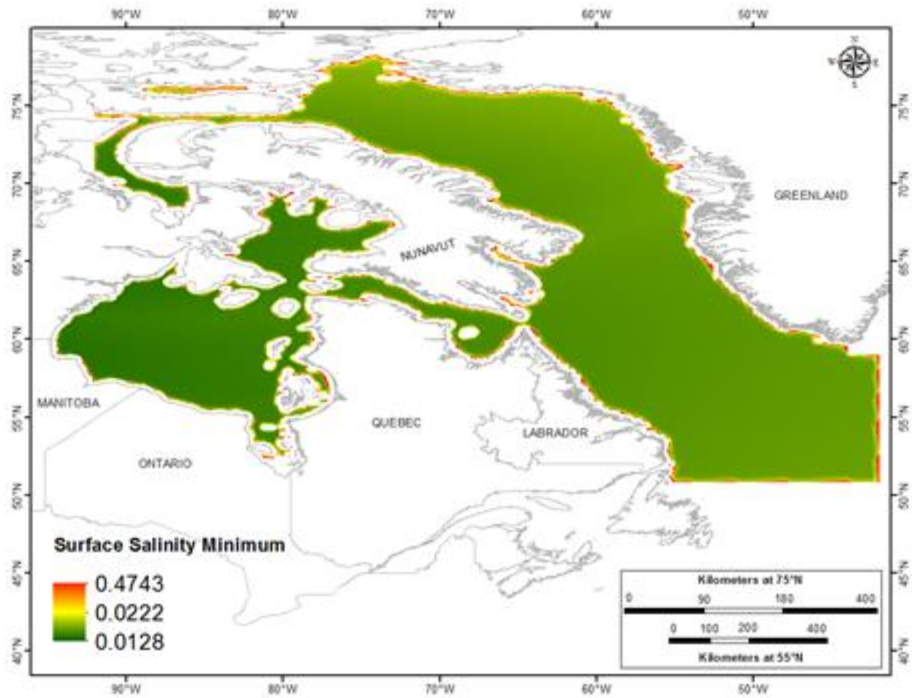


Figure 119. Prediction standard error surface of Surface Salinity Minimum.

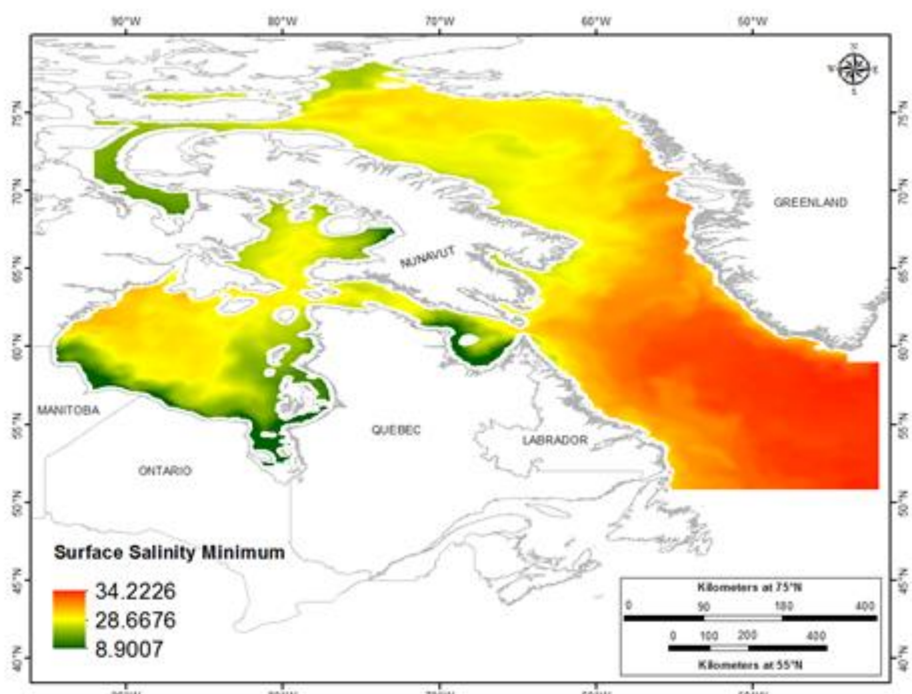


Figure 120. Interpolated prediction surface of Surface Salinity Minimum.

## Surface Salinity Maximum

This variable displayed a left-skewed, leptokurtic distribution prior to interpolation (Table 49, Figure 121). The data were lower than predicted by a normal distribution at both tails, while mid-values were slightly higher than the reference line (Figure 122). These areas of under- and over-prediction showed spatial pattern over the region (Figure 122).

The semivariogram showed moderate autocorrelation present in the data (Figure 123). The kriged model showed a very good fit between measured and predicted values (Figure 123). Fair performance of the model was indicated by the cross-validation results (Table 50). Variability in the predictions was underestimated, as indicated by the Standardized Root-Mean-Square Error greater than 1. The error map showed lower error in Hudson Bay compared to Baffin Bay and Davis Strait, with higher error along the edges of the study extent and in the most northern areas (Figure 124). The kriged surface is presented in Figure 125.

Table 49. Distributional properties of Surface Salinity Maximum.

| **Property** | **Value** |
|---|---:|
| Number of Observations | 16491 |
| Minimum | 24.206 |
| Maximum | 35.425 |
| Mean | 33.611 |
| Median | 33.635 |
| Standard Deviation | 1.013 |
| Skewness | -0.992 |
| Kurtosis | 6.043 |

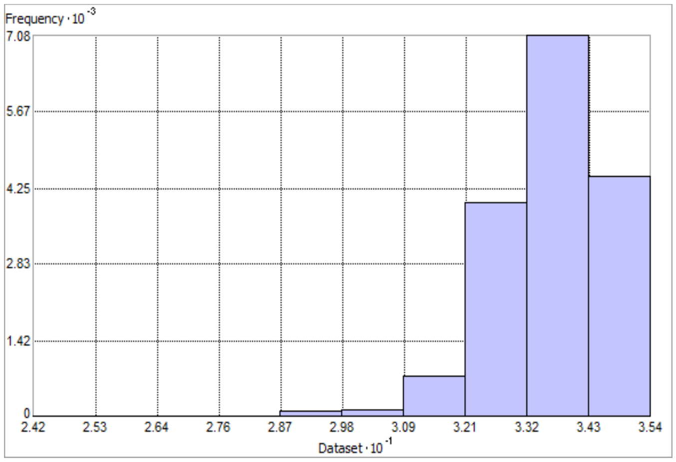


Figure 121. Distribution of Surface Salinity Maximum. Histogram was illustrated using 10 bins. X axis is shown at $10^{-1}$; Y axis is shown at $10^{-3}$.

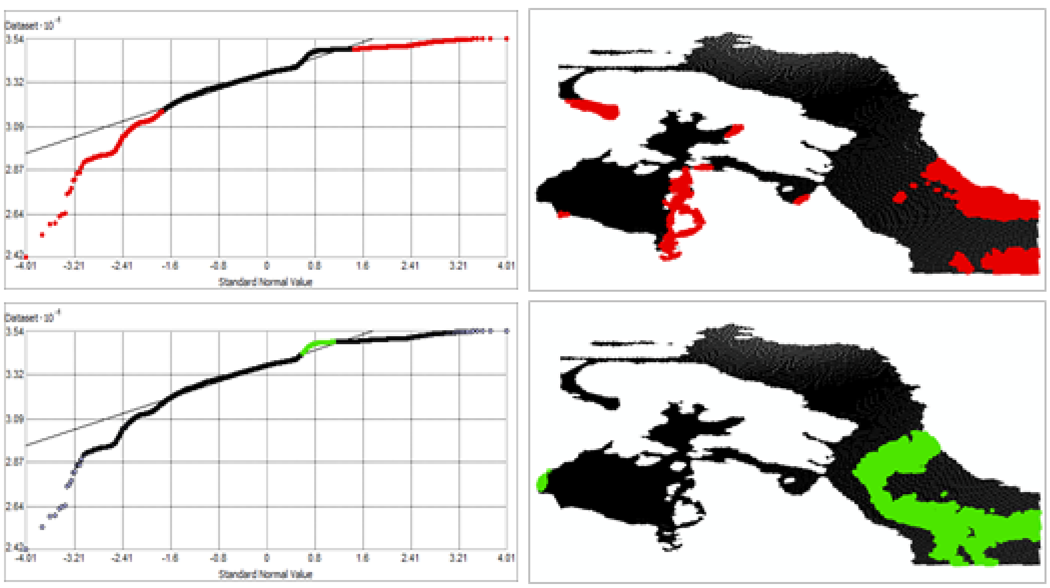


Figure 122. Normal Q-Q plot for data values of Surface Salinity Maximum. Points falling under (top right panel) and over (bottom right panel) the reference line are mapped.

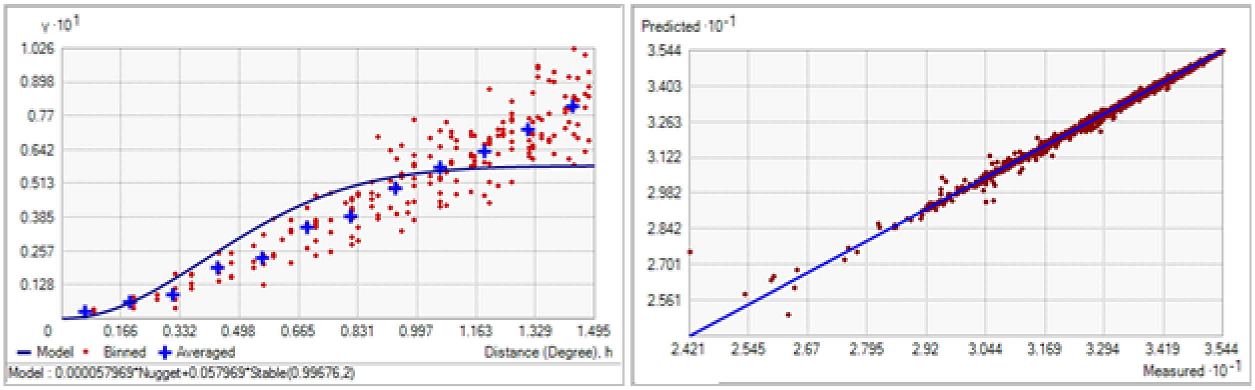


Figure 123. Left panel: Semivariogram of Surface Salinity Maximum. Binned values are shown as red dots; average points are shown as blue crosses; the model fit to the averaged values is shown as a blue line. Lag size: 0.125 degrees; number of lags: 12; Parameter: 2; Range: 0.997 degrees; Partial Sill: 0.058. Right panel: Scatterplot of predicted values versus observed values for the model of Surface Salinity Maximum.

Table 50. Results of cross-validation of the kriged model for Surface Salinity Maximum.

| **Prediction Error** | **Value** |
|---|---|
| Number of Observations | 16491 |
| Overall Mean Error | $3.467 \times 10^{-4}$ |
| Root Mean Square Prediction Error | 0.045 |
| Standardized Mean | 0.011 |
| Standardized Root Mean Square Prediction Error | 2.809 |
| Average Standard Error | 0.013 |

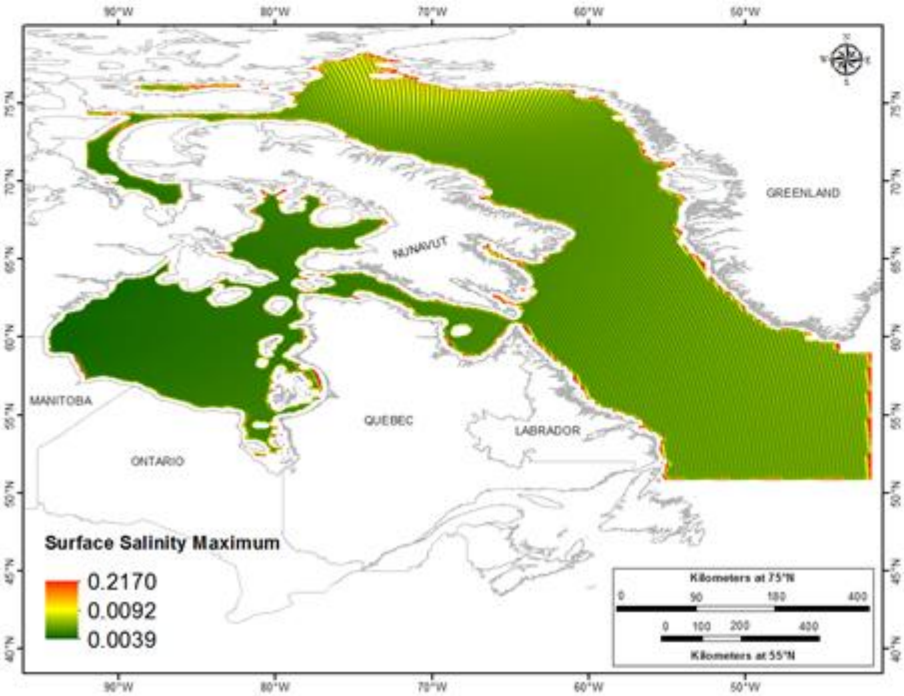


Figure 124. Prediction standard error surface of Surface Salinity Maximum.

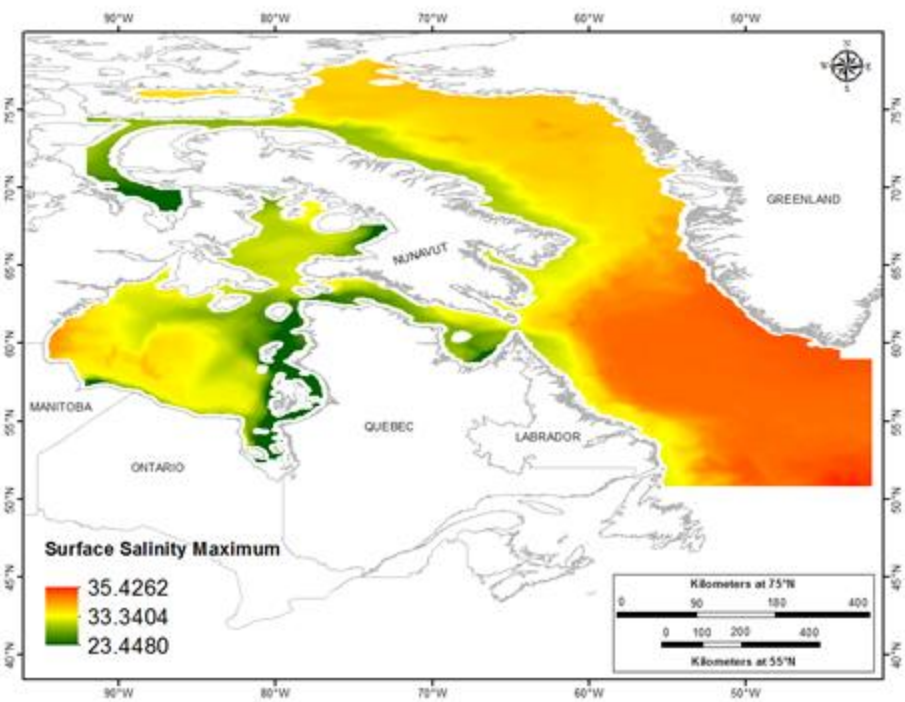


Figure 125. Interpolated prediction surface of Surface Salinity Maximum.

**Surface Salinity Range**

This variable displayed a right-skewed, leptokurtic distribution prior to interpolation (Table 51, Figure 126). The data were higher than predicted by a normal distribution at both tails, while mid-values were slightly lower than the reference line (Figure 127). These areas of under- and over-prediction showed spatial pattern over the region (Figure 127).

The semivariogram showed moderate autocorrelation present in the data (Figure 128). The kriged model showed a very good fit between measured and predicted values (Figure 128). Fair performance of the model was indicated by the cross-validation results (Table 52). Variability in the predictions was underestimated, as indicated by the Standardized Root-Mean-Square Error greater than 1. The error map showed lower error in Hudson Bay compared to Baffin Bay and Davis Strait, with higher error along the edges of the study extent and in the most northern areas (Figure 129). The kriged surface is presented in Figure 130.

Table 51. Distributional properties of Surface Salinity Range.

| Property | Value |
|---|---:|
| Number of Observations | 16491 |
| Minimum | 0.687 |
| Maximum | 18.245 |
| Mean | 4.041 |
| Median | 4.164 |
| Standard Deviation | 1.989 |
| Skewness | 0.997 |
| Kurtosis | 6.330 |

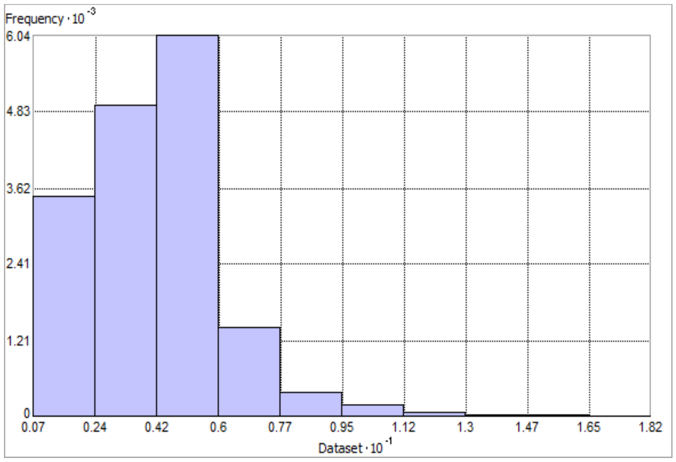


Figure 126. Distribution of Surface Salinity Range. Histogram was illustrated using 10 bins. X axis is shown at $10^{-1}$; Y axis is shown at $10^{-3}$.

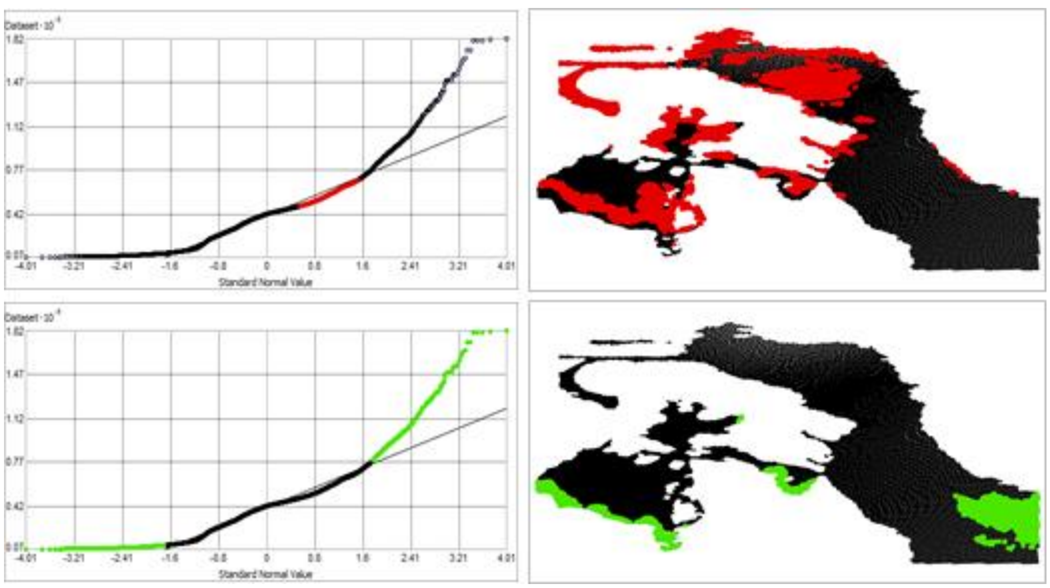

Figure 127. Normal Q-Q plot for data values of Surface Salinity Range. Points falling under (top right panel) and over (bottom right panel) the reference line are mapped.

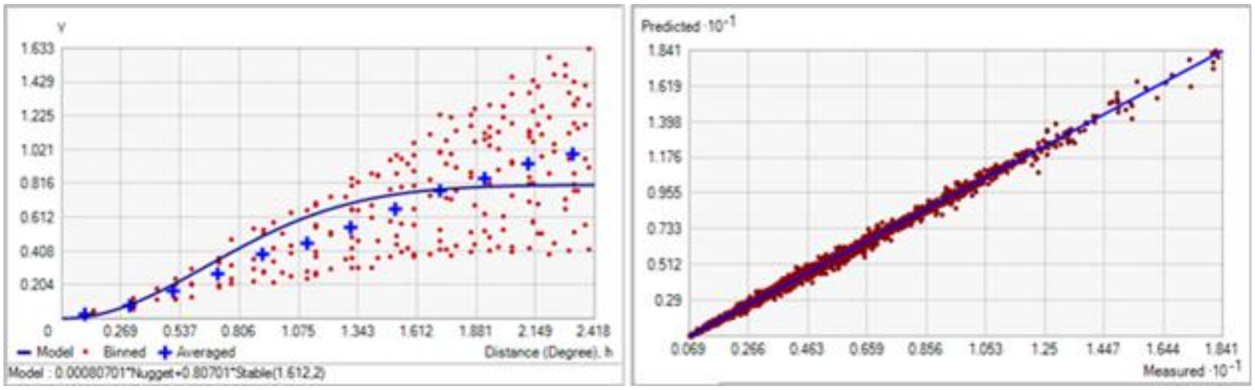


Figure 128. Left panel: Semivariogram of Surface Salinity Range. Binned values are shown as red dots; average points are shown as blue crosses; the model fit to the averaged values is shown as a blue line. Lag size: 0.202 degrees; number of lags: 12; Parameter: 2; Range: 1.612 degrees; Partial Sill: 0.807. Right panel: Scatterplot of predicted values versus observed values for the model of Surface Salinity Range.

Table 52. Results of cross-validation of the kriged model for Surface Salinity Range.

| **Prediction Error** | **Value** |
|---|---:|
| Number of Observations | 16491 |
| Overall Mean Error | $-5.052 \times 10^{-4}$ |
| Root Mean Square Prediction Error | 0.095 |
| Standardized Mean | $-4.803 \times 10^{-3}$ |
| Standardized Root Mean Square Prediction Error | 2.664 |
| Average Standard Error | 0.035 |

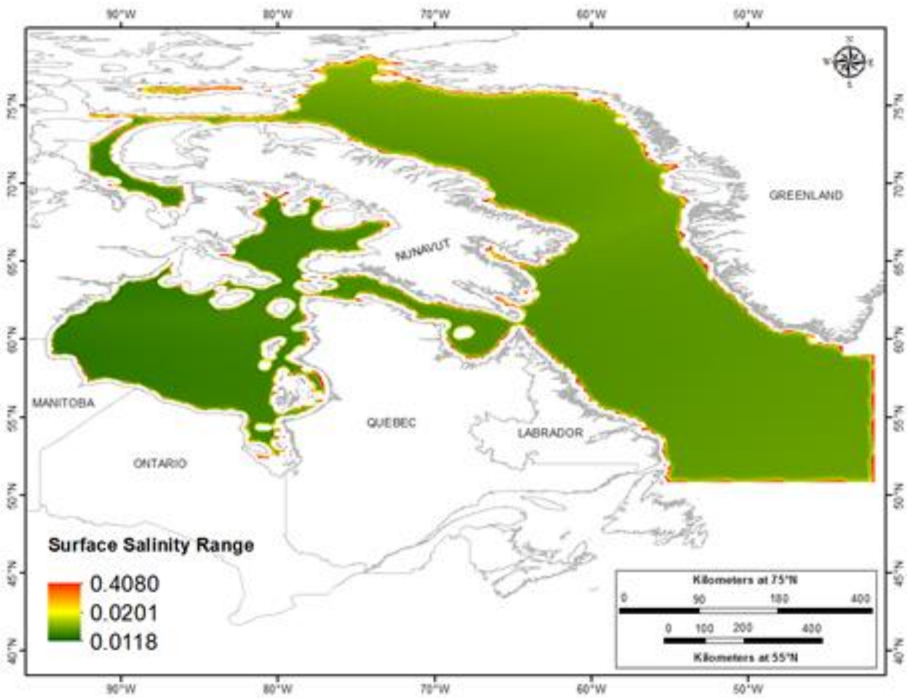


Figure 129. Prediction standard error surface of Surface Salinity Range.

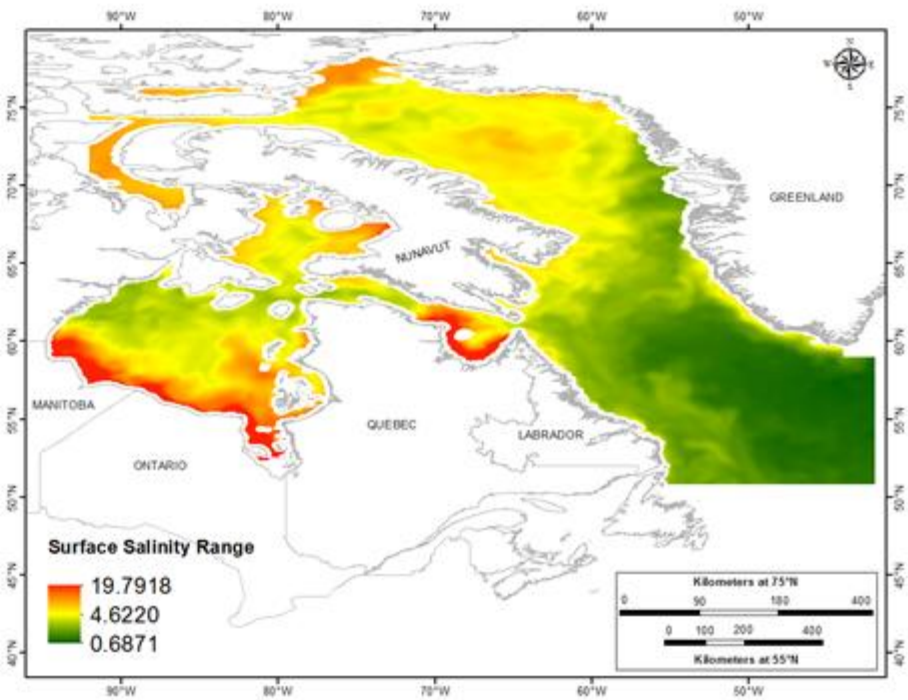


Figure 130. Interpolated prediction surface of Surface Salinity Range.

**Surface Salinity Average Minimum**

This variable displayed a left-skewed, leptokurtic distribution prior to interpolation (Table 53, Figure 131). The data were lower than predicted by a normal distribution at both tails, while mid-values were slightly higher than the reference line (Figure 132). These areas of under- and over-prediction showed spatial pattern over the region (Figure 132).

The semivariogram showed moderate autocorrelation present in the data (Figure 133). The kriged model showed a very good fit between measured and predicted values (Figure 133). Good performance of the model was indicated by the cross-validation results (Table 54). The error map showed lower error in Hudson Bay compared to Baffin Bay and Davis Strait, with higher error along the edges of the study extent and in the most northern areas (Figure 134). The kriged surface is presented in Figure 135.

Table 53. Distributional properties of Surface Salinity Average Minimum.

| **Property** | **Value** |
|---|---:|
| Number of Observations | 16491 |
| Minimum | 10.599 |
| Maximum | 34.541 |
| Mean | 30.792 |
| Median | 30.580 |
| Standard Deviation | 2.409 |
| Skewness | -0.825 |
| Kurtosis | 5.842 |

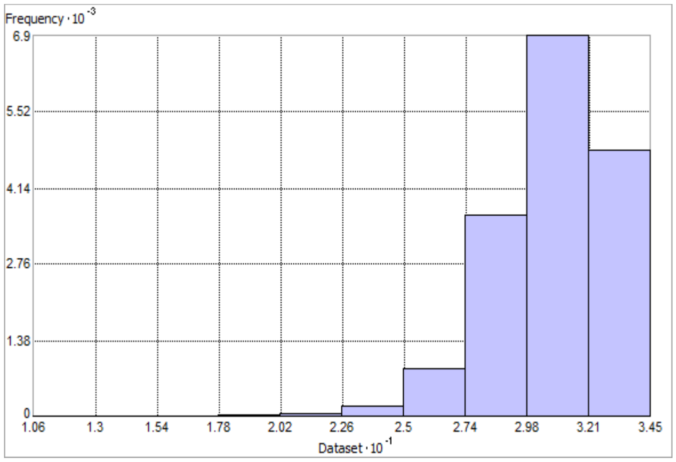


Figure 131. Distribution of Surface Salinity Average Minimum. Histogram was illustrated using 10 bins. X axis is shown at $10^{-1}$; Y axis is shown at $10^{-3}$.

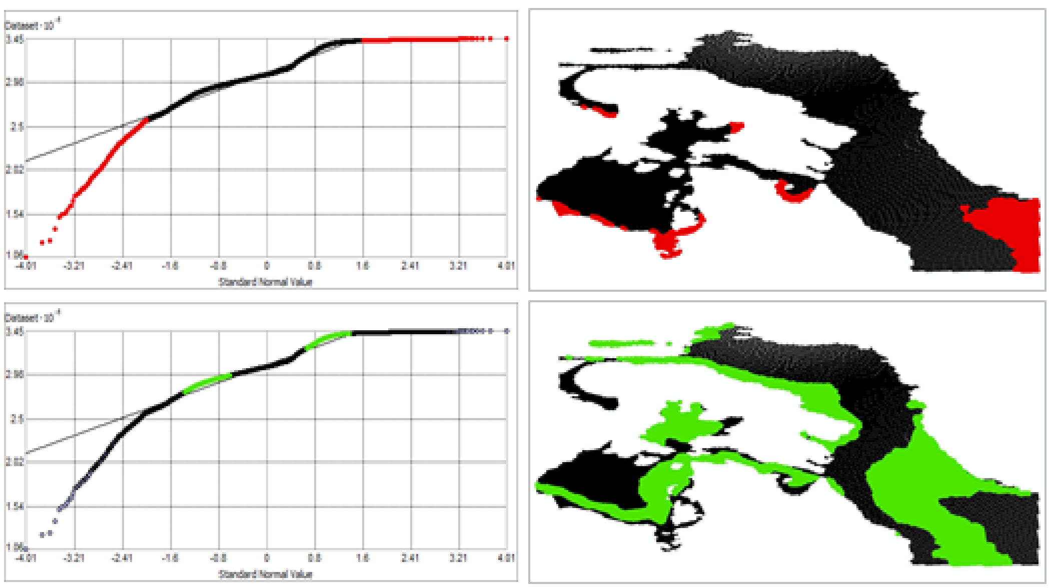

Figure 132. Normal Q-Q plot for data values of Surface Salinity Average Minimum. Points falling under (top right panel) and over (bottom right panel) the reference line are mapped.

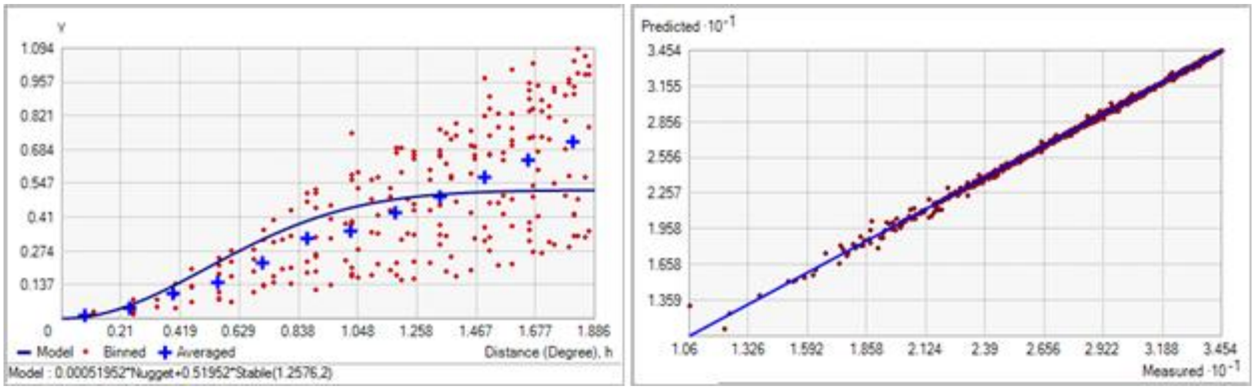


Figure 133. Left panel: Semivariogram of Surface Salinity Average Minimum. Binned values are shown as red dots; average points are shown as blue crosses; the model fit to the averaged values is shown as a blue line. Lag size: 0.157 degrees; number of lags: 12; Parameter: 2; Range: 1.258 degrees; Partial Sill: 0.519. Right panel: Scatterplot of predicted values versus observed values for the model of Surface Salinity Average Minimum.

Table 54. Results of cross-validation of the kriged model for Surface Salinity Average Minimum.

| **Prediction Error** | **Value** |
|---|---:|
| Number of Observations | 16491 |
| Overall Mean Error | $9.942 \times 10^{-4}$ |
| Root Mean Square Prediction Error | 0.047 |
| Standardized Mean | 0.015 |
| Standardized Root Mean Square Prediction Error | 1.147 |
| Average Standard Error | 0.032 |

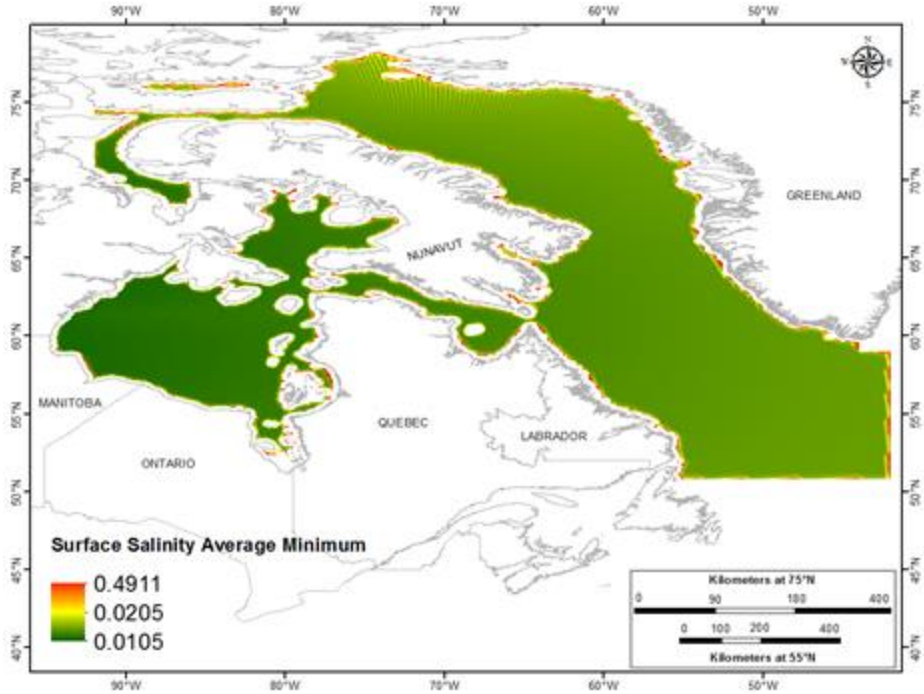


Figure 134. Prediction standard error surface of Surface Salinity Average Minimum.

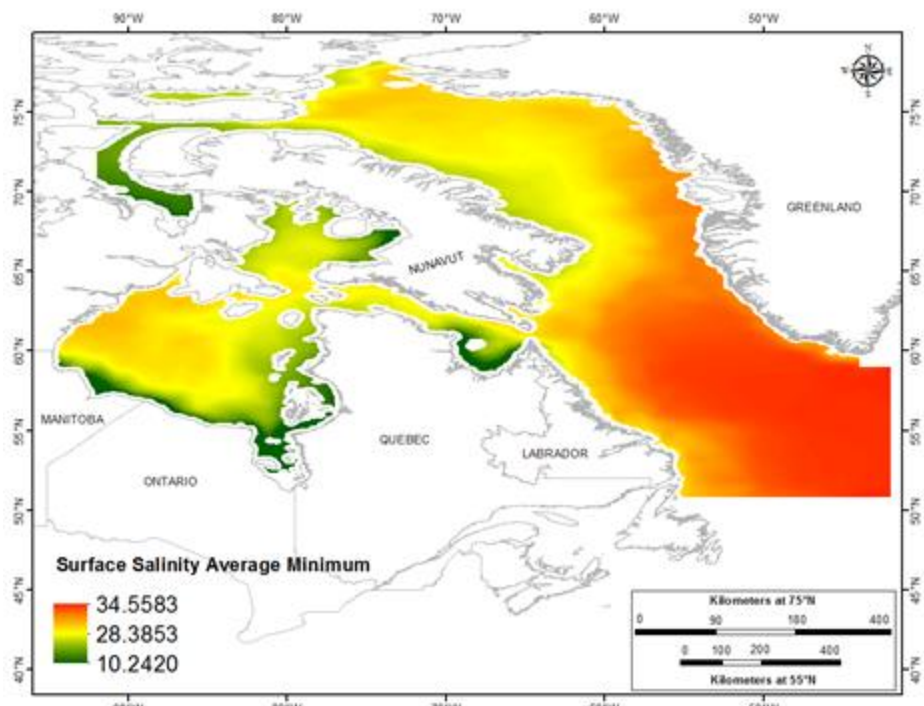


Figure 135. Interpolated prediction surface of Surface Salinity Average Minimum.

**Surface Salinity Average Maximum**

This variable displayed a left-skewed, leptokurtic distribution prior to interpolation (Table 55, Figure 136). The data were lower than predicted by a normal distribution at both tails, while mid-values were slightly higher than the reference line (Figure 137). These areas of under- and over-prediction showed spatial pattern over the region (Figure 137).

The semivariogram showed weak autocorrelation present in the data (Figure 138). The kriged model showed a very good fit between measured and predicted values (Figure 138). Good performance of the model was indicated by the cross-validation results (Table 56). The error map showed lower error in Hudson Bay compared to Baffin Bay and Davis Strait, with higher error along the edges of the study extent and in the most northern areas (Figure 139). The kriged surface is presented in Figure 140.

Table 55. Distributional properties of Surface Salinity Average Maximum.

| **Property** | **Value** |
|---|---:|
| Number of Observations | 16491 |
| Minimum | 18.067 |
| Maximum | 35.173 |
| Mean | 33.159 |
| Median | 33.151 |
| Standard Deviation | 1.258 |
| Skewness | -1.272 |
| Kurtosis | 9.542 |

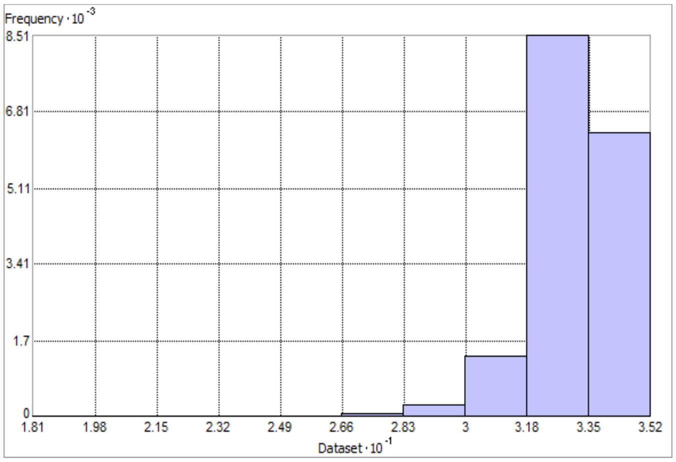


Figure 136. Distribution of Surface Salinity Average Maximum. Histogram was illustrated using 10 bins. X axis is shown at $10^{-1}$; Y axis is shown at $10^{-3}$.

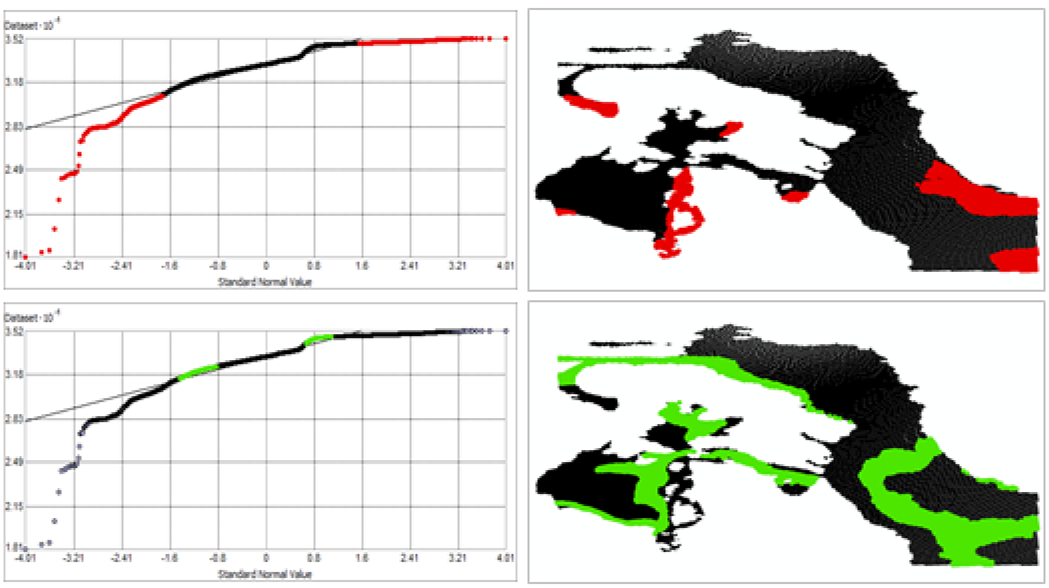

Figure 137. Normal Q-Q plot for data values of Surface Salinity Average Maximum. Points falling under (top right panel) and over (bottom right panel) the reference line are mapped.

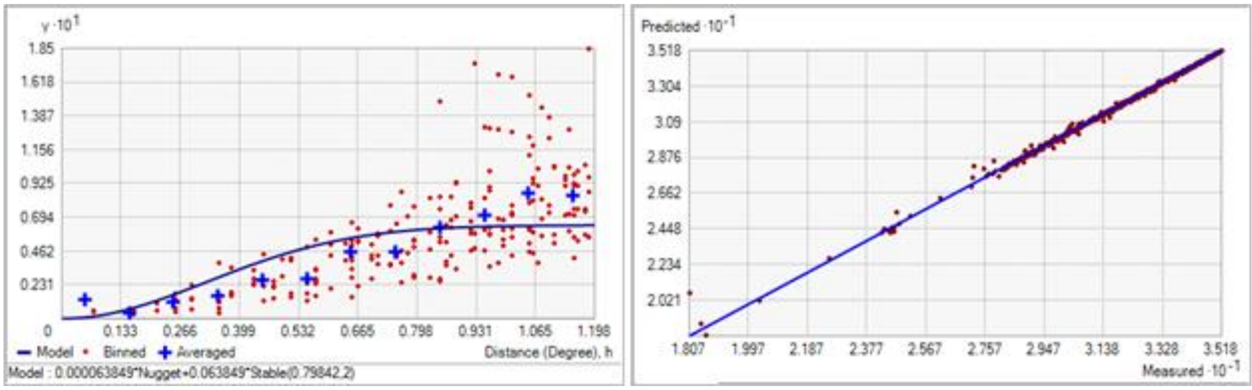


Figure 138. Left panel: Semivariogram of Surface Salinity Average Maximum. Binned values are shown as red dots; average points are shown as blue crosses; the model fit to the averaged values is shown as a blue line. Lag size: 0.100 degrees; number of lags: 12; Parameter: 2; Range: 0.798 degrees; Partial Sill: 0.064. Right panel: Scatterplot of predicted values versus observed values for the model of Surface Salinity Average Maximum.

Table 56. Results of cross-validation of the kriged model for Surface Salinity Average Maximum.

| **Prediction Error** | **Value** |
|---|---|
| Number of Observations | 16491 |
| Overall Mean Error | $3.744 \times 10^{-4}$ |
| Root Mean Square Prediction Error | 0.030 |
| Standardized Mean | $7.390 \times 10^{-3}$ |
| Standardized Root Mean Square Prediction Error | 1.202 |
| Average Standard Error | 0.017 |

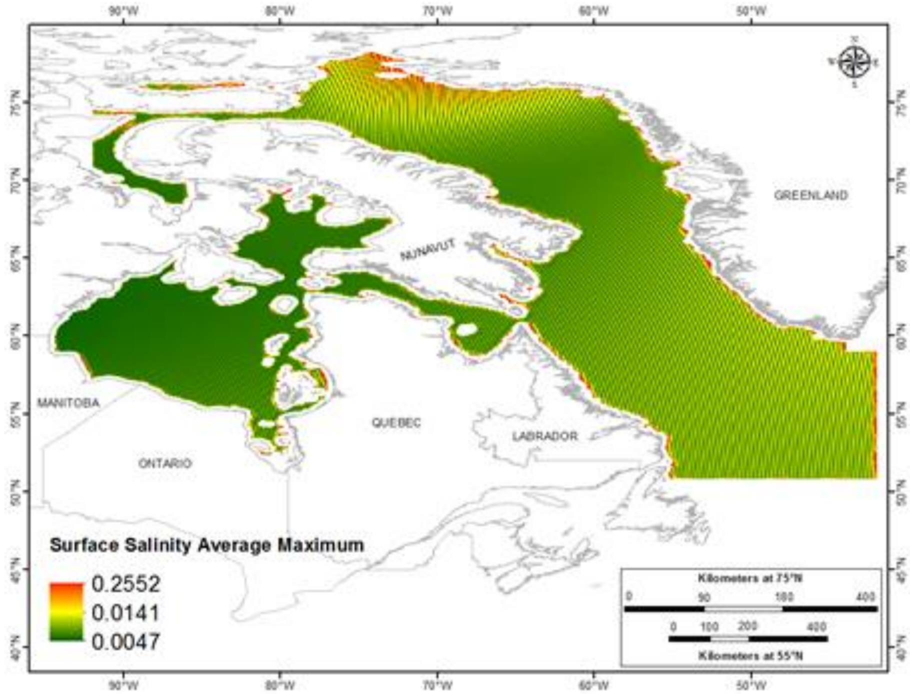


Figure 139. Prediction standard error surface of Surface Salinity Average Maximum.

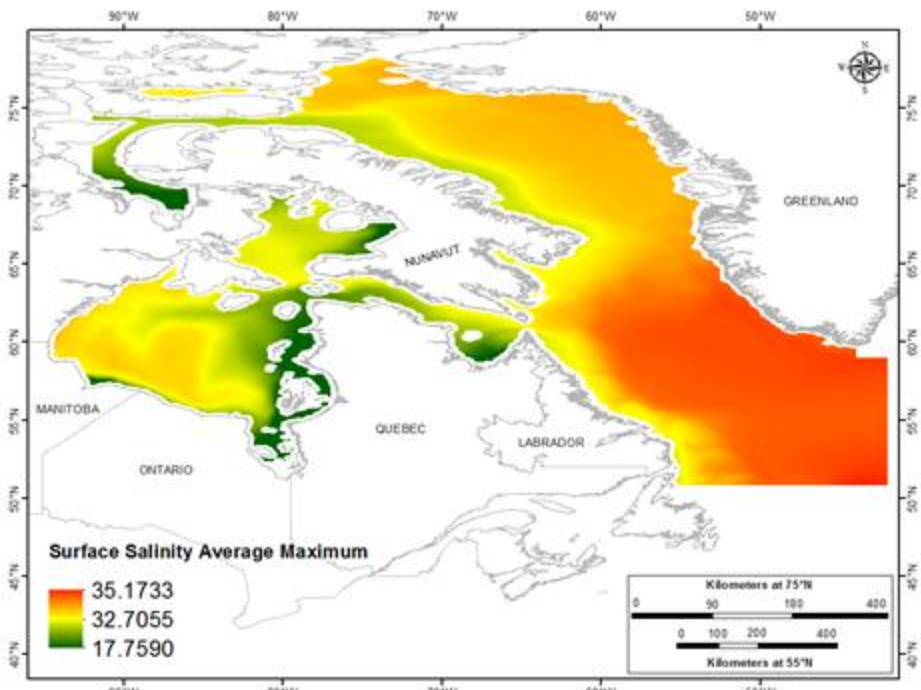


Figure 140. Interpolated prediction surface of Surface Salinity Average Maximum.

**Surface Salinity Average Range**

This variable displayed a right-skewed, leptokurtic distribution prior to interpolation (Table 57, Figure 141). The data were higher than predicted by a normal distribution at both tails, while mid-values were slightly lower than the reference line (Figure 142). These areas of under- and over-prediction showed spatial pattern over the region (Figure 142).

The semivariogram showed moderate autocorrelation present in the data (Figure 143). The kriged model showed a very good fit between measured and predicted values (Figure 143). Good performance of the model was indicated by the cross-validation results (Table 58). The error map showed lower error in Hudson Bay compared to Baffin Bay and Davis Strait, with higher error along the edges of the study extent and in the most northern areas (Figure 144). The kriged surface is presented in Figure 145.

Table 57. Distributional properties of Surface Salinity Average Range.

| **Property** | **Value** |
|---|---:|
| Number of Observations | 16491 |
| Minimum | 0.292 |
| Maximum | 14.429 |
| Mean | 2.367 |
| Median | 2.314 |
| Standard Deviation | 1.390 |
| Skewness | 1.492 |
| Kurtosis | 9.236 |

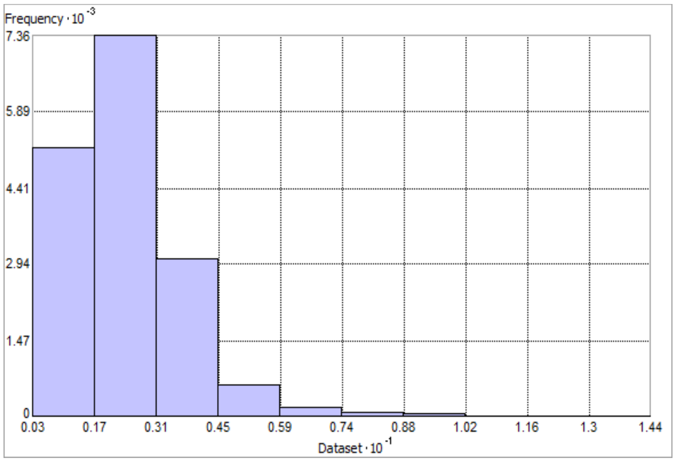

Figure 141. Distribution of Surface Salinity Average Range. Histogram was illustrated using 10 bins. X axis is shown at $10^{-1}$; Y axis is shown at $10^{-3}$.

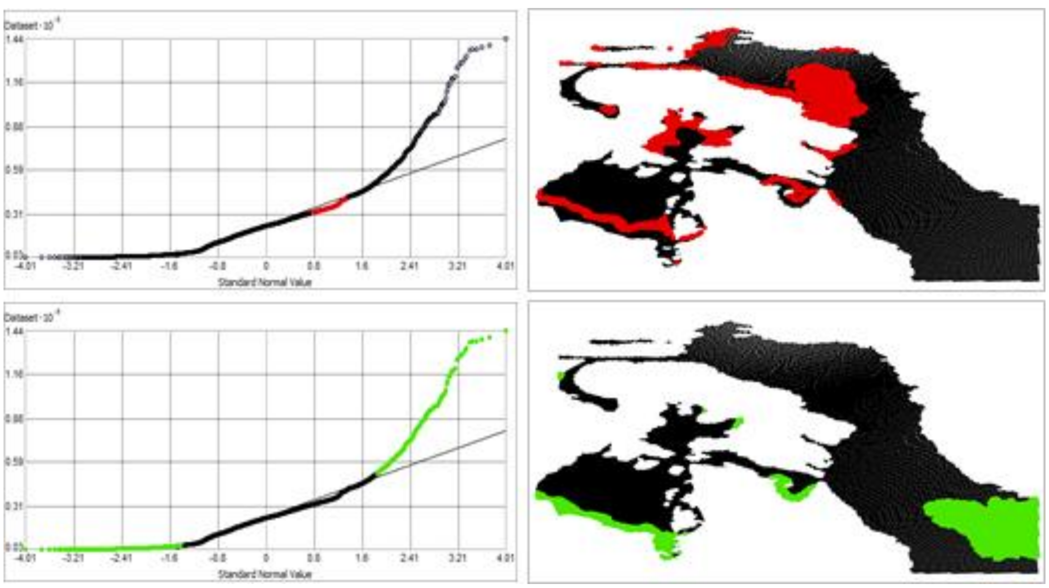
Figure 142. Normal Q-Q plot for data values of Surface Salinity Average Range. Points falling under (top right panel) and over (bottom right panel) the reference line are mapped.

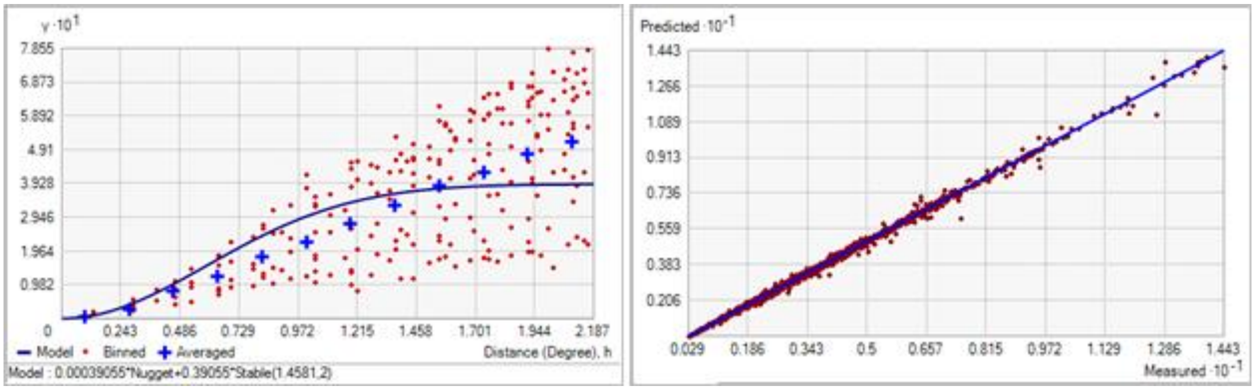


Figure 143. Left panel: Semivariogram of Surface Salinity Average Range. Binned values are shown as red dots; average points are shown as blue crosses; the model fit to the averaged values is shown as a blue line. Lag size: 0.182 degrees; number of lags: 12; Parameter: 2; Range: 1.458 degrees; Partial Sill: 0.391. Right panel: Scatterplot of predicted values versus observed values for the model of Surface Salinity Average Range.

Table 58. Results of cross-validation of the kriged model for Surface Salinity Average Range.

| **Prediction Error** | **Value** |
|---|---|
| Number of Observations | 16491 |
| Overall Mean Error | $-5.955 \times 10^{-4}$ |
| Root Mean Square Prediction Error | 0.040 |
| Standardized Mean | $-9.766 \times 10^{-3}$ |
| Standardized Root Mean Square Prediction Error | 1.280 |
| Average Standard Error | 0.026 |

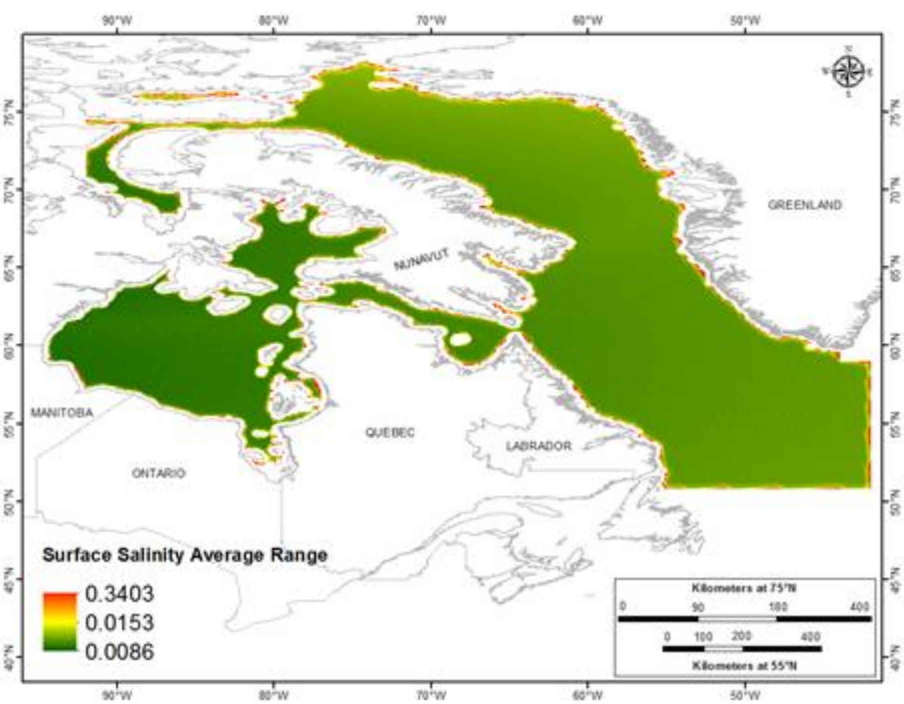


Figure 144. Prediction standard error surface of Surface Salinity Average Range.

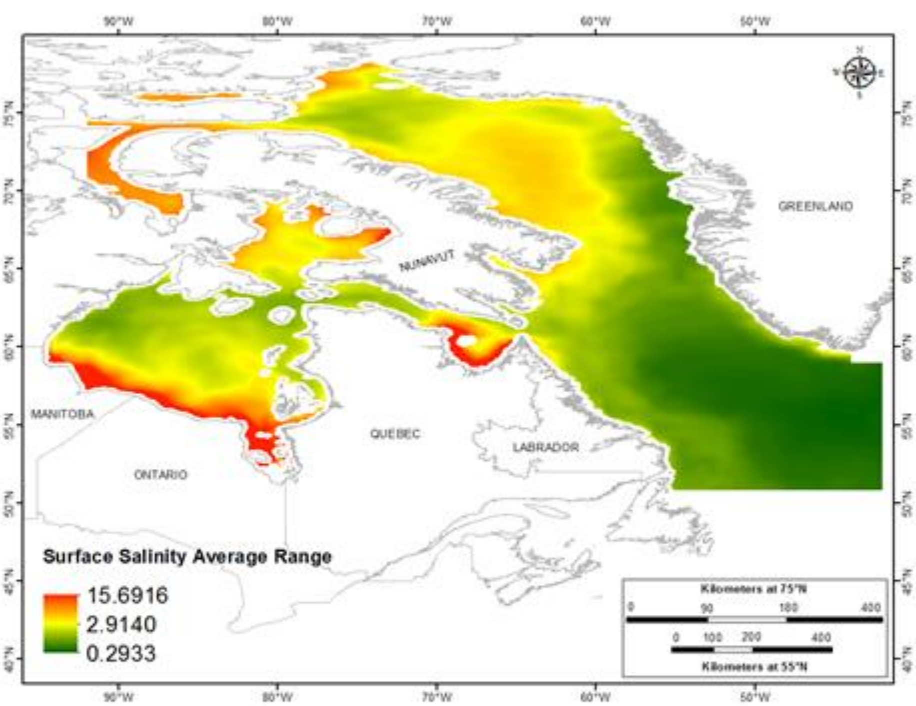


Figure 145. Interpolated prediction surface of Surface Salinity Average Range.

## Current Speed

Filter- and suspension-feeding fauna such as corals and sponges are often associated with areas of higher near-bottom current regimes (Genin et al., 1986; Ginn et al., 2000; Klitgaard et al., 1997). Current speed determines the rate at which food particles reach benthic species through both vertical and horizontal transmission. Excurrent flow rates through glass sponges in the Straight of Georgia were strongly and positively correlated with bottom currents (Leys et al., 2011), which provided a large proportion of the overall food intake in the sponges. Mass sponge occurrences off the Faroe Islands were found to be associated with the shelf break or areas where the bottom slope matches the slope required for the propagation of internal tidal waves (Kitgaard et al., 1997). In these regions, bottom currents were elevated, thus enhancing resuspension and transportation of particles.

### Bottom Current Mean

This variable displayed a right-skewed, leptokurtic distribution prior to interpolation (Table 59, Figure 146). The data were higher than predicted by a normal distribution at both tails, while mid-values were slightly lower than the reference line (Figure 147). These areas of under- and over-prediction showed little spatial pattern over the region (Figure 147).

The semivariogram showed moderate autocorrelation present in the data (Figure 148). The kriged model showed a poor fit between measured and predicted values (Figure 148). Very good performance of the model was indicated by the cross-validation results (Table 60). The error map showed lower error in Hudson Bay compared to Baffin Bay and Davis Strait, with higher error along the edges of the study extent and in the most northern areas (Figure 149). The kriged surface is presented in Figure 150.

Table 59. Distributional properties of Bottom Current Mean (m $s^{-1}$).

| Property | Value |
|---|---:|
| Number of Observations | 16257 |
| Minimum | $3.050 \times 10^{-4}$ |
| Maximum | 0.266 |
| Mean | 0.024 |
| Median | 0.017 |
| Standard Deviation | 0.023 |
| Skewness | 2.720 |
| Kurtosis | 15.291 |

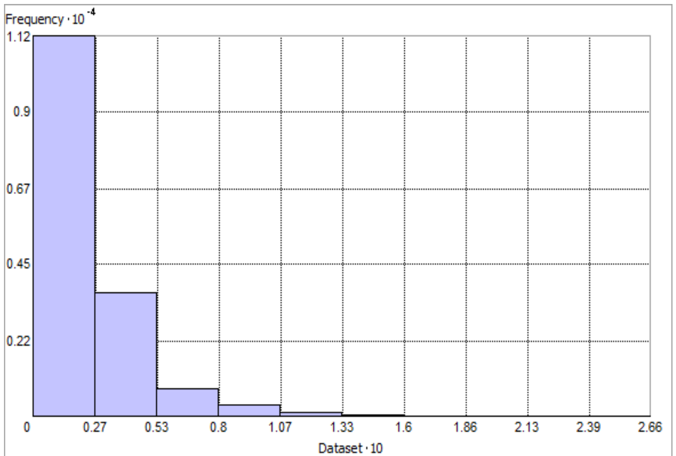


Figure 146. Distribution of Bottom Current Mean (m $s^{-1}$). Histogram was illustrated using 10 bins. X axis is shown at 10; Y axis is shown at $10^{-4}$.

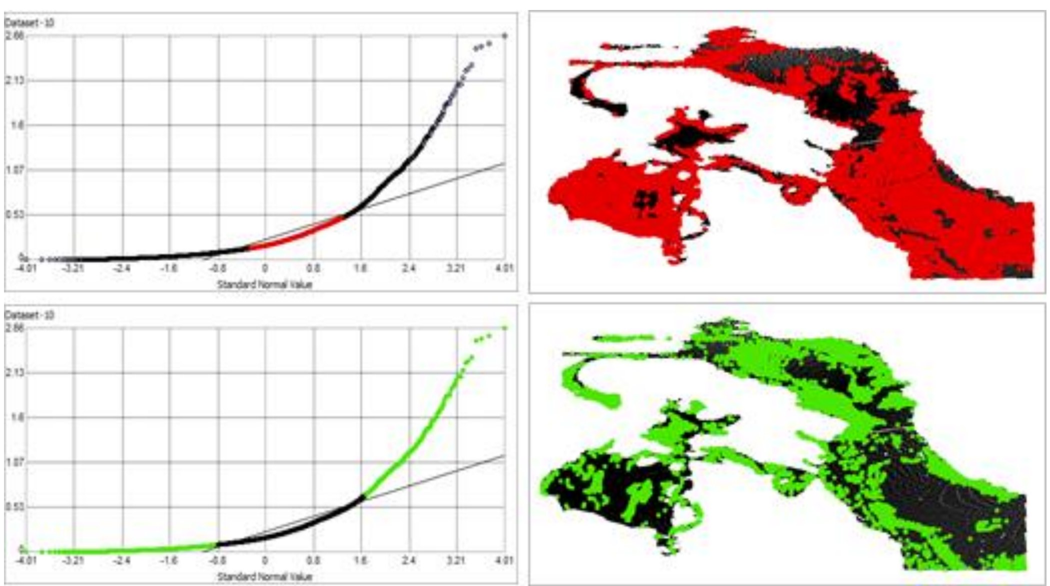

Figure 147. Normal Q-Q plot for data values of Bottom Current Mean (m $s^{-1}$). Points falling under (top right panel) and over (bottom right panel) the reference line are mapped.

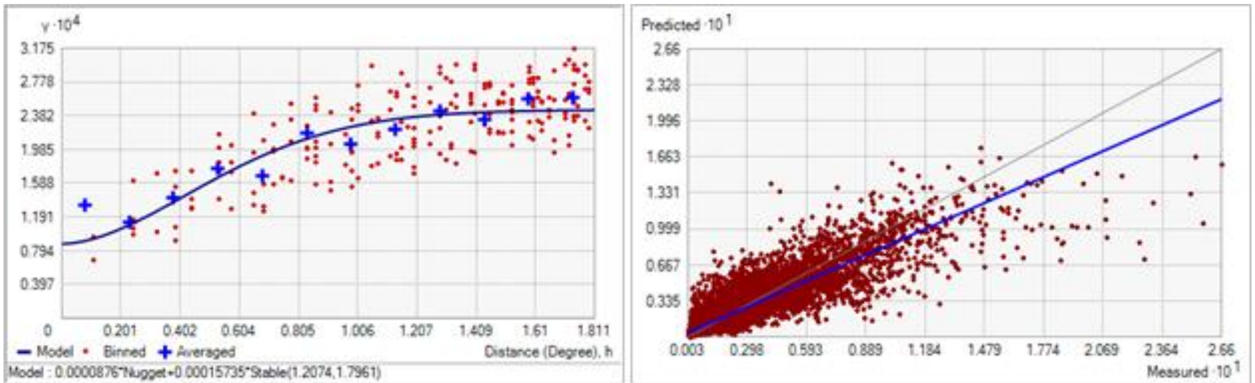


Figure 148. Left panel: Semivariogram of Bottom Current Mean (m $s^{-1}$). Binned values are shown as red dots; average points are shown as blue crosses; the model fit to the averaged values is shown as a blue line. Lag size: 0.151 degrees; number of lags: 12; Parameter: 1.796; Range: 1.207 degrees; Partial Sill: 1.573 x $10^{-4}$. Right panel: Scatterplot of predicted values versus observed values for the model of Bottom Current Mean (m $s^{-1}$).

Table 60. Results of cross-validation of the kriged model for Bottom Current Mean (m $s^{-1}$).

| **Prediction Error** | **Value** |
|---|---:|
| Number of Observations | 16257 |
| Overall Mean Error | 4.078 x $10^{-6}$ |
| Root Mean Square Prediction Error | 0.010 |
| Standardized Mean | 3.426 x $10^{-4}$ |
| Standardized Root Mean Square Prediction Error | 1.003 |
| Average Standard Error | 0.010 |

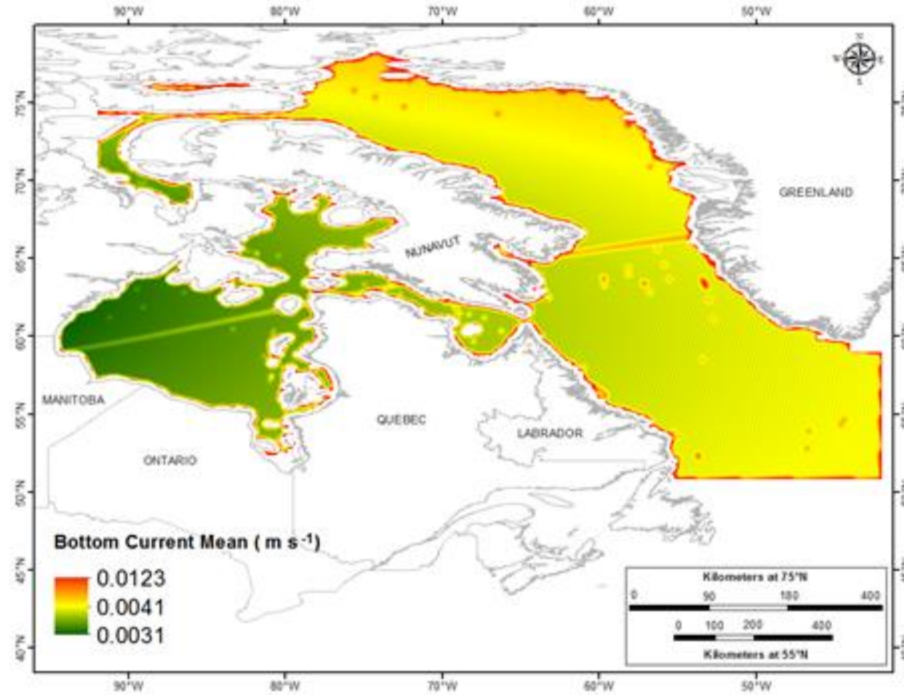


Figure 149. Prediction standard error surface of Bottom Current Mean (m $s^{-1}$).

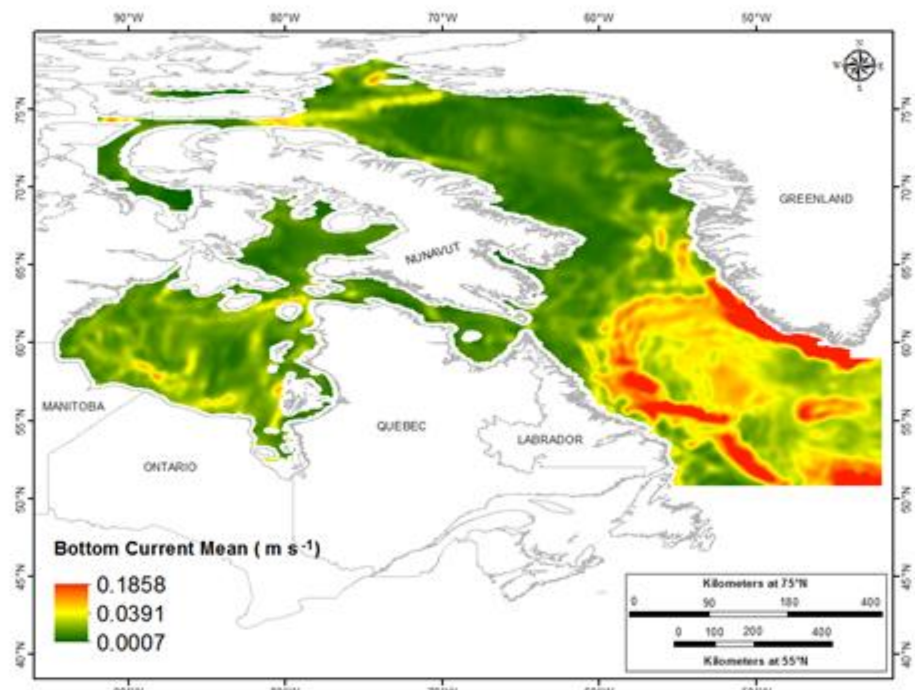


Figure 150. Interpolated prediction surface of Bottom Current Mean (m $s^{-1}$).

**Bottom Current Minimum**

This variable displayed a right-skewed, extremely leptokurtic distribution prior to interpolation and outlying data in the upper range (Table 61, Figure 151). The data were higher than predicted by a normal distribution at both tails, while mid-values were lower than the reference line (Figure 152). These areas of under- and over-prediction showed spatial pattern over the region (Figure 152).

The semivariogram showed autocorrelation present in the data (Figure 153). The kriged model showed a poor fit between measured and predicted values (Figure 153). Good performance of the model was indicated by the cross-validation results (Table 62). The error map showed lower error in Hudson Bay compared to Baffin Bay and Davis Strait, and higher error along the edges of the study extent and in the most northern areas (Figure 154). The kriged surface is presented in Figure 155.

Table 61. Distributional properties of Bottom Current Minimum (m $s^{-1}$).

| **Property** | **Value** |
|---|---:|
| Number of Observations | 16257 |
| Minimum | $1.000 \times 10^{-6}$ |
| Maximum | 0.149 |
| Mean | $2.482 \times 10^{-3}$ |
| Median | $6.250 \times 10^{-4}$ |
| Standard Deviation | $7.868 \times 10^{-3}$ |
| Skewness | 7.546 |
| Kurtosis | 77.951 |

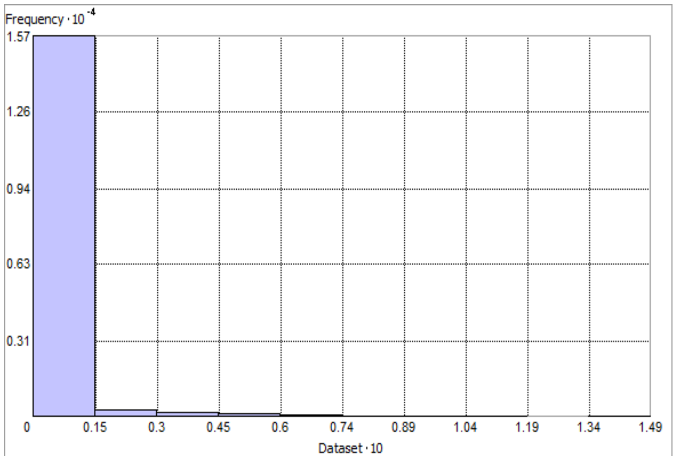

Figure 151. Distribution of Bottom Current Minimum (m $s^{-1}$). Histogram was illustrated using 10 bins. X axis is shown at 10; Y axis is shown at $10^{-4}$.

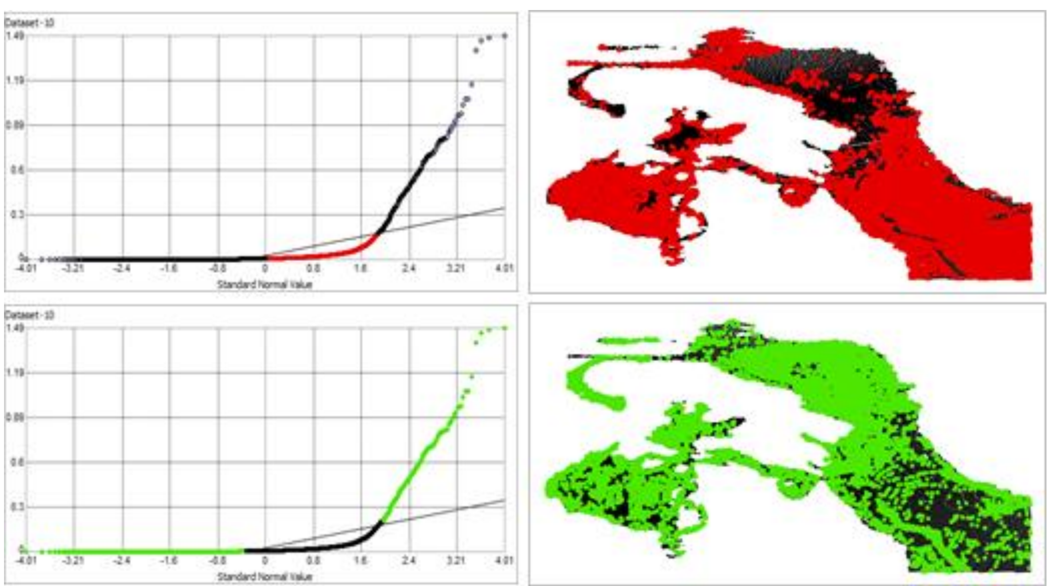

Figure 152. Normal Q-Q plot for data values of Bottom Current Minimum (m $s^{-1}$). Points falling under (top right panel) and over (bottom right panel) the reference line are mapped.

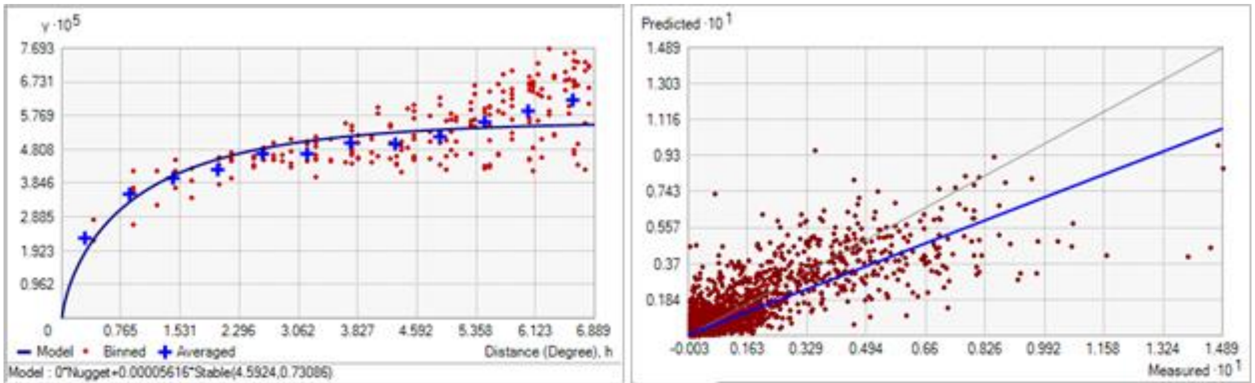


Figure 153. Left panel: Semivariogram of Bottom Current Minimum (m $s^{-1}$). Binned values are shown as red dots; average points are shown as blue crosses; the model fit to the averaged values is shown as a blue line. Lag size: 0.574 degrees; number of lags: 12; Parameter: 0.731; Range: 4.592 degrees; Partial Sill: 5.616 x $10^{-5}$. Right panel: Scatterplot of predicted values versus observed values for the model of Bottom Current Minimum (m $s^{-1}$).

Table 62. Results of cross-validation of the kriged model for Bottom Current Minimum (m $s^{-1}$).

| **Prediction Error** | **Value** |
|---|---:|
| Number of Observations | 16257 |
| Overall Mean Error | 5.008 x $10^{-6}$ |
| Root Mean Square Prediction Error | 4.011 x $10^{-3}$ |
| Standardized Mean | 7.523 x $10^{-4}$ |
| Standardized Root Mean Square Prediction Error | 1.078 |
| Average Standard Error | 3.633 x $10^{-3}$ |

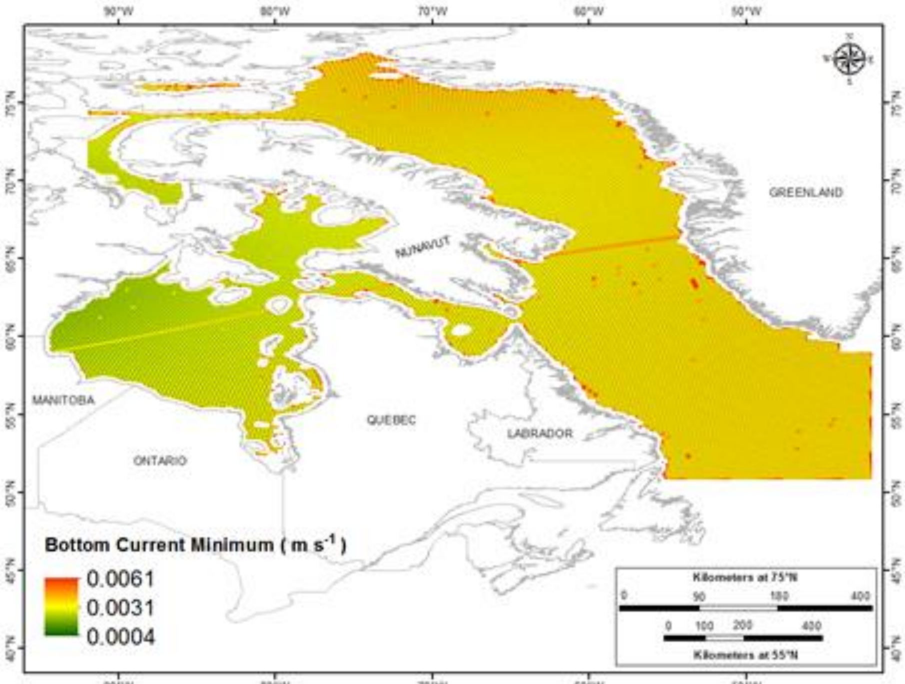


Figure 154. Prediction standard error surface of Bottom Current Minimum (m $s^{-1}$).

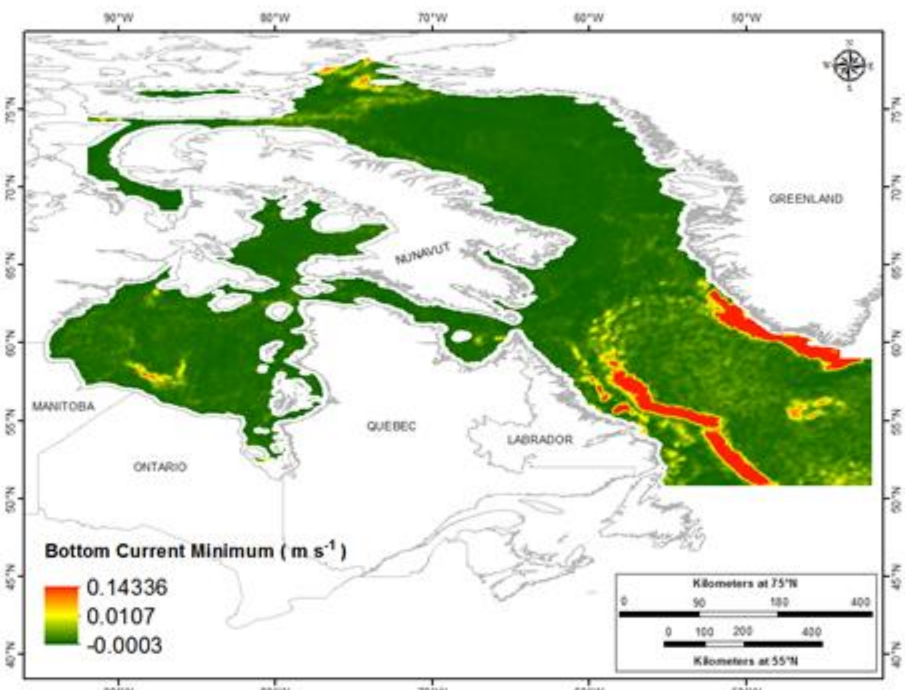


Figure 155. Interpolated prediction surface of Bottom Current Minimum (m $s^{-1}$).

**Bottom Current Maximum**

This variable displayed a right-skewed, leptokurtic distribution prior to interpolation and outlying data in the upper range (Table 63, Figure 156). The data were higher than predicted by a normal distribution at both tails, while mid-values were lower than the reference line (Figure 157). These areas of under- and over-prediction showed little spatial pattern over the region (Figure 157).

The semivariogram showed moderate autocorrelation present in the data (Figure 158). The kriged model showed a poor fit between measured and predicted values (Figure 158). Very good performance of the model was indicated by the cross-validation results (Table 64). The error map showed lower error in Hudson Bay compared to Baffin Bay and Davis Strait, and higher error along the edges of the study extent (Figure 159). The kriged surface is presented in Figure 160.

Table 63. Distributional properties of Bottom Current Maximum (m $s^{-1}$).

| **Property** | **Value** |
|---|---:|
| Number of Observations | 16257 |
| Minimum | $1.290 \times 10^{-3}$ |
| Maximum | 0.589 |
| Mean | 0.077 |
| Median | 0.062 |
| Standard Deviation | 0.056 |
| Skewness | 1.419 |
| Kurtosis | 5.864 |

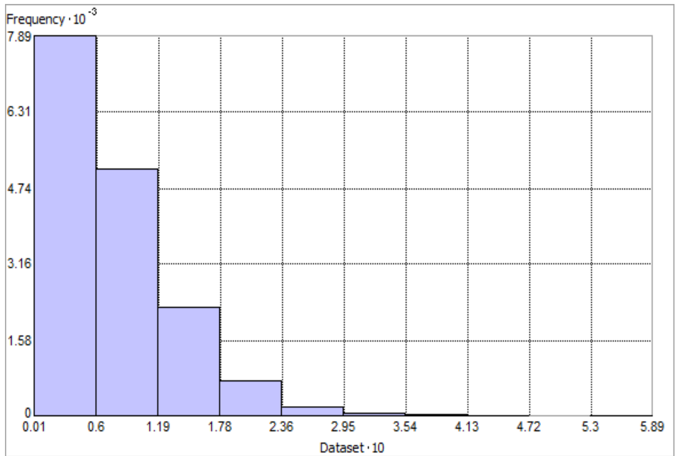


Figure 156. Distribution of Bottom Current Maximum (m $s^{-1}$). Histogram was illustrated using 10 bins. X axis is shown at 10; Y axis is shown at $10^{-3}$.

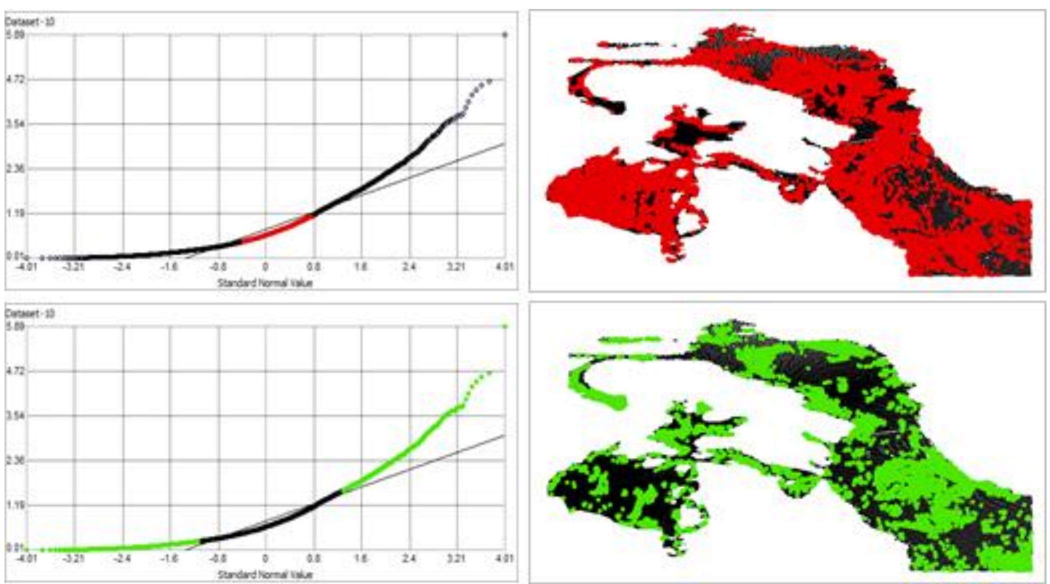

Figure 157. Normal Q-Q plot for data values of Bottom Current Maximum (m $s^{-1}$). Points falling under (top right panel) and over (bottom right panel) the reference line are mapped.

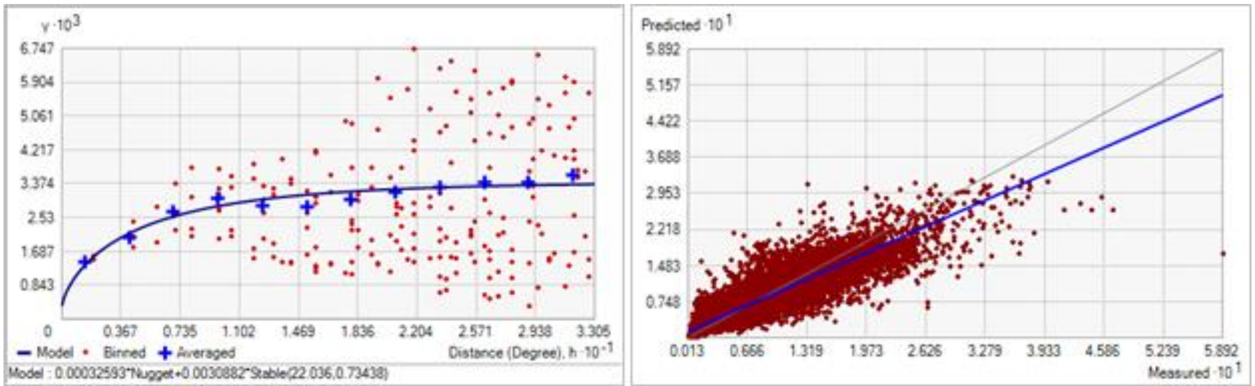


Figure 158. Left panel: Semivariogram of Bottom Current Maximum (m $s^{-1}$). Binned values are shown as red dots; average points are shown as blue crosses; the model fit to the averaged values is shown as a blue line. Lag size: 2.754 degrees; number of lags: 12; Parameter: 0.734; Range: 22.036 degrees; Partial Sill: 3.088 x $10^{-3}$. Right panel: Scatterplot of predicted values versus observed values for the model of Bottom Current Maximum (m $s^{-1}$).

Table 64. Results of cross-validation of the kriged model for Bottom Current Maximum (m $s^{-1}$).

| **Prediction Error** | **Value** |
|---|---|
| Number of Observations | 16257 |
| Overall Mean Error | -9.683 x $10^{-6}$ |
| Root Mean Square Prediction Error | 0.025 |
| Standardized Mean | -1.818 x $10^{-4}$ |
| Standardized Root Mean Square Prediction Error | 1.007 |
| Average Standard Error | 0.025 |

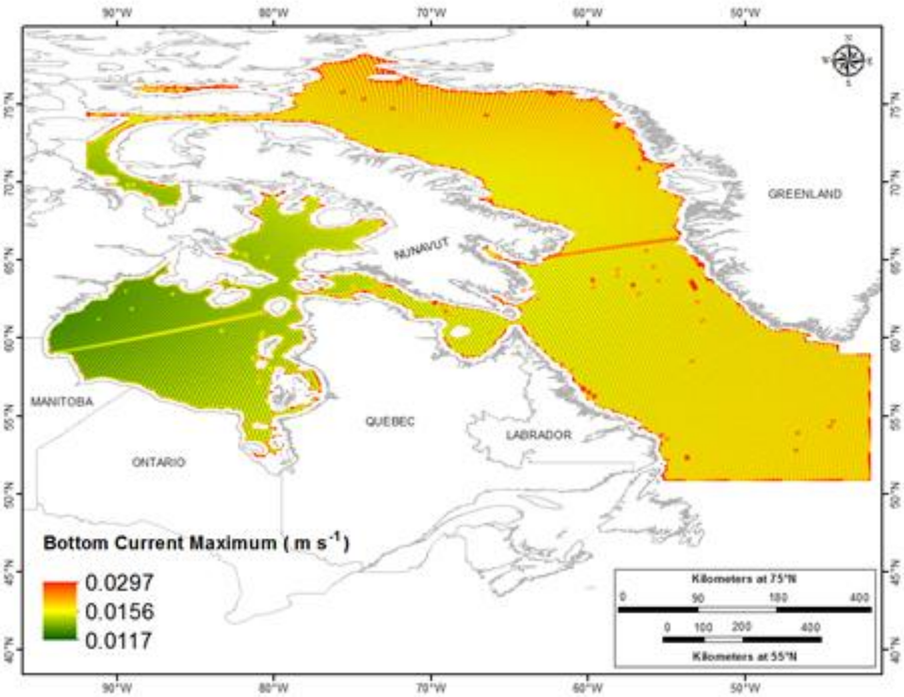


Figure 159. Prediction standard error surface of Bottom Current Maximum (m $s^{-1}$).

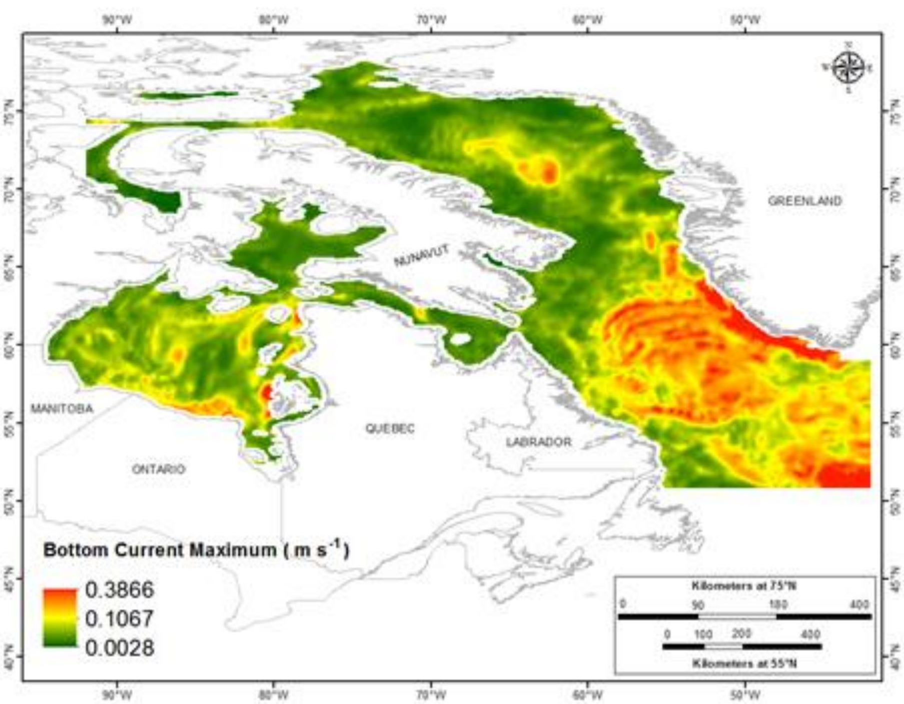


Figure 160. Interpolated prediction surface of Bottom Current Maximum (m $s^{-1}$).

**Bottom Current Range**

This variable displayed a right-skewed, leptokurtic distribution prior to interpolation and outlying data in the upper range (Table 65, Figure 161). The data were higher than predicted by a normal distribution at both tails, while mid-values were lower than the reference line (Figure 162). These areas of under- and over-prediction showed little spatial pattern over the region (Figure 162).

The semivariogram showed moderate autocorrelation present in the data (Figure 163). The kriged model showed a poor fit between measured and predicted values (Figure 163). Very good performance of the model was indicated by the cross-validation results (Table 66). The error map showed lower error in Hudson Bay compared to Baffin Bay and Davis Strait, and higher error along the edges of the study extent (Figure 164). The kriged surface is presented in Figure 165.

Table 65. Distributional properties of Bottom Current Range ($m\ s^{-1}$).

| **Property** | **Value** |
|---|---:|
| Number of Observations | 16257 |
| Minimum | $1.264 \times 10^{-3}$ |
| Maximum | 0.517 |
| Mean | 0.075 |
| Median | 0.061 |
| Standard Deviation | 0.053 |
| Skewness | 1.328 |
| Kurtosis | 5.262 |

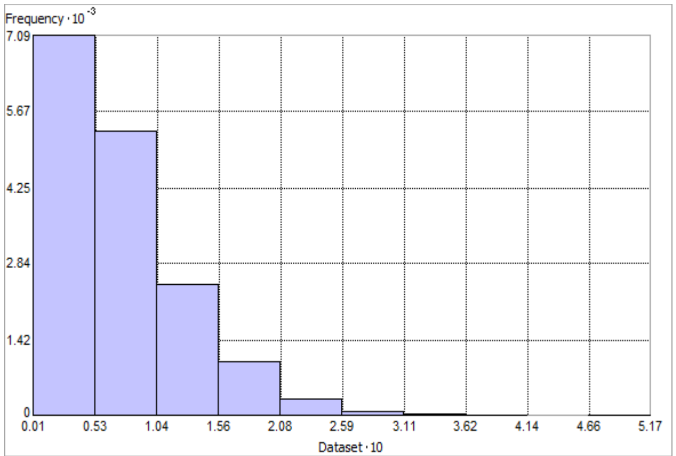


Figure 161. Distribution of Bottom Current Range (m $s^{-1}$). Histogram was illustrated using 10 bins. X axis is shown at 10; Y axis is shown at $10^{-3}$.

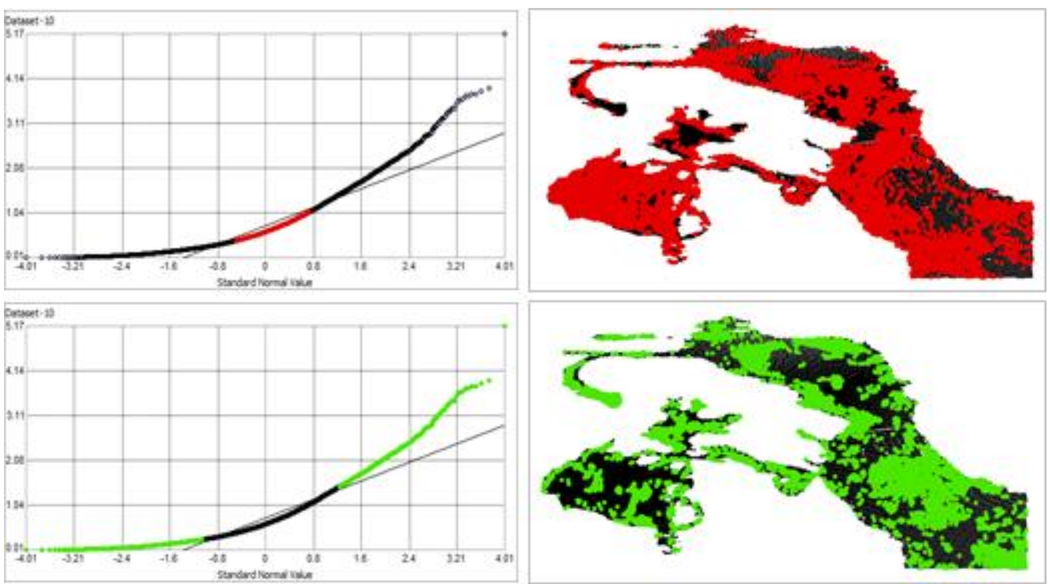


Figure 162. Normal Q-Q plot for data values of Bottom Current Range (m $s^{-1}$). Points falling under (top right panel) and over (bottom right panel) the reference line are mapped.

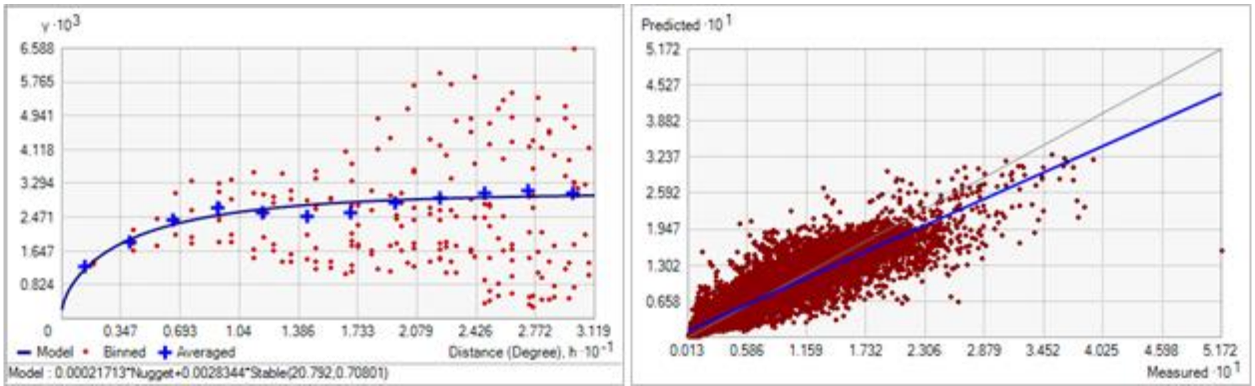


Figure 163. Left panel: Semivariogram of Bottom Current Range (m $s^{-1}$). Binned values are shown as red dots; average points are shown as blue crosses; the model fit to the averaged values is shown as a blue line. Lag size: 2.599 degrees; number of lags: 12; Parameter: 0.708; Range: 20.792 degrees; Partial Sill: 2.834 x $10^{-3}$. Right panel: Scatterplot of predicted values versus observed values for the model of Bottom Current Range (m $s^{-1}$).

Table 66. Results of cross-validation of the kriged model for Bottom Current Range (m $s^{-1}$).

| **Prediction Error** | **Value** |
|---|---|
| Number of Observations | 16257 |
| Overall Mean Error | -1.445 x $10^{-5}$ |
| Root Mean Square Prediction Error | 0.024 |
| Standardized Mean | -2.843 x $10^{-4}$ |
| Standardized Root Mean Square Prediction Error | 1.045 |
| Average Standard Error | 0.023 |

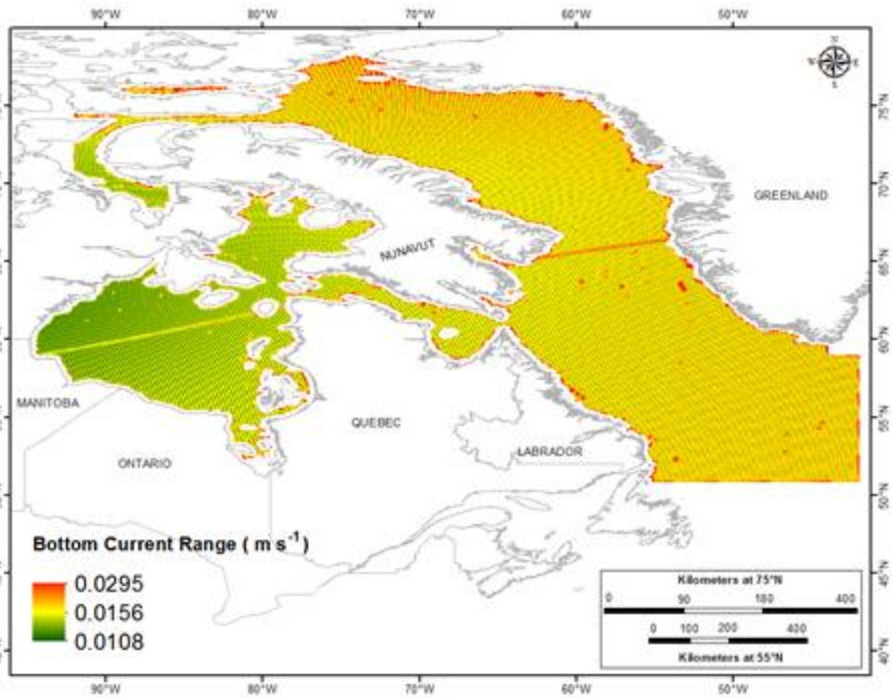


Figure 164. Prediction standard error surface of Bottom Current Range (m $s^{-1}$).

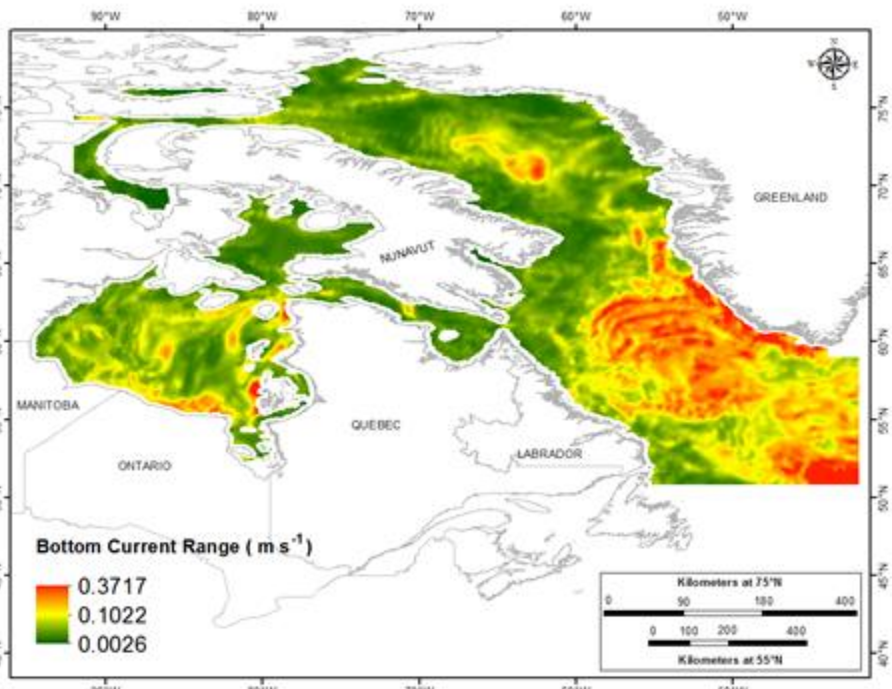


Figure 165. Interpolated prediction surface of Bottom Current Range (m $s^{-1}$).

**Bottom Current Average Minimum**

This variable displayed a right-skewed, extremely leptokurtic distribution prior to interpolation and outlying data in the upper range (Table 67, Figure 166). The data were higher than predicted by a normal distribution at both tails, while mid-values were lower than the reference line (Figure 167). These areas of under- and over-prediction showed spatial pattern over the region (Figure 167).

The semivariogram showed moderate autocorrelation present in the data (Figure 168). The kriged model showed a poor fit between measured and predicted values (Figure 168). Very good performance of the model was indicated by the cross-validation results (Table 68). The error map showed lower error in Hudson Bay compared to Baffin Bay and Davis Strait, and higher error along the edges of the study extent (Figure 169). The kriged surface is presented in Figure 170.

Table 67. Distributional properties of Bottom Current Average Minimum (m $s^{-1}$).

| **Property** | **Value** |
|---|---:|
| Number of Observations | 16257 |
| Minimum | $2.900 \times 10^{-5}$ |
| Maximum | 0.196 |
| Mean | $8.233 \times 10^{-3}$ |
| Median | $3.974 \times 10^{-3}$ |
| Standard Deviation | 0.014 |
| Skewness | 4.750 |
| Kurtosis | 34.270 |

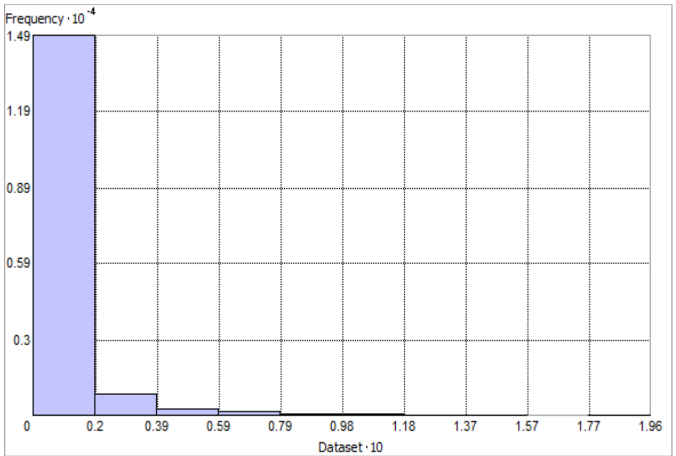


Figure 166. Distribution of Bottom Current Average Minimum (m $s^{-1}$). Histogram was illustrated using 10 bins. X axis is shown at 10; Y axis is shown at $10^{-4}$.

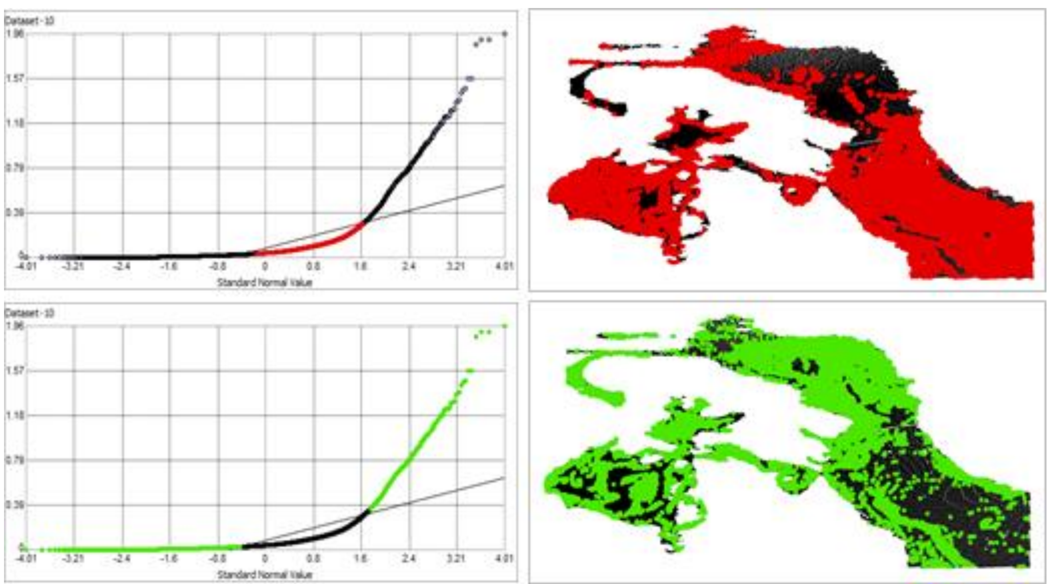

Figure 167. Normal Q-Q plot for data values of Bottom Current Average Minimum (m $s^{-1}$). Points falling under (top right panel) and over (bottom right panel) the reference line are mapped.

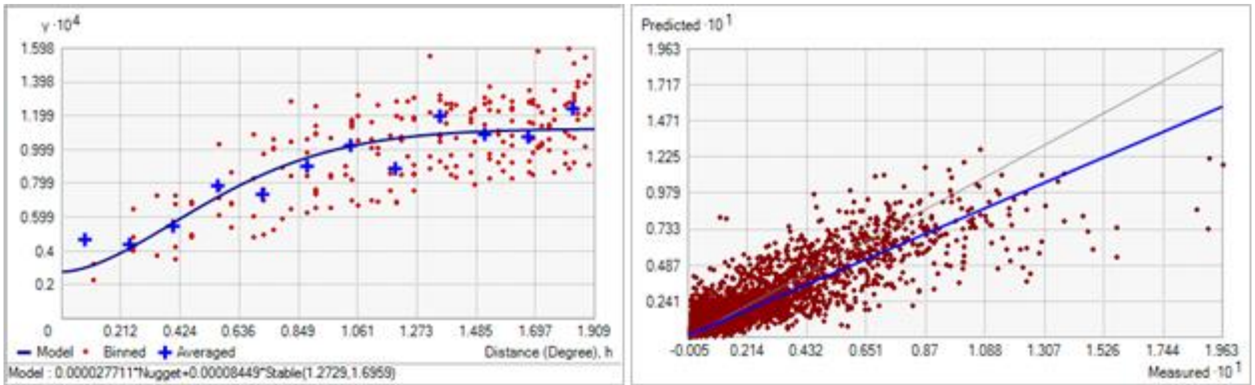

Figure 168. Left panel: Semivariogram of Bottom Current Average Minimum (m $s^{-1}$). Binned values are shown as red dots; average points are shown as blue crosses; the model fit to the averaged values is shown as a blue line. Lag size: 0.159 degrees; number of lags: 12; Parameter: 1.696; Range: 1.273 degrees; Partial Sill: $8.449 \times 10^{-5}$. Right panel: Scatterplot of predicted values versus observed values for the model of Bottom Current Average Minimum (m $s^{-1}$).

Table 68. Results of cross-validation of the kriged model for Bottom Current Average Minimum (m $s^{-1}$).

| **Prediction Error** | **Value** |
|---|---:|
| Number of Observations | 16257 |
| Overall Mean Error | $4.524 \times 10^{-6}$ |
| Root Mean Square Prediction Error | $6.199 \times 10^{-3}$ |
| Standardized Mean | $4.946 \times 10^{-4}$ |
| Standardized Root Mean Square Prediction Error | 1.013 |
| Average Standard Error | $6.038 \times 10^{-3}$ |

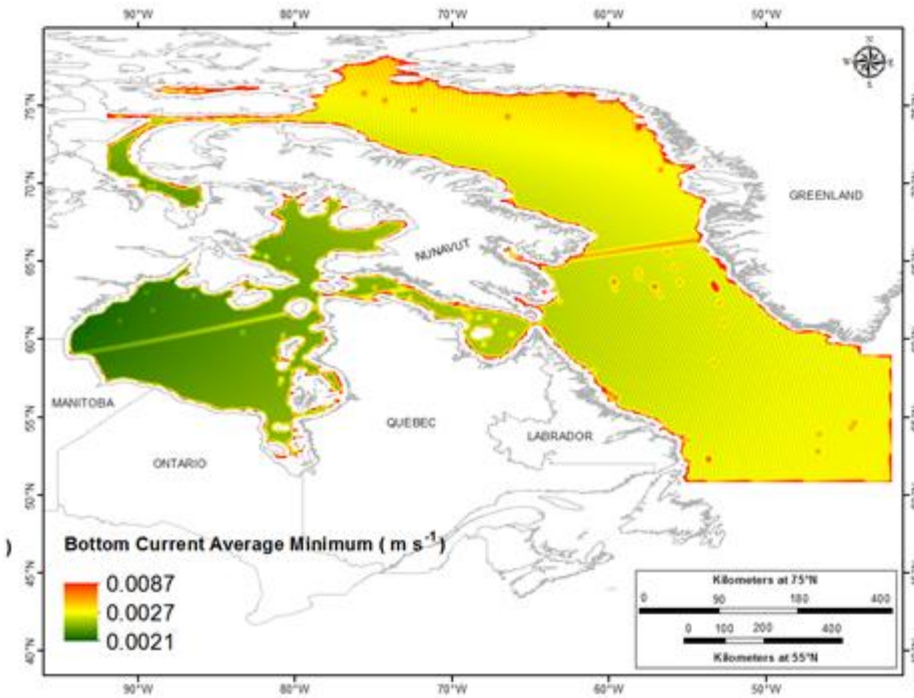


Figure 169. Prediction standard error surface of Bottom Current Average Minimum (m s$^{-1}$).

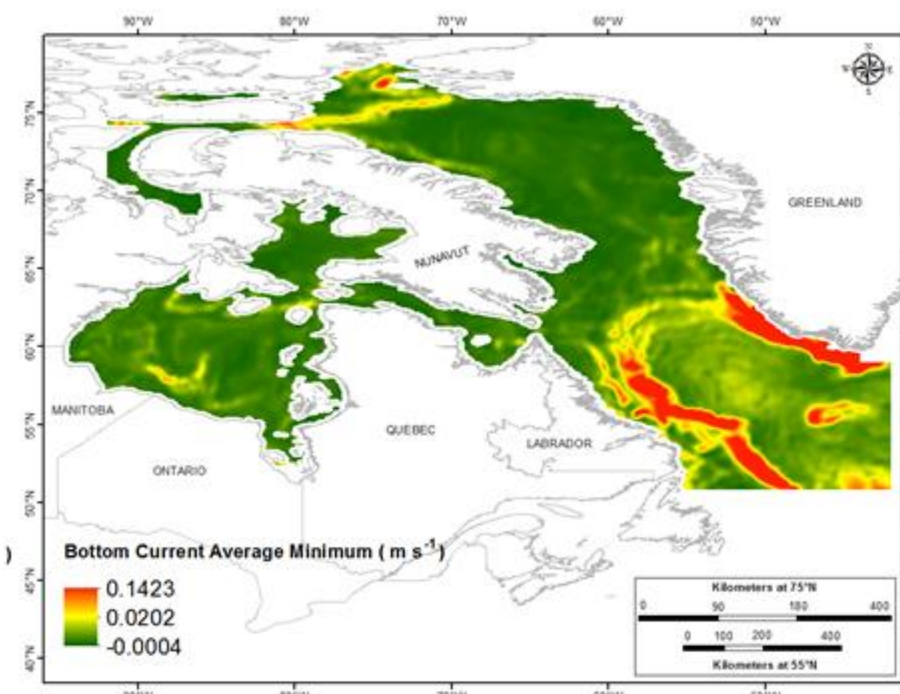


Figure 170. Interpolated prediction surface of Bottom Current Average Minimum (m s$^{-1}$).

**Bottom Current Average Maximum**

This variable displayed a right-skewed, leptokurtic distribution prior to interpolation (Table 69, Figure 171). The data were higher than predicted by a normal distribution at both tails, while mid-values were lower than the reference line (Figure 172). These areas of under- and over-prediction showed little spatial pattern over the region (Figure 172).

The semivariogram showed moderate autocorrelation present in the data (Figure 173). The kriged model showed a poor fit between measured and predicted values (Figure 173). Very good performance of the model was indicated by the cross-validation results (Table 70). The error map showed lower error in Hudson Bay compared to Baffin Bay and Davis Strait, and higher error along the edges of the study extent (Figure 174). The kriged surface is presented in Figure 175.

Table 69. Distributional properties of Bottom Current Average Maximum (m $s^{-1}$).

| **Property** | **Value** |
|---|---:|
| Number of Observations | 16257 |
| Minimum | $7.020 \times 10^{-4}$ |
| Maximum | 0.390 |
| Mean | 0.048 |
| Median | 0.037 |
| Standard Deviation | 0.038 |
| Skewness | 1.750 |
| Kurtosis | 8.180 |

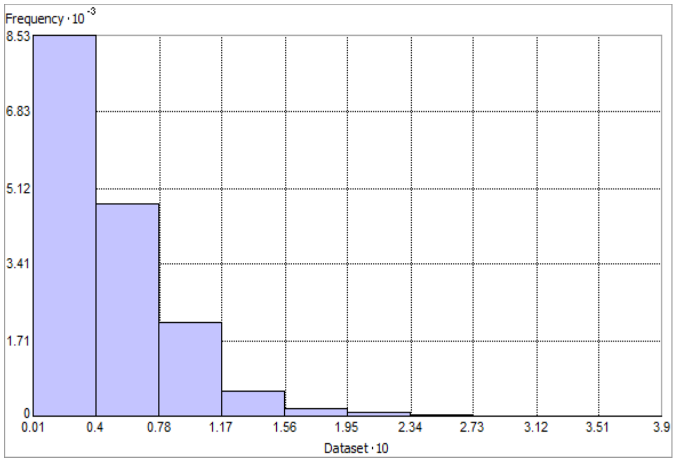


Figure 171. Distribution of Bottom Current Average Maximum (m $s^{-1}$). Histogram was illustrated using 10 bins. X axis is shown at 10; Y axis is shown at $10^{-3}$.

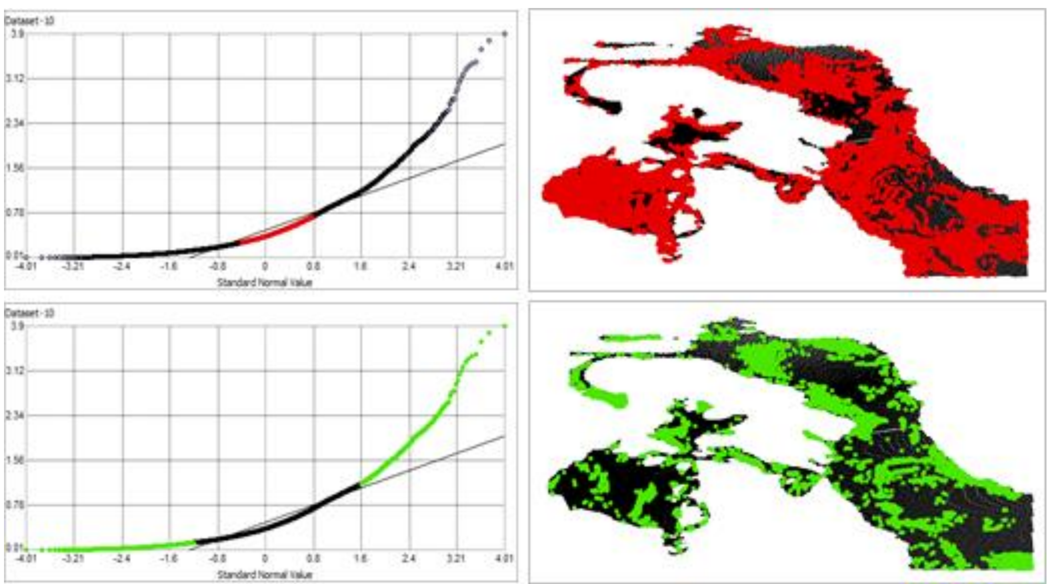

Figure 172. Normal Q-Q plot for data values of Bottom Current Average Maximum (m $s^{-1}$). Points falling under (top right panel) and over (bottom right panel) the reference line are mapped.

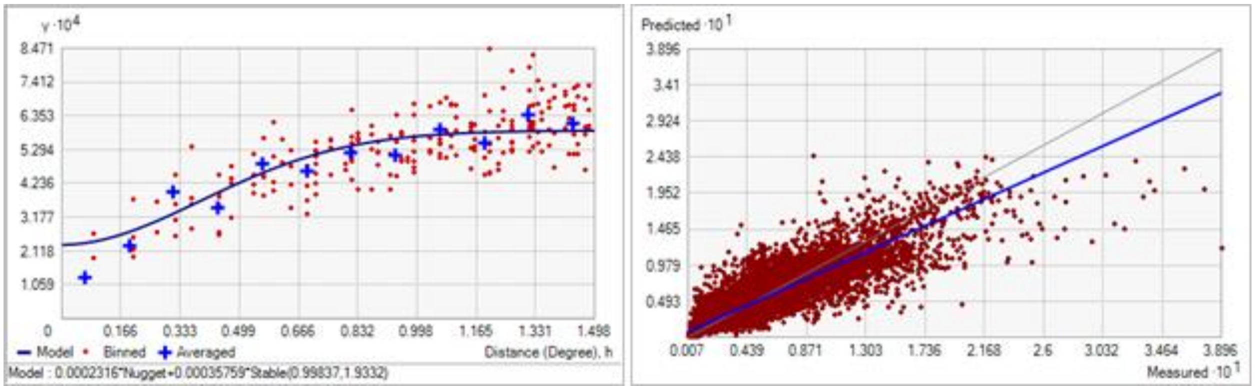


Figure 173. Left panel: Semivariogram of Bottom Current Average Maximum (m $s^{-1}$). Binned values are shown as red dots; average points are shown as blue crosses; the model fit to the averaged values is shown as a blue line. Lag size: 0.125 degrees; number of lags: 12; Parameter: 1.933; Range: 0.998 degrees; Partial Sill: $3.576 \times 10^{-4}$. Right panel: Scatterplot of predicted values versus observed values for the model of Bottom Current Average Maximum (m $s^{-1}$).

Table 70. Results of cross-validation of the kriged model for Bottom Current Average Maximum (m $s^{-1}$).

| **Prediction Error** | **Value** |
|---|---:|
| Number of Observations | 16257 |
| Overall Mean Error | $3.966 \times 10^{-6}$ |
| Root Mean Square Prediction Error | 0.017 |
| Standardized Mean | $3.576 \times 10^{-4}$ |
| Standardized Root Mean Square Prediction Error | 1.010 |
| Average Standard Error | 0.017 |

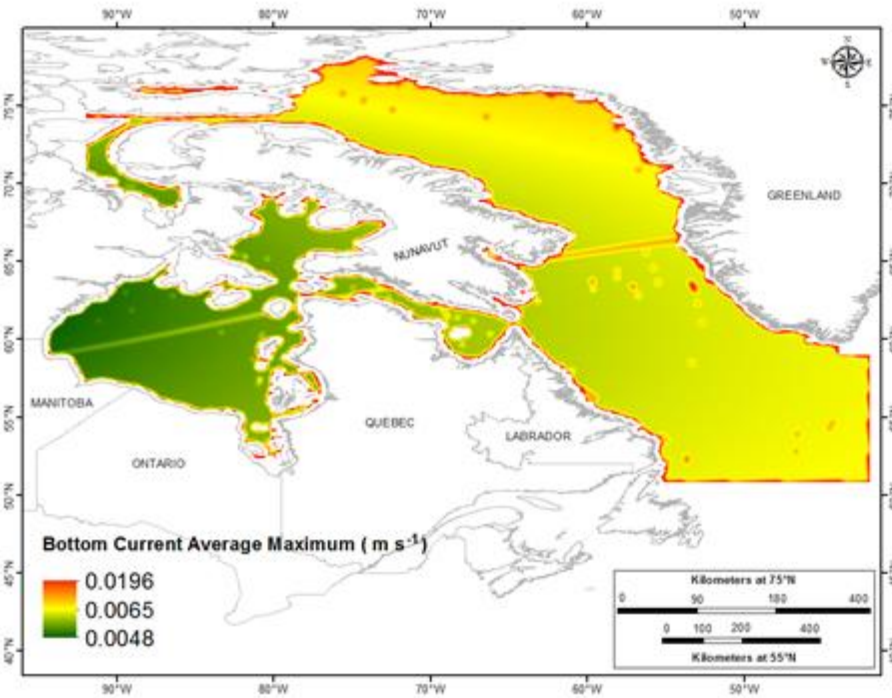


Figure 174. Prediction standard error surface of Bottom Current Average Maximum (m $s^{-1}$).

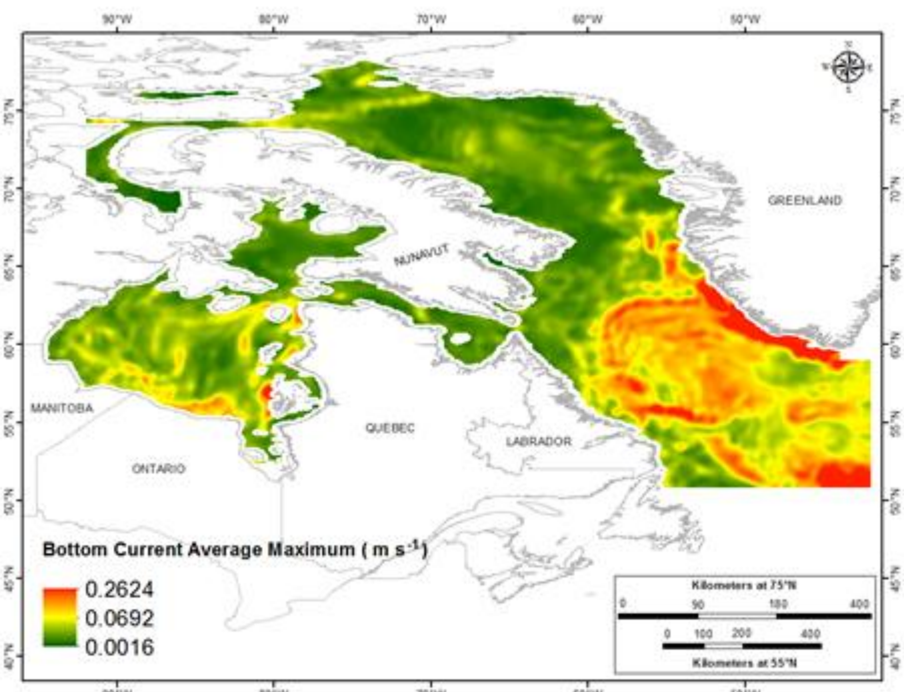


Figure 175. Interpolated prediction surface of Bottom Current Average Maximum (m $s^{-1}$).

**Bottom Current Average Range**

This variable displayed a right-skewed, leptokurtic distribution prior to interpolation (Table 71, Figure 176). The data were higher than predicted by a normal distribution at both tails, while mid-values were lower than the reference line (Figure 177). These areas of under- and over-prediction showed little spatial pattern over the region (Figure 177).

The semivariogram showed moderate autocorrelation present in the data (Figure 178). The kriged model showed a poor fit between measured and predicted values (Figure 178). Very good performance of the model was indicated by the cross-validation results (Table 72). The error map showed lower error in Hudson Bay compared to Baffin Bay and Davis Strait, and higher error along the edges of the study extent (Figure 179). The kriged surface is presented in Figure 180.

Table 71. Distributional properties of Bottom Current Average Range (m $s^{-1}$).

| **Property** | **Value** |
|---|---:|
| Number of Observations | 16257 |
| Minimum | $5.940 \times 10^{-4}$ |
| Maximum | 0.266 |
| Mean | 0.040 |
| Median | 0.032 |
| Standard Deviation | 0.029 |
| Skewness | 1.408 |
| Kurtosis | 5.830 |

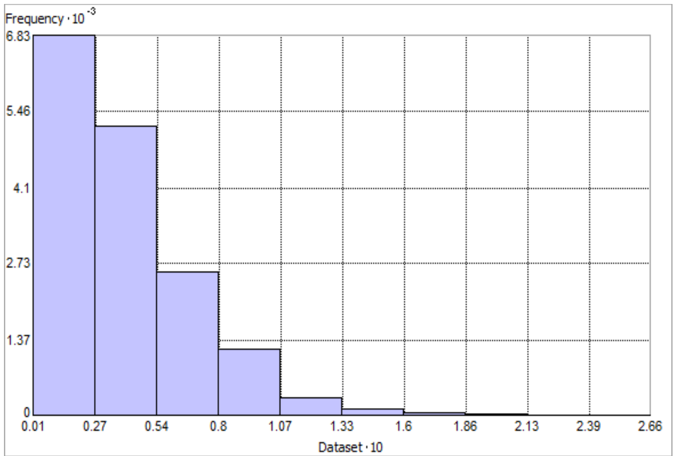


Figure 176. Distribution of Bottom Current Average Range (m $s^{-1}$). Histogram was illustrated using 10 bins. X axis is shown at 10; Y axis is shown at $10^{-3}$.

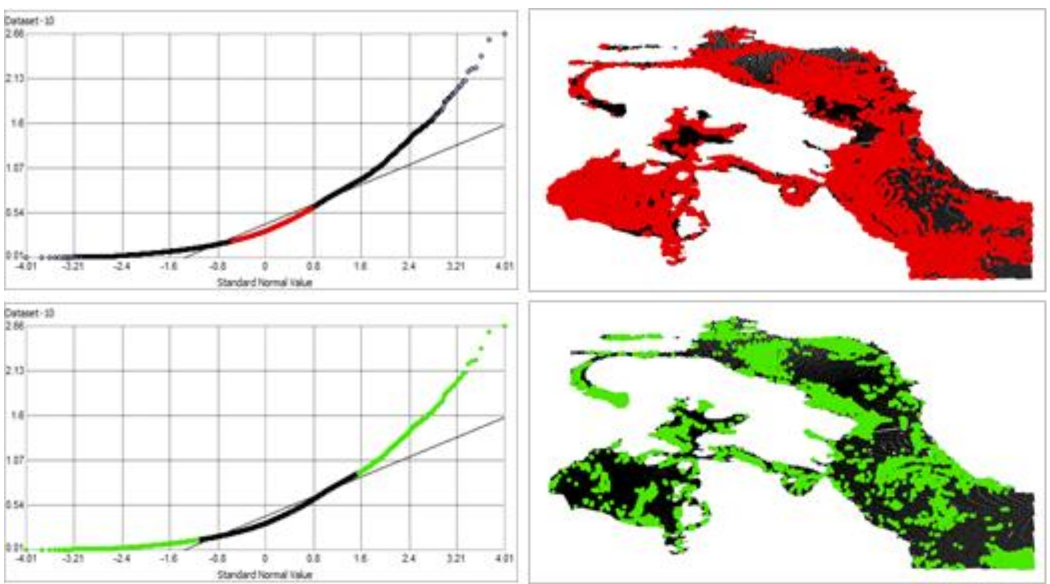

Figure 177. Normal Q-Q plot for data values of Bottom Current Average Range (m $s^{-1}$). Points falling under (top right panel) and over (bottom right panel) the reference line are mapped.

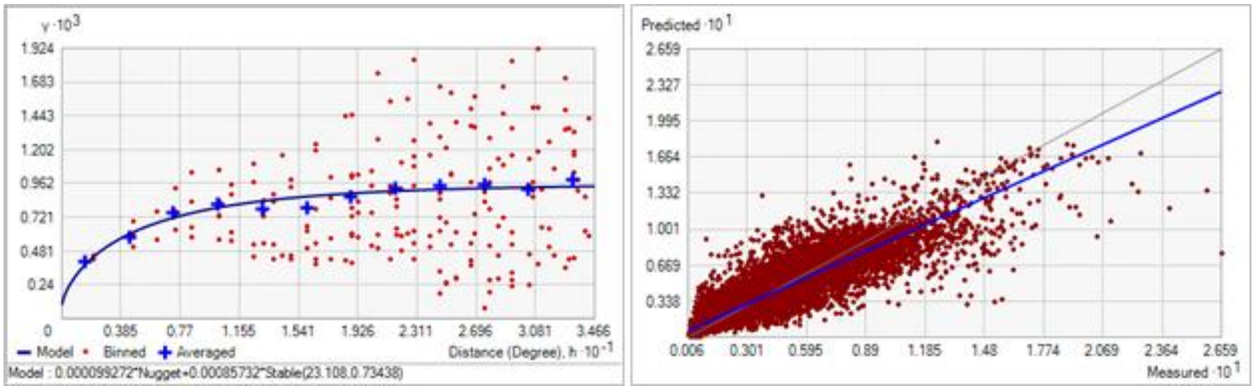


Figure 178. Left panel: Semivariogram of Bottom Current Average Range (m $s^{-1}$). Binned values are shown as red dots; average points are shown as blue crosses; the model fit to the averaged values is shown as a blue line. Lag size: 2.889 degrees; number of lags: 12; Parameter: 0.734; Range: 23.108 degrees; Partial Sill: $8.573 \times 10^{-4}$. Right panel: Scatterplot of predicted values versus observed values for the model of Bottom Current Average Range (m $s^{-1}$).

Table 72. Results of cross-validation of the kriged model for Bottom Current Average Range (m $s^{-1}$).

| **Prediction Error** | **Value** |
|---|---:|
| Number of Observations | 16257 |
| Overall Mean Error | $-7.277 \times 10^{-6}$ |
| Root Mean Square Prediction Error | 0.013 |
| Standardized Mean | $-3.011 \times 10^{-4}$ |
| Standardized Root Mean Square Prediction Error | 0.967 |
| Average Standard Error | 0.013 |

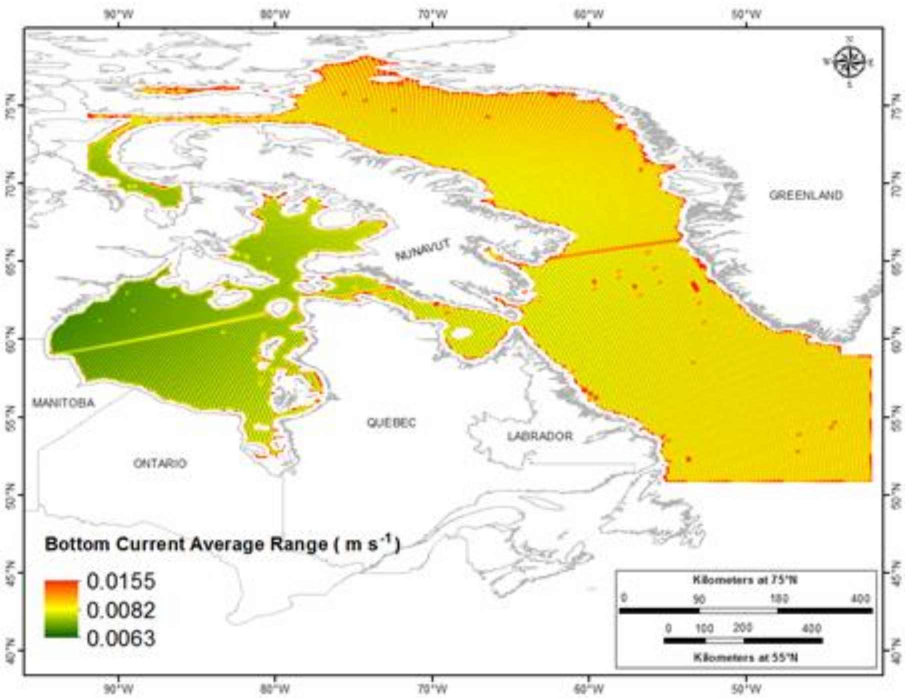


Figure 179. Prediction standard error surface of Bottom Current Average Range (m $s^{-1}$).

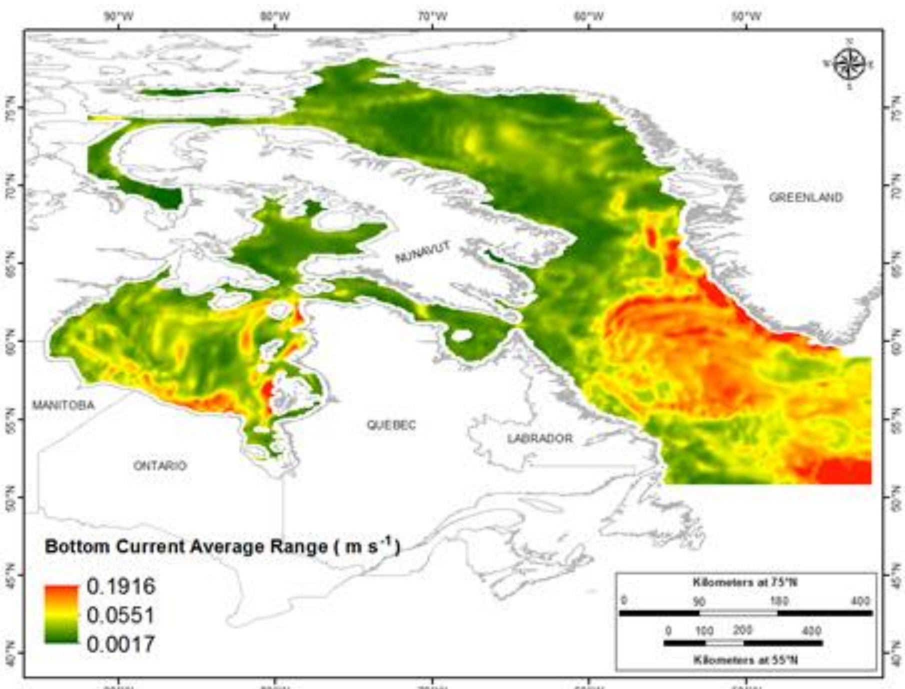


Figure 180. Interpolated prediction surface of Bottom Current Average Range (m $s^{-1}$).

**Surface Current Mean**

This variable displayed a right-skewed, leptokurtic distribution prior to interpolation (Table 73, Figure 181). The data were higher than predicted by a normal distribution at both tails, while mid-values were lower than the reference line (Figure 182). These areas of under- and over-prediction showed spatial pattern over the region (Figure 182).

The semivariogram showed moderate autocorrelation present in the data (Figure 183). The kriged model showed a good fit between measured and predicted values (Figure 183). Fair performance of the model was indicated by the cross-validation results (Table 74). The error map showed lower error in Hudson Bay compared to Baffin Bay and Davis Strait, and higher error along the edges of the study extent (Figure 184). The kriged surface is presented in Figure 185.

Table 73. Distributional properties of Surface Current Mean (m $s^{-1}$).

| **Property** | **Value** |
|---|---:|
| Number of Observations | 16376 |
| Minimum | $7.070 \times 10^{-3}$ |
| Maximum | 0.636 |
| Mean | 0.071 |
| Median | 0.057 |
| Standard Deviation | 0.054 |
| Skewness | 2.943 |
| Kurtosis | 16.720 |

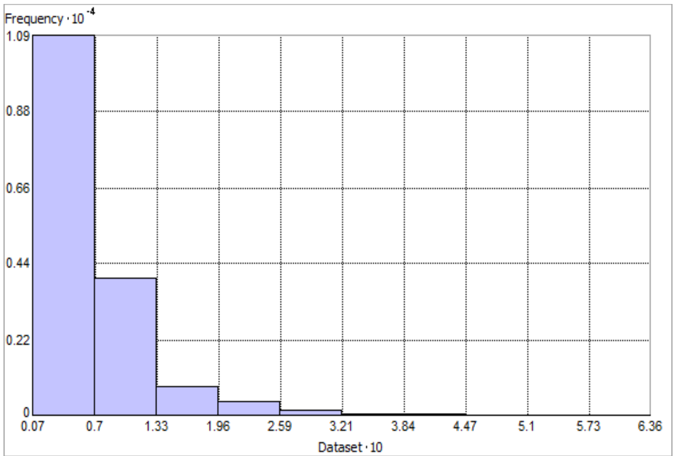


Figure 181. Distribution of Surface Current Mean (m $s^{-1}$). Histogram was illustrated using 10 bins. X axis is shown at 10; Y axis is shown at $10^{-4}$.

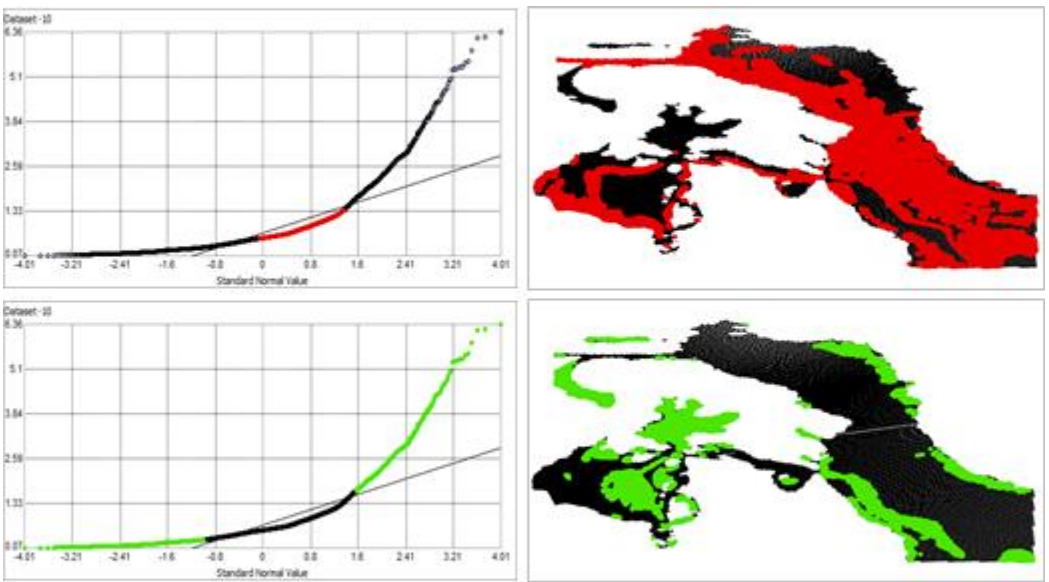

Figure 182. Normal Q-Q plot for data values of Surface Current Mean (m $s^{-1}$). Points falling under (top right panel) and over (bottom right panel) the reference line are mapped.

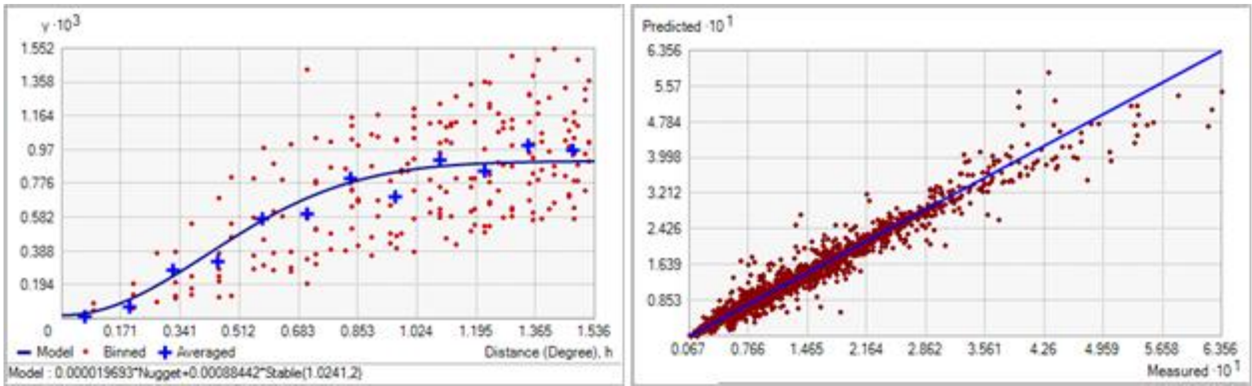

Figure 183. Left panel: Semivariogram of Surface Current Mean (m $s^{-1}$). Binned values are shown as red dots; average points are shown as blue crosses; the model fit to the averaged values is shown as a blue line. Lag size: 0.128 degrees; number of lags: 12; Parameter: 2; Range: 1.024 degrees; Partial Sill: 8.844 x $10^{-4}$. Right panel: Scatterplot of predicted values versus observed values for the model of Surface Current Mean (m $s^{-1}$).

Table 74. Results of cross-validation of the kriged model for Surface Current Mean (m $s^{-1}$).

| **Prediction Error** | **Value** |
|---|---|
| Number of Observations | 16376 |
| Overall Mean Error | -8.683 x $10^{-6}$ |
| Root Mean Square Prediction Error | 7.406 x $10^{-3}$ |
| Standardized Mean | 4.377 x $10^{-5}$ |
| Standardized Root Mean Square Prediction Error | 1.325 |
| Average Standard Error | 5.377 x $10^{-3}$ |

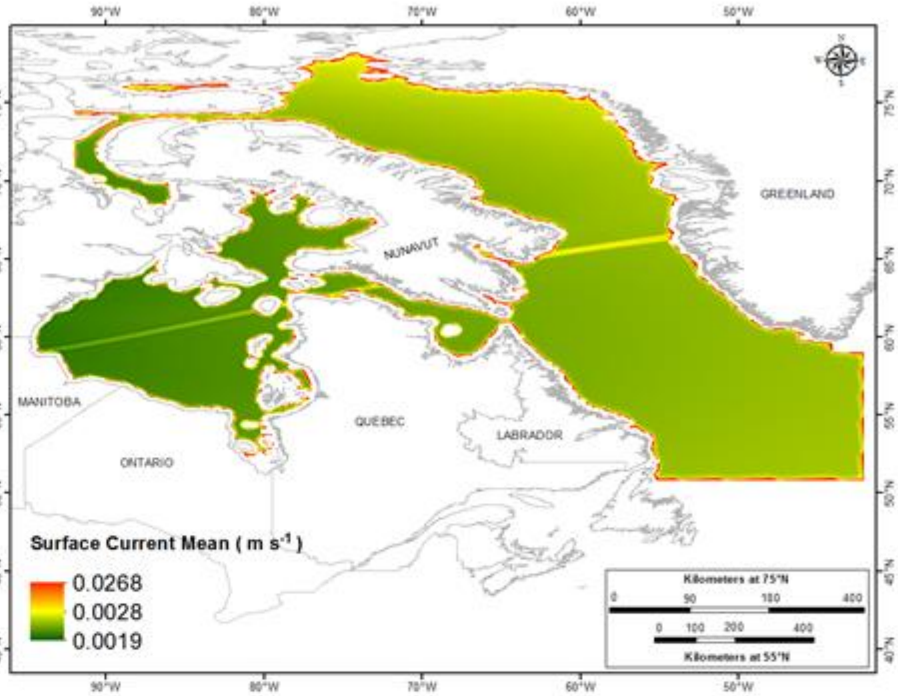


Figure 184. Prediction standard error surface of Surface Current Mean (m $s^{-1}$).

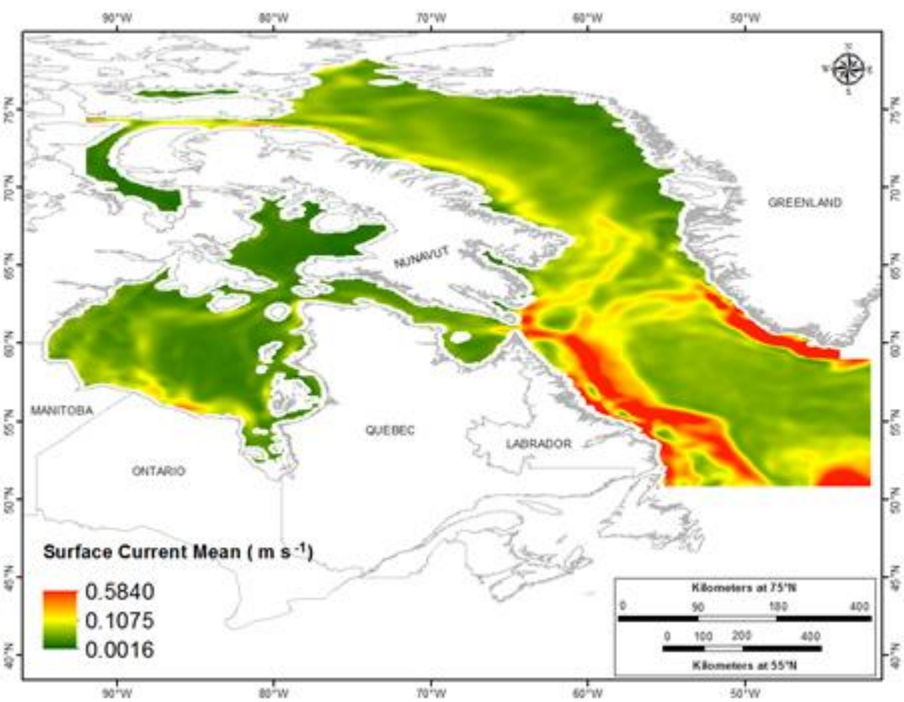


Figure 185. Interpolated prediction surface of Surface Current Mean (m $s^{-1}$).

### Surface Current Minimum

This variable displayed a right-skewed, extremely leptokurtic distribution prior to interpolation and outlying data in the upper range (Table 75, Figure 186). The data were higher than predicted by a normal distribution at both tails, while mid-values were lower than the reference line (Figure 187). These areas of under- and over-prediction showed little spatial pattern over the region (Figure 187).

The semivariogram showed moderate autocorrelation present in the data (Figure 188). Aside from a few outliers, the kriged model showed a good fit between measured and predicted values (Figure 188). Fair performance of the model was indicated by the cross-validation results (Table 76). The error map showed lower error in Hudson Bay compared to Baffin Bay and Davis Strait, and higher error along the edges of the study extent (Figure 189). The kriged surface is presented in Figure 190.

Table 75. Distributional properties of Surface Current Minimum (m $s^{-1}$).

| **Property** | **Value** |
|---|---:|
| Number of Observations | 16376 |
| Minimum | $2.100 \times 10^{-5}$ |
| Maximum | 0.374 |
| Mean | $8.243 \times 10^{-3}$ |
| Median | $3.214 \times 10^{-3}$ |
| Standard Deviation | 0.019 |
| Skewness | 6.356 |
| Kurtosis | 60.916 |

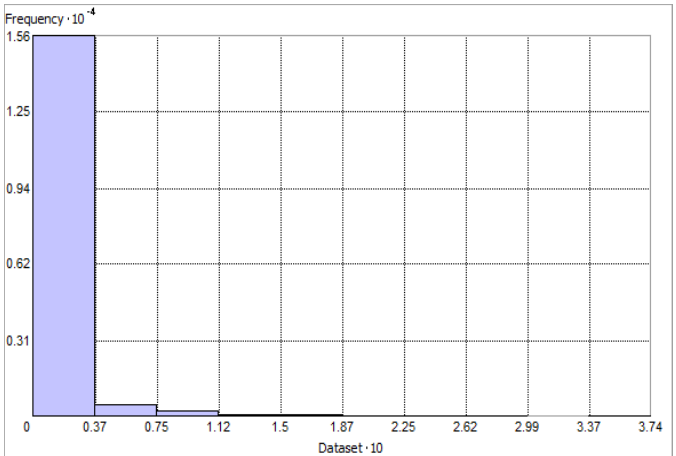


Figure 186. Distribution of Surface Current Minimum (m $s^{-1}$). Histogram was illustrated using 10 bins. X axis is shown at 10; Y axis is shown at $10^{-4}$.

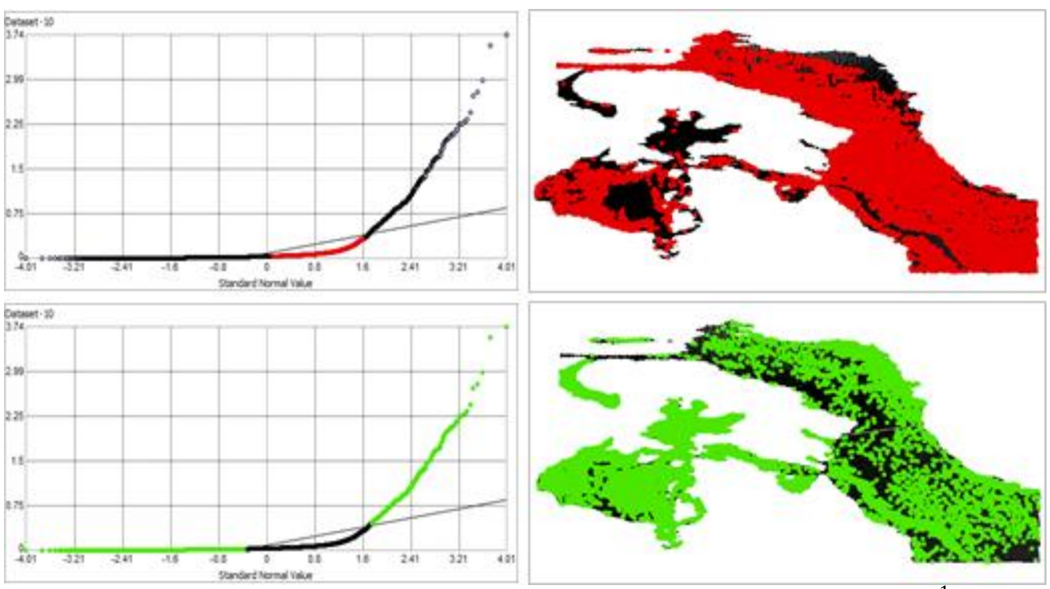

Figure 187. Normal Q-Q plot for data values of Surface Current Minimum (m $s^{-1}$). Points falling under (top right panel) and over (bottom right panel) the reference line are mapped.

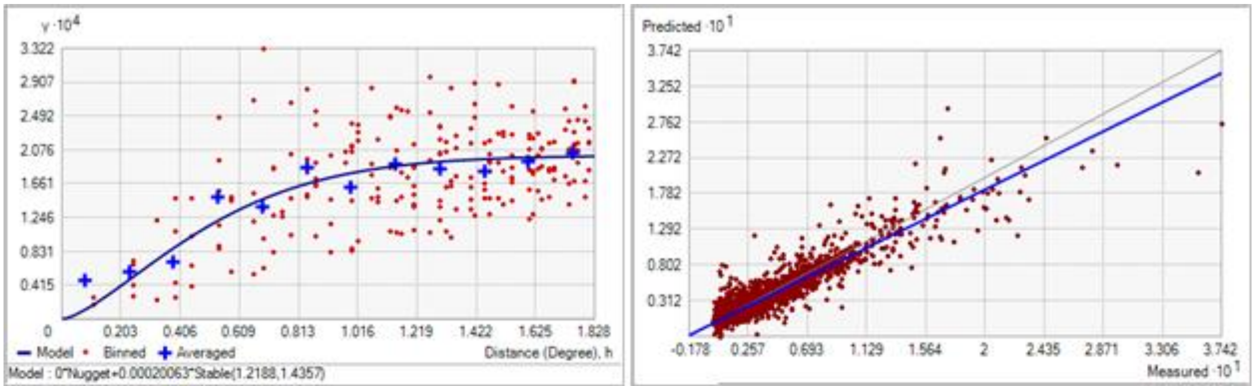

Figure 188. Left panel: Semivariogram of Surface Current Minimum (m $s^{-1}$). Binned values are shown as red dots; average points are shown as blue crosses; the model fit to the averaged values is shown as a blue line. Lag size: 0.152 degrees; number of lags: 12; Parameter: 1.436; Range: 1.219 degrees; Partial Sill: 2.006 x $10^{-4}$. Right panel: Scatterplot of predicted values versus observed values for the model of Surface Current Minimum (m $s^{-1}$).

Table 76. Results of cross-validation of the kriged model for Surface Current Minimum (m $s^{-1}$).

| **Prediction Error** | **Value** |
|---|---:|
| Number of Observations | 16376 |
| Overall Mean Error | -3.017 x $10^{-6}$ |
| Root Mean Square Prediction Error | 5.960x $10^{-3}$ |
| Standardized Mean | -1.823 x $10^{-4}$ |
| Standardized Root Mean Square Prediction Error | 1.343 |
| Average Standard Error | 4.296 x $10^{-3}$ |

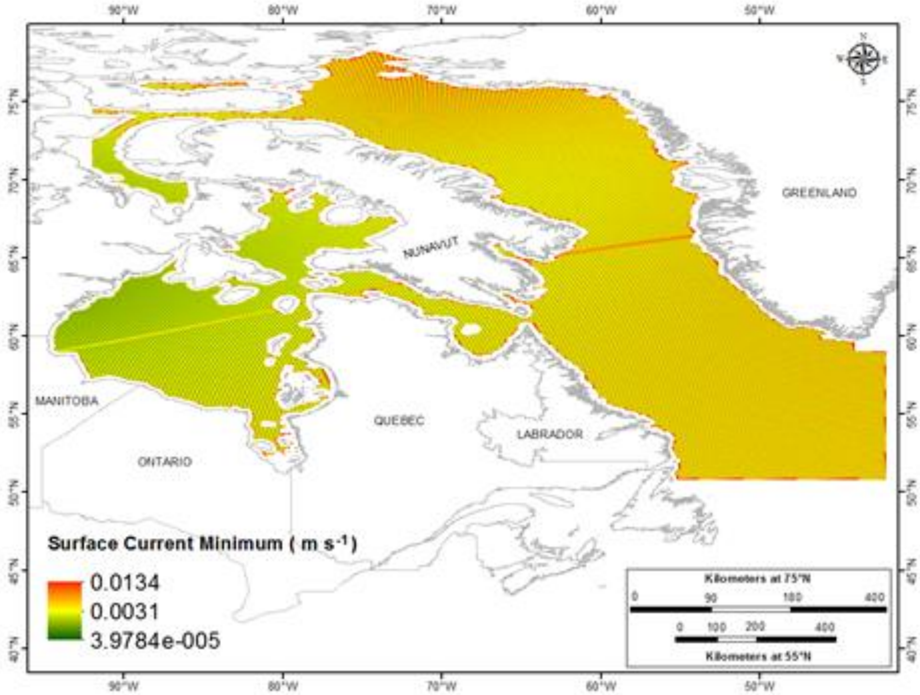


Figure 189. Prediction standard error surface of Surface Current Minimum (m $s^{-1}$).

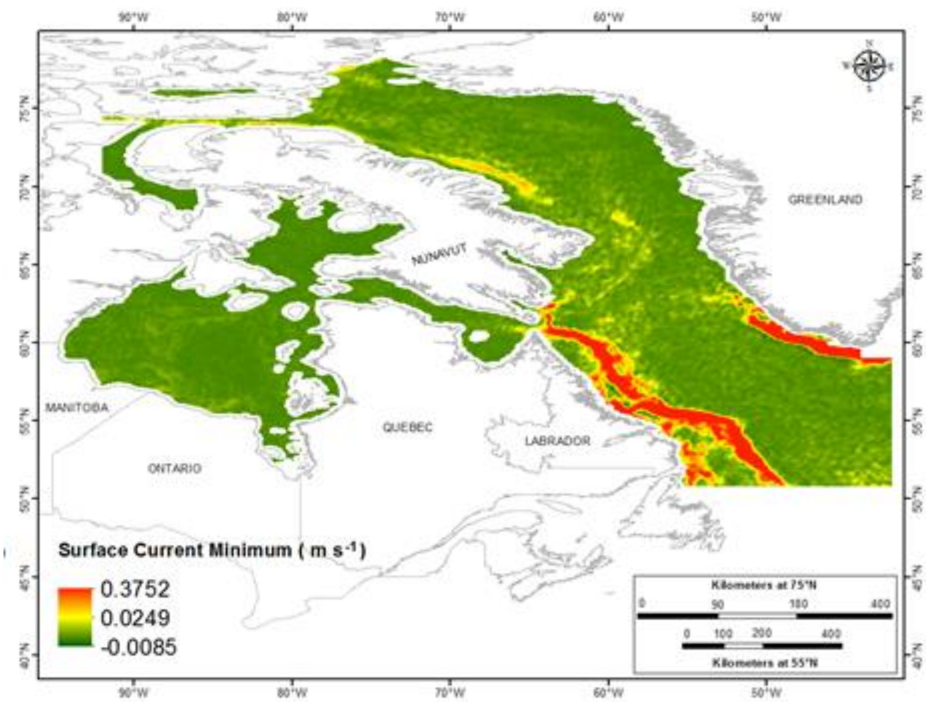


Figure 190. Interpolated prediction surface of Surface Current Minimum (m $s^{-1}$).

**Surface Current Maximum**

This variable displayed a right-skewed, leptokurtic distribution prior to interpolation (Table 77, Figure 191). The data were higher than predicted by a normal distribution at both tails, while mid-values were slightly lower than the reference line (Figure 192). These areas of under- and over-prediction showed spatial pattern over the region (Figure 192).

The semivariogram showed autocorrelation present in the data (Figure 193). The kriged model showed a good fit between measured and predicted values (Figure 193). Very good performance of the model was indicated by the cross-validation results (Table 78). The error map showed lower error in Hudson Bay compared to Baffin Bay and Davis Strait, with higher error along the edges of the study extent and in the most northern areas (Figure 194). The kriged surface is presented in Figure 195.

Table 77. Distributional properties of Surface Current Maximum (m $s^{-1}$).

| **Property** | **Value** |
|---|---:|
| Number of Observations | 16376 |
| Minimum | 0.029 |
| Maximum | 0.999 |
| Mean | 0.206 |
| Median | 0.189 |
| Standard Deviation | 0.105 |
| Skewness | 1.520 |
| Kurtosis | 7.387 |

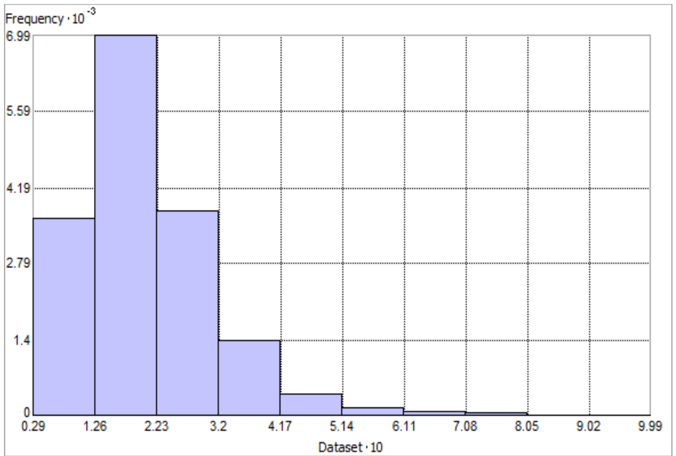


Figure 191. Distribution of Surface Current Maximum (m $s^{-1}$). Histogram was illustrated using 10 bins. X axis is shown at 10; Y axis is shown at $10^{-3}$.

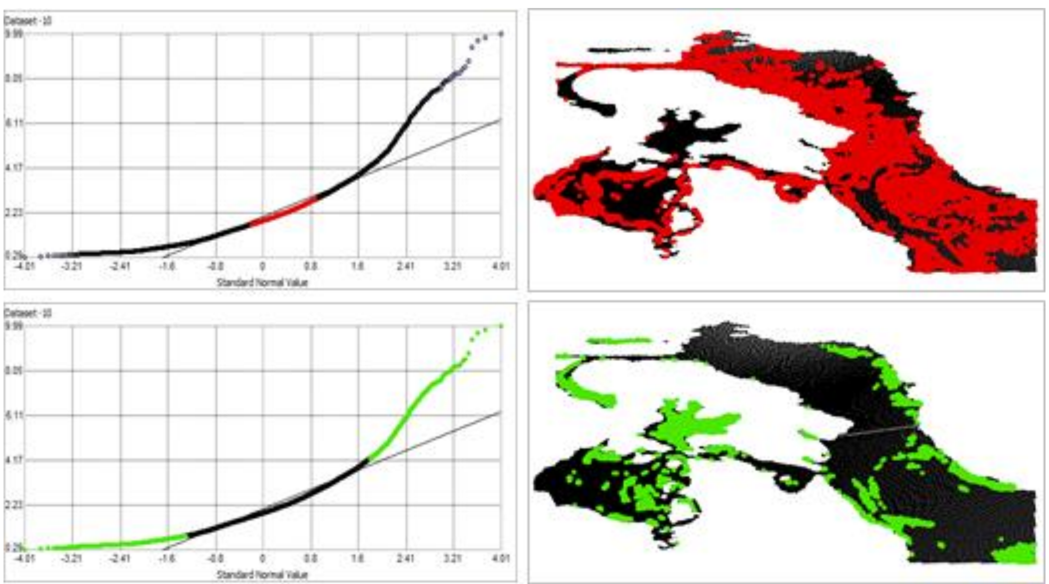


Figure 192. Normal Q-Q plot for data values of Surface Current Maximum (m $s^{-1}$). Points falling under (top right panel) and over (bottom right panel) the reference line are mapped.

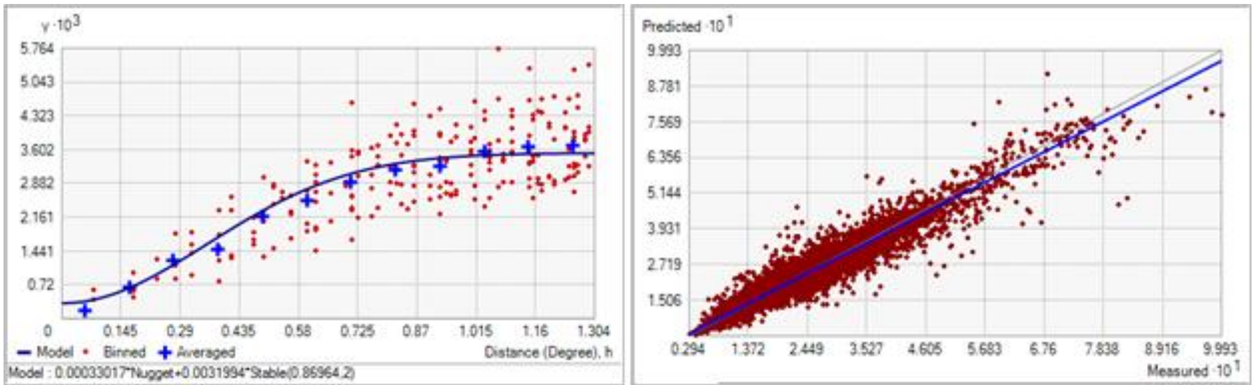

Figure 193. Left panel: Semivariogram of Surface Current Maximum (m $s^{-1}$). Binned values are shown as red dots; average points are shown as blue crosses; the model fit to the averaged values is shown as a blue line. Lag size: 0.109 degrees; number of lags: 12; Parameter: 2; Range: 0.870 degrees; Partial Sill: 3.199 x $10^{-3}$. Right panel: Scatterplot of predicted values versus observed values for the model of Surface Current Maximum (m $s^{-1}$).

Table 78. Results of cross-validation of the kriged model for Surface Current Maximum (m $s^{-1}$).

| **Prediction Error** | **Value** |
|---|---|
| Number of Observations | 16376 |
| Overall Mean Error | -6.189 x $10^{-5}$ |
| Root Mean Square Prediction Error | 0.025 |
| Standardized Mean | -5.143 x $10^{-4}$ |
| Standardized Root Mean Square Prediction Error | 1.142 |
| Average Standard Error | 0.021 |

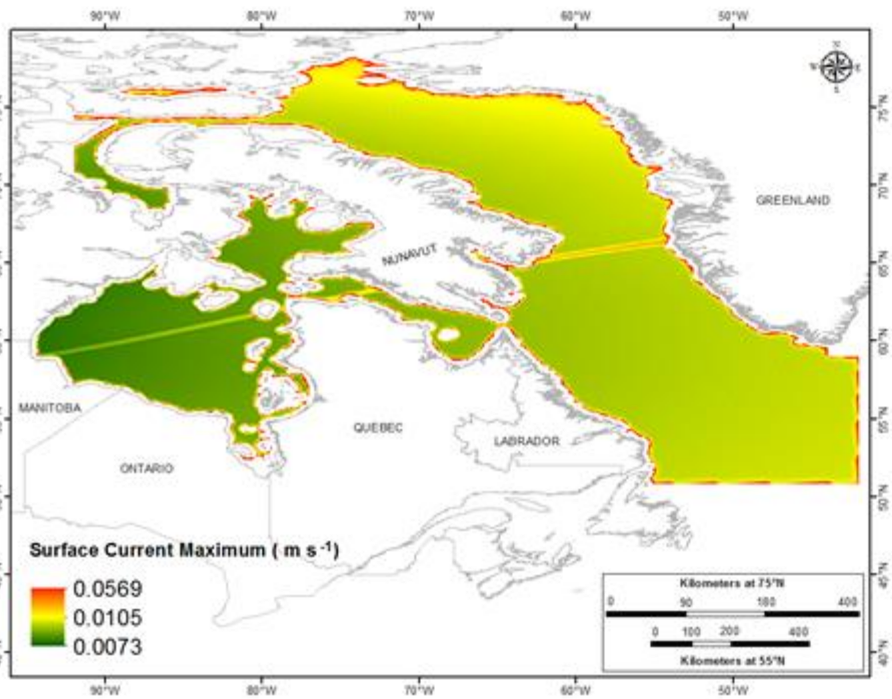


Figure 194. Prediction standard error surface of Surface Current Maximum (m $s^{-1}$).

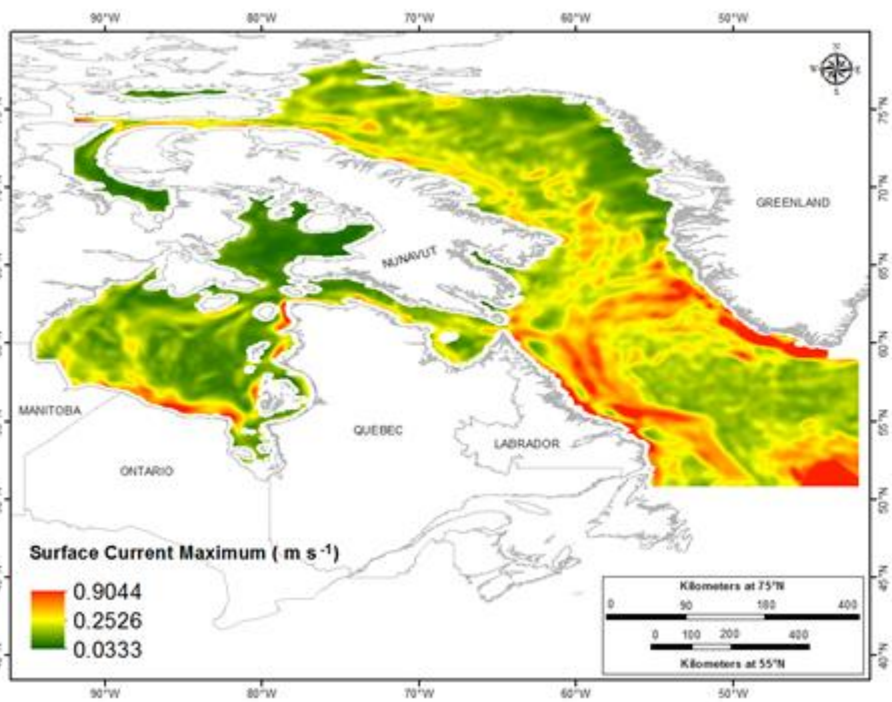


Figure 195. Interpolated prediction surface of Surface Current Maximum (m $s^{-1}$).

## Surface Current Range

This variable displayed a right-skewed, leptokurtic distribution prior to interpolation (Table 79, Figure 196). The data were higher than predicted by a normal distribution at both tails, while mid-values were slightly lower than the reference line (Figure 197). These areas of under- and over-prediction showed spatial pattern over the region (Figure 197).

The semivariogram showed moderate autocorrelation present in the data (Figure 198). The kriged model showed good fit between measured and predicted values (Figure 198). Very good performance of the model was indicated by the cross-validation results (Table 80). The error map showed lower error in Hudson Bay compared to Baffin Bay and Davis Strait, with higher error along the edges of the study extent and in the most northern areas (Figure 199). The kriged surface is presented in Figure 200.

Table 79. Distributional properties of Surface Current Range (m $s^{-1}$).

| **Property** | **Value** |
|---|---:|
| Number of Observations | 16376 |
| Minimum | 0.029 |
| Maximum | 0.822 |
| Mean | 0.198 |
| Median | 0.185 |
| Standard Deviation | 0.096 |
| Skewness | 1.345 |
| Kurtosis | 6.608 |

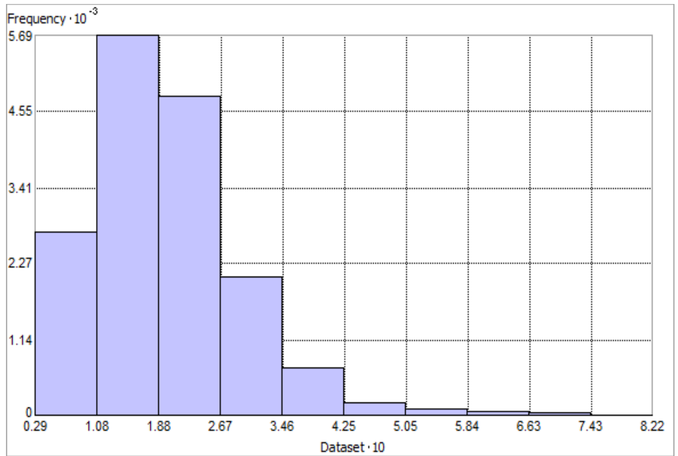


Figure 196. Distribution of Surface Current Range (m $s^{-1}$). Histogram was illustrated using 10 bins. X axis is shown at 10; Y axis is shown at $10^{-3}$.

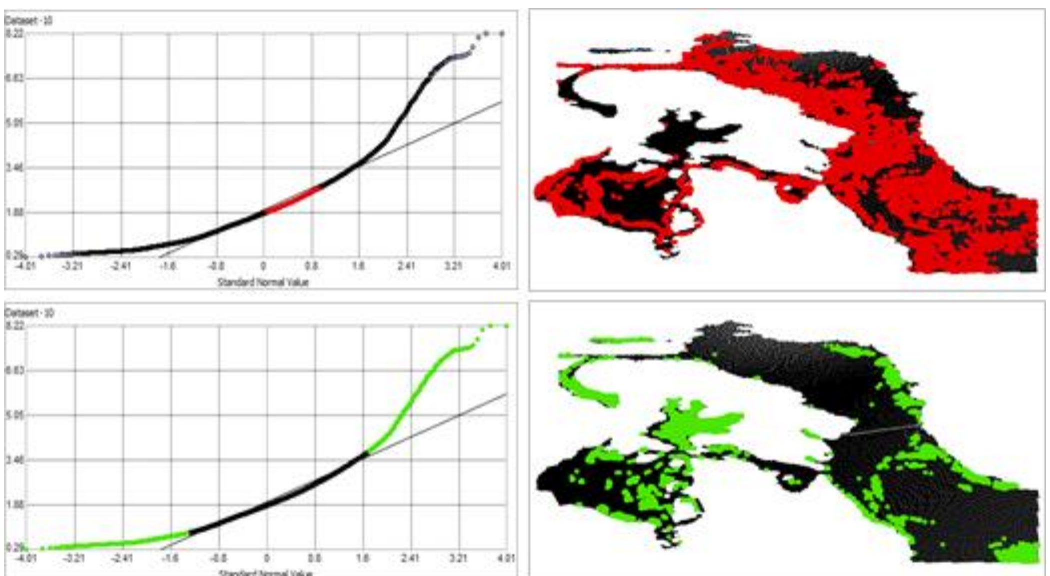


Figure 197. Normal Q-Q plot for data values of Surface Current Range (m $s^{-1}$). Points falling under (top right panel) and over (bottom right panel) the reference line are mapped.

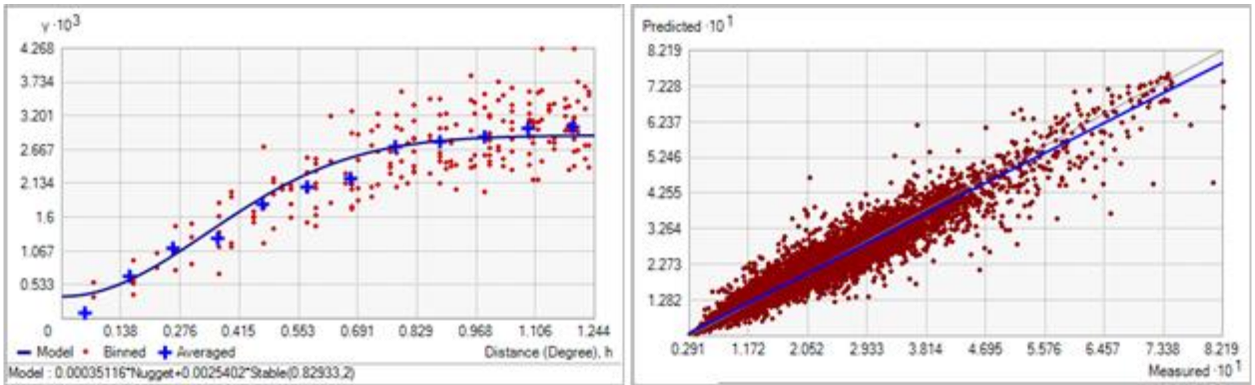


Figure 198. Left panel: Semivariogram of Surface Current Range (m $s^{-1}$). Binned values are shown as red dots; average points are shown as blue crosses; the model fit to the averaged values is shown as a blue line. Lag size: 0.104 degrees; number of lags: 12; Parameter: 2; Range: 0.829 degrees; Partial Sill: 2.540 x $10^{-3}$. Right panel: Scatterplot of predicted values versus observed values for the model of Surface Current Range (m $s^{-1}$).

Table 80. Results of cross-validation of the kriged model for Surface Current Range (m $s^{-1}$).

| **Prediction Error** | **Value** |
|---|---|
| Number of Observations | 16376 |
| Overall Mean Error | -6.828 x $10^{-5}$ |
| Root Mean Square Prediction Error | 0.025 |
| Standardized Mean | -7.758 x $10^{-4}$ |
| Standardized Root Mean Square Prediction Error | 1.110 |
| Average Standard Error | 0.022 |

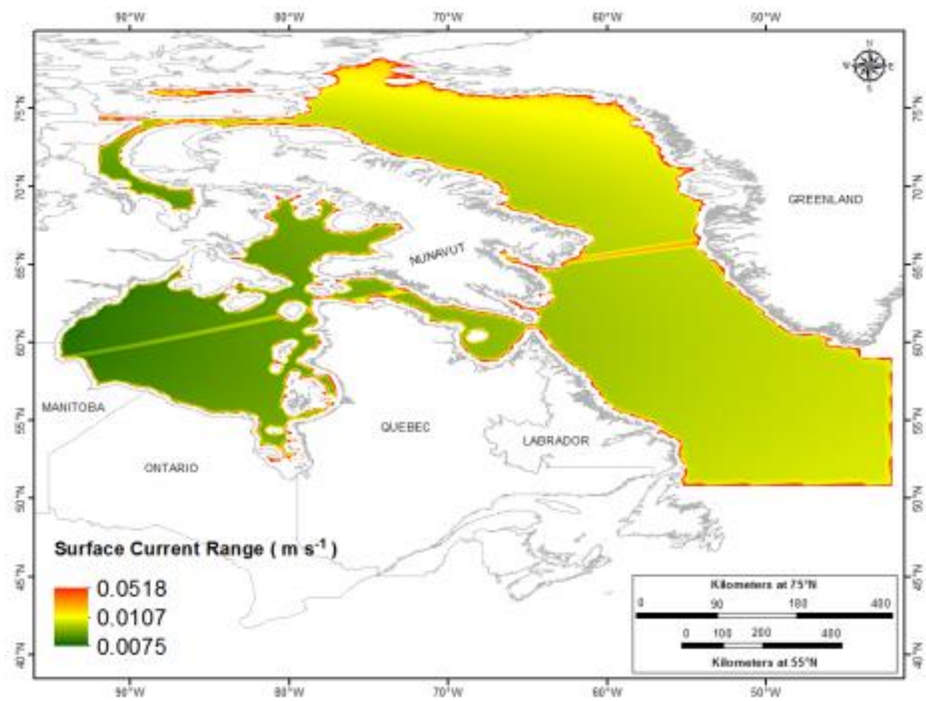


Figure 199. Prediction standard error surface of Surface Current Range (m $s^{-1}$).

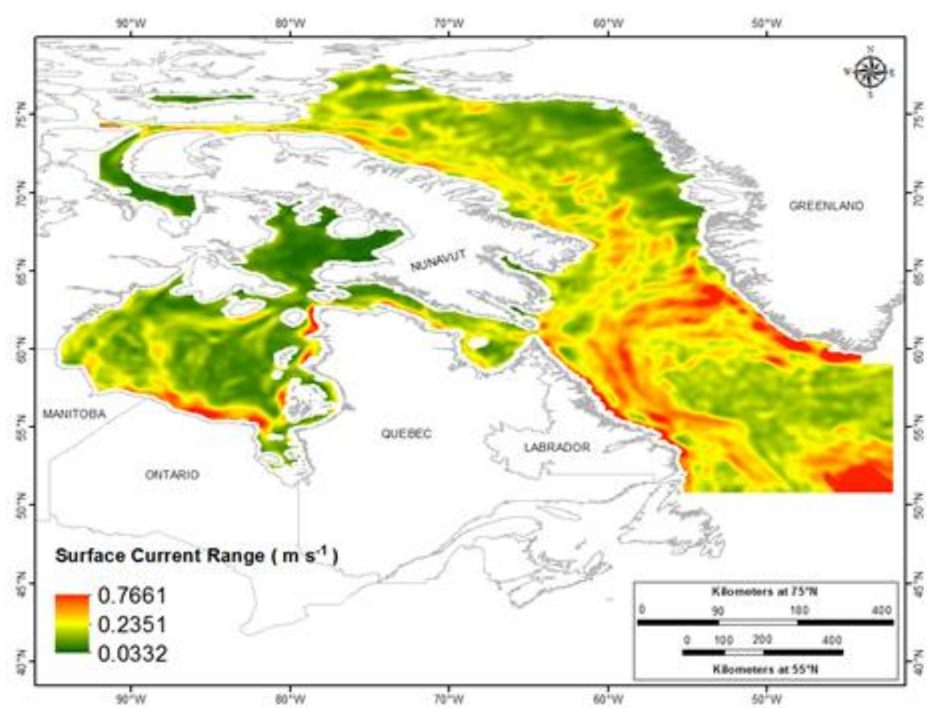


Figure 200. Interpolated prediction surface of Surface Current Range (m $s^{-1}$).

### Surface Current Average Minimum

This variable displayed a right-skewed, extremely leptokurtic distribution prior to interpolation (Table 81, Figure 201). The data were higher than predicted by a normal distribution at both tails, while mid-values were lower than the reference line (Figure 202). These areas of under- and over-prediction showed spatial pattern over the region (Figure 202).

The semivariogram showed moderate autocorrelation present in the data (Figure 203). The kriged model showed good fit between measured and predicted values (Figure 203). Very good performance of the model was indicated by the cross-validation results (Table 82). The error map showed lower error in Hudson Bay compared to Baffin Bay and Davis Strait, and higher error along the edges of the study extent (Figure 204). The kriged surface is presented in Figure 205.

Table 81. Distributional properties of Surface Current Average Minimum (m $s^{-1}$).

| **Property** | **Value** |
|---|---:|
| Number of Observations | 16376 |
| Minimum | $9.790 \times 10^{-4}$ |
| Maximum | 0.471 |
| Mean | 0.026 |
| Median | 0.016 |
| Standard Deviation | 0.035 |
| Skewness | 4.405 |
| Kurtosis | 30.354 |

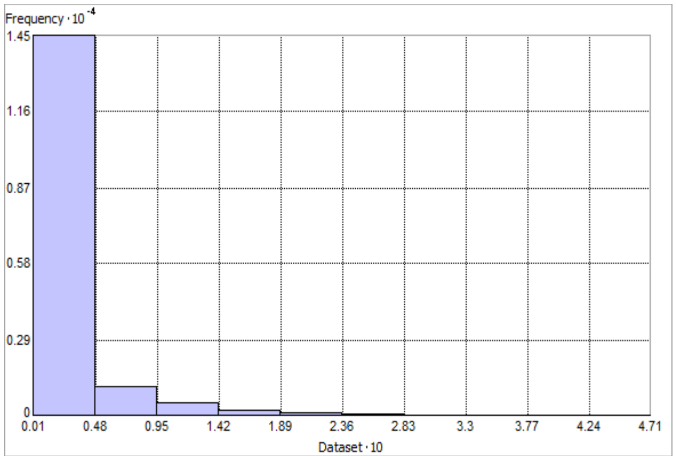


Figure 201. Distribution of Surface Current Average Minimum (m $s^{-1}$). Histogram was illustrated using 10 bins. X axis is shown at 10; Y axis is shown at $10^{-4}$.

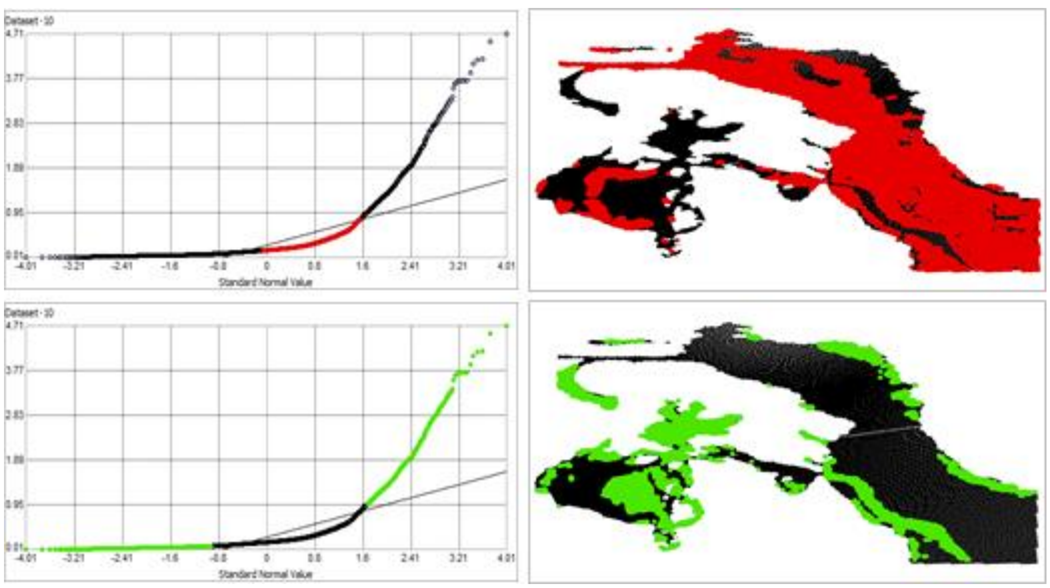

Figure 202. Normal Q-Q plot for data values of Surface Current Average Minimum (m $s^{-1}$). Points falling under (top right panel) and over (bottom right panel) the reference line are mapped.

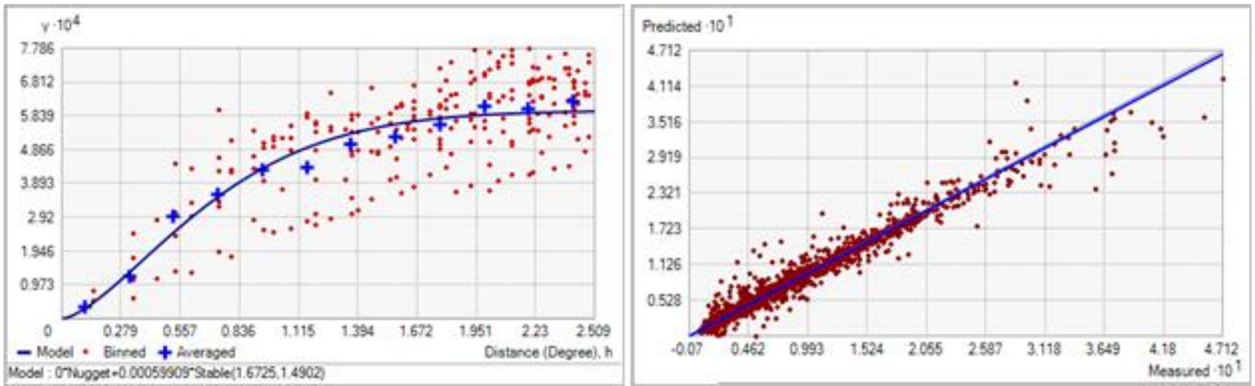


Figure 203. Left panel: Semivariogram of Surface Current Average Minimum (m $s^{-1}$). Binned values are shown as red dots; average points are shown as blue crosses; the model fit to the averaged values is shown as a blue line. Lag size: 0.209 degrees; number of lags: 12; Parameter: 1.490; Range: 1.672 degrees; Partial Sill: 5.991 x $10^{-4}$. Right panel: Scatterplot of predicted values versus observed values for the model of Surface Current Average Minimum (m $s^{-1}$).

Table 82. Results of cross-validation of the kriged model for Surface Current Average Minimum (m $s^{-1}$).

| Prediction Error | Value |
|---|---|
| Number of Observations | 16376 |
| Overall Mean Error | 1.453 x $10^{-6}$ |
| Root Mean Square Prediction Error | 5.123 x $10^{-3}$ |
| Standardized Mean | 1.396 x $10^{-4}$ |
| Standardized Root Mean Square Prediction Error | 0.930 |
| Average Standard Error | 5.206 x $10^{-3}$ |

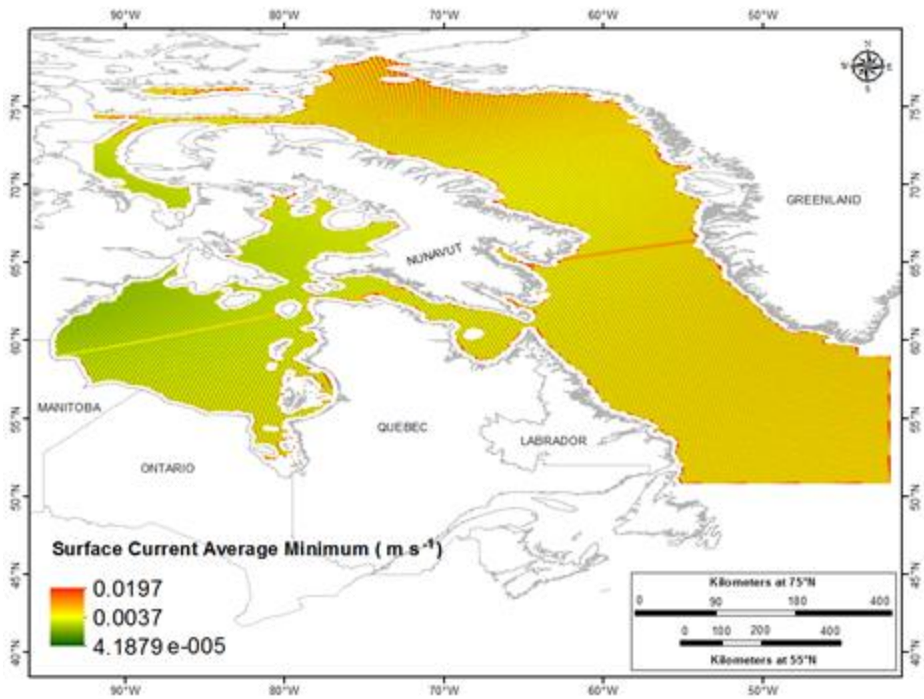


Figure 204. Prediction standard error surface of Surface Current Average Minimum (m $s^{-1}$).

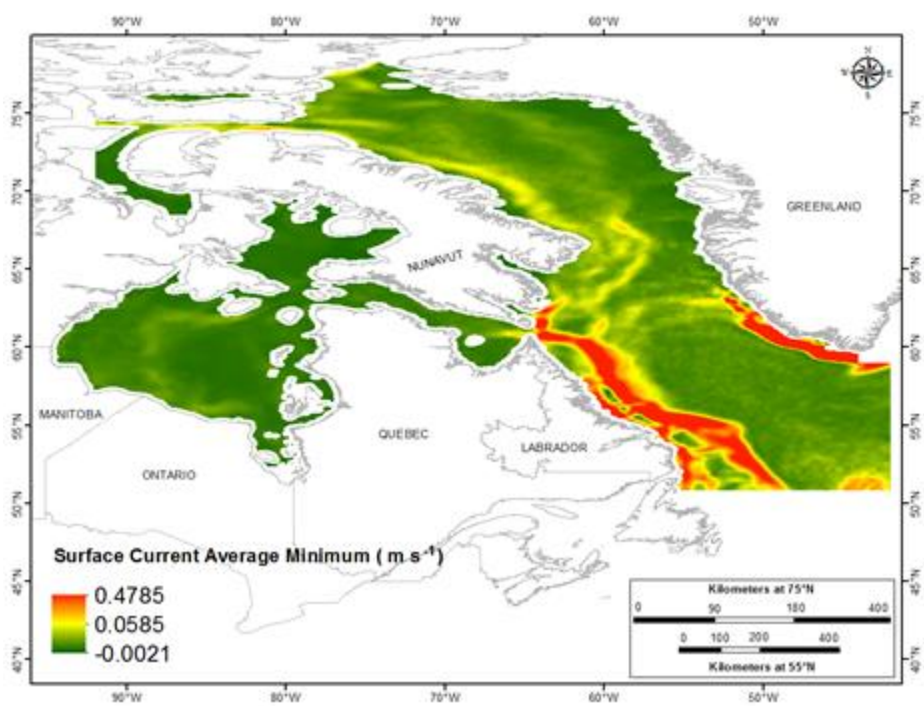


Figure 205. Interpolated prediction surface of Surface Current Average Minimum (m $s^{-1}$).

### Surface Current Average Maximum

This variable displayed a right-skewed, leptokurtic distribution prior to interpolation (Table 83, Figure 206). The data were higher than predicted by a normal distribution at both tails, while mid-values were lower than the reference line (Figure 207). These areas of under- and over-prediction showed spatial pattern over the region (Figure 207).

The semivariogram showed autocorrelation present in the data (Figure 208). The kriged model showed good fit between measured and predicted values (Figure 208). Very good performance of the model was indicated by the cross-validation results (Table 84). The error map showed lower error in Hudson Bay compared to Baffin Bay and Davis Strait, and higher error along the edges of the study extent (Figure 209). The kriged surface is presented in Figure 210.

Table 83. Distributional properties of Surface Current Average Maximum (m $s^{-1}$).

| **Property** | **Value** |
|---|---:|
| Number of Observations | 16376 |
| Minimum | 0.019 |
| Maximum | 0.832 |
| Mean | 0.136 |
| Median | 0.118 |
| Standard Deviation | 0.080 |
| Skewness | 2.035 |
| Kurtosis | 9.934 |

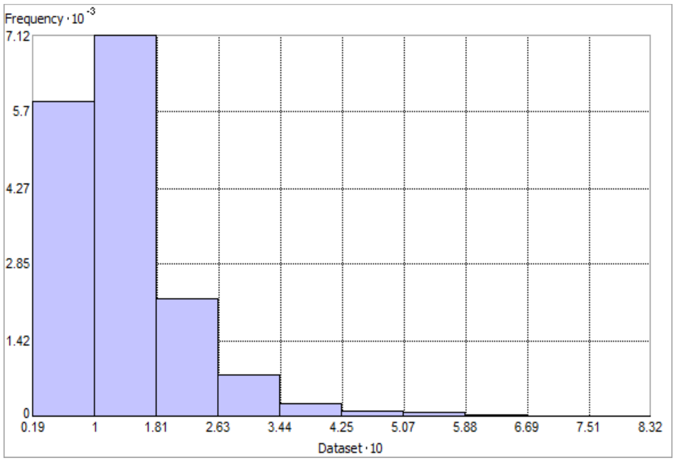

Figure 206. Distribution of Surface Current Average Maximum (m $s^{-1}$). Histogram was illustrated using 10 bins. X axis is shown at 10; Y axis is shown at $10^{-3}$.

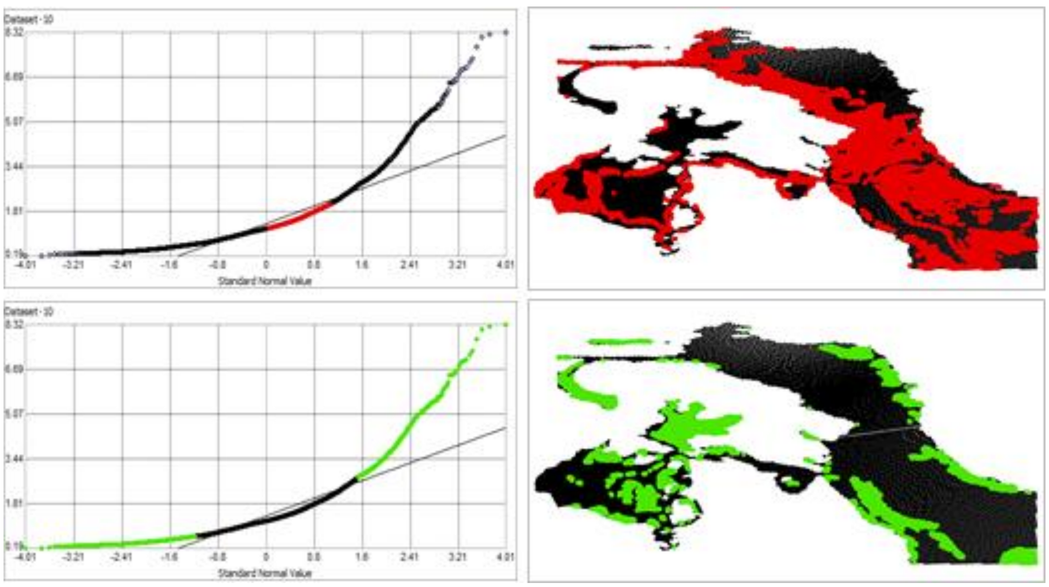
Figure 207. Normal Q-Q plot for data values of Surface Current Average Maximum (m $s^{-1}$). Points falling under (top right panel) and over (bottom right panel) the reference line are mapped.

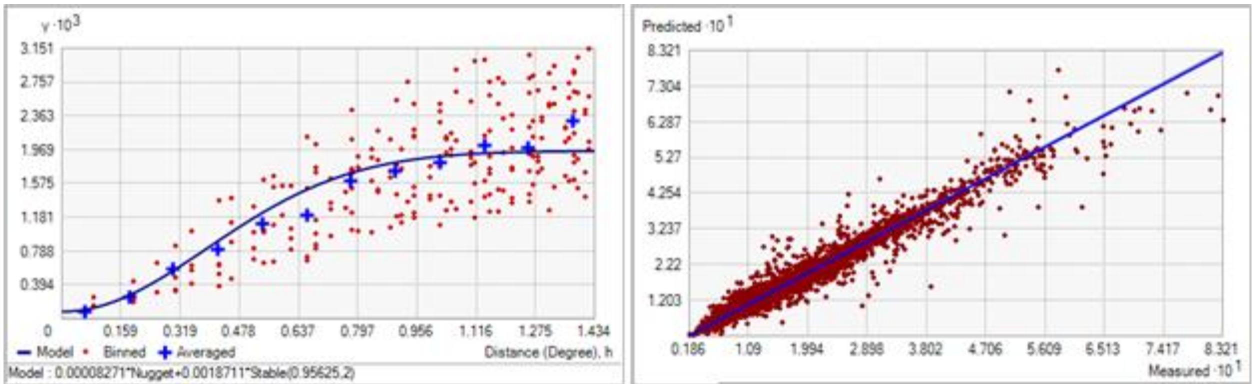

Figure 208. Left panel: Semivariogram of Surface Current Average Maximum (m $s^{-1}$). Binned values are shown as red dots; average points are shown as blue crosses; the model fit to the averaged values is shown as a blue line. Lag size: 0.120 degrees; number of lags: 12; Parameter: 2; Range: 0.956 degrees; Partial Sill: 1.871 x $10^{-3}$. Right panel: Scatterplot of predicted values versus observed values for the model of Surface Current Average Maximum (m $s^{-1}$).

Table 84. Results of cross-validation of the kriged model for Surface Current Average Maximum (m $s^{-1}$).

| **Prediction Error** | **Value** |
|---|---|
| Number of Observations | 16376 |
| Overall Mean Error | -4.683 x $10^{-5}$ |
| Root Mean Square Prediction Error | 0.013 |
| Standardized Mean | -8.298 x $10^{-4}$ |
| Standardized Root Mean Square Prediction Error | 1.093 |
| Average Standard Error | 0.011 |

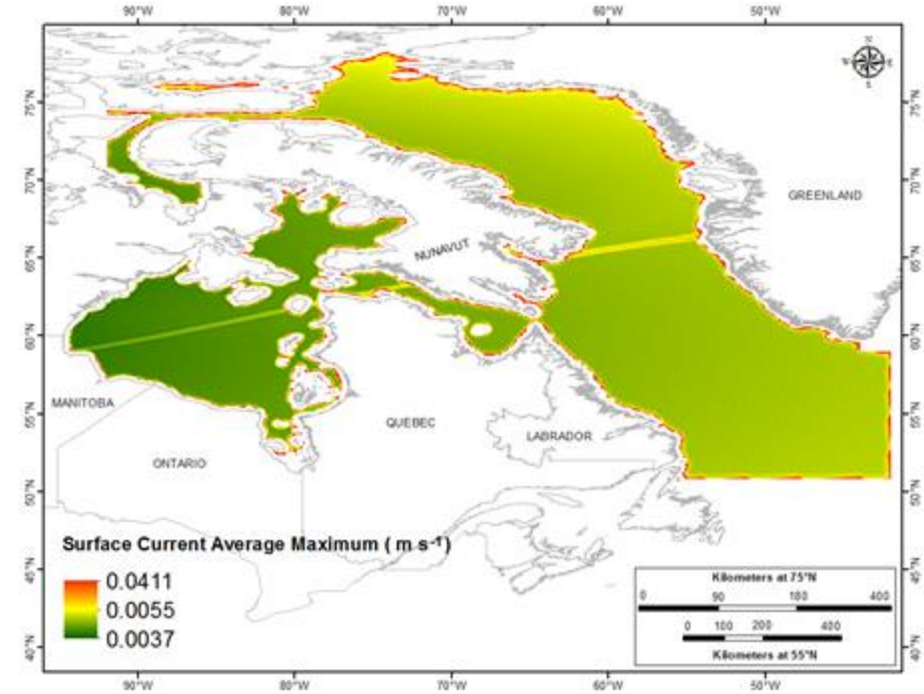


Figure 209. Prediction standard error surface of Surface Current Average Maximum (m $s^{-1}$).

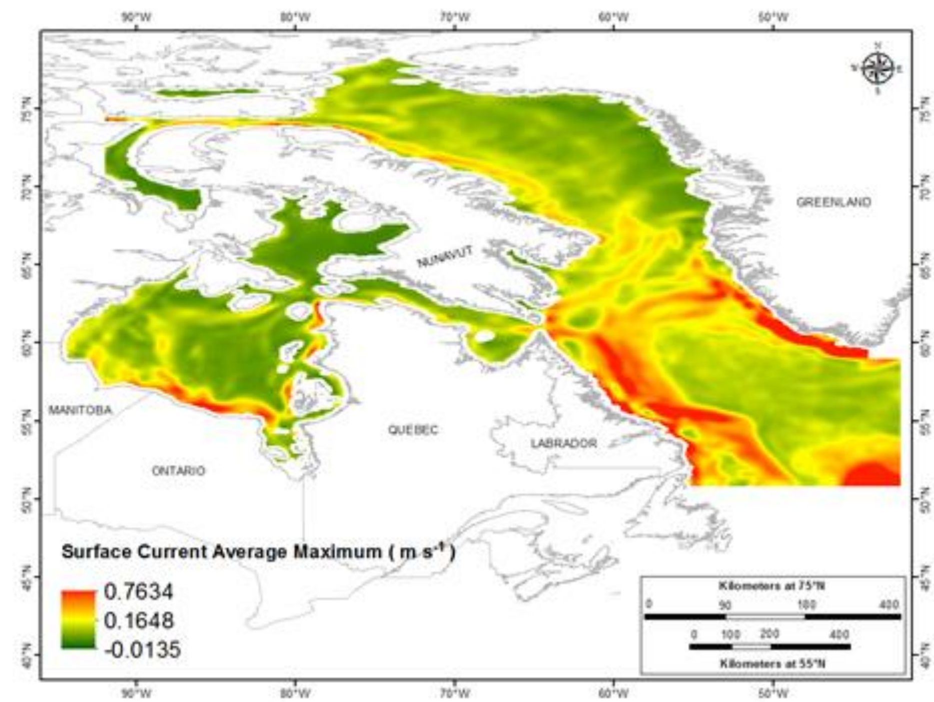


Figure 210. Interpolated prediction surface of Surface Current Average Maximum (m $s^{-1}$).

**Surface Current Average Range**

This variable displayed a right-skewed, leptokurtic distribution prior to interpolation (Table 85, Figure 211). The data were higher than predicted by a normal distribution at both tails, while mid-values were lower than the reference line (Figure 212). These areas of under- and over-prediction showed spatial pattern over the region (Figure 212).

The semivariogram showed autocorrelation present in the data (Figure 213). The kriged model showed good fit between measured and predicted values (Figure 213). Very good performance of the model was indicated by the cross-validation results (Table 86). The error map showed lower error in Hudson Bay compared to Baffin Bay and Davis Strait, and higher error along the edges of the study extent (Figure 214). The kriged surface is presented in Figure 215.

Table 85. Distributional properties of Surface Current Average Range (m $s^{-1}$).

| **Property** | **Value** |
|---|---|
| Number of Observations | 16376 |
| Minimum | 0.017 |
| Maximum | 0.499 |
| Mean | 0.110 |
| Median | 0.100 |
| Standard Deviation | 0.057 |
| Skewness | 1.748 |
| Kurtosis | 8.632 |

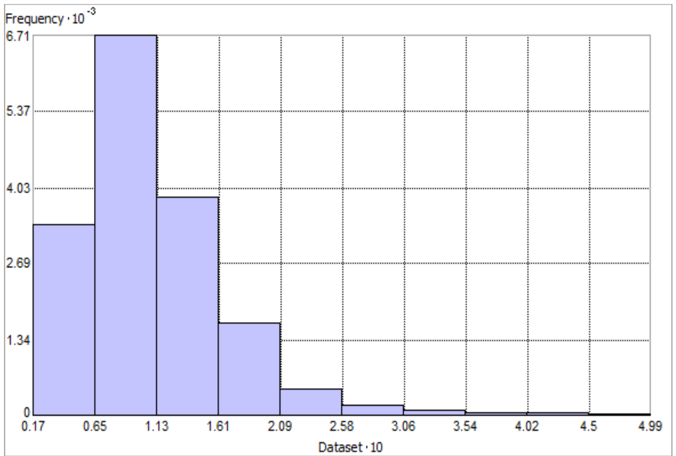


Figure 211. Distribution of Surface Current Average Range (m $s^{-1}$). Histogram was illustrated using 10 bins. X axis is shown at 10; Y axis is shown at $10^{-3}$.

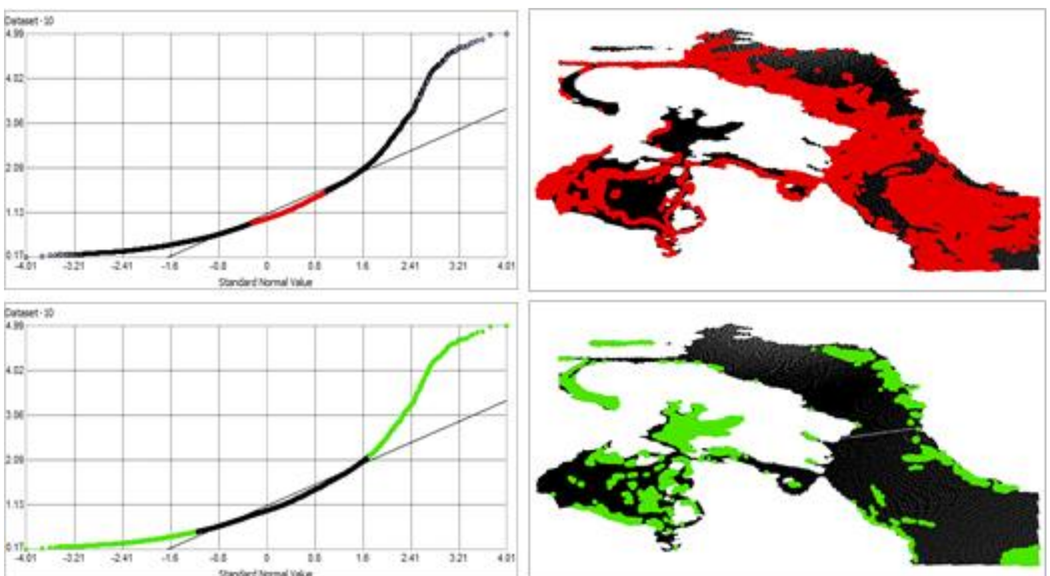

Figure 212. Normal Q-Q plot for data values of Surface Current Average Range (m $s^{-1}$). Points falling under (top right panel) and over (bottom right panel) the reference line are mapped.

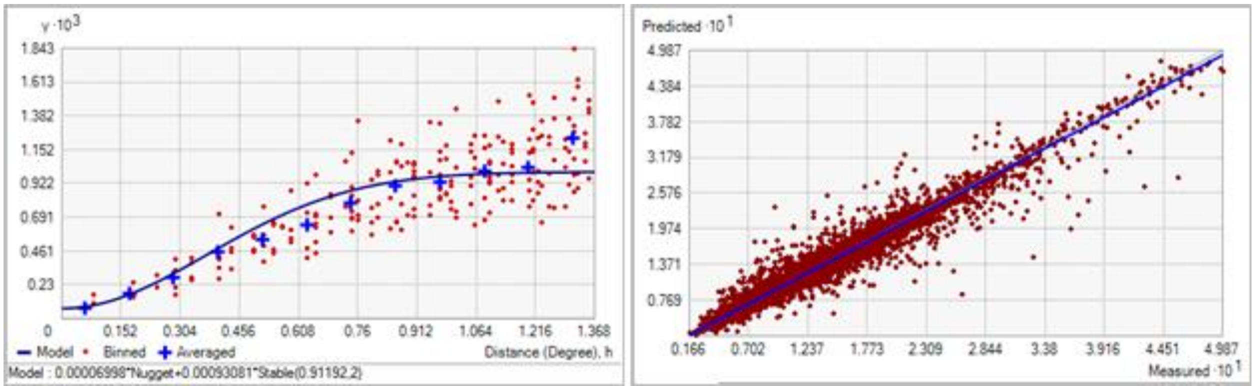


Figure 213. Left panel: Semivariogram of Surface Current Average Range (m $s^{-1}$). Binned values are shown as red dots; average points are shown as blue crosses; the model fit to the averaged values is shown as a blue line. Lag size: 0.114 degrees; number of lags: 12; Parameter: 2; Range: 0.912 degrees; Partial Sill: $9.308 \times 10^{-4}$. Right panel: Scatterplot of predicted values versus observed values for the model of Surface Current Average Range (m $s^{-1}$).

Table 86. Results of cross-validation of the kriged model for Surface Current Average Range (m $s^{-1}$).

| **Prediction Error** | **Value** |
|---|---:|
| Number of Observations | 16376 |
| Overall Mean Error | $-4.803 \times 10^{-5}$ |
| Root Mean Square Prediction Error | 0.011 |
| Standardized Mean | $-1.023 \times 10^{-3}$ |
| Standardized Root Mean Square Prediction Error | 0.997 |
| Average Standard Error | 0.010 |

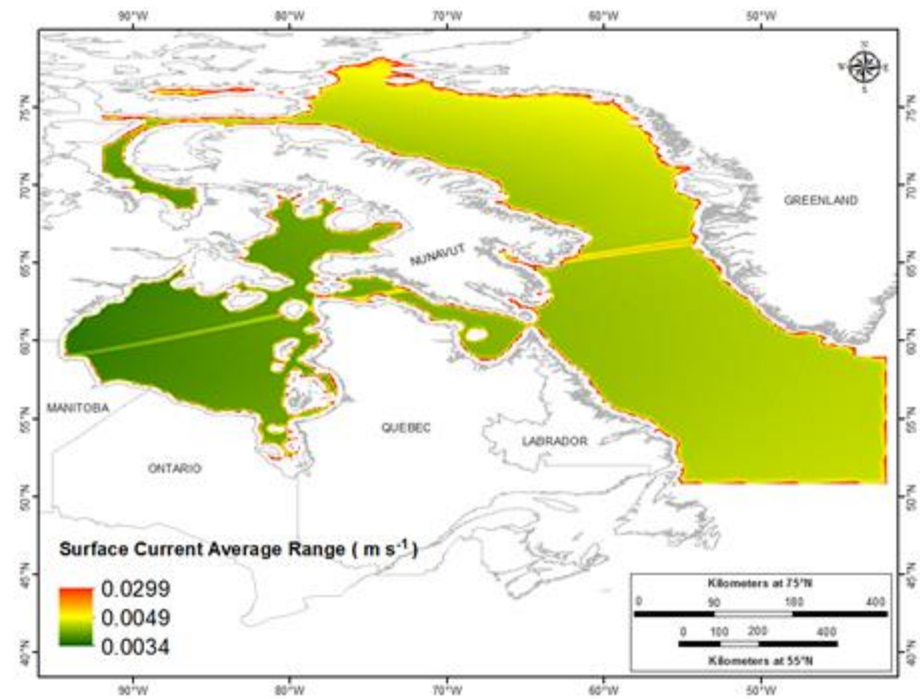


Figure 214. Prediction standard error surface of Surface Current Average Range (m $s^{-1}$).

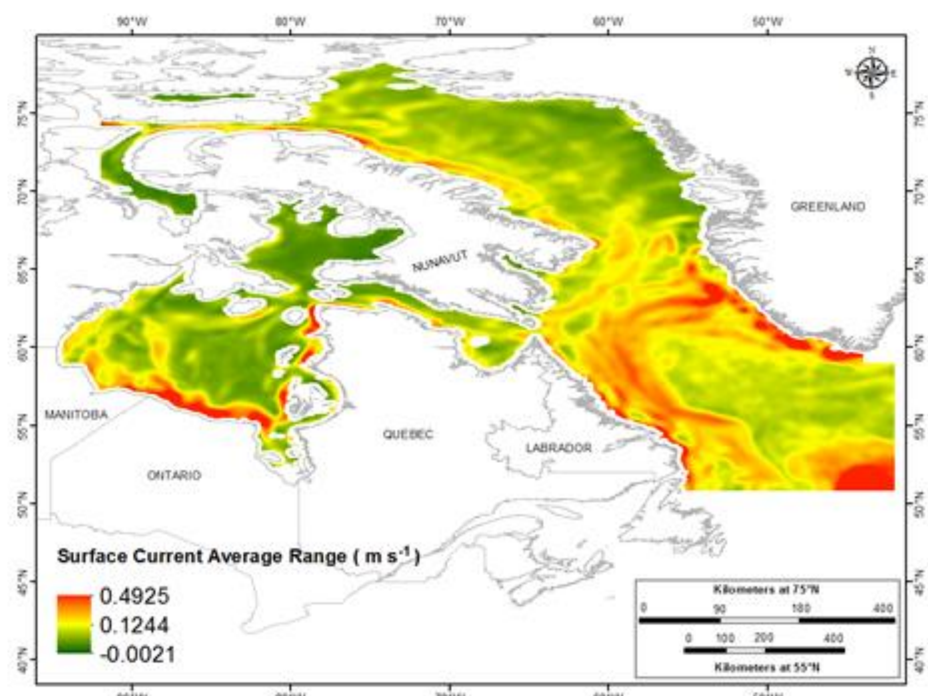


Figure 215. Interpolated prediction surface of Surface Current Average Range (m $s^{-1}$).

## Bottom Shear

Bottom shear stress reflects friction pressure on the seabed. Its unit is Pa or pascal, which is equivalent to one newton (1 N) of force over one meter squared. Shear stress near the seabed causes sediment erosion and affects vertical mixing and conditions conducive to sediment deposition (Cheng et al., 1999).

### Bottom Shear Mean

This variable displayed a right-skewed, extremely leptokurtic distribution prior to interpolation (Table 87, Figure 216). The data were higher than predicted by a normal distribution at both tails, while mid-values were slightly lower than the reference line (Figure 217). These areas of under- and over-prediction showed little spatial pattern over the region (Figure 217).

The semivariogram showed very weak autocorrelation present in the data (Figure 218). The kriged model showed poor fit between measured and predicted values (Figure 218). Very good performance of the model was indicated by the cross-validation results (Table 88). The error map showed lower error in Hudson Bay compared to Baffin Bay and Davis Strait, and higher error along the edges of the study extent (Figure 219). The kriged surface is presented in Figure 220.

Table 87. Distributional properties of Bottom Shear Mean (Pa).

| **Property** | **Value** |
|---|---:|
| Number of Observations | 16257 |
| Minimum | $1.080 \times 10^{-4}$ |
| Maximum | 0.278 |
| Mean | 0.010 |
| Median | $6.303 \times 10^{-3}$ |
| Standard Deviation | 0.014 |
| Skewness | 5.939 |
| Kurtosis | 67.933 |

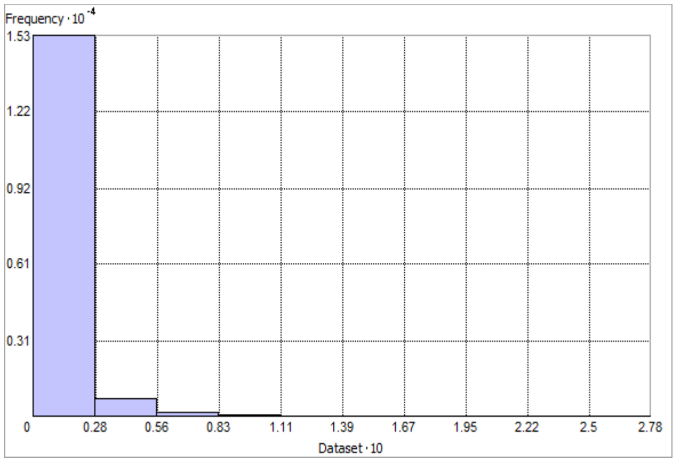


Figure 216. Distribution of Bottom Shear Mean (Pa). Histogram was illustrated using 10 bins. X axis is shown at 10; Y axis is shown at $10^{-4}$.

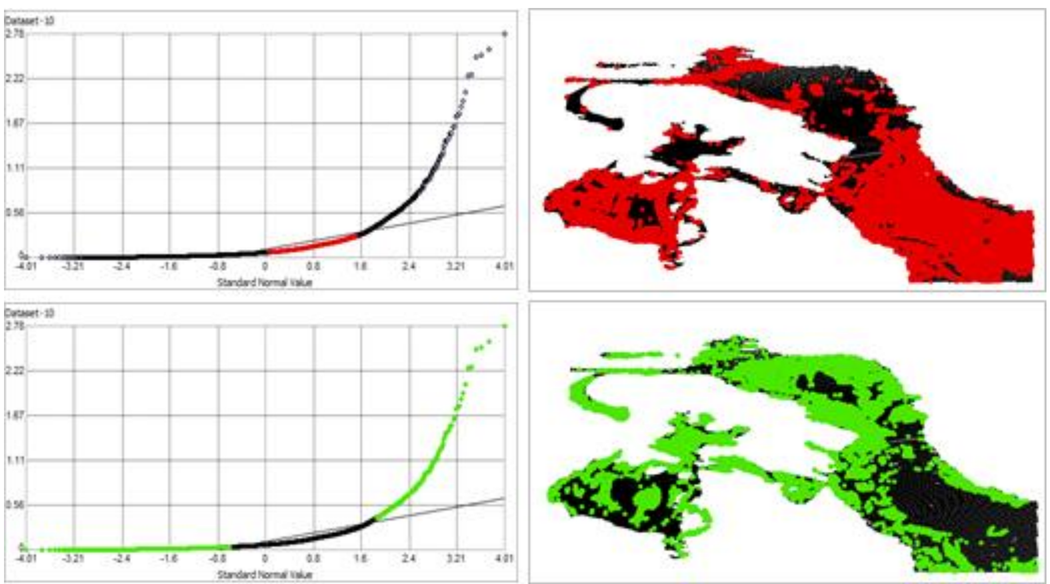

Figure 217. Normal Q-Q plot for data values of Bottom Shear Mean (Pa). Points falling under (top right panel) and over (bottom right panel) the reference line are mapped.

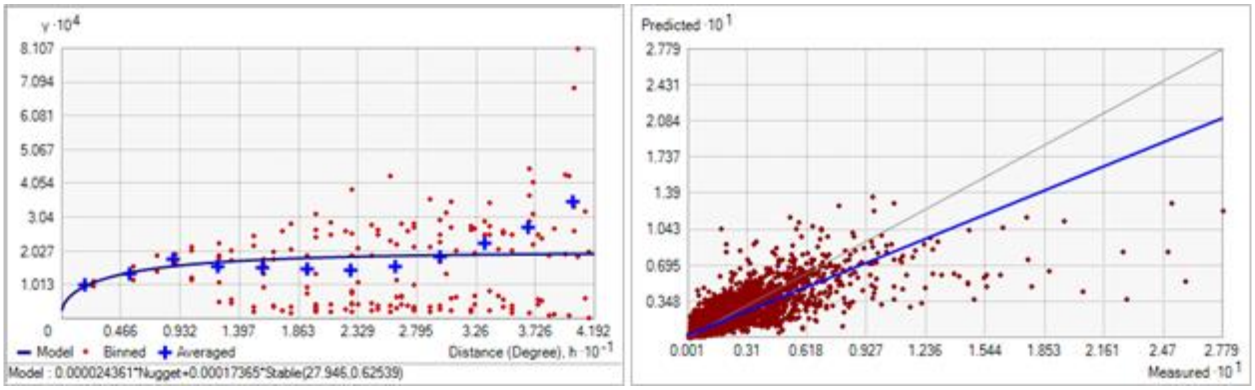


Figure 218. Left panel: Semivariogram of Bottom Shear Mean (Pa). Binned values are shown as red dots; average points are shown as blue crosses; the model fit to the averaged values is shown as a blue line. Lag size: 3.493 degrees; number of lags: 12; Parameter: 0.625; Range: 27.946 degrees; Partial Sill: 1.737 x $10^{-4}$. Right panel: Scatterplot of predicted values versus observed values for the model of Bottom Shear Mean (Pa).

Table 88. Results of cross-validation of the kriged model for Bottom Shear Mean (Pa).

| **Prediction Error** | **Value** |
|---|---:|
| Number of Observations | 16257 |
| Overall Mean Error | 1.436 x $10^{-6}$ |
| Root Mean Square Prediction Error | 7.488 x $10^{-3}$ |
| Standardized Mean | 1.278 x $10^{-4}$ |
| Standardized Root Mean Square Prediction Error | 1.065 |
| Average Standard Error | 6.939 x $10^{-3}$ |

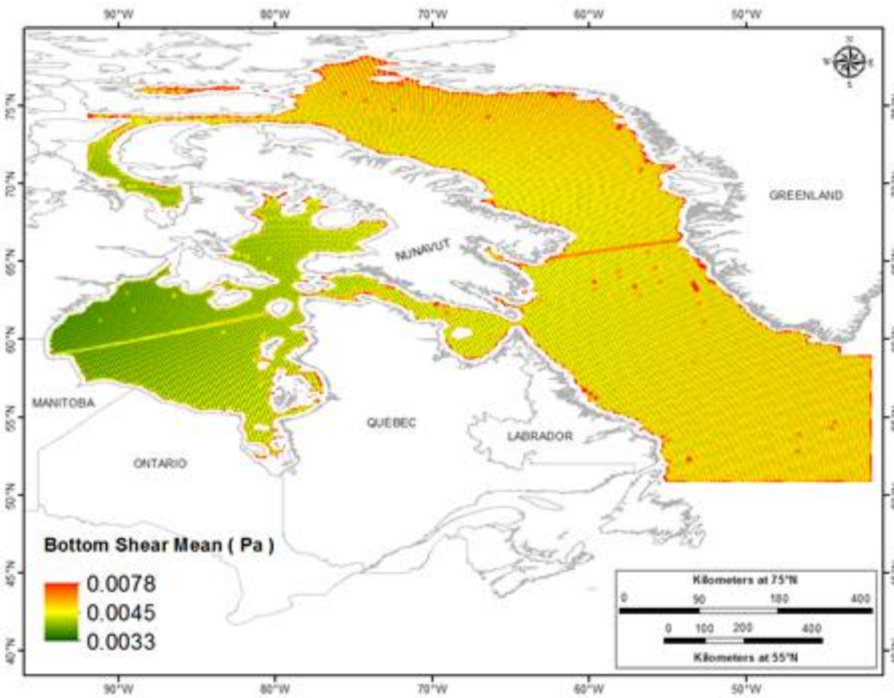


Figure 219. Prediction standard error surface of Bottom Shear Mean (Pa).

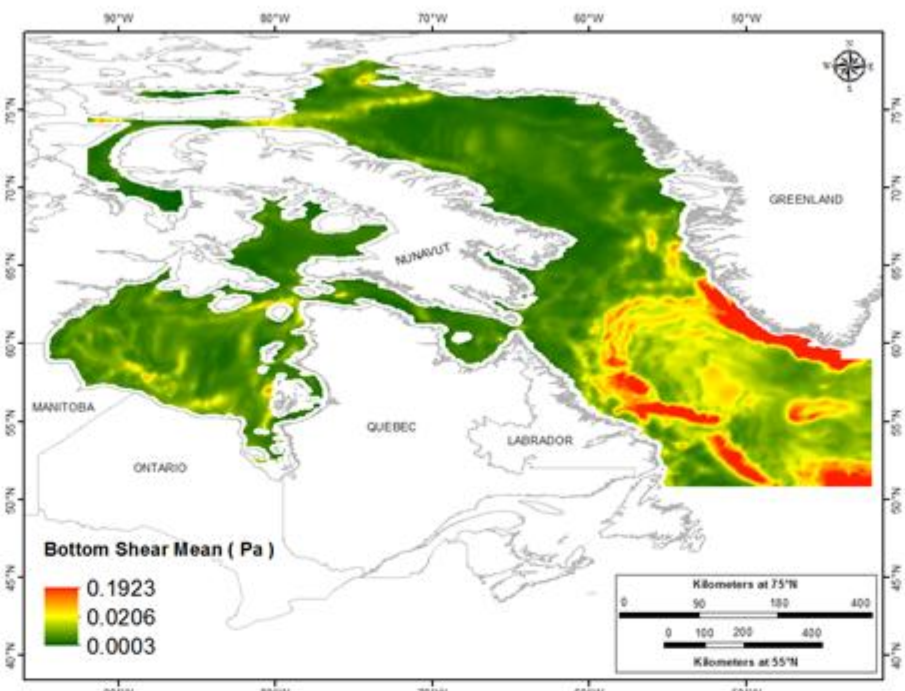


Figure 220. Interpolated prediction surface of Bottom Shear Mean (Pa).

## Bottom Shear Minimum

This variable displayed a right-skewed, extremely leptokurtic distribution prior to interpolation (Table 89, Figure 221). The data were higher than predicted by a normal distribution at both tails, while mid-values were lower than the reference line (Figure 222). These areas of under- and over-prediction showed little spatial pattern over the region (Figure 222).

The semivariogram showed moderate autocorrelation present in the data (Figure 223). The kriged model showed poor fit between measured and predicted values (Figure 223). Good performance of the model was indicated by the cross-validation results (Table 90). The error map showed lower error in Hudson Bay compared to Baffin Bay and Davis Strait, and higher error along the edges of the study extent (Figure 224). The kriged surface is presented in Figure 225.

Table 89. Distributional properties of Bottom Shear Minimum (Pa).

| **Property** | **Value** |
|---|---:|
| Number of Observations | 16257 |
| Minimum | $1.00 \times 10^{-6}$ |
| Maximum | 0.095 |
| Mean | $9.440 \times 10^{-4}$ |
| Median | $2.210 \times 10^{-4}$ |
| Standard Deviation | $3.451 \times 10^{-3}$ |
| Skewness | 10.587 |
| Kurtosis | 176.440 |

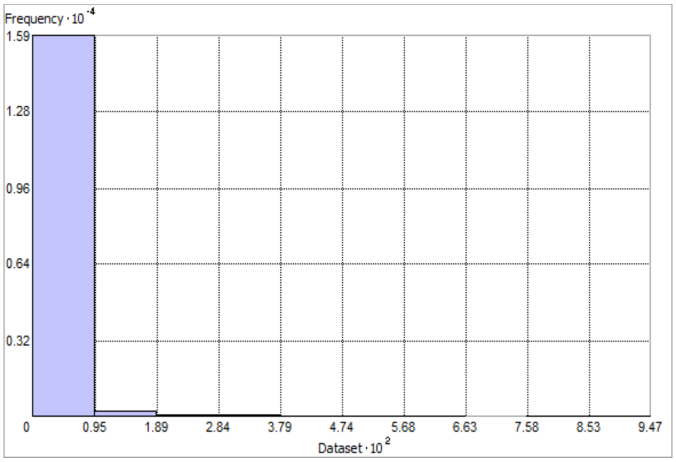


Figure 221. Distribution of Bottom Shear Minimum (Pa). Histogram was illustrated using 10 bins. X axis is shown at $10^2$; Y axis is shown at $10^{-4}$.

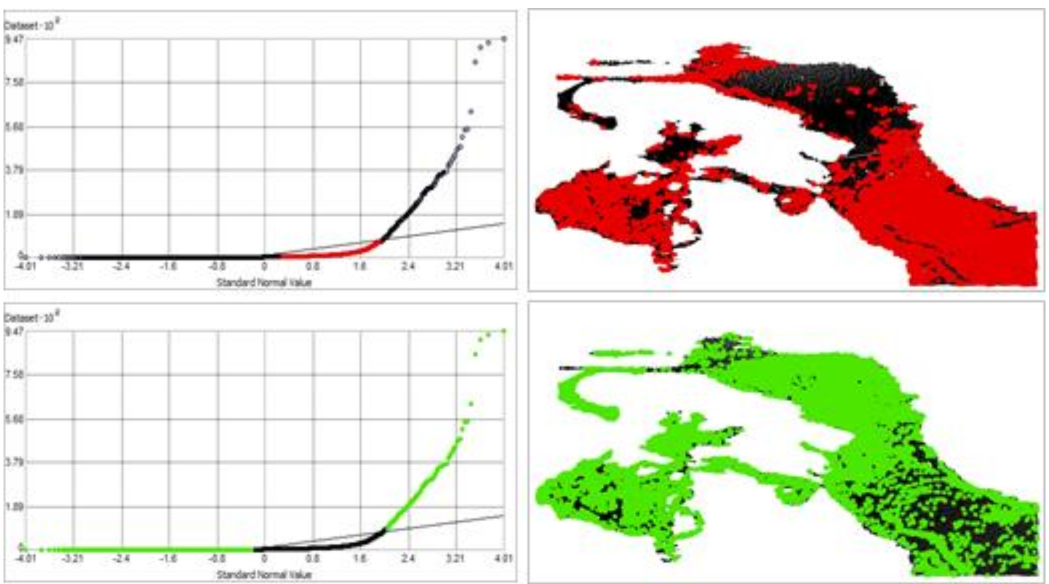

Figure 222. Normal Q-Q plot for data values of Bottom Shear Minimum (Pa). Points falling under (top right panel) and over (bottom right panel) the reference line are mapped.

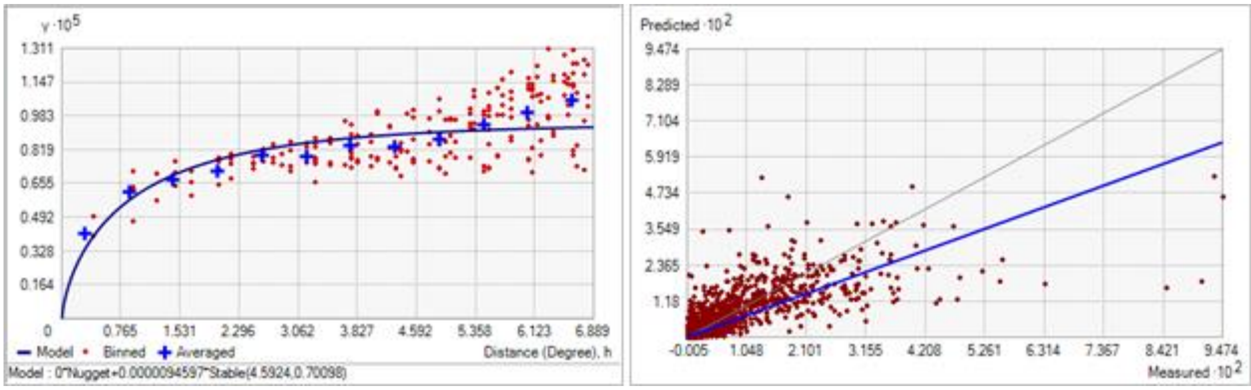


Figure 223. Left panel: Semivariogram of Bottom Shear Minimum (Pa). Binned values are shown as red dots; average points are shown as blue crosses; the model fit to the averaged values is shown as a blue line. Lag size: 0.574 degrees; number of lags: 12; Parameter: 0.701; Range: 4.592 degrees; Partial Sill: 9.460 x $10^{-6}$. Right panel: Scatterplot of predicted values versus observed values for the model of Bottom Shear Minimum (Pa).

Table 90. Results of cross-validation of the kriged model for Bottom Shear Minimum (Pa).

| **Prediction Error** | **Value** |
|---|---|
| Number of Observations | 16257 |
| Overall Mean Error | 2.495 x $10^{-6}$ |
| Root Mean Square Prediction Error | 1.995 x $10^{-3}$ |
| Standardized Mean | 8.883 x $10^{-4}$ |
| Standardized Root Mean Square Prediction Error | 1.243 |
| Average Standard Error | 1.567 x $10^{-3}$ |

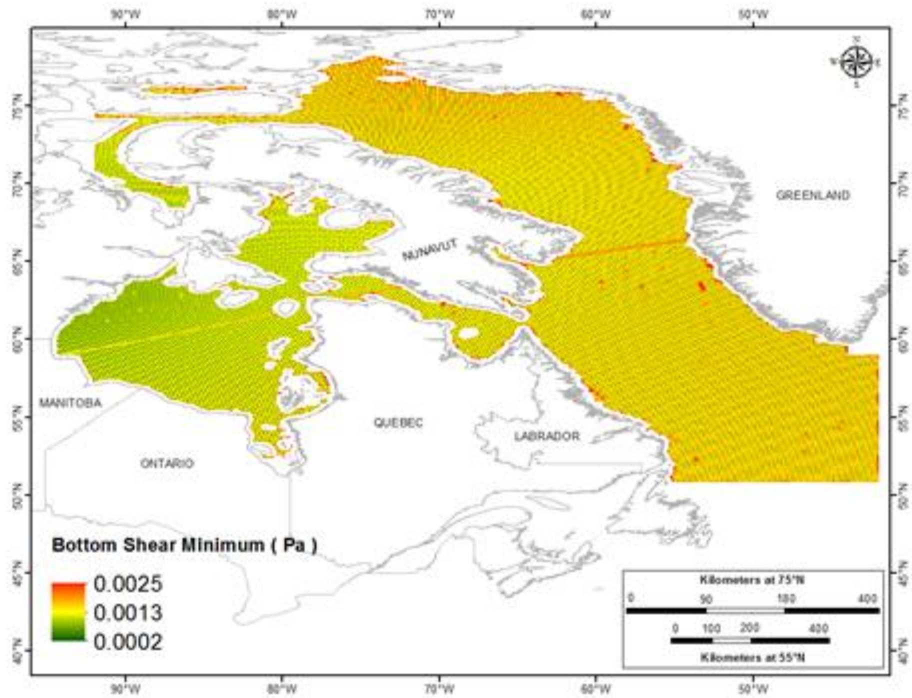


Figure 224. Prediction standard error surface of Bottom Shear Minimum (Pa).

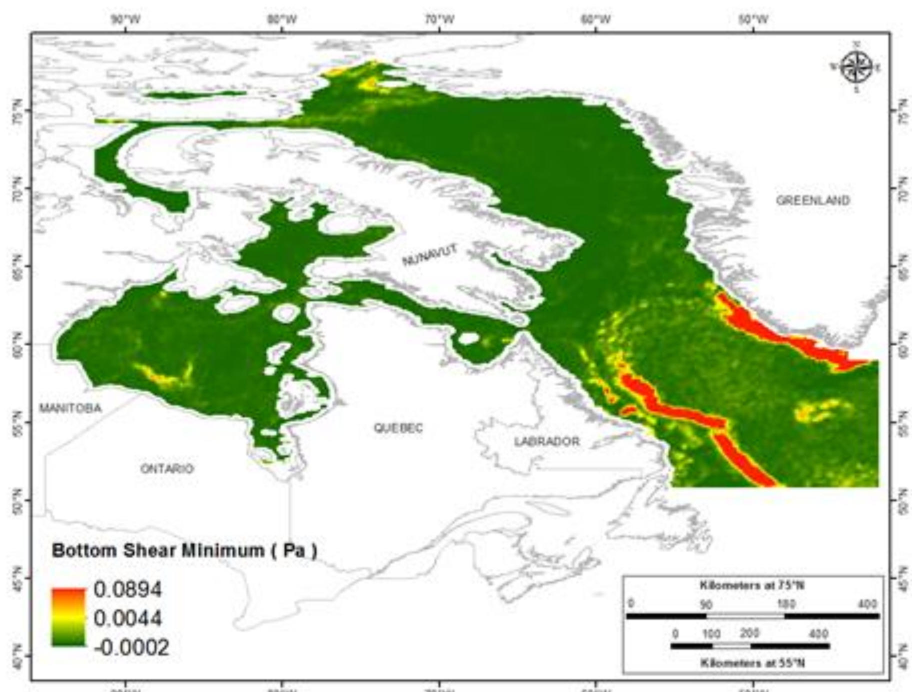


Figure 225. Interpolated prediction surface of Bottom Shear Minimum (Pa).

**Bottom Shear Maximum**

This variable displayed a right-skewed, leptokurtic distribution prior to interpolation (Table 91, Figure 226). The data were higher than predicted by a normal distribution at both tails, while mid-values were slightly lower than the reference line (Figure 227). These areas of under- and over-prediction showed little spatial pattern over the region (Figure 227).

The semivariogram showed moderate autocorrelation present in the data (Figure 228). The kriged model showed poor fit between measured and predicted values (Figure 228). Very good performance of the model was indicated by the cross-validation results (Table 92). The error map showed lower error in Hudson Bay compared to Baffin Bay and Davis Strait, and higher error along the edges of the study extent (Figure 229). The kriged surface is presented in Figure 230.

Table 91. Distributional properties of Bottom Shear Maximum (Pa).

| **Property** | **Value** |
|---|---:|
| Number of Observations | 16257 |
| Minimum | $4.570 \times 10^{-4}$ |
| Maximum | 1.249 |
| Mean | 0.044 |
| Median | 0.026 |
| Standard Deviation | 0.053 |
| Skewness | 4.105 |
| Kurtosis | 39.871 |

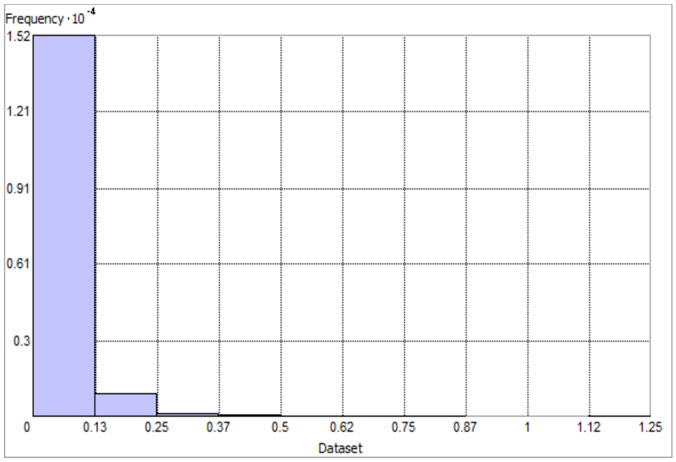

Figure 226. Distribution of Bottom Shear Maximum (Pa). Histogram was illustrated using 10 bins. Y axis is shown at $10^{-4}$.

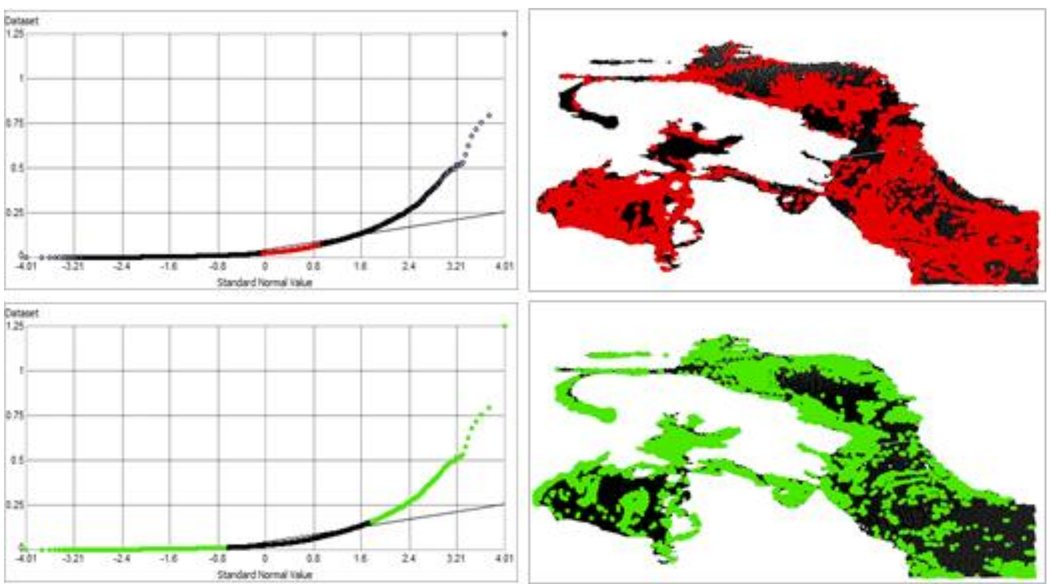

Figure 227. Normal Q-Q plot for data values of Bottom Shear Maximum (Pa). Points falling under (top right panel) and over (bottom right panel) the reference line are mapped.

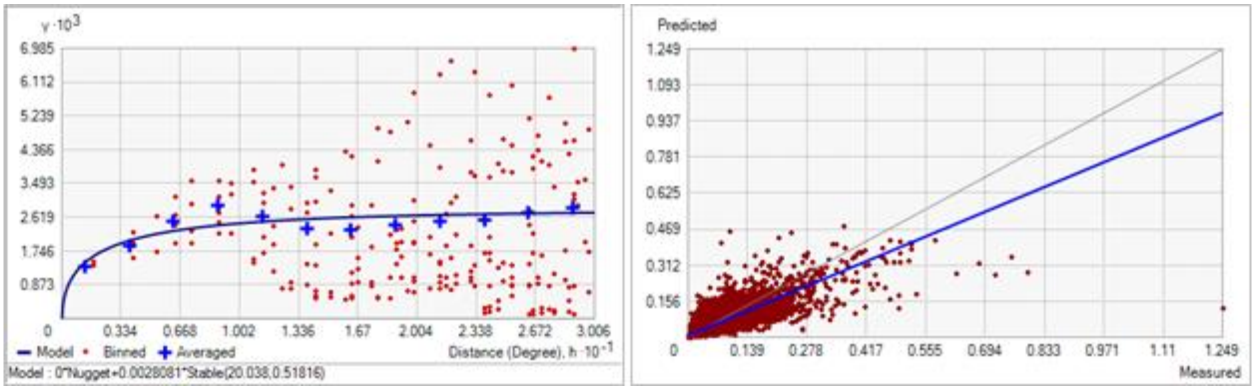


Figure 228. Left panel: Semivariogram of Bottom Shear Maximum (Pa). Binned values are shown as red dots; average points are shown as blue crosses; the model fit to the averaged values is shown as a blue line. Lag size: 2.505 degrees; number of lags: 12; Parameter: 0.518; Range: 20.038 degrees; Partial Sill: $2.808 \times 10^{-3}$. Right panel: Scatterplot of predicted values versus observed values for the model of Bottom Shear Maximum (Pa).

Table 92. Results of cross-validation of the kriged model for Bottom Shear Maximum (Pa).

| **Prediction Error** | **Value** |
|---|---:|
| Number of Observations | 16257 |
| Overall Mean Error | $-1.514 \times 10^{-5}$ |
| Root Mean Square Prediction Error | 0.029 |
| Standardized Mean | $-3.175 \times 10^{-4}$ |
| Standardized Root Mean Square Prediction Error | 1.082 |
| Average Standard Error | 0.026 |

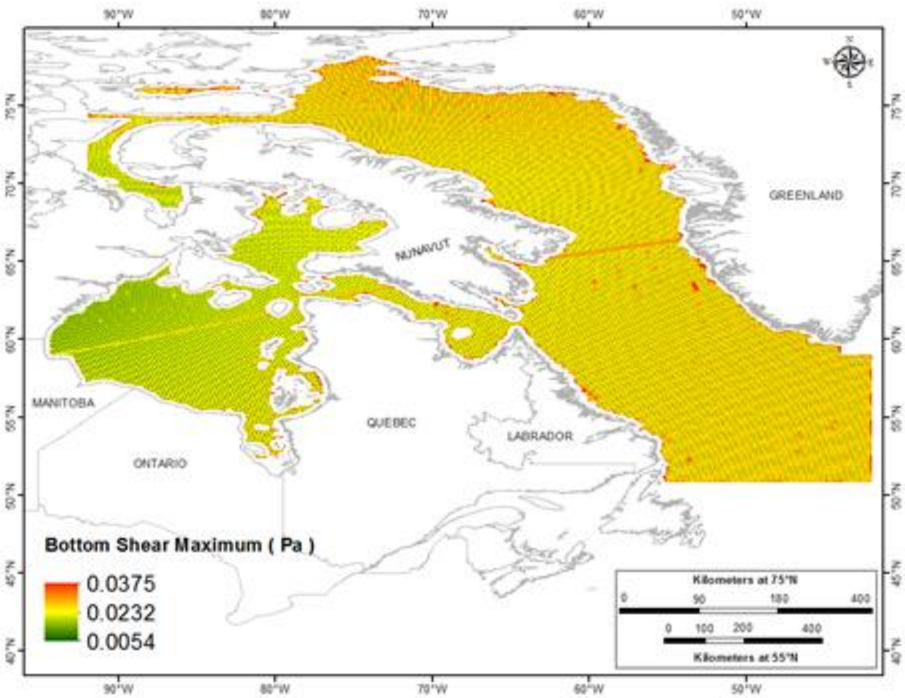


Figure 229. Prediction standard error surface of Bottom Shear Maximum (Pa).

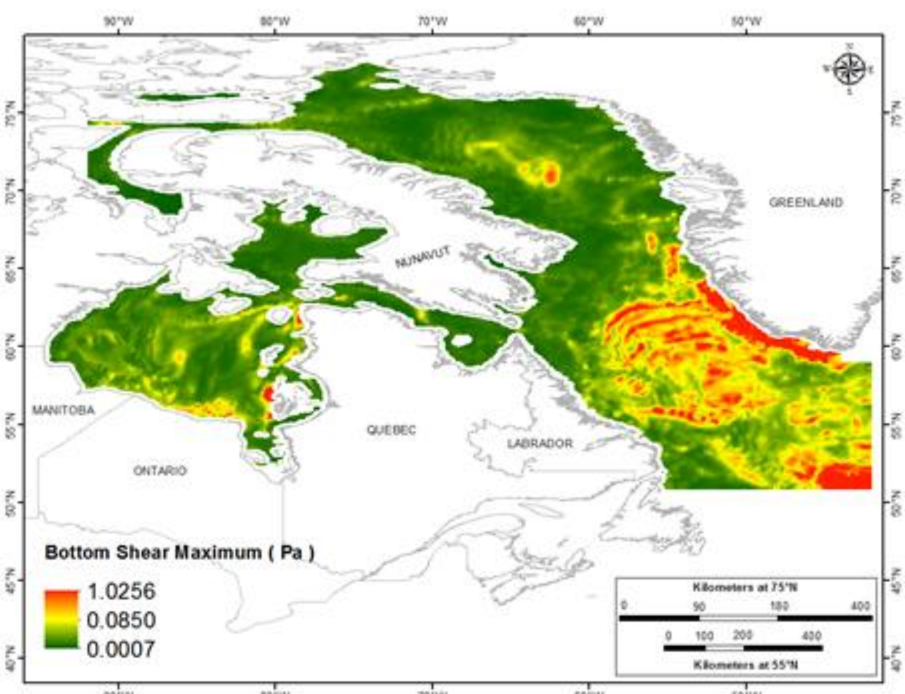


Figure 230. Interpolated prediction surface of Bottom Shear Maximum (Pa).

## Bottom Shear Range

This variable displayed a right-skewed, leptokurtic distribution prior to interpolation (Table 93, Figure 231). The data were higher than predicted by a normal distribution at both tails, while mid-values were lower than the reference line (Figure 232). These areas of under- and over-prediction showed little spatial pattern over the region (Figure 232).

The semivariogram showed moderate autocorrelation present in the data (Figure 233). The kriged model showed poor fit between measured and predicted values (Figure 233). Good performance of the model was indicated by the cross-validation results (Table 94). The error map showed lower error in Hudson Bay compared to Baffin Bay and Davis Strait, and higher error along the edges of the study extent (Figure 234). The kriged surface is presented in Figure 235.

Table 93. Distributional properties of Bottom Shear Range (Pa).

| **Property** | **Value** |
|---|---:|
| Number of Observations | 16257 |
| Minimum | $4.550 \times 10^{-4}$ |
| Maximum | 1.217 |
| Mean | 0.043 |
| Median | 0.025 |
| Standard Deviation | 0.051 |
| Skewness | 4.017 |
| Kurtosis | 38.580 |

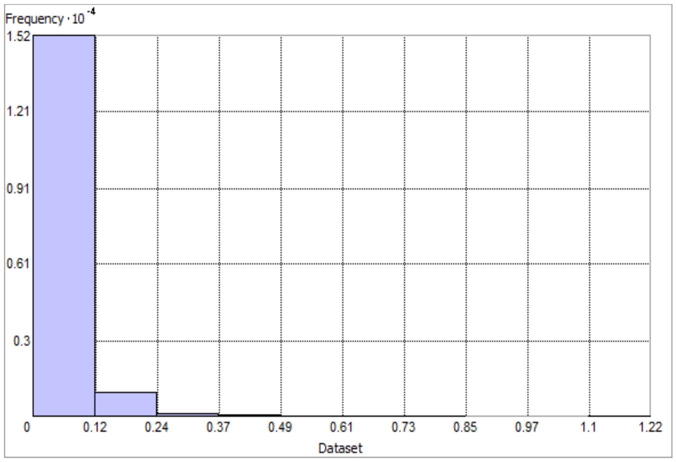

Figure 231. Distribution of Bottom Shear Range (Pa). Histogram was illustrated using 10 bins. Y axis is shown at $10^{-4}$.

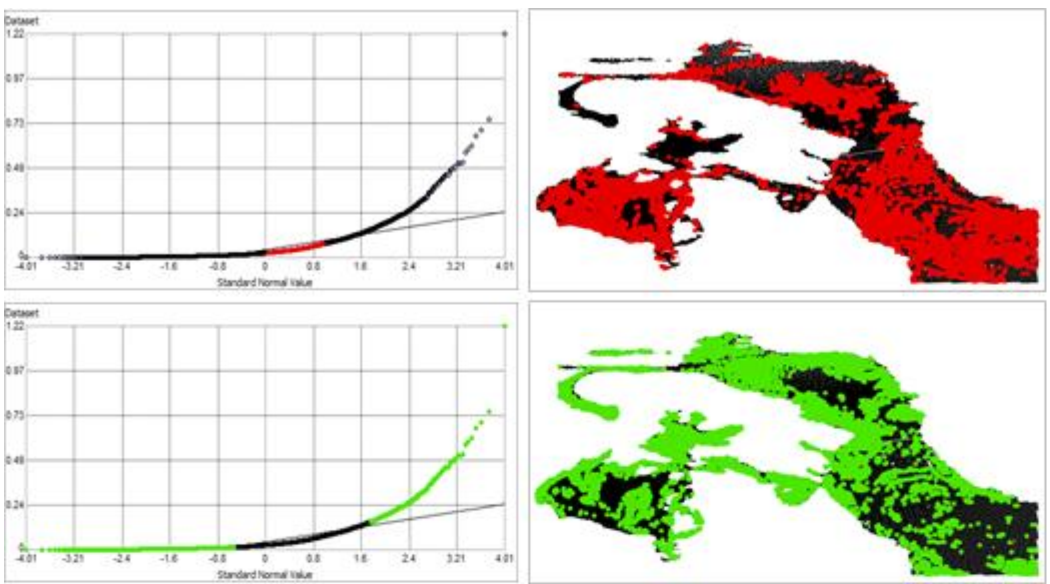

Figure 222. Normal Q-Q plot for data values of Bottom Shear Range (Pa). Points falling under (top right panel) and over (bottom right panel) the reference line are mapped.

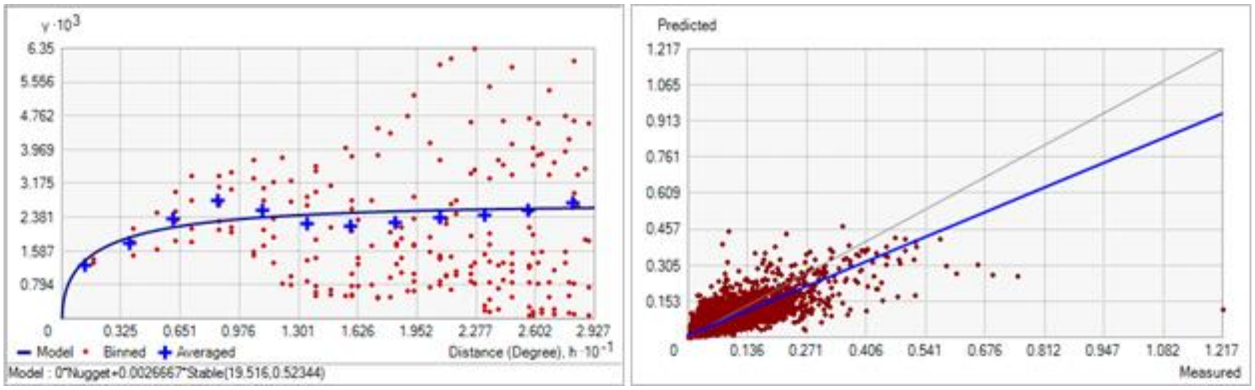


Figure 233. Left panel: Semivariogram of Bottom Shear Range (Pa). Binned values are shown as red dots; average points are shown as blue crosses; the model fit to the averaged values is shown as a blue line. Lag size: 2.439 degrees; number of lags: 12; Parameter: 0.523; Range: 19.516 degrees; Partial Sill: $2.667 \times 10^{-3}$. Right panel: Scatterplot of predicted values versus observed values for the model of Bottom Shear Range (Pa).

Table 94. Results of cross-validation of the kriged model for Bottom Shear Range (Pa).

| **Prediction Error** | **Value** |
|---|---:|
| Number of Observations | 16257 |
| Overall Mean Error | $-1.743 \times 10^{-5}$ |
| Root Mean Square Prediction Error | 0.028 |
| Standardized Mean | $-3.800 \times 10^{-4}$ |
| Standardized Root Mean Square Prediction Error | 1.085 |
| Average Standard Error | 0.025 |

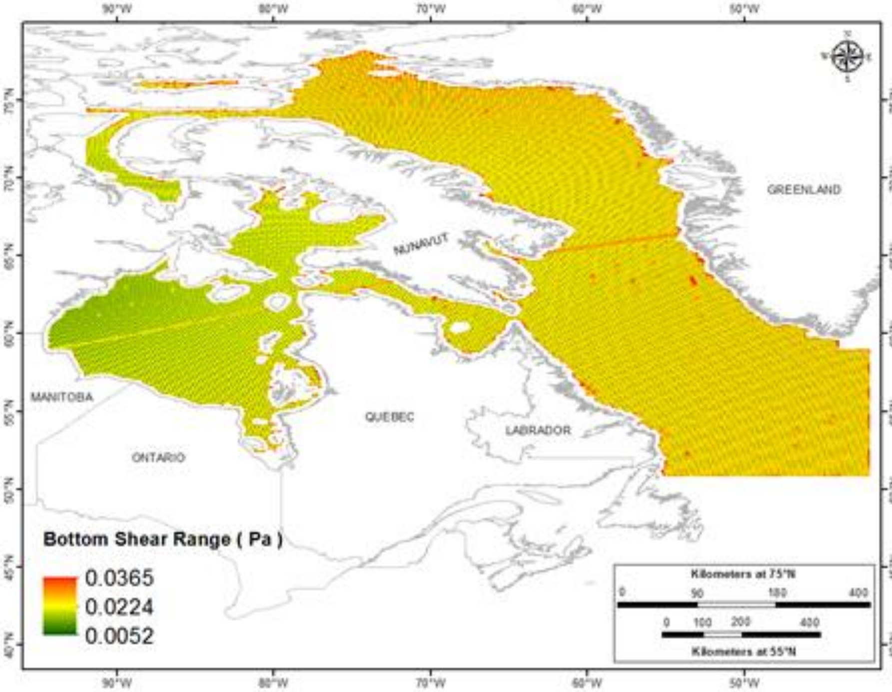


Figure 234. Prediction standard error surface of Bottom Shear Range (Pa).

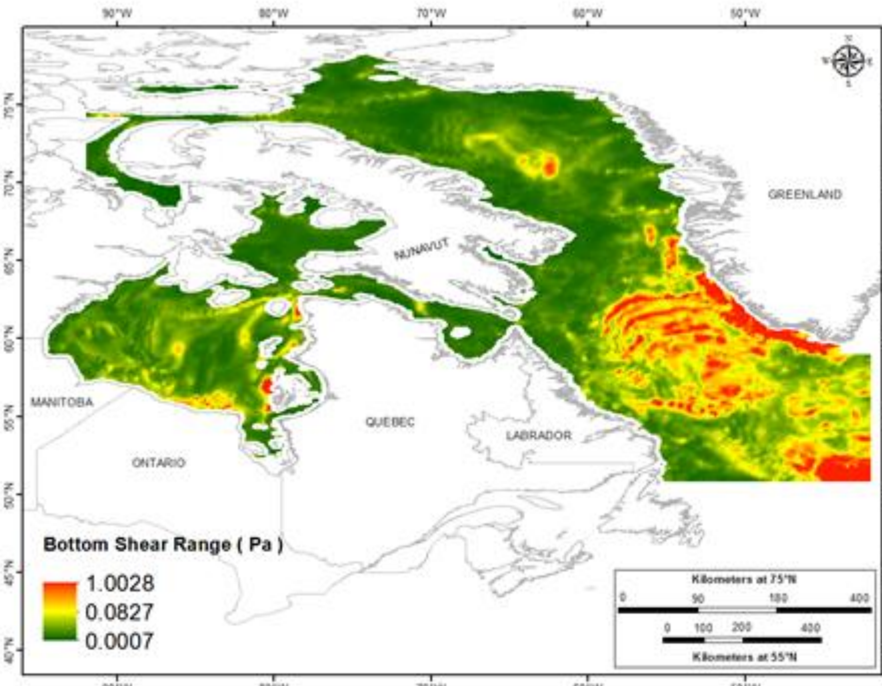


Figure 235. Interpolated prediction surface of Bottom Shear Range (Pa).

**Bottom Shear Average Minimum**

This variable displayed a right-skewed, extremely leptokurtic distribution prior to interpolation (Table 95, Figure 236). The data were higher than predicted by a normal distribution at both tails, while mid-values were lower than the reference line (Figure 237). These areas of under- and over-prediction showed spatial pattern over the region (Figure 237).

The semivariogram showed moderate autocorrelation present in the data (Figure 238). The kriged model showed poor fit between measured and predicted values (Figure 238). Very good performance of the model was indicated by the cross-validation results (Table 96). The error map showed lower error in Hudson Bay compared to Baffin Bay and Davis Strait, and higher error along the edges of the study extent (Figure 239). The kriged surface is presented in Figure 240.

Table 95. Distributional properties of Bottom Shear Average Minimum (Pa).

| **Property** | **Value** |
|---|---:|
| Number of Observations | 16257 |
| Minimum | $1.100 \times 10^{-5}$ |
| Maximum | 0.155 |
| Mean | $3.224 \times 10^{-3}$ |
| Median | $1.411 \times 10^{-3}$ |
| Standard Deviation | $6.729 \times 10^{-3}$ |
| Skewness | 7.674 |
| Kurtosis | 98.884 |

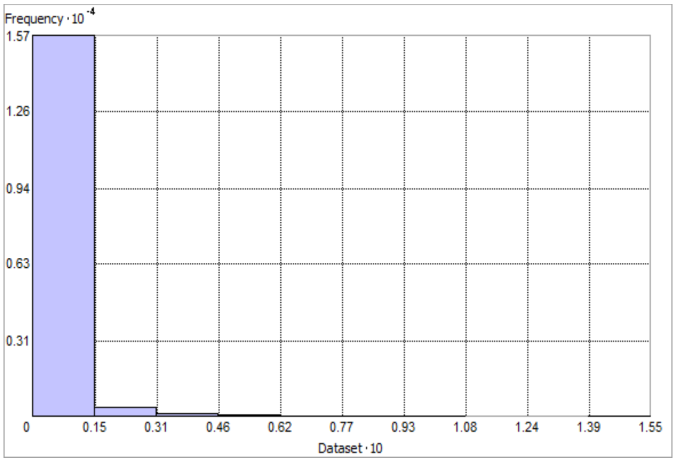


Figure 236. Distribution of Bottom Shear Average Minimum (Pa). Histogram was illustrated using 10 bins. X axis is shown at 10; Y axis is shown at $10^{-4}$.

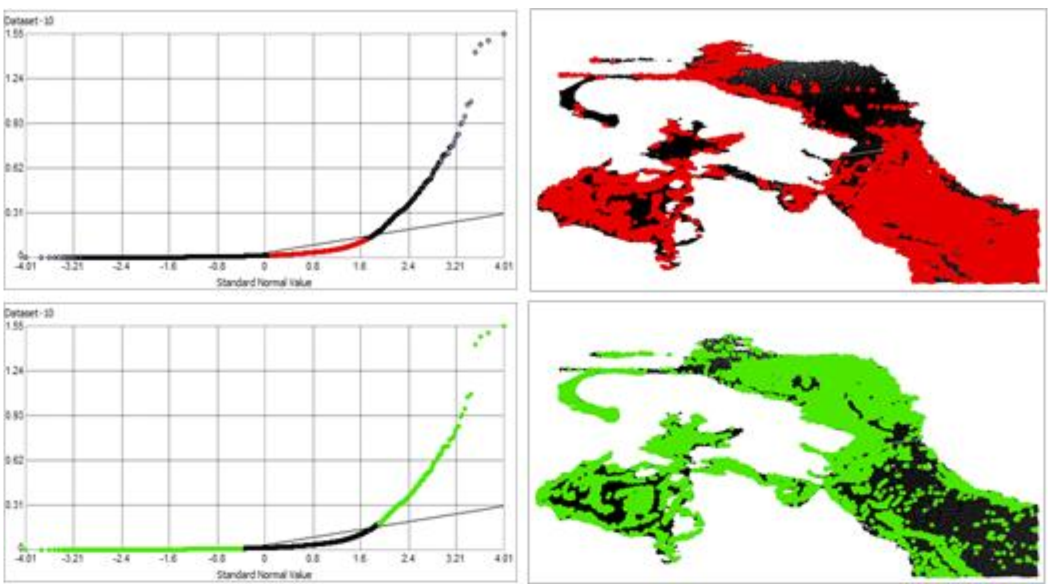

Figure 237. Normal Q-Q plot for data values of Bottom Shear Average Minimum (Pa). Points falling under (top right panel) and over (bottom right panel) the reference line are mapped.

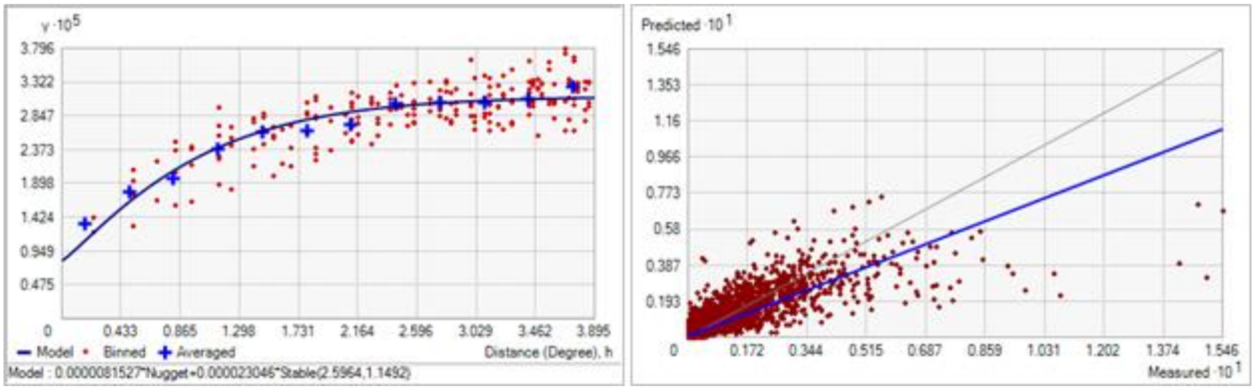


Figure 238. Left panel: Semivariogram of Bottom Shear Average Minimum (Pa). Binned values are shown as red dots; average points are shown as blue crosses; the model fit to the averaged values is shown as a blue line. Lag size: 0.235 degrees; number of lags: 12; Parameter: 1.149; Range: 2.596 degrees; Partial Sill: 2.305 x $10^{-5}$. Right panel: Scatterplot of predicted values versus observed values for the model of Bottom Shear Average Minimum (Pa).

Table 96. Results of cross-validation of the kriged model for Bottom Shear Average Minimum (Pa).

| Prediction Error | Value |
|---|---:|
| Number of Observations | 16257 |
| Overall Mean Error | 2.275 x $10^{-6}$ |
| Root Mean Square Prediction Error | 3.632 x $10^{-3}$ |
| Standardized Mean | 4.053 x $10^{-4}$ |
| Standardized Root Mean Square Prediction Error | 1.046 |
| Average Standard Error | 3.427 x $10^{-3}$ |

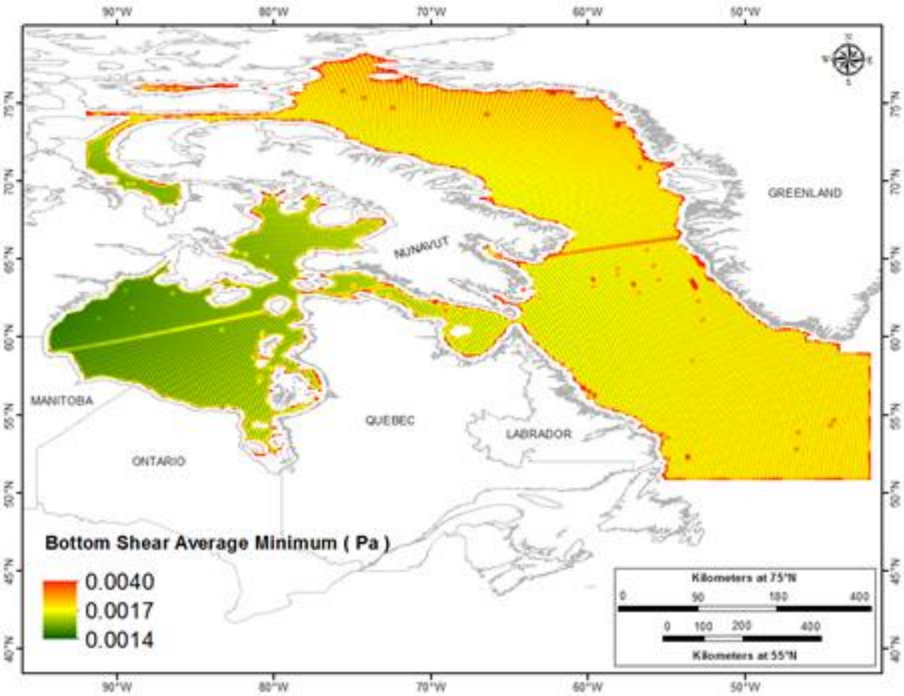


Figure 239. Prediction standard error surface of Bottom Shear Average Minimum (Pa).

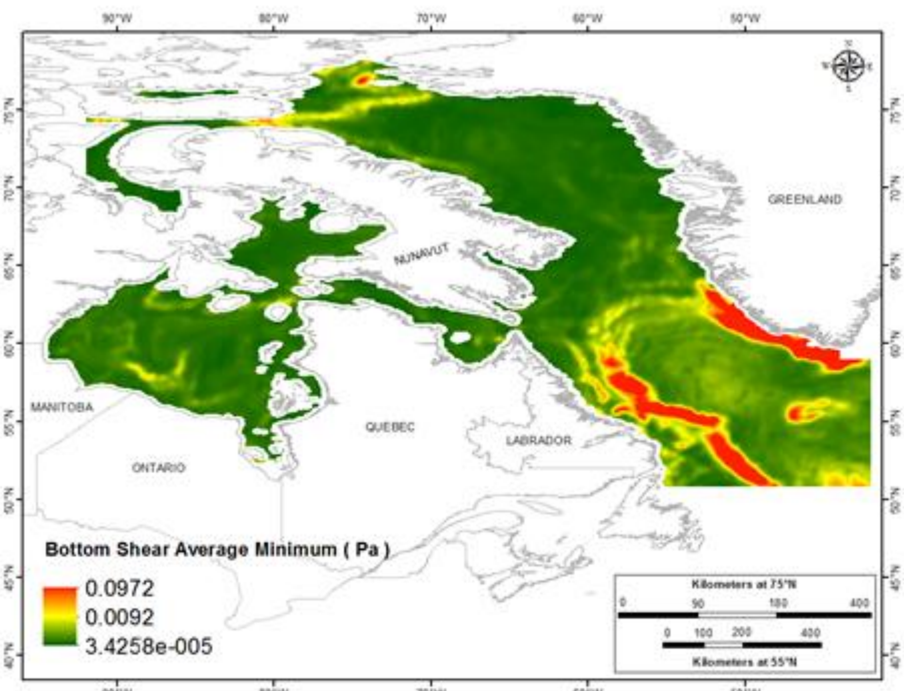


Figure 240. Interpolated prediction surface of Bottom Shear Average Minimum (Pa).

**Bottom Shear Average Maximum**

This variable displayed a right-skewed, extremely leptokurtic distribution prior to interpolation (Table 97, Figure 241). The data were higher than predicted by a normal distribution at both tails, while mid-values were lower than the reference line (Figure 242). These areas of under- and over-prediction showed spatial pattern over the region (Figure 242).

The semivariogram showed moderate autocorrelation present in the data (Figure 243). The kriged model showed poor fit between measured and predicted values (Figure 243). Very good performance of the model was indicated by the cross-validation results (Table 98). The error map showed lower error in Hudson Bay compared to Baffin Bay and Davis Strait, and higher error along the edges of the study extent (Figure 244). The kriged surface is presented in Figure 245.

Table 97. Distributional properties of Bottom Shear Average Maximum (Pa).

| **Property** | **Value** |
|---|---:|
| Number of Observations | 16257 |
| Minimum | $2.490 \times 10^{-4}$ |
| Maximum | 0.580 |
| Mean | 0.023 |
| Median | 0.014 |
| Standard Deviation | 0.028 |
| Skewness | 4.947 |
| Kurtosis | 53.176 |

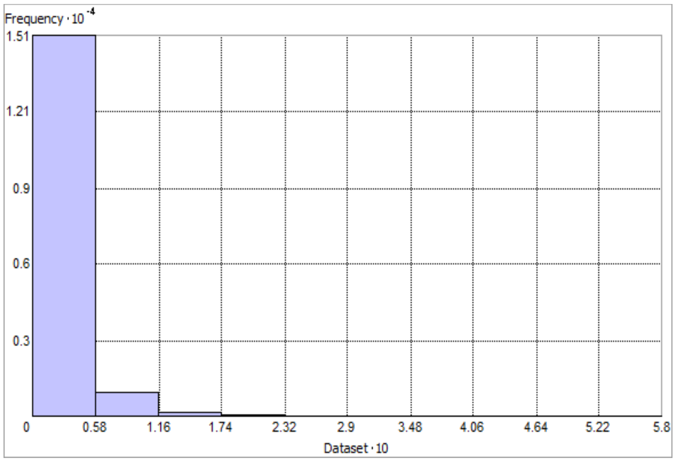

Figure 241. Distribution of Bottom Shear Average Maximum (Pa). Histogram was illustrated using 10 bins. X axis is shown at 10; Y axis is shown at $10^{-4}$.

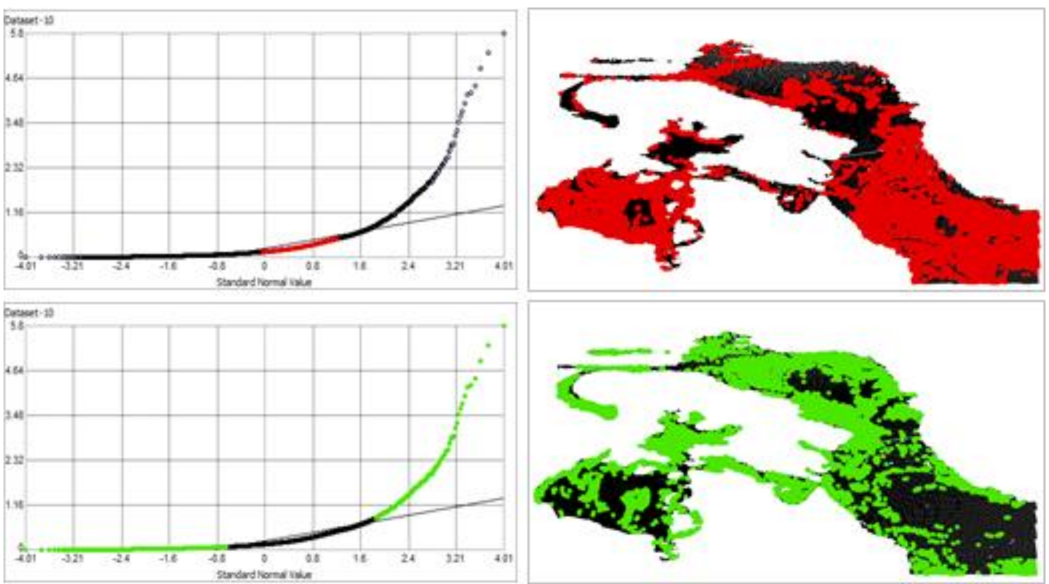
Figure 242. Normal Q-Q plot for data values of Bottom Shear Average Maximum (Pa). Points falling under (top right panel) and over (bottom right panel) the reference line are mapped.

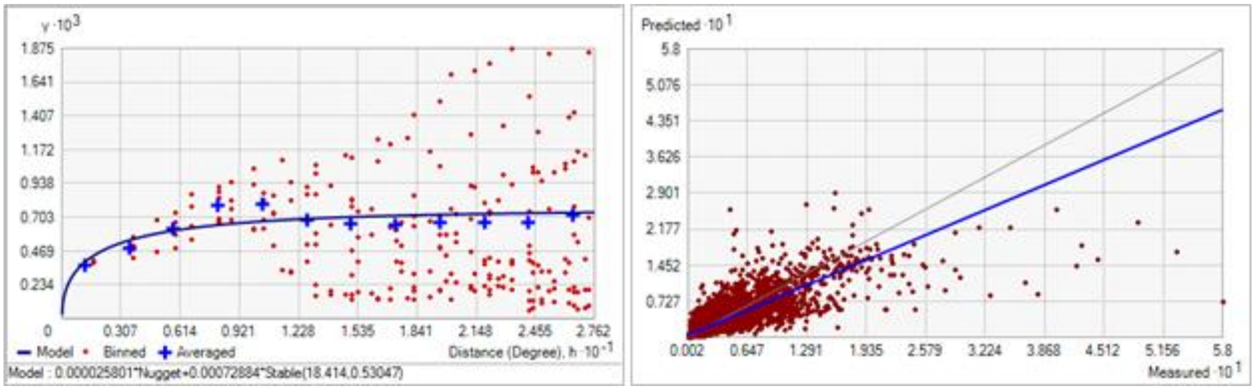

Figure 243. Left panel: Semivariogram of Bottom Shear Average Maximum (Pa). Binned values are shown as red dots; average points are shown as blue crosses; the model fit to the averaged values is shown as a blue line. Lag size: 2.302 degrees; number of lags: 12; Parameter: 0.530; Range: 18.414 degrees; Partial Sill: 7.288 x $10^{-4}$. Right panel: Scatterplot of predicted values versus observed values for the model of Bottom Shear Average Maximum (Pa).

Table 98. Results of cross-validation of the kriged model for Bottom Shear Average Maximum (Pa).

| **Prediction Error** | **Value** |
|---|---:|
| Number of Observations | 16257 |
| Overall Mean Error | -3.591 x $10^{-6}$ |
| Root Mean Square Prediction Error | 0.015 |
| Standardized Mean | -1.417 x $10^{-4}$ |
| Standardized Root Mean Square Prediction Error | 1.048 |
| Average Standard Error | 0.014 |

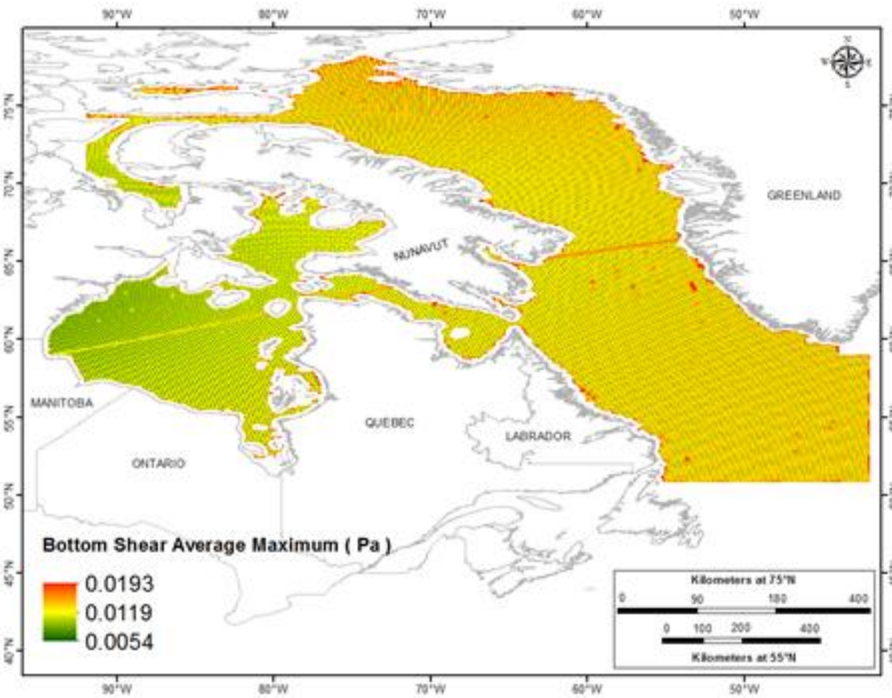


Figure 244. Prediction standard error surface of Bottom Shear Average Maximum (Pa).

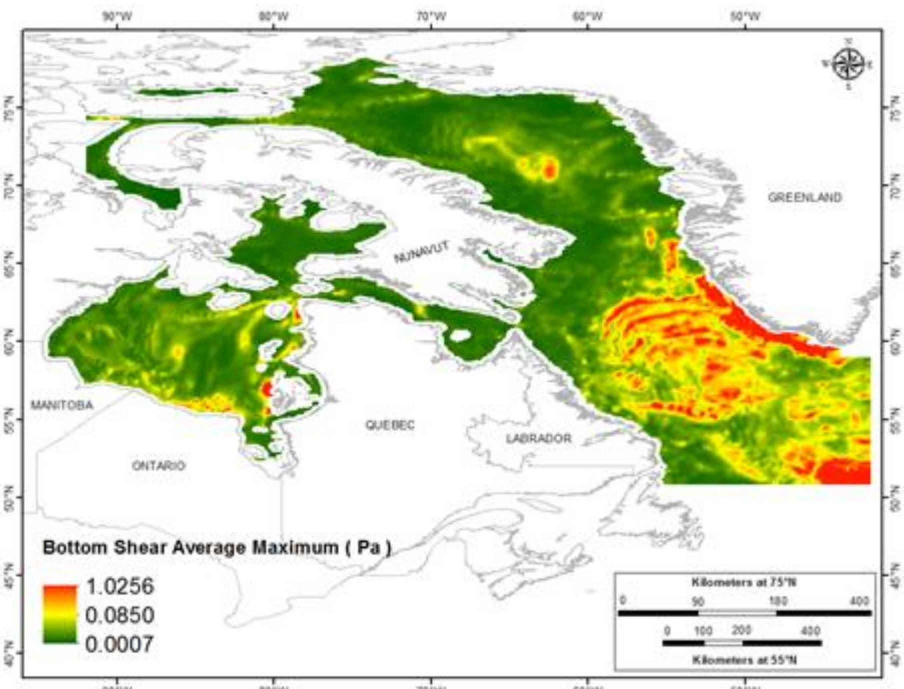


Figure 245. Interpolated prediction surface of Bottom Shear Average Maximum (Pa).

## Bottom Shear Average Range

This variable displayed a right-skewed, extremely leptokurtic distribution prior to interpolation (Table 99, Figure 246). The data were higher than predicted by a normal distribution at both tails, while mid-values were slightly lower than the reference line (Figure 247). These areas of under- and over-prediction showed little spatial pattern over the region (Figure 247).

The semivariogram showed very weak autocorrelation present in the data (Figure 248). The kriged model showed poor fit between measured and predicted values (Figure 248). Good performance of the model was indicated by the cross-validation results (Table 100). The error map showed lower error in Hudson Bay compared to Baffin Bay and Davis Strait, and higher error along the edges of the study extent (Figure 249). The kriged surface is presented in Figure 250.

Table 99. Distributional properties of Bottom Shear Average Range (Pa).

| **Property** | **Value** |
|---|---:|
| Number of Observations | 16257 |
| Minimum | $2.110 \times 10^{-4}$ |
| Maximum | 0.508 |
| Mean | 0.020 |
| Median | 0.013 |
| Standard Deviation | 0.023 |
| Skewness | 4.596 |
| Kurtosis | 48.795 |

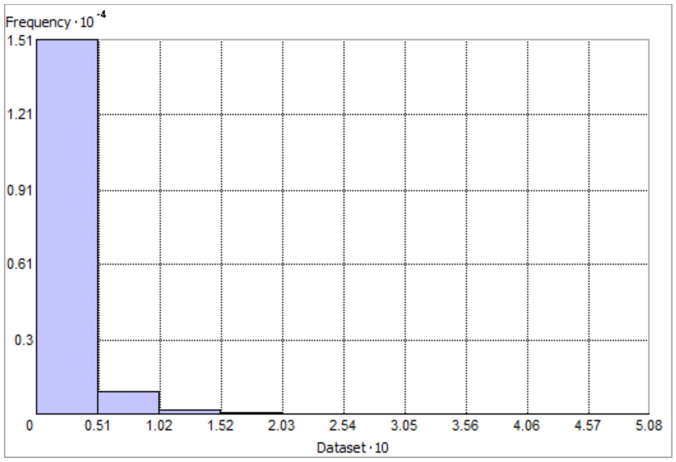


Figure 246. Distribution of Bottom Shear Average Range (Pa). Histogram was illustrated using 10 bins. X axis is shown at 10; Y axis is shown at $10^{-4}$.

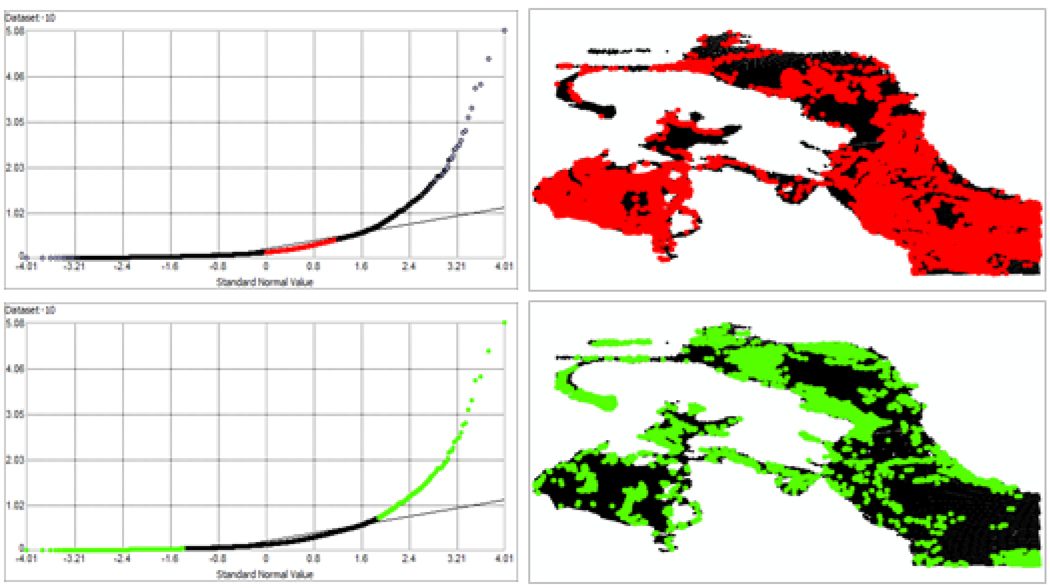

Figure 247. Normal Q-Q plot for data values of Bottom Shear Average Range (Pa). Points falling under (top right panel) and over (bottom right panel) the reference line are mapped.

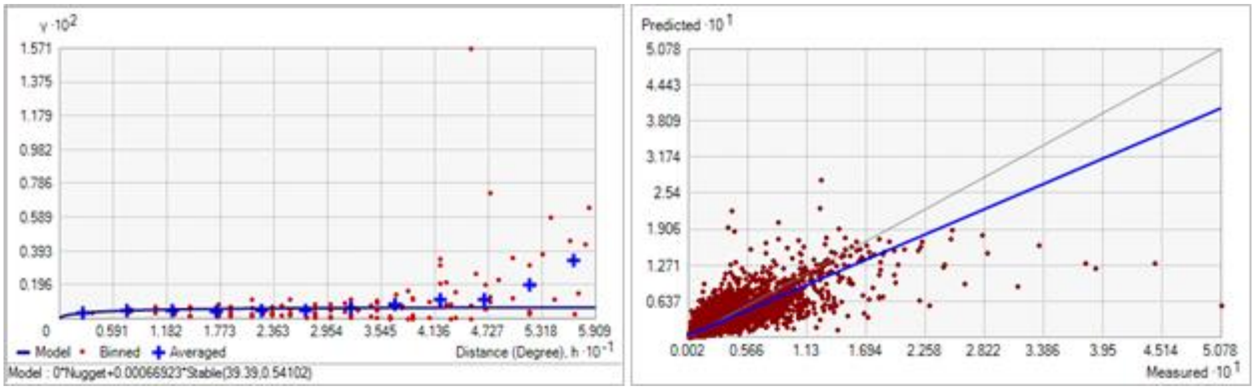


Figure 248. Left panel: Semivariogram of Bottom Shear Average Range (Pa). Binned values are shown as red dots; average points are shown as blue crosses; the model fit to the averaged values is shown as a blue line. Lag size: 4.924 degrees; number of lags: 12; Parameter: 0.541; Range: 39.390 degrees; Partial Sill: 6.692 x $10^{-4}$. Right panel: Scatterplot of predicted values versus observed values for the model of Bottom Shear Average Range (Pa).

Table 100. Results of cross-validation of the kriged model for Bottom Shear Average Range (Pa).

| **Prediction Error** | **Value** |
|---|---:|
| Number of Observations | 16257 |
| Overall Mean Error | -6.535 x $10^{-6}$ |
| Root Mean Square Prediction Error | 0.013 |
| Standardized Mean | -3.276 x $10^{-4}$ |
| Standardized Root Mean Square Prediction Error | 1.224 |
| Average Standard Error | 0.010 |

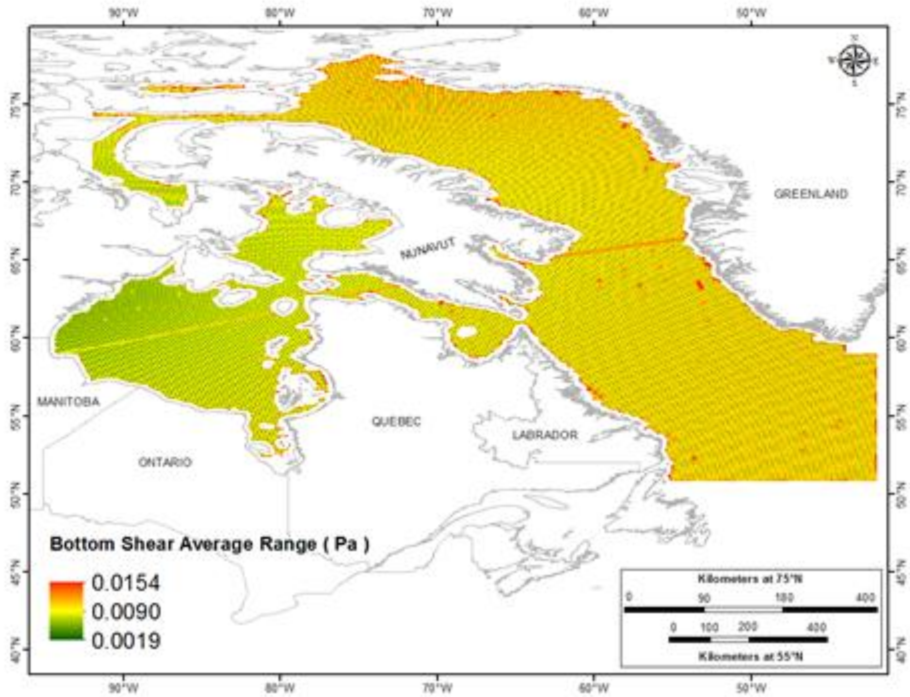


Figure 249. Prediction standard error surface of Bottom Shear Average Range (Pa).

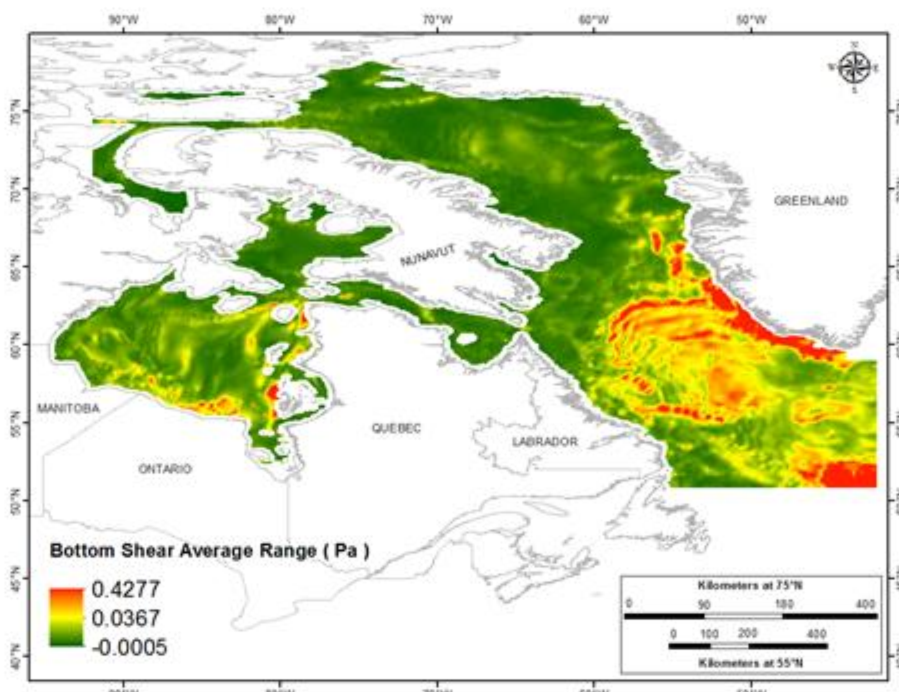


Figure 250. Interpolated prediction surface of Bottom Shear Average Range (Pa).

## Maximum Seasonal Mixed Layer Depth

Maximum mixed layer depth, or, the depth at which surface vertical mixing dissipates, is a near-universal feature of the open ocean (de Boyer Montégut et al., 2004). Within this mixed layer, salinity, temperature, and density are nearly uniform, a phenomenon caused by surface forcing, lateral advection, and internal wave processes that vary on diurnal, intra-seasonal, seasonal, and inter-annual scales (de Boyer Montégut et al., 2004). The depth of this mixed zone can show large spatial variability, ranging from less than 20 m in the summer hemisphere, to more than 500 m in the winter hemisphere at subpolar latitudes (de Boyer Montégut et al., 2004). The mixed layer depth has a significant influence on primary production in the surface waters. As the mixed layer depth increases it entrains nutrients from deeper waters below, supplying additional nutrients for primary production (Polovina et al., 1995; Carstensen et al., 2002).

### Maximum Spring Mixed Layer Depth

This variable displayed a right-skewed, leptokurtic distribution prior to interpolation (Table 101, Figure 251). The data were higher than predicted by a normal distribution at both tails, while mid-values were lower than the reference line (Figure 252). These areas of under- and over-prediction showed spatial pattern over the region (Figure 252).

The semivariogram showed moderate autocorrelation present in the data (Figure 253). The kriged model showed good fit between measured and predicted values (Figure 253). Very good performance of the model was indicated by the cross-validation results (Table 102). The error map showed lower error in Hudson Bay compared to Baffin Bay and Davis Strait, and higher error along the edges of the study extent (Figure 254). The kriged surface is presented in Figure 255.

Table 101. Distributional properties of Maximum Spring Mixed Layer Depth (m).

| Property | Value |
|---|---:|
| Number of Observations | 16376 |
| Minimum | 10.768 |
| Maximum | 2135.600 |
| Mean | 143.750 |
| Median | 59.046 |
| Standard Deviation | 240.630 |
| Skewness | 3.509 |
| Kurtosis | 16.990 |

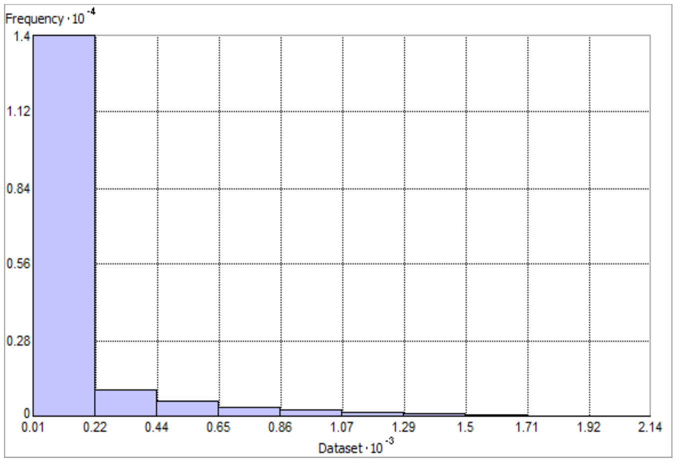


Figure 251. Distribution of Maximum Spring Mixed Layer Depth (m). Histogram was illustrated using 10 bins. X axis is shown at $10^{-3}$; Y axis is shown at $10^{-4}$.

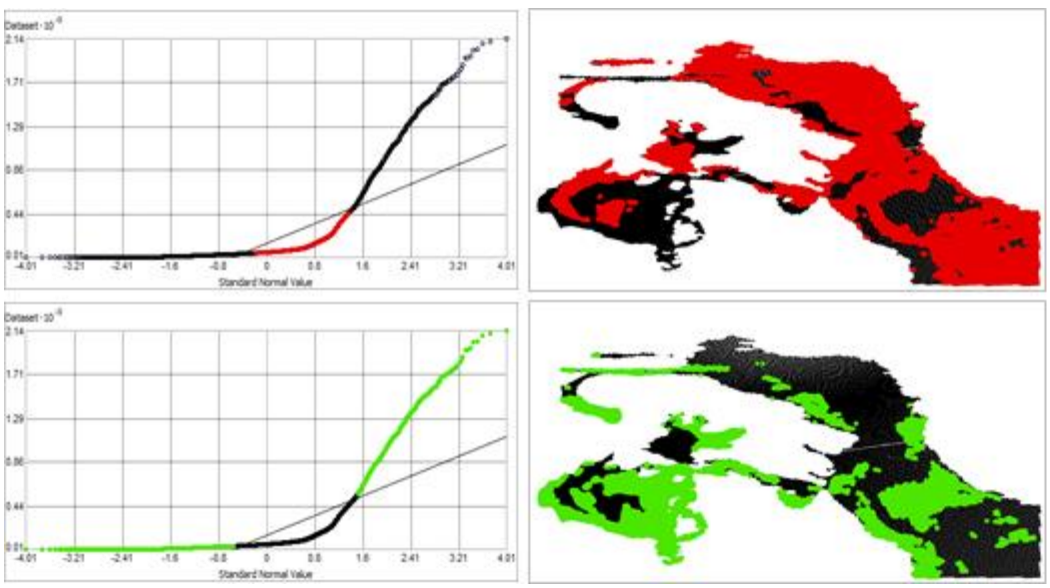

Figure 252. Normal Q-Q plot for data values of Maximum Spring Mixed Layer Depth (m). Points falling under (top right panel) and over (bottom right panel) the reference line are mapped.

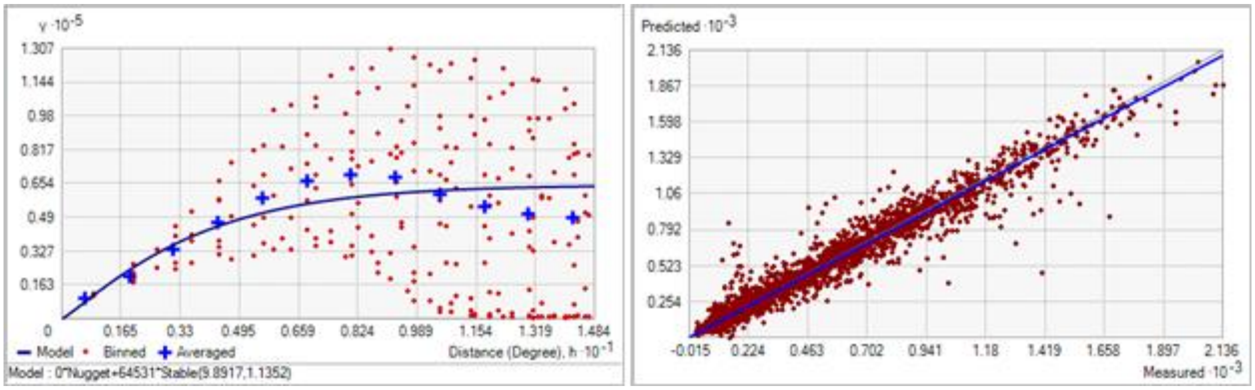

Figure 253. Left panel: Semivariogram of Maximum Spring Mixed Layer Depth (m). Binned values are shown as red dots; average points are shown as blue crosses; the model fit to the averaged values is shown as a blue line. Lag size: 1.236 degrees; number of lags: 12; Parameter: 1.135; Range: 9.892 degrees; Partial Sill: 64530.930. Right panel: Scatterplot of predicted values versus observed values for the model of Maximum Spring Mixed Layer Depth (m).

Table 102. Results of cross-validation of the kriged model for Maximum Spring Mixed Layer Depth (m).

| **Prediction Error** | **Value** |
|---|---|
| Number of Observations | 16376 |
| Overall Mean Error | -0.024 |
| Root Mean Square Prediction Error | 37.362 |
| Standardized Mean | $-4.621 \times 10^{-4}$ |
| Standardized Root Mean Square Prediction Error | 1.001 |
| Average Standard Error | 36.541 |

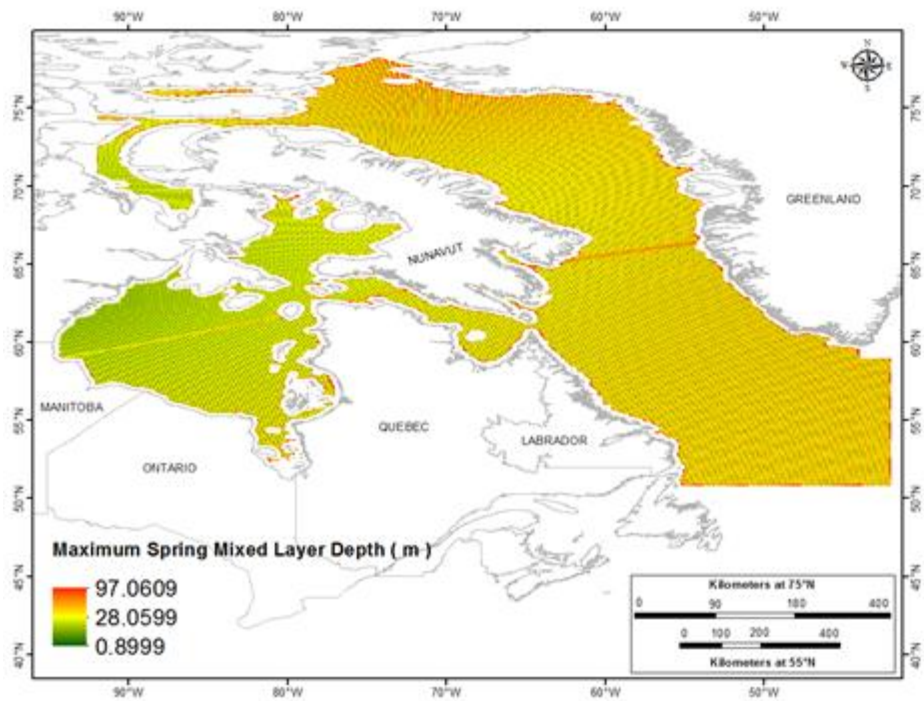


Figure 254. Prediction standard error surface of Maximum Spring Mixed Layer Depth (m).

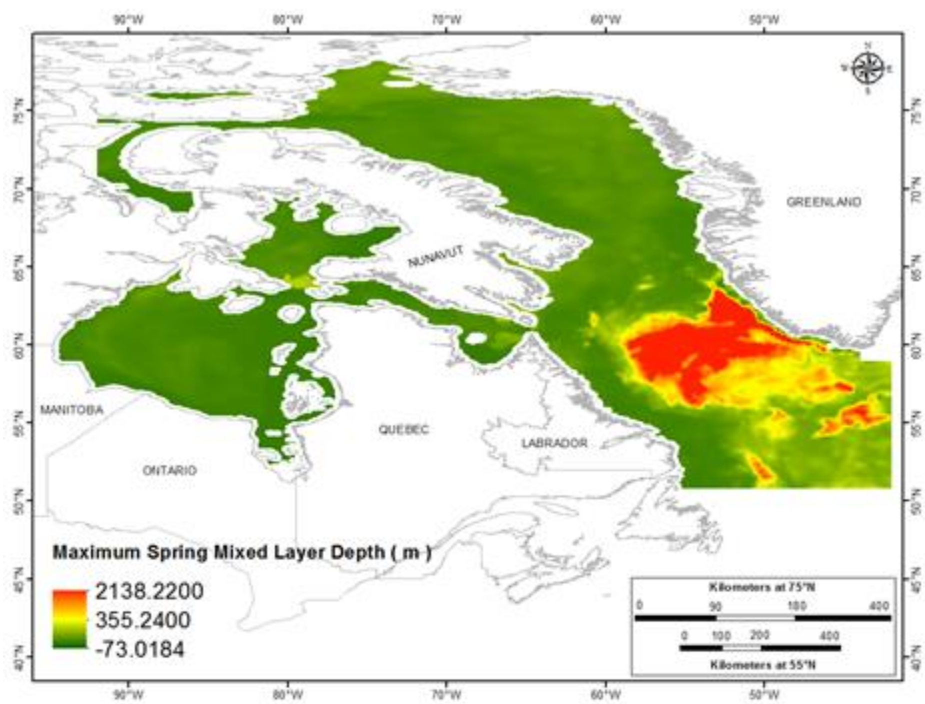


Figure 255. Interpolated prediction surface of Maximum Spring Mixed Layer Depth (m).

## Maximum Summer Mixed Layer Depth

This variable displayed a right-skewed, extremely leptokurtic distribution prior to interpolation (Table 103, Figure 256). The data were higher than predicted by a normal distribution at both tails, while mid-values were lower than the reference line (Figure 257). These areas of under- and over-prediction showed spatial pattern over the region (Figure 257).

The semivariogram showed autocorrelation present in the data (Figure 258). The kriged model showed good fit between measured and predicted values (Figure 258). Good performance of the model was indicated by the cross-validation results (Table 104). The error map showed lower error in Hudson Bay compared to Baffin Bay and Davis Strait, and higher error along the edges of the study extent (Figure 259). The kriged surface is presented in Figure 260.

Table 103. Distributional properties of Maximum Summer Mixed Layer Depth (m).

| **Property** | **Value** |
|---|---:|
| Number of Observations | 16376 |
| Minimum | 10.768 |
| Maximum | 495.000 |
| Mean | 26.078 |
| Median | 18.131 |
| Standard Deviation | 22.030 |
| Skewness | 8.452 |
| Kurtosis | 132.750 |

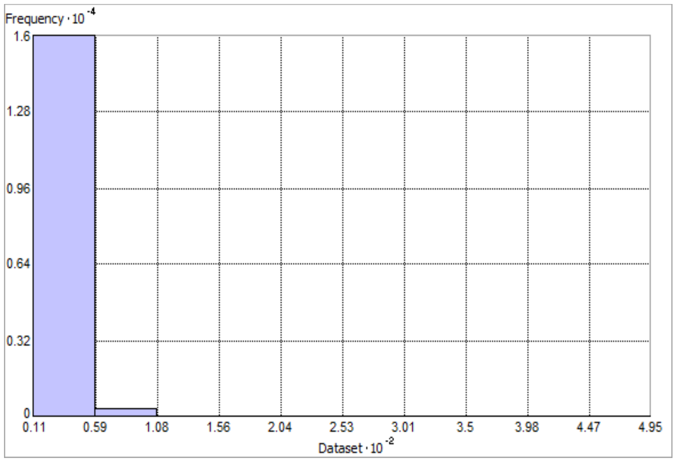


Figure 256. Distribution of Maximum Summer Mixed Layer Depth (m). Histogram was illustrated using 10 bins. X axis is shown at $10^{-2}$; Y axis is shown at $10^{-4}$.

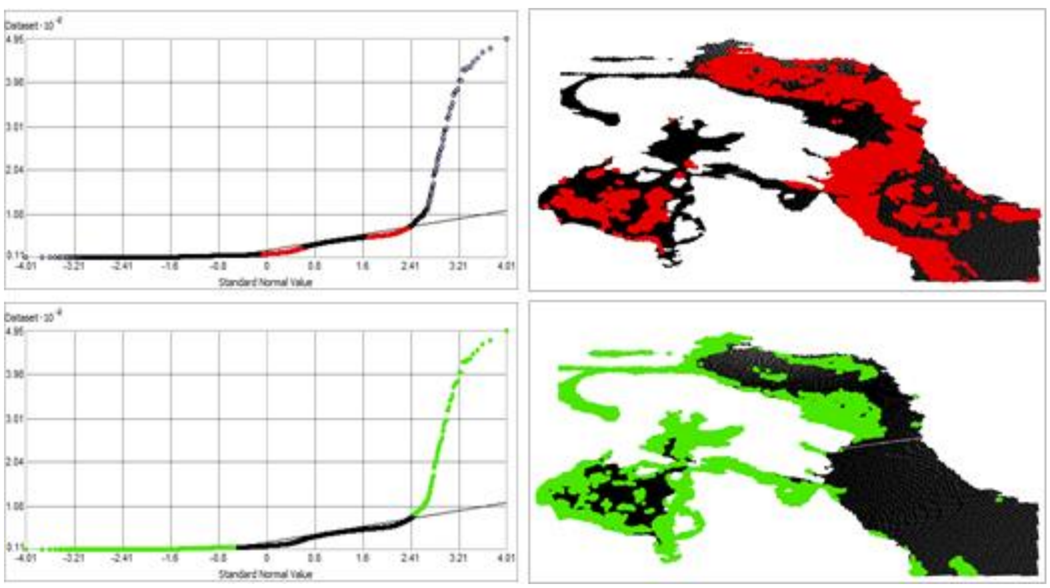

Figure 257. Normal Q-Q plot for data values of Maximum Summer Mixed Layer Depth (m). Points falling under (top right panel) and over (bottom right panel) the reference line are mapped.

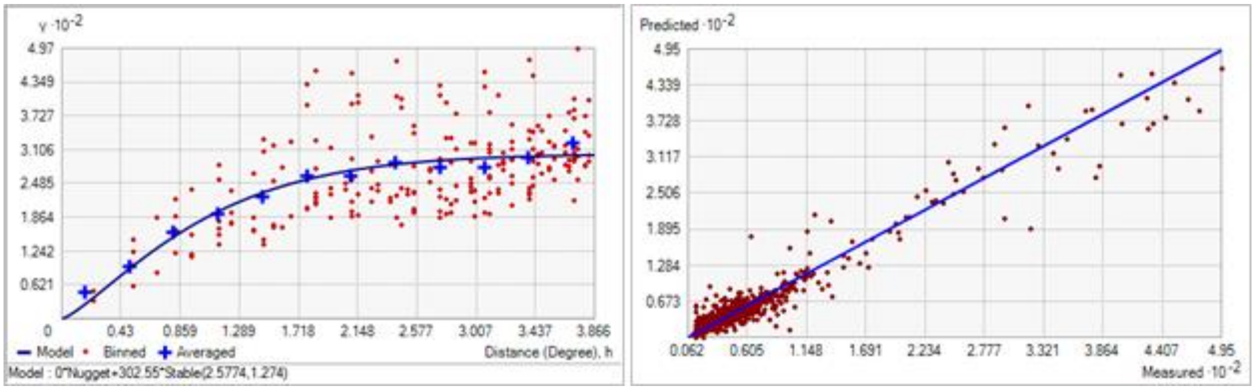

Figure 258. Left panel: Semivariogram of Maximum Summer Mixed Layer Depth (m). Binned values are shown as red dots; average points are shown as blue crosses; the model fit to the averaged values is shown as a blue line. Lag size: 0.322 degrees; number of lags: 12; Parameter: 1.274; Range: 2.577 degrees; Partial Sill: 302.546. Right panel: Scatterplot of predicted values versus observed values for the model of Maximum Summer Mixed Layer Depth (m).

Table 104. Results of cross-validation of the kriged model for Maximum Summer Mixed Layer Depth (m).

| Prediction Error | Value |
|---|---:|
| Number of Observations | 16376 |
| Overall Mean Error | $8.466 \times 10^{-4}$ |
| Root Mean Square Prediction Error | 4.076 |
| Standardized Mean | $4.353 \times 10^{-5}$ |
| Standardized Root Mean Square Prediction Error | 0.929 |
| Average Standard Error | 4.163 |

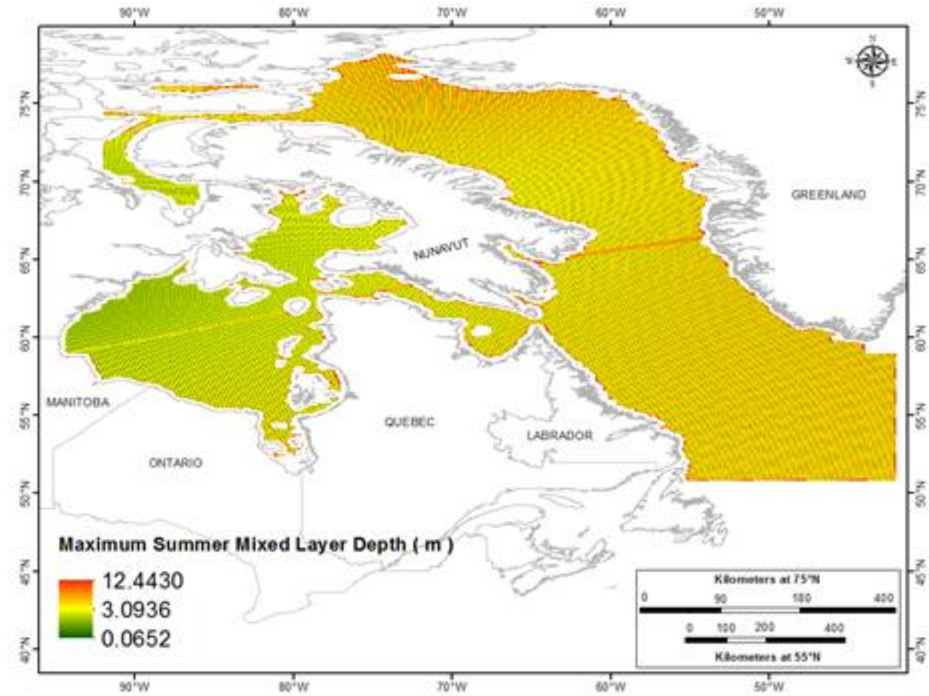


Figure 259. Prediction standard error surface of Maximum Summer Mixed Layer Depth (m).

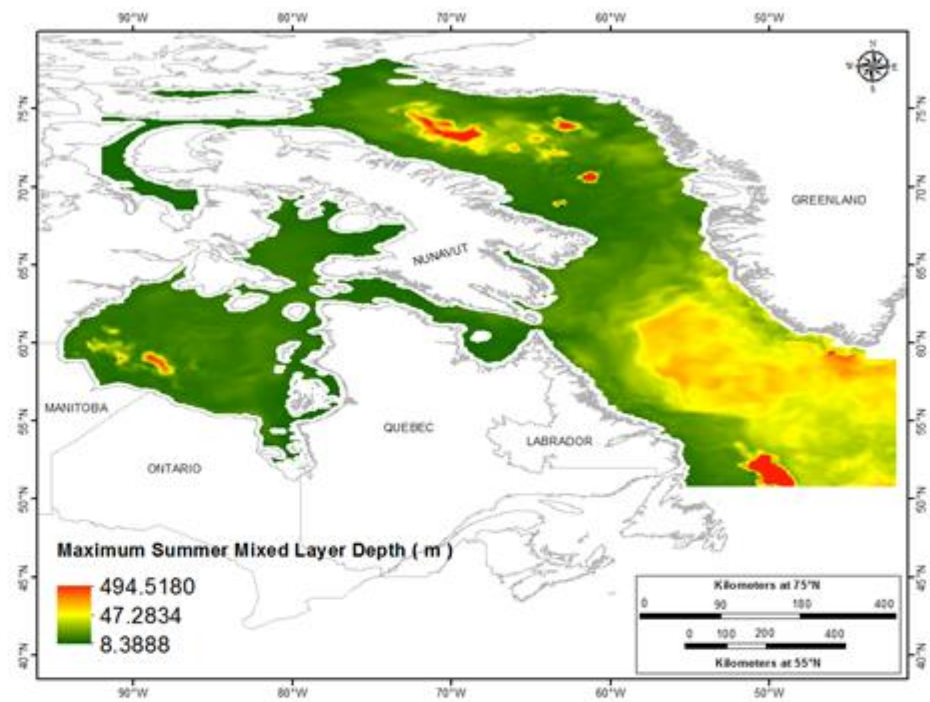


Figure 260. Interpolated prediction surface of Maximum Summer Mixed Layer Depth (m).

## Maximum Fall Mixed Layer Depth

This variable displayed a right-skewed, extremely leptokurtic distribution prior to interpolation (Table 105, Figure 261). The data were higher than predicted by a normal distribution at both tails, while mid-values were lower than the reference line (Figure 262). These areas of under- and over-prediction showed spatial pattern over the region (Figure 262).

The semivariogram showed moderate autocorrelation present in the data (Figure 263). The kriged model showed good fit between measured and predicted values (Figure 263). Good performance of the model was indicated by the cross-validation results (Table 106). The error map showed lower error in Hudson Bay compared to Baffin Bay and Davis Strait, and higher error along the edges of the study extent (Figure 264). The kriged surface is presented in Figure 265.

Table 105. Distributional properties of Maximum Fall Mixed Layer Depth (m).

| **Property** | **Value** |
|---|---:|
| Number of Observations | 16376 |
| Minimum | 11.099 |
| Maximum | 2463.100 |
| Mean | 91.004 |
| Median | 42.431 |
| Standard Deviation | 165.88 |
| Skewness | 7.593 |
| Kurtosis | 77.499 |

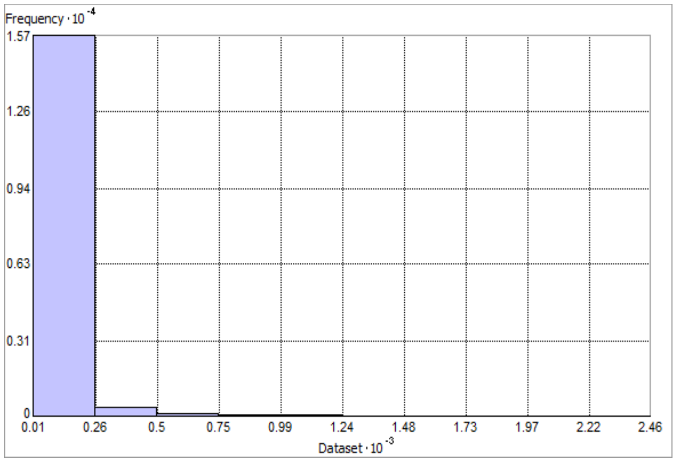


Figure 261. Distribution of Maximum Fall Mixed Layer Depth (m). Histogram was illustrated using 10 bins. X axis is shown at $10^{-3}$; Y axis is shown at $10^{-4}$.

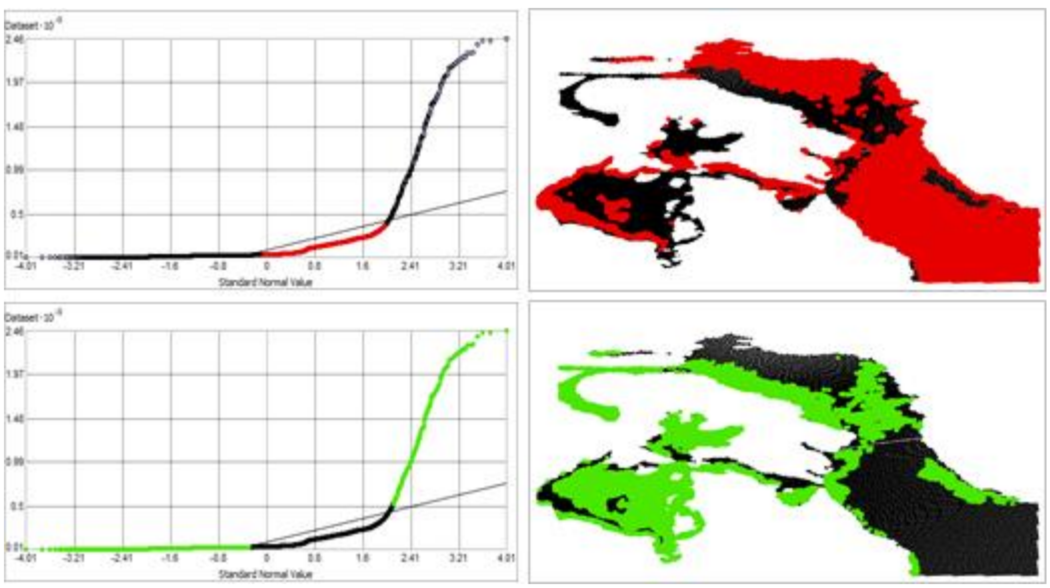

Figure 262. Normal Q-Q plot for data values of Maximum Fall Mixed Layer Depth (m). Points falling under (top right panel) and over (bottom right panel) the reference line are mapped.

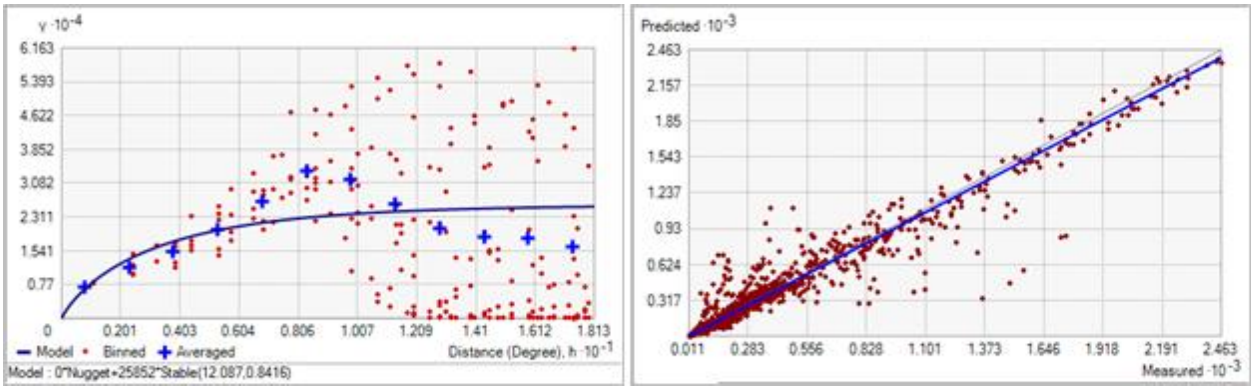

Figure 263. Left panel: Semivariogram of Maximum Fall Mixed Layer Depth (m). Binned values are shown as red dots; average points are shown as blue crosses; the model fit to the averaged values is shown as a blue line. Lag size: 1.511 degrees; number of lags: 12; Parameter: 0.842; Range: 12.087 degrees; Partial Sill: 25851.890. Right panel: Scatterplot of predicted values versus observed values for the model of Maximum Fall Mixed Layer Depth (m).

Table 106. Results of cross-validation of the kriged model for Maximum Fall Mixed Layer Depth (m).

| **Prediction Error** | **Value** |
|---|---|
| Number of Observations | 16376 |
| Overall Mean Error | 0.016 |
| Root Mean Square Prediction Error | 33.946 |
| Standardized Mean | $8.774 \times 10^{-5}$ |
| Standardized Root Mean Square Prediction Error | 0.769 |
| Average Standard Error | 43.112 |

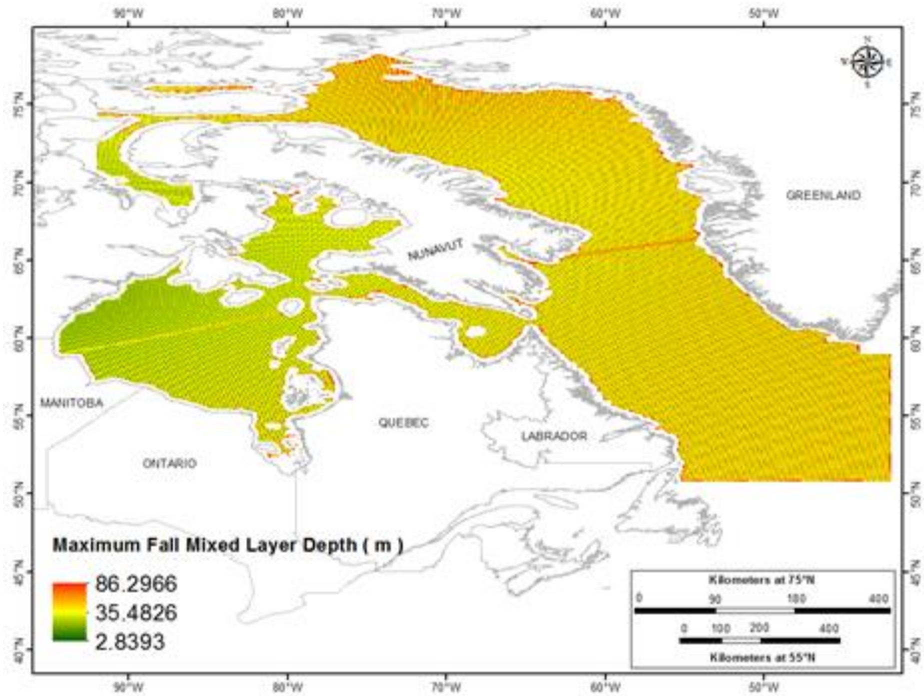


Figure 264. Prediction standard error surface of Maximum Fall Mixed Layer Depth (m).

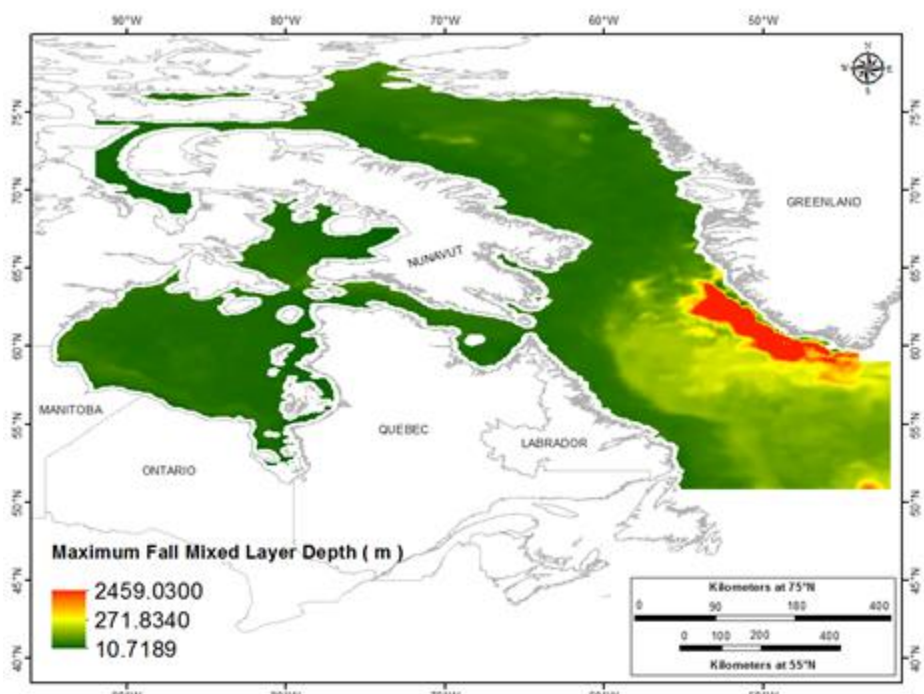


Figure 265. Interpolated prediction surface of Maximum Fall Mixed Layer Depth (m).

**Maximum Winter Mixed Layer Depth**

This variable displayed a right-skewed, leptokurtic distribution prior to interpolation (Table 107, Figure 266). The data were higher than predicted by a normal distribution at both tails, while mid-values were lower than the reference line (Figure 267). These areas of under- and over-prediction showed spatial pattern over the region (Figure 267).

The semivariogram showed moderate autocorrelation present in the data (Figure 268). The kriged model showed good fit between measured and predicted values (Figure 268). Fair performance of the model was indicated by the cross-validation results (Table 108), with underestimation of the variability of the predictions as indicated by a Standardized Root-Mean-Square Error higher than 1. The error map showed lower error in Hudson Bay compared to Baffin Bay and Davis Strait, and higher error along the edges of the study extent (Figure 269). The kriged surface is presented in Figure 270.

Table 107. Distributional properties of Maximum Winter Mixed Layer Depth (m).

| **Property** | **Value** |
|---|---:|
| Number of Observations | 16376 |
| Minimum | 10.768 |
| Maximum | 3036.500 |
| Mean | 315.330 |
| Median | 68.410 |
| Standard Deviation | 581.190 |
| Skewness | 2.389 |
| Kurtosis | 7.548 |

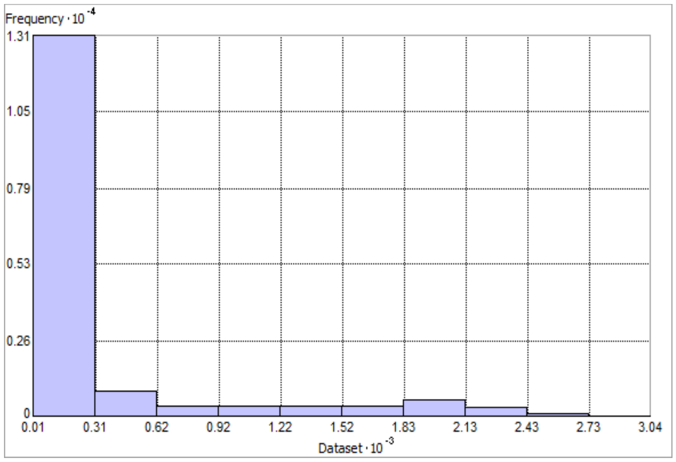


Figure 266. Distribution of Maximum Winter Mixed Layer Depth (m). Histogram was illustrated using 10 bins. X axis is shown at $10^{-3}$; Y axis is shown at $10^{-4}$.

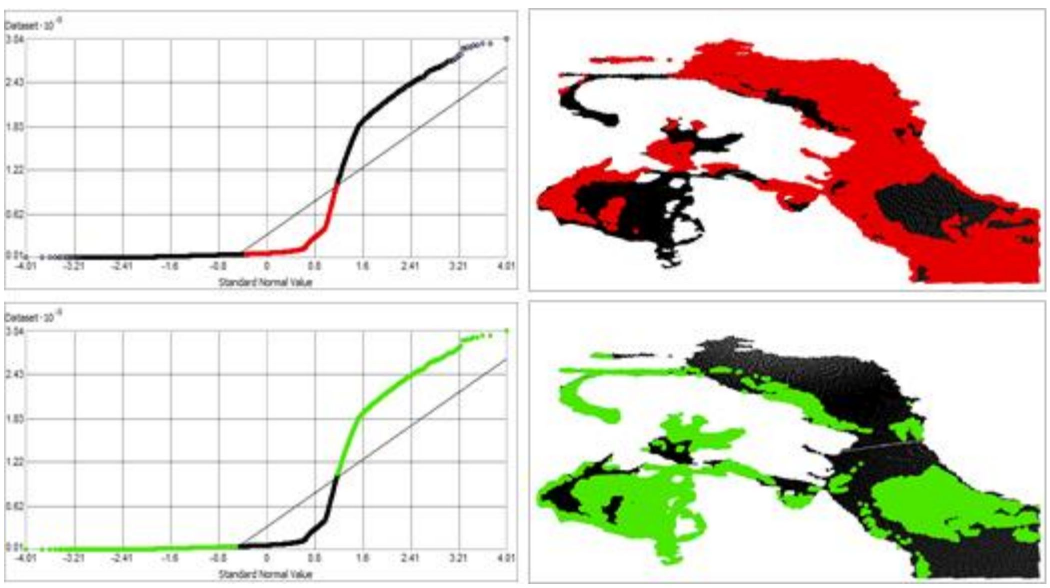

Figure 267. Normal Q-Q plot for data values of Maximum Winter Mixed Layer Depth (m). Points falling under (top right panel) and over (bottom right panel) the reference line are mapped.

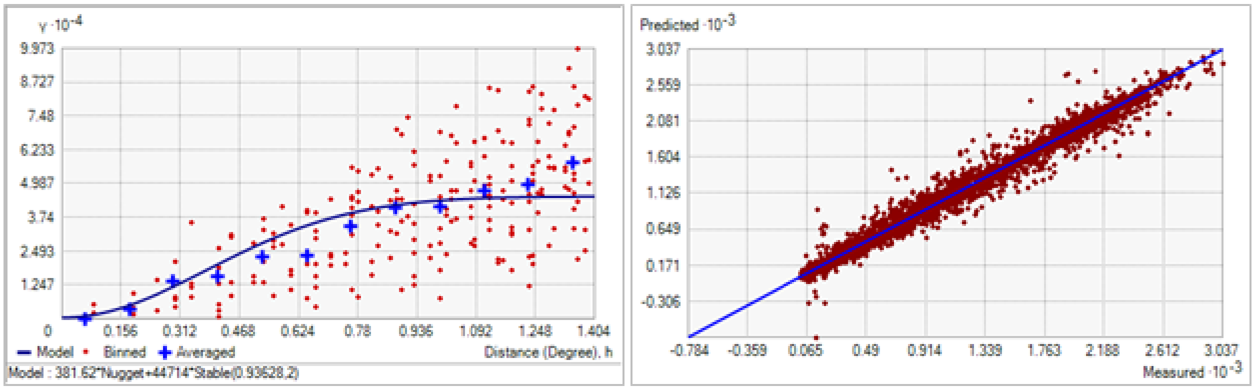


Figure 268. Left panel: Semivariogram of Maximum Winter Mixed Layer Depth (m). Binned values are shown as red dots; average points are shown as blue crosses; the model fit to the averaged values is shown as a blue line. Lag size: 0.117 degrees; number of lags: 12; Parameter: 2; Range: 0.936 degrees; Partial Sill: 44714.130. Right panel: Scatterplot of predicted values versus observed values for the model of Maximum Winter Mixed Layer Depth (m).

Table 108. Results of cross-validation of the kriged model for Maximum Winter Mixed Layer Depth (m).

| **Prediction Error** | **Value** |
|---|---:|
| Number of Observations | 16376 |
| Overall Mean Error | -0.041 |
| Root Mean Square Prediction Error | 51.859 |
| Standardized Mean | $1.256 \times 10^{-4}$ |
| Standardized Root Mean Square Prediction Error | 2.001 |
| Average Standard Error | 26.141 |

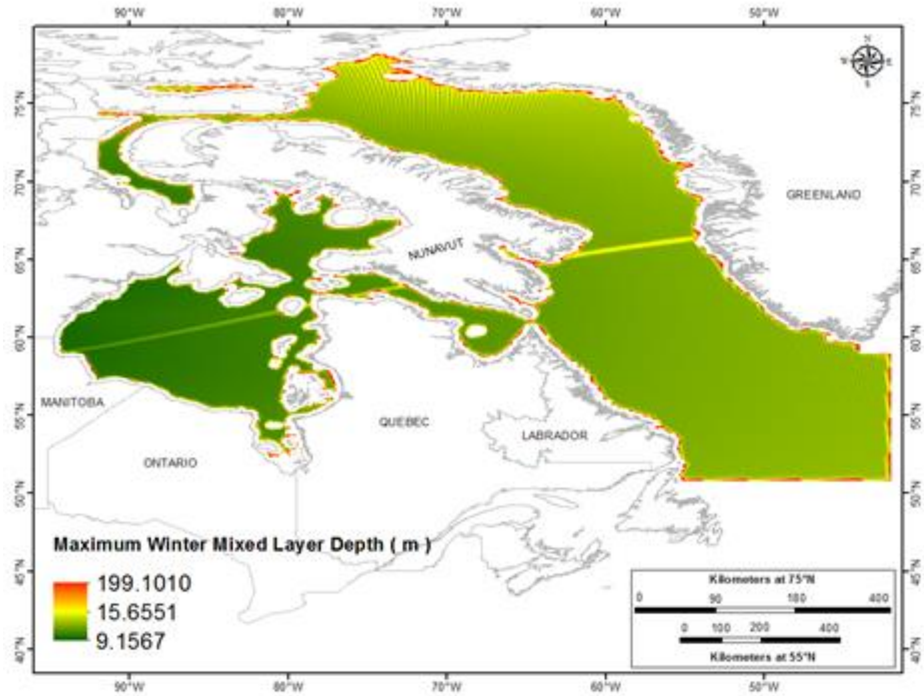


Figure 269. Prediction standard error surface of Maximum Winter Mixed Layer Depth (m).

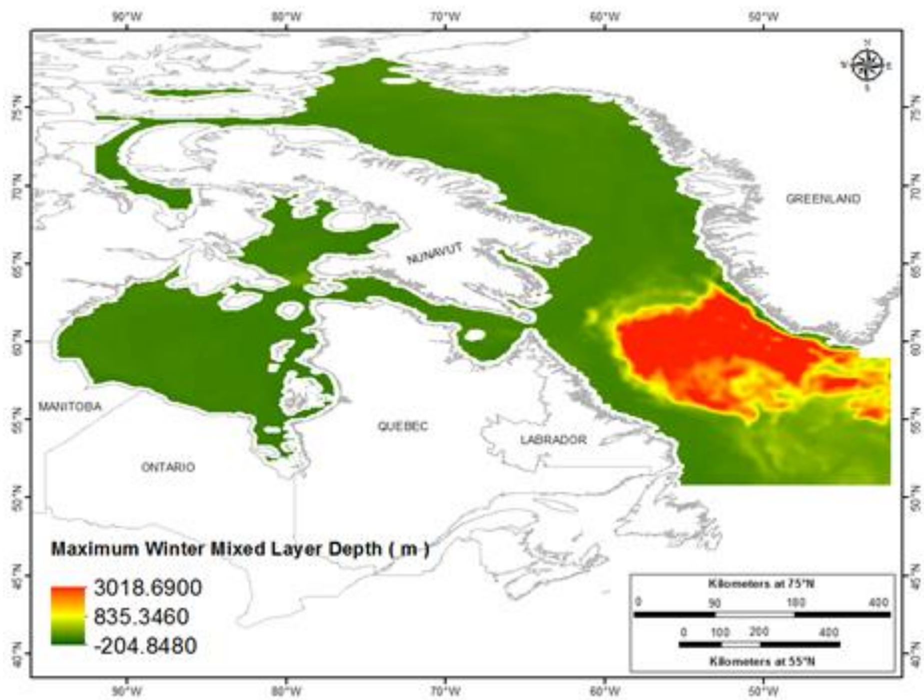


Figure 270. Interpolated prediction surface of Maximum Winter Mixed Layer Depth (m).

**Maximum Average Spring Mixed Layer Depth**

This variable displayed a right-skewed, leptokurtic distribution prior to interpolation (Table 109, Figure 271). The data were higher than predicted by a normal distribution at both tails, while mid-values were lower than the reference line (Figure 272). These areas of under- and over-prediction showed spatial pattern over the region (Figure 272).

The semivariogram showed moderate autocorrelation present in the data (Figure 273). The kriged model showed good fit between measured and predicted values (Figure 273). Good performance of the model was indicated by the cross-validation results (Table 110). The error map showed lower error in Hudson Bay compared to Baffin Bay and Davis Strait, and higher error along the edges of the study extent (Figure 274). The kriged surface is presented in Figure 275.

Table 109. Distributional properties of Maximum Average Spring Mixed Layer Depth (m).

| **Property** | **Value** |
|---|---:|
| Number of Observations | 16376 |
| Minimum | 10.768 |
| Maximum | 688.440 |
| Mean | 52.846 |
| Median | 32.658 |
| Standard Deviation | 61.182 |
| Skewness | 3.718 |
| Kurtosis | 21.944 |

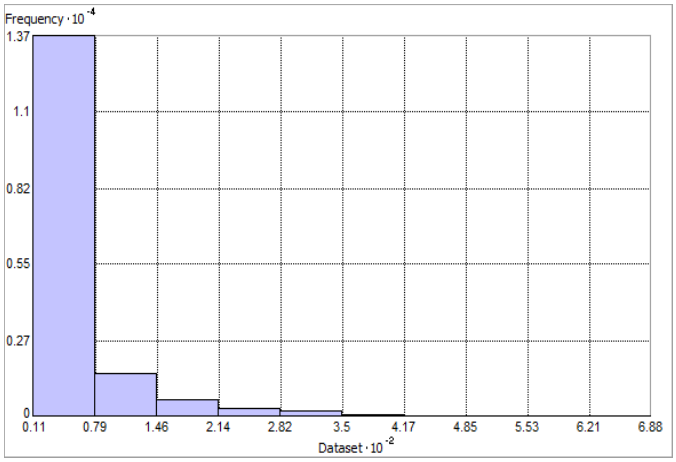


Figure 271. Distribution of Maximum Average Spring Mixed Layer Depth (m). Histogram was illustrated using 10 bins. X axis is shown at $10^{-2}$; Y axis is shown at $10^{-4}$.

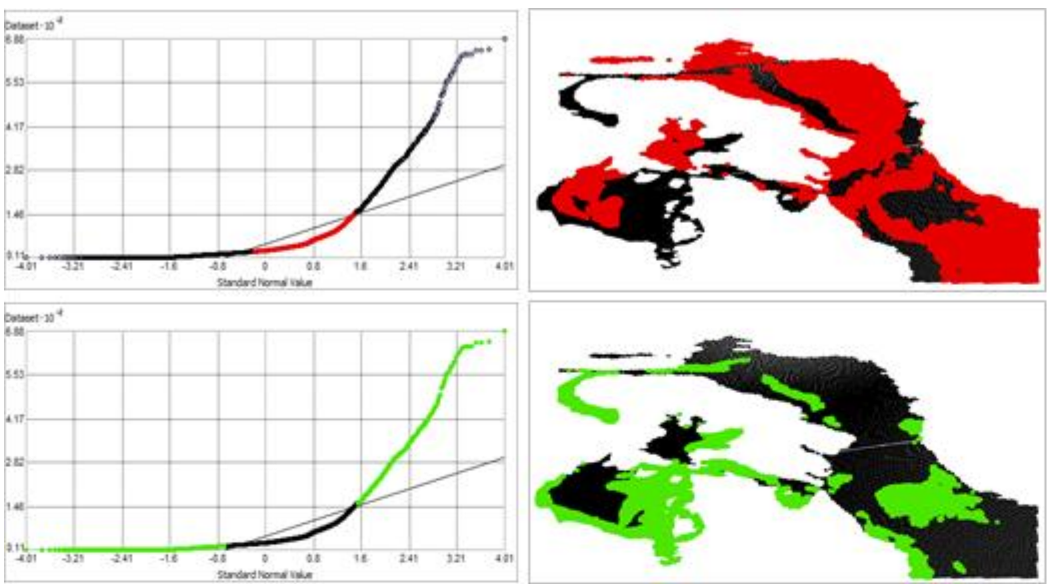

Figure 272. Normal Q-Q plot for data values of Maximum Average Spring Mixed Layer Depth (m). Points falling under (top right panel) and over (bottom right panel) the reference line are mapped.

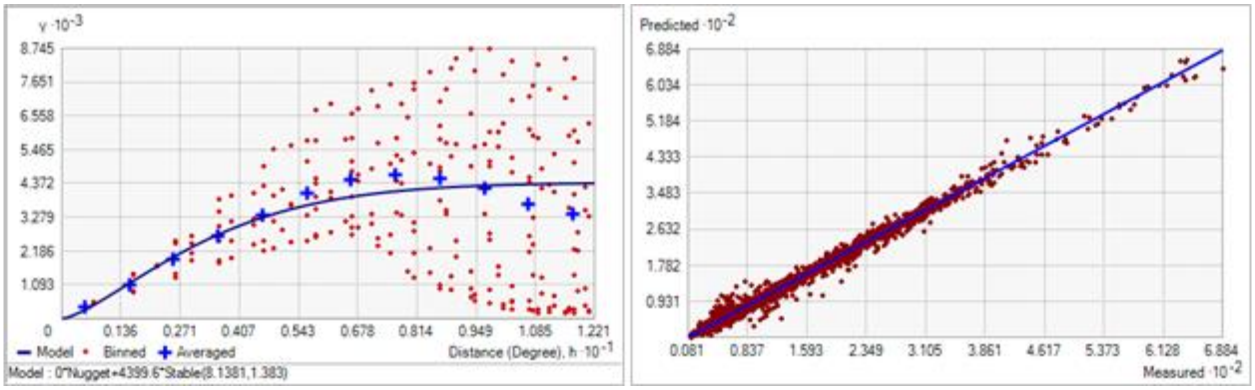


Figure 273. Left panel: Semivariogram of Maximum Average Spring Mixed Layer Depth (m). Binned values are shown as red dots; average points are shown as blue crosses; the model fit to the averaged values is shown as a blue line. Lag size: 1.017 degrees; number of lags: 12; Parameter: 1.383; Range: 8.138 degrees; Partial Sill: 4399.551. Right panel: Scatterplot of predicted values versus observed values for the model of Maximum Average Spring Mixed Layer Depth (m).

Table 110. Results of cross-validation of the kriged model for Maximum Average Spring Mixed Layer Depth (m).

| **Prediction Error** | **Value** |
|---|---:|
| Number of Observations | 16376 |
| Overall Mean Error | $-6.368 \times 10^{-3}$ |
| Root Mean Square Prediction Error | 4.340 |
| Standardized Mean | $-5.602 \times 10^{-4}$ |
| Standardized Root Mean Square Prediction Error | 0.747 |
| Average Standard Error | 5.656 |

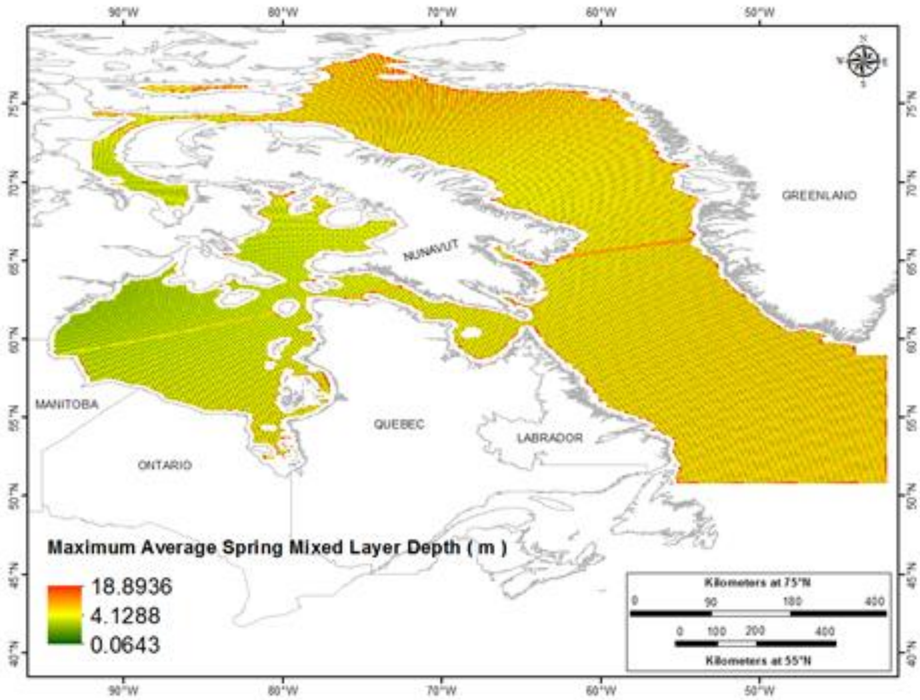


Figure 274. Prediction standard error surface of Maximum Average Spring Mixed Layer Depth (m).

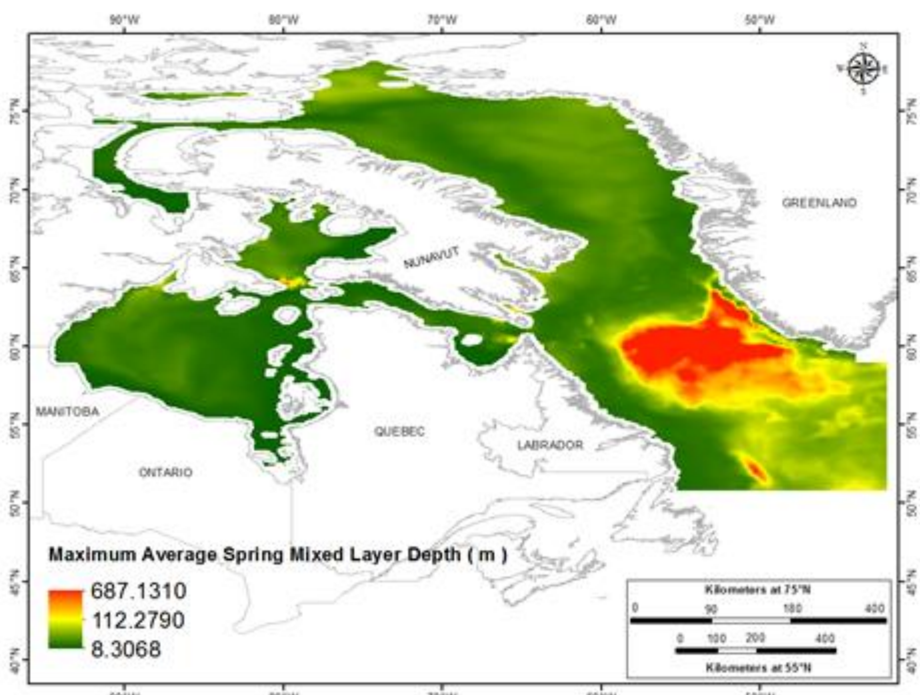


Figure 275. Interpolated prediction surface of Maximum Average Spring Mixed Layer Depth (m).

## Maximum Average Summer Mixed Layer Depth

This variable displayed a right-skewed, leptokurtic distribution prior to interpolation (Table 111, Figure 276). The data were greater than predicted by a normal distribution at the lowest and the highest, and upper mid-range values, and lower than predicted at lower mid-range values (Figure 277). These areas of under- and over-prediction showed a strong spatial pattern over the region (Figure 277).

The semivariogram showed weak autocorrelation present in the data (Figure 278). The kriged model showed good fit between measured and predicted values (Figure 278). Fair performance of the model was indicated by the cross-validation results (Table 112). The error map showed lower error in Hudson Bay compared to Baffin Bay and Davis Strait, and higher error along the edges of the study extent and in northern Baffin Bay (Figure 279). The kriged surface is presented in Figure 280.

Table 111. Distributional properties of Maximum Average Summer Mixed Layer Depth (m).

| Property | Value |
|---|---:|
| Number of Observations | 16376 |
| Minimum | 10.768 |
| Maximum | 71.450 |
| Mean | 17.144 |
| Median | 13.318 |
| Standard Deviation | 7.758 |
| Skewness | 1.371 |
| Kurtosis | 3.769 |

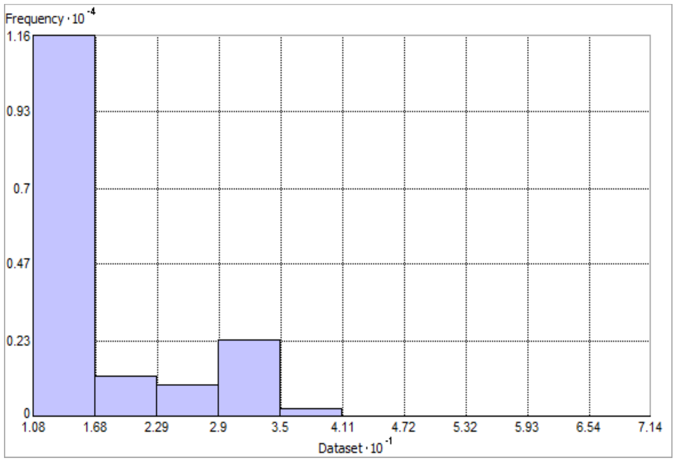


Figure 276. Distribution of Maximum Average Summer Mixed Layer Depth (m). Histogram was illustrated using 10 bins. X axis is shown at $10^{-1}$; Y axis is shown at $10^{-4}$.

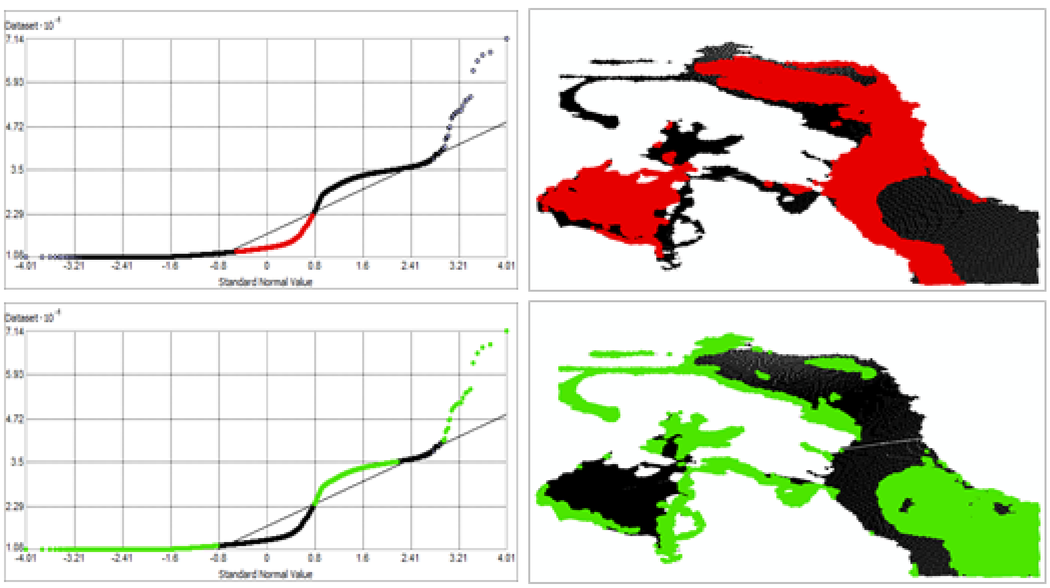


Figure 277. Normal Q-Q plot for data values of Maximum Average Summer Mixed Layer Depth (m). Points falling under (top right panel) and over (bottom right panel) the reference line are mapped.

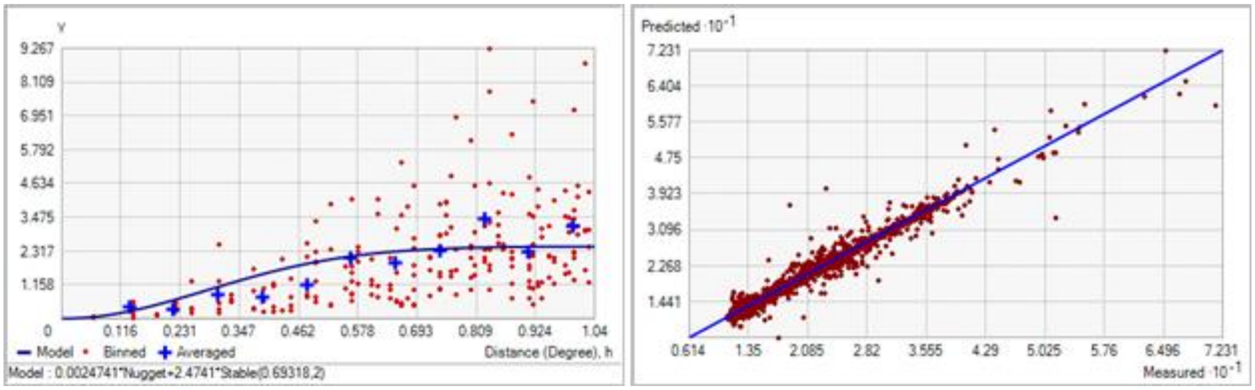


Figure 278. Left panel: Semivariogram of Maximum Average Summer Mixed Layer Depth (m). Binned values are shown as red dots; average points are shown as blue crosses; the model fit to the averaged values is shown as a blue line. Lag size: 0.087 degrees; number of lags: 12; Parameter: 2; Range: 0.693 degrees; Partial Sill: 2.474. Right panel: Scatterplot of predicted values versus observed values for the model of Maximum Average Summer Mixed Layer Depth (m).

Table 112. Results of cross-validation of the kriged model for Maximum Average Summer Mixed Layer Depth (m).

| **Prediction Error** | **Value** |
|---|---|
| Number of Observations | 16376 |
| Overall Mean Error | $1.003 \times 10^{-3}$ |
| Root Mean Square Prediction Error | 0.559 |
| Standardized Mean | $2.101 \times 10^{-3}$ |
| Standardized Root Mean Square Prediction Error | 5.407 |
| Average Standard Error | 0.129 |

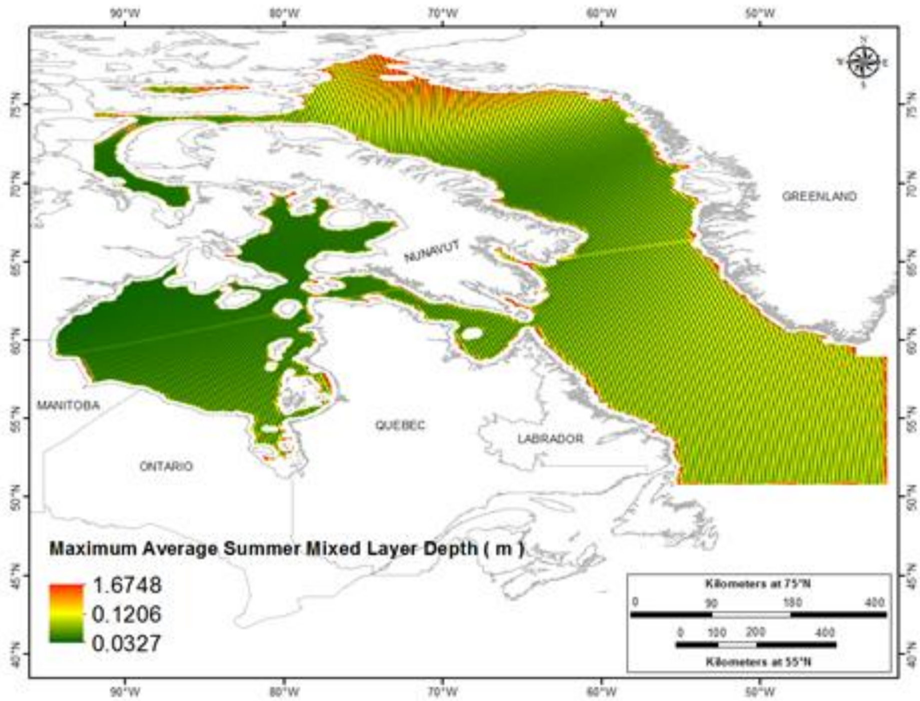


Figure 279. Prediction standard error surface of Maximum Average Summer Mixed Layer Depth (m).

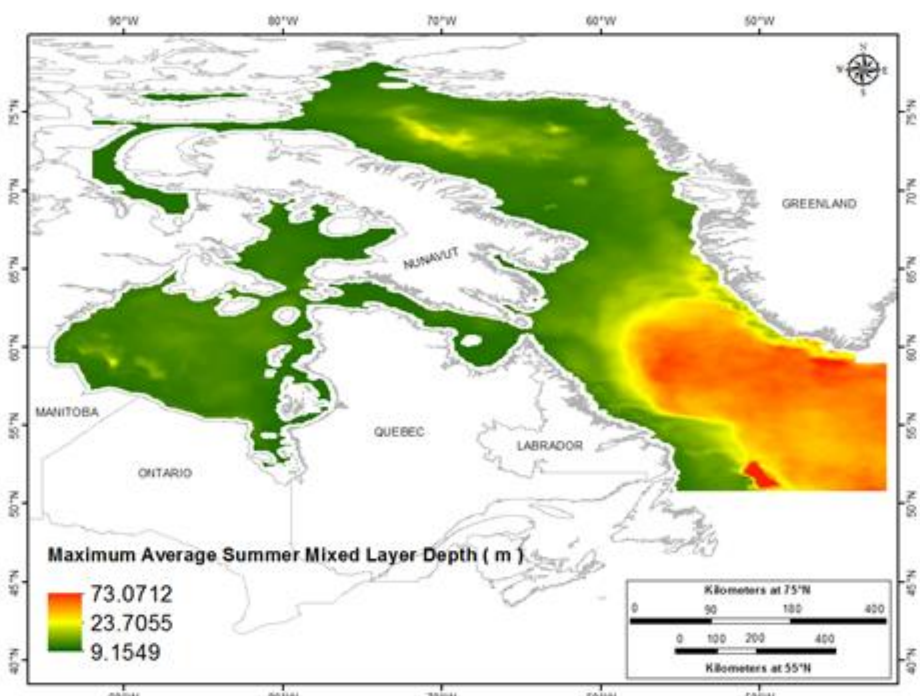


Figure 280. Interpolated prediction surface of Maximum Average Summer Mixed Layer Depth (m).

**Maximum Average Fall Mixed Layer Depth**

This variable displayed a right-skewed, extremely leptokurtic distribution prior to interpolation (Table 113, Figure 281). The data were higher than predicted by a normal distribution at both tails, while mid-values were lower than the reference line (Figure 282). These areas of under- and over-prediction showed a strong spatial pattern over the region (Figure 282).

The semivariogram showed autocorrelation present in the data (Figure 283). The kriged model showed good fit between measured and predicted values (Figure 283). Fair performance of the model was indicated by the cross-validation results (Table 114). The error map showed lower error in Hudson Bay compared to Baffin Bay and Davis Strait, and higher error along the edges of the study extent (Figure 284). The kriged surface is presented in Figure 285.

Table 113. Distributional properties of Maximum Average Fall Mixed Layer Depth (m).

| **Property** | **Value** |
|---|---:|
| Number of Observations | 16376 |
| Minimum | 10.884 |
| Maximum | 898.050 |
| Mean | 50.671 |
| Median | 28.843 |
| Standard Deviation | 61.793 |
| Skewness | 5.949 |
| Kurtosis | 56.735 |

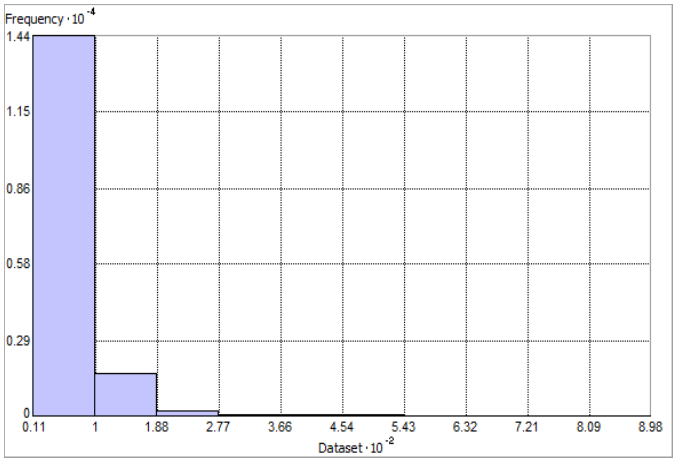


Figure 281. Distribution of Maximum Average Fall Mixed Layer Depth (m). Histogram was illustrated using 10 bins. X axis is shown at $10^{-2}$; Y axis is shown at $10^{-4}$.

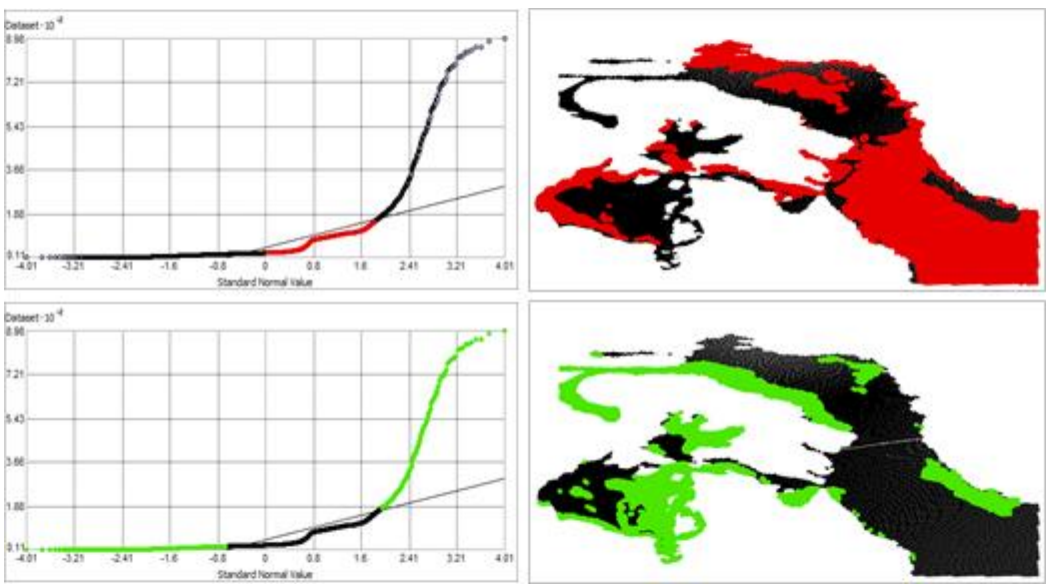

Figure 282. Normal Q-Q plot for data values of Maximum Average Fall Mixed Layer Depth (m). Points falling under (top right panel) and over (bottom right panel) the reference line are mapped.

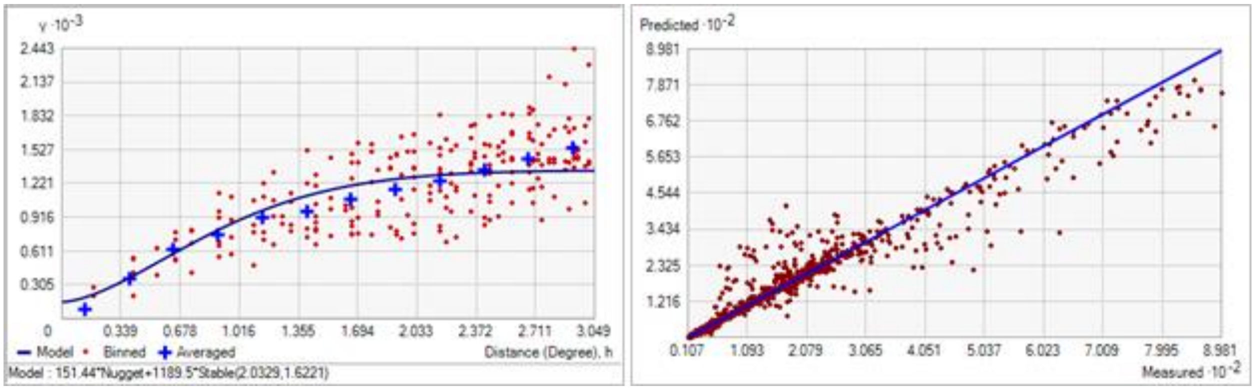


Figure 283. Left panel: Semivariogram of Maximum Average Fall Mixed Layer Depth (m). Binned values are shown as red dots; average points are shown as blue crosses; the model fit to the averaged values is shown as a blue line. Lag size: 0.254 degrees; number of lags: 12; Parameter: 1.622; Range: 2.033 degrees; Partial Sill: 1189.452. Right panel: Scatterplot of predicted values versus observed values for the model of Maximum Average Fall Mixed Layer Depth (m).

Table 114. Results of cross-validation of the kriged model for Maximum Average Fall Mixed Layer Depth (m).

| **Prediction Error** | **Value** |
|---|---:|
| Number of Observations | 16376 |
| Overall Mean Error | -0.012 |
| Root Mean Square Prediction Error | 11.126 |
| Standardized Mean | $-9.535 \times 10^{-4}$ |
| Standardized Root Mean Square Prediction Error | 0.761 |
| Average Standard Error | 14.433 |

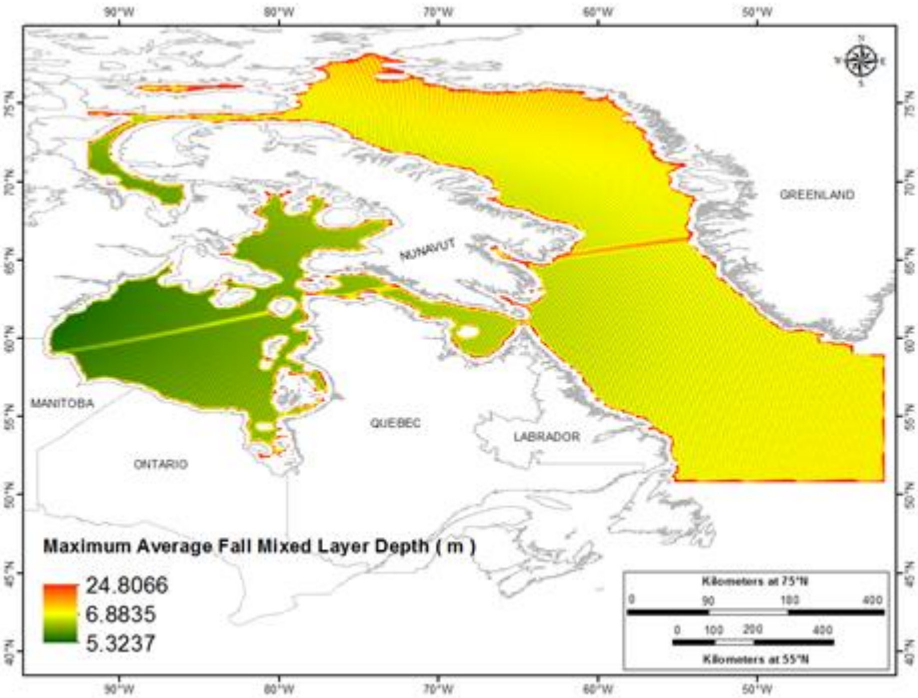


Figure 284. Prediction standard error surface of Maximum Average Fall Mixed Layer Depth (m).

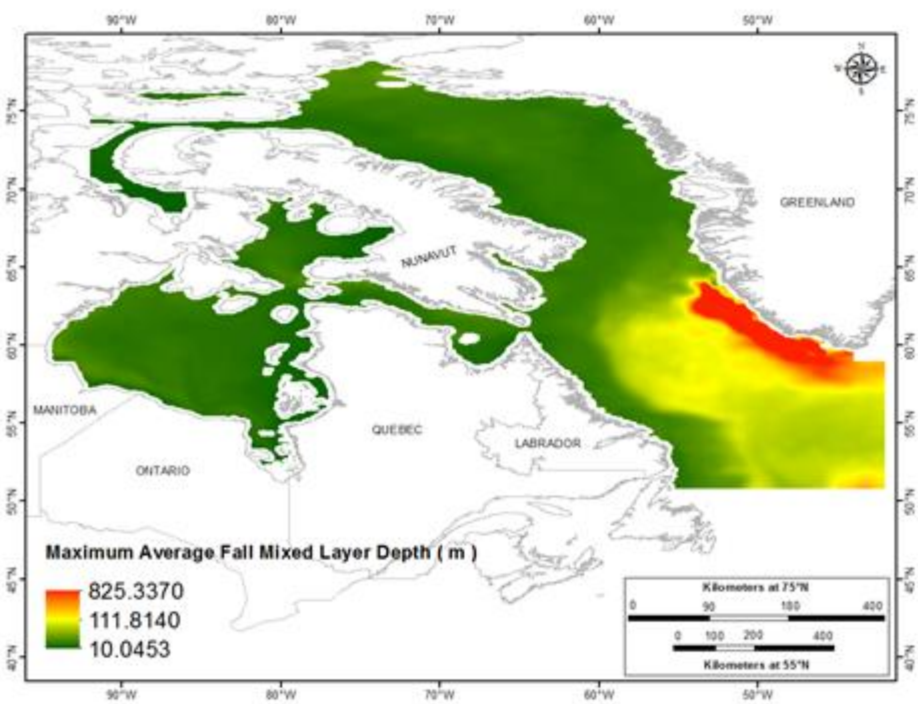


Figure 285. Interpolated prediction surface of Maximum Average Fall Mixed Layer Depth (m).

### Maximum Average Winter Mixed Layer Depth

This variable displayed a right-skewed, leptokurtic distribution prior to interpolation (Table 115, Figure 286). The data were higher than predicted by a normal distribution at both tails, while mid-values were lower than the reference line (Figure 287). These areas of under- and over-prediction showed a strong spatial pattern over the region (Figure 287).

The semivariogram showed weak autocorrelation present in the data (Figure 288). The kriged model showed good fit between measured and predicted values (Figure 288). Fair performance of the model was indicated by the cross-validation results (Table 116). The error map showed lower error in Hudson Bay compared to Baffin Bay and Davis Strait, and higher error along the edges of the study extent (Figure 289). The kriged surface is presented in Figure 290.

Table 115. Distributional properties of Maximum Average Winter Mixed Layer Depth (m).

| **Property** | **Value** |
|---|---:|
| Number of Observations | 16376 |
| Minimum | 10.768 |
| Maximum | 2183.800 |
| Mean | 122.720 |
| Median | 43.956 |
| Standard Deviation | 214.390 |
| Skewness | 3.820 |
| Kurtosis | 22.146 |

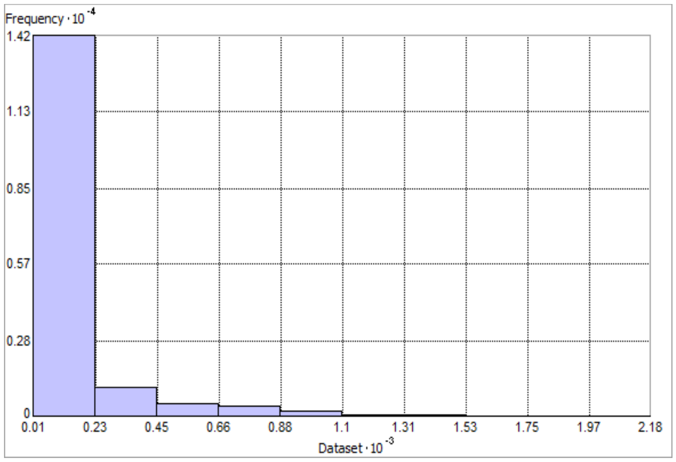


Figure 286. Distribution of Maximum Average Winter Mixed Layer Depth (m). Histogram was illustrated using 10 bins. X axis is shown at $10^{-3}$; Y axis is shown at $10^{-4}$.

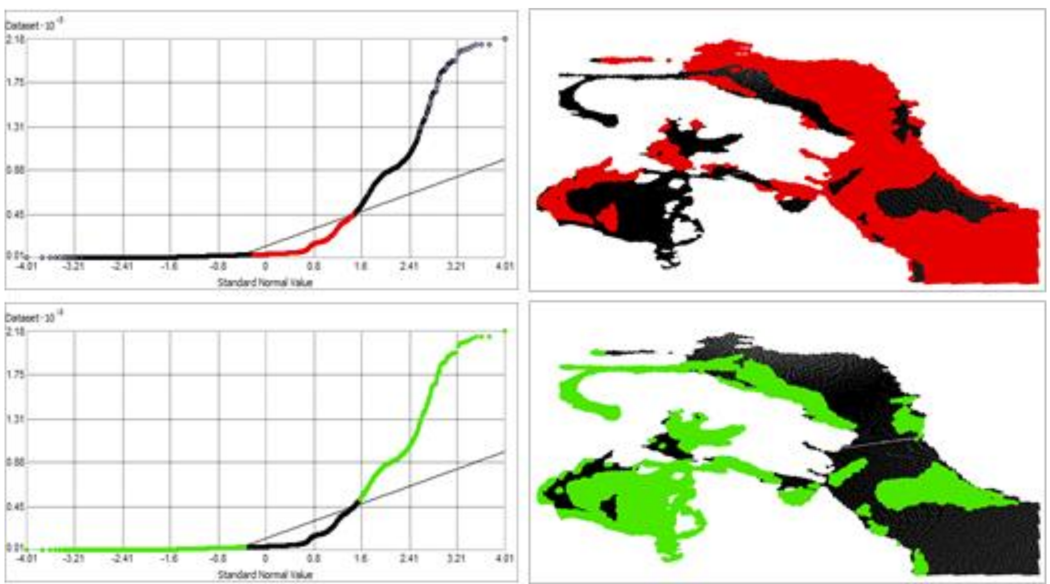

Figure 287. Normal Q-Q plot for data values of Maximum Average Winter Mixed Layer Depth (m). Points falling under (top right panel) and over (bottom right panel) the reference line are mapped.

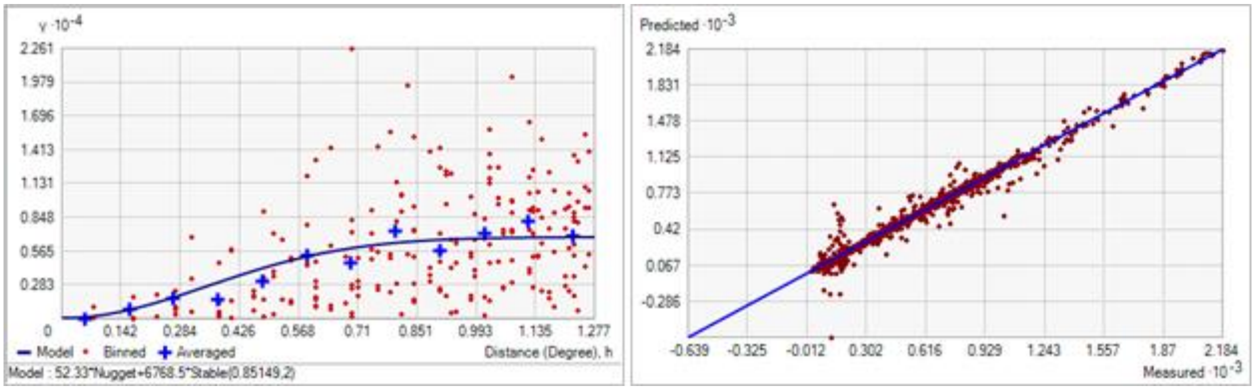

Figure 288. Left panel: Semivariogram of Maximum Average Winter Mixed Layer Depth (m). Binned values are shown as red dots; average points are shown as blue crosses; the model fit to the averaged values is shown as a blue line. Lag size: 0.106 degrees; number of lags: 12; Parameter: 2; Range: 0.851 degrees; Partial Sill: 6768.481. Right panel: Scatterplot of predicted values versus observed values for the model of Maximum Average Winter Mixed Layer Depth (m).

Table 116. Results of cross-validation of the kriged model for Maximum Average Winter Mixed Layer Depth (m).

| **Prediction Error** | **Value** |
|---|---:|
| Number of Observations | 16376 |
| Overall Mean Error | -0.056 |
| Root Mean Square Prediction Error | 17.368 |
| Standardized Mean | $-1.996 \times 10^{-3}$ |
| Standardized Root Mean Square Prediction Error | 1.593 |
| Average Standard Error | 10.337 |

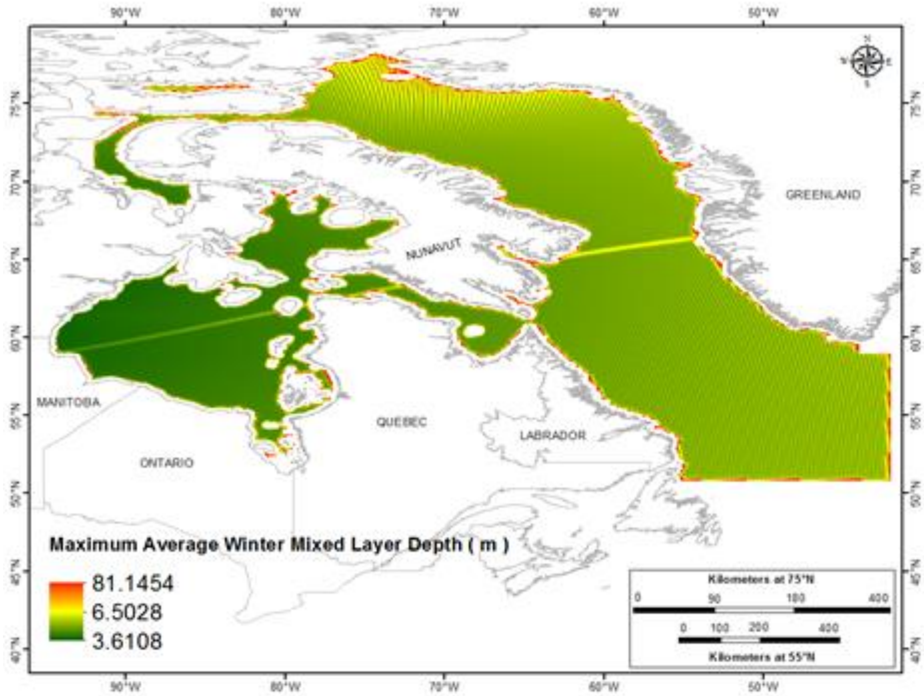


Figure 289. Prediction standard error surface of Maximum Average Winter Mixed Layer Depth (m).

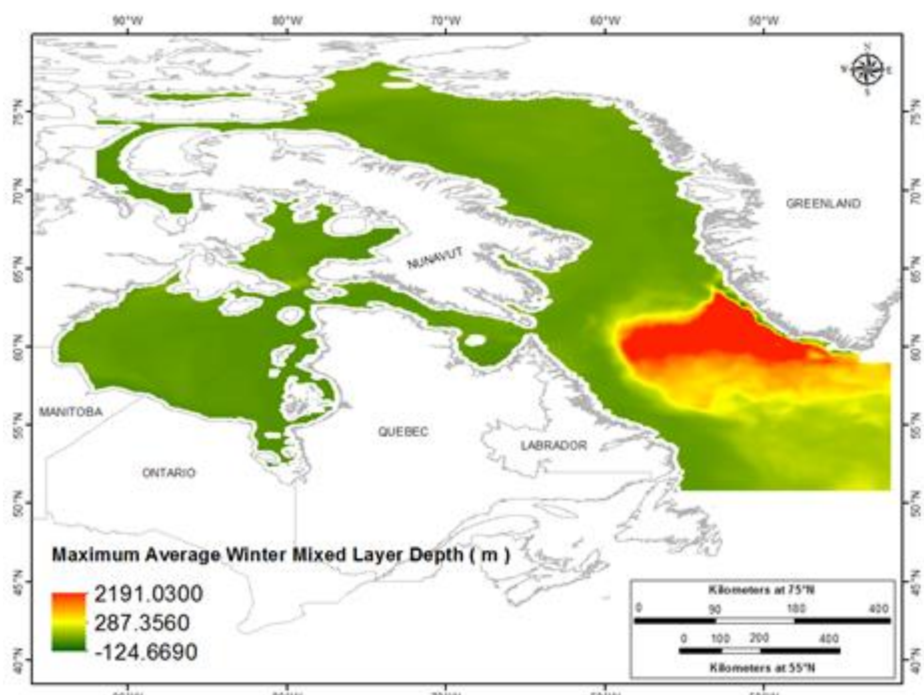


Figure 290. Interpolated prediction surface of Maximum Average Winter Mixed Layer Depth (m).

## Sea Surface Chlorophyll *a*

Sea surface chlorophyll *a* concentration is a proxy for phytoplankton biomass and is therefore related to the vertical flux of particulate organic carbon and food supply to the seafloor (Lutz et al., 2007). Gradients in food supply have often been identified as the main factor in controlling changes in benthic biomass, diversity, distribution, and zonation in the deep sea (Levin et al., 2001; Carney, 2005; Soltwedel et al., 2009; MacDonald et al., 2010; Papiol et al., 2012). In the northwest Atlantic, surface chlorophyll *a* has shown to be an important determinant in generalized linear models of megafaunal abundance and richness (Beazley et al. 2013) and was an important variable in random forest models predicting the presence of *Geodia* sponge and sponge grounds (Knudby et al., 2013). The spring phytoplankton bloom is thought to be a controlling factor in the reproductive cycles of several deep-sea corals (Sun et al., 2010a; 2010b; 2011; Mercier and Hamel, 2011) and sponges (Spetland et al., 2007) in the North Atlantic. Therefore, we expect that seasonal rather than annual measures of chlorophyll *a* will be more important in species distribution models.

### Spring Chlorophyll *a* Mean

This variable displayed a right-skewed, extremely leptokurtic distribution with outlying data in the upper range prior to interpolation (Table 117, Figure 291). The data were higher than predicted by a normal distribution at both tails, while mid-values were slightly lower than the reference line (Figure 292). These areas of under- and over-prediction showed little spatial pattern over the region (Figure 292).

The semivariogram showed very weak autocorrelation present in the data (Figure 293). The kriged model showed poor fit between measured and predicted values (Figure 293). Very good performance of the model was indicated by the cross-validation results (Table 118). The error map showed patches of high error across the study extent, particularly east off Baffin Island and in Foxe Basin (Figure 294). The kriged surface is presented in Figure 295.

Table 117. Distributional properties of Spring Chlorophyll *a* Mean (mg $m^{-3}$).

| Property | Value |
|---|---:|
| Number of Observations | 62911 |
| Minimum | 0.217 |
| Maximum | 25.219 |
| Mean | 1.155 |
| Median | 0.962 |
| Standard Deviation | 0.780 |
| Skewness | 6.934 |
| Kurtosis | 136.230 |

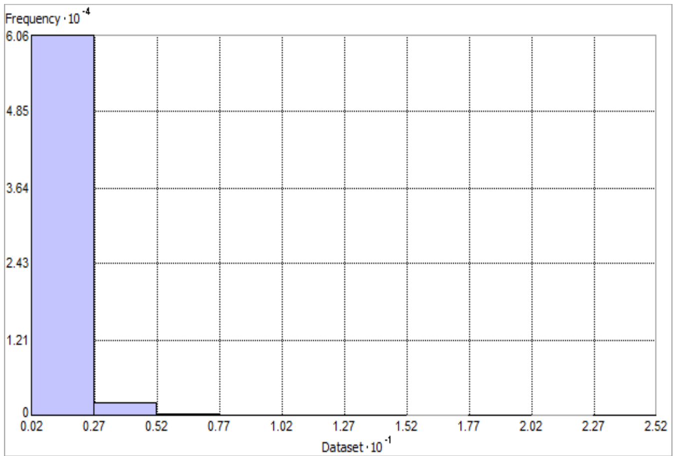


Figure 291. Distribution of Spring Chlorophyll *a* Mean (mg m$^{-3}$). Histogram was illustrated using 10 bins. X axis is shown at $10^{-1}$; Y axis is shown at $10^{-4}$.

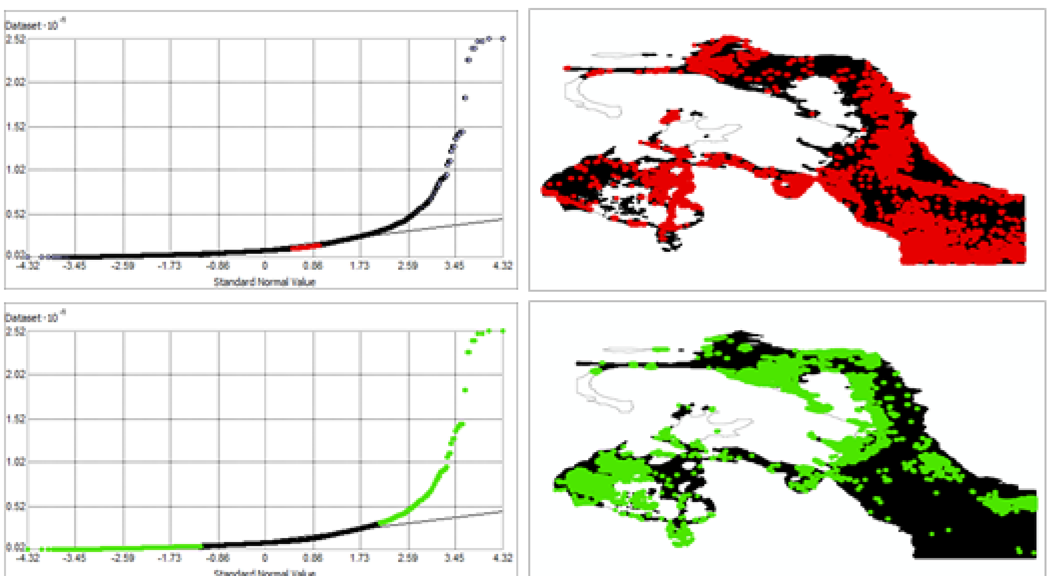


Figure 292. Normal Q-Q plot for data values of Spring Chlorophyll *a* Mean (mg m$^{-3}$). Points falling under (top right panel) and over (bottom right panel) the reference line are mapped.

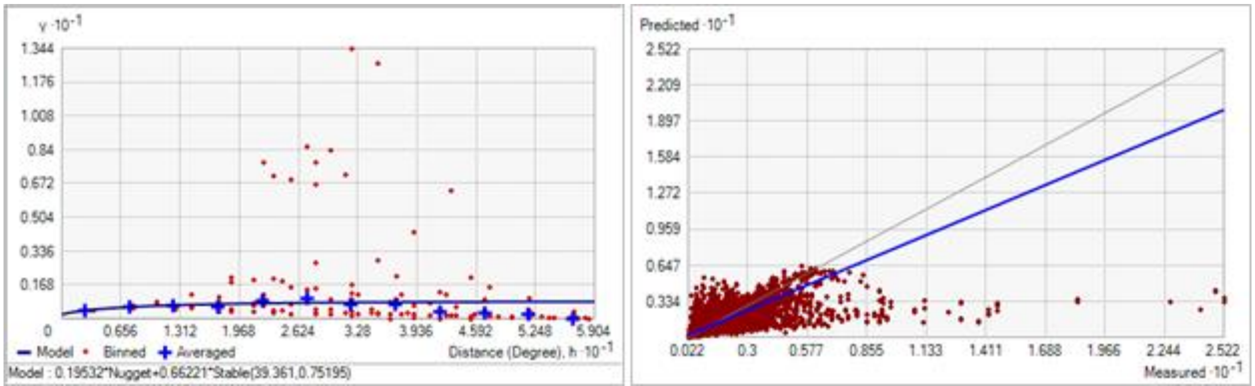

Figure 293. Left panel: Semivariogram of Spring Chlorophyll *a* Mean (mg $m^{-3}$). Binned values are shown as red dots; average points are shown as blue crosses; the model fit to the averaged values is shown as a blue line. Lag size: 4.920 degrees; number of lags: 12; Parameter: 0.752; Range: 39.361 degrees; Partial Sill: 0.662. Right panel: Scatterplot of predicted values versus observed values for the model of Spring Chlorophyll *a* Mean (mg $m^{-3}$).

Table 118. Results of cross-validation of the kriged model for Spring Chlorophyll *a* Mean (mg $m^{-3}$).

| Prediction Error | Value |
|---|---|
| Number of Observations | 62911 |
| Overall Mean Error | $1.659 \times 10^{-4}$ |
| Root Mean Square Prediction Error | 0.491 |
| Standardized Mean | $4.065 \times 10^{-4}$ |
| Standardized Root Mean Square Prediction Error | 1.023 |
| Average Standard Error | 0.478 |

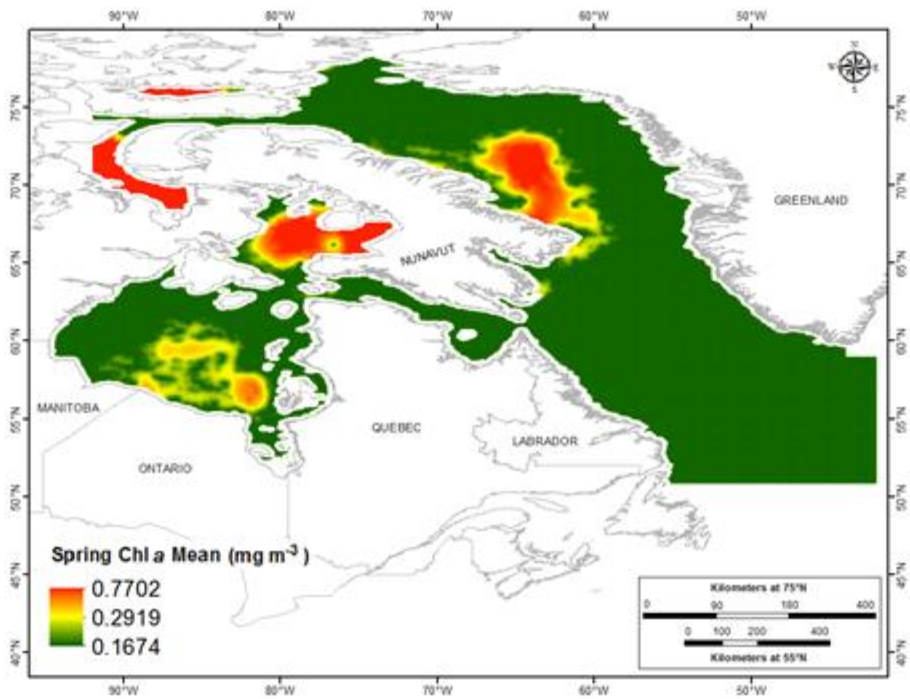


Figure 294. Prediction standard error surface of Spring Chlorophyll *a* Mean (mg m$^{-3}$).

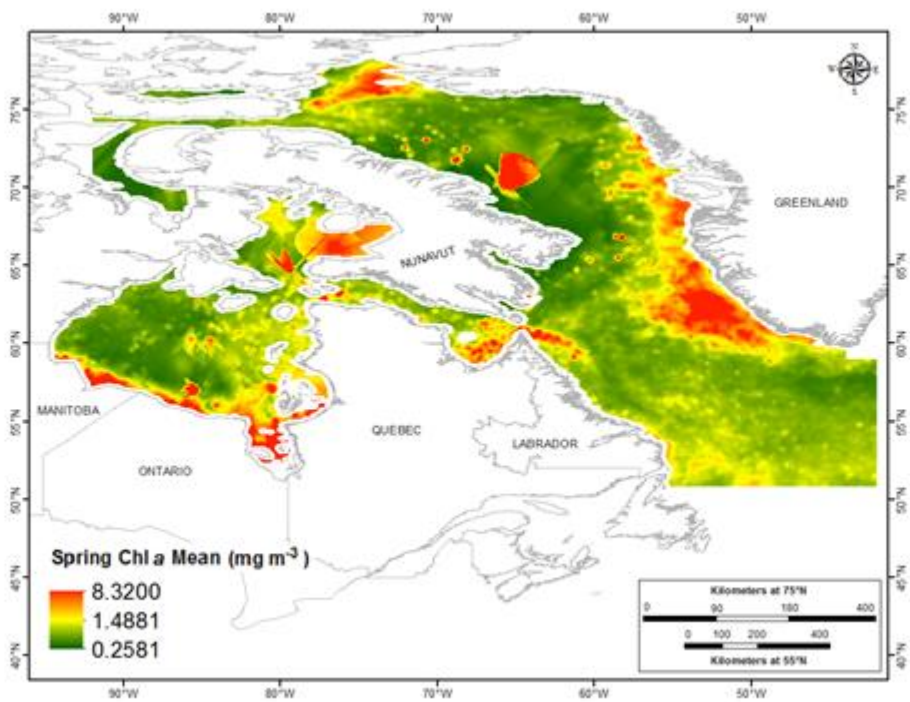


Figure 295. Interpolated prediction surface of Spring Chlorophyll *a* Mean (mg m$^{-3}$).

## Spring Chlorophyll *a* Minimum

This variable displayed a right-skewed, extremely leptokurtic distribution with outlying data in the upper range prior to interpolation (Table 119, Figure 296). The data were higher than predicted by a normal distribution at both tails, while mid-values were slightly lower than the reference line (Figure 297). These areas of under- and over-prediction showed a spatial pattern over the region (Figure 297).

The semivariogram showed autocorrelation present in the data (Figure 298). The kriged model showed moderate fit between measured and predicted values (Figure 298). Very good performance of the model was indicated by the cross-validation results (Table 120). The error map showed patches of high error across the study extent, particularly off Baffin Island, Foxe Basin, south of Hudson Bay and in the Gulf of Boothia (Figure 299). The kriged surface is presented in Figure 300.

Table 119. Distributional properties of Spring Chlorophyll *a* Minimum (mg $m^{-3}$).

| **Property** | **Value** |
|---|---:|
| Number of Observations | 62911 |
| Minimum | 0.025 |
| Maximum | 10.788 |
| Mean | 0.371 |
| Median | 0.303 |
| Standard Deviation | 0.294 |
| Skewness | 6.667 |
| Kurtosis | 105.650 |

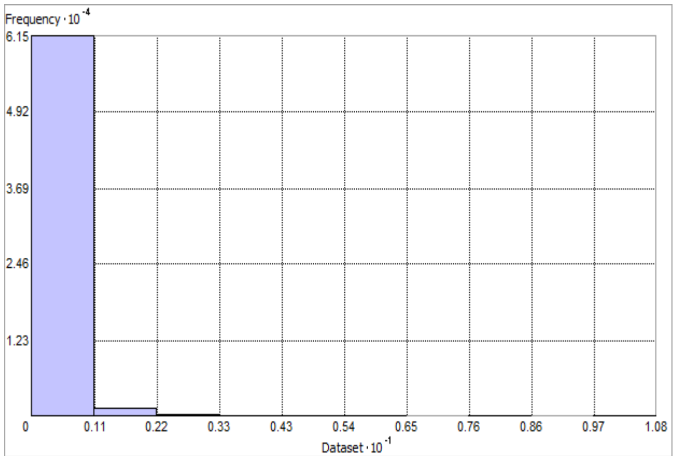

Figure 296. Distribution of Spring Chlorophyll *a* Minimum (mg m$^{-3}$). Histogram was illustrated using 10 bins. X axis is shown at $10^{-1}$; Y axis is shown at $10^{-4}$.

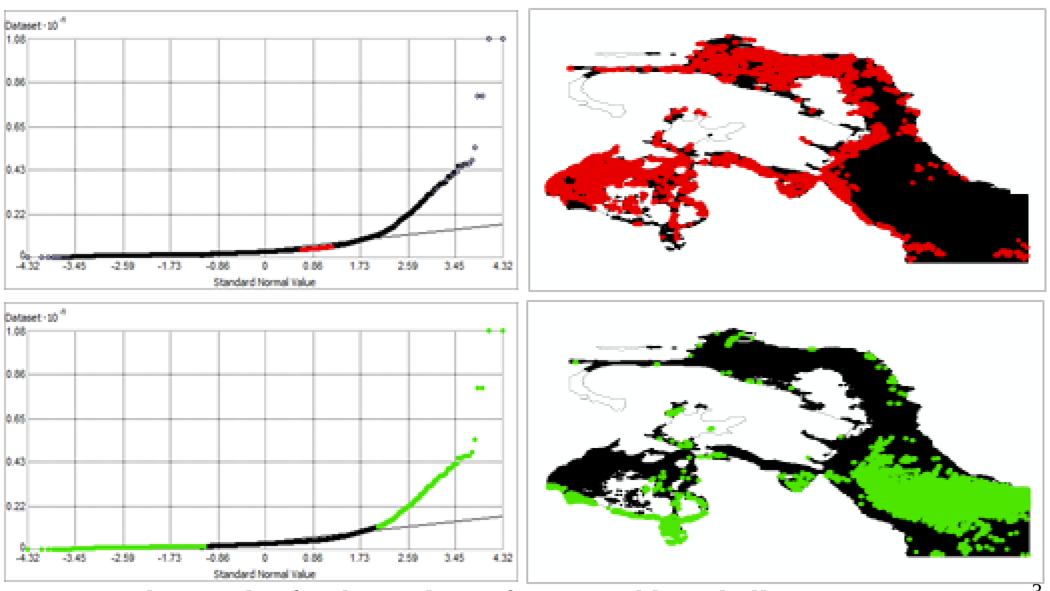

Figure 297. Normal Q-Q plot for data values of Spring Chlorophyll *a* Minimum (mg m$^{-3}$). Points falling under (top right panel) and over (bottom right panel) the reference line are mapped.

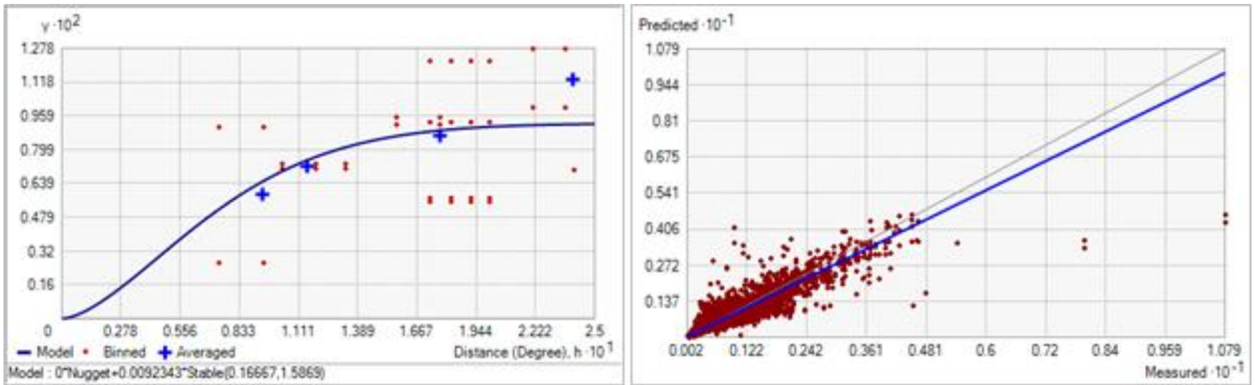

Figure 298. Left panel: Semivariogram of Spring Chlorophyll *a* Minimum (mg m$^{-3}$). Binned values are shown as red dots; average points are shown as blue crosses; the model fit to the averaged values is shown as a blue line. Lag size: 0.021 degrees; number of lags: 12; Parameter: 1.587; Range: 0.167 degrees; Partial Sill: 9.234 x 10$^{-3}$. Right panel: Scatterplot of predicted values versus observed values for the model of Spring Chlorophyll *a* Minimum (mg m$^{-3}$).

Table 120. Results of cross-validation of the kriged model for Spring Chlorophyll *a* Minimum (mg m$^{-3}$).

| **Prediction Error** | **Value** |
|---|---:|
| Number of Observations | 62911 |
| Overall Mean Error | -2.412 x 10$^{-5}$ |
| Root Mean Square Prediction Error | 0.101 |
| Standardized Mean | -3.218 x 10$^{-5}$ |
| Standardized Root Mean Square Prediction Error | 1.298 |
| Average Standard Error | 0.075 |

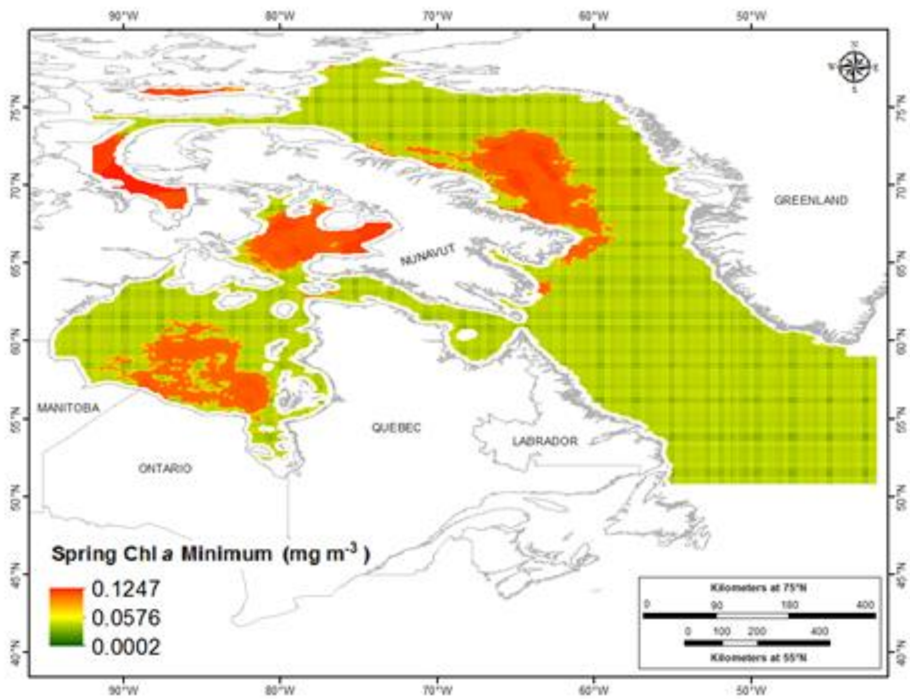


Figure 299. Prediction standard error surface of Spring Chlorophyll *a* Minimum (mg $m^{-3}$).

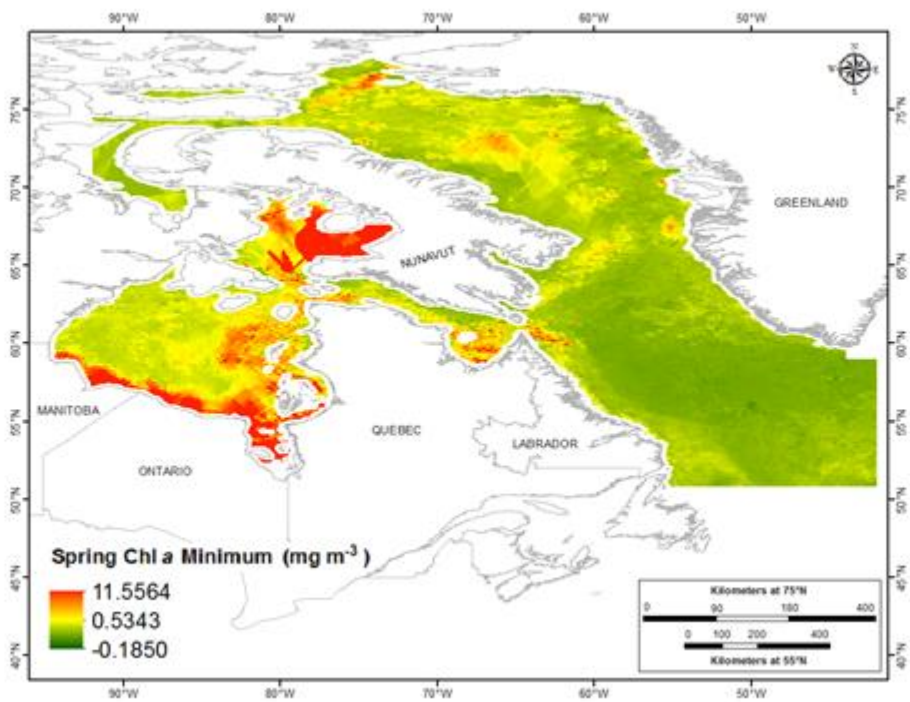


Figure 300. Interpolated prediction surface of Spring Chlorophyll *a* Minimum (mg $m^{-3}$).

## Spring Chlorophyll *a* Maximum

This variable displayed a right-skewed, extremely leptokurtic distribution prior to interpolation (Table 121, Figure 301). The data were higher than predicted by a normal distribution at both tails, while mid-values were slightly lower than the reference line (Figure 302). These areas of under- and over-prediction showed spatial pattern over the region (Figure 302).

The semivariogram showed autocorrelation present in the data (Figure 303). The kriged model showed poor fit between measured and predicted values (Figure 303). Good performance of the model was indicated by the cross-validation results (Table 122). The error map showed patches of high error across the study extent, particularly off Baffin Island, Foxe Basin, south of Hudson Bay and in the Gulf of Boothia (Figure 304). The kriged surface is presented in Figure 305.

Table 121. Distributional properties of Spring Chlorophyll *a* Maximum (mg $m^{-3}$).

| **Property** | **Value** |
|---|---:|
| Number of Observations | 62911 |
| Minimum | 0.232 |
| Maximum | 98.423 |
| Mean | 4.023 |
| Median | 2.506 |
| Standard Deviation | 4.937 |
| Skewness | 5.079 |
| Kurtosis | 53.261 |

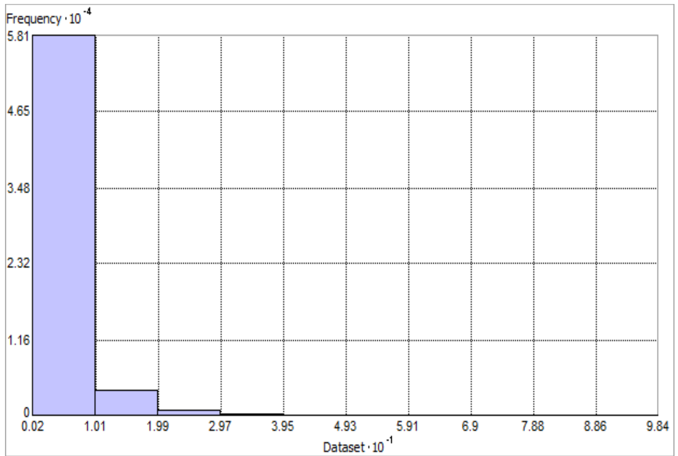


Figure 301. Distribution of Spring Chlorophyll *a* Maximum (mg m$^{-3}$). Histogram was illustrated using 10 bins. X axis is shown at $10^{-1}$; Y axis is shown at $10^{-4}$.

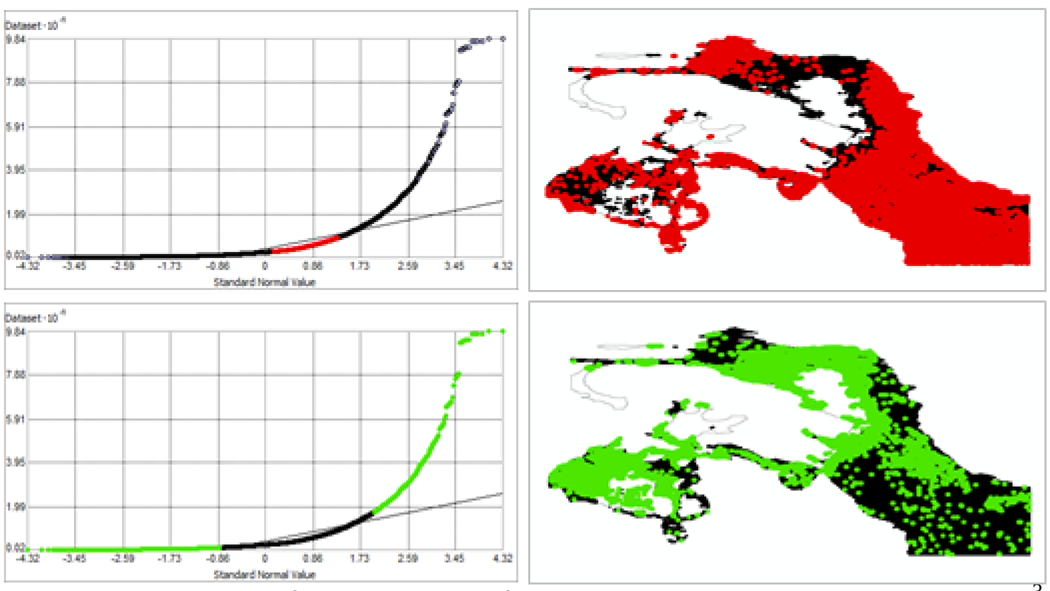


Figure 302. Normal Q-Q plot for data values of Spring Chlorophyll *a* Maximum (mg m$^{-3}$). Points falling under (top right panel) and over (bottom right panel) the reference line are mapped.

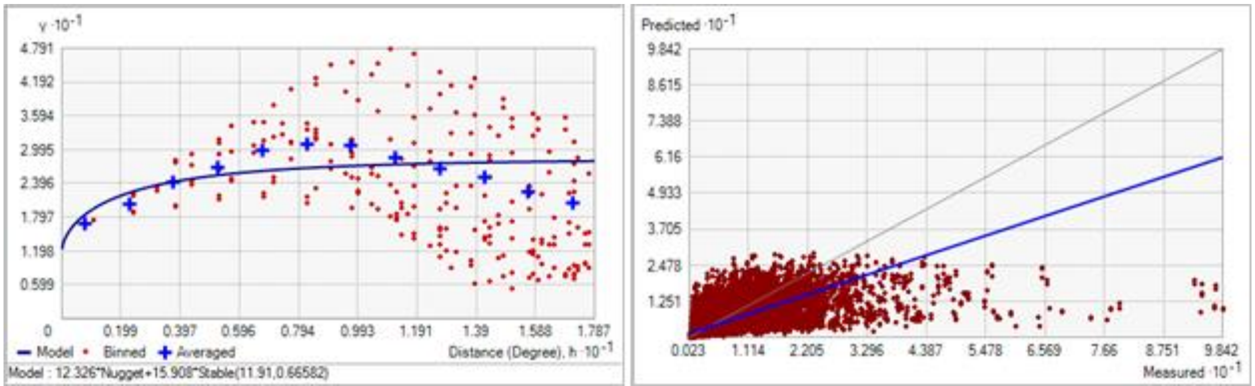

Figure 303. Left panel: Semivariogram of Spring Chlorophyll *a* Maximum (mg $m^{-3}$). Binned values are shown as red dots; average points are shown as blue crosses; the model fit to the averaged values is shown as a blue line. Lag size: 1.489 degrees; number of lags: 12; Parameter: 0.666; Range: 11.910 degrees; Partial Sill: 15.908. Right panel: Scatterplot of predicted values versus observed values for the model of Spring Chlorophyll *a* Maximum (mg $m^{-3}$).

Table 122. Results of cross-validation of the kriged model for Spring Chlorophyll *a* Maximum (mg $m^{-3}$).

| **Prediction Error** | **Value** |
|---|---:|
| Number of Observations | 62911 |
| Overall Mean Error | $6.692 \times 10^{-5}$ |
| Root Mean Square Prediction Error | 3.484 |
| Standardized Mean | $2.463 \times 10^{-5}$ |
| Standardized Root Mean Square Prediction Error | 0.902 |
| Average Standard Error | 3.866 |

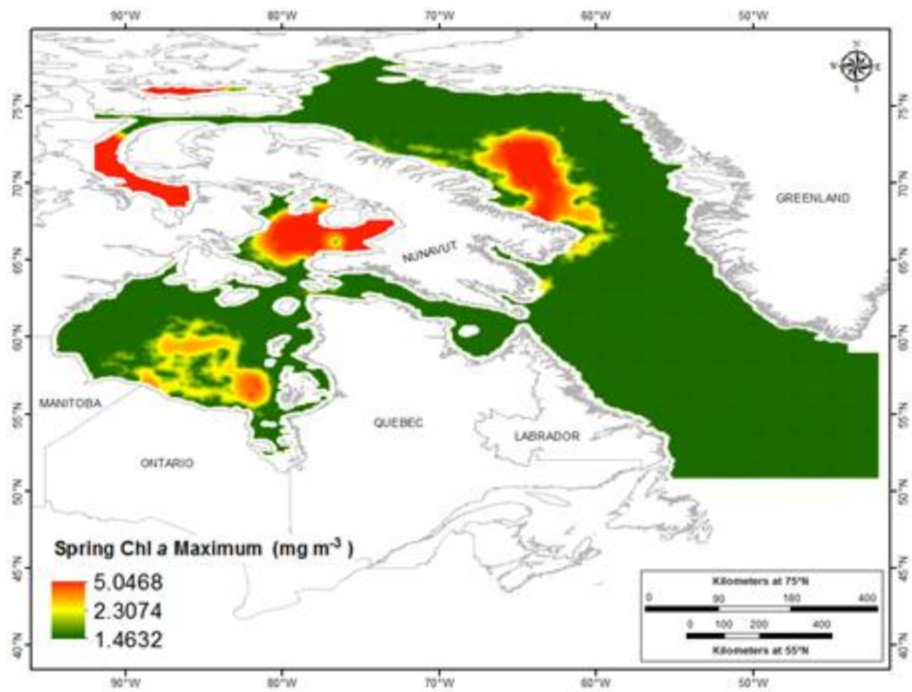


Figure 304. Prediction standard error surface of Spring Chlorophyll *a* Maximum (mg $m^{-3}$).

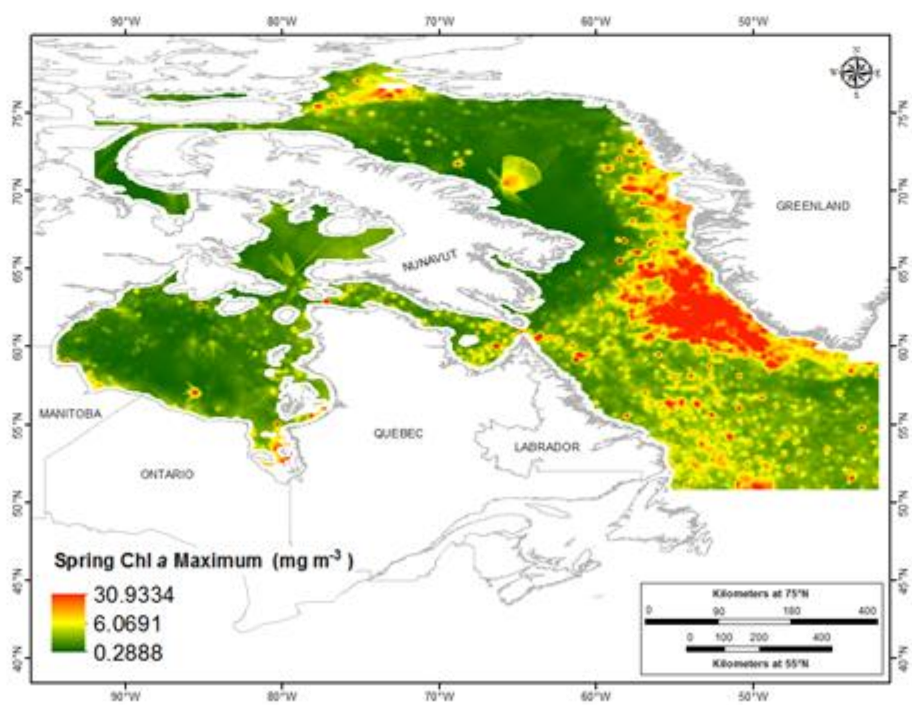


Figure 305. Interpolated prediction surface of Spring Chlorophyll *a* Maximum (mg $m^{-3}$).

**Spring Chlorophyll *a* Range**

This variable displayed a right-skewed, extremely leptokurtic distribution prior to interpolation (Table 123, Figure 306). The data were higher than predicted by a normal distribution at both tails, while mid-values were slightly lower than the reference line (Figure 307). These areas of under- and over-prediction showed strong spatial pattern over the region (Figure 307).

The semivariogram showed weak autocorrelation present in the data (Figure 308). The kriged model showed poor fit between measured and predicted values (Figure 308). Good performance of the model was indicated by the cross-validation results (Table 124). The error map showed patches of high error across the study extent, particularly off Baffin Island, Foxe Basin, south of Hudson Bay and in the Gulf of Boothia (Figure 309). The kriged surface is presented in Figure 310.

Table 123. Distributional properties of Spring Chlorophyll *a* Range (mg $m^{-3}$).

| **Property** | **Value** |
|---|---:|
| Number of Observations | 62911 |
| Minimum | $3.001 \times 10^{-5}$ |
| Maximum | 98.108 |
| Mean | 3.653 |
| Median | 2.180 |
| Standard Deviation | 4.960 |
| Skewness | 5.023 |
| Kurtosis | 52.382 |

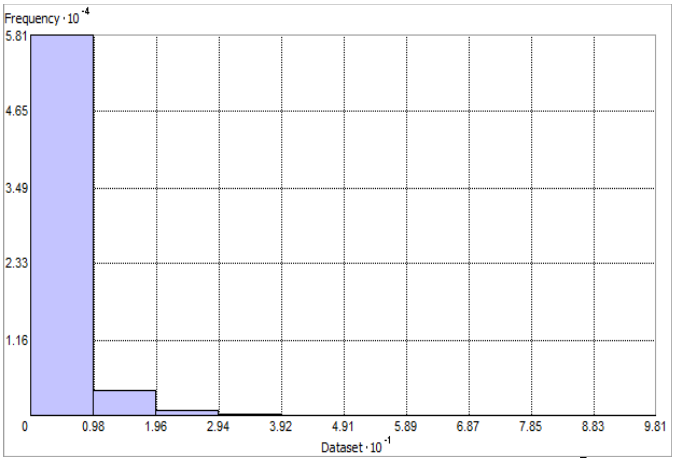


Figure 306. Distribution of Spring Chlorophyll *a* Range (mg m$^{-3}$). Histogram was illustrated using 10 bins. X axis is shown at $10^{-1}$; Y axis is shown at $10^{-4}$.

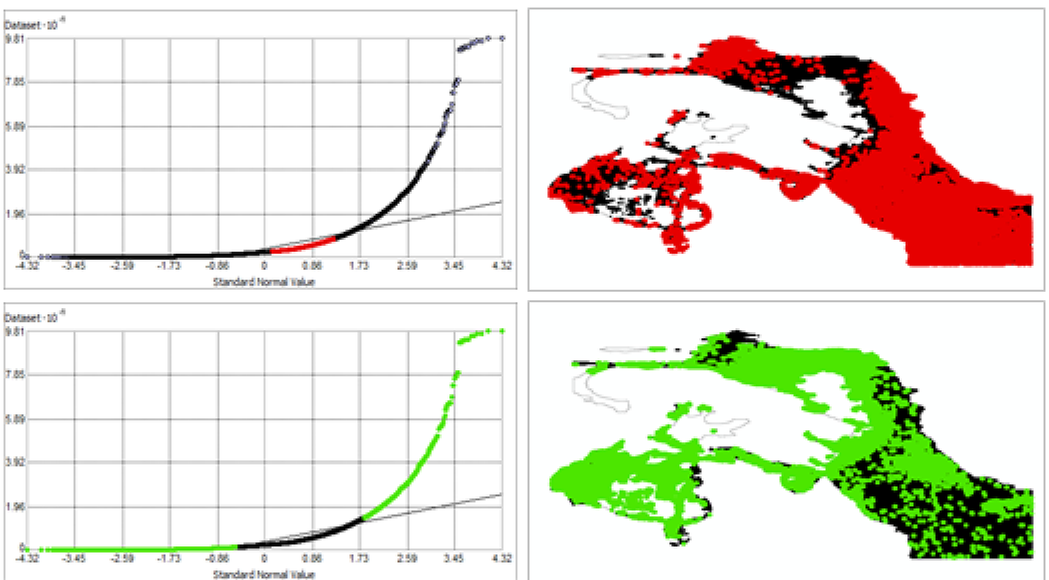

Figure 307. Normal Q-Q plot for data values of Spring Chlorophyll *a* Range (mg m$^{-3}$). Points falling under (top right panel) and over (bottom right panel) the reference line are mapped.

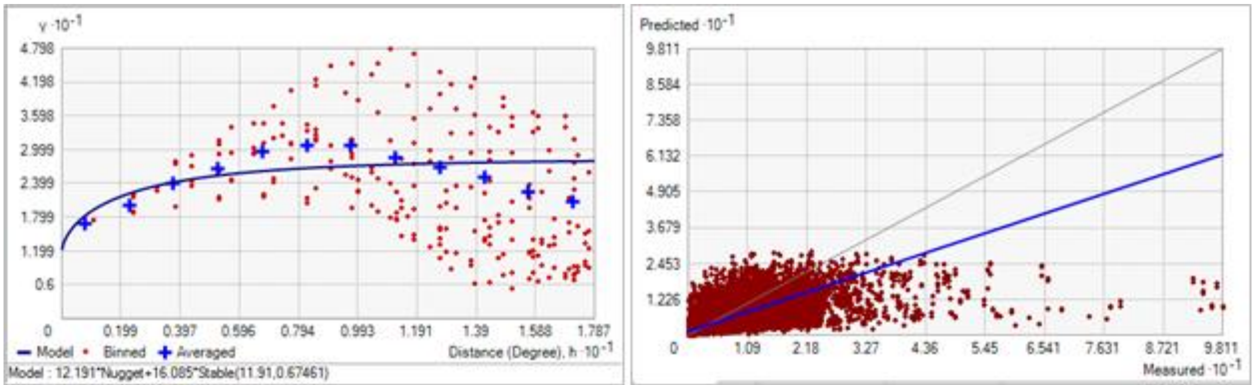


Figure 308. Left panel: Semivariogram of Spring Chlorophyll *a* Range (mg $m^{-3}$). Binned values are shown as red dots; average points are shown as blue crosses; the model fit to the averaged values is shown as a blue line. Lag size: 1.489 degrees; number of lags: 12; Parameter: 0.675; Range: 11.910 degrees; Partial Sill: 16.085. Right panel: Scatterplot of predicted values versus observed values for the model of Spring Chlorophyll *a* Range (mg $m^{-3}$).

Table 124. Results of cross-validation of the kriged model for Spring Chlorophyll *a* Range (mg $m^{-3}$).

| **Prediction Error** | **Value** |
|---|---:|
| Number of Observations | 62911 |
| Overall Mean Error | $3.099 \times 10^{-5}$ |
| Root Mean Square Prediction Error | 3.482 |
| Standardized Mean | $1.272 \times 10^{-5}$ |
| Standardized Root Mean Square Prediction Error | 0.907 |
| Average Standard Error | 3.840 |

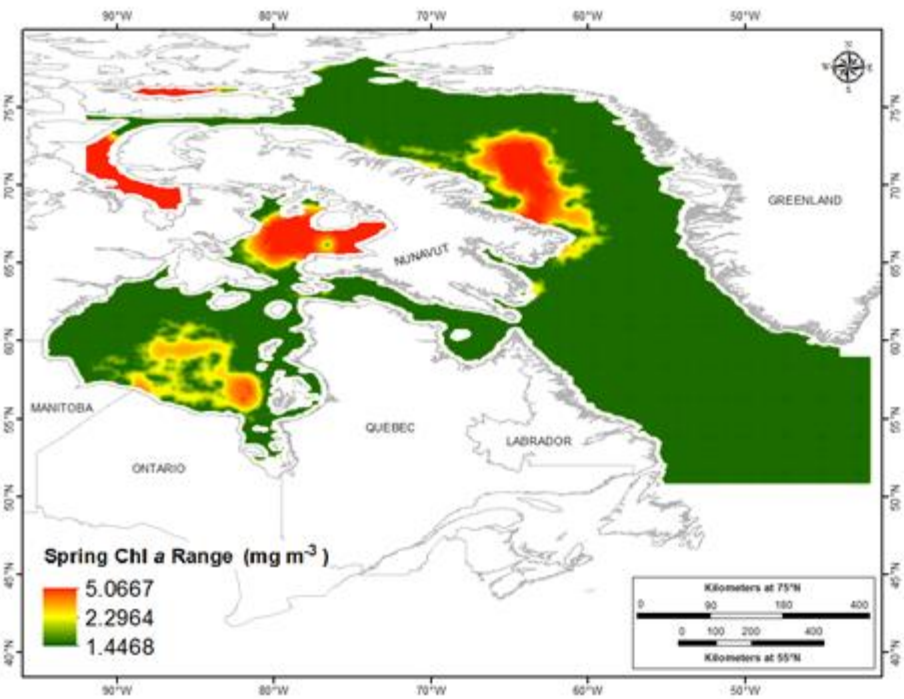


Figure 309. Prediction standard error surface of Spring Chlorophyll *a* Range (mg m$^{-3}$).

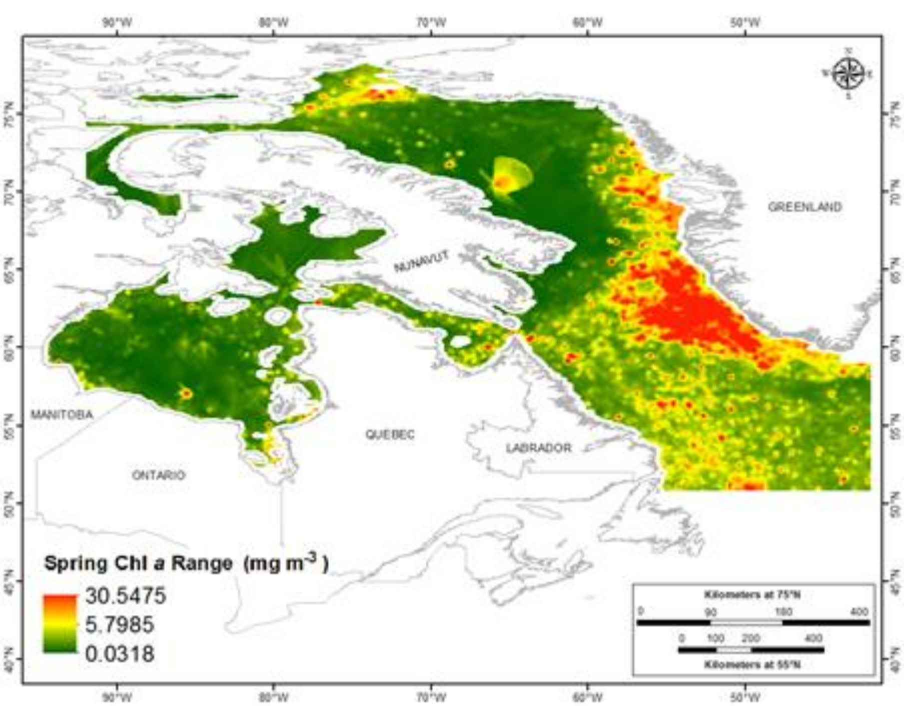


Figure 310. Interpolated prediction surface of Spring Chlorophyll *a* Range (mg m$^{-3}$).

**Summer Chlorophyll *a* Mean**

This variable displayed a right-skewed, leptokurtic distribution with outlying data in the upper range prior to interpolation (Table 125, Figure 311). The data were higher than predicted by a normal distribution at both tails, while mid-values were slightly lower than the reference line (Figure 312). These areas of under- and over-prediction showed spatial pattern over the region (Figure 312).

The semivariogram showed autocorrelation present in the data (Figure 313). The kriged model showed a good fit between measured and predicted values (Figure 313). Good performance of the model was indicated by the cross-validation results (Table 126). The error map displayed a grid-like pattern over the study extent (Figure 314). The kriged surface is presented in Figure 315.

Table 125. Distributional properties of Summer Chlorophyll *a* Mean (mg $m^{-3}$).

| **Property** | **Value** |
|---|---:|
| Number of Observations | 77369 |
| Minimum | 0.277 |
| Maximum | 8.013 |
| Mean | 0.699 |
| Median | 0.607 |
| Standard Deviation | 0.411 |
| Skewness | 3.935 |
| Kurtosis | 30.406 |

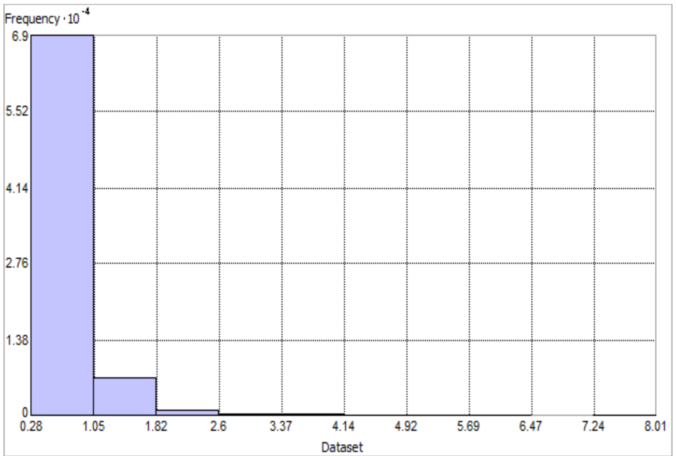

Figure 311. Distribution of Summer Chlorophyll *a* Mean (mg $m^{-3}$). Histogram was illustrated using 10 bins. Y axis is shown at $10^{-4}$.

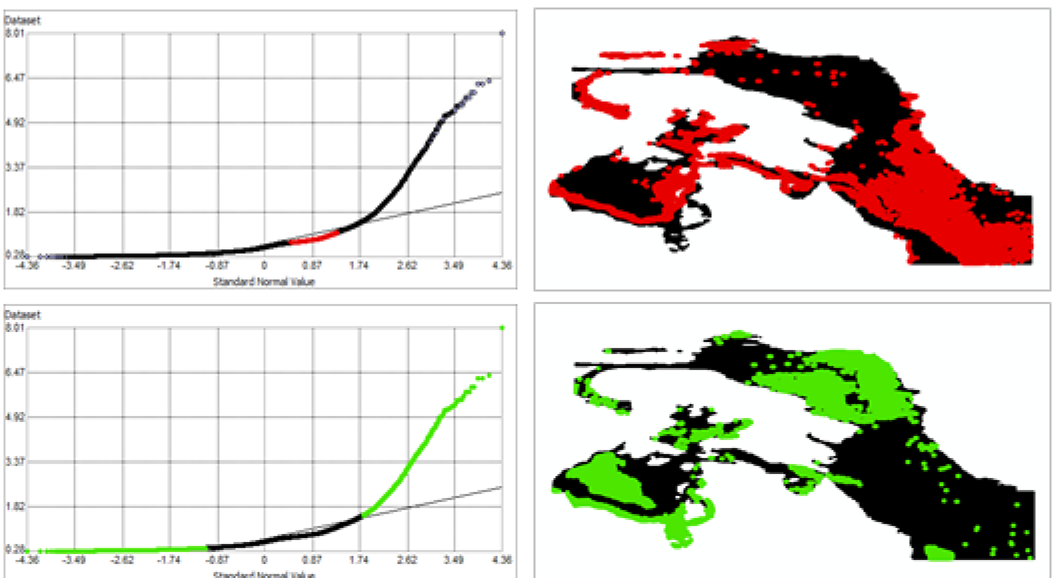

Figure 312. Normal Q-Q plot for data values of Summer Chlorophyll *a* Mean (mg $m^{-3}$). Points falling under (top right panel) and over (bottom right panel) the reference line are mapped.

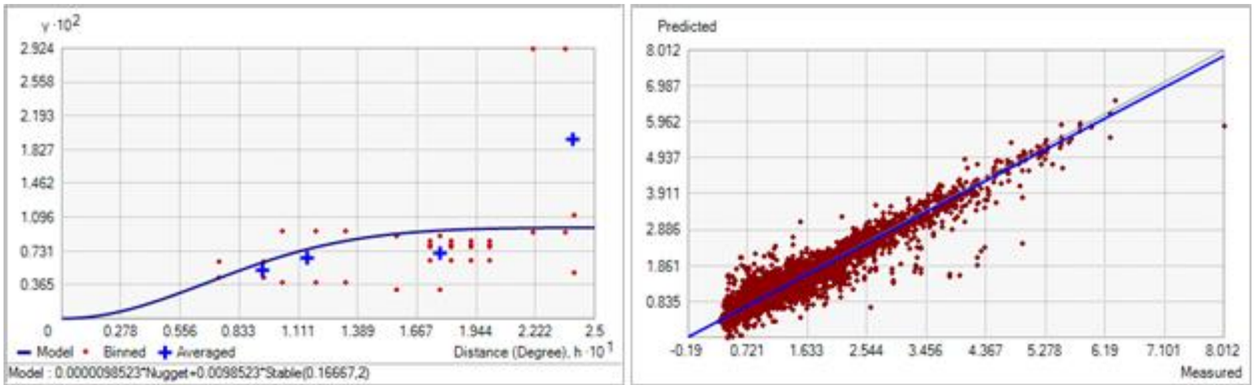

Figure 313. Left panel: Semivariogram of Summer Chlorophyll *a* Mean (mg $m^{-3}$). Binned values are shown as red dots; average points are shown as blue crosses; the model fit to the averaged values is shown as a blue line. Lag size: 0.021 degrees; number of lags: 12; Parameter: 2; Range: 0.167 degrees; Partial Sill: $9.852 \times 10^{-3}$. Right panel: Scatterplot of predicted values versus observed values for the model of Summer Chlorophyll *a* Mean (mg $m^{-3}$).

Table 126. Results of cross-validation of the kriged model for Summer Chlorophyll *a* Mean (mg $m^{-3}$).

| **Prediction Error** | **Value** |
|---|---:|
| Number of Observations | 77369 |
| Overall Mean Error | $-3.061 \times 10^{-4}$ |
| Root Mean Square Prediction Error | 0.086 |
| Standardized Mean | $-2.324 \times 10^{-3}$ |
| Standardized Root Mean Square Prediction Error | 1.593 |
| Average Standard Error | 0.052 |

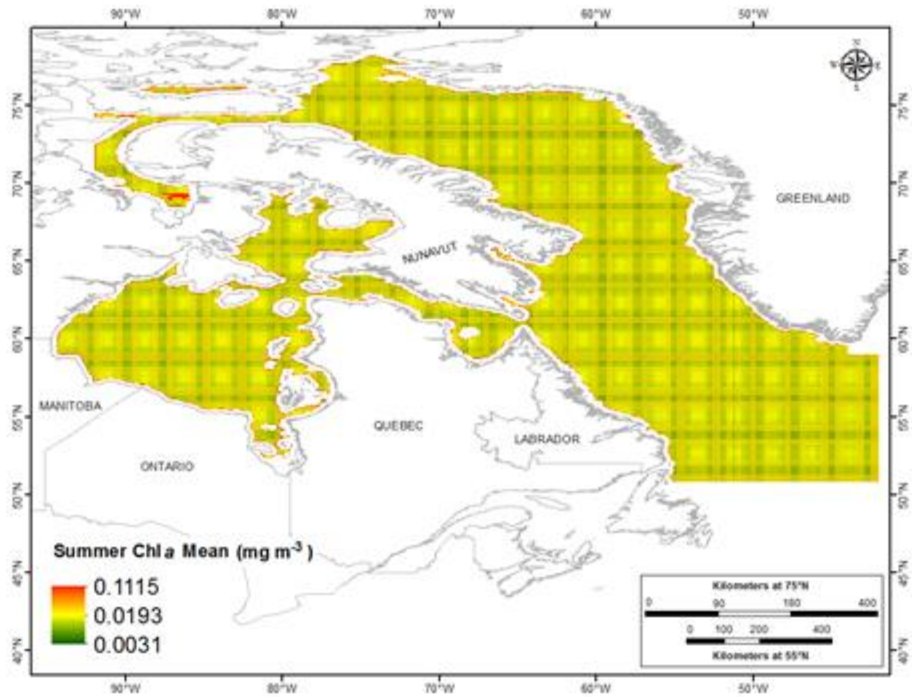


Figure 314. Prediction standard error surface of Summer Chlorophyll *a* Mean (mg m$^{-3}$).

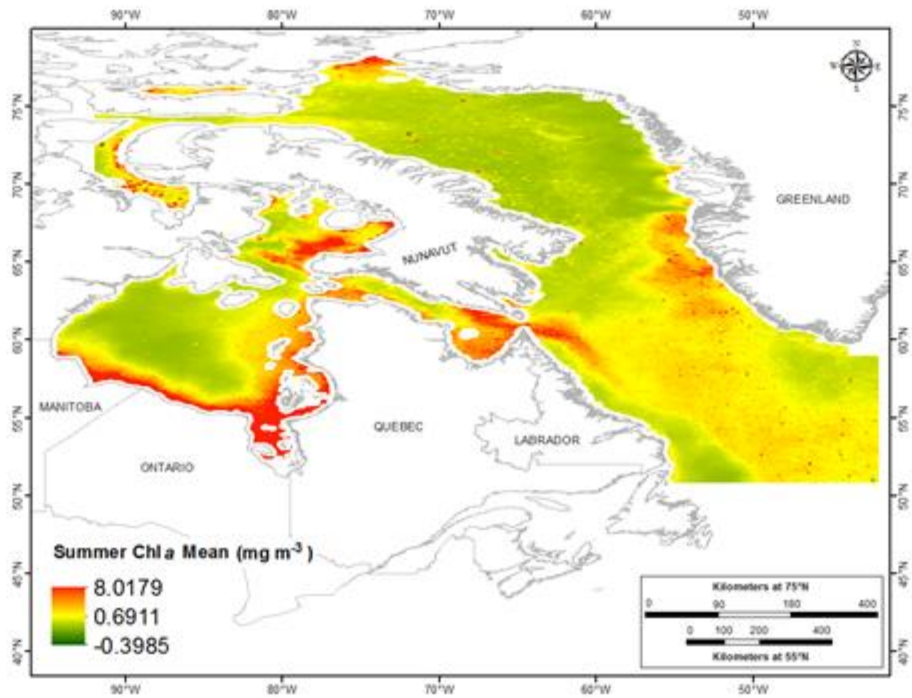


Figure 315. Interpolated prediction surface of Summer Chlorophyll *a* Mean (mg m$^{-3}$).

### Summer Chlorophyll *a* Minimum

This variable displayed a right-skewed, extremely leptokurtic distribution prior to interpolation (Table 127, Figure 316). The data were higher than predicted by a normal distribution at both tails, while mid-values were slightly lower than the reference line (Figure 317). These areas of under- and over-prediction showed spatial pattern over the region (Figure 317).

The semivariogram showed autocorrelation present in the data (Figure 318). The kriged model showed a good fit between measured and predicted values (Figure 318). Good performance of the model was indicated by the cross-validation results (Table 128). The error map displayed a grid-like pattern over the study extent (Figure 319). The kriged surface is presented in Figure 320.

Table 127. Distributional properties of Summer Chlorophyll *a* Minimum (mg $m^{-3}$).

| **Property** | **Value** |
|---|---:|
| Number of Observations | 77369 |
| Minimum | 0.055 |
| Maximum | 4.214 |
| Mean | 0.343 |
| Median | 0.297 |
| Standard Deviation | 0.194 |
| Skewness | 5.907 |
| Kurtosis | 68.497 |

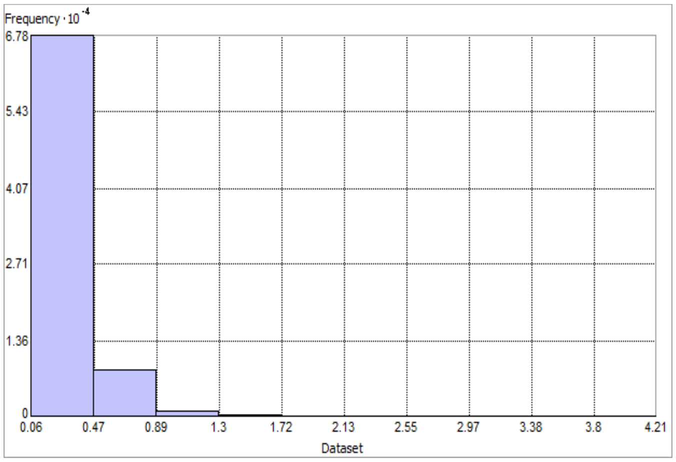


Figure 316. Distribution of Summer Chlorophyll *a* Minimum (mg m$^{-3}$). Histogram was illustrated using 10 bins. Y axis is shown at $10^{-4}$.

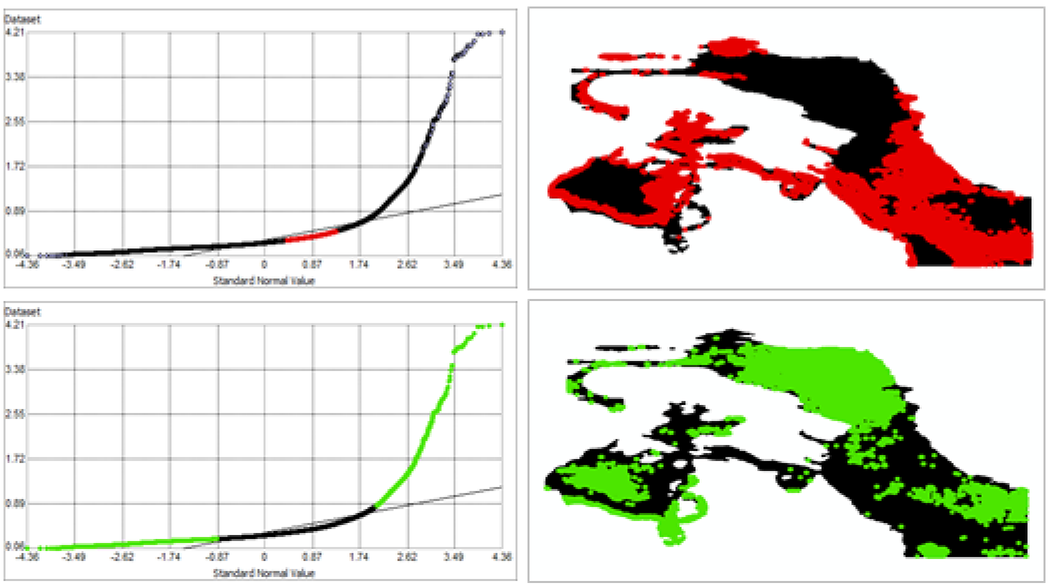

Figure 317. Normal Q-Q plot for data values of Summer Chlorophyll *a* Minimum (mg m$^{-3}$). Points falling under (top right panel) and over (bottom right panel) the reference line are mapped.

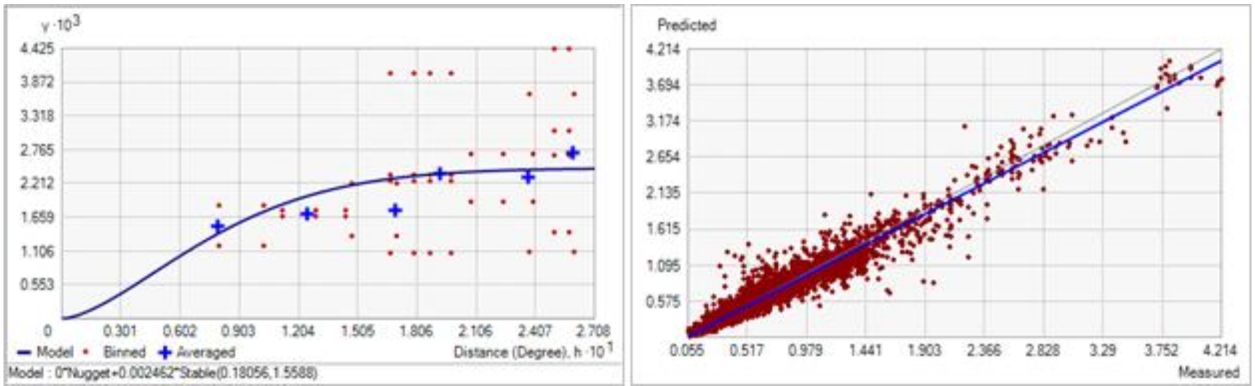


Figure 318. Left panel: Semivariogram of Summer Chlorophyll *a* Minimum (mg $m^{-3}$). Binned values are shown as red dots; average points are shown as blue crosses; the model fit to the averaged values is shown as a blue line. Lag size: 0.022 degrees; number of lags: 12; Parameter: 1.559; Range: 0.181 degrees; Partial Sill: 2.462 x $10^{-3}$. Right panel: Scatterplot of predicted values versus observed values for the model of Summer Chlorophyll *a* Minimum (mg $m^{-3}$).

Table 128. Results of cross-validation of the kriged model for Summer Chlorophyll *a* Minimum (mg $m^{-3}$).

| **Prediction Error** | **Value** |
|---|---:|
| Number of Observations | 77369 |
| Overall Mean Error | -1.551 x $10^{-4}$ |
| Root Mean Square Prediction Error | 0.038 |
| Standardized Mean | -2.648 x $10^{-3}$ |
| Standardized Root Mean Square Prediction Error | 1.016 |
| Average Standard Error | 0.037 |

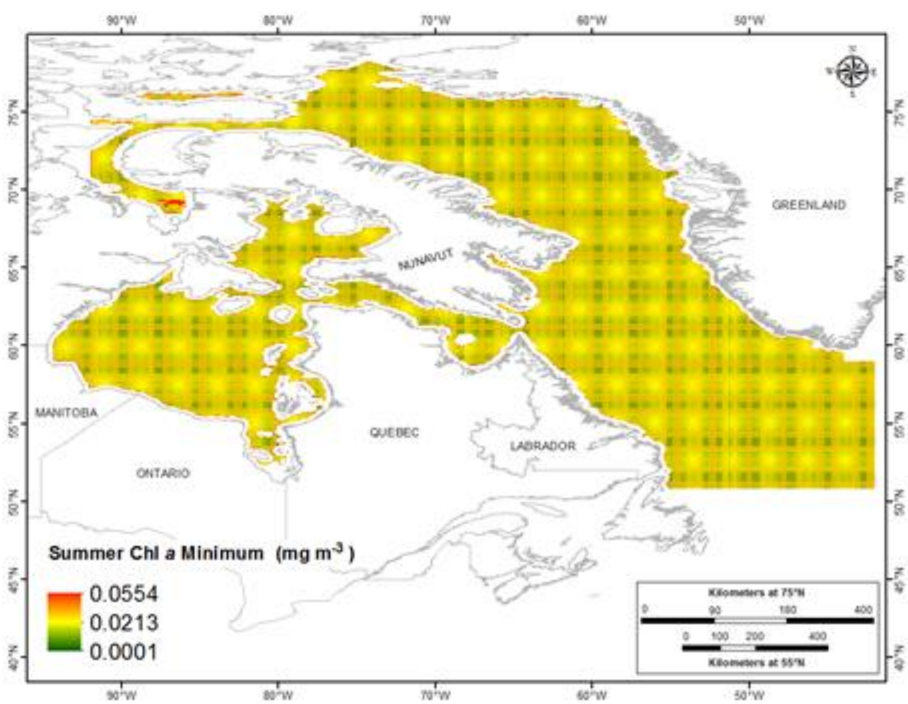


Figure 319. Prediction standard error surface of Summer Chlorophyll *a* Minimum (mg $m^{-3}$).

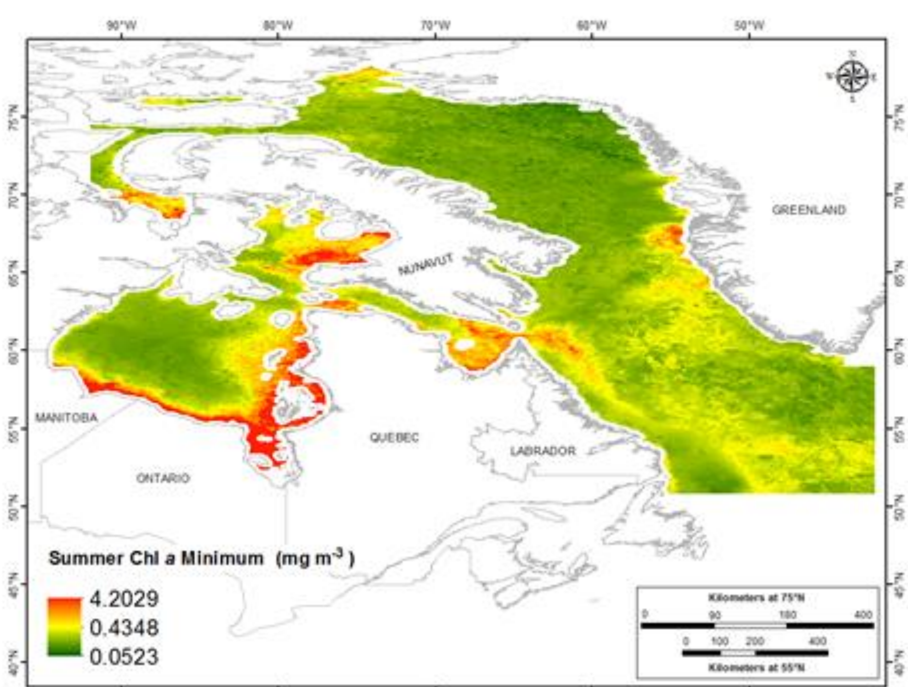


Figure 320. Interpolated prediction surface of Summer Chlorophyll *a* Minimum (mg $m^{-3}$).

**Summer Chlorophyll *a* Maximum**

This variable displayed a right-skewed, extremely leptokurtic distribution with outlying data in the upper range prior to interpolation (Table 129, Figure 321). The data were higher than predicted by a normal distribution at both tails, while mid-values were slightly lower than the reference line (Figure 322). These areas of under- and over-prediction showed spatial pattern over the region (Figure 322).

The semivariogram showed weak autocorrelation present in the data (Figure 323). The kriged model showed a poor fit between measured and predicted values (Figure 323). Good performance of the model was indicated by the cross-validation results (Table 130). The error map displayed a grid-like pattern over the study extent (Figure 324). The kriged surface is presented in Figure 325.

Table 129. Distributional properties of Summer Chlorophyll *a* Maximum (mg $m^{-3}$).

| **Property** | **Value** |
|---|---:|
| Number of Observations | 77369 |
| Minimum | 0.370 |
| Maximum | 82.209 |
| Mean | 1.770 |
| Median | 1.296 |
| Standard Deviation | 2.024 |
| Skewness | 9.741 |
| Kurtosis | 203.040 |

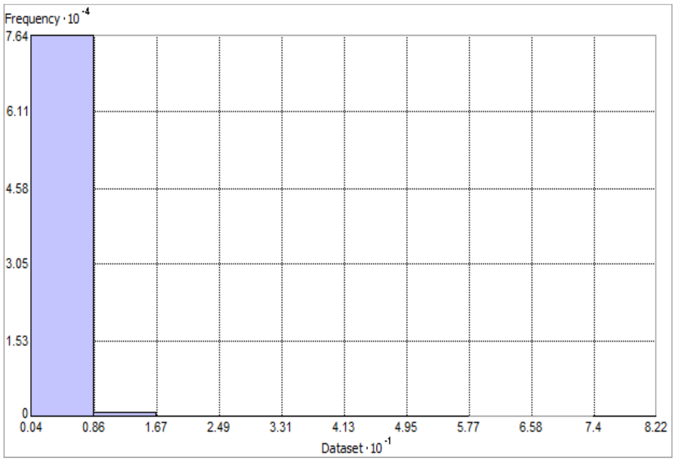


Figure 321. Distribution of Summer Chlorophyll *a* Maximum (mg m$^{-3}$). Histogram was illustrated using 10 bins. X axis is shown at $10^{-1}$; Y axis is shown at $10^{-4}$.

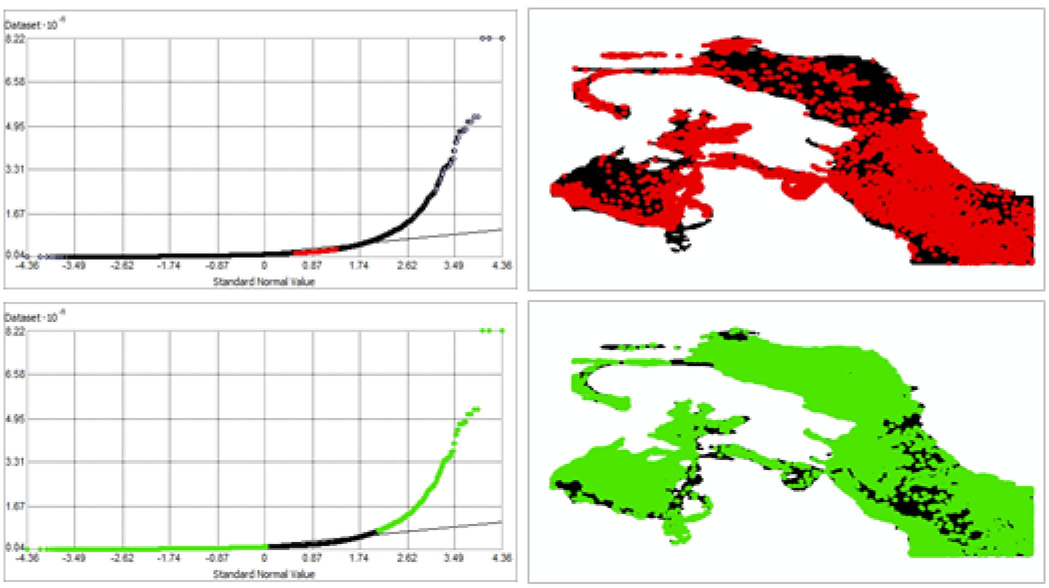

Figure 322. Normal Q-Q plot for data values of Summer Chlorophyll *a* Maximum (mg m$^{-3}$). Points falling under (top right panel) and over (bottom right panel) the reference line are mapped.

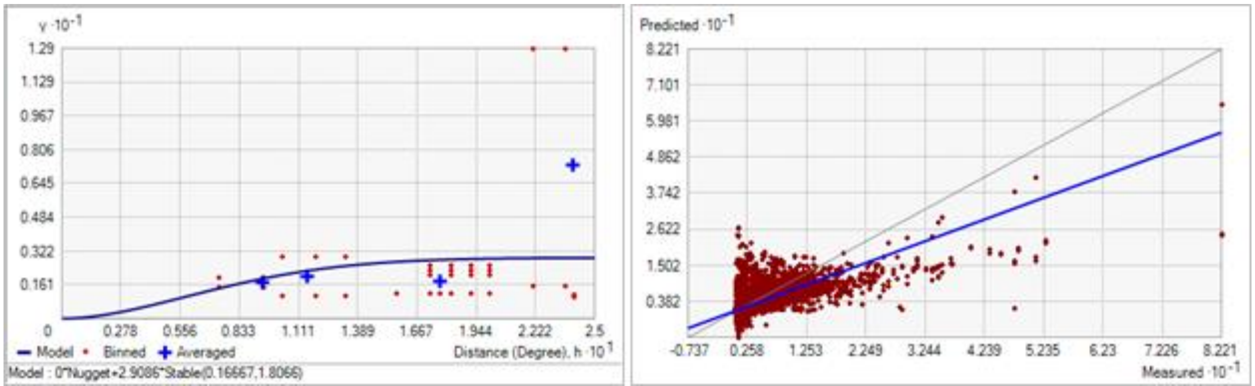

Figure 323. Left panel: Semivariogram of Summer Chlorophyll *a* Maximum (mg $m^{-3}$). Binned values are shown as red dots; average points are shown as blue crosses; the model fit to the averaged values is shown as a blue line. Lag size: 0.021 degrees; number of lags: 12; Parameter: 1.807; Range: 0.167 degrees; Partial Sill: 2.909. Right panel: Scatterplot of predicted values versus observed values for the model of Summer Chlorophyll *a* Maximum (mg $m^{-3}$).

Table 130. Results of cross-validation of the kriged model for Summer Chlorophyll *a* Maximum (mg $m^{-3}$).

| **Prediction Error** | **Value** |
|---|---:|
| Number of Observations | 77369 |
| Overall Mean Error | $-1.427 \times 10^{-4}$ |
| Root Mean Square Prediction Error | 1.343 |
| Standardized Mean | $-1.520 \times 10^{-6}$ |
| Standardized Root Mean Square Prediction Error | 1.164 |
| Average Standard Error | 1.153 |

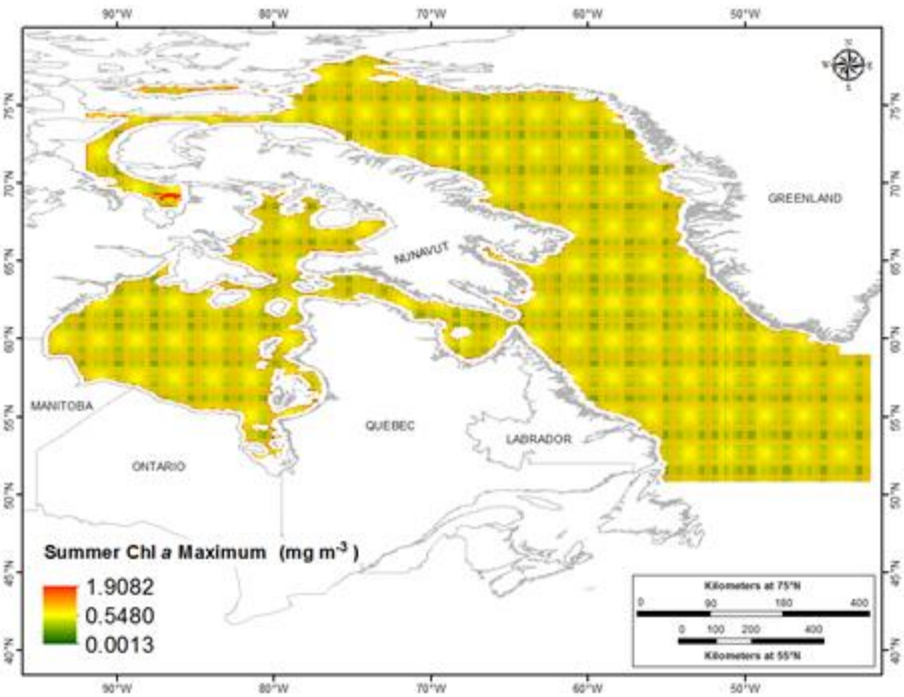


Figure 324. Prediction standard error surface of Summer Chlorophyll *a* Maximum (mg $m^{-3}$).

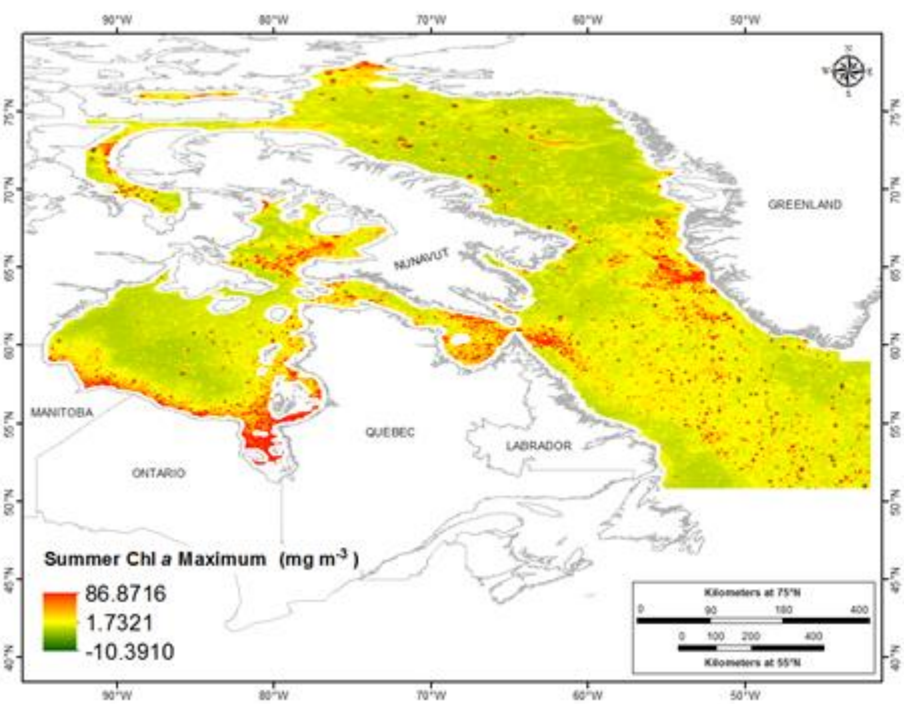


Figure 325. Interpolated prediction surface of Summer Chlorophyll *a* Maximum (mg $m^{-3}$).

**Summer Chlorophyll *a* Range**

This variable displayed a right-skewed, extremely leptokurtic distribution with outlying data in the upper range prior to interpolation (Table 131, Figure 326). The data were higher than predicted by a normal distribution at both tails, while mid-values were slightly lower than the reference line (Figure 327). These areas of under- and over-prediction showed spatial pattern over the region (Figure 327).

The semivariogram showed weak autocorrelation present in the data (Figure 328). The kriged model showed a poor fit between measured and predicted values (Figure 328). Good performance of the model was indicated by the cross-validation results (Table 132). The error map displayed a grid-like pattern over the study extent (Figure 329). The kriged surface is presented in Figure 330.

Table 131. Distributional properties of Summer Chlorophyll *a* Range (mg $m^{-3}$).

| **Property** | **Value** |
|---|---:|
| Number of Observations | 77369 |
| Minimum | $1.150 \times 10^{-3}$ |
| Maximum | 81.975 |
| Mean | 1.427 |
| Median | 0.970 |
| Standard Deviation | 1.950 |
| Skewness | 10.596 |
| Kurtosis | 233.710 |

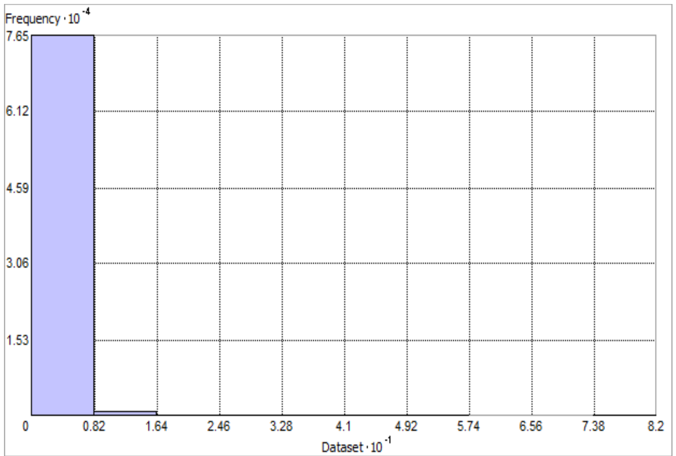

Figure 326. Distribution of Summer Chlorophyll *a* Range (mg m$^{-3}$). Histogram was illustrated using 10 bins. X axis is shown at $10^{-1}$; Y axis is shown at $10^{-4}$.

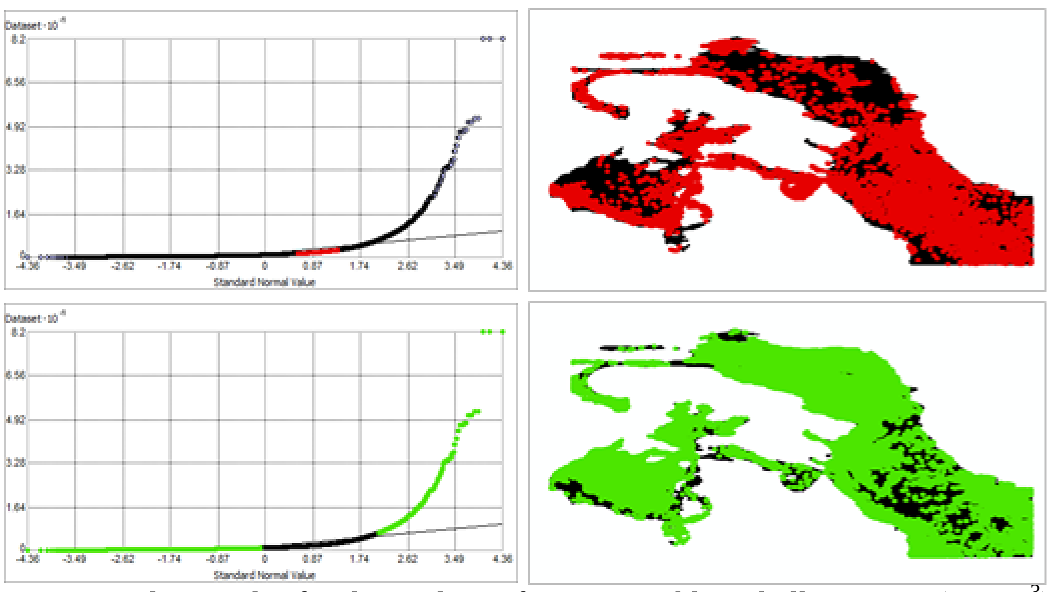
Figure 327. Normal Q-Q plot for data values of Summer Chlorophyll *a* Range (mg m$^{-3}$). Points falling under (top right panel) and over (bottom right panel) the reference line are mapped.

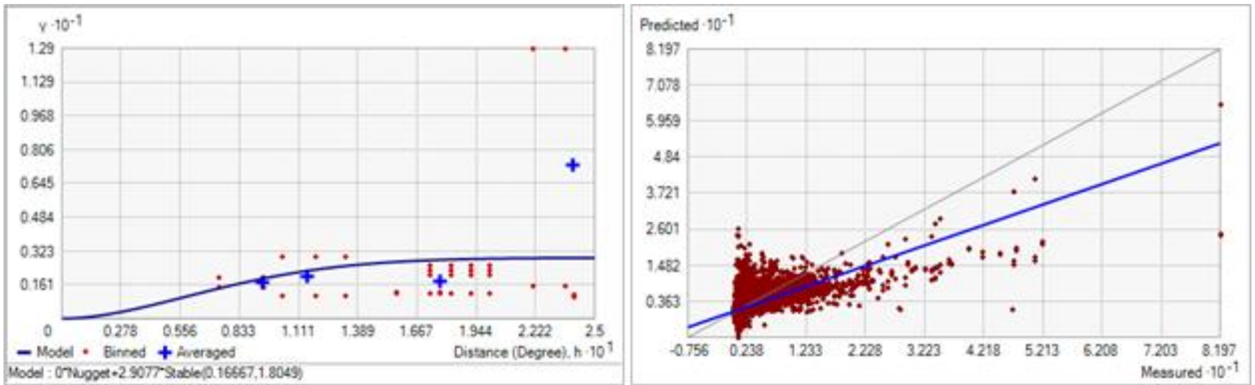


Figure 328. Left panel: Semivariogram of Summer Chlorophyll *a* Range (mg $m^{-3}$). Binned values are shown as red dots; average points are shown as blue crosses; the model fit to the averaged values is shown as a blue line. Lag size: 0.021 degrees; number of lags: 12; Parameter: 1.805; Range: 0.167 degrees; Partial Sill: 2.908. Right panel: Scatterplot of predicted values versus observed values for the model of Summer Chlorophyll *a* Range (mg $m^{-3}$).

Table 132. Results of cross-validation of the kriged model for Summer Chlorophyll *a* Range (mg $m^{-3}$).

| **Prediction Error** | **Value** |
|---|---:|
| Number of Observations | 77369 |
| Overall Mean Error | $5.356 \times 10^{-6}$ |
| Root Mean Square Prediction Error | 1.342 |
| Standardized Mean | $6.433 \times 10^{-6}$ |
| Standardized Root Mean Square Prediction Error | 1.162 |
| Average Standard Error | 1.154 |

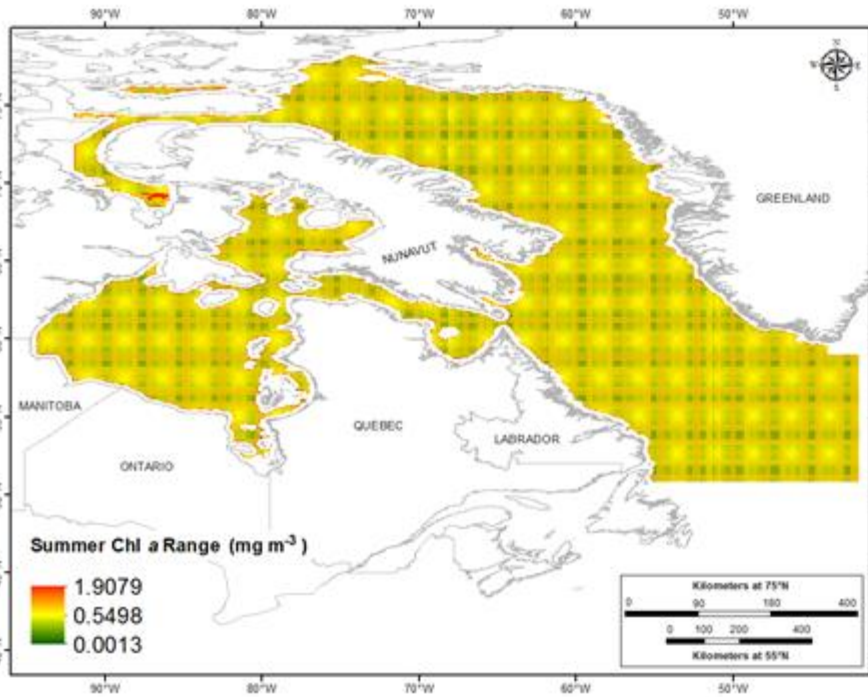


Figure 329. Prediction standard error surface of Spring Chlorophyll *a* Range (mg m$^{-3}$).

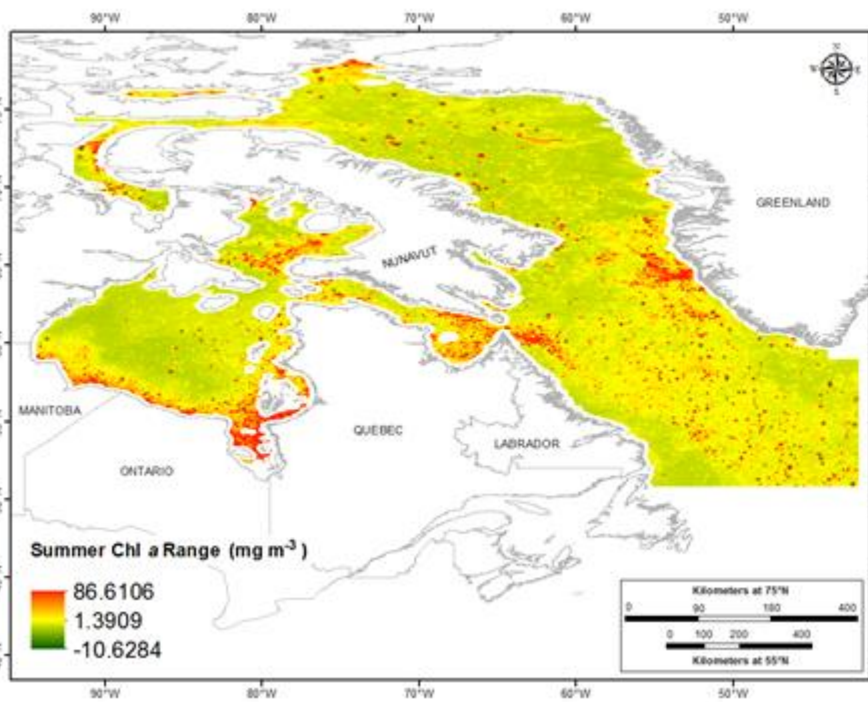


Figure 330. Interpolated prediction surface of Summer Chlorophyll *a* Range (mg m$^{-3}$).

**Annual Chlorophyll *a* Mean**

This variable displayed a right-skewed, extremely leptokurtic distribution with outlying data in the upper range prior to interpolation (Table 133, Figure 331). The data were higher than predicted by a normal distribution at both tails, while mid-values were slightly lower than the reference line (Figure 332). These areas of under- and over-prediction showed spatial pattern over the region (Figure 332).

The semivariogram showed autocorrelation present in the data (Figure 333). The kriged model showed a good fit between measured and predicted values (Figure 333). Good performance of the model was indicated by the cross-validation results (Table 134). The error map displayed a grid-like pattern over the study extent (Figure 334). The kriged surface is presented in Figure 335.

Table 133. Distributional properties of Annual Chlorophyll *a* Mean (mg $m^{-3}$).

| **Property** | **Value** |
|---|---:|
| Number of Observations | 77369 |
| Minimum | 0.289 |
| Maximum | 8.504 |
| Mean | 0.806 |
| Median | 0.723 |
| Standard Deviation | 0.457 |
| Skewness | 3.144 |
| Kurtosis | 21.812 |

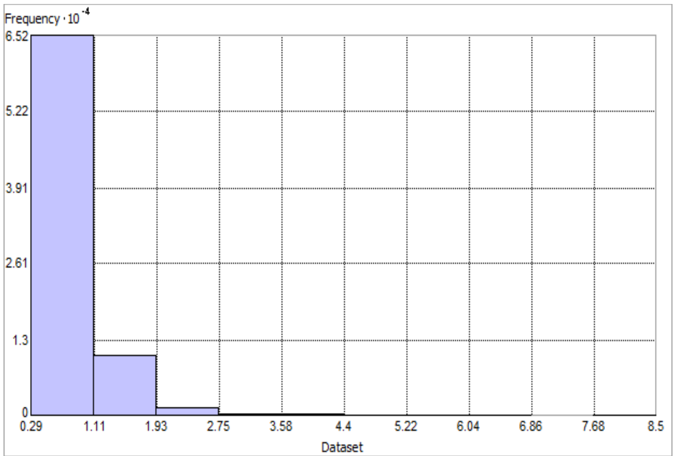


Figure 331. Distribution of Annual Chlorophyll *a* Mean (mg $m^{-3}$). Histogram was illustrated using 10 bins. Y axis is shown at $10^{-4}$.

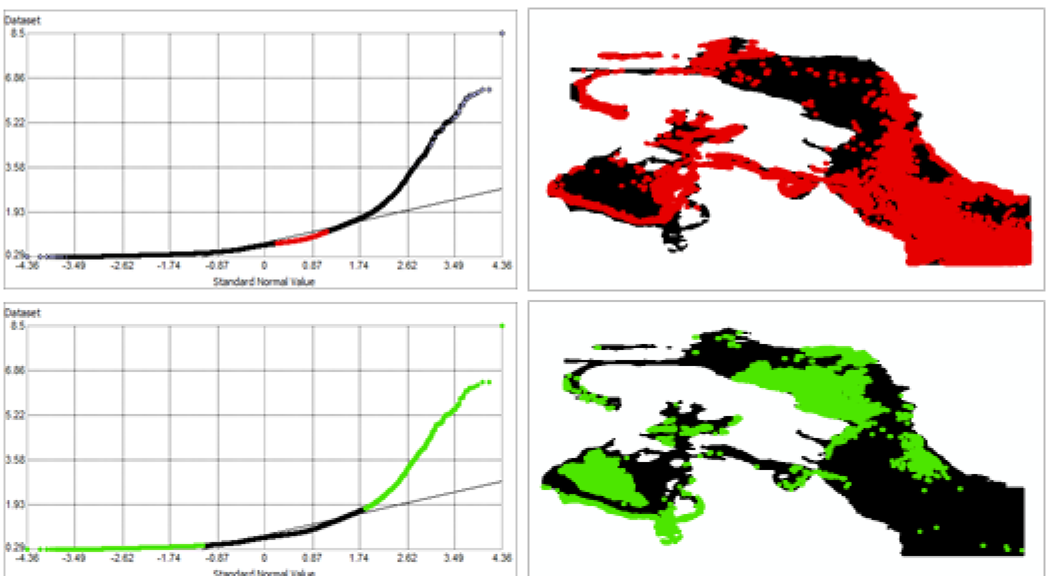


Figure 332. Normal Q-Q plot for data values of Annual Chlorophyll *a* Mean (mg $m^{-3}$). Points falling under (top right panel) and over (bottom right panel) the reference line are mapped.

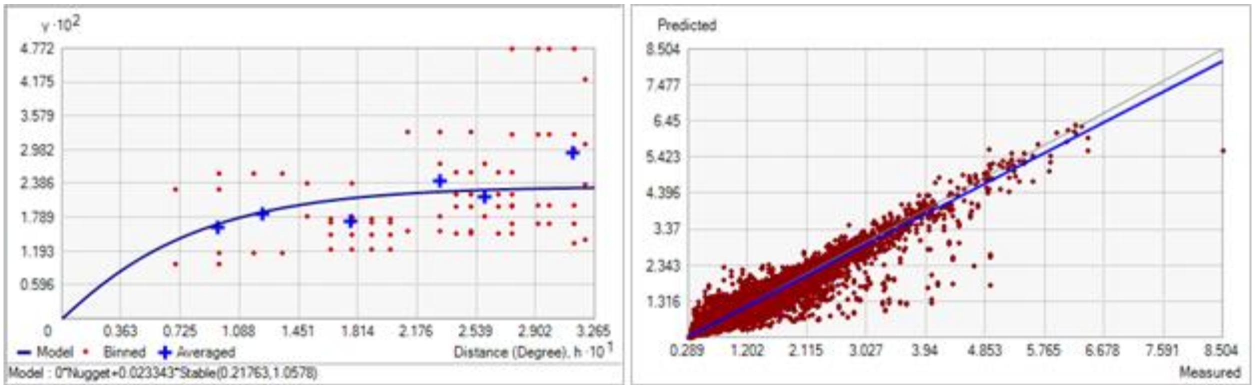

Figure 333. Left panel: Semivariogram of Annual Chlorophyll *a* Mean (mg $m^{-3}$). Binned values are shown as red dots; average points are shown as blue crosses; the model fit to the averaged values is shown as a blue line. Lag size: 0.027 degrees; number of lags: 12; Parameter: 1.058; Range: 0.218 degrees; Partial Sill: 0.023. Right panel: Scatterplot of predicted values versus observed values for the model of Annual Chlorophyll *a* Mean (mg $m^{-3}$).

Table 134. Results of cross-validation of the kriged model for Annual Chlorophyll *a* Mean (mg $m^{-3}$).

| **Prediction Error** | **Value** |
|---|---|
| Number of Observations | 77369 |
| Overall Mean Error | $-3.059 \times 10^{-4}$ |
| Root Mean Square Prediction Error | 0.114 |
| Standardized Mean | $-1.860 \times 10^{-3}$ |
| Standardized Root Mean Square Prediction Error | 0.887 |
| Average Standard Error | 0.128 |

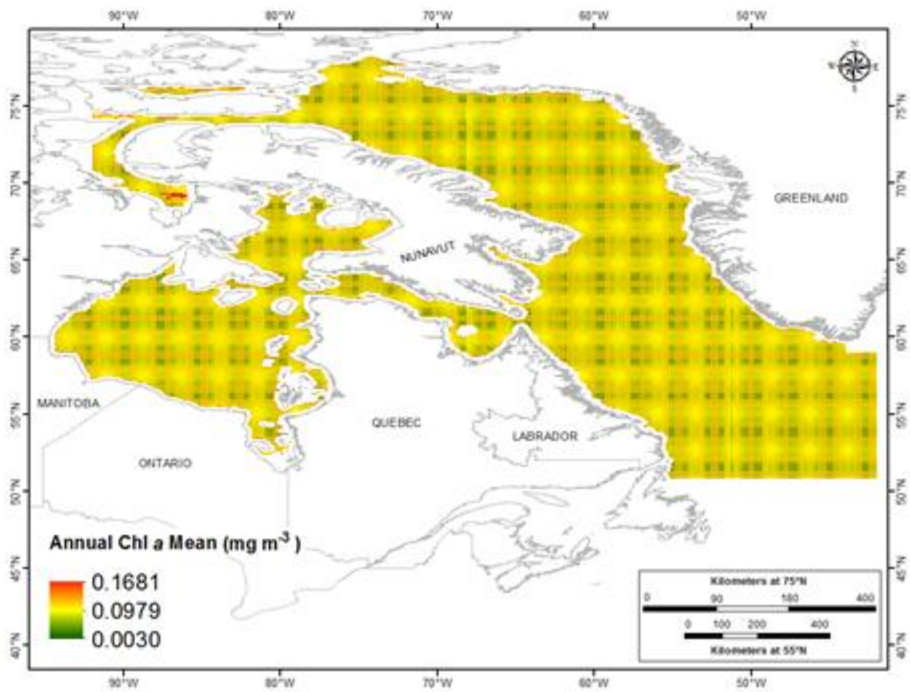


Figure 334. Prediction standard error surface of Annual Chlorophyll *a* Mean (mg $m^{-3}$).

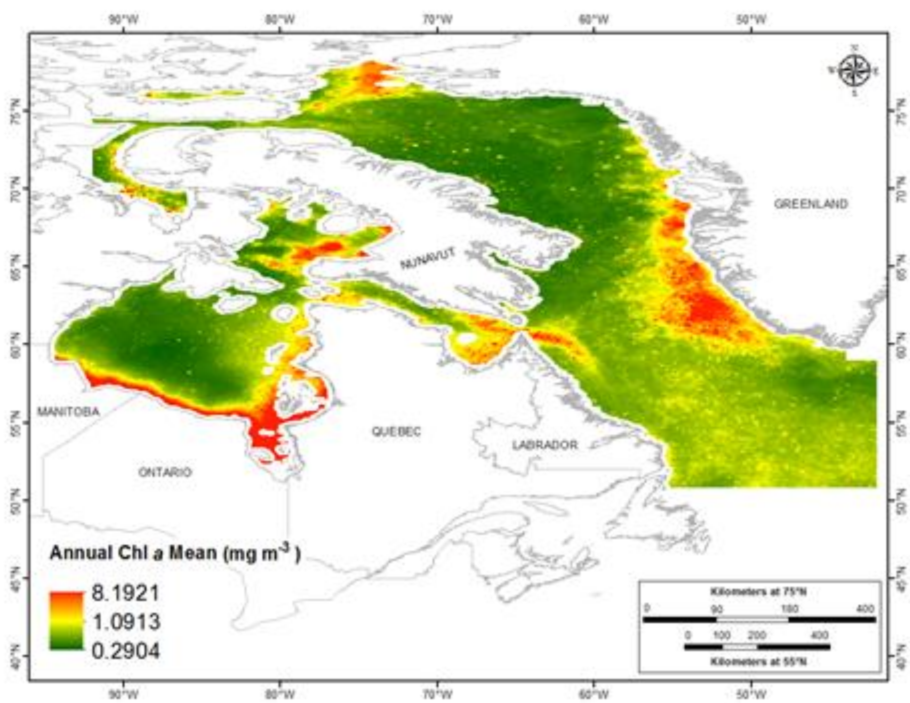


Figure 335. Interpolated prediction surface of Annual Chlorophyll *a* Mean (mg $m^{-3}$).

**Annual Chlorophyll *a* Minimum**

This variable displayed a right-skewed, extremely leptokurtic distribution prior to interpolation (Table 135, Figure 336). The data were higher than predicted by a normal distribution at both tails, while mid-values were slightly lower than the reference line (Figure 337). These areas of under- and over-prediction showed spatial pattern over the region (Figure 337).

The semivariogram showed weak autocorrelation present in the data (Figure 338). The kriged model showed a good fit between measured and predicted values (Figure 338). Good performance of the model was indicated by the cross-validation results (Table 136). The error map showed low error across the study area except along its boundaries (Figure 339). The kriged surface is presented in Figure 340.

Table 135. Distributional properties of Annual Chlorophyll *a* Minimum (mg $m^{-3}$).

| **Property** | **Value** |
|---|---:|
| Number of Observations | 77369 |
| Minimum | 0.023 |
| Maximum | 4.156 |
| Mean | 0.272 |
| Median | 0.236 |
| Standard Deviation | 0.181 |
| Skewness | 6.252 |
| Kurtosis | 74.928 |

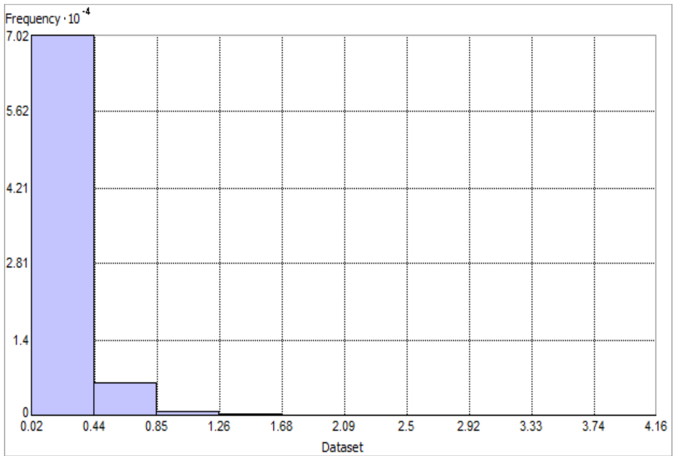


Figure 336. Distribution of Annual Chlorophyll *a* Minimum (mg m$^{-3}$). Histogram was illustrated using 10 bins. Y axis is shown at $10^{-4}$.

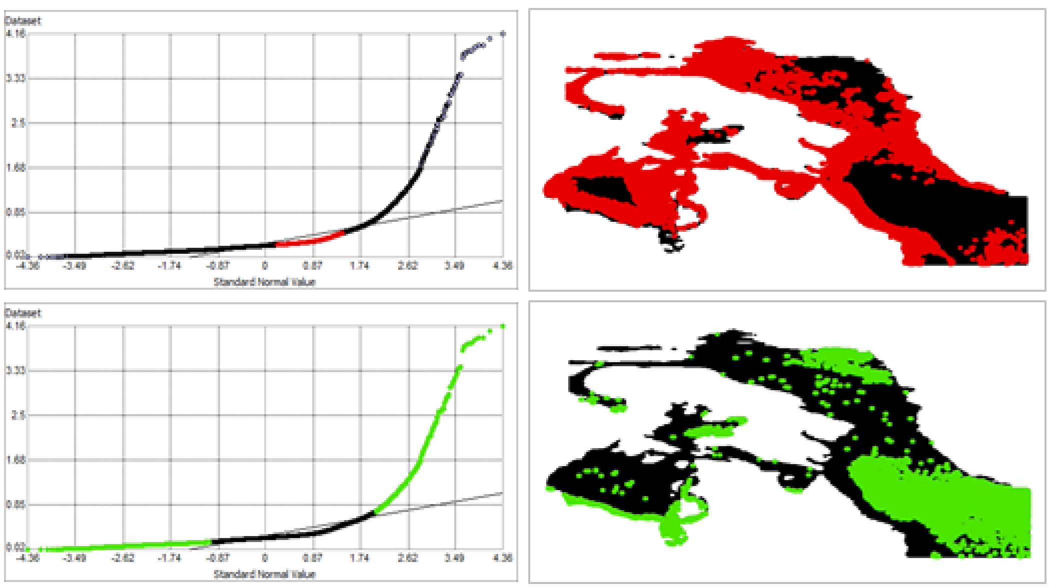


Figure 337. Normal Q-Q plot for data values of Annual Chlorophyll *a* Minimum (mg m$^{-3}$). Points falling under (top right panel) and over (bottom right panel) the reference line are mapped.

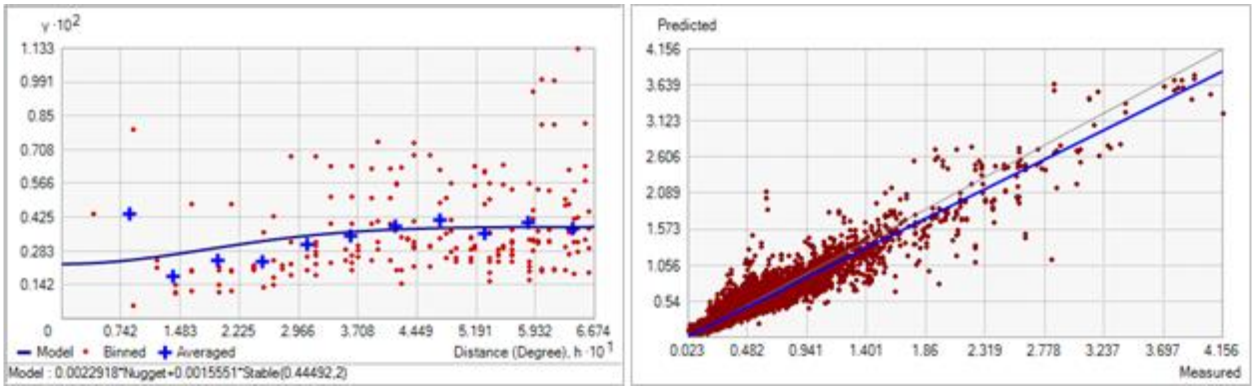


Figure 338. Left panel: Semivariogram of Annual Chlorophyll *a* Minimum (mg $m^{-3}$). Binned values are shown as red dots; average points are shown as blue crosses; the model fit to the averaged values is shown as a blue line. Lag size: 0.056 degrees; number of lags: 12; Parameter: 2; Range: 0.445 degrees; Partial Sill: 1.555 x $10^{-3}$. Right panel: Scatterplot of predicted values versus observed values for the model of Annual Chlorophyll *a* Minimum (mg $m^{-3}$).

Table 136. Results of cross-validation of the kriged model for Annual Chlorophyll *a* Minimum (mg $m^{-3}$).

| **Prediction Error** | **Value** |
|---|---:|
| Number of Observations | 77369 |
| Overall Mean Error | -6.915 x $10^{-5}$ |
| Root Mean Square Prediction Error | 0.048 |
| Standardized Mean | -9.483 x $10^{-4}$ |
| Standardized Root Mean Square Prediction Error | 0.939 |
| Average Standard Error | 0.051 |

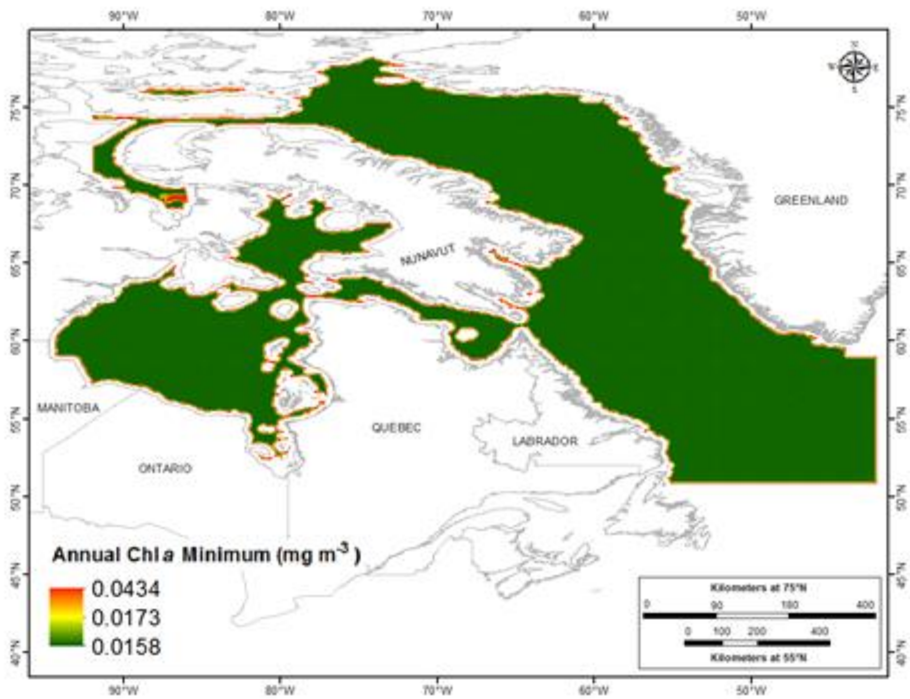


Figure 339. Prediction standard error surface of Annual Chlorophyll *a* Minimum (mg m$^{-3}$).

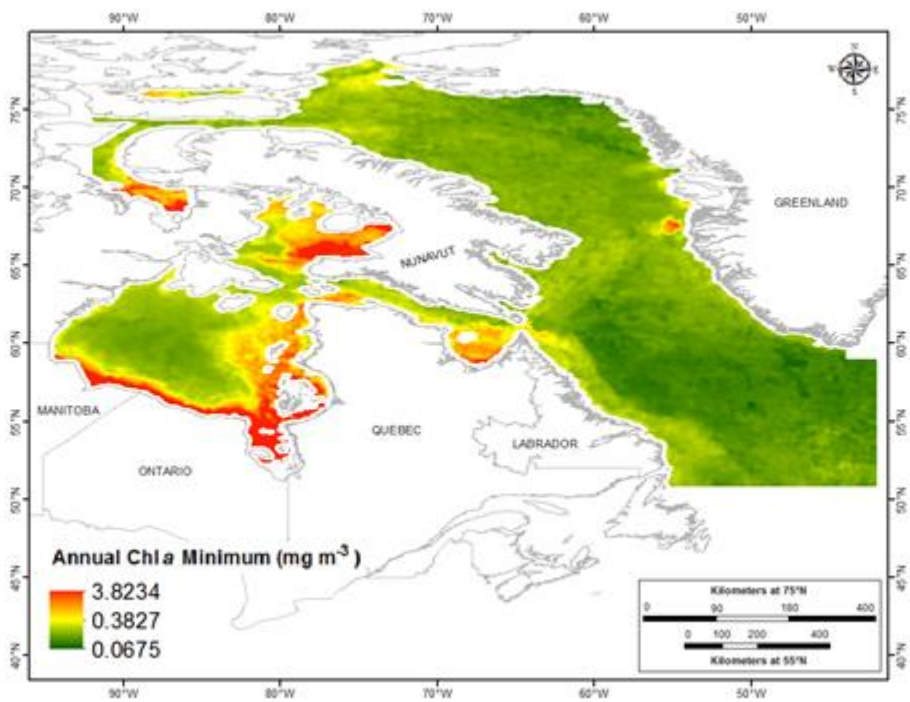


Figure 340. Interpolated prediction surface of Annual Chlorophyll *a* Minimum (mg m$^{-3}$).

**Annual Chlorophyll *a* Maximum**

This variable displayed a right-skewed, extremely leptokurtic distribution prior to interpolation (Table 137, Figure 341). The data were higher than predicted by a normal distribution at both tails, while mid-values were slightly lower than the reference line (Figure 342). These areas of under- and over-prediction showed spatial pattern over the region (Figure 342).

The semivariogram showed autocorrelation present in the data (Figure 343). The kriged model showed poor fit between measured and predicted values (Figure 343). Good performance of the model was indicated by the cross-validation results (Table 138). The error map displayed a grid-like pattern over the study extent (Figure 344). The kriged surface is presented in Figure 345.

Table 137. Distributional properties of Annual Chlorophyll *a* Maximum (mg $m^{-3}$).

| **Property** | **Value** |
|---|---:|
| Number of Observations | 77369 |
| Minimum | 0.370 |
| Maximum | 98.423 |
| Mean | 3.894 |
| Median | 2.409 |
| Standard Deviation | 4.483 |
| Skewness | 5.159 |
| Kurtosis | 53.817 |

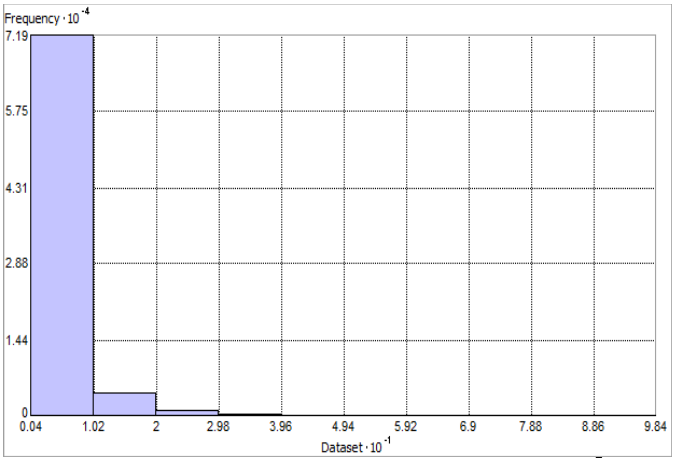


Figure 341. Distribution of Annual Chlorophyll *a* Maximum (mg $m^{-3}$). Histogram was illustrated using 10 bins. X axis is shown at $10^{-1}$; Y axis is shown at $10^{-4}$.

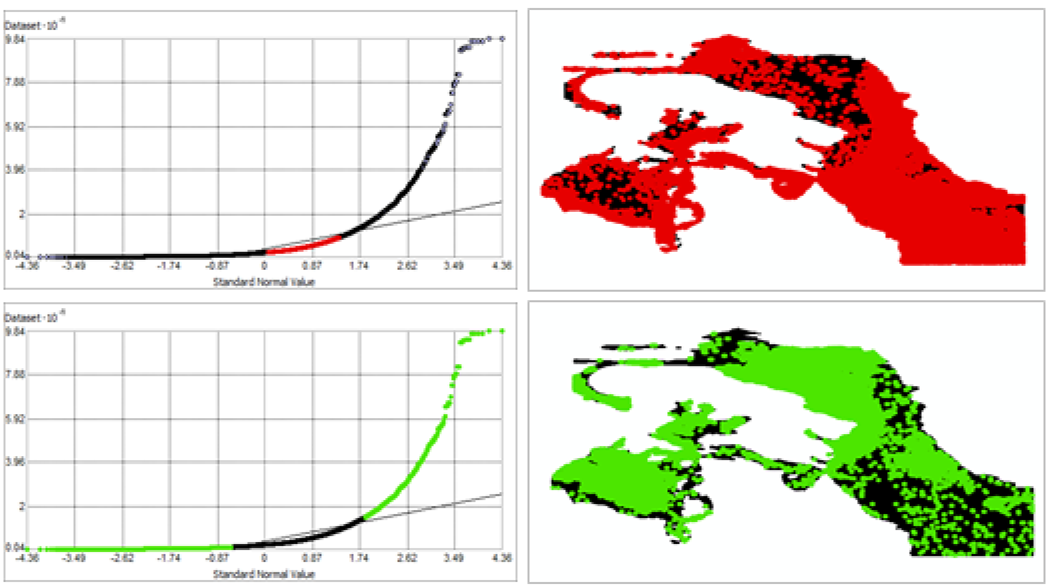

Figure 342. Normal Q-Q plot for data values of Annual Chlorophyll *a* Maximum (mg $m^{-3}$). Points falling under (top right panel) and over (bottom right panel) the reference line are mapped.

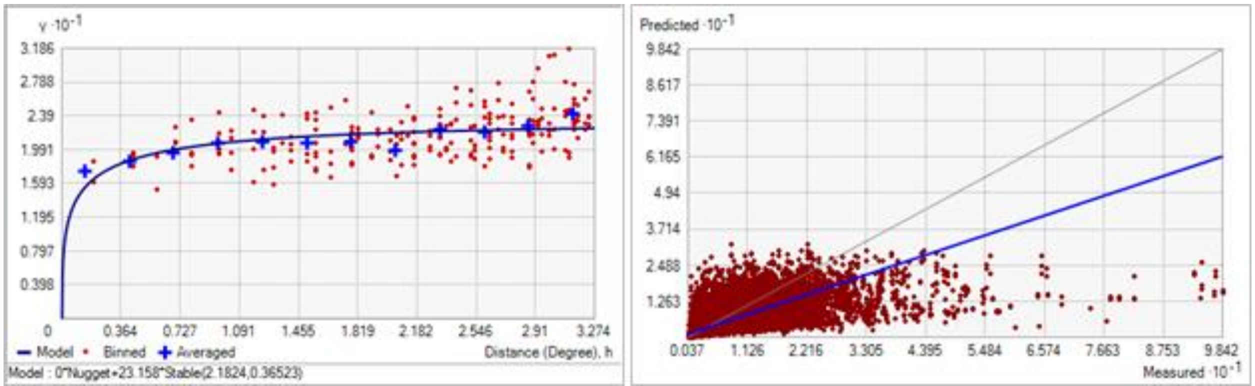

Figure 343. Left panel: Semivariogram of Annual Chlorophyll *a* Maximum (mg $m^{-3}$). Binned values are shown as red dots; average points are shown as blue crosses; the model fit to the averaged values is shown as a blue line. Lag size: 0.273 degrees; number of lags: 12; Parameter: 0.365; Range: 2.812 degrees; Partial Sill: 23.158. Right panel: Scatterplot of predicted values versus observed values for the model of Annual Chlorophyll *a* Maximum (mg $m^{-3}$).

Table 138. Results of cross-validation of the kriged model for Annual Chlorophyll *a* Maximum (mg $m^{-3}$).

| **Prediction Error** | **Value** |
|---|---:|
| Number of Observations | 77369 |
| Overall Mean Error | $-8.504 \times 10^{-6}$ |
| Root Mean Square Prediction Error | 3.357 |
| Standardized Mean | $1.005 \times 10^{-5}$ |
| Standardized Root Mean Square Prediction Error | 0.867 |
| Average Standard Error | 3.875 |

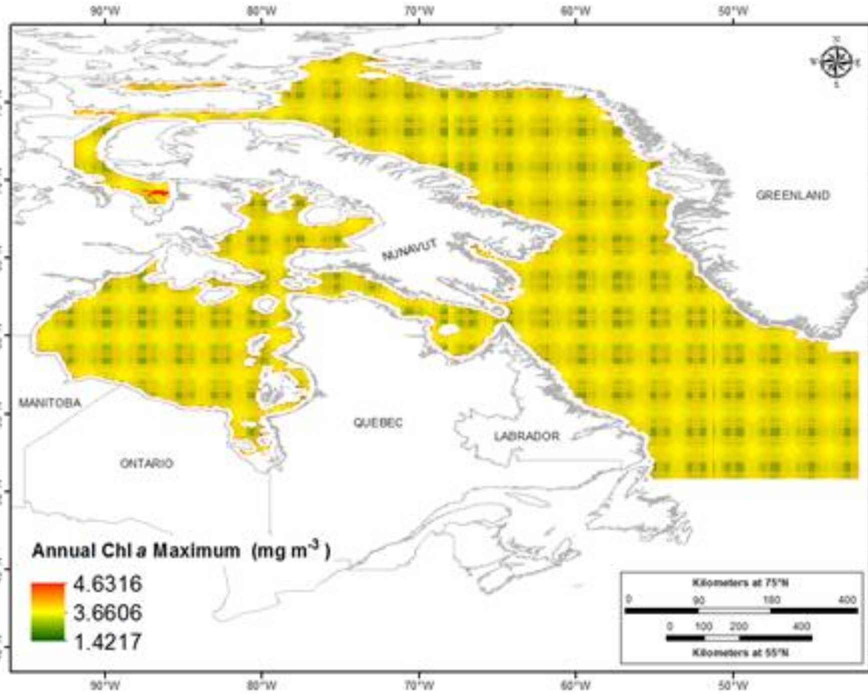


Figure 344. Prediction standard error surface of Annual Chlorophyll *a* Maximum (mg m$^{-3}$).

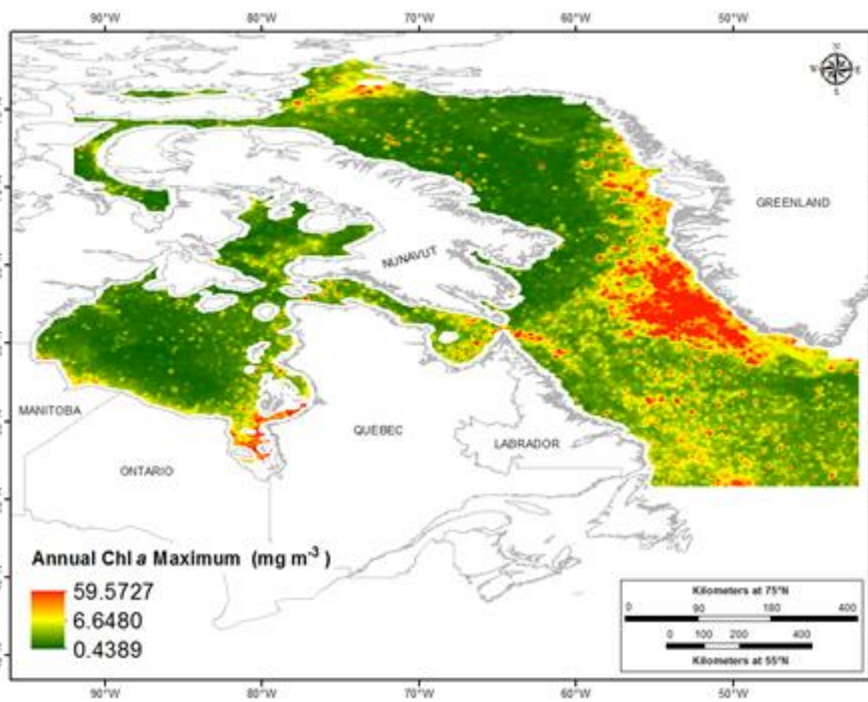


Figure 345. Interpolated prediction surface of Annual Chlorophyll *a* Maximum (mg m$^{-3}$).

## Annual Chlorophyll *a* Range

This variable displayed a right-skewed, extremely leptokurtic distribution prior to interpolation (Table 139, Figure 346). The data were higher than predicted by a normal distribution at both tails, while mid-values were slightly lower than the reference line (Figure 347). These areas of under- and over-prediction showed spatial pattern over the region (Figure 347).

The semivariogram showed autocorrelation present in the data (Figure 348). The kriged model showed poor fit between measured and predicted values (Figure 348). Good performance of the model was indicated by the cross-validation results (Table 140). The error map displayed a grid-like pattern over the study extent (Figure 349). The kriged surface is presented in Figure 350.

Table 139. Distributional properties of Annual Chlorophyll *a* Range (mg $m^{-3}$).

| **Property** | **Value** |
|---|---:|
| Number of Observations | 77369 |
| Minimum | $1.150 \times 10^{-3}$ |
| Maximum | 98.108 |
| Mean | 3.622 |
| Median | 2.157 |
| Standard Deviation | 4.838 |
| Skewness | 5.174 |
| Kurtosis | 54.027 |

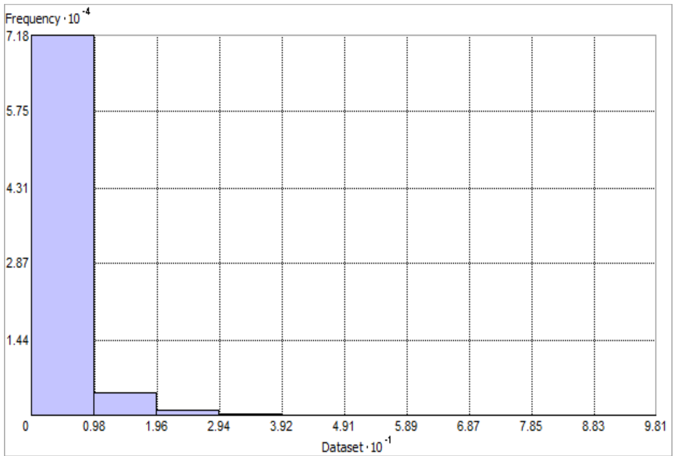


Figure 346. Distribution of Annual Chlorophyll *a* Range (mg m$^{-3}$). Histogram was illustrated using 10 bins. X axis is shown at $10^{-1}$; Y axis is shown at $10^{-4}$.

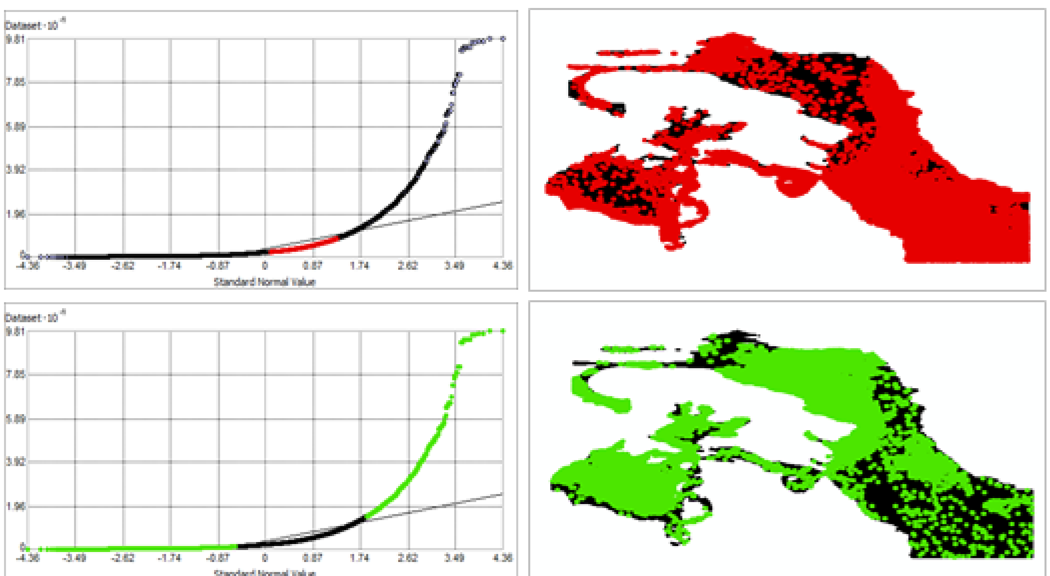

Figure 347. Normal Q-Q plot for data values of Annual Chlorophyll *a* Range (mg m$^{-3}$). Points falling under (top right panel) and over (bottom right panel) the reference line are mapped.

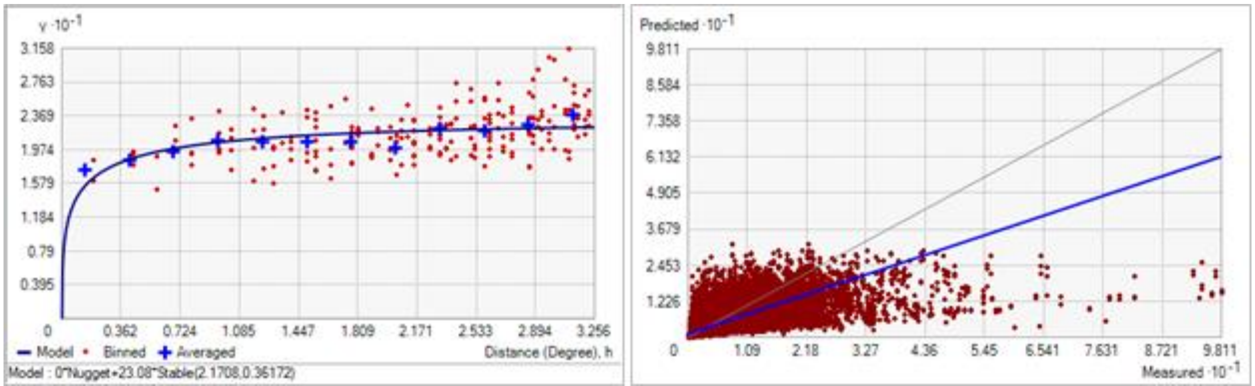

Figure 348. Left panel: Semivariogram of Annual Chlorophyll *a* Range (mg $m^{-3}$). Binned values are shown as red dots; average points are shown as blue crosses; the model fit to the averaged values is shown as a blue line. Lag size: 0.271 degrees; number of lags: 12; Parameter: 0.362; Range: 2.170 degrees; Partial Sill: 23.080. Right panel: Scatterplot of predicted values versus observed values for the model of Annual Chlorophyll *a* Range (mg $m^{-3}$).

Table 140. Results of cross-validation of the kriged model for Annual Chlorophyll *a* Range (mg $m^{-3}$).

| **Prediction Error** | **Value** |
|---|---:|
| Number of Observations | 77369 |
| Overall Mean Error | $9.777 \times 10^{-5}$ |
| Root Mean Square Prediction Error | 3.359 |
| Standardized Mean | $3.249 \times 10^{-5}$ |
| Standardized Root Mean Square Prediction Error | 0.865 |
| Average Standard Error | 3.884 |

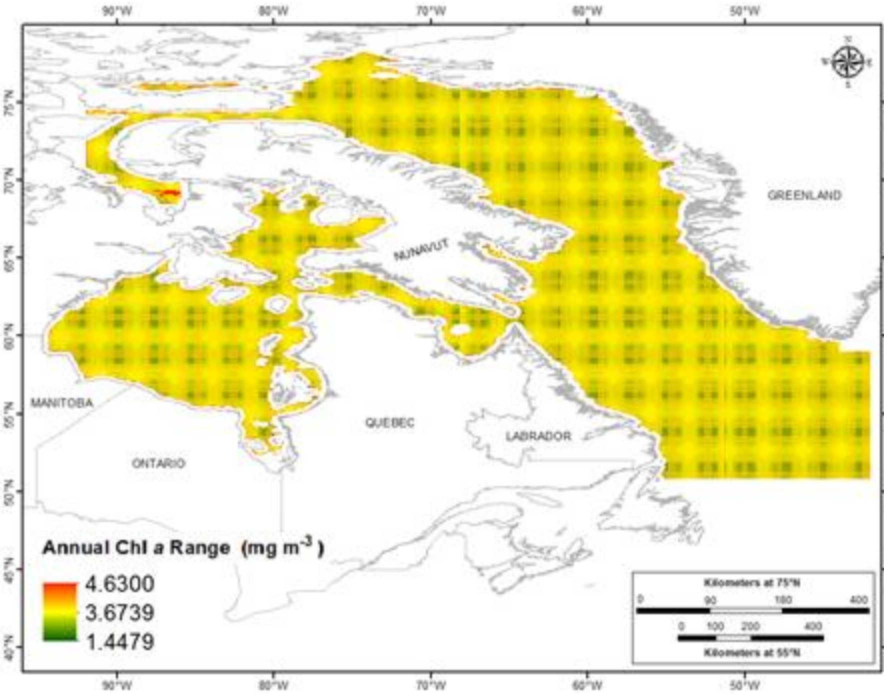


Figure 349. Prediction standard error surface of Annual Chlorophyll *a* Range (mg $m^{-3}$).

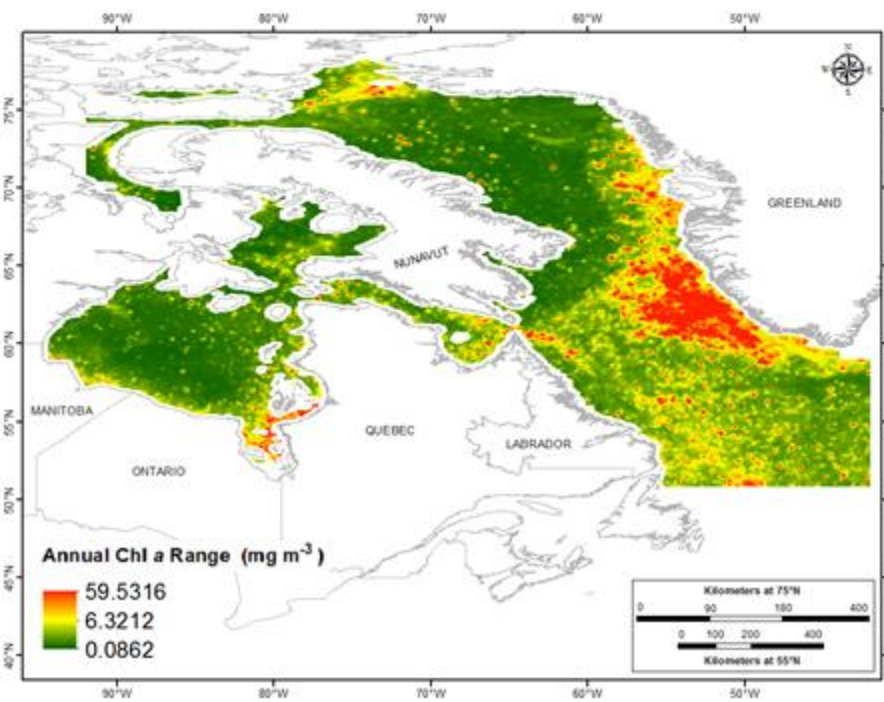


Figure 350. Interpolated prediction surface of Annual Chlorophyll *a* Range (mg $m^{-3}$).

# Primary Production

Primary production measures the rate at which atmospheric or aqueous carbon dioxide is converted to organic carbon by autotrophs (Bender et al., 1987) and relates more directly to the flux of particulate organic carbon and food supply to the seafloor than sea surface chlorophyll *a* concentration. However, as satellite-derived chlorophyll *a* is a main source of data used in the calculation of the primary production variables in this report, we expect these variables to be highly correlated.

### Spring Primary Production Mean

This variable had poor coverage over much of the study extent. It displayed a near-normal distribution prior to interpolation, with leptokurtosis (Table 141, Figure 351). The data were higher than predicted by a normal distribution at both tails however the mid-region was very well-predicted (Figure 352). Only a single data point fell below the reference line.

The semivariogram showed autocorrelation present in the data (Figure 353). The kriged model showed a good fit between measured and predicted values (Figure 353). Good performance of the model was indicated by the cross-validation results (Table 142). The error map was discontinuous and showed patches of high error in those areas where data points were scarce (Figure 354). The kriged surface is presented in Figure 355. Predictions were discontinuous in data-poor areas.

Table 141. Distributional properties of Spring Primary Production Mean (mg C $m^{-2}$ $day^{-1}$).

| **Property** | **Value** |
|---|---:|
| Number of Observations | 17007 |
| Minimum | 173.010 |
| Maximum | 1344.800 |
| Mean | 684.990 |
| Median | 667.710 |
| Standard Deviation | 107.120 |
| Skewness | 1.013 |
| Kurtosis | 4.671 |

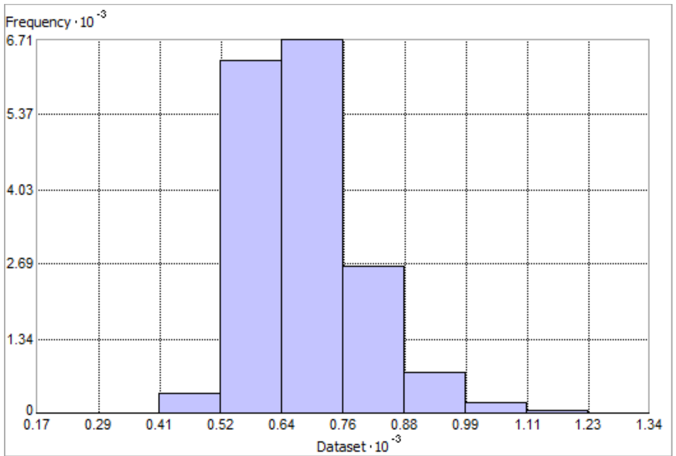


Figure 351. Distribution of Spring Primary Production Mean (mg C $m^{-2}$ $day^{-1}$). Histogram was illustrated using 10 bins. X axis is shown at $10^{-3}$; Y axis is shown at $10^{-3}$.

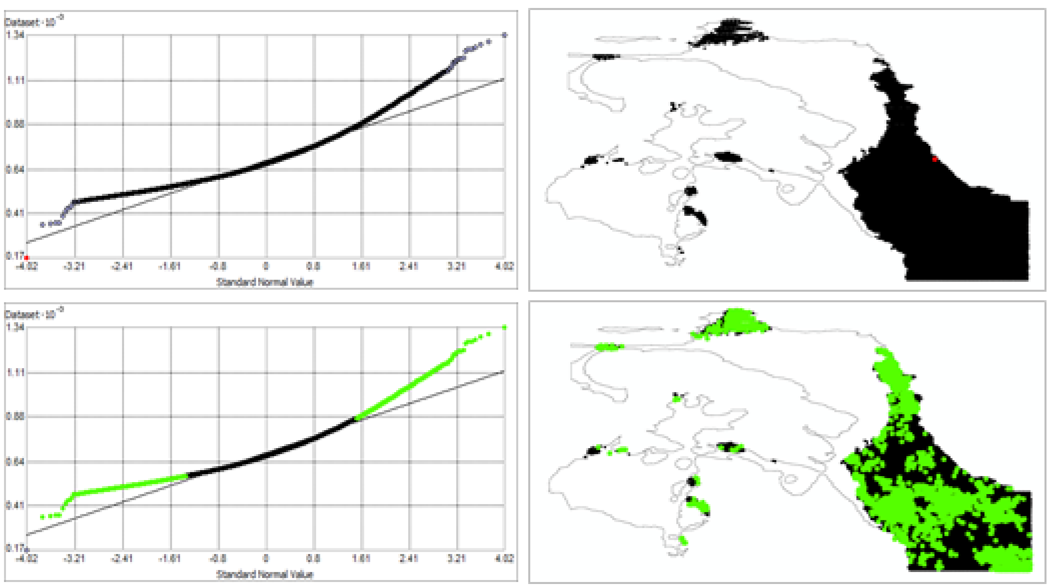

Figure 352. Normal Q-Q plot for data values of Spring Primary Production Mean (mg C $m^{-2}$ $day^{-1}$). Points falling under (top right panel) and over (bottom right panel) the reference line are mapped.

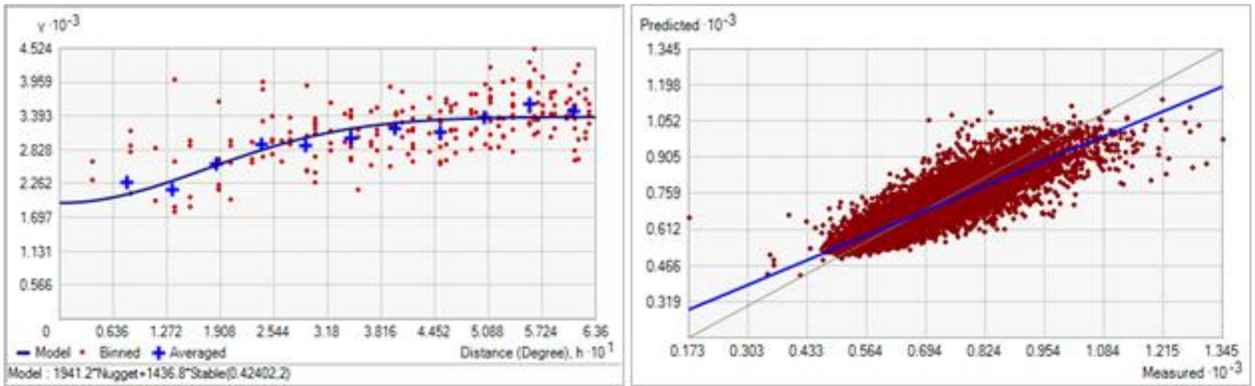


Figure 353. Left panel: Semivariogram of Spring Primary Production Mean (mg C $m^{-2}$ $day^{-1}$). Binned values are shown as red dots; average points are shown as blue crosses; the model fit to the averaged values is shown as a blue line. Lag size: 0.053 degrees; number of lags: 12; Parameter: 2; Range: 0.424 degrees; Partial Sill: 1436.812. Right panel: Scatterplot of predicted values versus observed values for the model of Spring Primary Production Mean (mg C $m^{-2}$ $day^{-1}$).

Table 142. Results of cross-validation of the kriged model for Spring Primary Production Mean (mg C $m^{-2}$ $day^{-1}$).

| **Prediction Error** | **Value** |
|---|---|
| Number of Observations | 17007 |
| Overall Mean Error | 0.027 |
| Root Mean Square Prediction Error | 53.093 |
| Standardized Mean | $4.773 \times 10^{-4}$ |
| Standardized Root Mean Square Prediction Error | 1.076 |
| Average Standard Error | 48.782 |

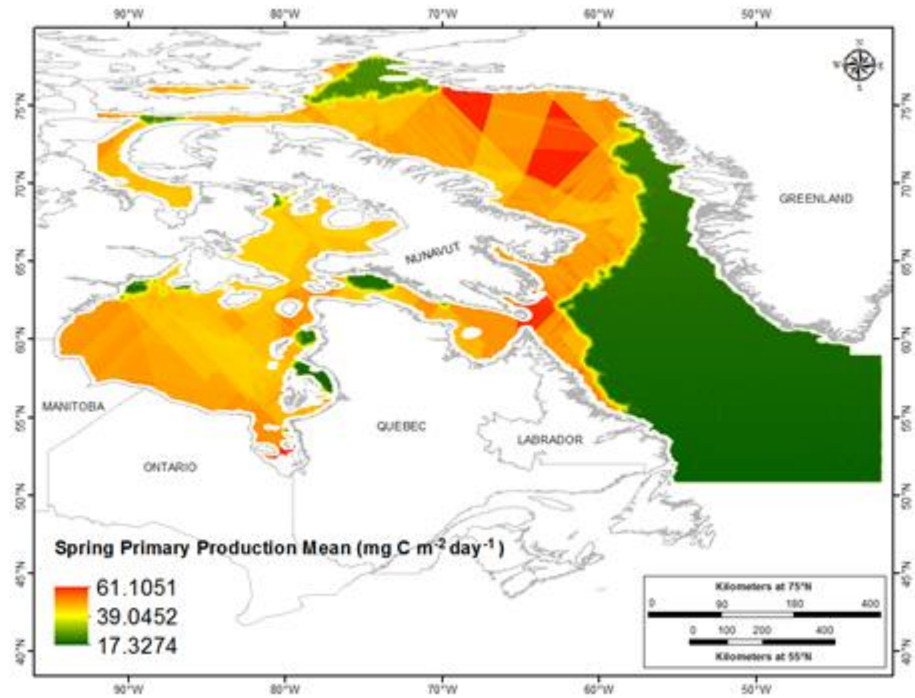


Figure 354. Prediction standard error surface of Spring Primary Production Mean (mg C $m^{-2}$ $day^{-1}$).

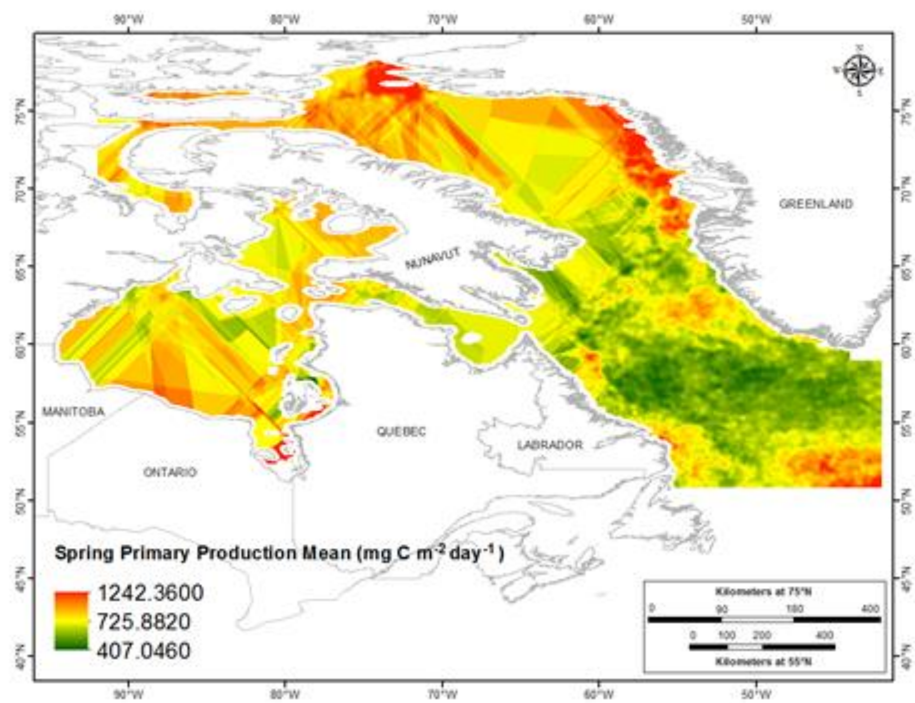


Figure 355. Interpolated prediction surface of Spring Primary Production Mean (mg C $m^{-2}$ $day^{-1}$).

**Spring Primary Production Minimum**

This variable had poor coverage over much of the study extent. It displayed a near-normal distribution prior to interpolation, with slight skewness (Table 143, Figure 356). The data were higher than predicted by a normal distribution at both tails however the mid-region was very well-predicted (Figure 357). These areas of under- and over-prediction showed no strong spatial pattern over the region (Figure 357).

The semivariogram showed autocorrelation present in the data (Figure 358). The kriged model showed a good fit between measured and predicted values (Figure 358). Very good performance of the model was indicated by the cross-validation results (Table 144). The error map was discontinuous and showed patches of high error in those areas where data points were scarce (Figure 359). The kriged surface is presented in Figure 360. Predictions were discontinuous in data-poor areas.

Table 143. Distributional properties of Spring Primary Production Minimum (mg C $m^{-2}$ $day^{-1}$).

| **Property** | **Value** |
|---|---:|
| Number of Observations | 17007 |
| Minimum | 39.890 |
| Maximum | 1038.500 |
| Mean | 356.740 |
| Median | 326.770 |
| Standard Deviation | 136.520 |
| Skewness | 0.772 |
| Kurtosis | 3.086 |

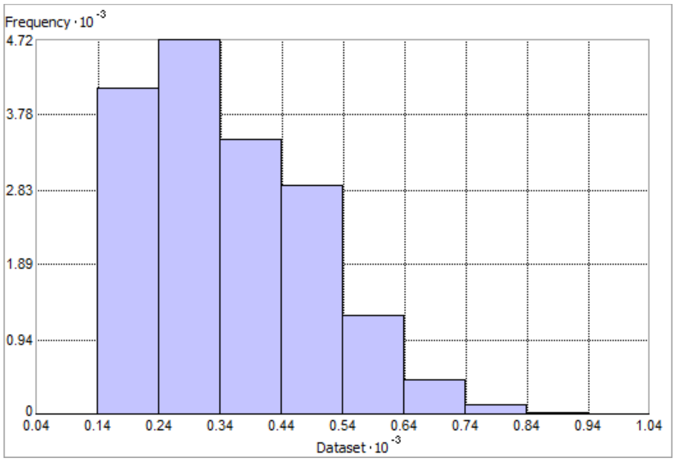


Figure 356. Distribution of Spring Primary Production Minimum (mg C $m^{-2}$ $day^{-1}$). Histogram was illustrated using 10 bins. X axis is shown at $10^{-3}$; Y axis is shown at $10^{-3}$.

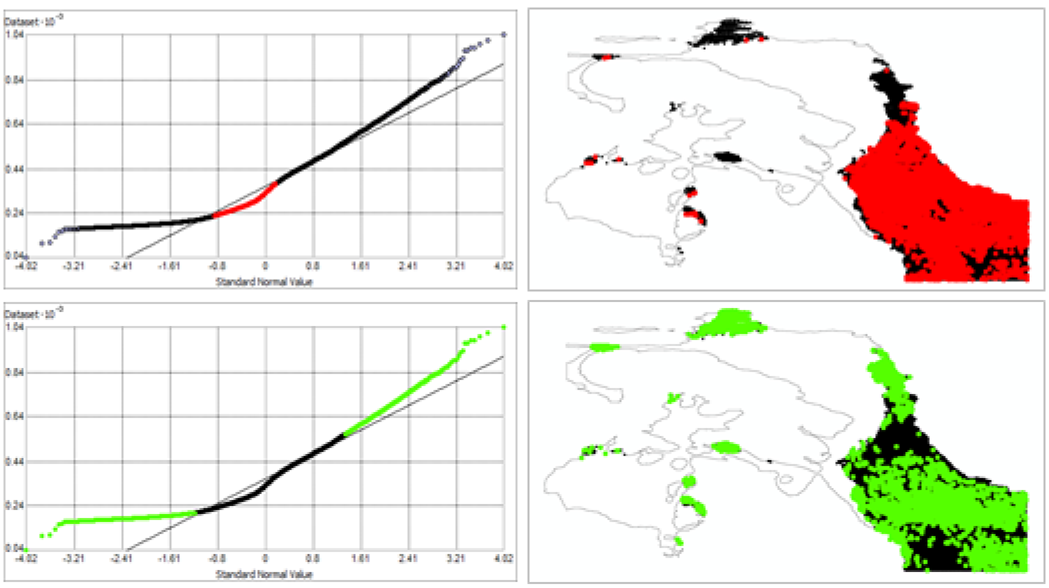

Figure 357. Normal Q-Q plot for data values of Spring Primary Production Minimum (mg C $m^{-2}$ $day^{-1}$). Points falling under (top right panel) and over (bottom right panel) the reference line are mapped.

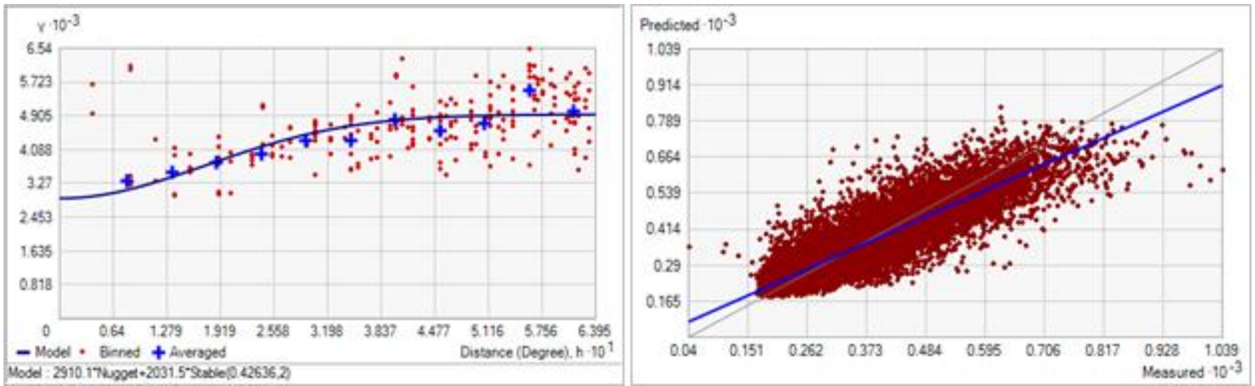


Figure 358. Left panel: Semivariogram of Spring Primary Production Minimum (mg C $m^{-2}$ $day^{-1}$). Binned values are shown as red dots; average points are shown as blue crosses; the model fit to the averaged values is shown as a blue line. Lag size: 0.053 degrees; number of lags: 12; Parameter: 2; Range: 0.426 degrees; Partial Sill: 2031.490. Right panel: Scatterplot of predicted values versus observed values for the model of Spring Primary Production Minimum (mg C $m^{-2}$ $day^{-1}$).

Table 144. Results of cross-validation of the kriged model for Spring Primary Production Minimum (mg C $m^{-2}$ $day^{-1}$).

| **Prediction Error** | **Value** |
|---|---:|
| Number of Observations | 17007 |
| Overall Mean Error | 0.059 |
| Root Mean Square Prediction Error | 61.362 |
| Standardized Mean | $7.975 \times 10^{-4}$ |
| Standardized Root Mean Square Prediction Error | 1.024 |
| Average Standard Error | 59.532 |

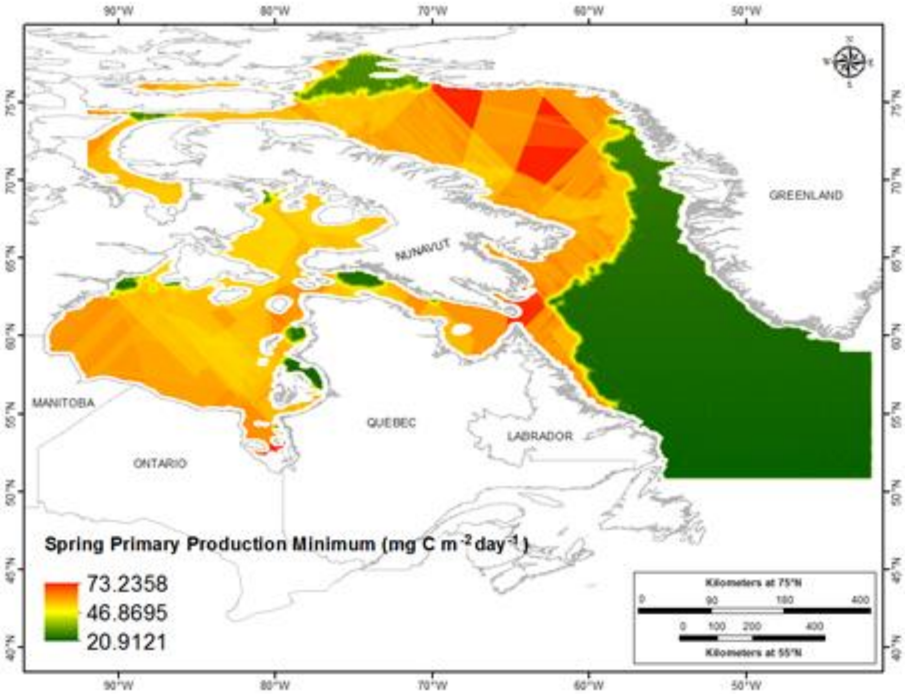


Figure 359. Prediction standard error surface of Spring Primary Production Minimum (mg C m$^{-2}$ day$^{-1}$).

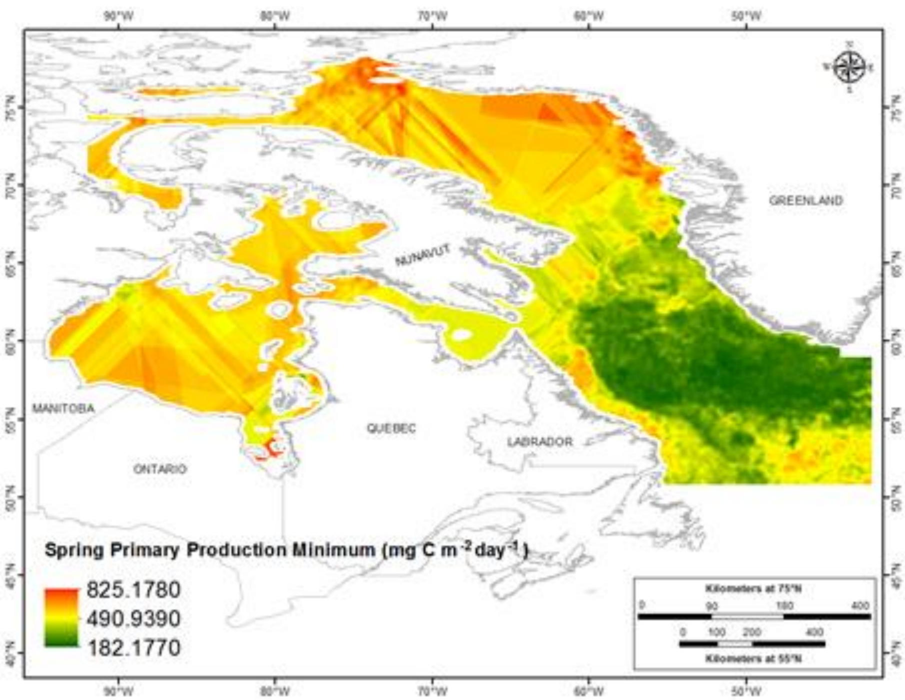


Figure 360. Interpolated prediction surface of Spring Primary Production Minimum (mg C m$^{-2}$ day$^{-1}$).

### Spring Primary Production Maximum

This variable had poor coverage over much of the study extent. It displayed a slightly skewed, leptokurtic distribution prior to interpolation (Table 145, Figure 361). The data were higher than predicted by a normal distribution at both tails however the mid-region was well-predicted, with some data points falling just below the reference line (Figure 362). These areas of under- and over-prediction showed no strong spatial pattern over the region (Figure 362).

The semivariogram showed weak autocorrelation present in the data (Figure 363). The kriged model showed good fit between measured and predicted values (Figure 363). Good performance of the model was indicated by the cross-validation results (Table 146). The error map was discontinuous and showed patches of high error in those areas where data points were scarce (Figure 364). The kriged surface is presented in Figure 365. Predictions were discontinuous in data-poor areas.

Table 145. Distributional properties of Spring Primary Production Maximum (mg C $m^{-2}$ $day^{-1}$).

| Property | Value |
|---|---:|
| Number of Observations | 17007 |
| Minimum | 426.800 |
| Maximum | 3163.600 |
| Mean | 1085.900 |
| Median | 1043.100 |
| Standard Deviation | 232.360 |
| Skewness | 0.984 |
| Kurtosis | 4.472 |

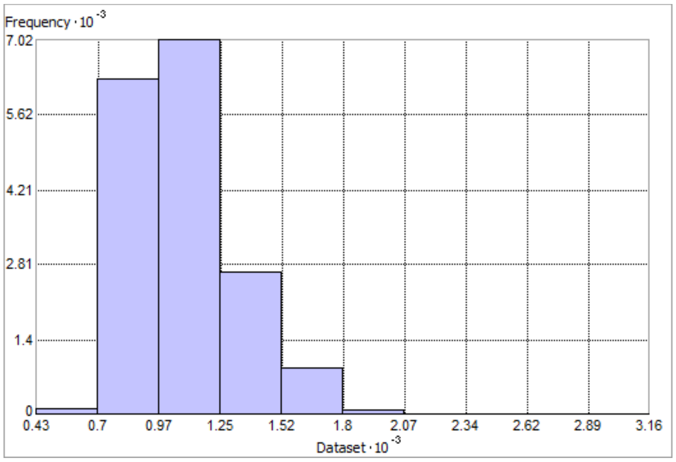


Figure 361. Distribution of Spring Primary Production Maximum (mg C m$^{-2}$ day$^{-1}$). Histogram was illustrated using 10 bins. X axis is shown at $10^{-3}$; Y axis is shown at $10^{-3}$.

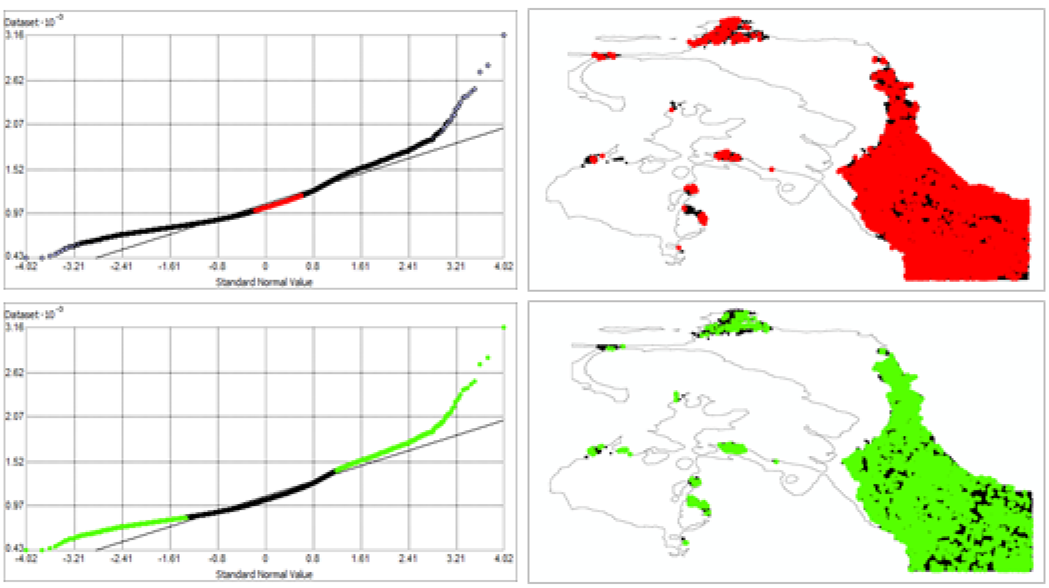

Figure 362. Normal Q-Q plot for data values of Spring Primary Production Maximum (mg C m$^{-2}$ day$^{-1}$). Points falling under (top right panel) and over (bottom right panel) the reference line are mapped.

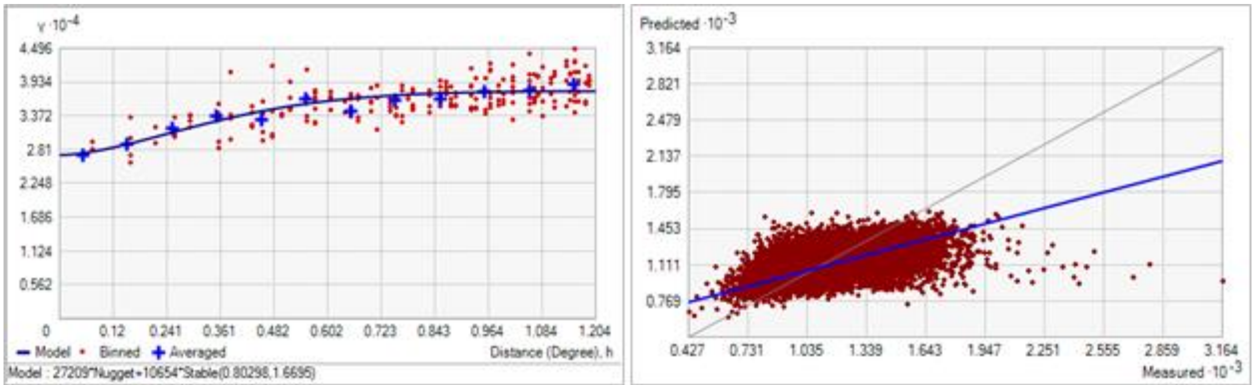


Figure 363. Left panel: Semivariogram of Spring Primary Production Maximum (mg C $m^{-2}$ $day^{-1}$). Binned values are shown as red dots; average points are shown as blue crosses; the model fit to the averaged values is shown as a blue line. Lag size: 0.100 degrees; number of lags: 12; Parameter: 1.670; Range: 0.823 degrees; Partial Sill: 10654.160. Right panel: Scatterplot of predicted values versus observed values for the model of Spring Primary Production Maximum (mg C $m^{-2}$ $day^{-1}$).

Table 146. Results of cross-validation of the kriged model for Spring Primary Production Maximum (mg C $m^{-2}$ $day^{-1}$).

| **Prediction Error** | **Value** |
|---|---|
| Number of Observations | 17007 |
| Overall Mean Error | -0.047 |
| Root Mean Square Prediction Error | 178.937 |
| Standardized Mean | $-2.725 \times 10^{-4}$ |
| Standardized Root Mean Square Prediction Error | 1.028 |
| Average Standard Error | 173.744 |

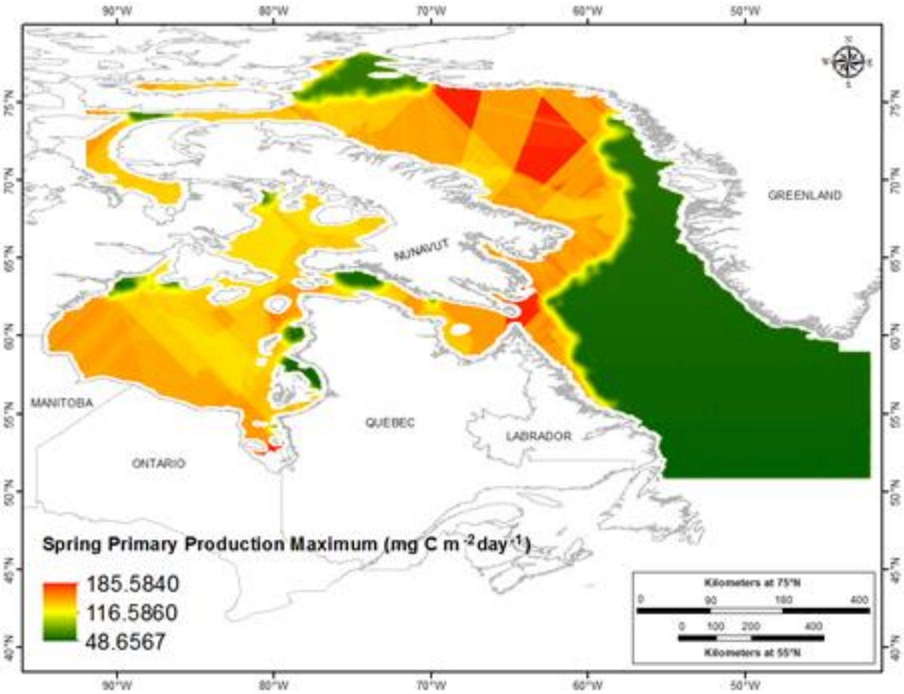


Figure 364. Prediction standard error surface of Spring Primary Production Maximum (mg C m$^{-2}$ day$^{-1}$).

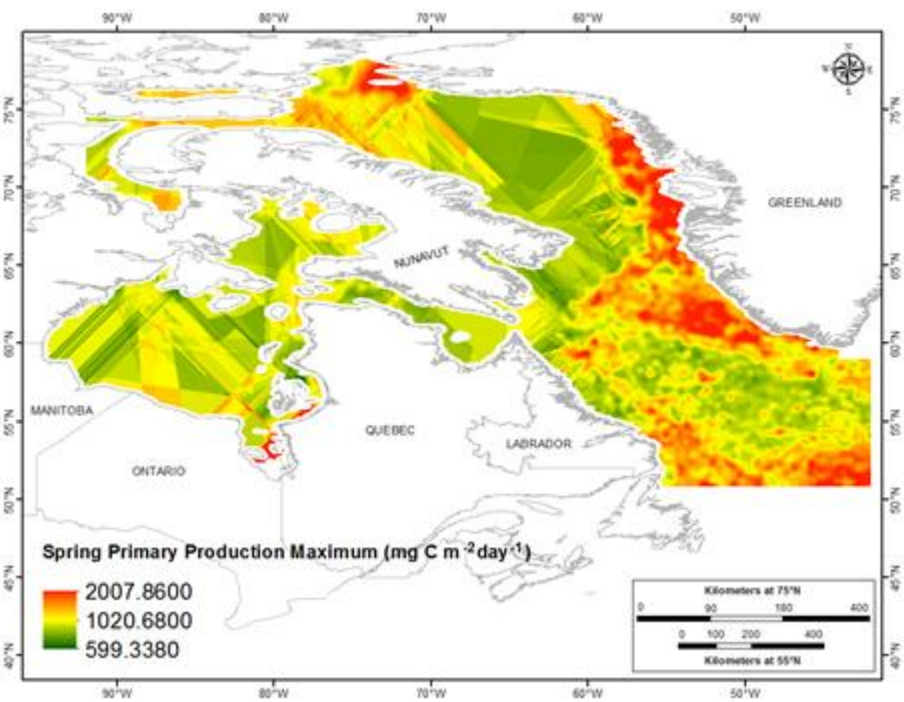


Figure 365. Interpolated prediction surface of Spring Primary Production Maximum (mg C m$^{-2}$ day$^{-1}$).

**Spring Primary Production Range**

This variable had poor coverage over much of the study extent. It displayed a near-normal distribution prior to interpolation, with slight skew and leptokurtosis (Table 147, Figure 366). The data were higher than predicted by a normal distribution, and no points fell under the reference line (Figure 367). These areas of over-prediction showed no strong spatial pattern over the region (Figure 367).

The semivariogram showed autocorrelation present in the data (Figure 368). The kriged model showed a poor fit between measured and predicted values (Figure 368). Nonetheless very good performance of the model was indicated by the cross-validation results (Table 148). The error map was discontinuous and showed patches of high error in those areas where data points were scarce (Figure 369). The kriged surface is presented in Figure 370. Predictions were discontinuous in data-poor areas.

Table 147. Distributional properties of Spring Primary Production Range (mg C $m^{-2}$ $day^{-1}$).

| **Property** | **Value** |
|---|---:|
| Number of Observations | 17007 |
| Minimum | 36.480 |
| Maximum | 2727.700 |
| Mean | 729.180 |
| Median | 705.700 |
| Standard Deviation | 242.390 |
| Skewness | 0.582 |
| Kurtosis | 4.538 |

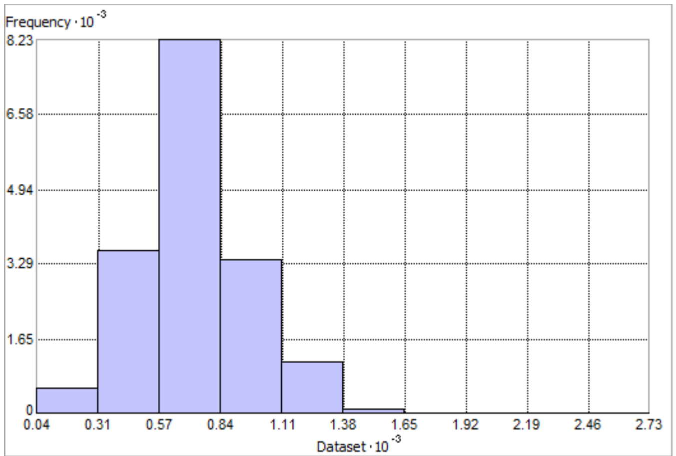


Figure 366. Distribution of Spring Primary Production Range (mg C m$^{-2}$ day$^{-1}$). Histogram was illustrated using 10 bins. X axis is shown at $10^{-3}$; Y axis is shown at $10^{-3}$.

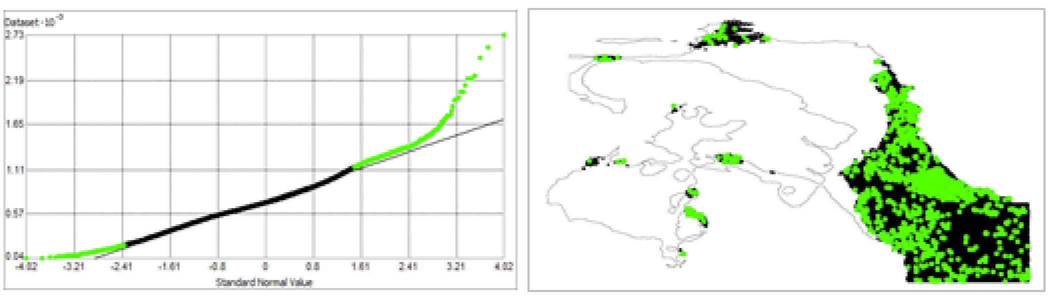


Figure 367. Normal Q-Q plot for data values of Spring Primary Production Range (mg C m$^{-2}$ day$^{-1}$). Points falling over the reference line are mapped; no points fall under the reference line.

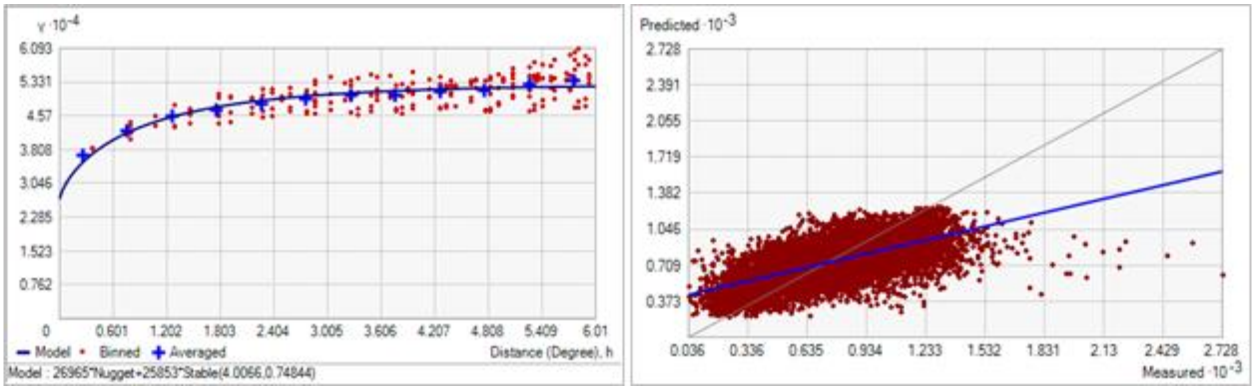


Figure 368. Left panel: Semivariogram of Spring Primary Production Range (mg C $m^{-2}$ $day^{-1}$). Binned values are shown as red dots; average points are shown as blue crosses; the model fit to the averaged values is shown as a blue line. Lag size: 0.501 degrees; number of lags: 12; Parameter: 0.748; Range: 4.007 degrees; Partial Sill: 25852.560. Right panel: Scatterplot of predicted values versus observed values for the model of Spring Primary Production Range (mg C $m^{-2}$ $day^{-1}$).

Table 148. Results of cross-validation of the kriged model for Spring Primary Production Range (mg C $m^{-2}$ $day^{-1}$).

| **Prediction Error** | **Value** |
|---|---:|
| Number of Observations | 17007 |
| Overall Mean Error | -0.082 |
| Root Mean Square Prediction Error | 188.334 |
| Standardized Mean | $-4.377 \times 10^{-4}$ |
| Standardized Root Mean Square Prediction Error | 1.017 |
| Average Standard Error | 184.791 |

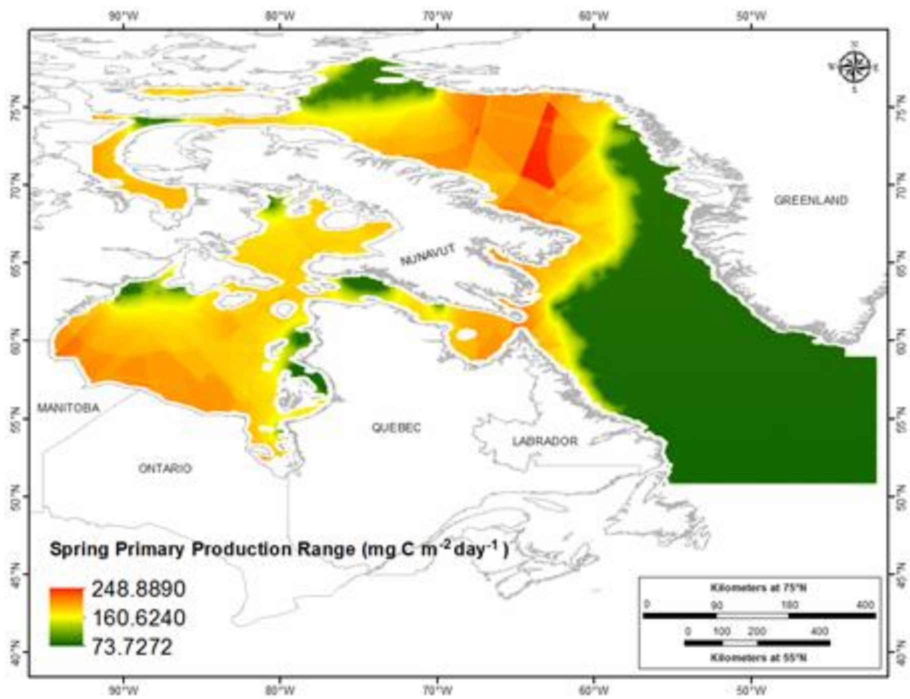


Figure 369. Prediction standard error surface of Spring Primary Production Range (mg C $m^{-2}$ $day^{-1}$).

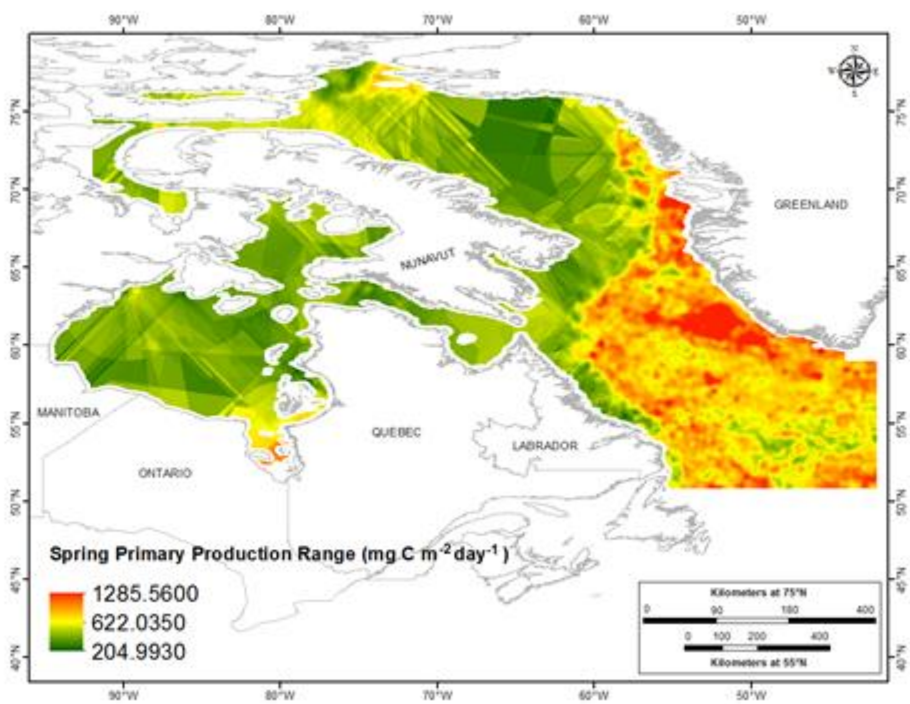


Figure 370. Interpolated prediction surface of Spring Primary Production Range (mg C $m^{-2}$ $day^{-1}$).

### Spring Primary Production Average Minimum

This variable had poor coverage over much of the study extent. It displayed a near-normal distribution prior to interpolation (Table 149, Figure 371). The data were higher than predicted by a normal distribution, and no points fell under the reference line (Figure 372). These areas of over-prediction showed no strong spatial pattern over the region (Figure 372).

The semivariogram showed autocorrelation present in the data (Figure 373). The kriged model showed a good fit between measured and predicted values (Figure 373). Nonetheless very good performance of the model was indicated by the cross-validation results (Table 150). The error map was discontinuous and showed patches of high error in those areas where data points were scarce (Figure 374). The kriged surface is presented in Figure 375. Predictions were discontinuous in data-poor areas.

Table 149. Distributional properties of Spring Primary Production Average Minimum (mg C $m^{-2}$ $day^{-1}$).

| **Property** | **Value** |
|---|---:|
| Number of Observations | 17007 |
| Minimum | 64.068 |
| Maximum | 1167.100 |
| Mean | 492.070 |
| Median | 486.910 |
| Standard Deviation | 125.320 |
| Skewness | 0.535 |
| Kurtosis | 3.402 |

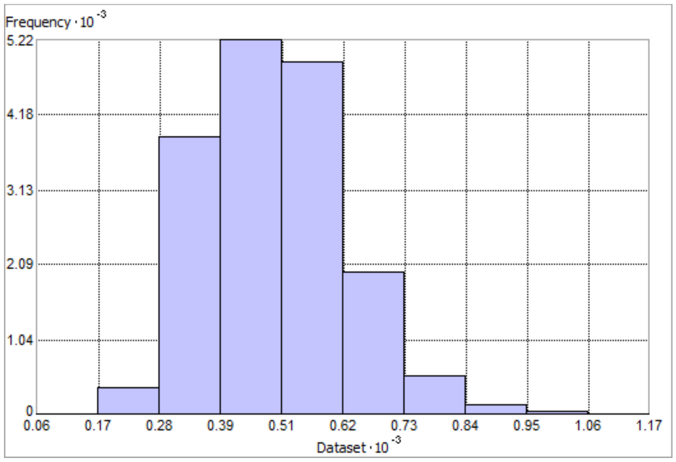


Figure 371. Distribution of Spring Primary Production Average Minimum (mg C $m^{-2}$ $day^{-1}$). Histogram was illustrated using 10 bins. X axis is shown at $10^{-3}$; Y axis is shown at $10^{-3}$.

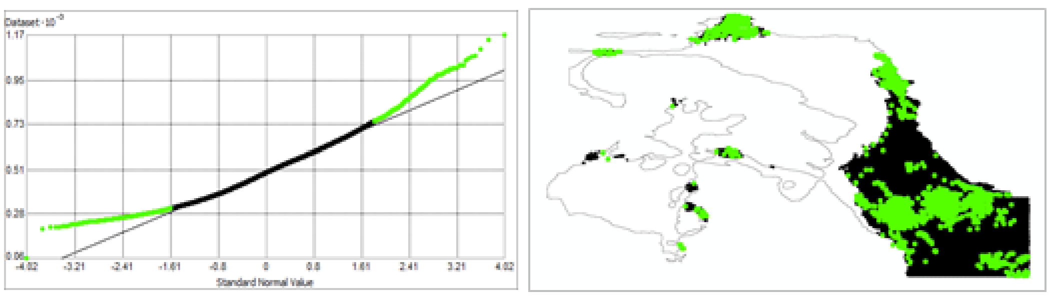

Figure 372. Normal Q-Q plot for data values of Spring Primary Production Average Minimum (mg C $m^{-2}$ $day^{-1}$). Points falling over the reference line are mapped; no points fall under the reference line.

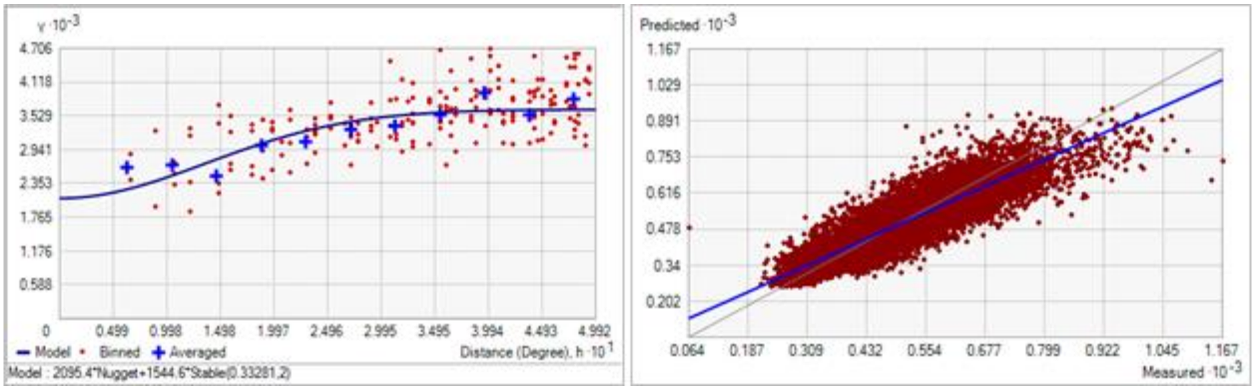

Figure 373. Left panel: Semivariogram of Spring Primary Production Average Minimum (mg C $m^{-2}$ $day^{-1}$). Binned values are shown as red dots; average points are shown as blue crosses; the model fit to the averaged values is shown as a blue line. Lag size: 0.042 degrees; number of lags: 12; Parameter: 2; Range: 0.333 degrees; Partial Sill: 1544.585. Right panel: Scatterplot of predicted values versus observed values for the model of Spring Primary Production Average Minimum (mg C $m^{-2}$ $day^{-1}$).

Table 150. Results of cross-validation of the kriged model for Spring Primary Production Average Minimum (mg C $m^{-2}$ $day^{-1}$).

| **Prediction Error** | **Value** |
|---|---|
| Number of Observations | 17007 |
| Overall Mean Error | 0.023 |
| Root Mean Square Prediction Error | 54.929 |
| Standardized Mean | $3.654 \times 10^{-4}$ |
| Standardized Root Mean Square Prediction Error | 1.039 |
| Average Standard Error | 52.460 |

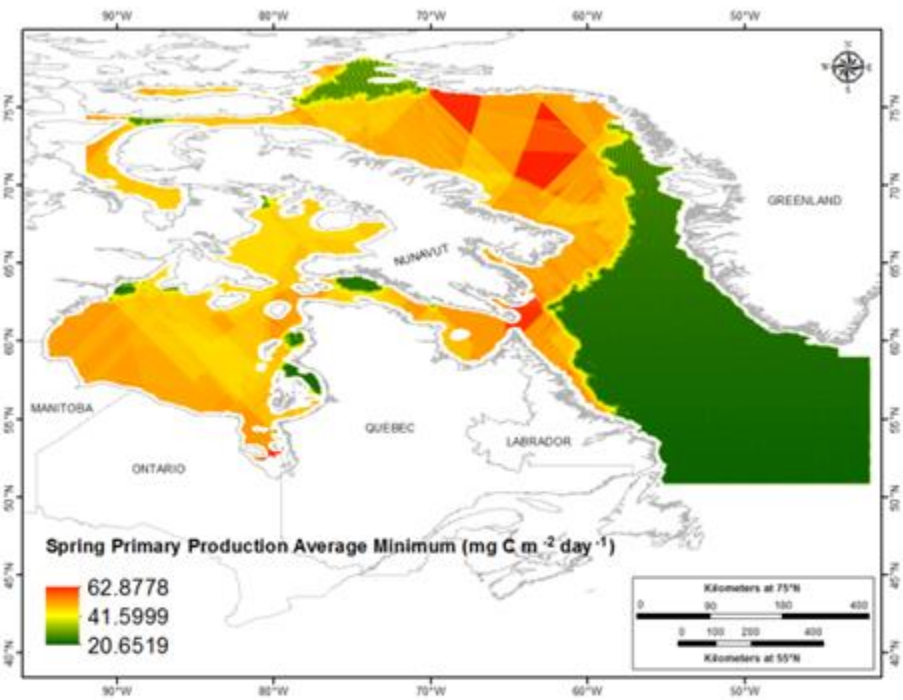


Figure 374. Prediction standard error surface of Spring Primary Production Average Minimum (mg C $m^{-2}$ $day^{-1}$).

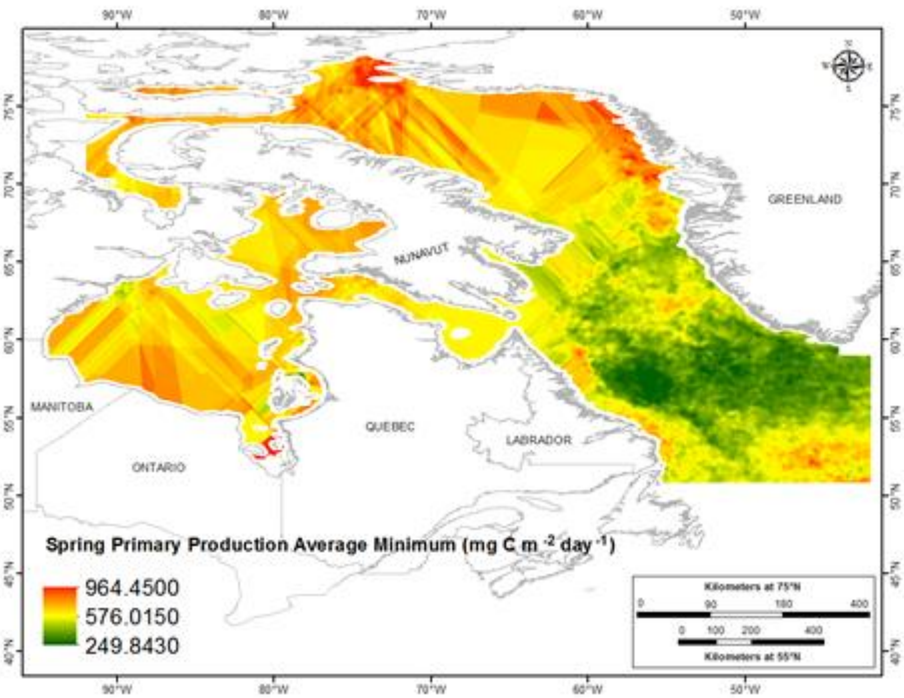


Figure 375. Interpolated prediction surface of Spring Primary Production Average Minimum (mg C $m^{-2}$ $day^{-1}$).

## Spring Primary Production Average Maximum

This variable had poor coverage over much of the study extent. It displayed a near-normal distribution prior to interpolation, with slight skew and leptokurtosis (Table 151, Figure 376). The data were higher than predicted by a normal distribution at both tails however the mid-region was well-predicted with some points falling below the reference line (Figure 377). These areas of under- and over-prediction showed no spatial pattern over the region (Figure 377).

The semivariogram showed autocorrelation present in the data (Figure 378). The kriged model showed poor fit between measured and predicted values (Figure 378). Nonetheless, very good performance of the model was indicated by the cross-validation results (Table 152). The error map was discontinuous and showed patches of high error in those areas where data points were scarce (Figure 379). The kriged surface is presented in Figure 380. Predictions were discontinuous in data-poor areas.

Table 151. Distributional properties of Spring Primary Production Average Maximum (mg C $m^{-2}$ $day^{-1}$).

| **Property** | **Value** |
|---|---:|
| Number of Observations | 17007 |
| Minimum | 349.330 |
| Maximum | 1753.000 |
| Mean | 875.120 |
| Median | 848.680 |
| Standard Deviation | 132.770 |
| Skewness | 1.059 |
| Kurtosis | 4.990 |

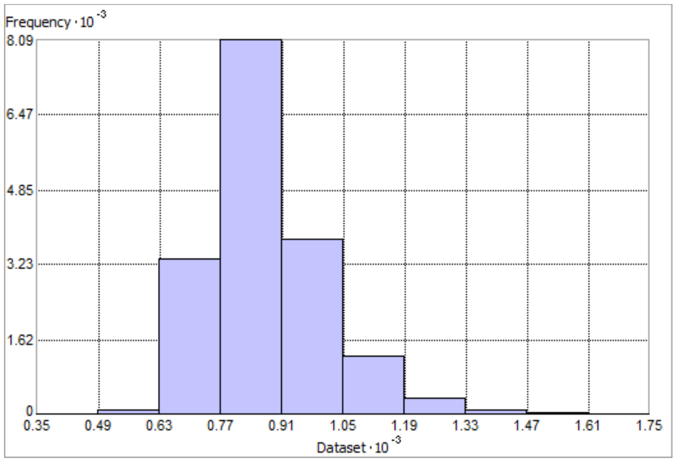


Figure 376. Distribution of Spring Primary Production Average Maximum (mg C m$^{-2}$ day$^{-1}$). Histogram was illustrated using 10 bins. X axis is shown at $10^{-3}$; Y axis is shown at $10^{-3}$.

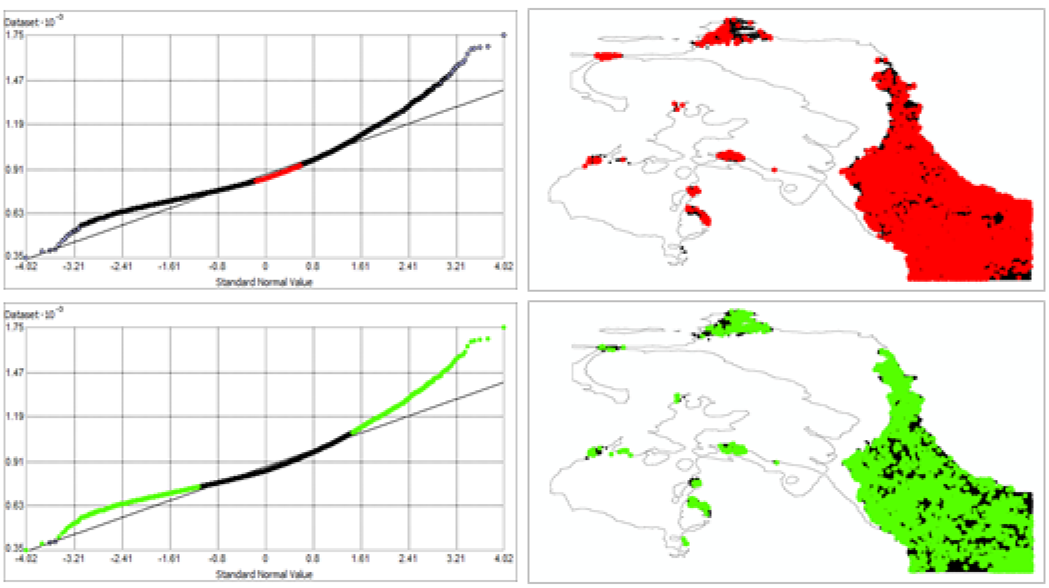


Figure 377. Normal Q-Q plot for data values of Spring Primary Production Average Maximum (mg C m$^{-2}$ day$^{-1}$). Points falling under (top right panel) and over (bottom right panel) the reference line are mapped.

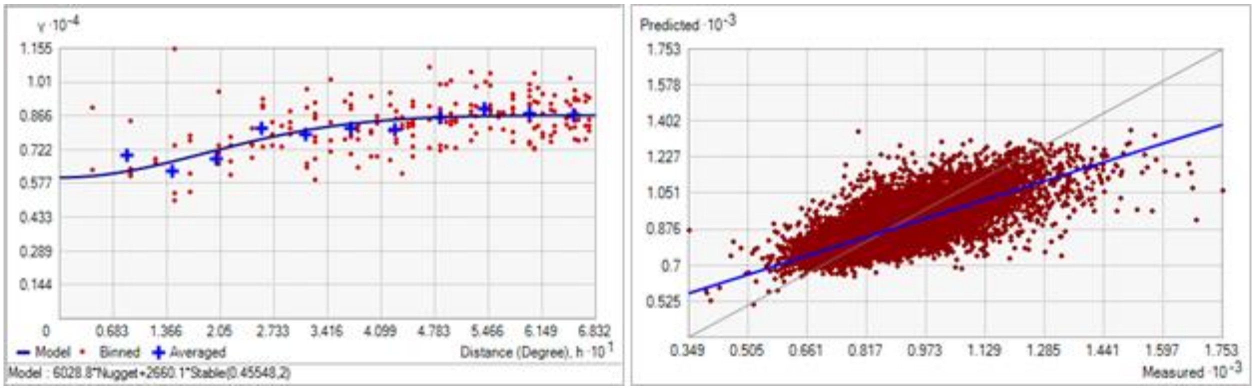

Figure 378. Left panel: Semivariogram of Spring Primary Production Average Maximum (mg C $m^{-2}$ $day^{-1}$). Binned values are shown as red dots; average points are shown as blue crosses; the model fit to the averaged values is shown as a blue line. Lag size: 0.057 degrees; number of lags: 12; Parameter: 2; Range: 0.455 degrees; Partial Sill: 2660.101. Right panel: Scatterplot of predicted values versus observed values for the model of Spring Primary Production Average Maximum (mg C $m^{-2}$ $day^{-1}$).

Table 152. Results of cross-validation of the kriged model for Spring Primary Production Average Maximum (mg C $m^{-2}$ $day^{-1}$).

| **Prediction Error** | **Value** |
|---|---:|
| Number of Observations | 17007 |
| Overall Mean Error | 0.012 |
| Root Mean Square Prediction Error | 87.644 |
| Standardized Mean | $1.281 \times 10^{-4}$ |
| Standardized Root Mean Square Prediction Error | 1.041 |
| Average Standard Error | 83.602 |

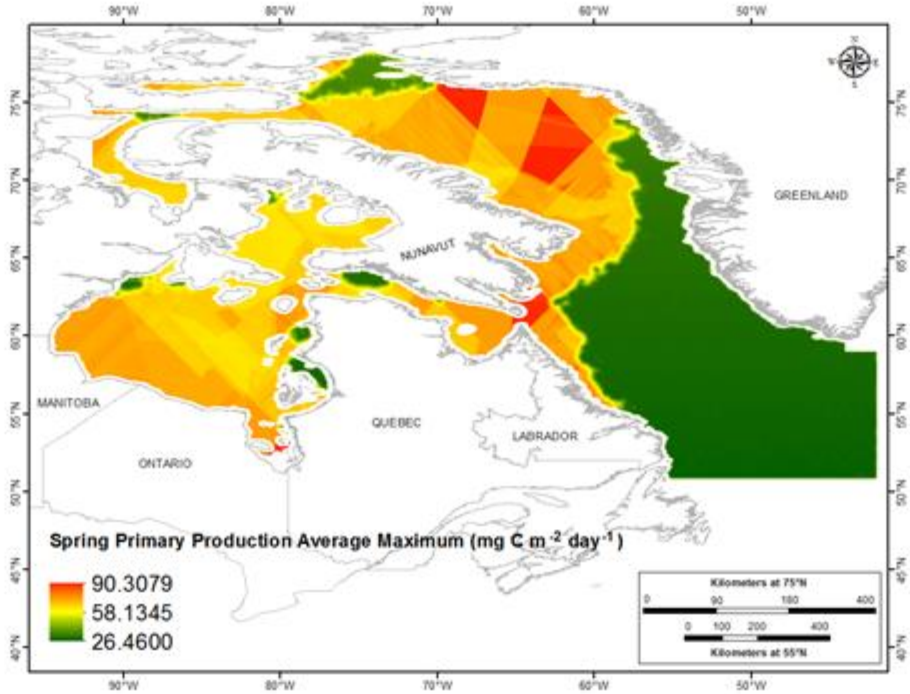


Figure 379. Prediction standard error surface of Spring Primary Production Average Maximum (mg C $m^{-2}$ $day^{-1}$).

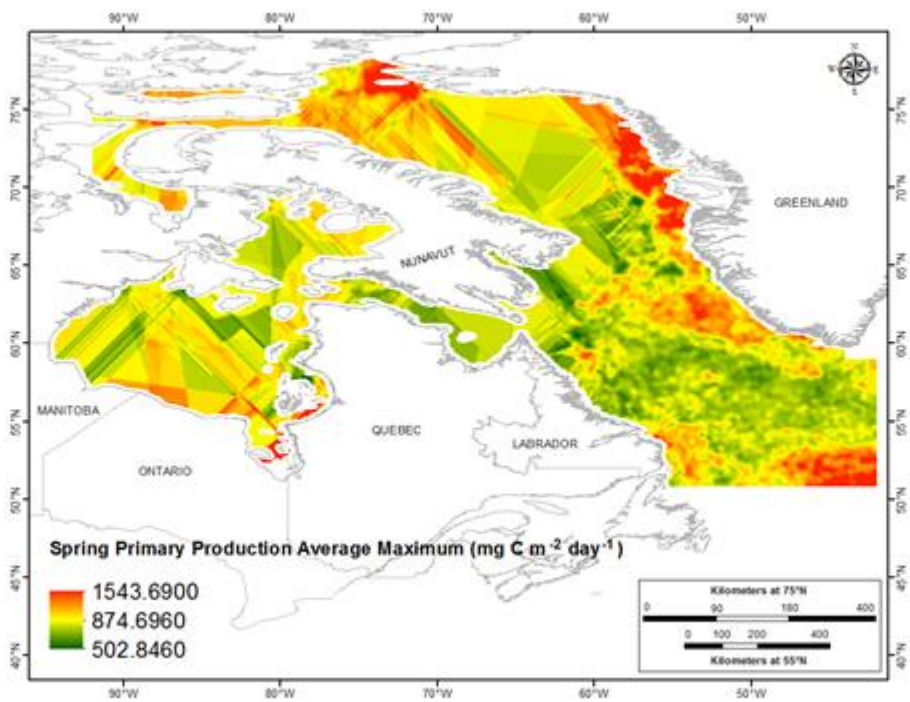


Figure 380. Interpolated prediction surface of Spring Primary Production Average Maximum (mg C $m^{-2}$ $day^{-1}$).

## Spring Primary Production Average Range

This variable had poor coverage over much of the study extent. It displayed a near-normal distribution prior to interpolation, with slight skew and leptokurtosis (Table 153, Figure 381). The data were higher than predicted by a normal distribution, and no points fell under the reference line (Figure 382). These areas of over-prediction showed no strong spatial pattern over the region (Figure 382).

The semivariogram showed weak autocorrelation present in the data (Figure 383). The kriged model showed a fair fit between measured and predicted values (Figure 383). Nonetheless, very good performance of the model was indicated by the cross-validation results (Table 154). The error map was discontinuous and showed patches of high error in those areas where data points were scarce (Figure 384). The kriged surface is presented in Figure 385. Predictions were discontinuous in data-poor areas.

Table 153. Distributional properties of Spring Primary Production Average Range (mg C $m^{-2}$ $day^{-1}$).

| **Property** | **Value** |
|---|---:|
| Number of Observations | 17007 |
| Minimum | 1.42 |
| Maximum | 1127.200 |
| Mean | 383.050 |
| Median | 379.940 |
| Standard Deviation | 130.200 |
| Skewness | 0.191 |
| Kurtosis | 3.389 |

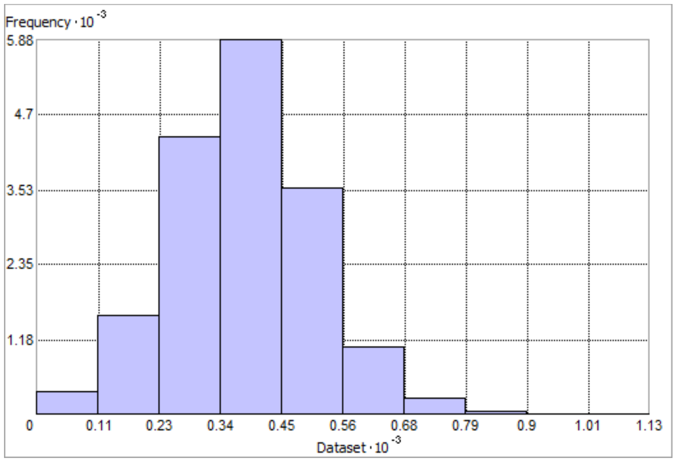


Figure 381. Distribution of Spring Primary Production Average Range (mg C $m^{-2}$ $day^{-1}$). Histogram was illustrated using 10 bins. X axis is shown at $10^{-3}$; Y axis is shown at $10^{-3}$.

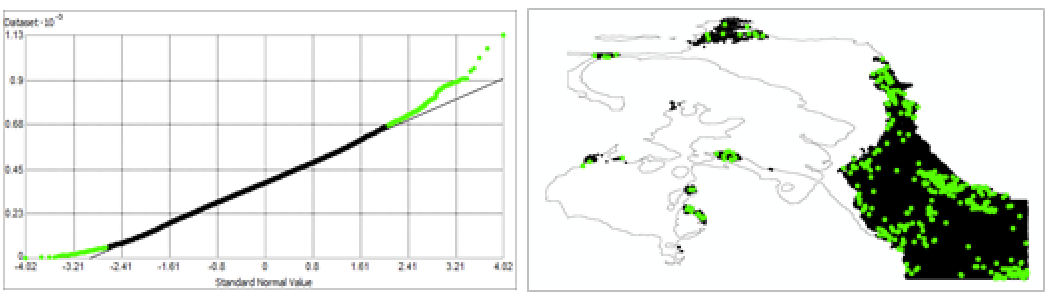


Figure 382. Normal Q-Q plot for data values of Spring Primary Production Average Range (mg C $m^{-2}$ $day^{-1}$). Points falling over the reference line are mapped; no points fall under the reference line.

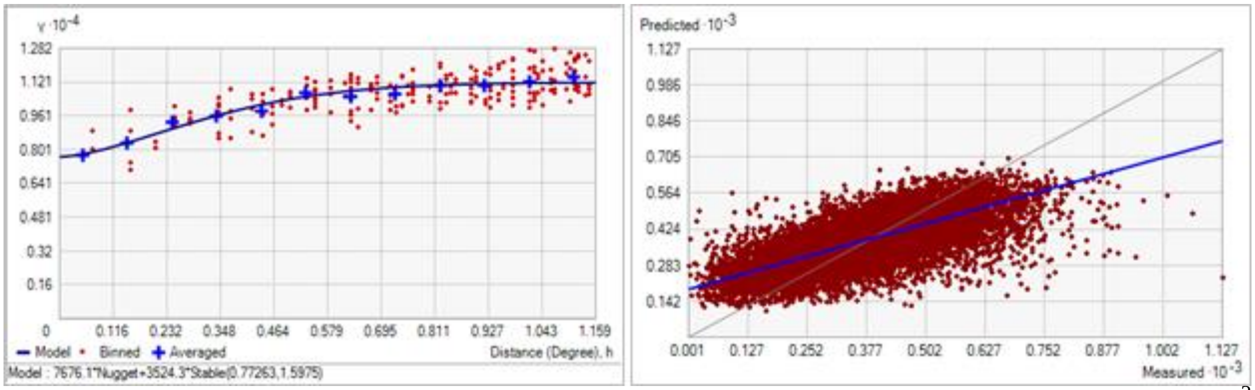

Figure 383. Left panel: Semivariogram of Spring Primary Production Average Range (mg C $m^{-2}$ $day^{-1}$). Binned values are shown as red dots; average points are shown as blue crosses; the model fit to the averaged values is shown as a blue line. Lag size: 0.097 degrees; number of lags: 12; Parameter: 1.597; Range: 0.773 degrees; Partial Sill: 3524.317. Right panel: Scatterplot of predicted values versus observed values for the model of Spring Primary Production Average Range (mg C $m^{-2}$ $day^{-1}$).

Table 154. Results of cross-validation of the kriged model for Spring Primary Production Average Range (mg C $m^{-2}$ $day^{-1}$).

| **Prediction Error** | **Value** |
|---|---|
| Number of Observations | 17007 |
| Overall Mean Error | -0.035 |
| Root Mean Square Prediction Error | 95.453 |
| Standardized Mean | $-3.781 \times 10^{-4}$ |
| Standardized Root Mean Square Prediction Error | 1.020 |
| Average Standard Error | 93.237 |

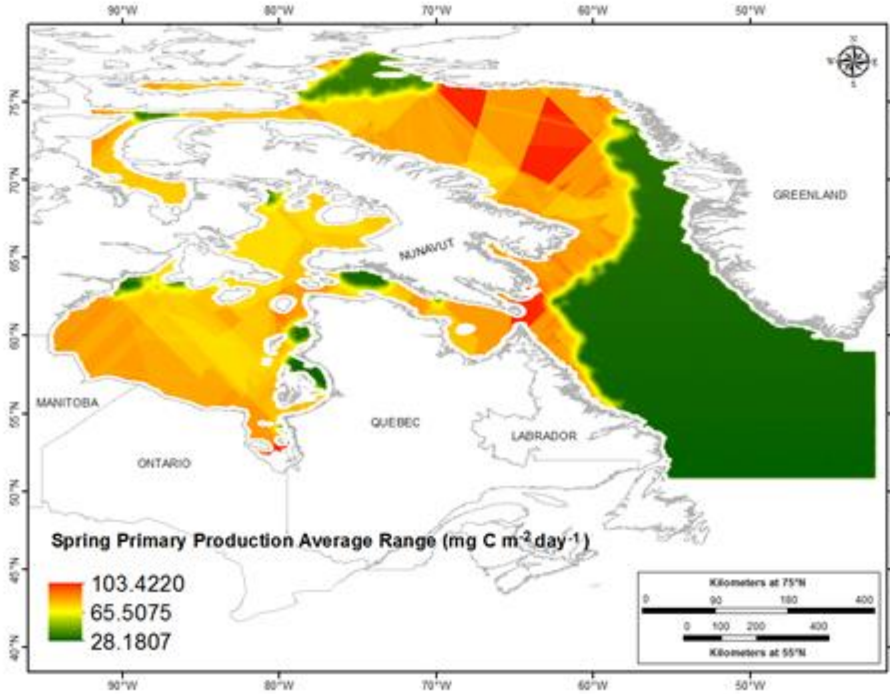


Figure 384. Prediction standard error surface of Spring Primary Production Average Range (mg C $m^{-2}$ $day^{-1}$).

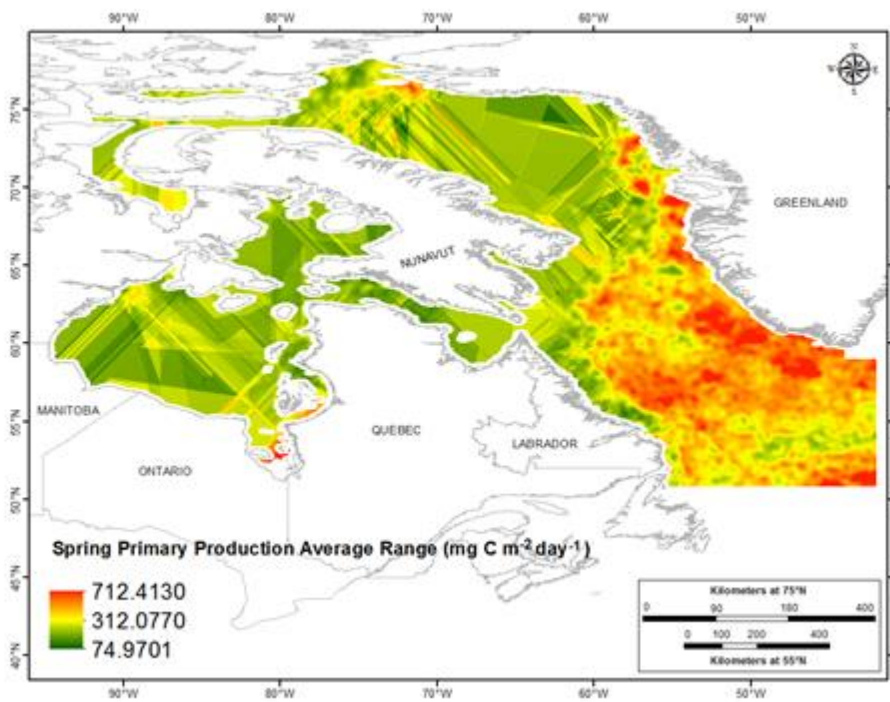


Figure 385. Interpolated prediction surface of Spring Primary Production Average Range (mg C $m^{-2}$ $day^{-1}$).

## Summer Primary Production Mean

This variable had good coverage over the study extent and displayed a near-normal distribution prior to interpolation (Table 155, Figure 386). The data were lower than predicted by a normal distribution at both tails, while mid-values were slightly higher in the upper mid-range values (Figure 387). These areas of under- and over-prediction showed spatial pattern over the region (Figure 387).

The semivariogram showed moderate autocorrelation present in the data (Figure 388). The kriged model showed a good fit between measured and predicted values (Figure 388). Good performance of the model was indicated by the cross-validation results (Table 156). The error map showed moderate error in the northern portion of the study extent, with patches of high error interspersed (Figure 389). The kriged surface is presented in Figure 390.

Table 155. Distributional properties of Summer Primary Production Mean (mg C $m^{-2}$ $day^{-1}$).

| **Property** | **Value** |
|---|---:|
| Number of Observations | 33872 |
| Minimum | 94.012 |
| Maximum | 1083.600 |
| Mean | 658.900 |
| Median | 653.610 |
| Standard Deviation | 115.980 |
| Skewness | 0.176 |
| Kurtosis | 3.186 |

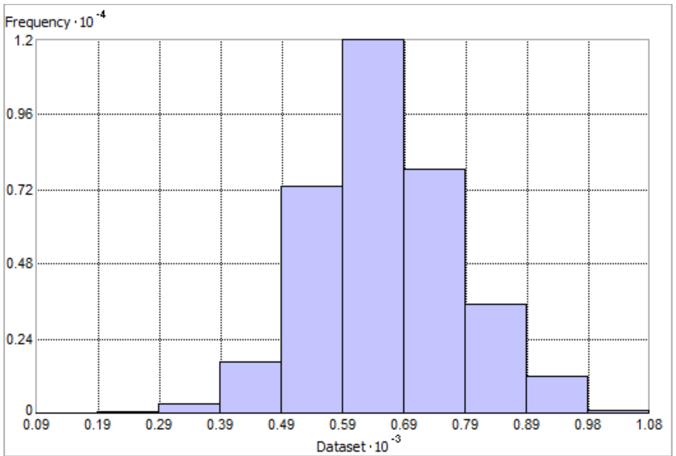

Figure 386. Distribution of Summer Primary Production Mean (mg C m$^{-2}$ day$^{-1}$). Histogram was illustrated using 10 bins. X axis is shown at $10^{-3}$; Y axis is shown at $10^{-4}$.

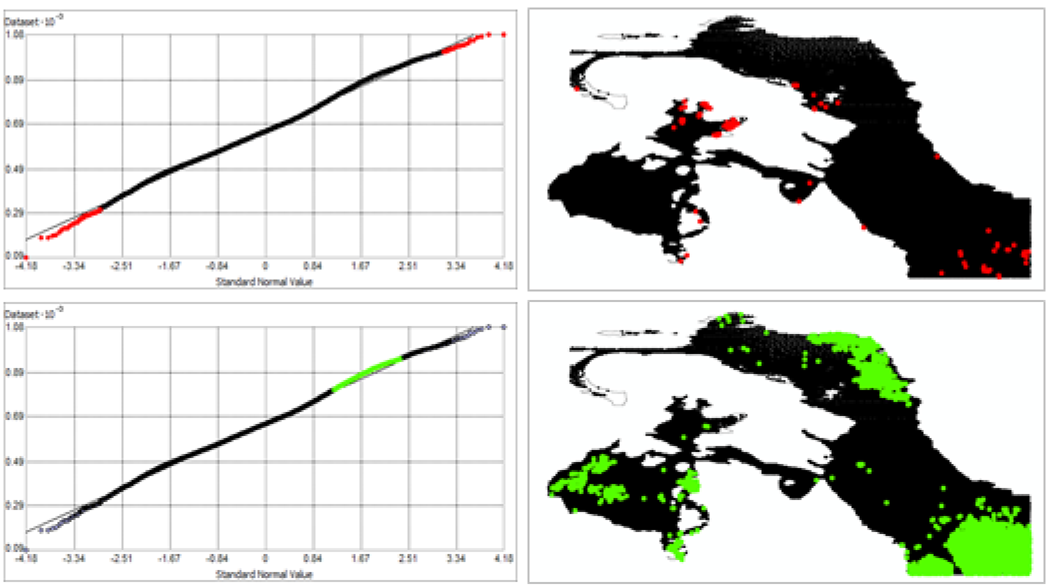
Figure 387. Normal Q-Q plot for data values of Summer Primary Production Mean (mg C m$^{-2}$ day$^{-1}$). Points falling under (top right panel) and over (bottom right panel) the reference line are mapped.

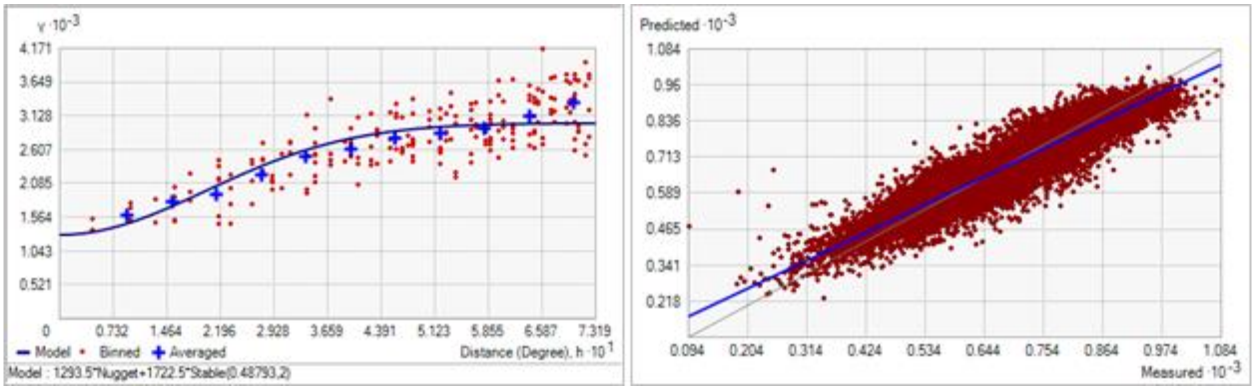

Figure 388. Left panel: Semivariogram of Summer Primary Production Mean (mg C $m^{-2}$ $day^{-1}$). Binned values are shown as red dots; average points are shown as blue crosses; the model fit to the averaged values is shown as a blue line. Lag size: 0.061 degrees; number of lags: 12; Parameter: 2; Range: 0.488 degrees; Partial Sill: 1722.462 Right panel: Scatterplot of predicted values versus observed values for the model of Summer Primary Production Mean (mg C $m^{-2}$ $day^{-1}$).

Table 156. Results of cross-validation of the kriged model for Summer Primary Production Mean (mg C $m^{-2}$ $day^{-1}$).

| **Prediction Error** | **Value** |
|---|---:|
| Number of Observations | 33872 |
| Overall Mean Error | 0.068 |
| Root Mean Square Prediction Error | 43.090 |
| Standardized Mean | $1.211 \times 10^{-3}$ |
| Standardized Root Mean Square Prediction Error | 1.061 |
| Average Standard Error | 40.421 |

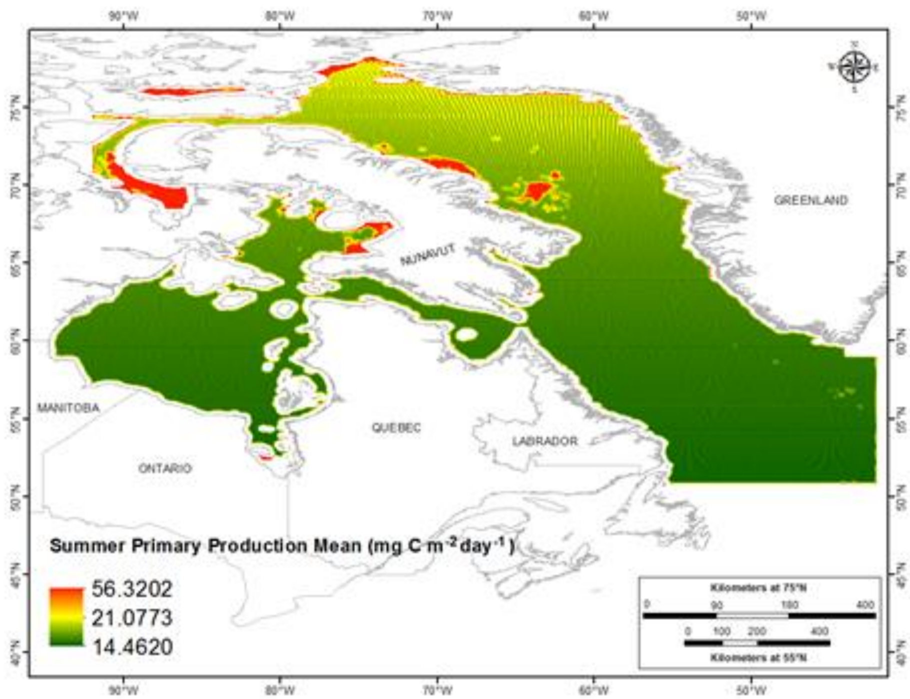


Figure 389. Prediction standard error surface of Summer Primary Production Mean (mg C $m^{-2}$ $day^{-1}$).

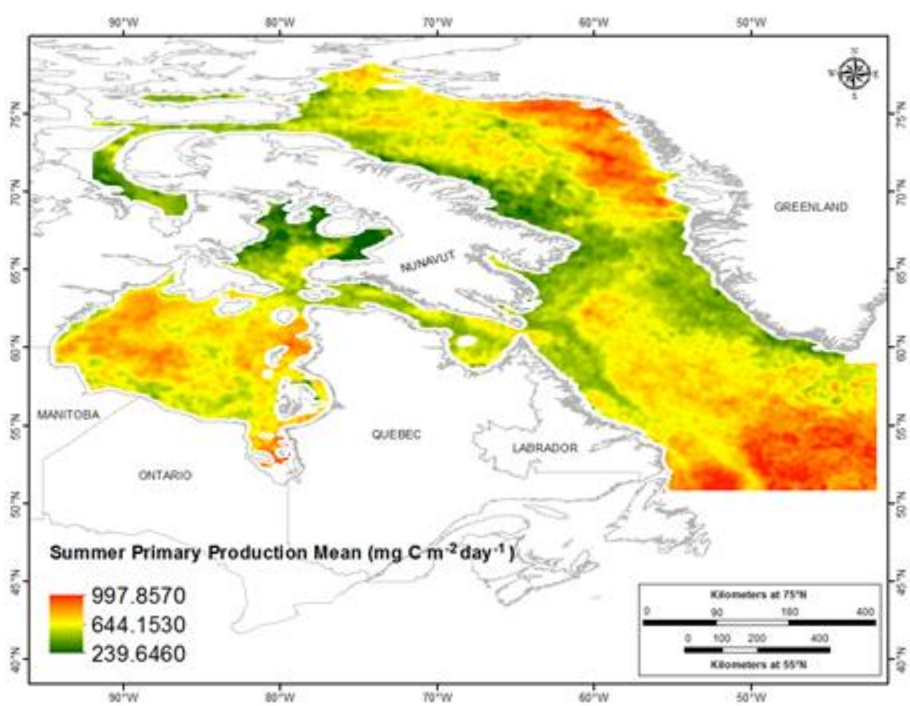


Figure 390. Interpolated prediction surface of Summer Primary Production Mean (mg C $m^{-2}$ $day^{-1}$).

**Summer Primary Production Minimum**

This variable had good coverage over the study extent and displayed a near-normal distribution prior to interpolation (Table 157, Figure 391). The data were higher than predicted by a normal distribution at both tails, with no data points falling under the reference line (Figure 392). These areas over-prediction showed some spatial pattern over the region (Figure 392).

The semivariogram showed moderate autocorrelation present in the data (Figure 393). The kriged model showed a good fit between measured and predicted values (Figure 393). Very good performance of the model was indicated by the cross-validation results (Table 158). The error map showed moderate error in the northern portion of the study extent, with patches of high error interspersed (Figure 394). The kriged surface is presented in Figure 395.

Table 157. Distributional properties of Summer Primary Production Minimum (mg C $m^{-2}$ $day^{-1}$).

| **Property** | **Value** |
|---|---:|
| Number of Observations | 33872 |
| Minimum | 44.610 |
| Maximum | 848.49 |
| Mean | 370.920 |
| Median | 367.550 |
| Standard Deviation | 110.260 |
| Skewness | 0.517 |
| Kurtosis | 3.300 |

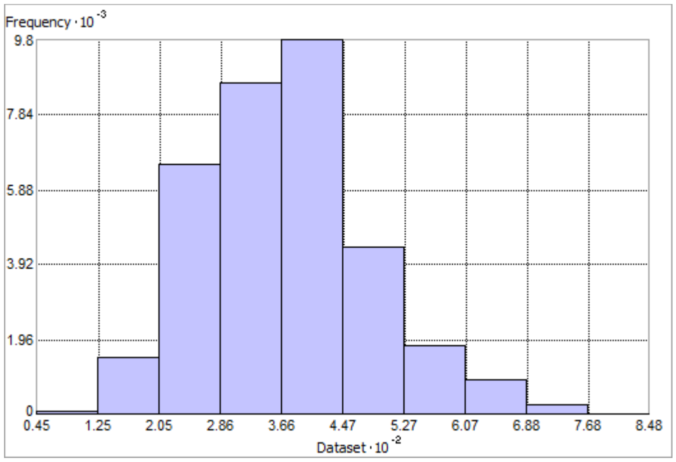


Figure 391. Distribution of Summer Primary Production Minimum (mg C $m^{-2}$ $day^{-1}$). Histogram was illustrated using 10 bins. X axis is shown at $10^{-2}$; Y axis is shown at $10^{-3}$.

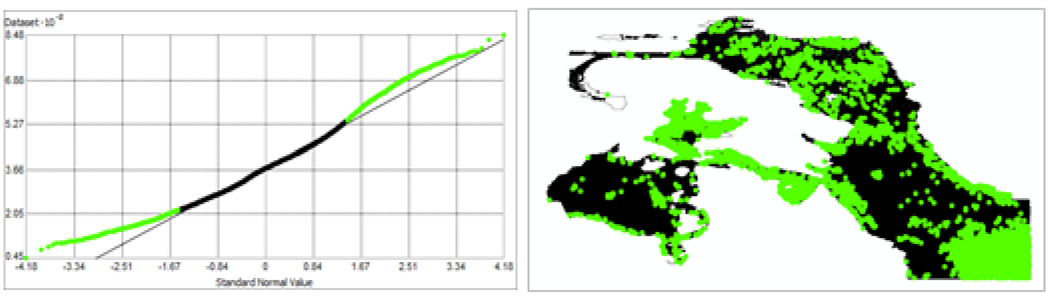

Figure 392. Normal Q-Q plot for data values of Summer Primary Production Minimum (mg C $m^{-2}$ $day^{-1}$). Points falling over the reference line are mapped; no points fall under the reference line.

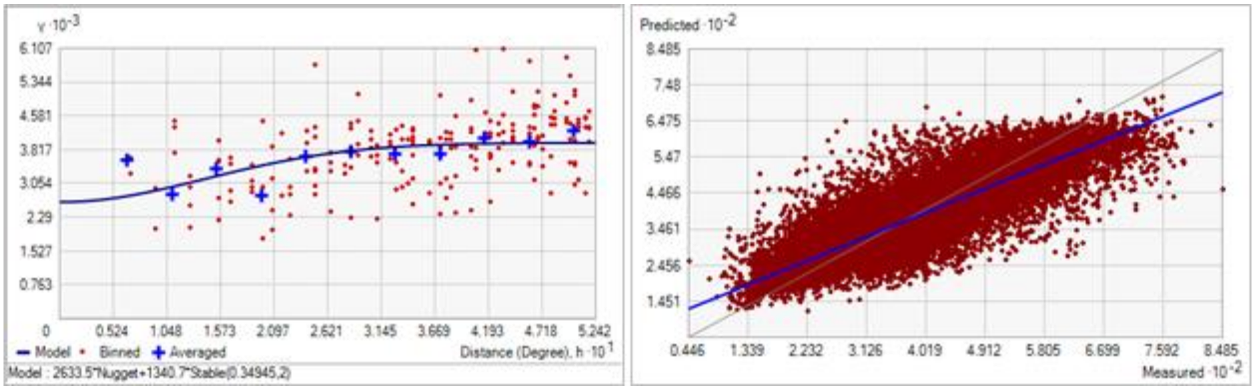


Figure 393. Left panel: Semivariogram of Summer Primary Production Minimum (mg C $m^{-2}$ $day^{-1}$). Binned values are shown as red dots; average points are shown as blue crosses; the model fit to the averaged values is shown as a blue line. Lag size: 0.044 degrees; number of lags: 12; Parameter: 2; Range: 0.350 degrees; Partial Sill: 1340.729 Right panel: Scatterplot of predicted values versus observed values for the model of Summer Primary Production Minimum (mg C $m^{-2}$ $day^{-1}$).

Table 158. Results of cross-validation of the kriged model for Summer Primary Production Minimum (mg C $m^{-2}$ $day^{-1}$).

| **Prediction Error** | **Value** |
|---|---|
| Number of Observations | 33872 |
| Overall Mean Error | 0.057 |
| Root Mean Square Prediction Error | 58.631 |
| Standardized Mean | $8.434 \times 10^{-3}$ |
| Standardized Root Mean Square Prediction Error | 1.019 |
| Average Standard Error | 57.482 |

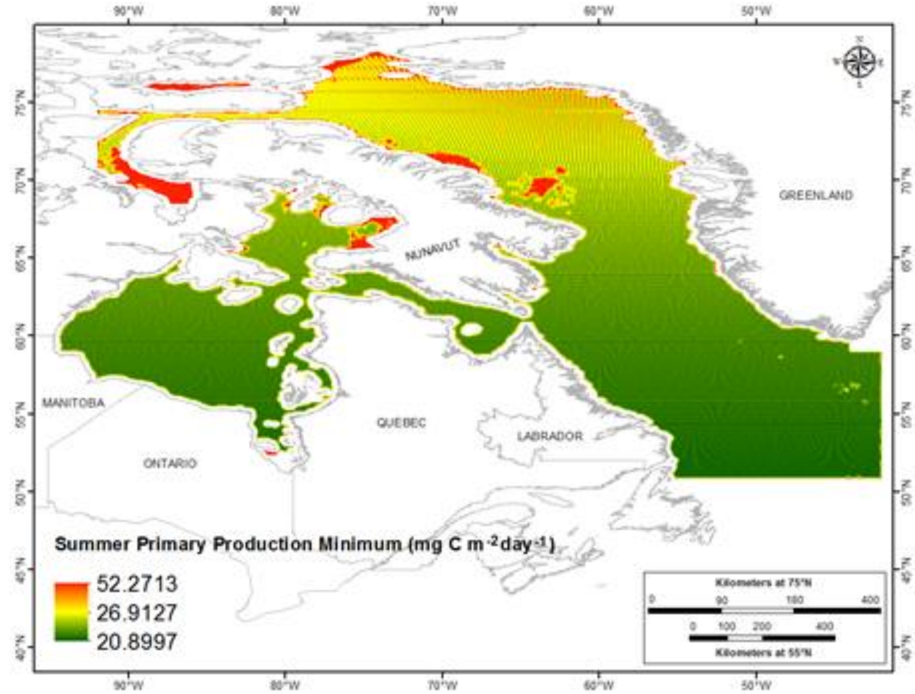


Figure 394. Prediction standard error surface of Summer Primary Production Minimum (mg C $m^{-2}$ $day^{-1}$).

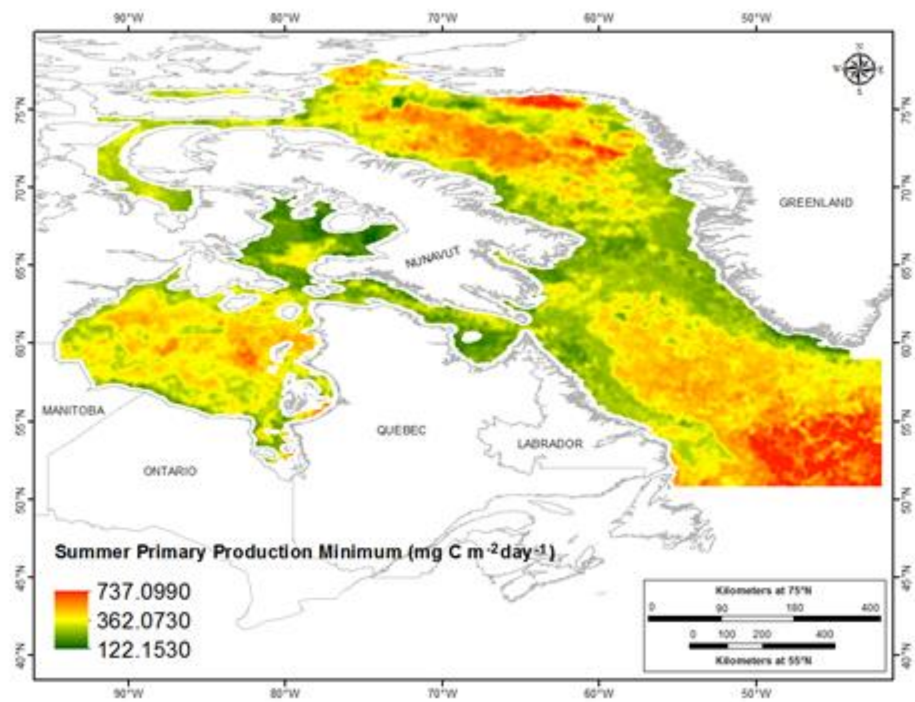


Figure 395. Interpolated prediction surface of Summer Primary Production Minimum (mg C $m^{-2}$ $day^{-1}$).

**Summer Primary Production Maximum**

This variable displayed a right-skewed, leptokurtic distribution prior to interpolation (Table 159, Figure 396). The data were higher than predicted by a normal distribution at both tails (Figure 397). No data points fell below the reference line. These areas of over-prediction showed no spatial pattern over the region (Figure 397).

The semivariogram showed weak autocorrelation present in the data (Figure 398). The kriged model showed poor fit between measured and predicted values (Figure 398). Very good performance of the model was indicated by the cross-validation results (Table 160). The error map showed moderate error in the northern portion of the study extent, with patches of high error interspersed (Figure 399). The kriged surface is presented in Figure 400.

Table 159. Distributional properties of Summer Primary Production Maximum (mg C $m^{-2}$ $day^{-1}$).

| **Property** | **Value** |
|---|---:|
| Number of Observations | 33872 |
| Minimum | 135.380 |
| Maximum | 2895.700 |
| Mean | 1031.600 |
| Median | 1014.400 |
| Standard Deviation | 213.980 |
| Skewness | 0.317 |
| Kurtosis | 3.596 |

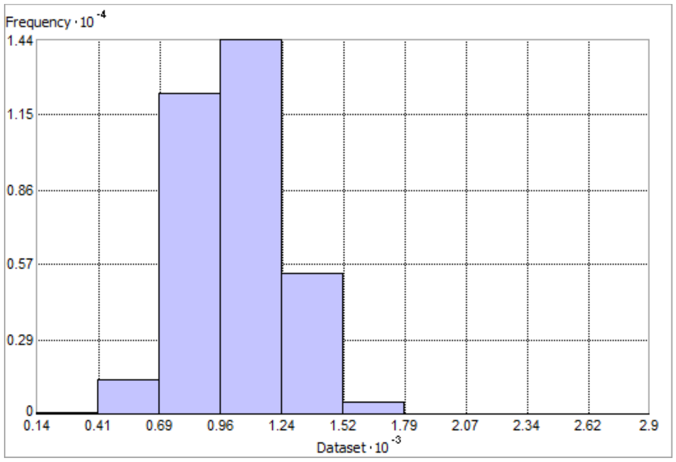


Figure 396. Distribution of Summer Primary Production Maximum (mg C $m^{-2}$ $day^{-1}$). Histogram was illustrated using 10 bins. X axis is shown at $10^{-3}$; Y axis is shown at $10^{-4}$.

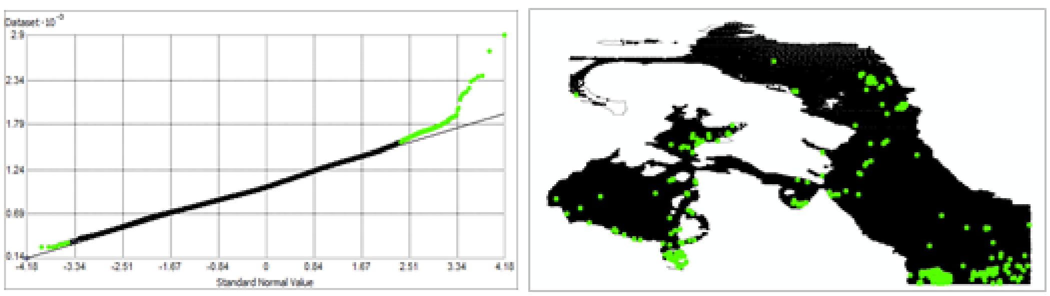

Figure 397. Normal Q-Q plot for data values of Summer Primary Production Maximum (mg C $m^{-2}$ $day^{-1}$). Points falling over the reference line are mapped; no points fall under the reference line.

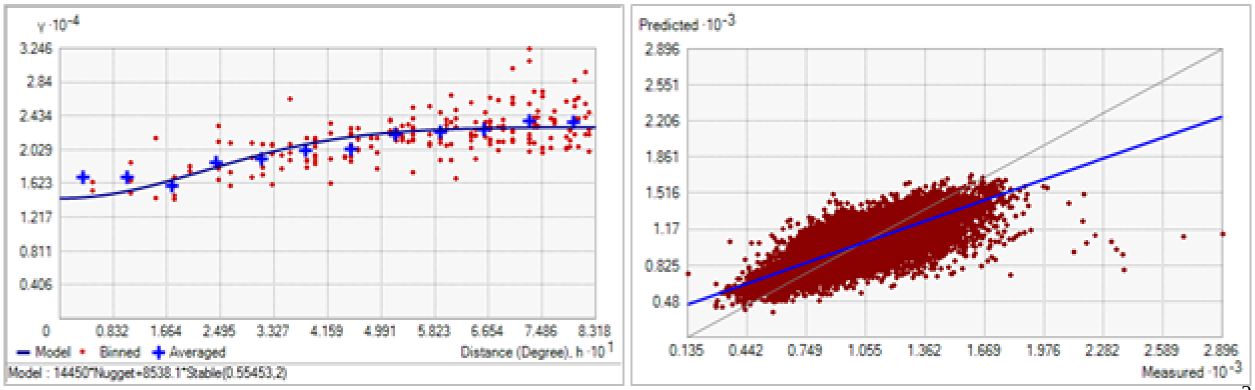


Figure 398. Left panel: Semivariogram of Summer Primary Production Maximum (mg C $m^{-2}$ $day^{-1}$). Binned values are shown as red dots; average points are shown as blue crosses; the model fit to the averaged values is shown as a blue line. Lag size: 0.069 degrees; number of lags: 12; Parameter: 2; Range: 0.555 degrees; Partial Sill: 8538.102 Right panel: Scatterplot of predicted values versus observed values for the model of Summer Primary Production Maximum (mg C $m^{-2}$ $day^{-1}$).

Table 160. Results of cross-validation of the kriged model for Summer Primary Production Maximum (mg C $m^{-2}$ $day^{-1}$).

| **Prediction Error** | **Value** |
|---|---|
| Number of Observations | 33872 |
| Overall Mean Error | 0.091 |
| Root Mean Square Prediction Error | 133.937 |
| Standardized Mean | $5.654 \times 10^{-4}$ |
| Standardized Root Mean Square Prediction Error | 1.036 |
| Average Standard Error | 129.108 |

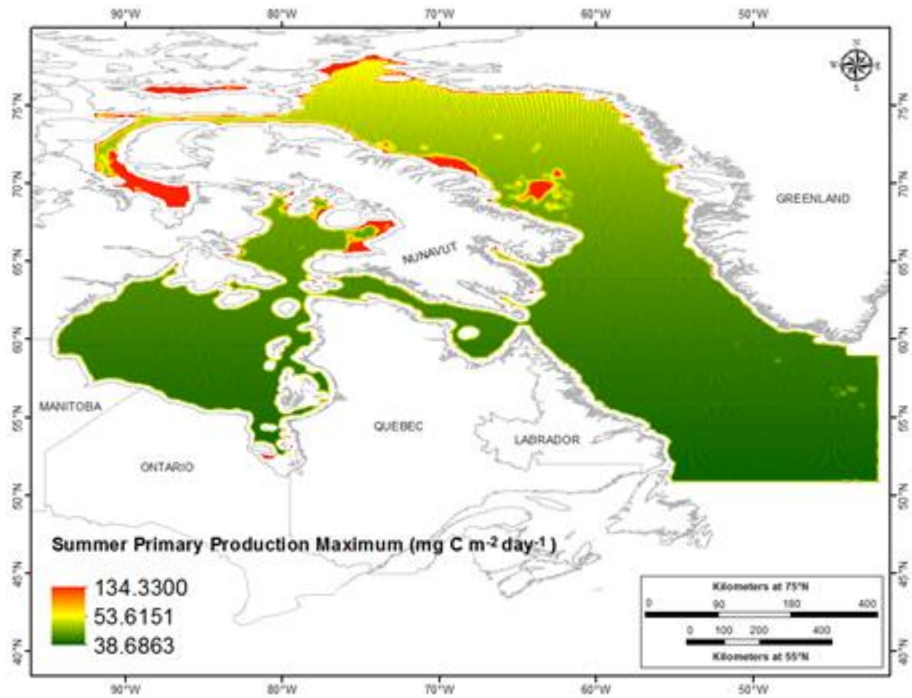


Figure 399. Prediction standard error surface of Summer Primary Production Maximum (mg C $m^{-2}$ $day^{-1}$).

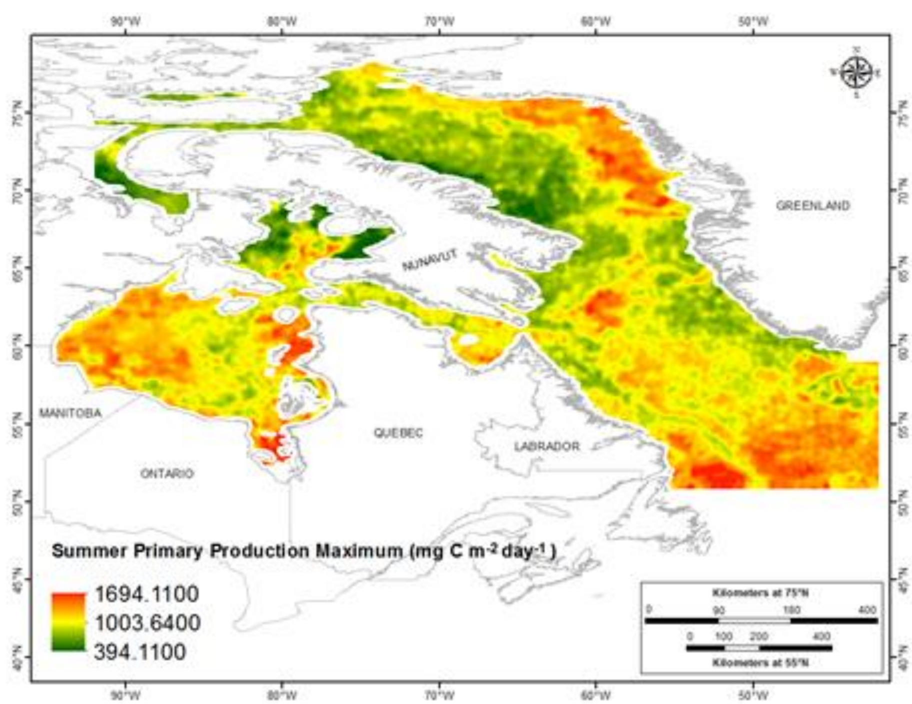


Figure 400. Interpolated prediction surface of Summer Primary Production Maximum (mg C $m^{-2}$ $day^{-1}$).

### Summer Primary Production Range

This variable displayed a right-skewed, leptokurtic distribution prior to interpolation (Table 161, Figure 401). The data were higher than predicted by a normal distribution at both tails (Figure 402). No data points fell below the reference line. These areas of over-prediction showed no strong spatial pattern over the region (Figure 402).

The semivariogram showed weak autocorrelation present in the data (Figure 403). The kriged model showed fair fit between measured and predicted values (Figure 403). Very good performance of the model was indicated by the cross-validation results (Table 162). The error map showed moderate error over much of the study extent, with patches of high error interspersed (Figure 404). The kriged surface is presented in Figure 405.

Table 161. Distributional properties of Summer Primary Production Range (mg C $m^{-2}$ $day^{-1}$).

| **Property** | **Value** |
|---|---:|
| Number of Observations | 33872 |
| Minimum | 16.860 |
| Maximum | 2523.500 |
| Mean | 660.650 |
| Median | 644.080 |
| Standard Deviation | 210.560 |
| Skewness | 0.475 |
| Kurtosis | 4.024 |

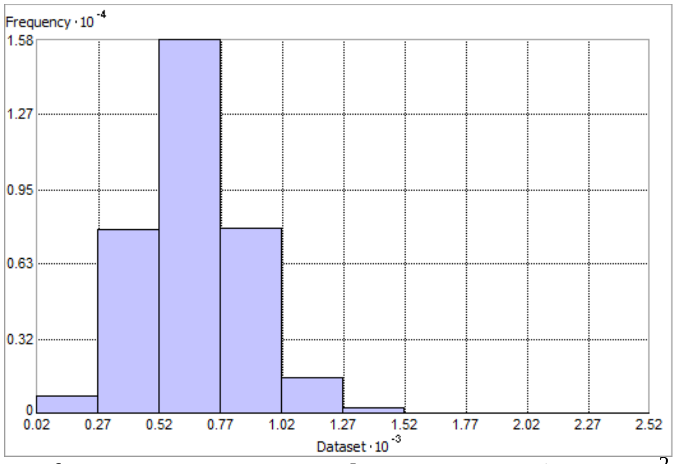

Figure 401. Distribution of Summer Primary Production Range (mg C $m^{-2}$ $day^{-1}$). Histogram was illustrated using 10 bins. X axis is shown at $10^{-3}$; Y axis is shown at $10^{-4}$.

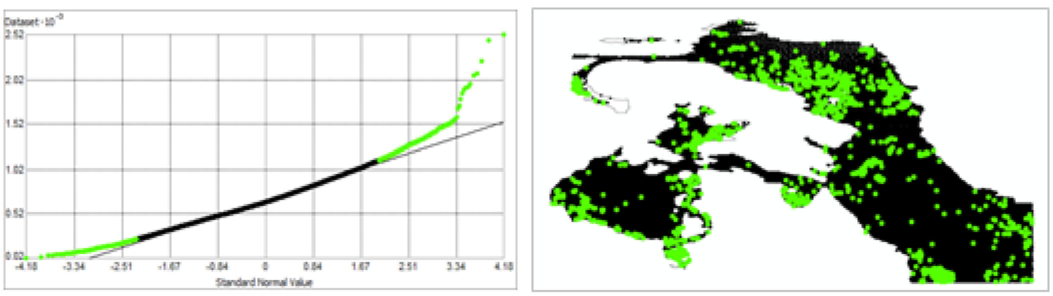

Figure 402. Normal Q-Q plot for data values of Summer Primary Production Range (mg C $m^{-2}$ $day^{-1}$). Points falling over the reference line are mapped; no points fall under the reference line.

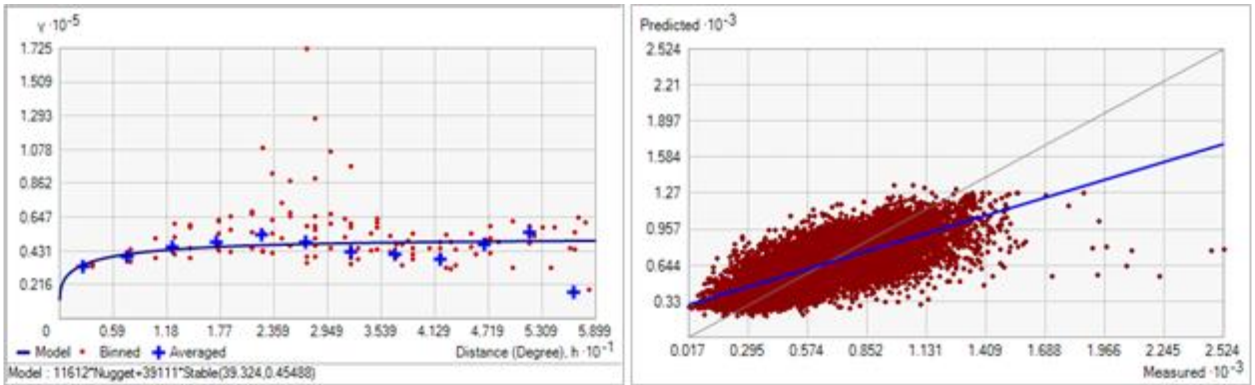

Figure 403. Left panel: Semivariogram of Summer Primary Production Range (mg C $m^{-2}$ $day^{-1}$). Binned values are shown as red dots; average points are shown as blue crosses; the model fit to the averaged values is shown as a blue line. Lag size: 4.195 degrees; number of lags: 12; Parameter: 0.455; Range: 39.324 degrees; Partial Sill: 39111.100 Right panel: Scatterplot of predicted values versus observed values for the model of Summer Primary Production Range (mg C $m^{-2}$ $day^{-1}$).

Table 162. Results of cross-validation of the kriged model for Summer Primary Production Range (mg C $m^{-2}$ $day^{-1}$).

| **Prediction Error** | **Value** |
|---|---:|
| Number of Observations | 33872 |
| Overall Mean Error | 0.025 |
| Root Mean Square Prediction Error | 145.592 |
| Standardized Mean | $1.128 \times 10^{-4}$ |
| Standardized Root Mean Square Prediction Error | 1.012 |
| Average Standard Error | 143.667 |

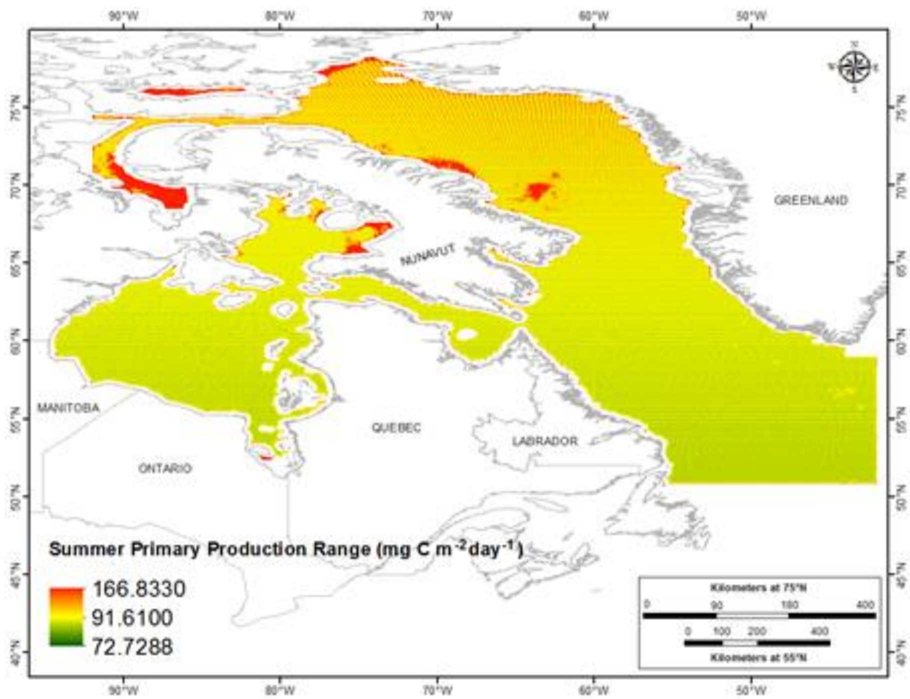


Figure 404. Prediction standard error surface of Summer Primary Production Range (mg C m$^{-2}$ day$^{-1}$).

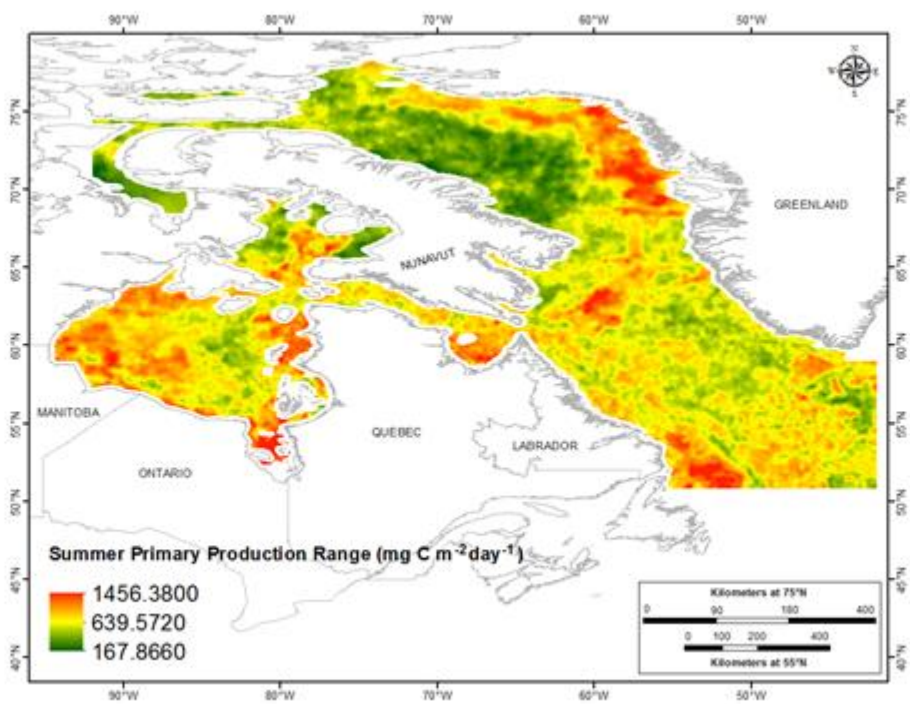


Figure 405. Interpolated prediction surface of Summer Primary Production Range (mg C m$^{-2}$ day$^{-1}$).

**Summer Primary Production Average Minimum**

This variable displayed a normal distribution prior to interpolation (Table 163, Figure 406). Few data points deviated from the 1:1 reference line in the Q-Q plot (Figure 407). These areas of over and under-prediction showed little spatial pattern over the region (Figure 407).

The semivariogram showed autocorrelation present in the data (Figure 408). The kriged model showed a good fit between measured and predicted values (Figure 408). Good performance of the model was indicated by the cross-validation results (Table 164). The error map showed moderate error in the northern portion of the study extent, with patches of high error interspersed (Figure 409). The kriged surface is presented in Figure 410.

Table 163. Distributional properties of Summer Primary Production Average Minimum (mg C $m^{-2}$ $day^{-1}$).

| **Property** | **Value** |
|---|---:|
| Number of Observations | 33872 |
| Minimum | 71.732 |
| Maximum | 933.640 |
| Mean | 502.040 |
| Median | 497.090 |
| Standard Deviation | 109.310 |
| Skewness | 0.227 |
| Kurtosis | 3.014 |

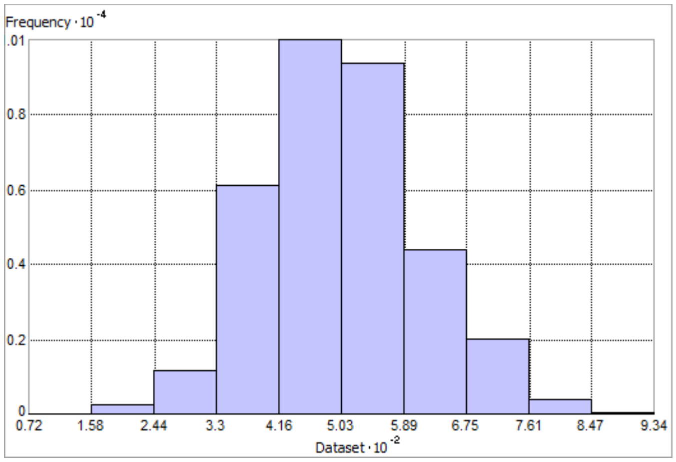


Figure 406. Distribution of Summer Primary Production Average Minimum (mg C $m^{-2}$ $day^{-1}$). Histogram was illustrated using 10 bins. X axis is shown at $10^{-2}$; Y axis is shown at $10^{-4}$.

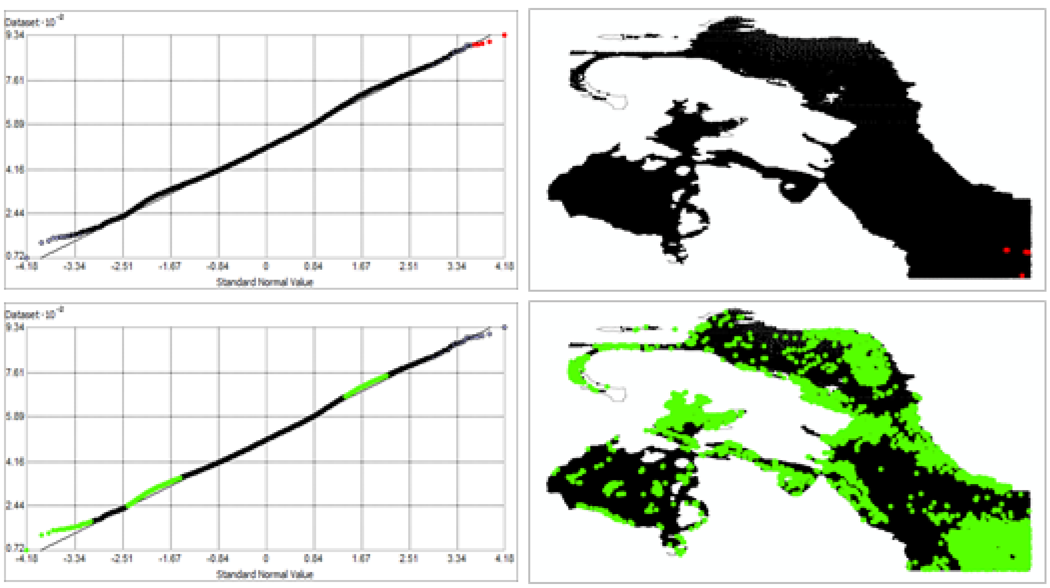

Figure 407. Normal Q-Q plot for data values of Summer Primary Production Average Minimum (mg C $m^{-2}$ $day^{-1}$). Points falling under (top right panel) and over (bottom right panel) the reference line are mapped.

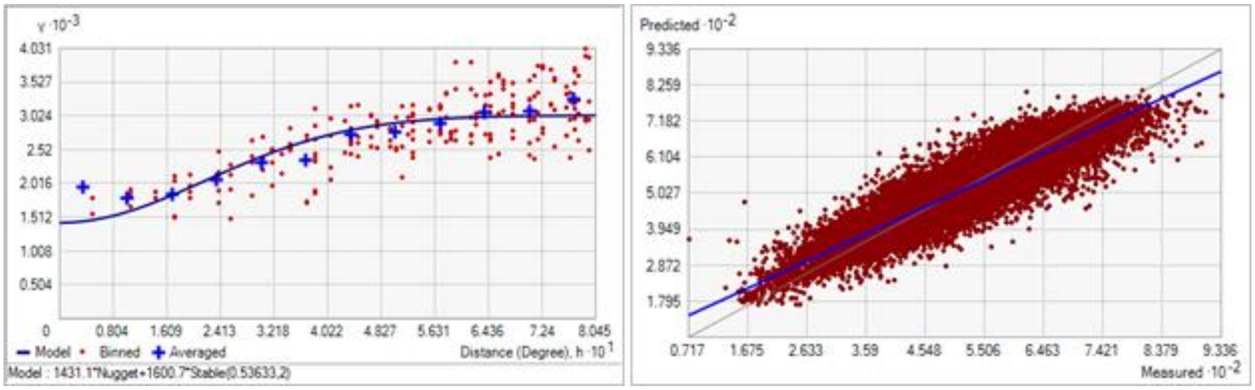


Figure 408. Left panel: Semivariogram of Summer Primary Production Average Minimum (mg C $m^{-2}$ $day^{-1}$). Binned values are shown as red dots; average points are shown as blue crosses; the model fit to the averaged values is shown as a blue line. Lag size: 0.067 degrees; number of lags: 12; Parameter: 2; Range: 0.536 degrees; Partial Sill: 1600.746 Right panel: Scatterplot of predicted values versus observed values for the model of Summer Primary Production Average Minimum (mg C $m^{-2}$ $day^{-1}$).

Table 164. Results of cross-validation of the kriged model for Summer Primary Production Average Minimum (mg C $m^{-2}$ $day^{-1}$).

| **Prediction Error** | **Value** |
|---|---:|
| Number of Observations | 33872 |
| Overall Mean Error | 0.058 |
| Root Mean Square Prediction Error | 44.955 |
| Standardized Mean | $1.068 \times 10^{-3}$ |
| Standardized Root Mean Square Prediction Error | 1.076 |
| Average Standard Error | 41.686 |

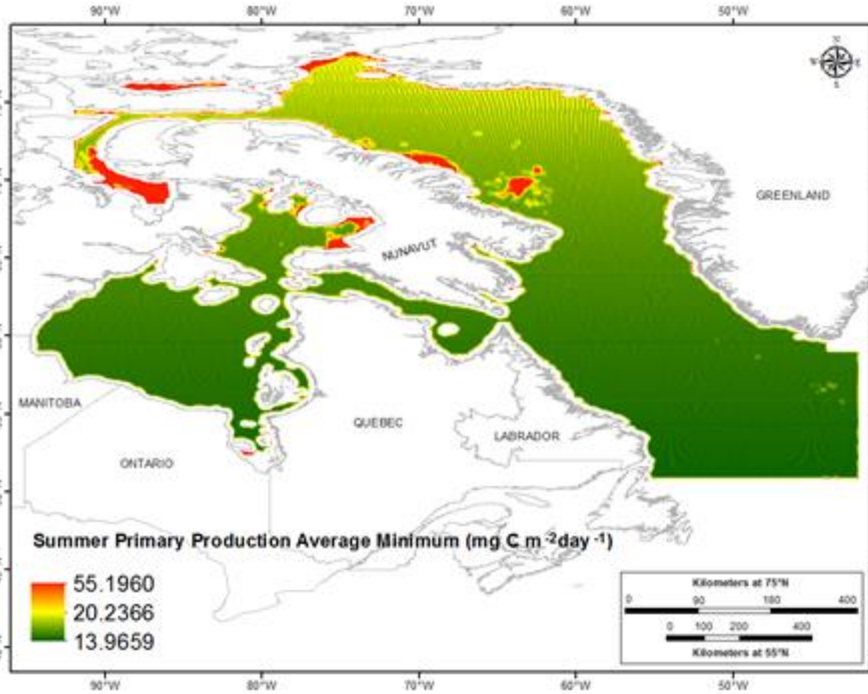


Figure 409. Prediction standard error surface of Summer Primary Production Average Minimum (mg C $m^{-2}$ $day^{-1}$).

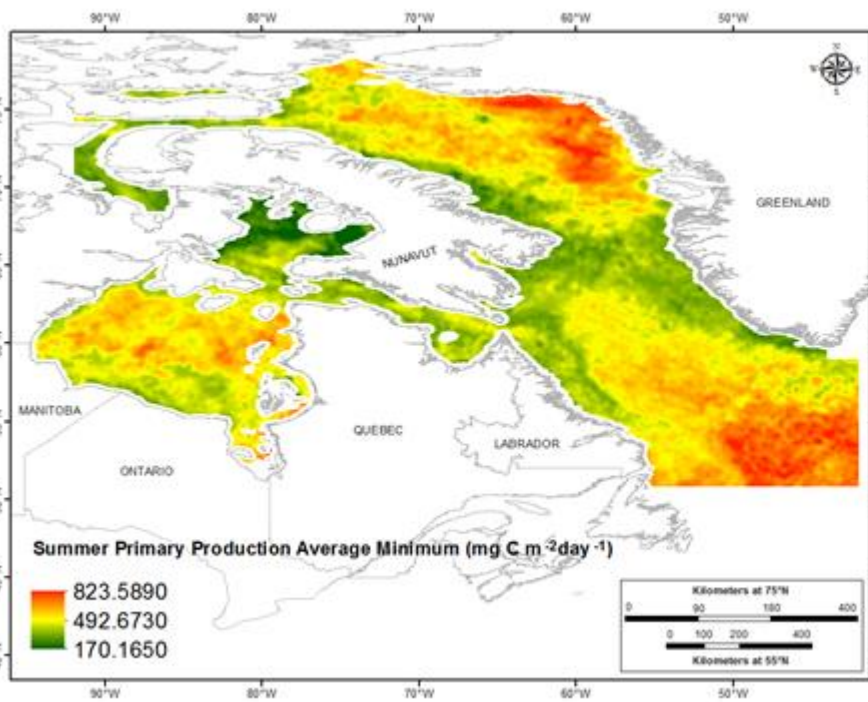


Figure 410. Interpolated prediction surface of Summer Primary Production Average Minimum (mg C $m^{-2}$ $day^{-1}$).

**Summer Primary Production Average Maximum**

This variable displayed a normal distribution prior to interpolation (Table 165, Figure 411). Few data points deviated from the 1:1 reference line in the Q-Q plot (Figure 412). These areas of over and under-prediction showed some spatial pattern over the region (Figure 412).

The semivariogram showed autocorrelation present in the data (Figure 413). The kriged model showed a good fit between measured and predicted values (Figure 413). Very good performance of the model was indicated by the cross-validation results (Table 166). The error map showed moderate error in the northern portion of the study extent, with patches of high error interspersed (Figure 414). The kriged surface is presented in Figure 415.

Table 165. Distributional properties of Summer Primary Production Average Maximum (mg C $m^{-2}$ $day^{-1}$).

| **Property** | **Value** |
|---|---:|
| Number of Observations | 33872 |
| Minimum | 114.300 |
| Maximum | 1458.900 |
| Mean | 817.940 |
| Median | 808.470 |
| Standard Deviation | 147.000 |
| Skewness | 0.256 |
| Kurtosis | 3.364 |

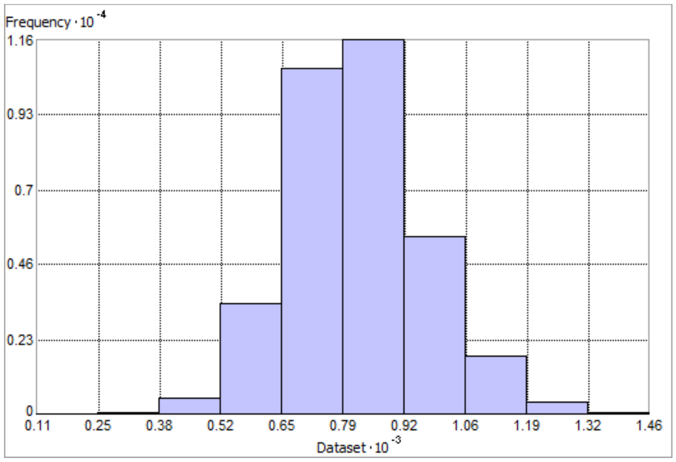


Figure 411. Distribution of Summer Primary Production Average Maximum (mg C $m^{-2}$ $day^{-1}$). Histogram was illustrated using 10 bins. X axis is shown at $10^{-3}$; Y axis is shown at $10^{-4}$.

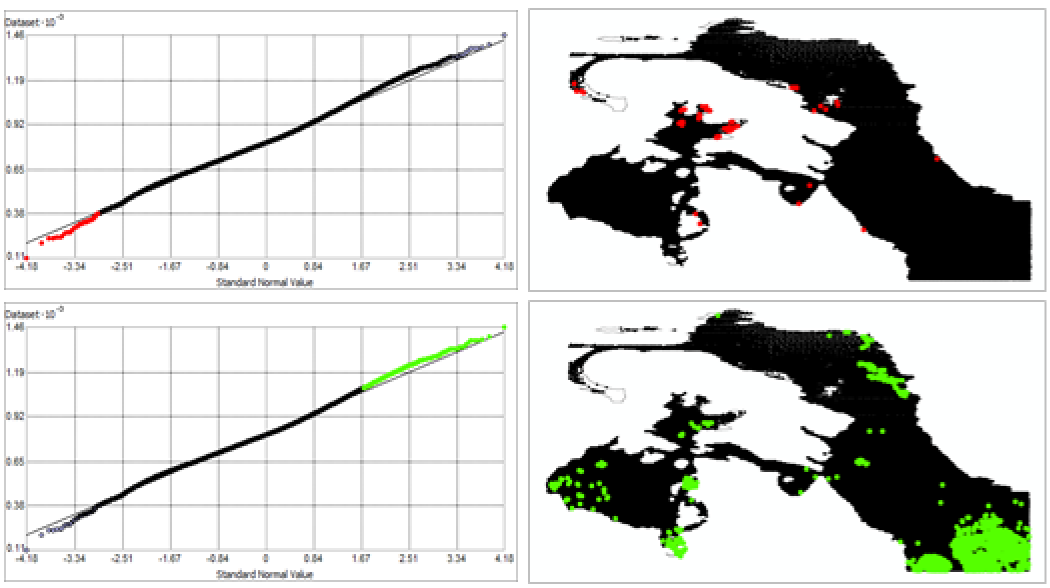

Figure 412. Normal Q-Q plot for data values of Summer Primary Production Average Maximum (mg C $m^{-2}$ $day^{-1}$). Points falling under (top right panel) and over (bottom right panel) the reference line are mapped.

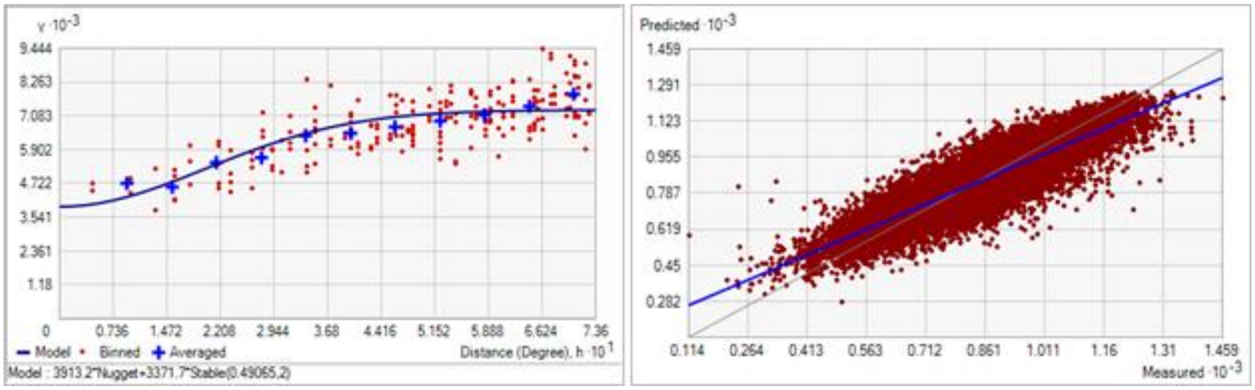


Figure 413. Left panel: Semivariogram of Summer Primary Production Average Maximum (mg C $m^{-2}$ $day^{-1}$). Binned values are shown as red dots; average points are shown as blue crosses; the model fit to the averaged values is shown as a blue line. Lag size: 0.061 degrees; number of lags: 12; Parameter: 2; Range: 0.491 degrees; Partial Sill: 3371.717 Right panel: Scatterplot of predicted values versus observed values for the model of Summer Primary Production Average Maximum (mg C $m^{-2}$ $day^{-1}$).

Table 166. Results of cross-validation of the kriged model for Summer Primary Production Average Maximum (mg C $m^{-2}$ $day^{-1}$).

| Prediction Error | Value |
|---|---|
| Number of Observations | 33872 |
| Overall Mean Error | 0.075 |
| Root Mean Square Prediction Error | 69.940 |
| Standardized Mean | $7.868 \times 10^{-4}$ |
| Standardized Root Mean Square Prediction Error | 1.011 |
| Average Standard Error | 68.955 |

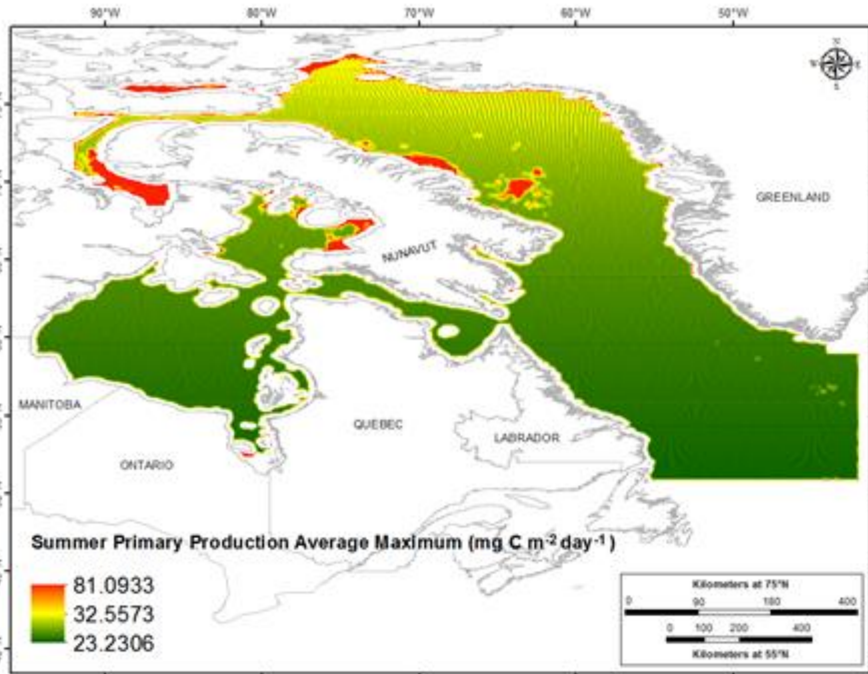


Figure 414. Prediction standard error surface of Summer Primary Production Average Maximum (mg C $m^{-2}$ $day^{-1}$).

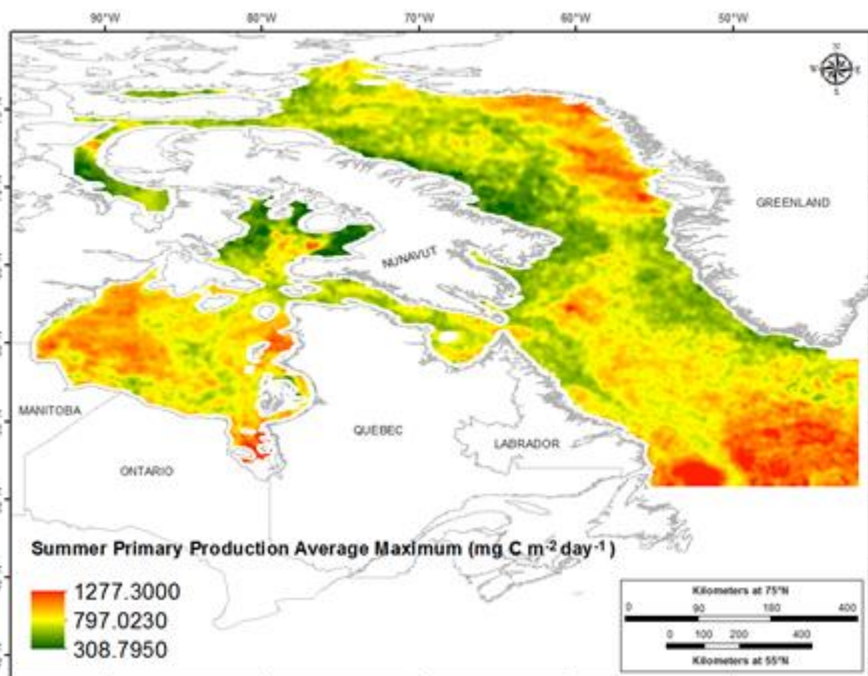


Figure 415. Interpolated prediction surface of Summer Primary Production Average Maximum (mg C $m^{-2}$ $day^{-1}$).

## Summer Primary Production Average Range

This variable displayed a slightly skewed and leptokurtic distribution prior to interpolation (Table 167, Figure 416). The data were higher than predicted by a normal distribution at both tails. No data points fell below the reference line. Mid-range values were well predicted (Figure 417). These areas of over-prediction showed no spatial pattern over the region (Figure 417).

The semivariogram showed weak autocorrelation present in the data (Figure 418). The kriged model showed fair fit between measured and predicted values (Figure 418). Very good performance of the model was indicated by the cross-validation results (Table 168). The error map showed moderate error in the northern portion of the study extent, with patches of high error interspersed (Figure 419). The kriged surface is presented in Figure 420.

Table 167. Distributional properties of Summer Primary Production Average Range (mg C $m^{-2}$ $day^{-1}$).

| Property | Value |
|---|---:|
| Number of Observations | 33872 |
| Minimum | 5.225 |
| Maximum | 924.880 |
| Mean | 315.900 |
| Median | 307.740 |
| Standard Deviation | 111.590 |
| Skewness | 0.464 |
| Kurtosis | 3.572 |

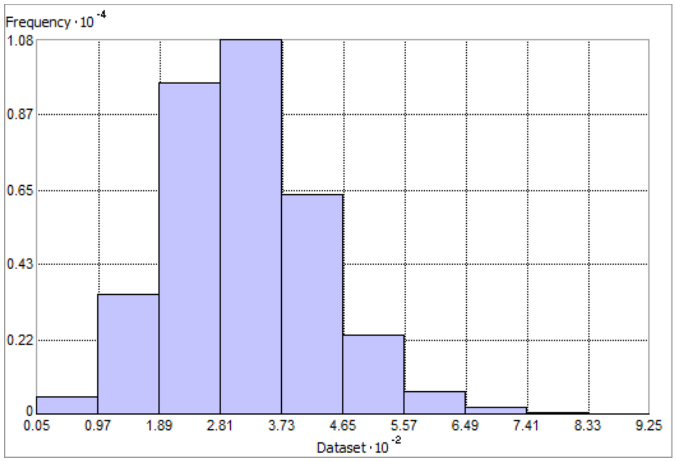


Figure 416. Distribution of Summer Primary Production Average Range (mg C $m^{-2}$ $day^{-1}$). Histogram was illustrated using 10 bins. X axis is shown at $10^{-2}$; Y axis is shown at $10^{-4}$.

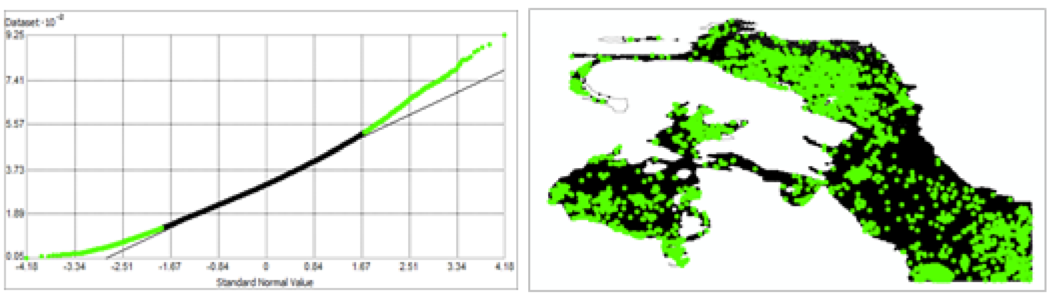

Figure 417. Normal Q-Q plot for data values of Summer Primary Production Average Range (mg C $m^{-2}$ $day^{-1}$). Points falling over the reference line are mapped; no points fall under the reference line.

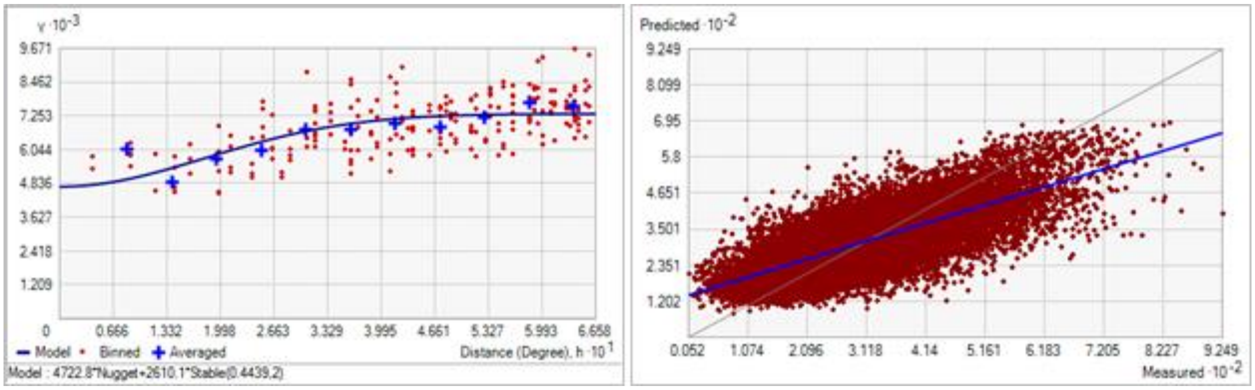


Figure 418. Left panel: Semivariogram of Summer Primary Production Average Range (mg C $m^{-2}$ $day^{-1}$). Binned values are shown as red dots; average points are shown as blue crosses; the model fit to the averaged values is shown as a blue line. Lag size: 0.055 degrees; number of lags: 12; Parameter: 1.597; Range: 0.444 degrees; Partial Sill: 2610.084. Right panel: Scatterplot of predicted values versus observed values for the model of Summer Primary Production Average Range (mg C $m^{-2}$ $day^{-1}$).

Table 168. Results of cross-validation of the kriged model for Summer Primary Production Average Range (mg C $m^{-2}$ $day^{-1}$).

| **Prediction Error** | **Value** |
|---|---|
| Number of Observations | 33872 |
| Overall Mean Error | 0.012 |
| Root Mean Square Prediction Error | 75.468 |
| Standardized Mean | $8.089 \times 10^{-5}$ |
| Standardized Root Mean Square Prediction Error | 1.002 |
| Average Standard Error | 75.213 |

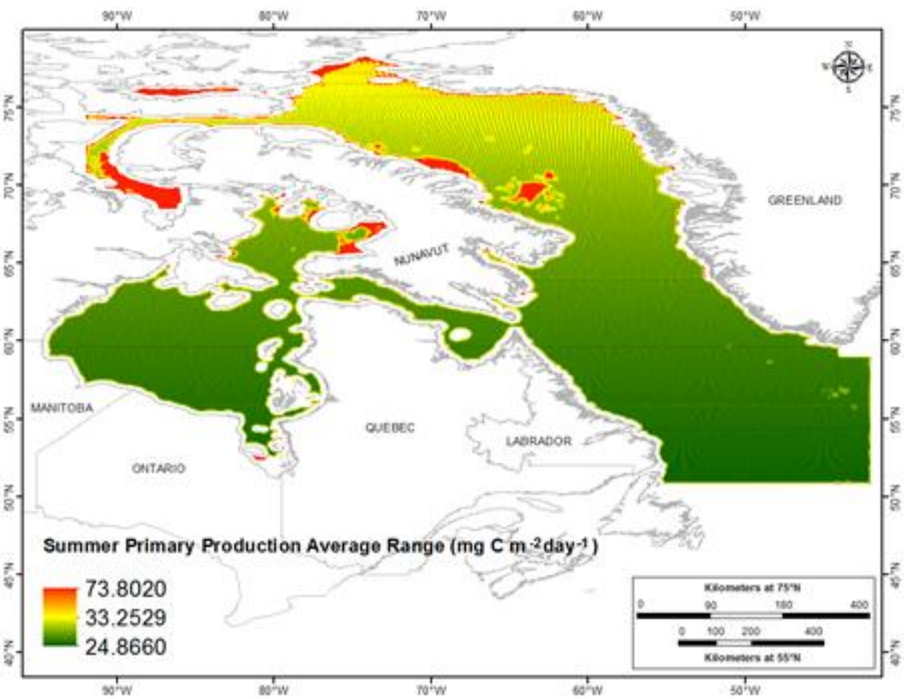


Figure 419. Prediction standard error surface of Summer Primary Production Average Range (mg C $m^{-2}$ $day^{-1}$).

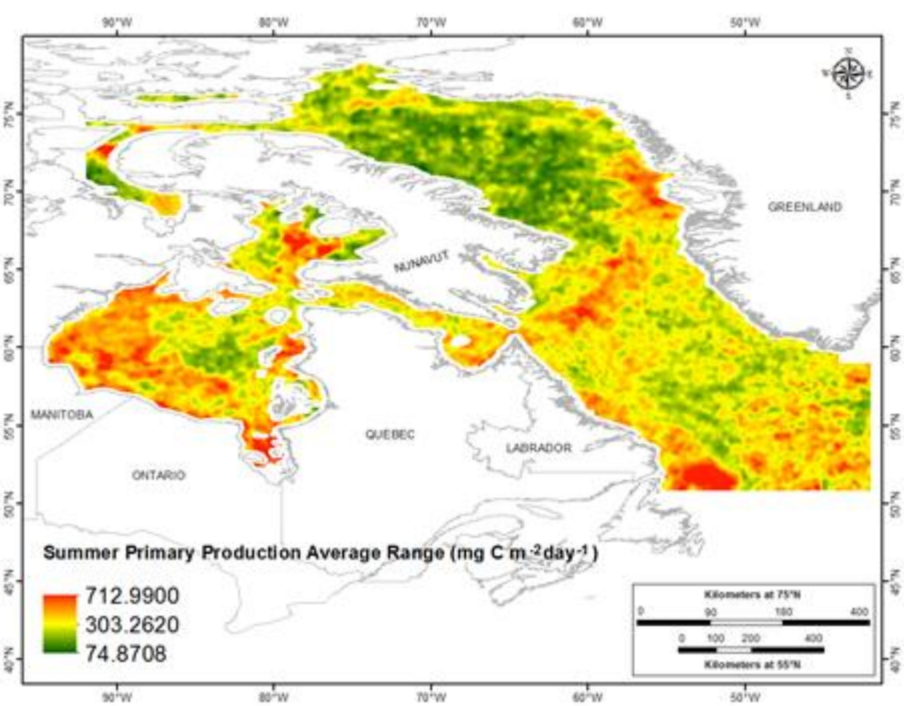


Figure 420. Interpolated prediction surface of Summer Primary Production Average Range (mg C $m^{-2}$ $day^{-1}$).

## Annual Primary Production Mean

This variable displayed a near-normal but slightly leptokurtic distribution prior to interpolation (Table 169, Figure 421). The data were higher than predicted by a normal distribution at the highest values and lower than predicted at the lowest values. Mid-range values were well predicted (Figure 422). These areas of over and under-prediction showed some spatial pattern over the region (Figure 422).

The semivariogram showed weak autocorrelation present in the data (Figure 423). The kriged model showed fair fit between measured and predicted values (Figure 423). Good performance of the model was indicated by the cross-validation results (Table 170). The error map showed moderate error in the northern portion of the study extent, with patches of high error interspersed (Figure 424). The kriged surface is presented in Figure 425.

Table 169. Distributional properties of Annual Primary Production Mean (mg C $m^{-2}$ $day^{-1}$).

| **Property** | **Value** |
|---|---:|
| Number of Observations | 33920 |
| Minimum | 128.970 |
| Maximum | 1039.300 |
| Mean | 636.700 |
| Median | 630.830 |
| Standard Deviation | 90.619 |
| Skewness | 0.022 |
| Kurtosis | 3.938 |

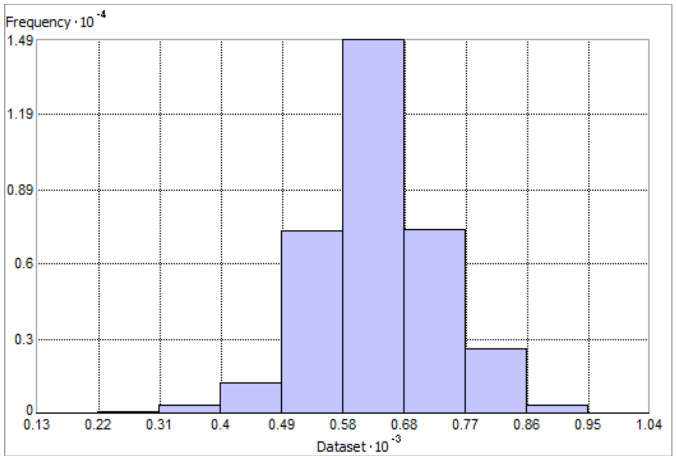


Figure 421. Distribution of Annual Primary Production Mean (mg C $m^{-2}$ $day^{-1}$). Histogram was illustrated using 10 bins. X axis is shown at $10^{-3}$; Y axis is shown at $10^{-4}$.

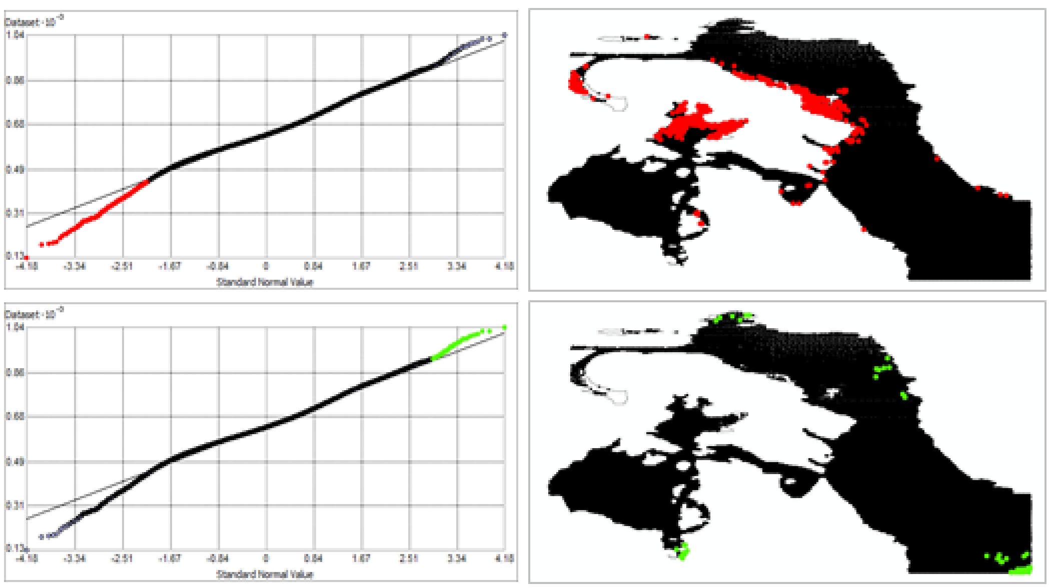

Figure 422. Normal Q-Q plot for data values of Annual Primary Production Mean (mg C $m^{-2}$ $day^{-1}$). Points falling under (top right panel) and over (bottom right panel) the reference line are mapped.

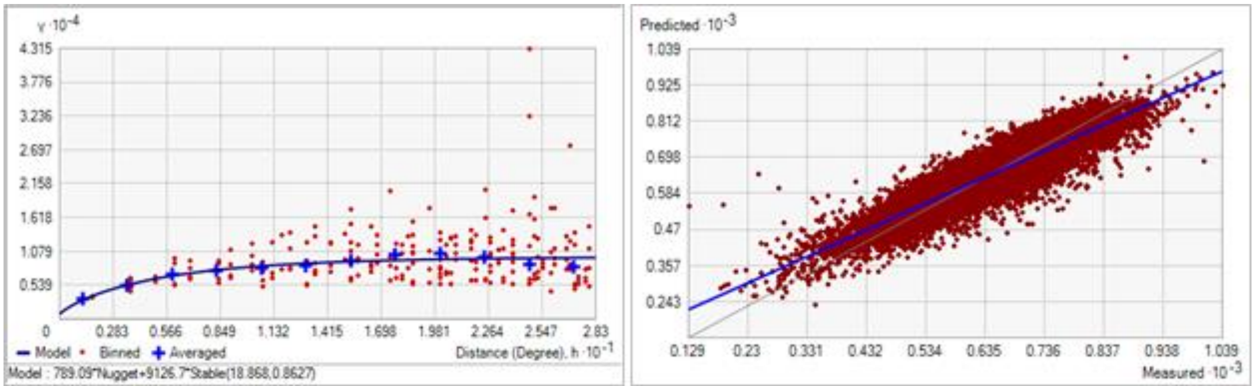

Figure 423. Left panel: Semivariogram of Annual Primary Production Mean (mg C $m^{-2}$ $day^{-1}$). Binned values are shown as red dots; average points are shown as blue crosses; the model fit to the averaged values is shown as a blue line. Lag size: 2.358 degrees; number of lags: 12; Parameter: 0.863; Range: 18.868 degrees; Partial Sill: 9126.734. Right panel: Scatterplot of predicted values versus observed values for the model of Annual Primary Production Mean (mg C $m^{-2}$ $day^{-1}$).

Table 170. Results of cross-validation of the kriged model for Annual Primary Production Mean (mg C $m^{-2}$ $day^{-1}$).

| **Prediction Error** | **Value** |
|---|---|
| Number of Observations | 33920 |
| Overall Mean Error | 0.025 |
| Root Mean Square Prediction Error | 38.029 |
| Standardized Mean | $2.632 \times 10^{-4}$ |
| Standardized Root Mean Square Prediction Error | 1.091 |
| Average Standard Error | 34.606 |

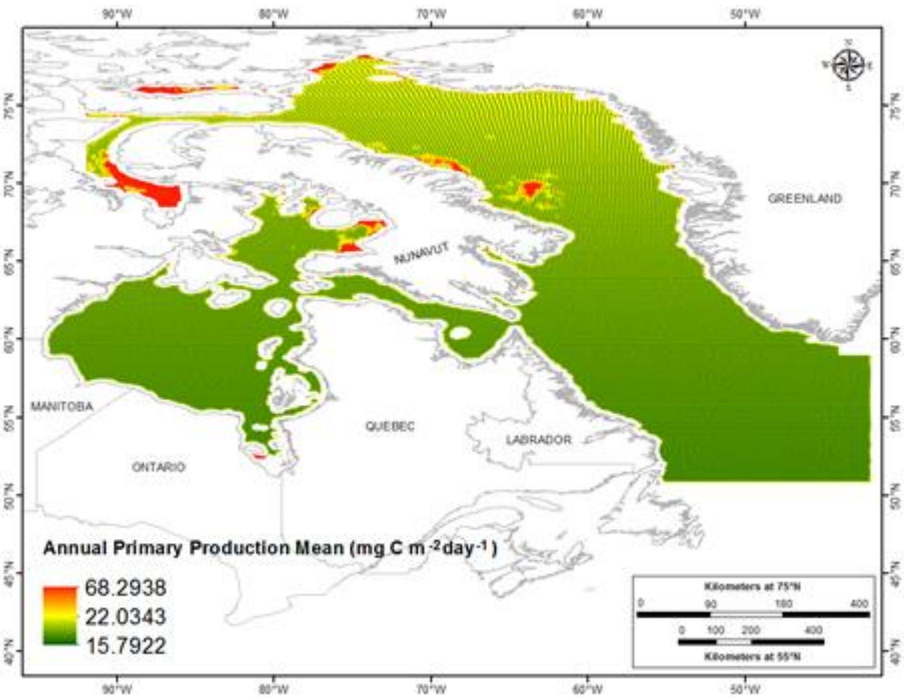


Figure 424. Prediction standard error surface of Annual Primary Production Mean (mg C $m^{-2}$ $day^{-1}$).

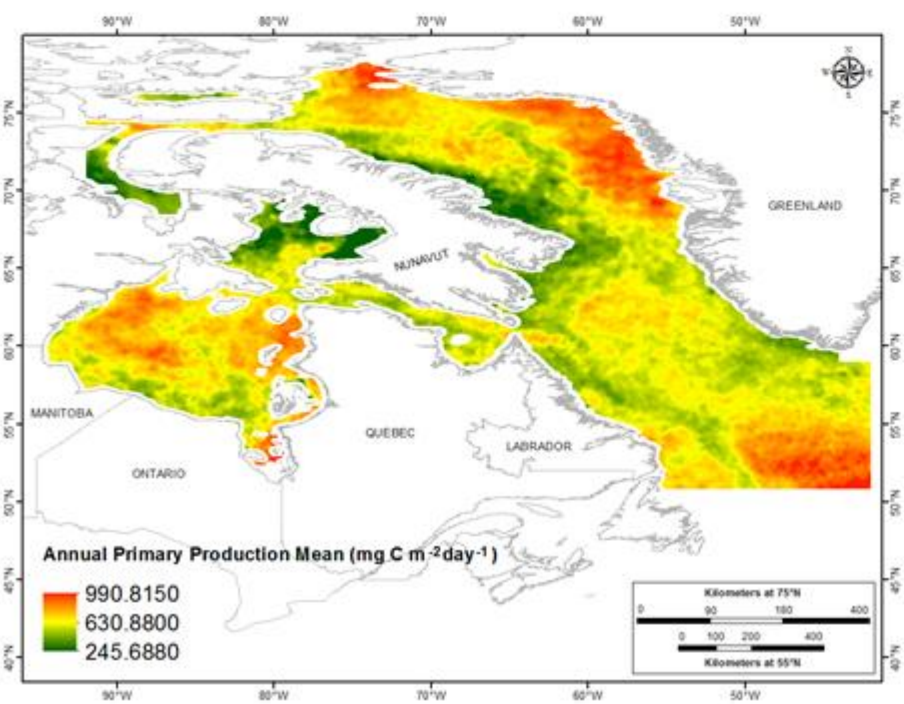


Figure 425. Interpolated prediction surface of Annual Primary Production Mean (mg C $m^{-2}$ $day^{-1}$).

## Annual Primary Production Minimum

This variable displayed a slightly skewed distribution prior to interpolation (Table 171, Figure 426). The data were higher than predicted by a normal distribution at both tails and slightly lower than predicted at mid-values (Figure 427). These areas of over and under-prediction showed little spatial pattern over the region (Figure 427).

The semivariogram showed autocorrelation present in the data (Figure 428). The kriged model showed good fit between measured and predicted values (Figure 428). Good performance of the model was indicated by the cross-validation results (Table 172). The error map showed moderate error in the northern portion of the study extent, with patches of high error interspersed (Figure 429). The kriged surface is presented in Figure 430.

Table 171. Distributional properties of Annual Primary Production Minimum (mg C $m^{-2}$ $day^{-1}$).

| Property | Value |
|---|---:|
| Number of Observations | 33920 |
| Minimum | 18.220 |
| Maximum | 774.380 |
| Mean | 259.110 |
| Median | 234.340 |
| Standard Deviation | 99.234 |
| Skewness | 0.839 |
| Kurtosis | 3.209 |

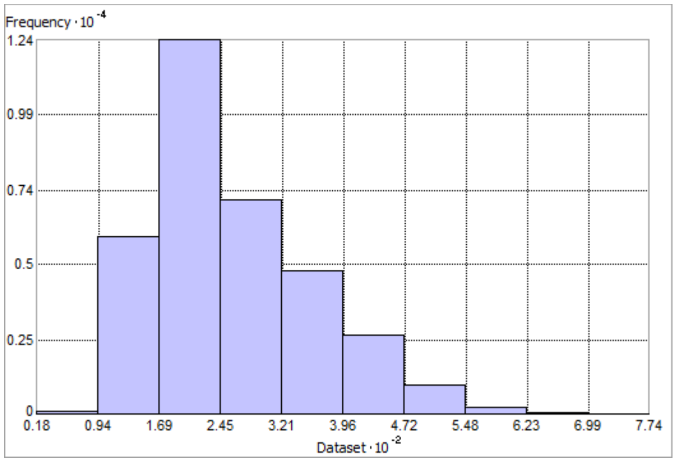

Figure 426. Distribution of Annual Primary Production Minimum (mg C $m^{-2}$ $day^{-1}$). Histogram was illustrated using 10 bins. X axis is shown at $10^{-2}$; Y axis is shown at $10^{-4}$.

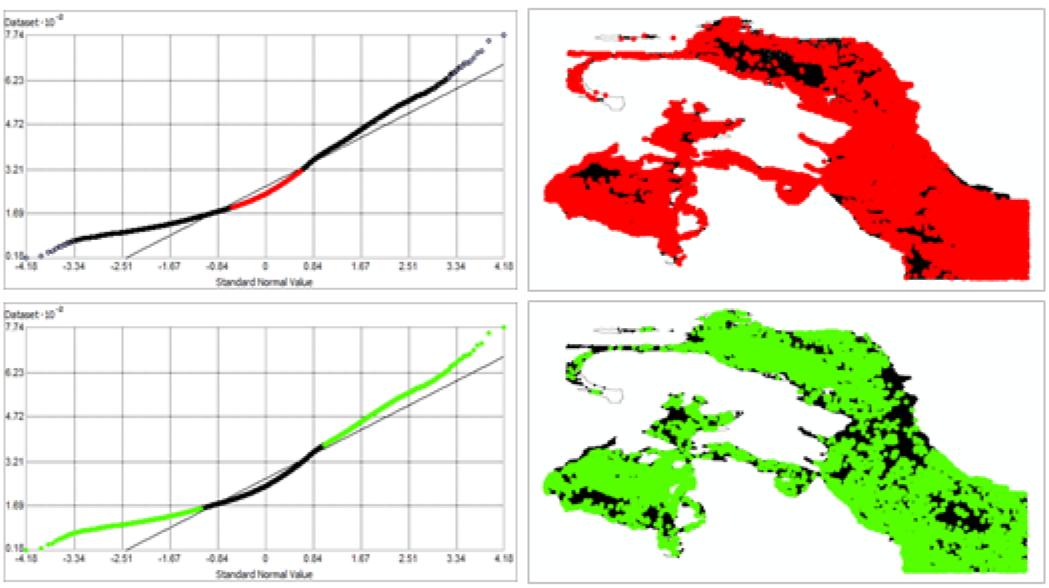

Figure 427. Normal Q-Q plot for data values of Annual Primary Production Minimum (mg C $m^{-2}$ $day^{-1}$). Points falling under (top right panel) and over (bottom right panel) the reference line are mapped.

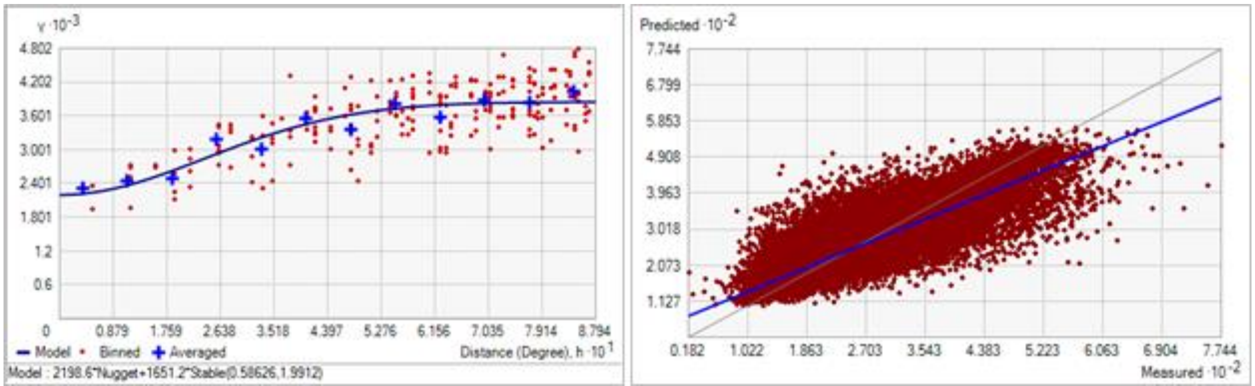

Figure 428. Left panel: Semivariogram of Annual Primary Production Minimum (mg C $m^{-2}$ $day^{-1}$). Binned values are shown as red dots; average points are shown as blue crosses; the model fit to the averaged values is shown as a blue line. Lag size: 2.358 degrees; number of lags: 12; Parameter: 0.863; Range: 18.868 degrees; Partial Sill: 9126.734. Right panel: Scatterplot of predicted values versus observed values for the model of Annual Primary Production Minimum (mg C $m^{-2}$ $day^{-1}$).

Table 172. Results of cross-validation of the kriged model for Annual Primary Production Minimum (mg C $m^{-2}$ $day^{-1}$).

| **Prediction Error** | **Value** |
|---|---|
| Number of Observations | 33920 |
| Overall Mean Error | 0.027 |
| Root Mean Square Prediction Error | 53.069 |
| Standardized Mean | $3.637 \times 10^{-4}$ |
| Standardized Root Mean Square Prediction Error | 1.048 |
| Average Standard Error | 50.520 |

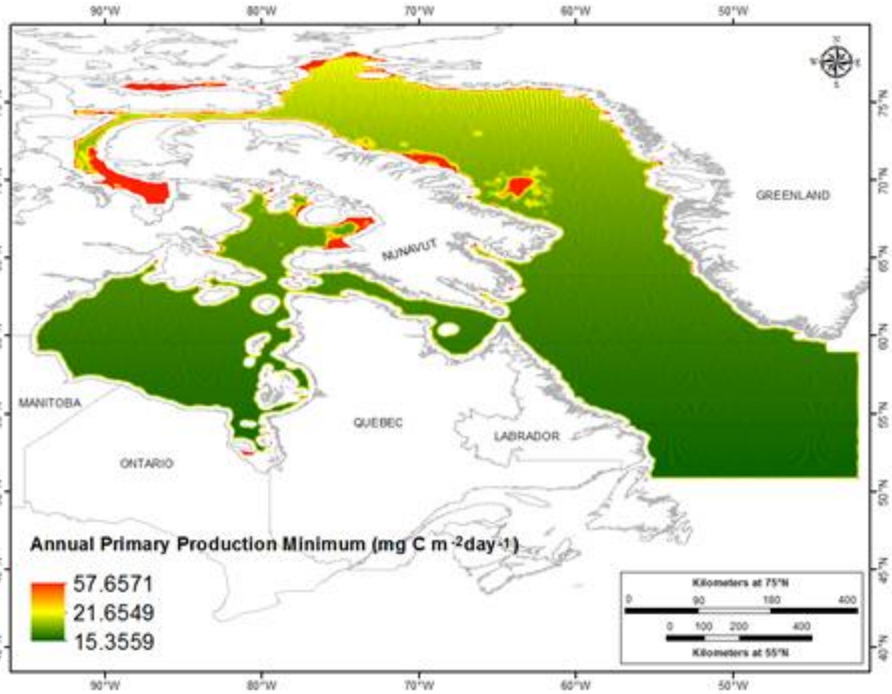


Figure 429. Prediction standard error surface of Annual Primary Production Minimum (mg C m$^{-2}$ day$^{-1}$).

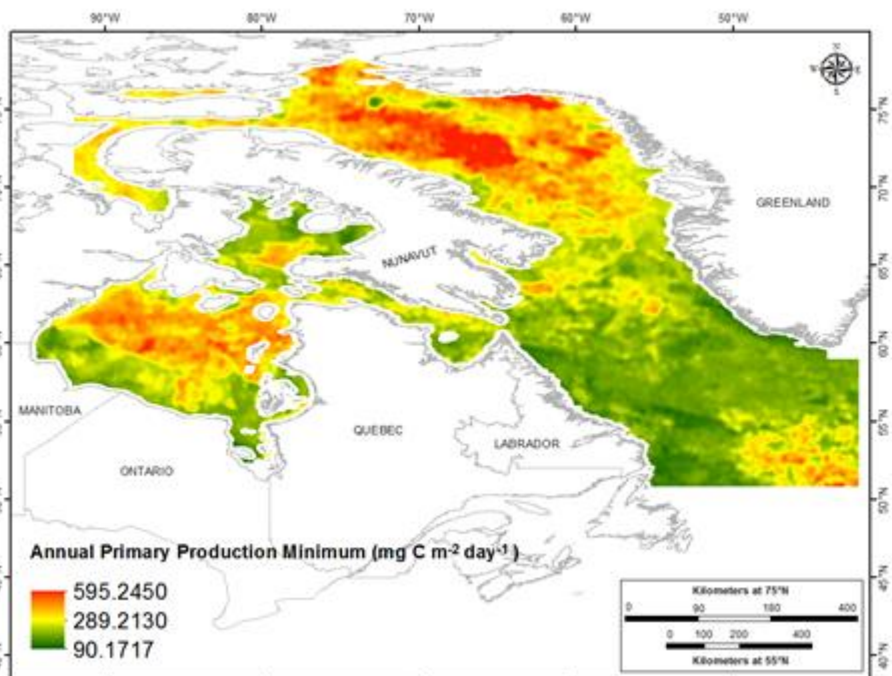


Figure 430. Interpolated prediction surface of Annual Primary Production Minimum (mg C m$^{-2}$ day$^{-1}$).

## Annual Primary Production Maximum

This variable displayed a right-skewed, leptokurtic distribution prior to interpolation (Table 173, Figure 431). The data were higher than predicted by a normal distribution at both tails, while mid-values followed the reference line (Figure 432). These areas of over-prediction showed little spatial pattern over the region (Figure 432).

The semivariogram showed very weak autocorrelation present in the data (Figure 433). The kriged model showed fair fit between measured and predicted values (Figure 433). Very good performance of the model was indicated by the cross-validation results (Table 174). The error map showed moderate error in the northern portion of the study extent, with patches of high error interspersed (Figure 434). The kriged surface is presented in Figure 435.

Table 173. Distributional properties of Annual Primary Production Maximum (mg C $m^{-2}$ $day^{-1}$).

| **Property** | **Value** |
|---|---:|
| Number of Observations | 33920 |
| Minimum | 279.220 |
| Maximum | 3378.800 |
| Mean | 1129.700 |
| Median | 1114.900 |
| Standard Deviation | 242.570 |
| Skewness | 0.566 |
| Kurtosis | 5.232 |

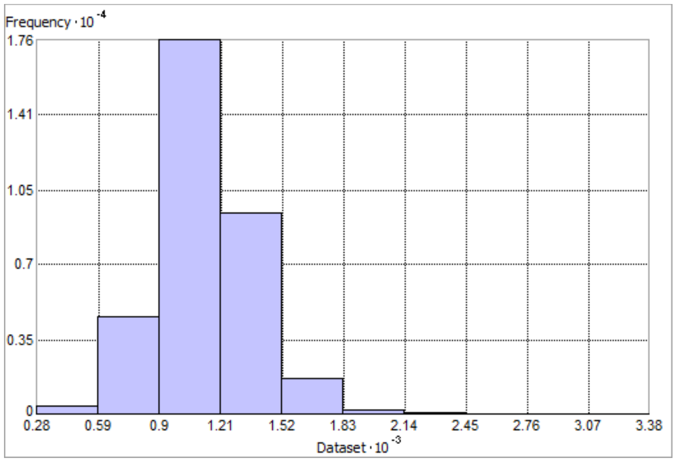


Figure 431. Distribution of Annual Primary Production Maximum (mg C m$^{-2}$ day$^{-1}$). Histogram was illustrated using 10 bins. X axis is shown at $10^{-3}$; Y axis is shown at $10^{-4}$.

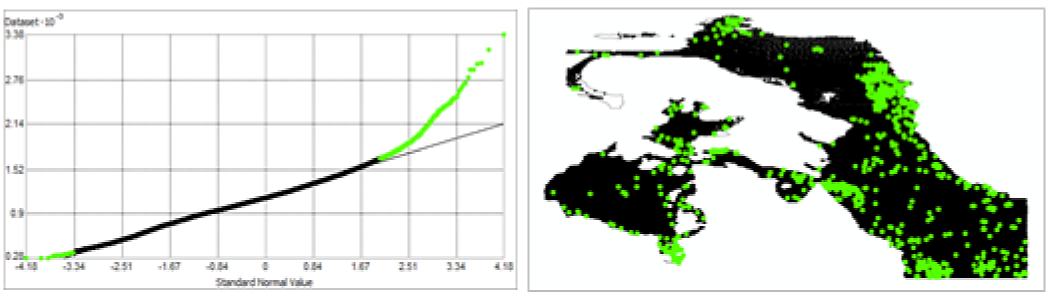

Figure 432. Normal Q-Q plot for data values of Annual Primary Production Maximum (mg C m$^{-2}$ day$^{-1}$). Points falling over the reference line are mapped; no points fall under the reference line.

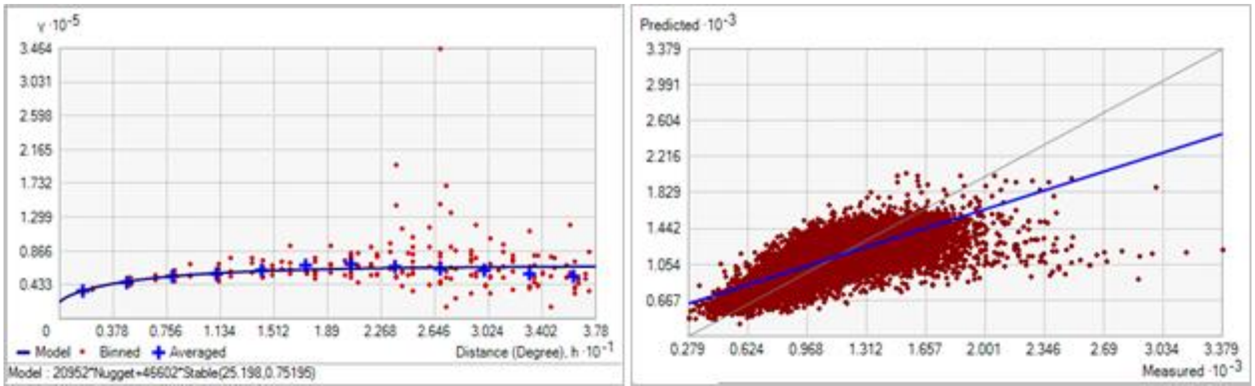

Figure 433. Left panel: Semivariogram of Annual Primary Production Maximum (mg C $m^{-2}$ $day^{-1}$). Binned values are shown as red dots; average points are shown as blue crosses; the model fit to the averaged values is shown as a blue line. Lag size: 3.150 degrees; number of lags: 12; Parameter: 0.752; Range: 25.198 degrees; Partial Sill: 46602.110. Right panel: Scatterplot of predicted values versus observed values for the model of Annual Primary Production Maximum (mg C $m^{-2}$ $day^{-1}$).

Table 174. Results of cross-validation of the kriged model for Annual Primary Production Maximum (mg C $m^{-2}$ $day^{-1}$).

| **Prediction Error** | **Value** |
|---|---:|
| Number of Observations | 33920 |
| Overall Mean Error | -0.043 |
| Root Mean Square Prediction Error | 166.018 |
| Standardized Mean | $-3.306 \times 10^{-4}$ |
| Standardized Root Mean Square Prediction Error | 1.049 |
| Average Standard Error | 158.026 |

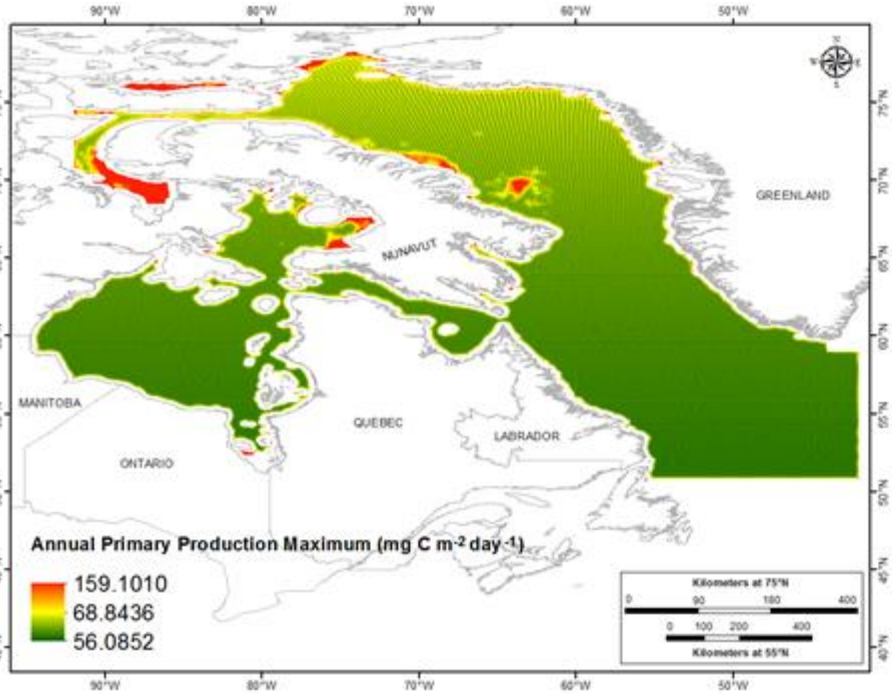


Figure 434. Prediction standard error surface of Annual Primary Production Maximum (mg C $m^{-2}$ $day^{-1}$).

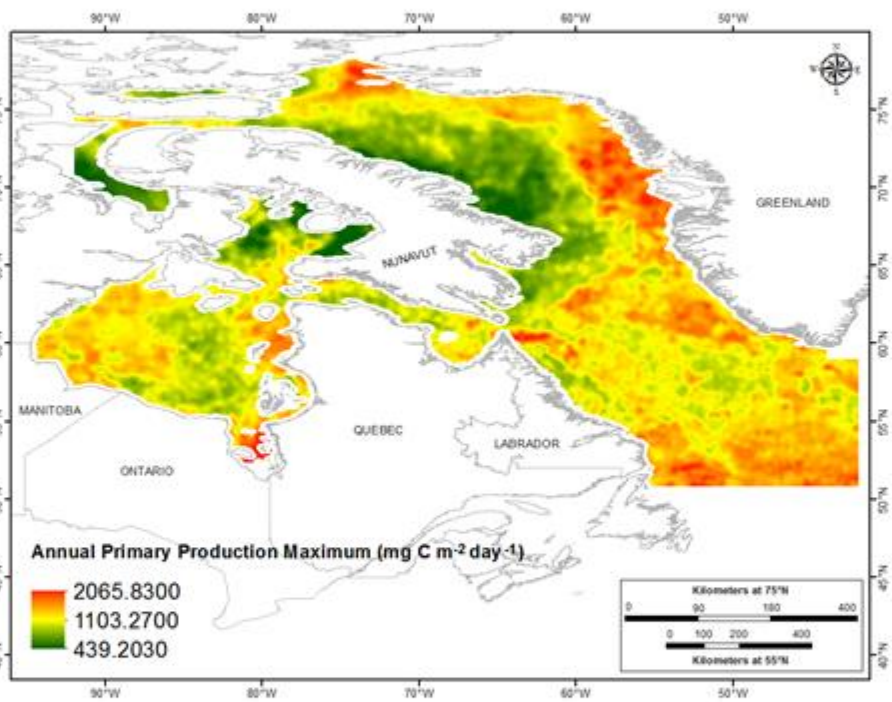


Figure 435. Interpolated prediction surface of Annual Primary Production Maximum (mg C $m^{-2}$ $day^{-1}$).

## Annual Primary Production Range

This variable displayed a right-skewed, leptokurtic distribution prior to interpolation (Table 175, Figure 436). The data were higher than predicted by a normal distribution at both tails, while mid-values followed the reference line (Figure 437). These areas of over-prediction showed little spatial pattern over the region (Figure 437).

The semivariogram showed autocorrelation present in the data (Figure 438). The kriged model showed fair fit between measured and predicted values (Figure 438). Good performance of the model was indicated by the cross-validation results (Table 176). The error map showed moderate error in the northern portion of the study extent, with patches of high error interspersed (Figure 439). The kriged surface is presented in Figure 440.

Table 175. Distributional properties of Annual Primary Production Range (mg C $m^{-2}$ $day^{-1}$).

| Property | Value |
|---|---:|
| Number of Observations | 33920 |
| Minimum | 30.100 |
| Maximum | 3110.100 |
| Mean | 870.600 |
| Median | 868.660 |
| Standard Deviation | 271.540 |
| Skewness | 0.289 |
| Kurtosis | 4.336 |

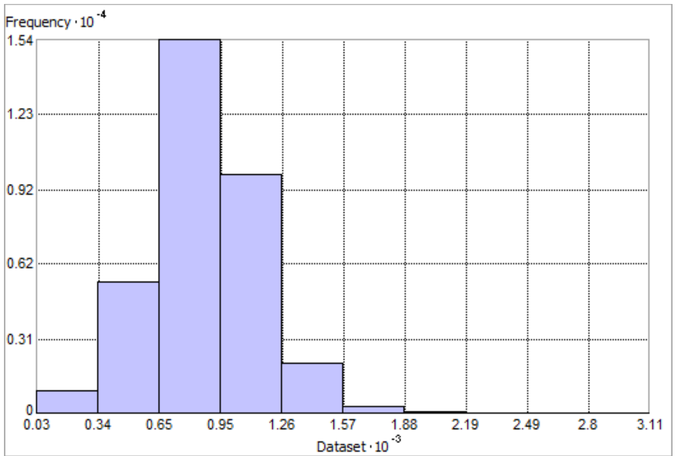


Figure 436. Distribution of Annual Primary Production Range (mg C m$^{-2}$ day$^{-1}$). Histogram was illustrated using 10 bins. X axis is shown at $10^{-3}$; Y axis is shown at $10^{-4}$.

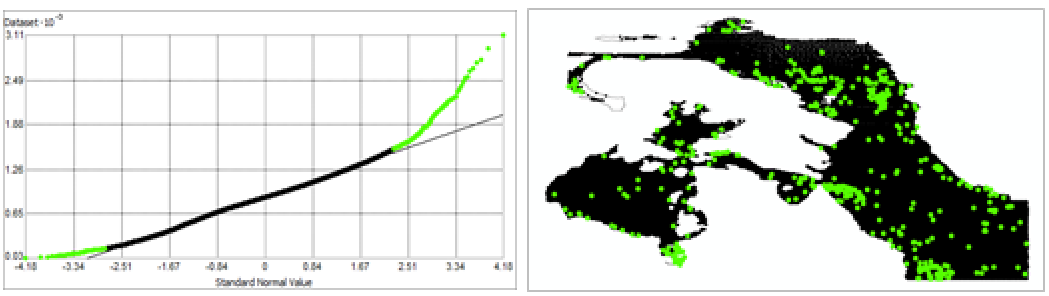

Figure 437. Normal Q-Q plot for data values of Annual Primary Production Range (mg C m$^{-2}$ day$^{-1}$). Points falling over the reference line are mapped; no points fall under the reference line.

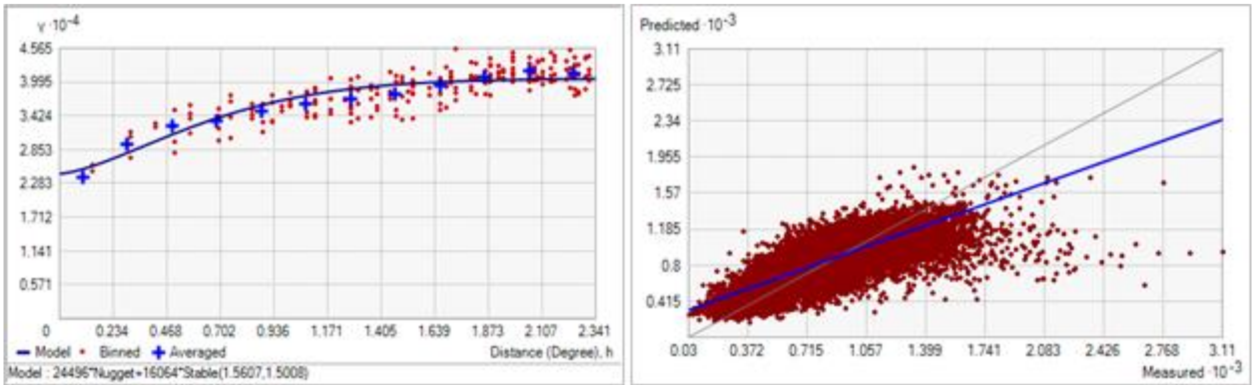


Figure 438. Left panel: Semivariogram of Annual Primary Production Range (mg C $m^{-2}$ $day^{-1}$). Binned values are shown as red dots; average points are shown as blue crosses; the model fit to the averaged values is shown as a blue line. Lag size: 0.195 degrees; number of lags: 12; Parameter: 1.501; Range: 1.561 degrees; Partial Sill: 16063.880. Right panel: Scatterplot of predicted values versus observed values for the model of Annual Primary Production Range (mg C $m^{-2}$ $day^{-1}$).

Table 176. Results of cross-validation of the kriged model for Annual Primary Production Range (mg C $m^{-2}$ $day^{-1}$).

| **Prediction Error** | **Value** |
|---|---:|
| Number of Observations | 33920 |
| Overall Mean Error | -0.038 |
| Root Mean Square Prediction Error | 174.505 |
| Standardized Mean | $-2.486 \times 10^{-4}$ |
| Standardized Root Mean Square Prediction Error | 1.061 |
| Average Standard Error | 164.330 |

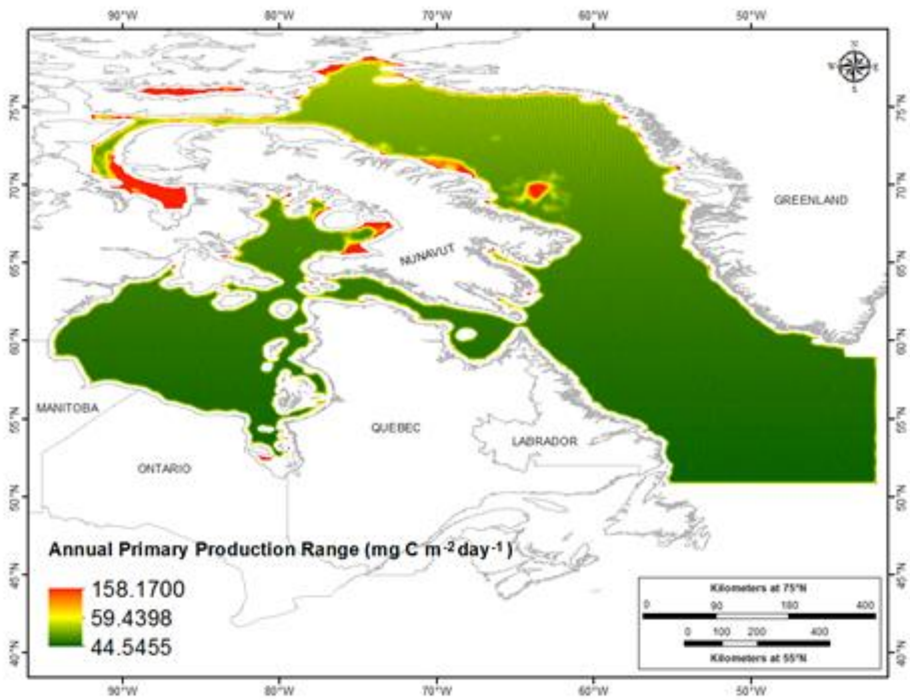


Figure 439. Prediction standard error surface of Annual Primary Production Range (mg C $m^{-2}$ $day^{-1}$).

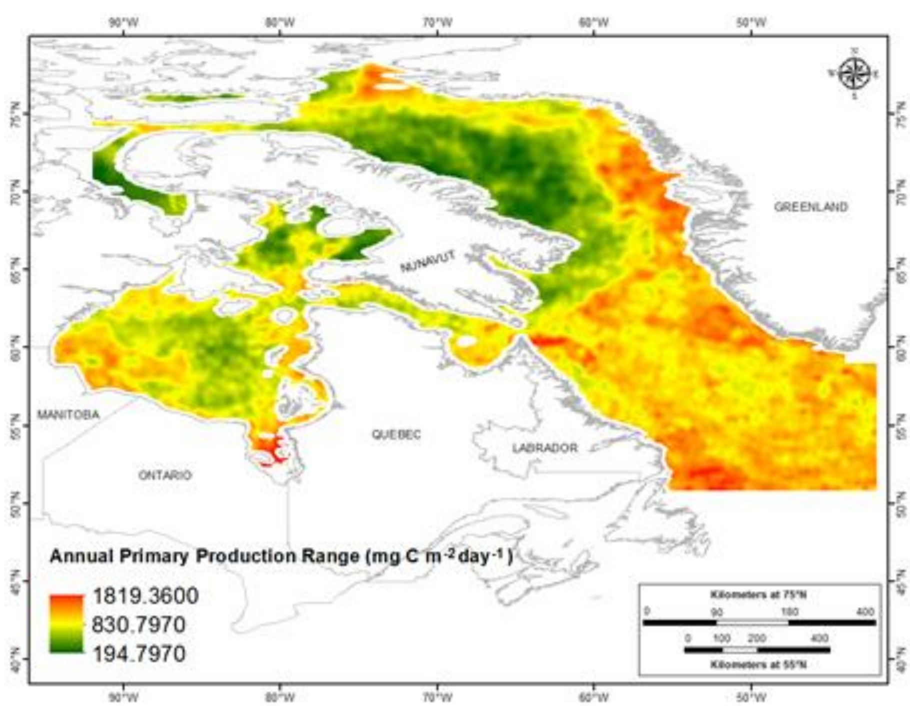


Figure 440. Interpolated prediction surface of Annual Primary Production Range (mg C $m^{-2}$ $day^{-1}$).

## Annual Primary Production Average Minimum

This variable displayed a near-normal distribution prior to interpolation (Table 177, Figure 441). The data were higher than predicted by a normal distribution at the lowest values and lower than predicted at the highest values, while mid-values followed the reference line (Figure 442). These areas of under and over-prediction showed spatial pattern over the region (Figure 442).

The semivariogram showed autocorrelation present in the data (Figure 443). The kriged model showed good fit between measured and predicted values (Figure 443). Very good performance of the model was indicated by the cross-validation results (Table 178). The error map showed moderate error in the northern portion of the study extent, with patches of high error interspersed (Figure 444). The kriged surface is presented in Figure 445.

Table 177. Distributional properties of Annual Primary Production Average Minimum (mg C $m^{-2}$ $day^{-1}$).

| **Property** | **Value** |
|---|---:|
| Number of Observations | 33920 |
| Minimum | 40.032 |
| Maximum | 795.840 |
| Mean | 400.200 |
| Median | 389.85 |
| Standard Deviation | 104.860 |
| Skewness | 0.339 |
| Kurtosis | 2.595 |

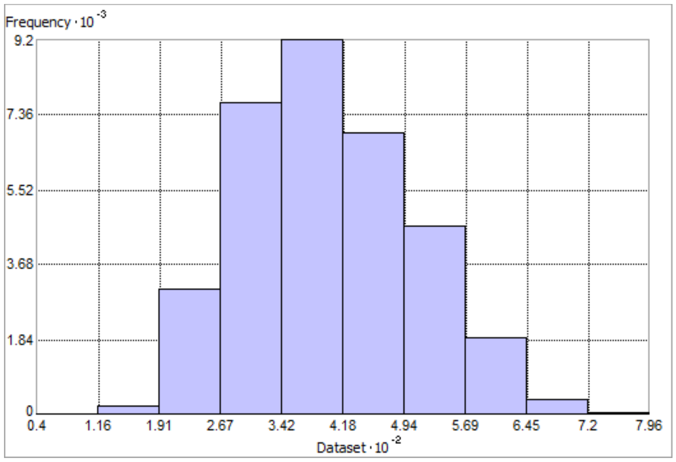


Figure 441. Distribution of Annual Primary Production Average Minimum (mg C $m^{-2}$ $day^{-1}$). Histogram was illustrated using 10 bins. X axis is shown at $10^{-2}$; Y axis is shown at $10^{-3}$.

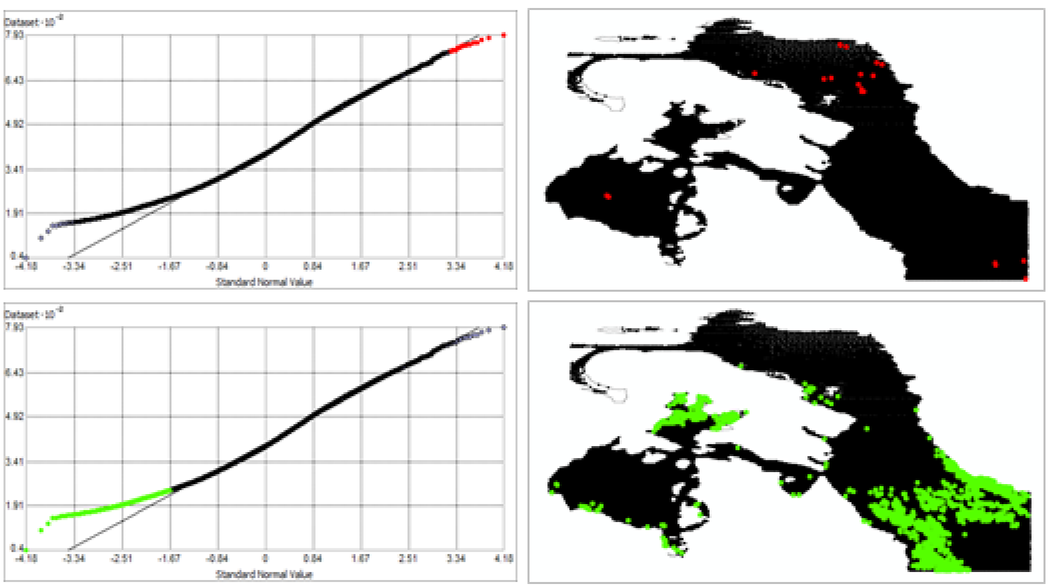


Figure 442. Normal Q-Q plot for data values of Annual Primary Production Average Minimum (mg C $m^{-2}$ $day^{-1}$). Points falling under (top right panel) and over (bottom right panel) the reference line are mapped.

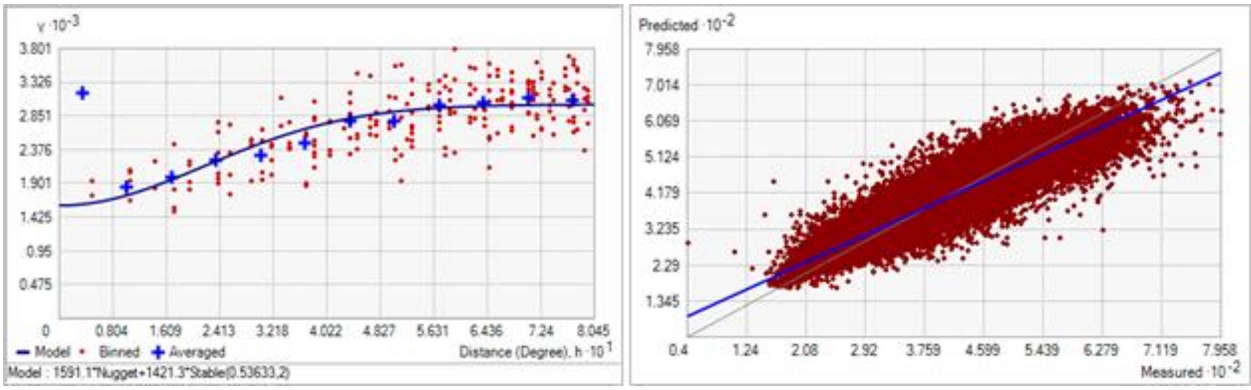


Figure 443. Left panel: Semivariogram of Annual Primary Production Average Minimum (mg C m$^{-2}$ day$^{-1}$). Binned values are shown as red dots; average points are shown as blue crosses; the model fit to the averaged values is shown as a blue line. Lag size: 0.067 degrees; number of lags: 12; Parameter: 2; Range: 0.536 degrees; Partial Sill: 1421.344. Right panel: Scatterplot of predicted values versus observed values for the model of Annual Primary Production Average Minimum (mg C m$^{-2}$ day$^{-1}$).

Table 178. Results of cross-validation of the kriged model for Annual Primary Production Average Minimum (mg C m$^{-2}$ day$^{-1}$).

| **Prediction Error** | **Value** |
|---|---:|
| Number of Observations | 33920 |
| Overall Mean Error | 0.043 |
| Root Mean Square Prediction Error | 43.524 |
| Standardized Mean | $7.260 \times 10^{-4}$ |
| Standardized Root Mean Square Prediction Error | 0.997 |
| Average Standard Error | 43.585 |

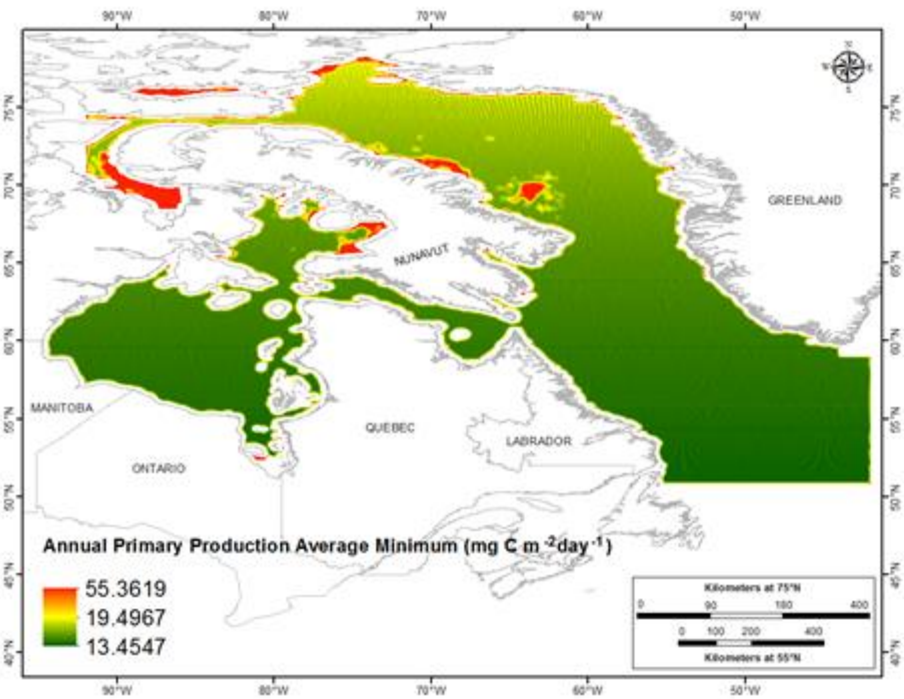


Figure 444. Prediction standard error surface of Annual Primary Production Average Minimum (mg C m$^{-2}$ day$^{-1}$).

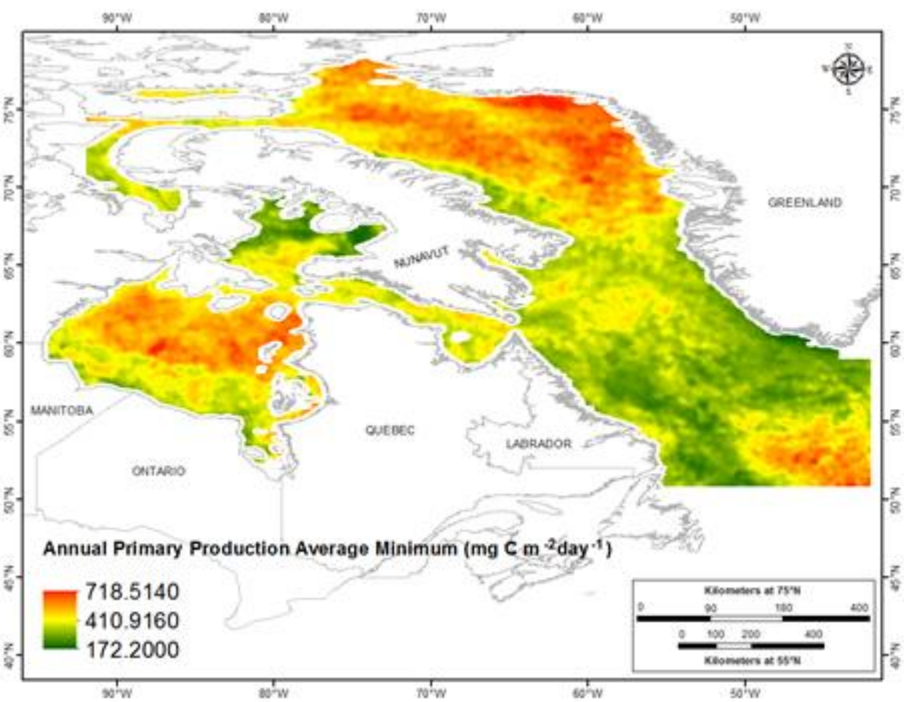


Figure 445. Interpolated prediction surface of Annual Primary Production Average Minimum (mg C m$^{-2}$ day$^{-1}$).

**Annual Primary Production Average Maximum**

This variable displayed a left-skewed, leptokurtic distribution prior to interpolation (Table 179, Figure 446). The data were higher than predicted by a normal distribution at the highest values and lower than predicted at the lowest values, while mid-values followed the reference line (Figure 447). These areas of under and over-prediction showed spatial pattern over the region (Figure 447).

The semivariogram showed autocorrelation present in the data (Figure 448). The kriged model showed a good fit between measured and predicted values (Figure 448). Good performance of the model was indicated by the cross-validation results (Table 180). The error map showed moderate error in the northern portion of the study extent, with patches of high error interspersed (Figure 449). The kriged surface is presented in Figure 450.

Table 179. Distributional properties of Annual Primary Production Average Maximum (mg C $m^{-2}$ $day^{-1}$).

| **Property** | **Value** |
|---|---:|
| Number of Observations | 33920 |
| Minimum | 208.690 |
| Maximum | 1725.600 |
| Mean | 886.880 |
| Median | 890.080 |
| Standard Deviation | 151.910 |
| Skewness | -0.138 |
| Kurtosis | 3.660 |

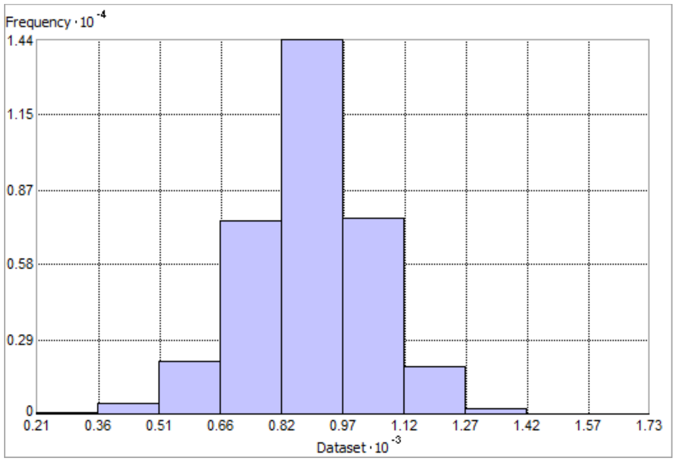

Figure 446. Distribution of Annual Primary Production Average Maximum (mg C $m^{-2}$ $day^{-1}$). Histogram was illustrated using 10 bins. X axis is shown at $10^{-3}$; Y axis is shown at $10^{-4}$.

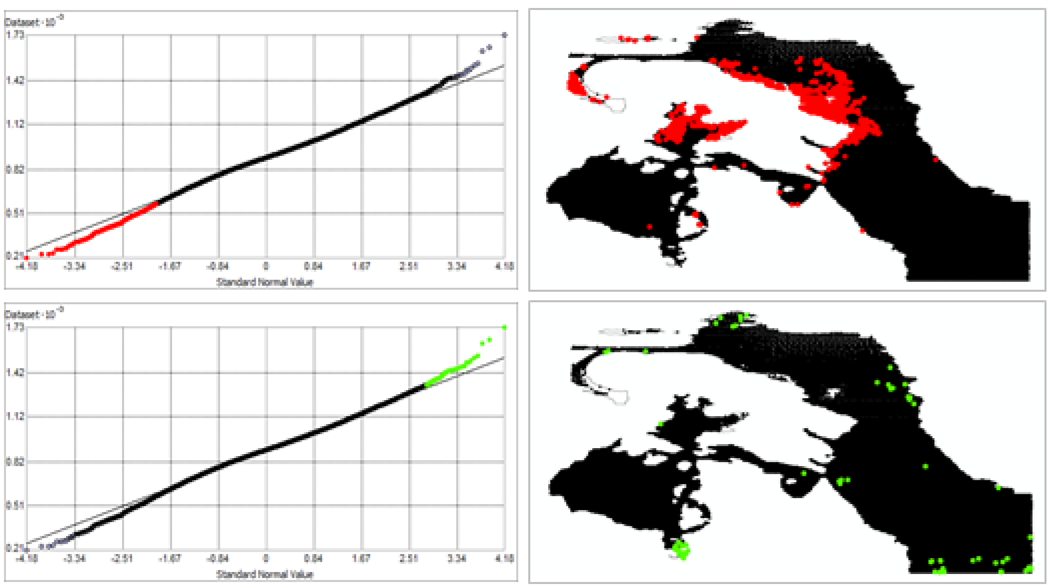
Figure 447. Normal Q-Q plot for data values of Annual Primary Production Average Maximum (mg C $m^{-2}$ $day^{-1}$). Points falling under (top right panel) and over (bottom right panel) the reference line are mapped.

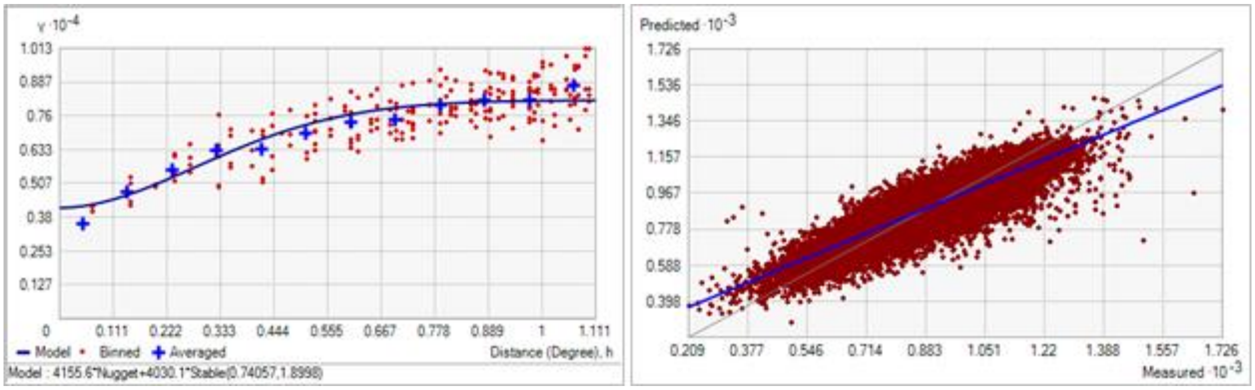


Figure 448. Left panel: Semivariogram of Annual Primary Production Average Maximum (mg C $m^{-2}$ $day^{-1}$). Binned values are shown as red dots; average points are shown as blue crosses; the model fit to the averaged values is shown as a blue line. Lag size: 0.093 degrees; number of lags: 12; Parameter: 1.900; Range: 0.741 degrees; Partial Sill: 4030.125. Right panel: Scatterplot of predicted values versus observed values for the model of Annual Primary Production Average Maximum (mg C $m^{-2}$ $day^{-1}$).

Table 180. Results of cross-validation of the kriged model for Annual Primary Production Average Maximum (mg C $m^{-2}$ $day^{-1}$).

| Prediction Error | Value |
|---|---|
| Number of Observations | 33920 |
| Overall Mean Error | 0.074 |
| Root Mean Square Prediction Error | 75.022 |
| Standardized Mean | $7.510 \times 10^{-4}$ |
| Standardized Root Mean Square Prediction Error | 1.081 |
| Average Standard Error | 69.126 |

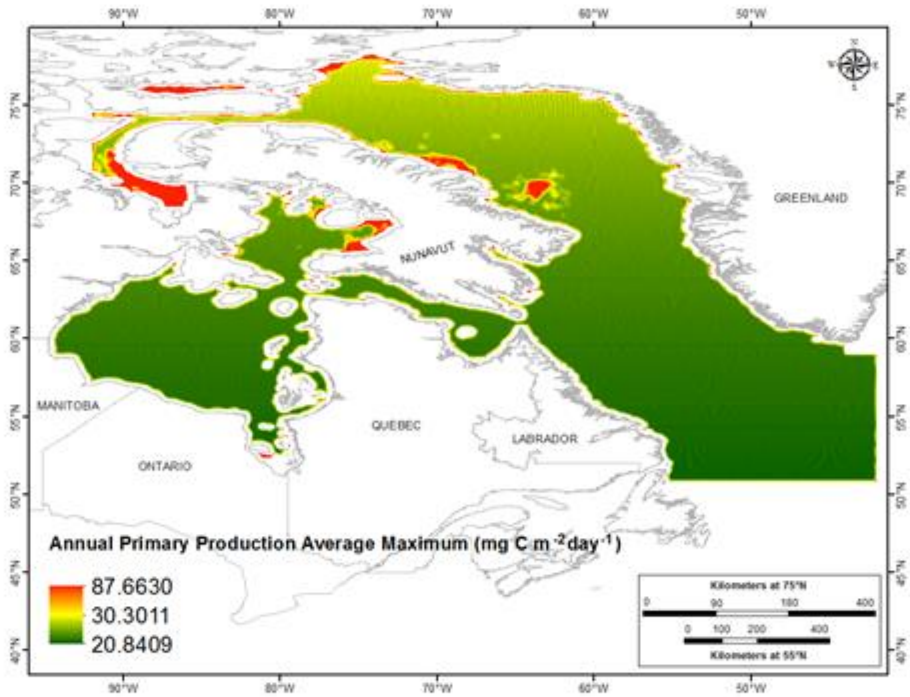


Figure 449. Prediction standard error surface of Annual Primary Production Average Maximum (mg C $m^{-2}$ $day^{-1}$).

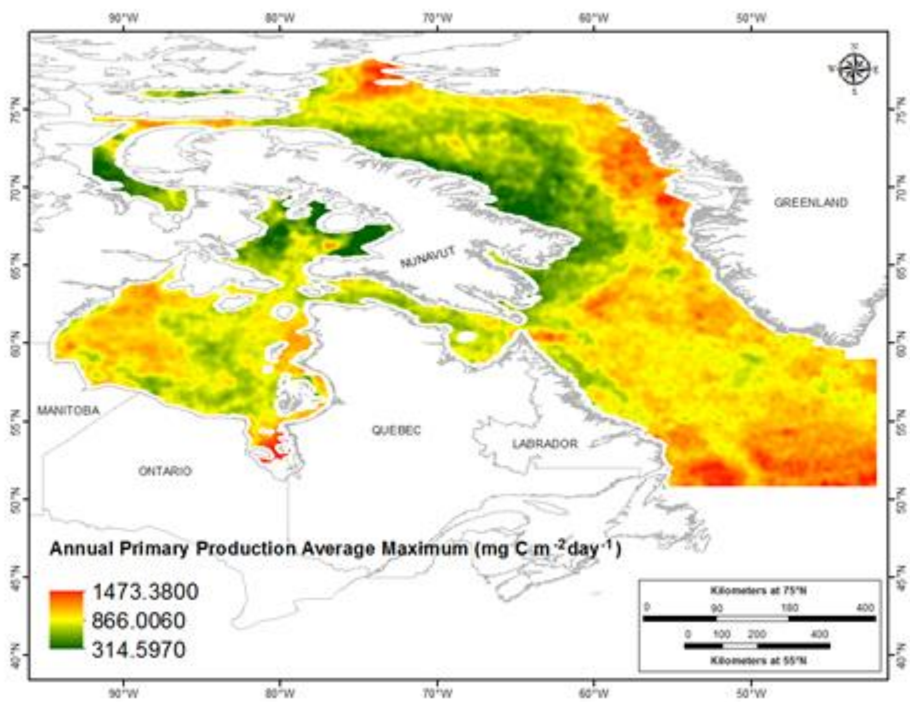


Figure 450. Interpolated prediction surface of Annual Primary Production Average Maximum (mg C $m^{-2}$ $day^{-1}$).

**Annual Primary Production Average Range**

This variable displayed a slightly right-skewed distribution prior to interpolation (Table 181, Figure 451). The data were higher than predicted by a normal distribution at both tails, while mid-values followed the reference line (Figure 452). These areas of over-prediction showed spatial pattern over the region (Figure 452).

The semivariogram showed moderate autocorrelation present in the data (Figure 453). The kriged model showed good fit between measured and predicted values (Figure 453). Good performance of the model was indicated by the cross-validation results (Table 182). The error map showed moderate error in the northern portion of the study extent, with patches of high error interspersed (Figure 454). The kriged surface is presented in Figure 455.

Table 181. Distributional properties of Annual Primary Production Average Range (mg C $m^{-2}$ $day^{-1}$).

| **Property** | **Value** |
|---|---:|
| Number of Observations | 33920 |
| Minimum | 4.535 |
| Maximum | 1486.600 |
| Mean | 486.680 |
| Median | 495.460 |
| Standard Deviation | 178.290 |
| Skewness | 0.019 |
| Kurtosis | 2.823 |

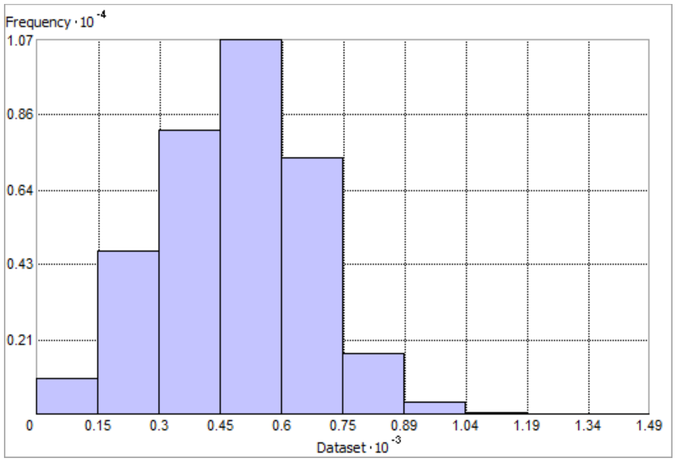


Figure 451. Distribution of Annual Primary Production Average Range (mg C m$^{-2}$ day$^{-1}$). Histogram was illustrated using 10 bins. X axis is shown at $10^{-3}$; Y axis is shown at $10^{-4}$.

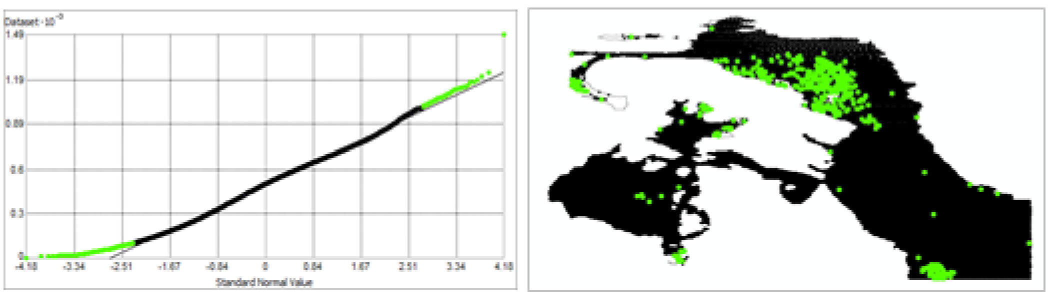


Figure 452. Normal Q-Q plot for data values of Annual Primary Production Average Range (mg C m$^{-2}$ day$^{-1}$). Points falling over the reference line are mapped; no points fall under the reference line.

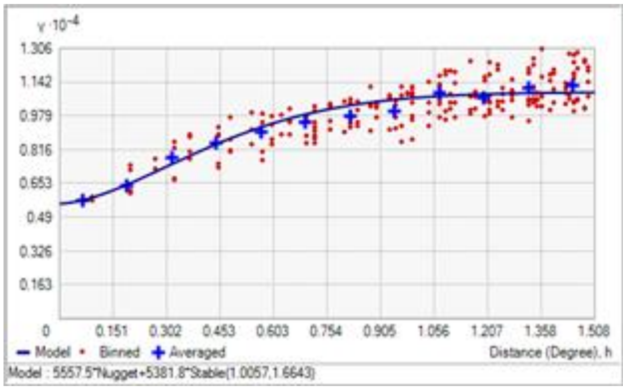

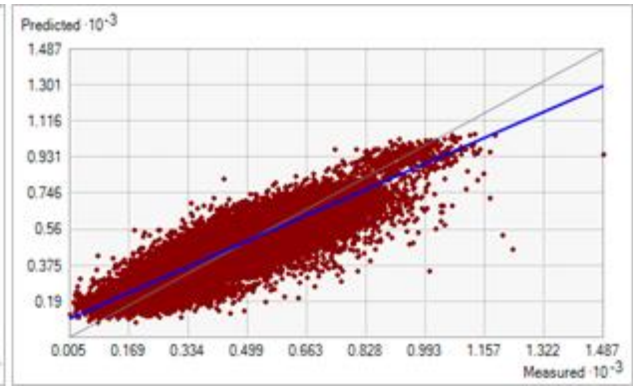

Figure 453. Left panel: Semivariogram of Annual Primary Production Average Range (mg C $m^{-2}$ $day^{-1}$). Binned values are shown as red dots; average points are shown as blue crosses; the model fit to the averaged values is shown as a blue line. Lag size: 0.126 degrees; number of lags: 12; Parameter: 1.664; Range: 1.006 degrees; Partial Sill: 5381.840. Right panel: Scatterplot of predicted values versus observed values for the model of Annual Primary Production Average Range (mg C $m^{-2}$ $day^{-1}$).

Table 182. Results of cross-validation of the kriged model for Annual Primary Production Average Range (mg C $m^{-2}$ $day^{-1}$).

| **Prediction Error** | **Value** |
|---|---:|
| Number of Observations | 33920 |
| Overall Mean Error | 0.031 |
| Root Mean Square Prediction Error | 83.098 |
| Standardized Mean | $2.681 \times 10^{-4}$ |
| Standardized Root Mean Square Prediction Error | 1.039 |
| Average Standard Error | 79.826 |

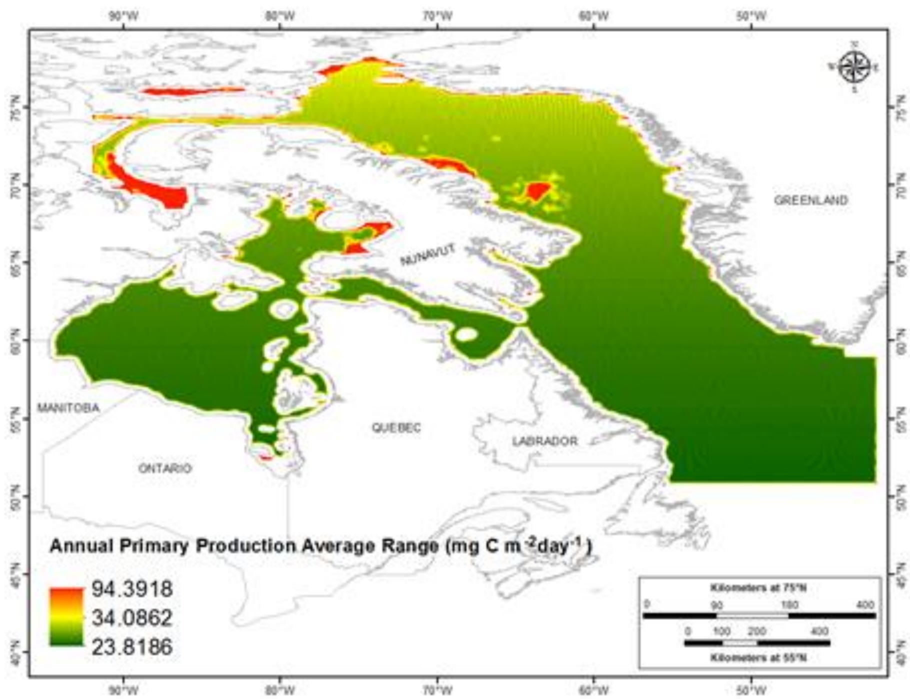


Figure 454. Prediction standard error surface of Annual Primary Production Average Range (mg C $m^{-2}$ $day^{-1}$).

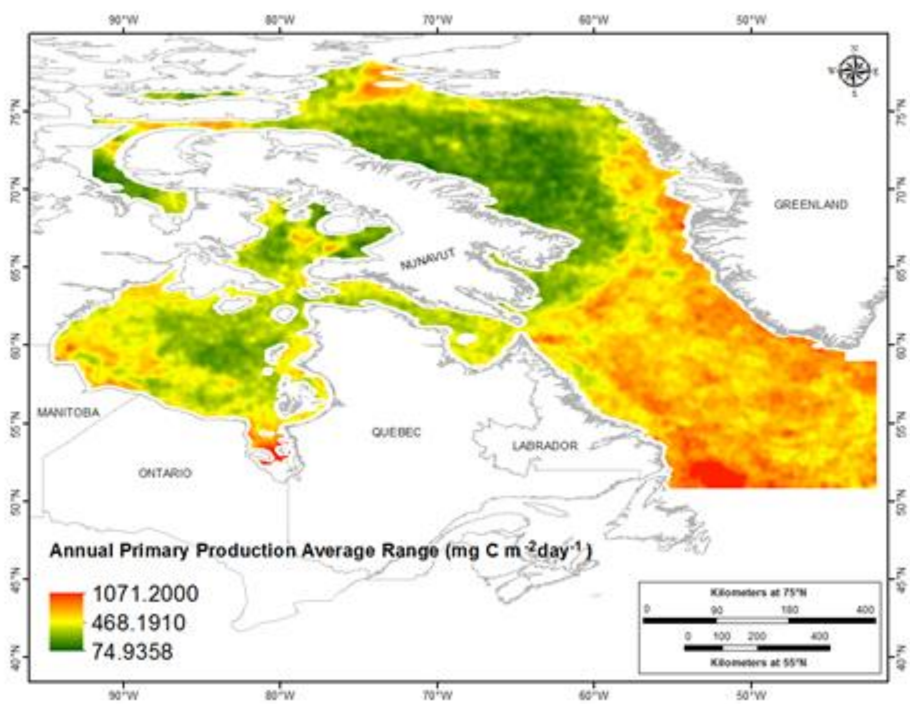


Figure 455. Interpolated prediction surface of Annual Primary Production Average Range (mg C $m^{-2}$ $day^{-1}$).

## Sea Ice Cover

Sea ice is an important driver of the physical marine environment in Arctic communities. As temperatures warm in the spring and summer, sea ice weakens, and is fragmented and transported offshore by wind (Clark et al., 2015). This phenomenon is referred to as sea ice ‘break out’ (Clark et al., 2015). This seasonal cycle of sea ice presence and absence can have an impact on the underlying physical marine environment through its regulation of light penetration, disturbance, and sedimentation. The seasonal extent and duration of sea ice is rapidly changing in the Arctic (Boé et al., 2009), and small changes in the timing of sea ice presence and absence can cause complete regime shifts in local benthic communities from invertebrate to algae-dominated states (Clark et al., 2013).

The sea ice cover values are presented as a fraction from 0 to 1, representing 0 to 100% ice cover.

### Spring Ice Cover Mean

This variable displayed a left-skewed, bimonal distribution prior to interpolation (Table 183, Figure 456). The data were higher than predicted by a normal distribution at the lowest and upper mid-values, while were lower than predicted at the highest and lower mid-values (Figure 457). These areas of over and under-prediction showed a strong spatial pattern over the region (Figure 457).

The semivariogram showed moderate autocorrelation present in the data (Figure 458). The kriged model showed very good fit between measured and predicted values (Figure 458). Good performance of the model was indicated by the cross-validation results (Table 184), although the Standardized Root-Mean-Square Prediction error was greater than 1 indicating that variability in the predictions has been underestimated. The error map showed lower error in all the study area except in Jones and Lancaster Sound (Figure 459). The kriged surface is presented in Figure 460.

Table 183. Distributional properties of Spring Ice Cover Mean.

| Property | Value |
|---|---:|
| Number of Observations | 526 |
| Minimum | 0.000 |
| Maximum | 0.996 |
| Mean | 0.529 |
| Median | 0.702 |
| Standard Deviation | 0.396 |
| Skewness | -0.361 |
| Kurtosis | 1.376 |

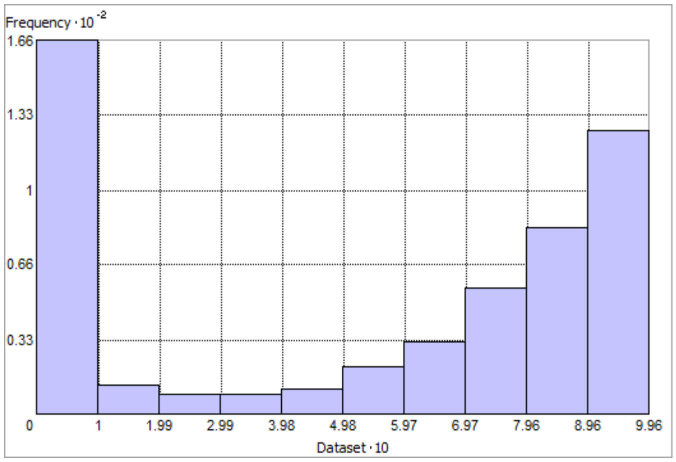

Figure 456. Distribution of Spring Ice Cover Mean Histogram was illustrated using 10 bins. X axis is shown at 10; Y axis is shown at $10^{-2}$.

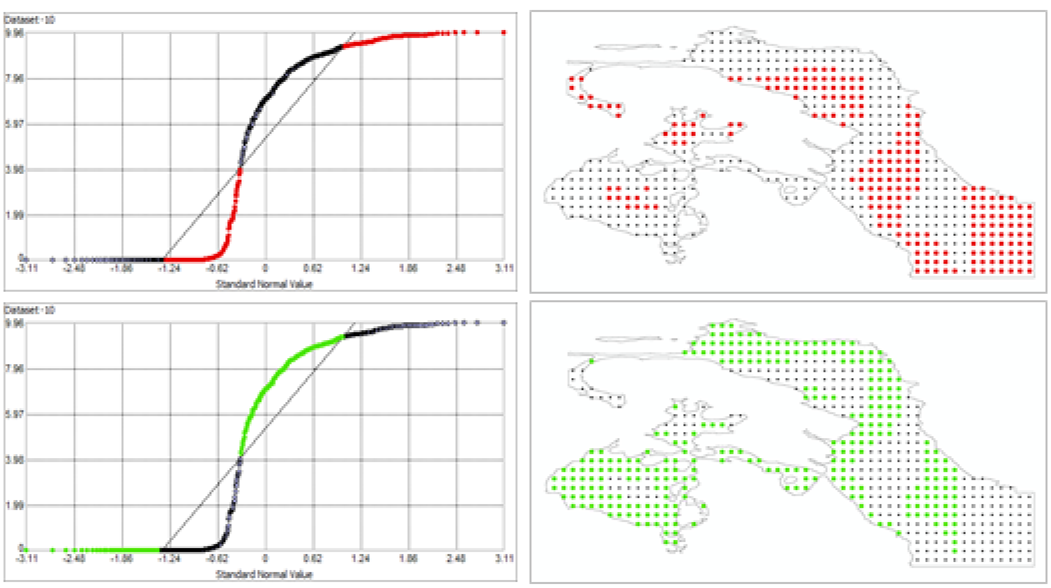
Figure 457. Normal Q-Q plot for data values of Spring Ice Cover Mean. Points falling under (top right panel) and over (bottom right panel) the reference line are mapped.

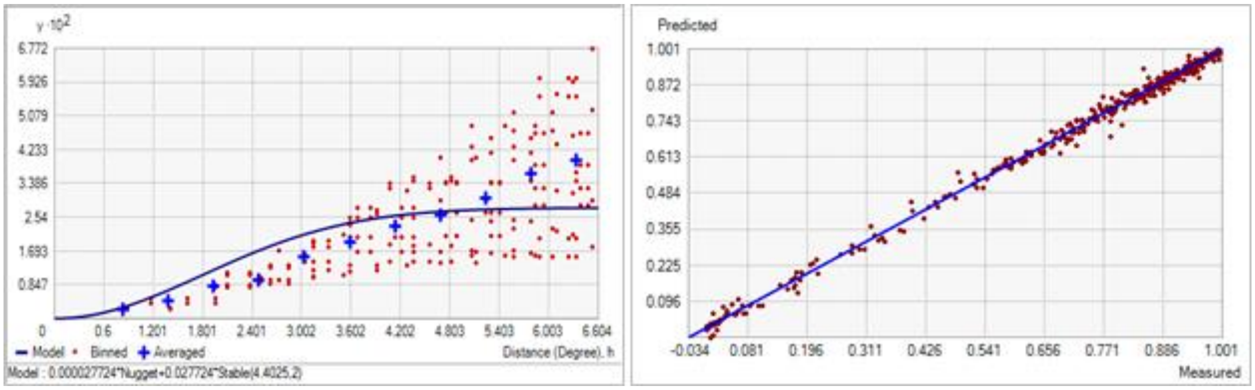


Figure 458. Left panel: Semivariogram of Spring Ice Cover Mean. Binned values are shown as red dots; average points are shown as blue crosses; the model fit to the averaged values is shown as a blue line. Lag size: 0.550 degrees; number of lags: 12; Parameter: 2; Range: 4.402 degrees; Partial Sill: 0.028. Right panel: Scatterplot of predicted values versus observed values for the model of Spring Ice Cover Mean.

Table 184. Results of cross-validation of the kriged model for Spring Ice Cover Mean.

| **Prediction Error** | **Value** |
|---|---:|
| Number of Observations | 526 |
| Overall Mean Error | $-5.048 \times 10^{-5}$ |
| Root Mean Square Prediction Error | 0.017 |
| Standardized Mean | 0.012 |
| Standardized Root Mean Square Prediction Error | 1.300 |
| Average Standard Error | 0.018 |

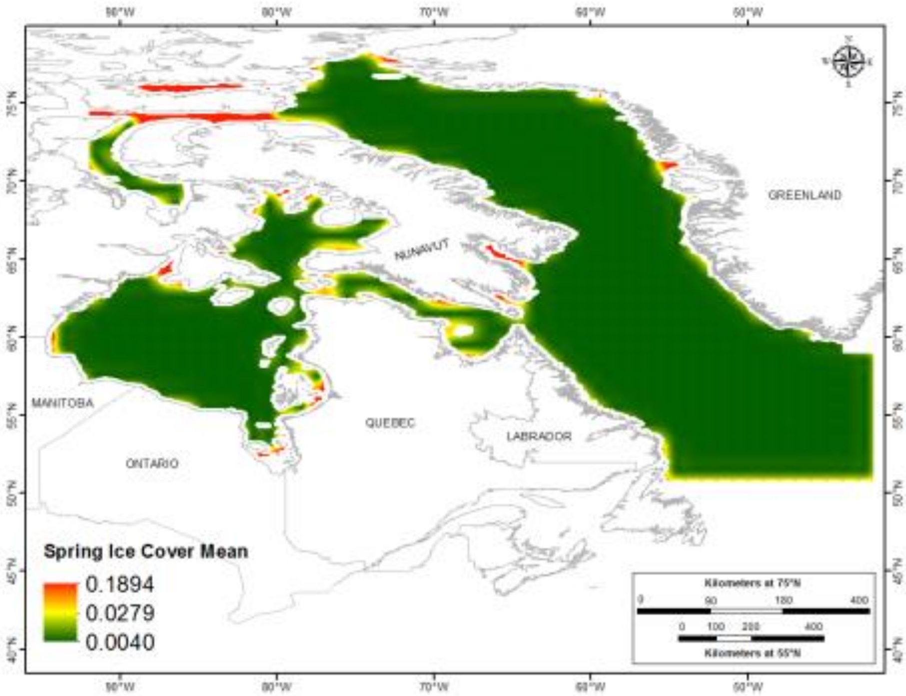


Figure 459. Prediction standard error surface of Spring Ice Cover Mean.

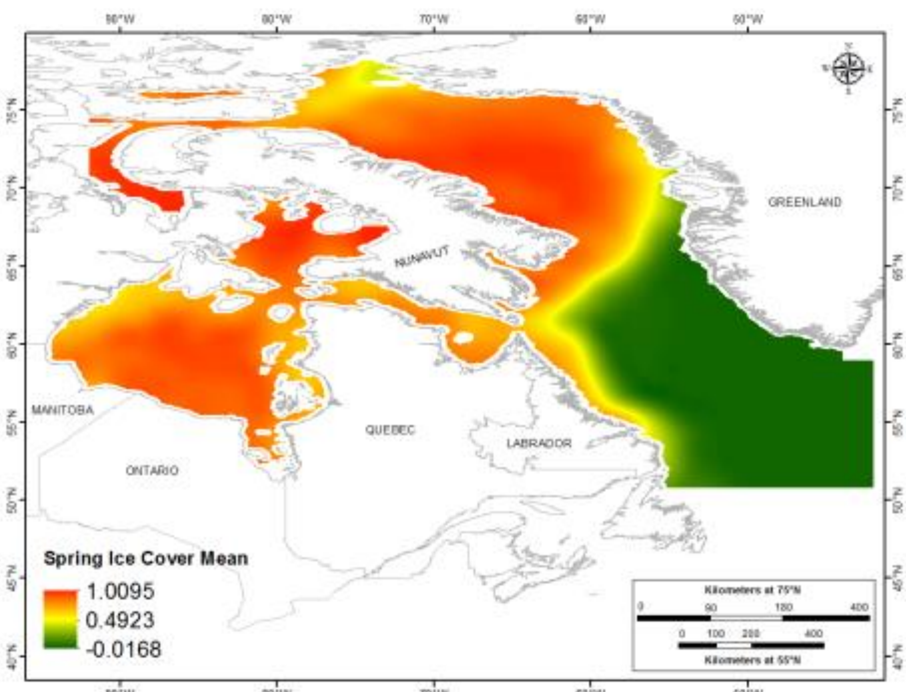


Figure 460. Interpolated prediction surface of Spring Ice Cover Mean.

**Spring Ice Cover Minimum**

This variable displayed a right-skewed, leptokurtic distribution prior to interpolation (Table 185, Figure 461). The data were higher than predicted by a normal distribution at both tails, while were lower than predicted at mid-values (Figure 462). These areas of over and under-prediction showed spatial pattern over the region (Figure 462).

The semivariogram showed moderate autocorrelation present in the data (Figure 463). The kriged model showed a good fit between measured and predicted values (Figure 463). Good performance of the model was indicated by the cross-validation results (Table 186). The error map showed a “bullseye” pattern with error increasing with distance from data points (Figure 464). The kriged surface is presented in Figure 465.

Table 185. Distributional properties of Spring Ice Cover Minimum.

| **Property** | **Value** |
|---|---:|
| Number of Observations | 526 |
| Minimum | 0.000 |
| Maximum | 0.950 |
| Mean | 0.160 |
| Median | 0.000 |
| Standard Deviation | 0.272 |
| Skewness | 1.659 |
| Kurtosis | 4.578 |

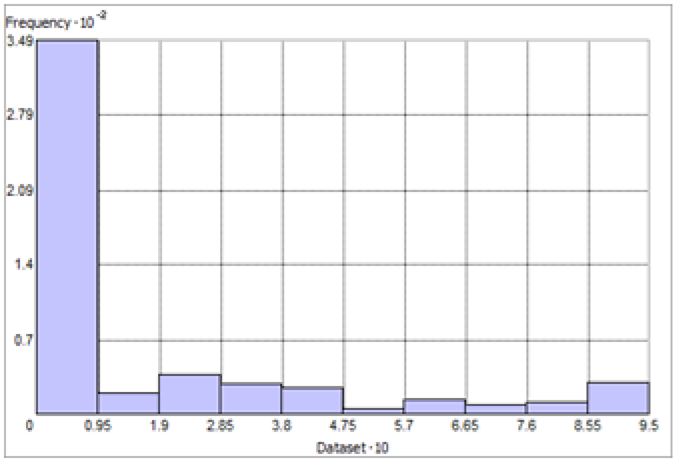


Figure 461. Distribution of Spring Ice Cover Minimum. Histogram was illustrated using 10 bins. X axis is shown at 10; Y axis is shown at $10^{-2}$.

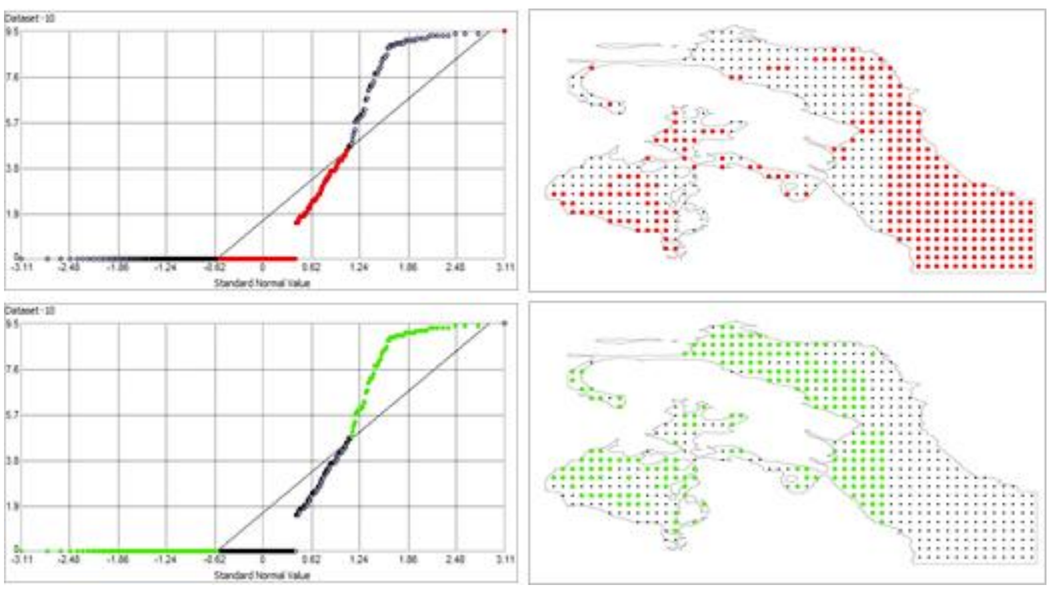

Figure 462. Normal Q-Q plot for data values of Spring Ice Cover Minimum. Points falling under (top right panel) and over (bottom right panel) the reference line are mapped.

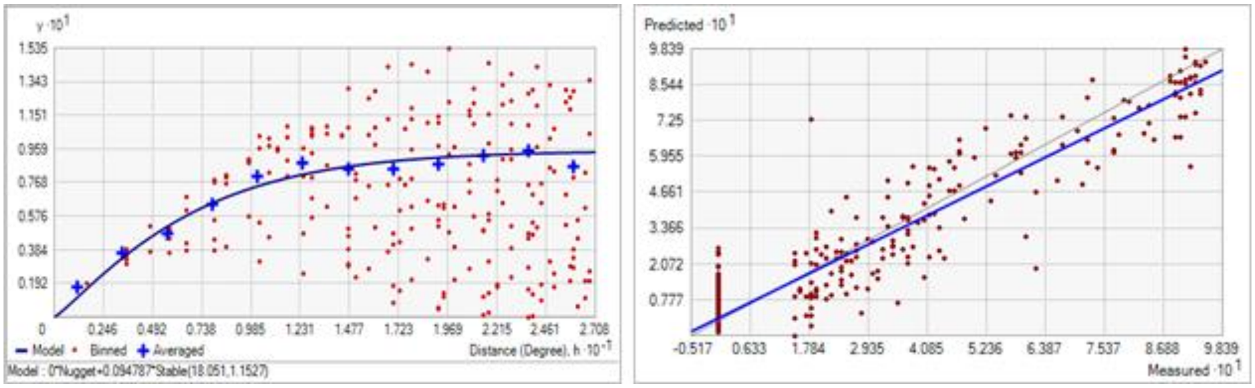

Figure 463. Left panel: Semivariogram of Spring Ice Cover Minimum. Binned values are shown as red dots; average points are shown as blue crosses; the model fit to the averaged values is shown as a blue line. Lag size: 2.256 degrees; number of lags: 12; Parameter: 1.153; Range: 18.050 degrees; Partial Sill: 0.095. Right panel: Scatterplot of predicted values versus observed values for the model of Spring Ice Cover Minimum.

Table 186. Results of cross-validation of the kriged model for Spring Ice Cover Minimum.

| **Prediction Error** | **Value** |
|---|---:|
| Number of Observations | 526 |
| Overall Mean Error | $-2.042 \times 10^{-4}$ |
| Root Mean Square Prediction Error | 0.083 |
| Standardized Mean | $-1.165 \times 10^{-3}$ |
| Standardized Root Mean Square Prediction Error | 0.908 |
| Average Standard Error | 0.085 |

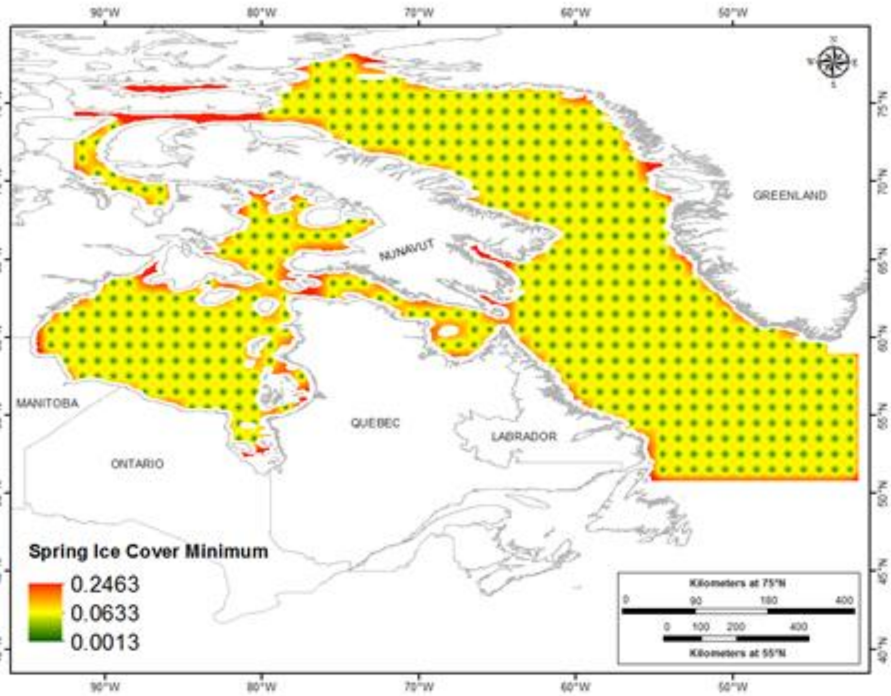


Figure 464. Prediction standard error surface of Spring Ice Cover Minimum.

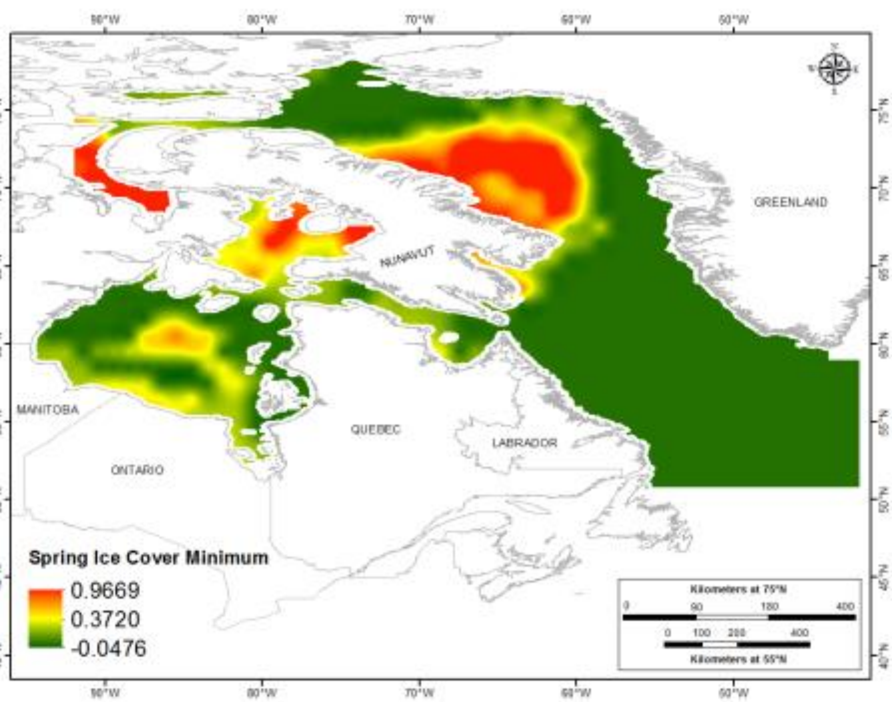


Figure 465. Interpolated prediction surface of Spring Ice Cover Minimum.

## Spring Ice Cover Maximum

This variable displayed a bimodal, platykurtic distribution prior to interpolation (Table 187, Figure 466). The data were higher than predicted by a normal distribution at the lowest and upper mid-values, and were lower than predicted at the highest and lower mid-values (Figure 467). These areas of over and under-prediction showed spatial pattern over the region (Figure 467).

The semivariogram showed moderate autocorrelation present in the data (Figure 468). The kriged model showed good fit between measured and predicted values (Figure 468). Fair performance of the model was indicated by the cross-validation results (Table 188), with underestimation in the variability of the predictions as indicated by the Standardized Root-Mean-Square Error greater than 1. The error map showed low error over much of the study extent with higher error in Lancaster Sound and in smaller inlets (Figure 469). The kriged surface is presented in Figure 470.

Table 187. Distributional properties of Spring Ice Cover Maximum.

| Property | Value |
|---|---:|
| Number of Observations | 526 |
| Minimum | 0.000 |
| Maximum | 1.000 |
| Mean | 0.723 |
| Median | 0.99 |
| Standard Deviation | 0.410 |
| Skewness | -1.053 |
| Kurtosis | 2.266 |

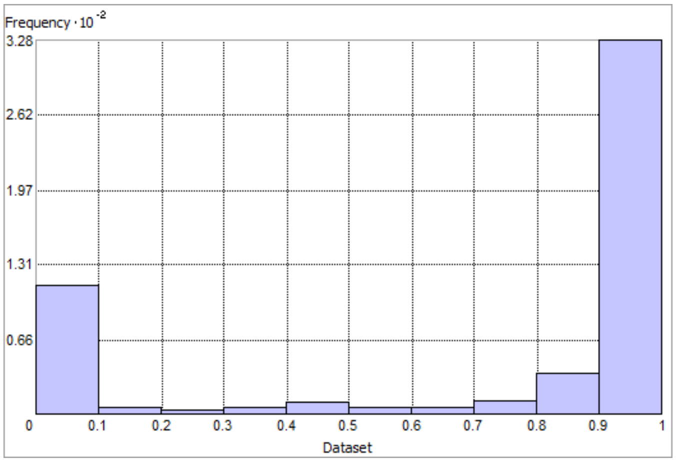

Figure 466. Distribution of Spring Ice Cover Maximum. Histogram was illustrated using 10 bins. Y axis is shown at $10^{-2}$.

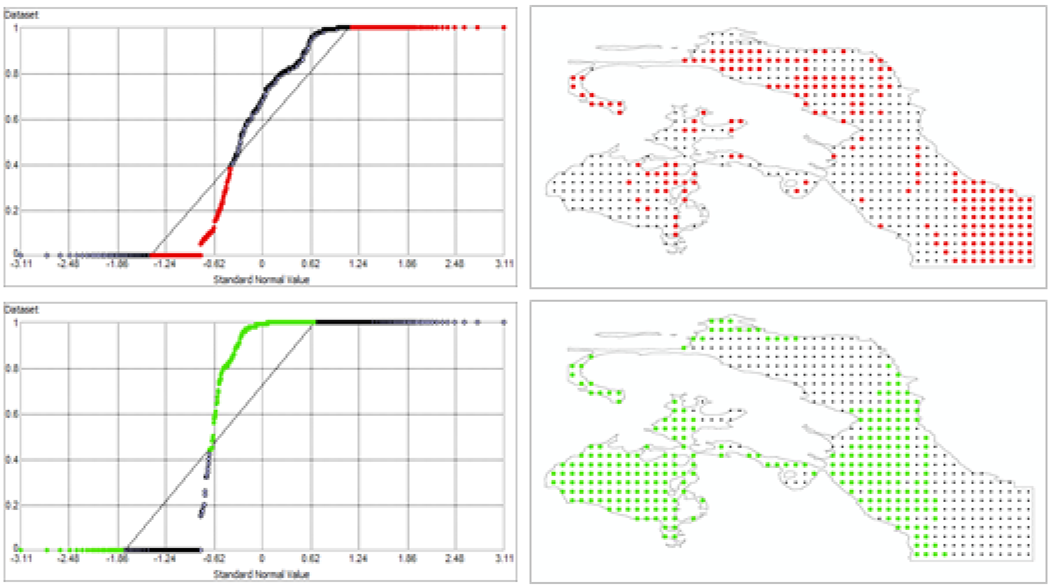
Figure 467. Normal Q-Q plot for data values of Spring Ice Cover Maximum. Points falling under (top right panel) and over (bottom right panel) the reference line are mapped.

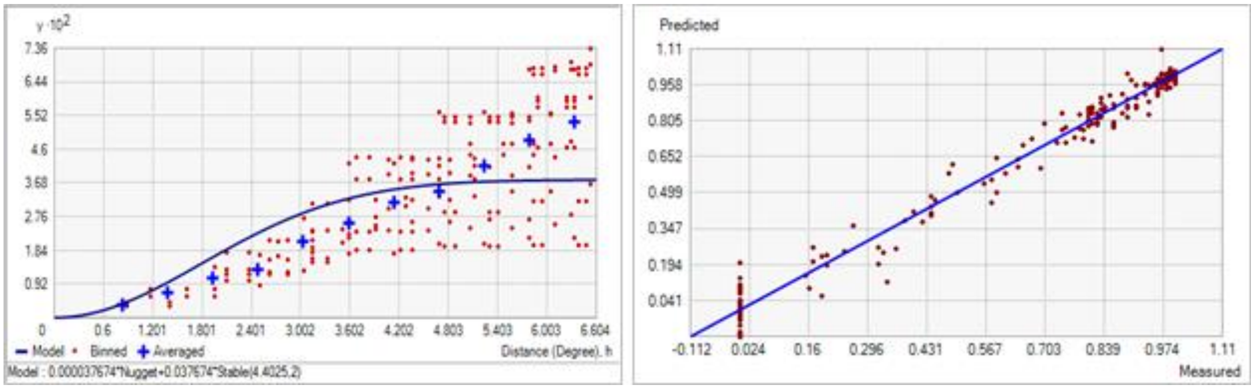


Figure 468. Left panel: Semivariogram of Spring Ice Cover Maximum. Binned values are shown as red dots; average points are shown as blue crosses; the model fit to the averaged values is shown as a blue line. Lag size: 0.550 degrees; number of lags: 12; Parameter: 2; Range: 4.402 degrees; Partial Sill: 0.038. Right panel: Scatterplot of predicted values versus observed values for the model of Spring Ice Cover Maximum.

Table 188. Results of cross-validation of the kriged model for Spring Ice Cover Maximum.

| **Prediction Error** | **Value** |
|---|---:|
| Number of Observations | 526 |
| Overall Mean Error | $3.211 \times 10^{-4}$ |
| Root Mean Square Prediction Error | 0.033 |
| Standardized Mean | $6.180 \times 10^{-4}$ |
| Standardized Root Mean Square Prediction Error | 2.775 |
| Average Standard Error | 0.021 |

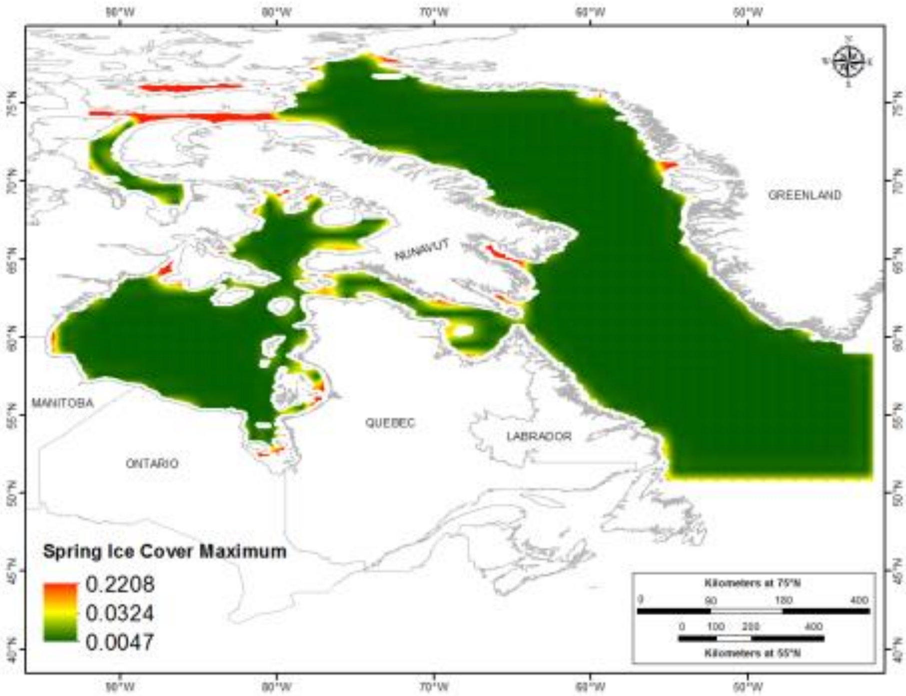


Figure 469. Prediction standard error surface of Spring Ice Cover Maximum.

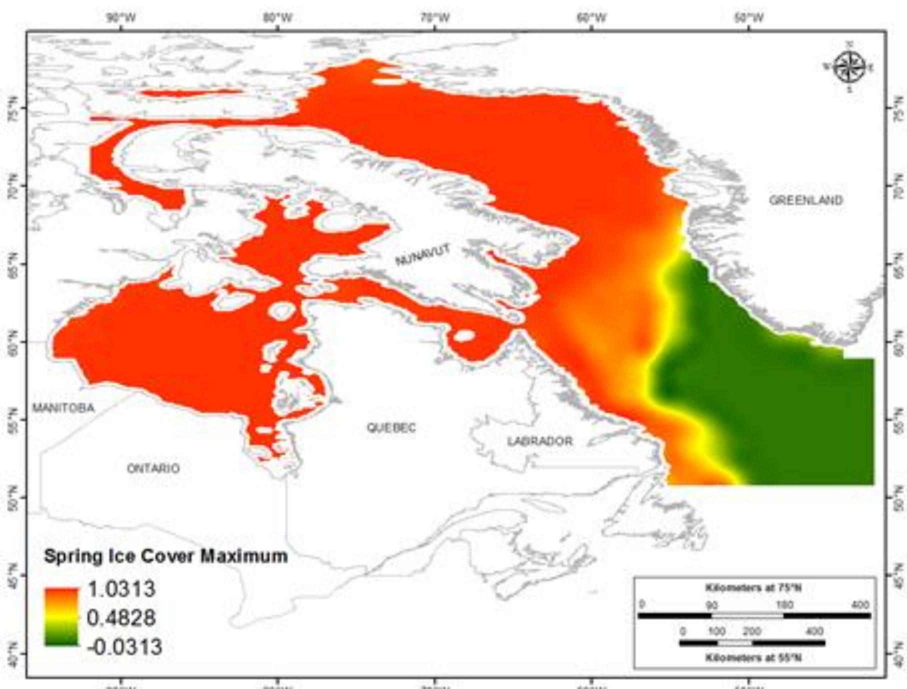


Figure 470. Interpolated prediction surface of Spring Ice Cover Maximum.

## Spring Ice Cover Range

This variable displayed a bimodal, platykurtic distribution prior to interpolation (Table 189, Figure 471). The data were higher than predicted by a normal distribution at the lowest and upper mid-values, and were lower than predicted at the highest and lower mid-values (Figure 472). These areas of over and under-prediction showed spatial pattern over the region (Figure 472).

The semivariogram showed moderate autocorrelation present in the data (Figure 473). The kriged model showed good fit between measured and predicted values (Figure 473). Very good performance of the model was indicated by the cross-validation results (Table 190). The error map showed a “bullseye” pattern with error decreasing with distance from data points (Figure 474). The kriged surface is presented in Figure 475.

Table 189. Distributional properties of Spring Ice Cover Range.

| **Property** | **Value** |
|---|---:|
| Number of Observations | 526 |
| Minimum | 0.000 |
| Maximum | 1.000 |
| Mean | 0.563 |
| Median | 0.680 |
| Standard Deviation | 0.392 |
| Skewness | -0.361 |
| Kurtosis | 1.517 |

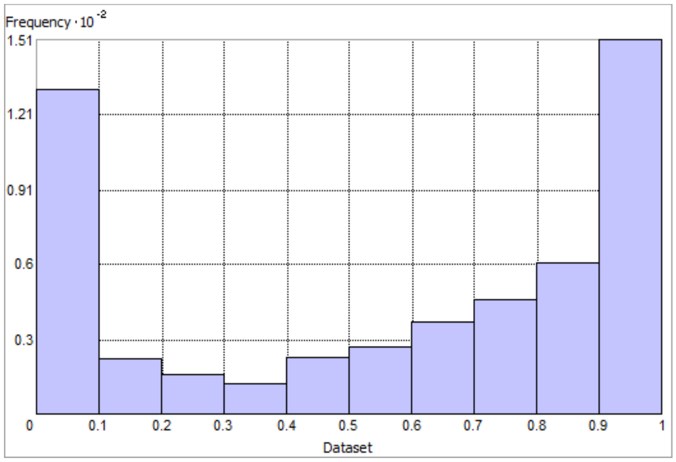


Figure 471. Distribution of Spring Ice Cover Range. Histogram was illustrated using 10 bins. Y axis is shown at $10^{-2}$.

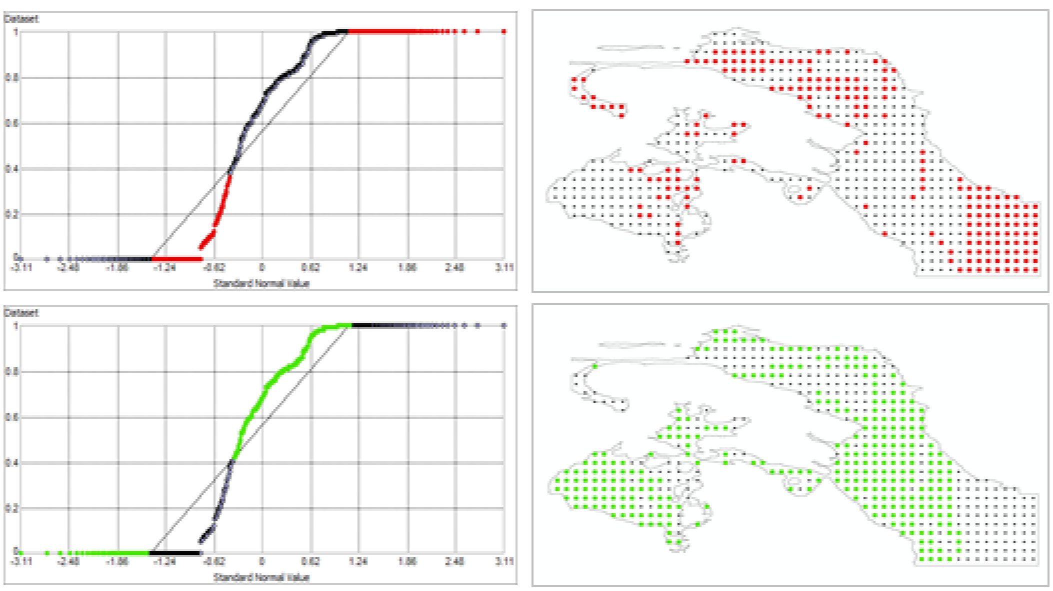

Figure 472. Normal Q-Q plot for data values of Spring Ice Cover Range. Points falling under (top right panel) and over (bottom right panel) the reference line are mapped.

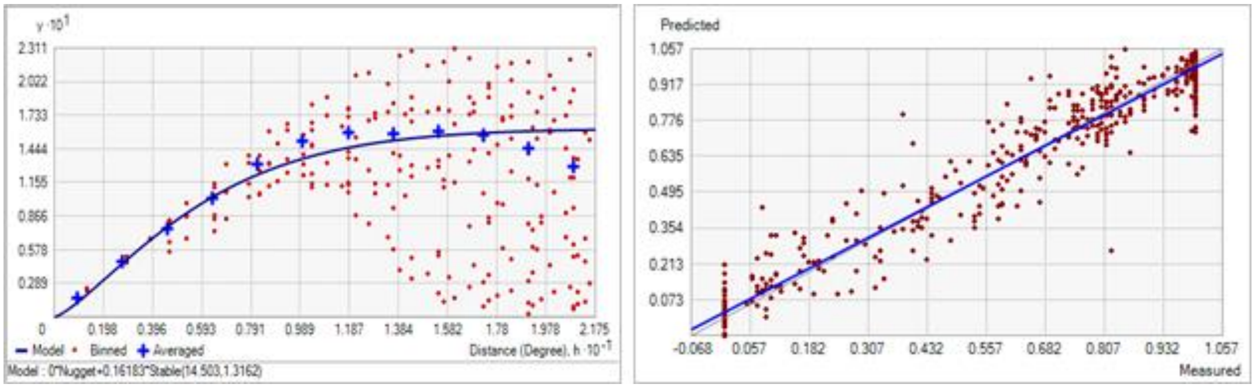

Figure 473. Left panel: Semivariogram of Spring Ice Cover Range. Binned values are shown as red dots; average points are shown as blue crosses; the model fit to the averaged values is shown as a blue line. Lag size: 1.813 degrees; number of lags: 12; Parameter: 1.316; Range: 14.503 degrees; Partial Sill: 0.162. Right panel: Scatterplot of predicted values versus observed values for the model of Spring Ice Cover Range.

Table 190. Results of cross-validation of the kriged model for Spring Ice Cover Range.

| Prediction Error | Value |
|---|---|
| Number of Observations | 526 |
| Overall Mean Error | $1.881 \times 10^{-4}$ |
| Root Mean Square Prediction Error | 0.090 |
| Standardized Mean | $9.383 \times 10^{-4}$ |
| Standardized Root Mean Square Prediction Error | 0.906 |
| Average Standard Error | 0.098 |

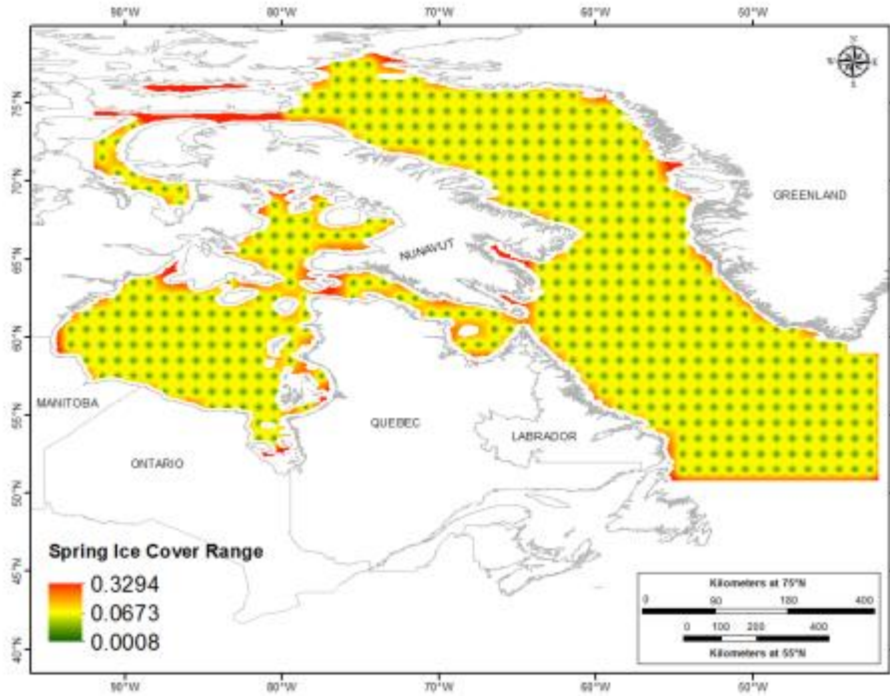


Figure 474. Prediction standard error surface of Spring Ice Cover Range.

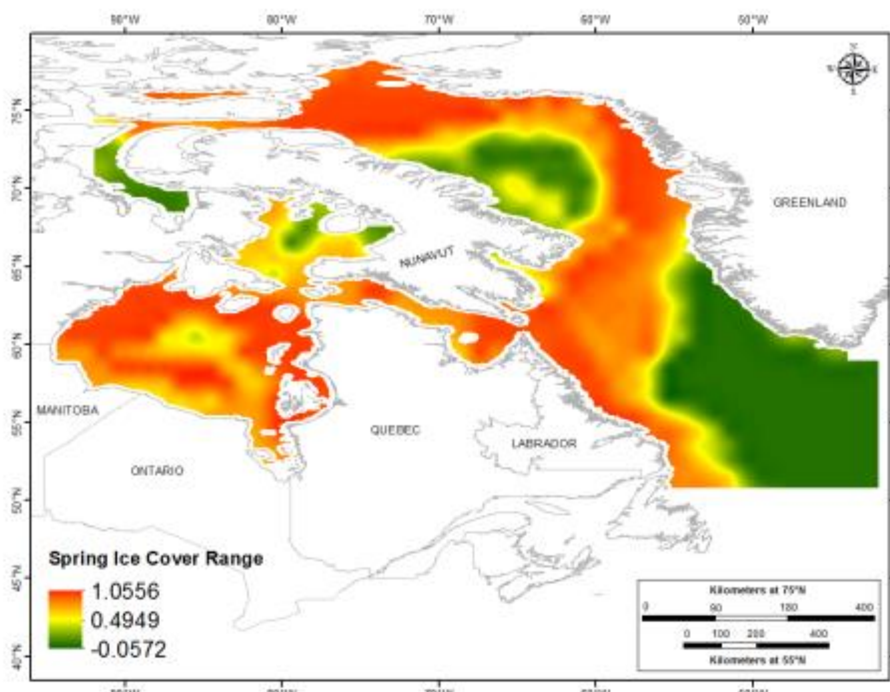


Figure 475. Interpolated prediction surface of Spring Ice Cover Range.

### Spring Ice Cover Average Minimum

This variable displayed a right-skewed, nearly bimodal distribution with kurtosis prior to interpolation (Table 191, Figure 476). The data were higher than predicted by a normal distribution at the lowest and upper mid-values, and were lower than predicted at the highest and lower mid-values (Figure 477). These areas of over and under-prediction showed spatial pattern over the region (Figure 477).

The semivariogram showed moderate autocorrelation present in the data (Figure 478). The kriged model showed good fit between measured and predicted values (Figure 478). Good performance of the model was indicated by the cross-validation results (Table 192), although variability in the predictions was underestimated as indicated by the Standardized Root-Mean-Square Error greater than 1. The error map showed lower error in Hudson Bay, Baffin Bay and Davis Strait, with higher error along the edges of the study extent and in Lancaster Sound (Figure 479). The kriged surface is presented in Figure 480.

Table 191. Distributional properties of Spring Ice Cover Average Minimum.

| **Property** | **Value** |
|---|---:|
| Number of Observations | 526 |
| Minimum | 0.000 |
| Maximum | 0.987 |
| Mean | 0.400 |
| Median | 0.386 |
| Standard Deviation | 0.367 |
| Skewness | 0.154 |
| Kurtosis | 1.391 |

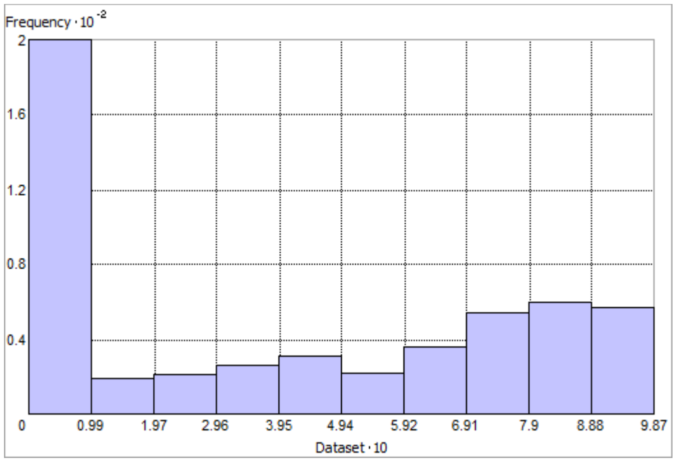


Figure 476. Distribution of Spring Ice Cover Average Minimum. Histogram was illustrated using 10 bins. X axis is shown at 10; Y axis is shown at $10^{-2}$.

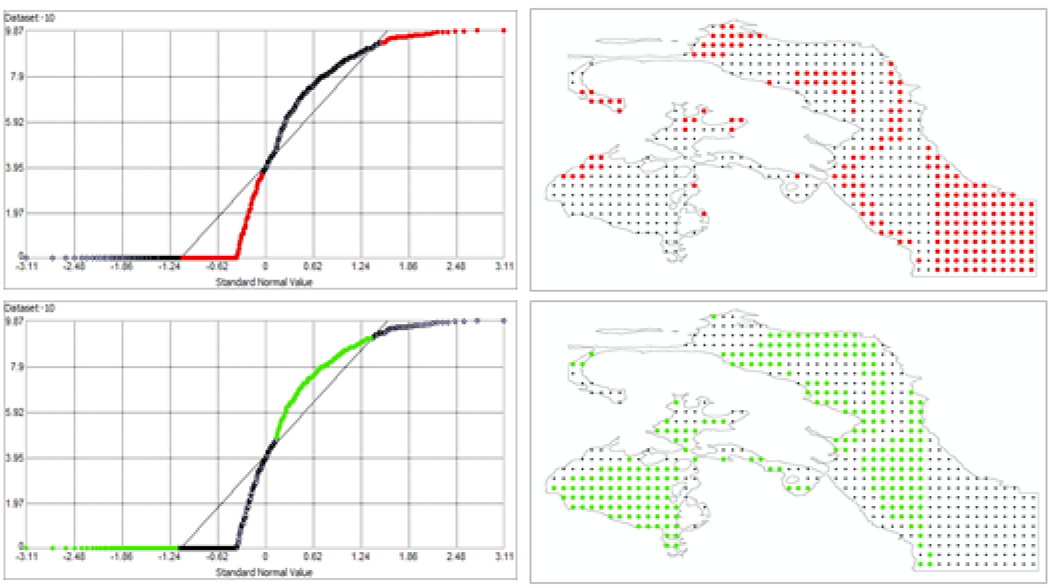

Figure 477. Normal Q-Q plot for data values of Spring Ice Cover Average Minimum. Points falling under (top right panel) and over (bottom right panel) the reference line are mapped.

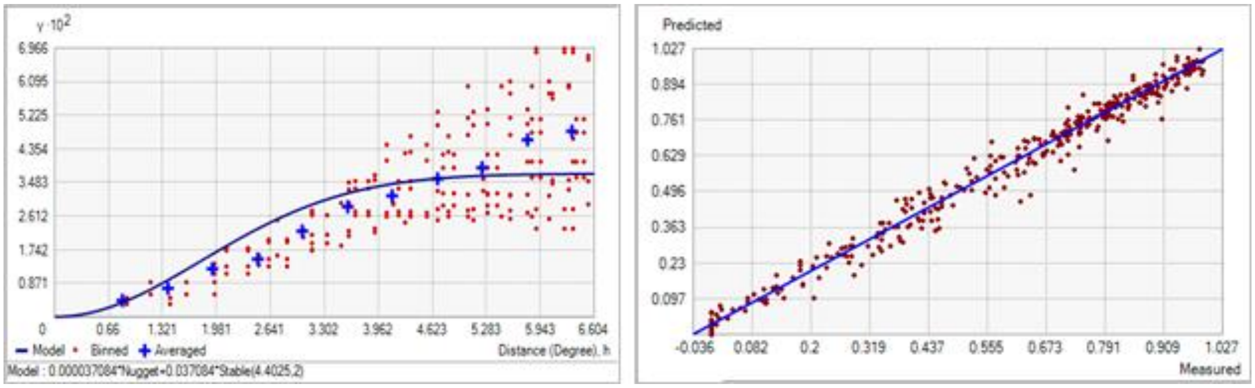


Figure 478. Left panel: Semivariogram of Spring Ice Cover Average Minimum. Binned values are shown as red dots; average points are shown as blue crosses; the model fit to the averaged values is shown as a blue line. Lag size: 0.550 degrees; number of lags: 12; Parameter: 2; Range: 4.402 degrees; Partial Sill: 0.037. Right panel: Scatterplot of predicted values versus observed values for the model of Spring Ice Cover Average Minimum.

Table 192. Results of cross-validation of the kriged model for Spring Ice Cover Average Minimum.

| **Prediction Error** | **Value** |
|---|---:|
| Number of Observations | 526 |
| Overall Mean Error | $-9.569 \times 10^{-4}$ |
| Root Mean Square Prediction Error | 0.033 |
| Standardized Mean | $-8.629 \times 10^{-3}$ |
| Standardized Root Mean Square Prediction Error | 1.905 |
| Average Standard Error | 0.021 |

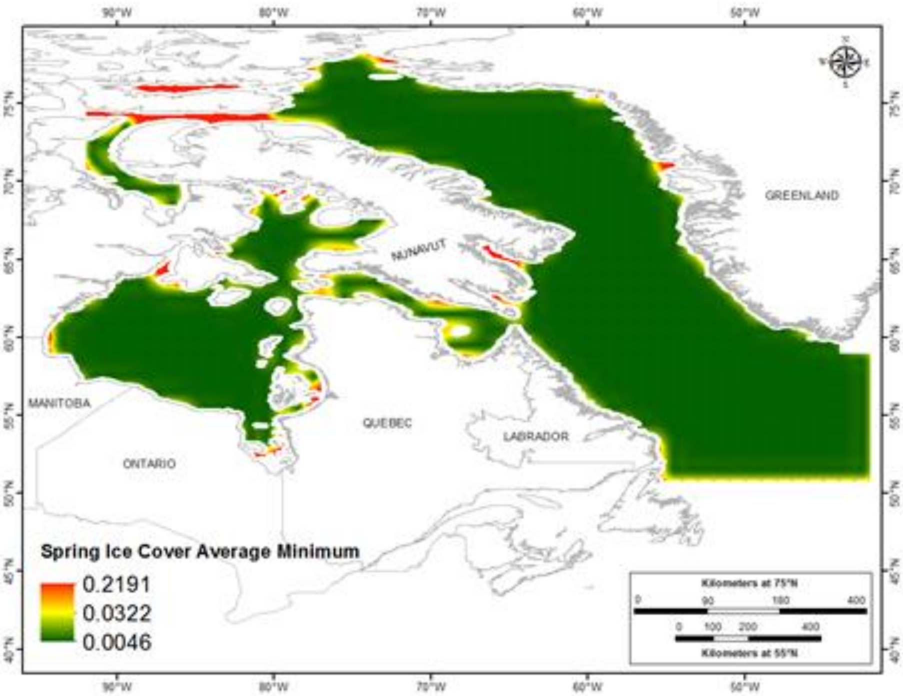


Figure 479. Prediction standard error surface of Spring Ice Cover Average Minimum.

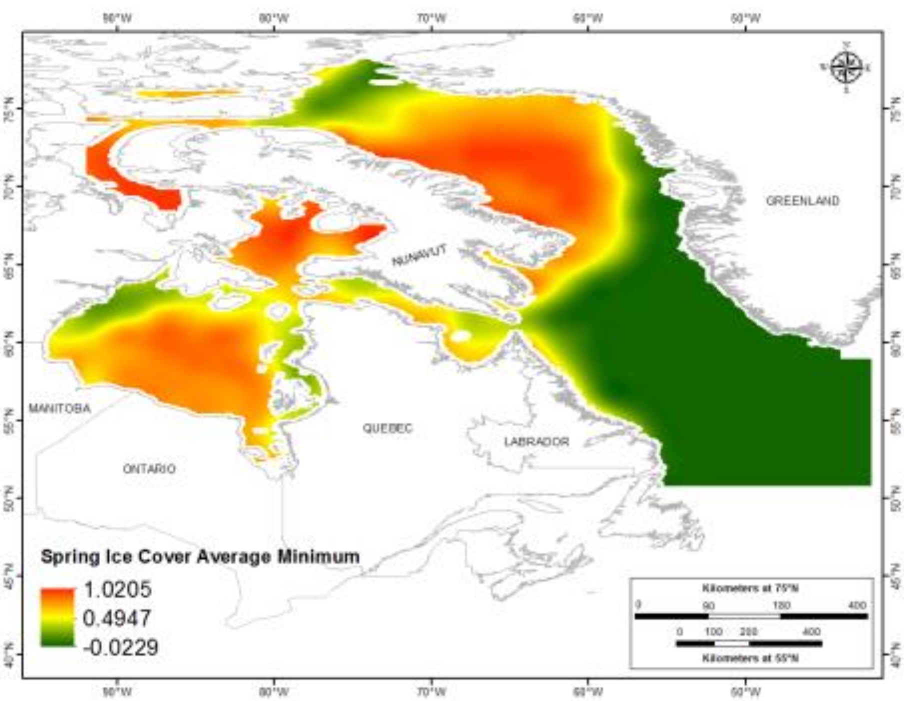


Figure 480. Interpolated prediction surface of Spring Ice Cover Average Minimum.

### Spring Ice Cover Average Maximum

This variable displayed a bimodal, platykurtic distribution prior to interpolation (Table 193, Figure 481). The data were higher than predicted by a normal distribution at the lowest and upper mid-values, and were lower than predicted at the highest and lower mid-values (Figure 482). These areas of over and under-prediction showed spatial pattern over the region (Figure 482).

The semivariogram showed moderate autocorrelation present in the data (Figure 483). The kriged model showed good fit between measured and predicted values (Figure 483). Good performance of the model was indicated by the cross-validation results (Table 194). The error map showed lower error in Hudson Bay and Baffin Bay compared with Davis Strait, with higher error along the edges of the study extent and in Lancaster Sound (Figure 484). The kriged surface is presented in Figure 485.

Table 193. Distributional properties of Spring Ice Cover Average Maximum.

| **Property** | **Value** |
|---|---:|
| Number of Observations | 526 |
| Minimum | 0.000 |
| Maximum | 1.000 |
| Mean | 0.633 |
| Median | 0.921 |
| Standard Deviation | 0.432 |
| Skewness | -0.636 |
| Kurtosis | 1.525 |

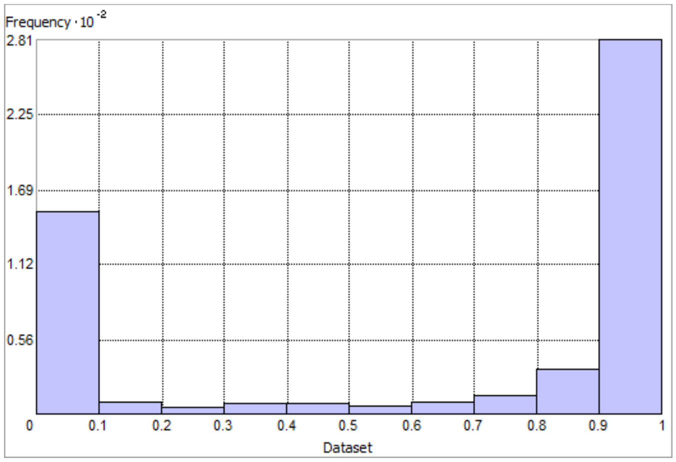

Figure 481. Distribution of Spring Ice Cover Average Maximum. Histogram was illustrated using 10 bins. Y axis is shown at $10^{-2}$.

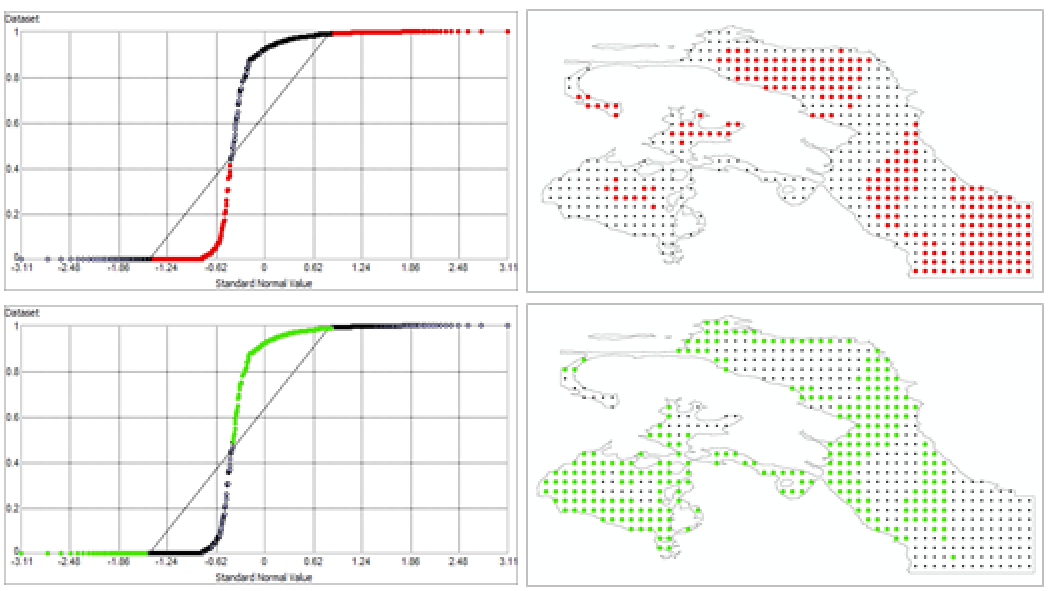


Figure 482. Normal Q-Q plot for data values of Spring Ice Cover Average Maximum. Points falling under (top right panel) and over (bottom right panel) the reference line are mapped.

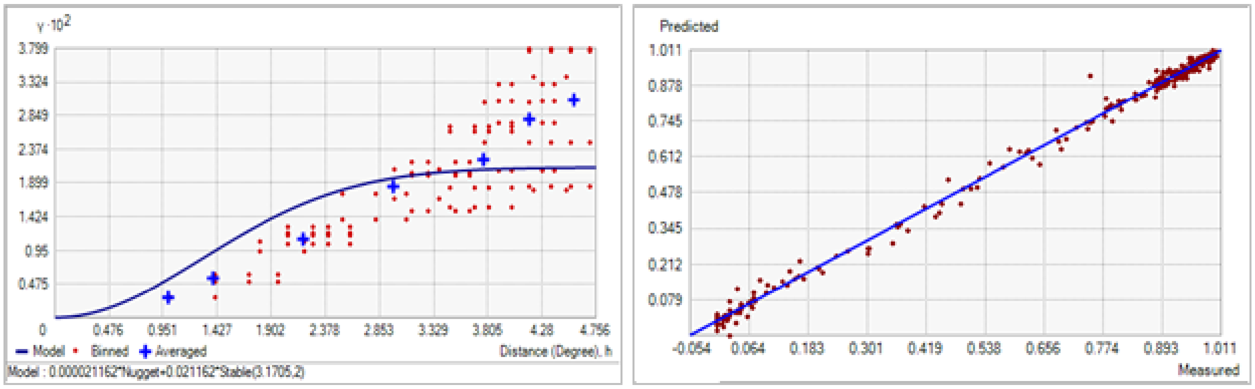


Figure 483. Left panel: Semivariogram of Spring Ice Cover Average Maximum. Binned values are shown as red dots; average points are shown as blue crosses; the model fit to the averaged values is shown as a blue line. Lag size: 0.396 degrees; number of lags: 12; Parameter: 2; Range: 3.170 degrees; Partial Sill: 0.021. Right panel: Scatterplot of predicted values versus observed values for the model of Spring Ice Cover Average Maximum.

Table 194. Results of cross-validation of the kriged model for Spring Ice Cover Average Maximum.

| **Prediction Error** | **Value** |
|---|---:|
| Number of Observations | 526 |
| Overall Mean Error | $2.166 \times 10^{-4}$ |
| Root Mean Square Prediction Error | 0.017 |
| Standardized Mean | -0.015 |
| Standardized Root Mean Square Prediction Error | 0.822 |
| Average Standard Error | 0.031 |

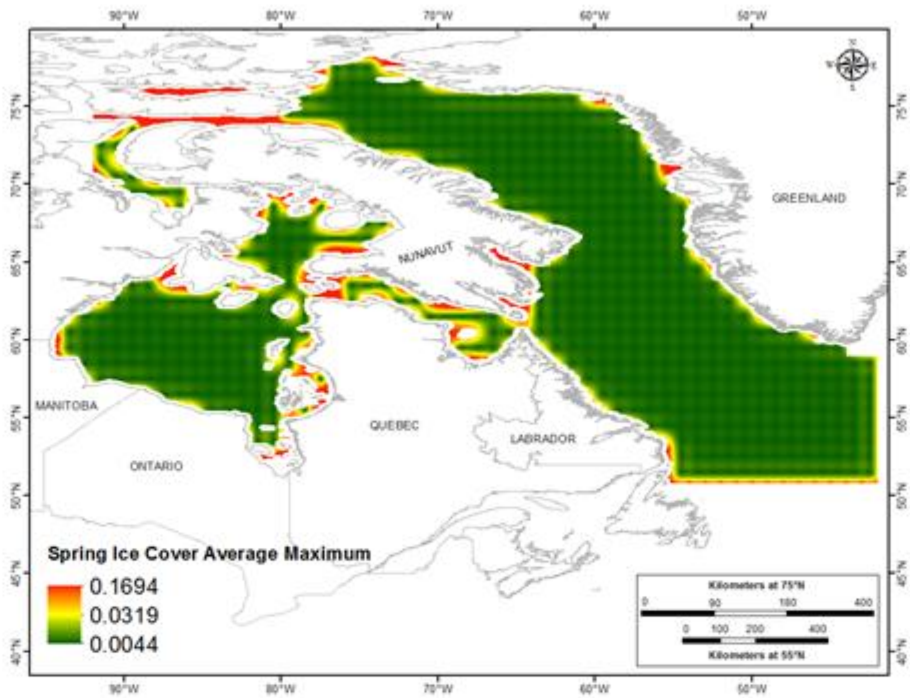


Figure 484. Prediction standard error surface of Spring Ice Cover Average Maximum.

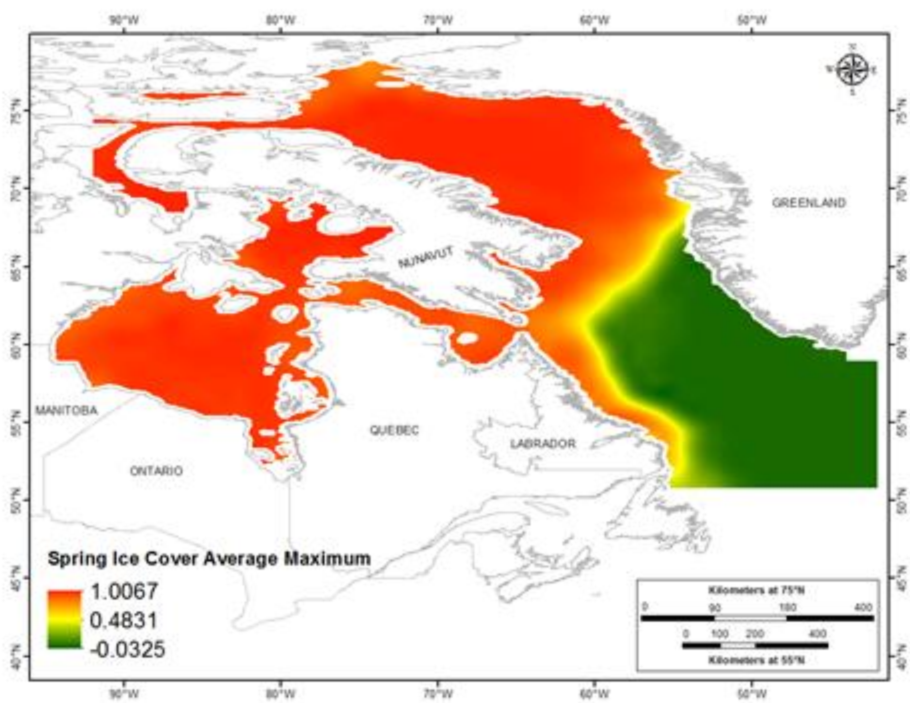


Figure 485. Interpolated prediction surface of Spring Ice Cover Average Maximum.

## Spring Ice Cover Average Range

This variable displayed a right-skewed, platykurtic distribution prior to interpolation (Table 195, Figure 486). The data were higher than predicted by a normal distribution at the lowest and upper mid-values, and were lower than predicted at the highest and lower mid-values (Figure 487). These areas of over and under-prediction showed spatial pattern over the region (Figure 487).

The semivariogram showed moderate autocorrelation present in the data (Figure 488). The kriged model showed a good fit between measured and predicted values (Figure 488). Good performance of the model was indicated by the cross-validation results (Table 196). The error map showed low error over much of the study extent with higher error in Lancaster Sound and along some coastal regions (Figure 489). The kriged surface is presented in Figure 490.

Table 195. Distributional properties of Spring Ice Cover Average Range.

| Property | Value |
|---|---:|
| Number of Observations | 526 |
| Minimum | 0.000 |
| Maximum | 0.856 |
| Mean | 0.233 |
| Median | 0.166 |
| Standard Deviation | 0.228 |
| Skewness | 0.738 |
| Kurtosis | 2.375 |

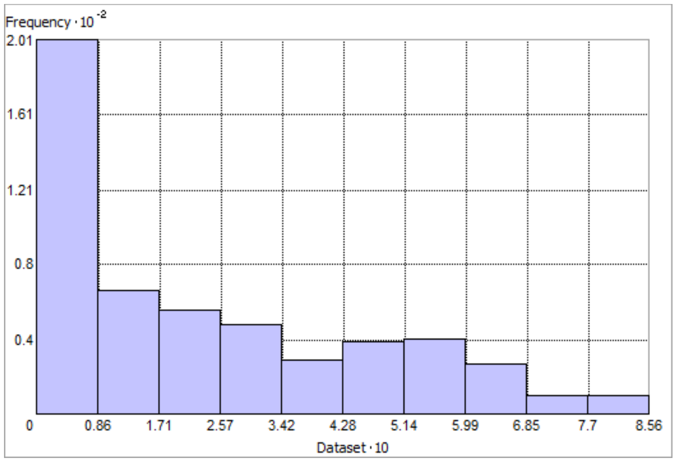


Figure 486. Distribution of Spring Ice Cover Average Range. Histogram was illustrated using 10 bins. X axis is shown at 10; Y axis is shown at $10^{-2}$.

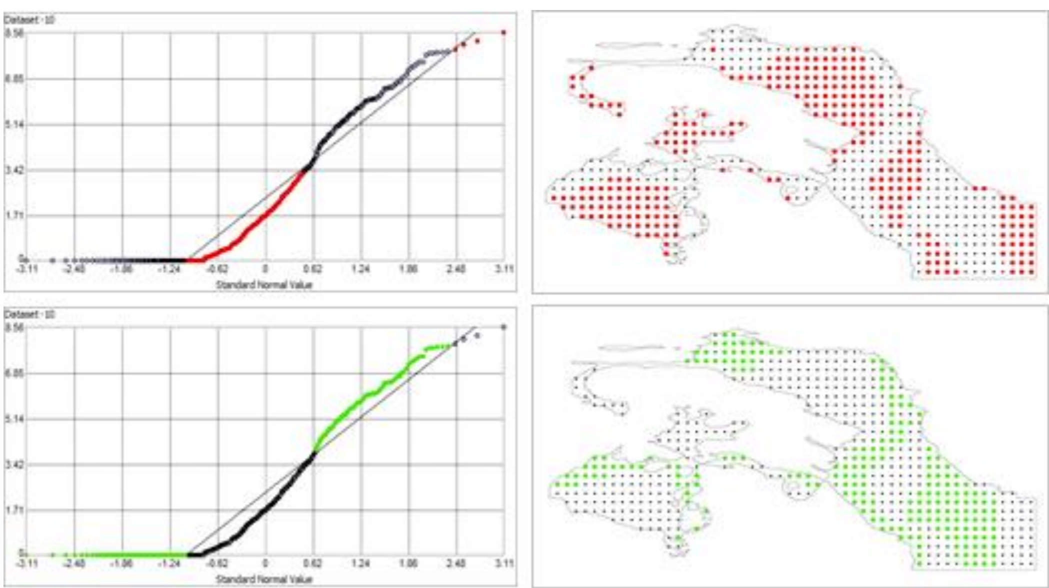

Figure 487. Normal Q-Q plot for data values of Spring Ice Cover Average Range. Points falling under (top right panel) and over (bottom right panel) the reference line are mapped.

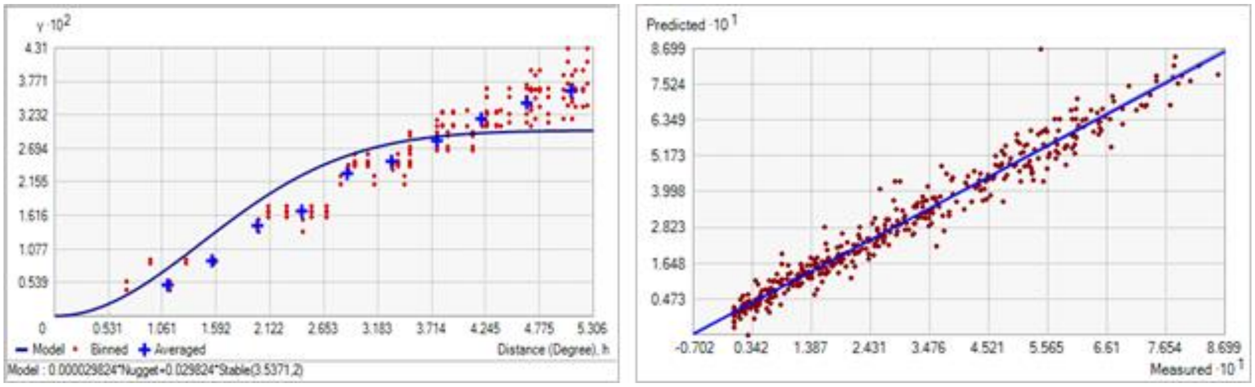


Figure 488. Left panel: Semivariogram of Spring Ice Cover Average Range. Binned values are shown as red dots; average points are shown as blue crosses; the model fit to the averaged values is shown as a blue line. Lag size: 0.442 degrees; number of lags: 12; Parameter: 2; Range: 3.537 degrees; Partial Sill: 0.030. Right panel: Scatterplot of predicted values versus observed values for the model of Spring Ice Cover Average Range.

Table 196. Results of cross-validation of the kriged model for Spring Ice Cover Average Range.

| **Prediction Error** | **Value** |
|---|---:|
| Number of Observations | 526 |
| Overall Mean Error | $4.853 \times 10^{-4}$ |
| Root Mean Square Prediction Error | 0.038 |
| Standardized Mean | -0.037 |
| Standardized Root Mean Square Prediction Error | 1.691 |
| Average Standard Error | 0.031 |

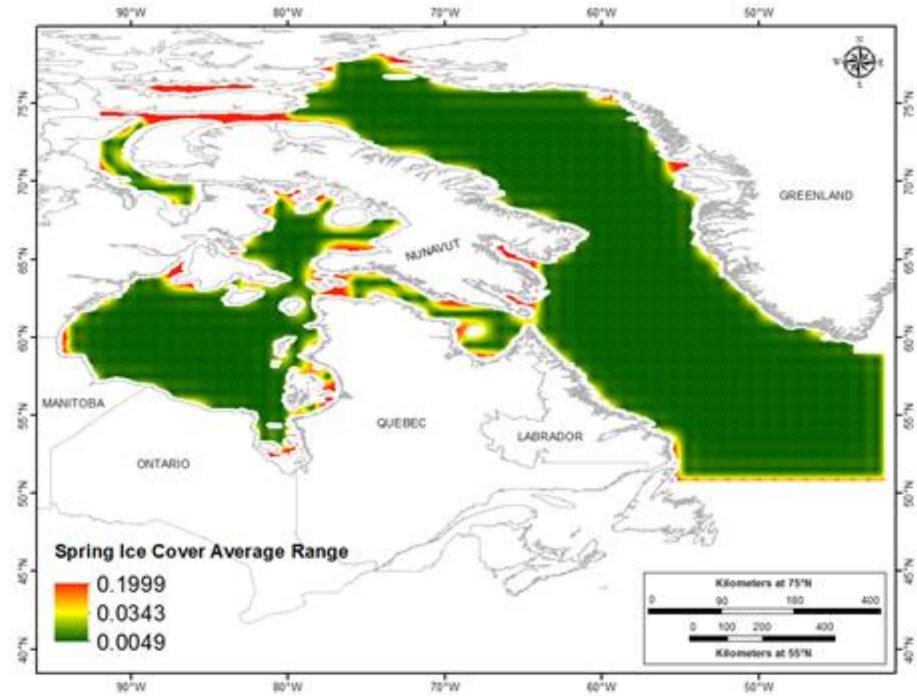

Figure 489. Prediction standard error surface of Spring Ice Cover Average Range.

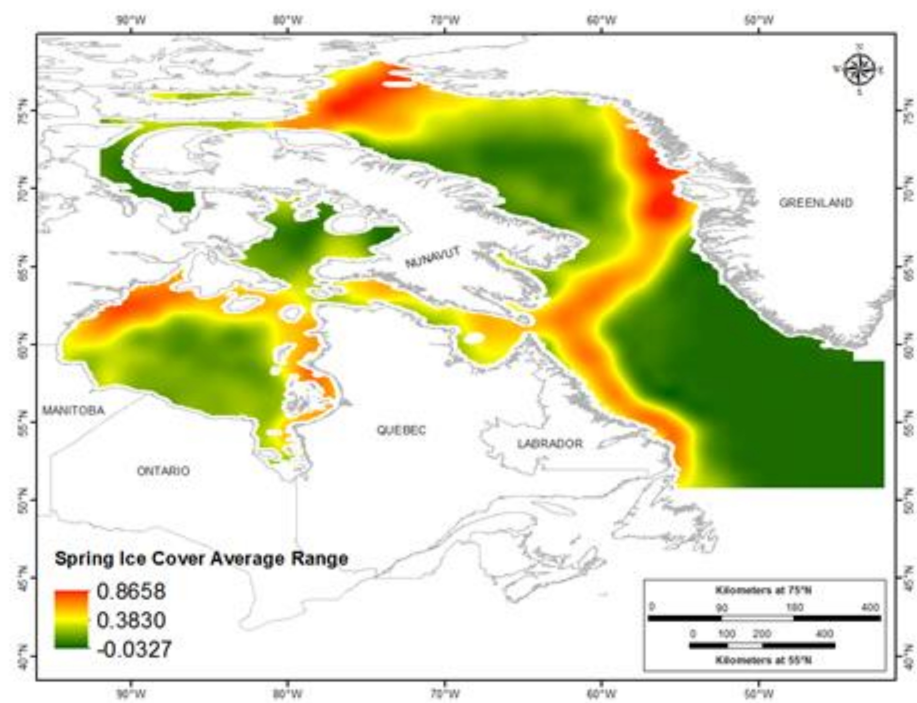

Figure 490. Interpolated prediction surface of Spring Ice Cover Average Range.

**Fall Ice Cover Mean**

This variable displayed a right-skewed, platykurtic distribution prior to interpolation (Table 197, Figure 491). The data were higher than predicted by a normal distribution at the lowest and upper mid-values, and were lower than predicted at the highest and lower mid-values (Figure 492). These areas of over and under-prediction showed spatial pattern over the region (Figure 492).

The semivariogram showed relatively weak autocorrelation present in the data (Figure 493). The kriged model showed good fit between measured and predicted values (Figure 493). Fair to poor performance of the model was indicated by the cross-validation results (Table 198), with underestimation of the variability in the predictions as indicated by the Standardized Root-Mean-Square Error higher than 1. The error map showed low error in all the study extent, with higher error in Lancaster Sound and other coastal regions (Figure 494). The kriged surface is presented in Figure 495.

Table 197. Distributional properties of Fall Ice Cover Mean.

| **Property** | **Value** |
|---|---:|
| Number of Observations | 526 |
| Minimum | 0.000 |
| Maximum | 0.856 |
| Mean | 0.256 |
| Median | 0.234 |
| Standard Deviation | 0.257 |
| Skewness | 0.552 |
| Kurtosis | 2.035 |

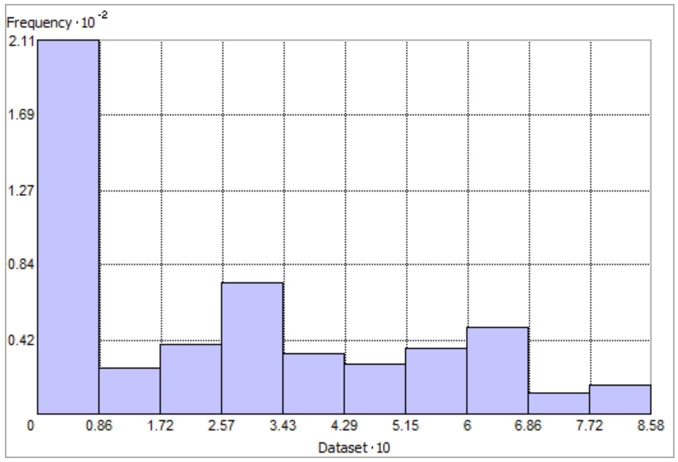


Figure 491. Distribution of Fall Ice Cover Mean. Histogram was illustrated using 10 bins. X axis is shown at 10; Y axis is shown at $10^{-2}$.

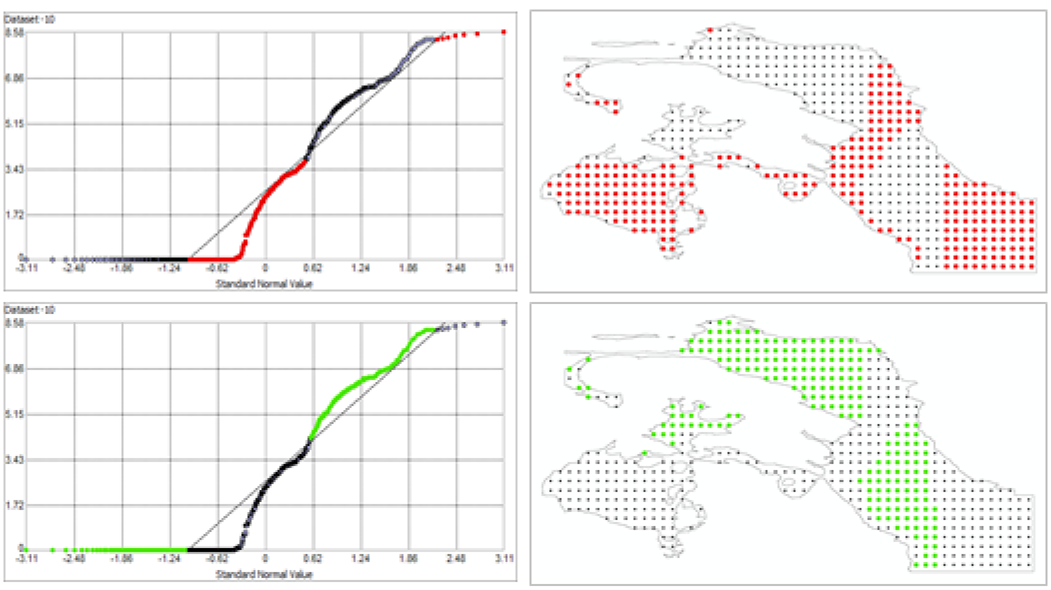


Figure 492. Normal Q-Q plot for data values of Fall Ice Cover Mean. Points falling under (top right panel) and over (bottom right panel) the reference line are mapped.

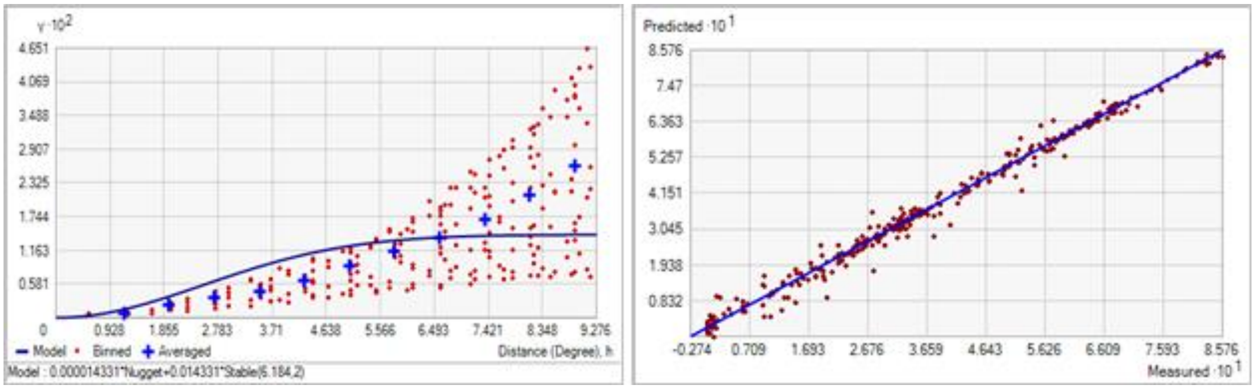


Figure 493. Left panel: Semivariogram of Fall Ice Cover Mean. Binned values are shown as red dots; average points are shown as blue crosses; the model fit to the averaged values is shown as a blue line. Lag size: 0.773 degrees; number of lags: 12; Parameter: 2; Range: 6.184 degrees; Partial Sill: 0.014. Right panel: Scatterplot of predicted values versus observed values for the model of Fall Ice Cover Mean.

Table 198. Results of cross-validation of the kriged model for Fall Ice Cover Mean.

| **Prediction Error** | **Value** |
|---|---:|
| Number of Observations | 526 |
| Overall Mean Error | $-1.876 \times 10^{-4}$ |
| Root Mean Square Prediction Error | 0.019 |
| Standardized Mean | -0.016 |
| Standardized Root Mean Square Prediction Error | 2.610 |
| Average Standard Error | $7.427 \times 10^{-3}$ |

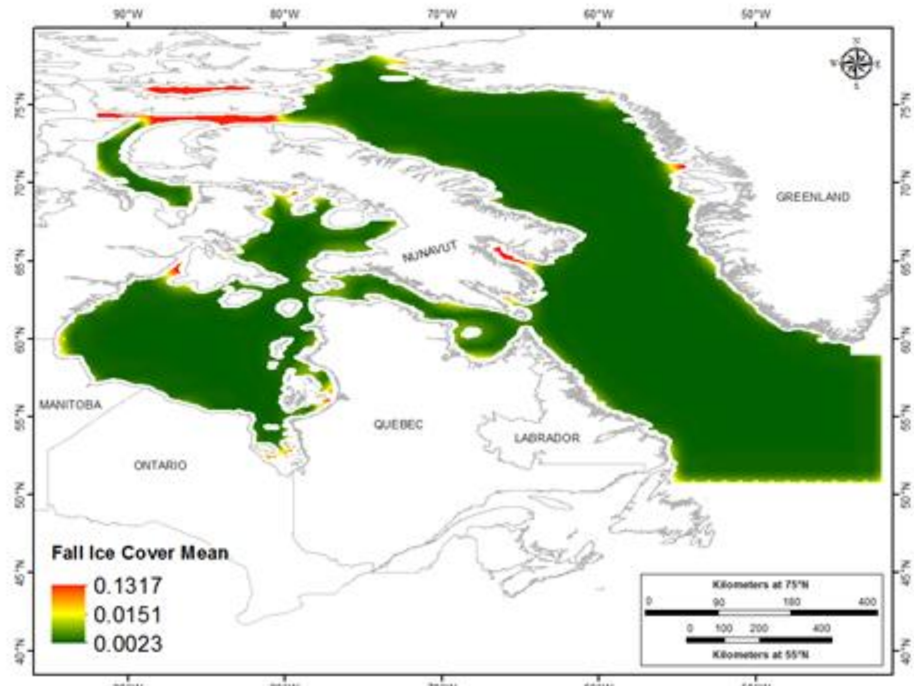


Figure 494. Prediction standard error surface of Fall Ice Cover Mean.

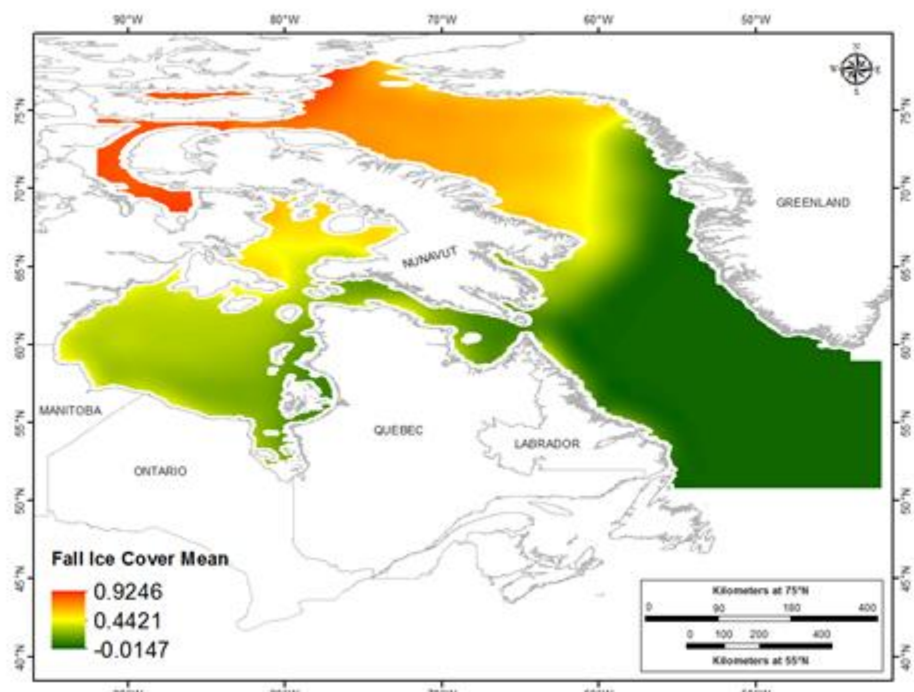


Figure 495. Interpolated prediction surface of Fall Ice Cover Mean.

## Fall Ice Cover Minimum

This variable displayed an extremely right-skewed, leptokurtic distribution with outlying data in the upper range prior to interpolation (Table 199, Figure 496). The data were higher than predicted by a normal distribution at both tails, and were lower than predicted at mid-values (Figure 497). These areas of over and under-prediction showed strong spatial pattern over the region (Figure 497).

The semivariogram showed autocorrelation present in the data (Figure 498). The kriged model showed poor fit between measured and predicted values (Figure 498). Nonetheless, good performance of the model was indicated by the cross-validation results (Table 200). The error map showed a "bullseye" pattern with error increasing with distance from data points (Figure 499). The kriged surface is presented in Figure 500.

Table 199. Distributional properties of Fall Ice Cover Minimum.

| **Property** | **Value** |
|---|---:|
| Number of Observations | 526 |
| Minimum | 0.000 |
| Maximum | 0.500 |
| Mean | $3.441 \times 10^{-3}$ |
| Median | 0.000 |
| Standard Deviation | 0.033 |
| Skewness | 11.152 |
| Kurtosis | 141.560 |

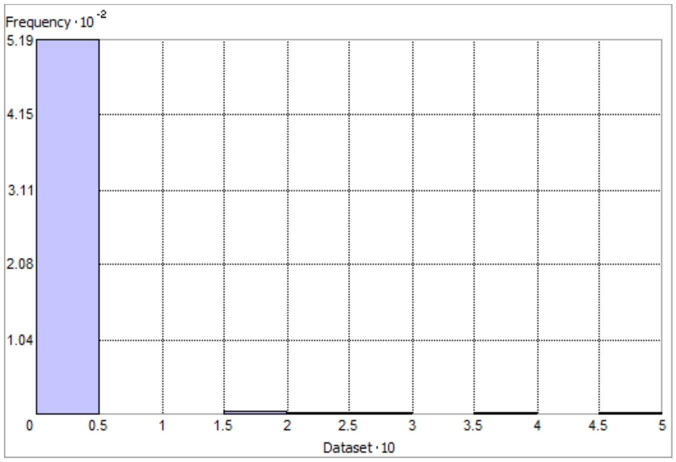


Figure 496. Distribution of Fall Ice Cover Minimum. Histogram was illustrated using 10 bins. X axis is shown at 10; Y axis is shown at $10^{-2}$.

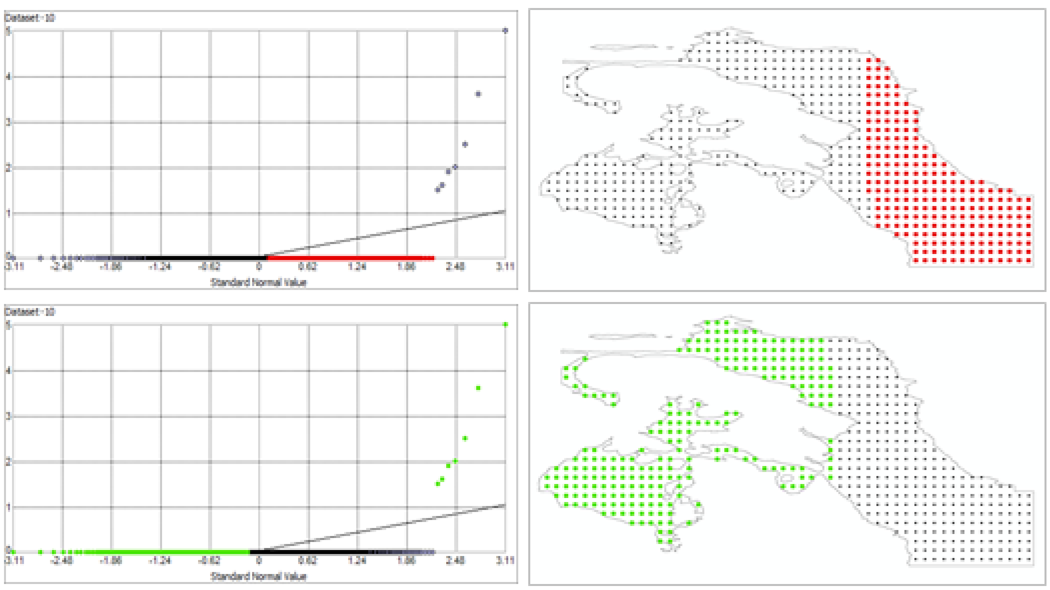

Figure 497. Normal Q-Q plot for data values of Fall Ice Cover Minimum. Points falling under (top right panel) and over (bottom right panel) the reference line are mapped.

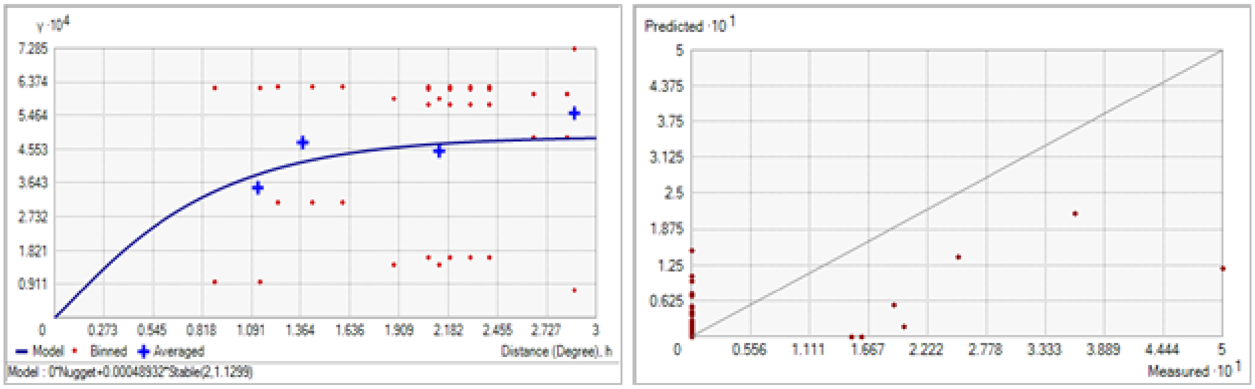


Figure 498. Left panel: Semivariogram of Fall Ice Cover Minimum. Binned values are shown as red dots; average points are shown as blue crosses; the model fit to the averaged values is shown as a blue line. Lag size: 0.250 degrees; number of lags: 12; Parameter: 1.130; Range: 2 degrees; Partial Sill: 4.893 x $10^{-4}$. Right panel: Scatterplot of predicted values versus observed values for the model of Fall Ice Cover Minimum.

Table 200. Results of cross-validation of the kriged model for Fall Ice Cover Minimum.

| **Prediction Error** | **Value** |
|---|---:|
| Number of Observations | 526 |
| Overall Mean Error | -4.107 x $10^{-4}$ |
| Root Mean Square Prediction Error | 0.026 |
| Standardized Mean | -0.015 |
| Standardized Root Mean Square Prediction Error | 1.205 |
| Average Standard Error | 0.020 |

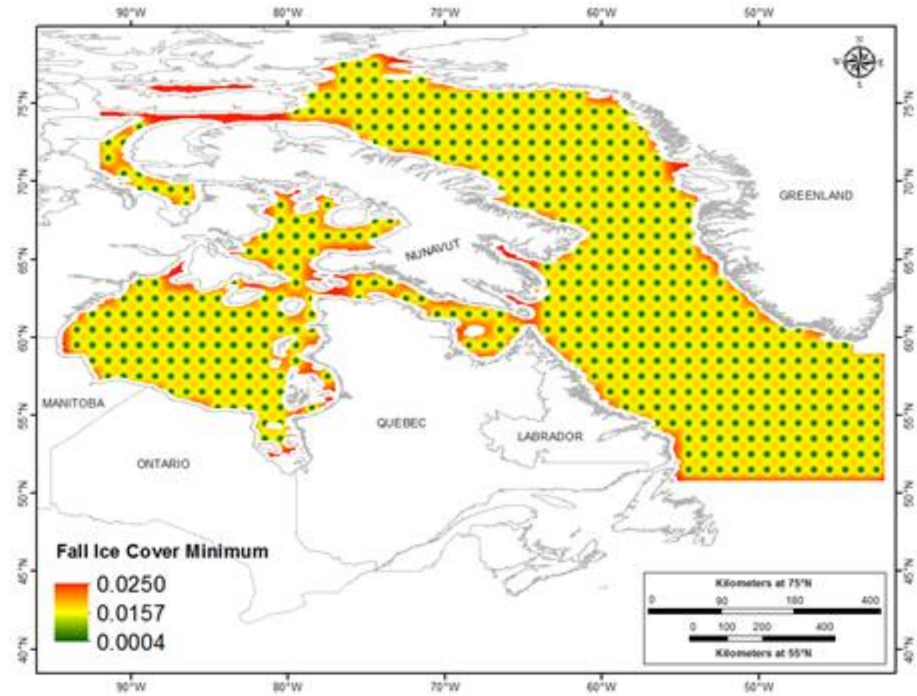


Figure 499. Prediction standard error surface of Fall Ice Cover Minimum.

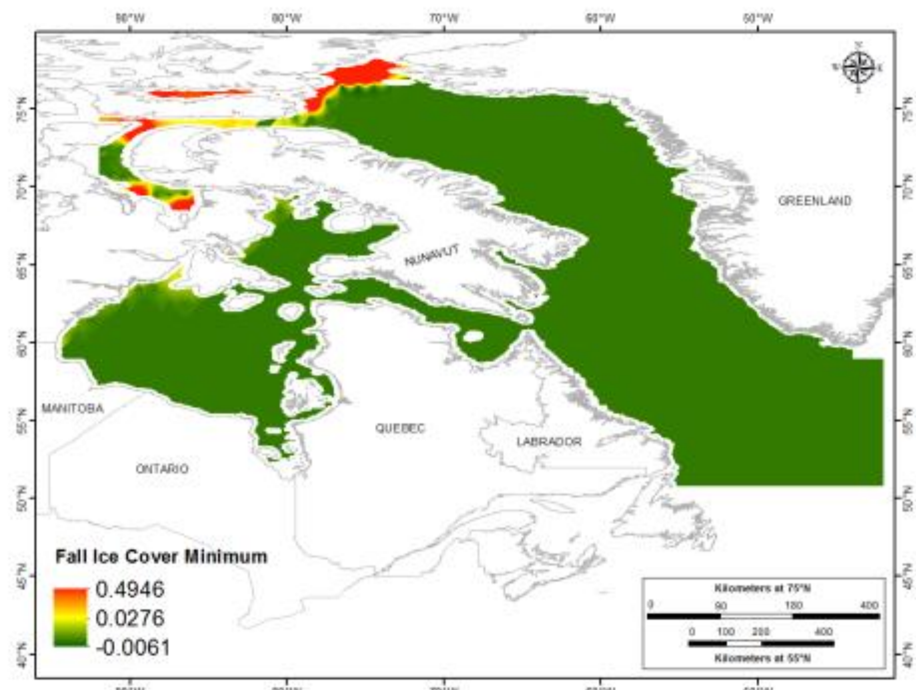


Figure 500. Interpolated prediction surface of Fall Ice Cover Minimum.

## Fall Ice Cover Maximum

This variable displayed a bimodal, platykurtic distribution prior to interpolation (Table 201, Figure 501). The data were greater than predicted by a normal distribution at the lowest and upper mid-range values, and lower than predicted at the highest and lower mid-range values (Figure 502). These areas of over and under-prediction showed a strong spatial pattern over the region (Figure 502).

The semivariogram showed autocorrelation present in the data (Figure 503). The kriged model showed good fit between measured and predicted values (Figure 503). Poor performance of the model was indicated by the cross-validation results (Table 202), with a Standardized Root-Mean-Square Error higher than 1, indicating that variability in the predictions was underestimated. The error map showed lower error across the study extent, with high error in Lancaster Sound and other coastal areas (Figure 504). The kriged surface is presented in Figure 505.

Table 201. Distributional properties of Fall Ice Cover Maximum.

| **Property** | **Value** |
|---|---:|
| Number of Observations | 526 |
| Minimum | 0.000 |
| Maximum | 1.000 |
| Mean | 0.601 |
| Median | 0.935 |
| Standard Deviation | 0.459 |
| Skewness | -0.469 |
| Kurtosis | 1.304 |

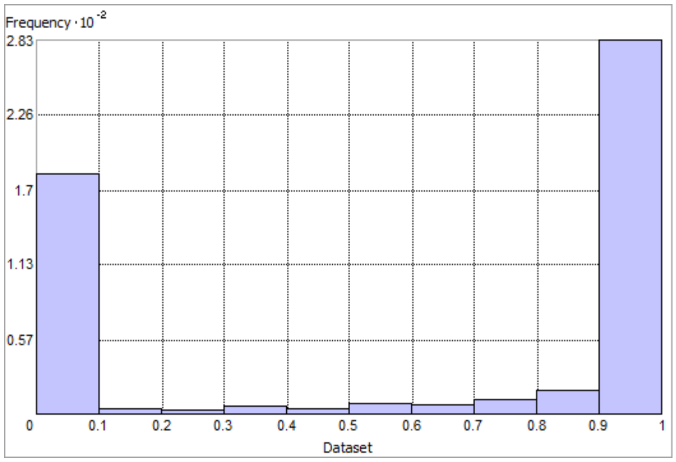


Figure 501. Distribution of Fall Ice Cover Maximum. Histogram was illustrated using 10 bins. Y axis is shown at $10^{-2}$.

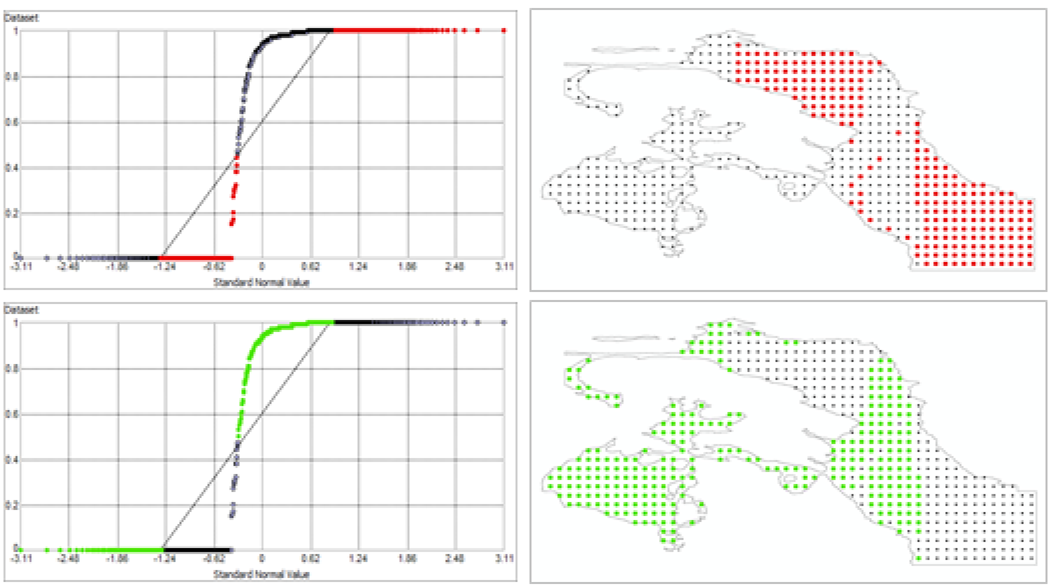


Figure 502. Normal Q-Q plot for data values of Fall Ice Cover Maximum. Points falling under (top right panel) and over (bottom right panel) the reference line are mapped.

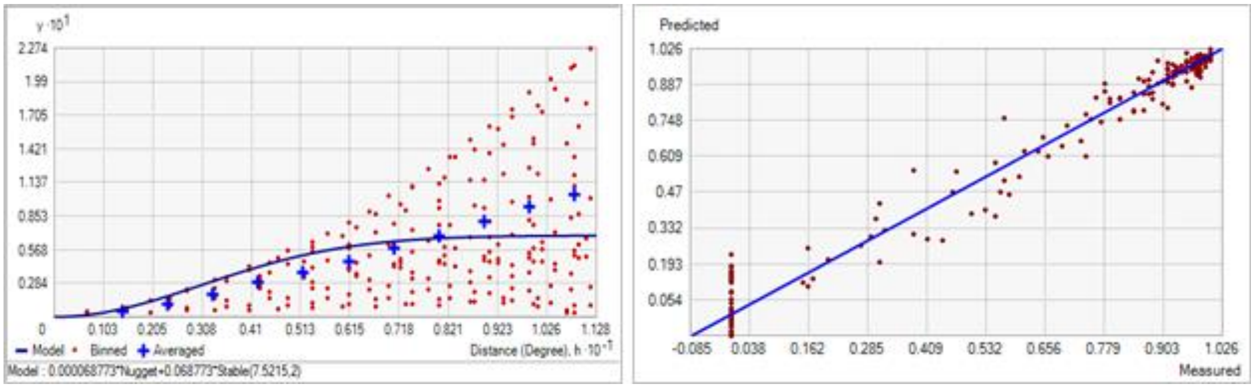

Figure 503. Left panel: Semivariogram of Fall Ice Cover Maximum. Binned values are shown as red dots; average points are shown as blue crosses; the model fit to the averaged values is shown as a blue line. Lag size: 0.940 degrees; number of lags: 12; Parameter: 2; Range: 7.521 degrees; Partial Sill: 0.069. Right panel: Scatterplot of predicted values versus observed values for the model of Fall Ice Cover Maximum.

Table 202. Results of cross-validation of the kriged model for Fall Ice Cover Maximum.

| Prediction Error | Value |
|---|---:|
| Number of Observations | 526 |
| Overall Mean Error | $9.188 \times 10^{-4}$ |
| Root Mean Square Prediction Error | 0.037 |
| Standardized Mean | 0.043 |
| Standardized Root Mean Square Prediction Error | 3.380 |
| Average Standard Error | 0.013 |

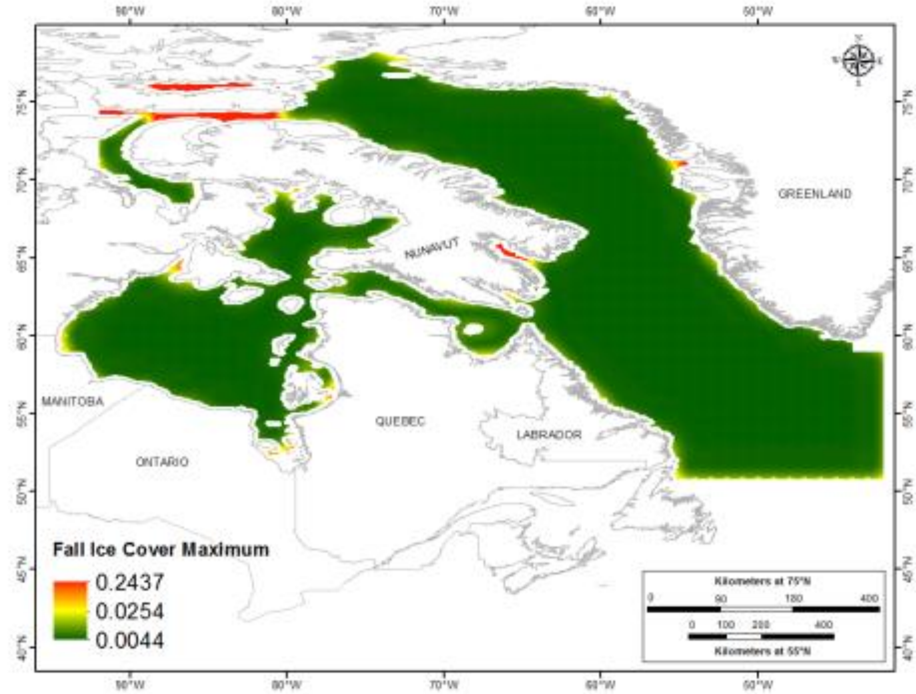


Figure 504. Prediction standard error surface of Fall Ice Cover Maximum.

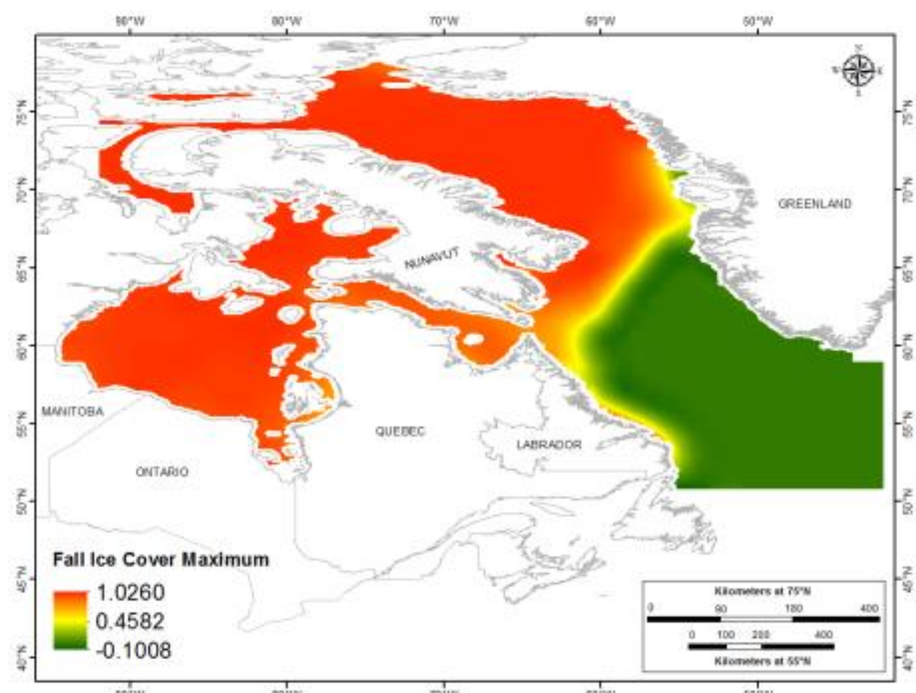


Figure 505. Interpolated prediction surface of Fall Ice Cover Maximum.

**Fall Ice Cover Range**

This variable displayed a bimodal, platykurtic distribution prior to interpolation (Table 203, Figure 506). The data were greater than predicted by a normal distribution at the lowest and upper mid-range values, and lower than predicted at the highest and lower mid-range values (Figure 507). These areas of over and under-prediction showed spatial pattern over the region (Figure 507).

The semivariogram showed autocorrelation present in the data (Figure 508). The kriged model showed good fit between measured and predicted values (Figure 508). Poor performance of the model was indicated by the cross-validation results (Table 204), with a Standardized Root-Mean-Square Error higher than 1, indicating that variability in the predictions was underestimated. The error map showed lower error across the study extent, with high error in Lancaster Sound and other coastal areas (Figure 509). The kriged surface is presented in Figure 510.

Table 203. Distributional properties of Fall Ice Cover Range.

| **Property** | **Value** |
|---|---:|
| Number of Observations | 526 |
| Minimum | 0.000 |
| Maximum | 1.000 |
| Mean | 0.598 |
| Median | 0.920 |
| Standard Deviation | 0.457 |
| Skewness | -0.459 |
| Kurtosis | 1.303 |

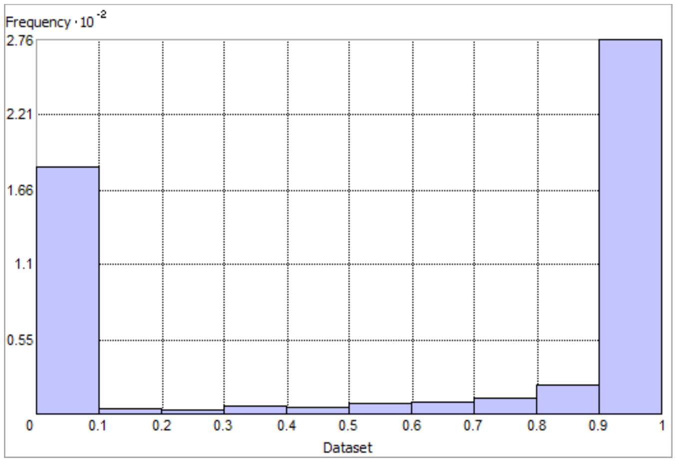


Figure 506. Distribution of Fall Ice Cover Range. Histogram was illustrated using 10 bins. Y axis is shown at $10^{-2}$.

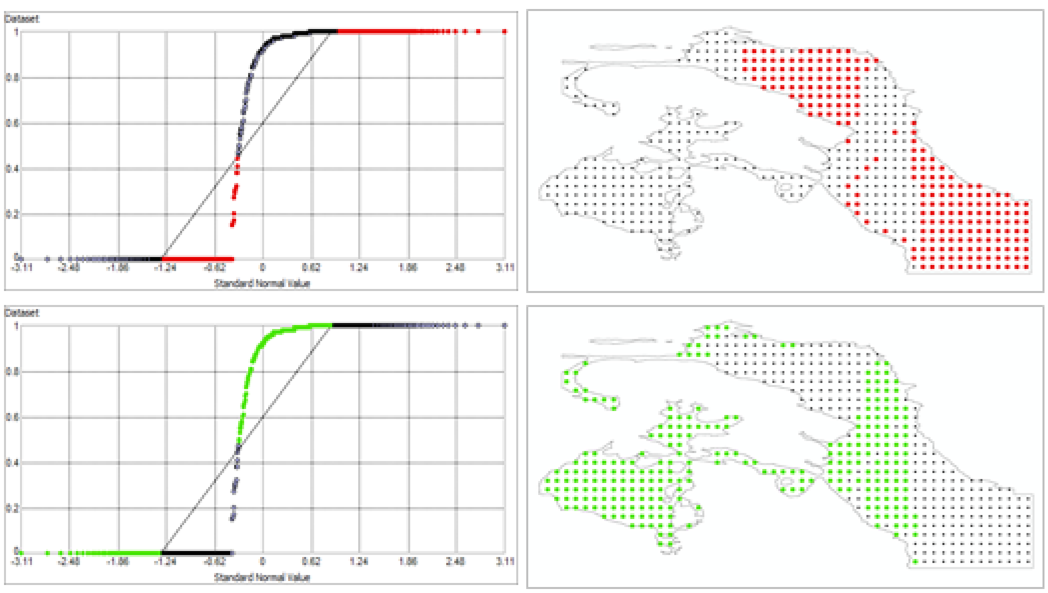

Figure 507. Normal Q-Q plot for data values of Fall Ice Cover Range. Points falling under (top right panel) and over (bottom right panel) the reference line are mapped.

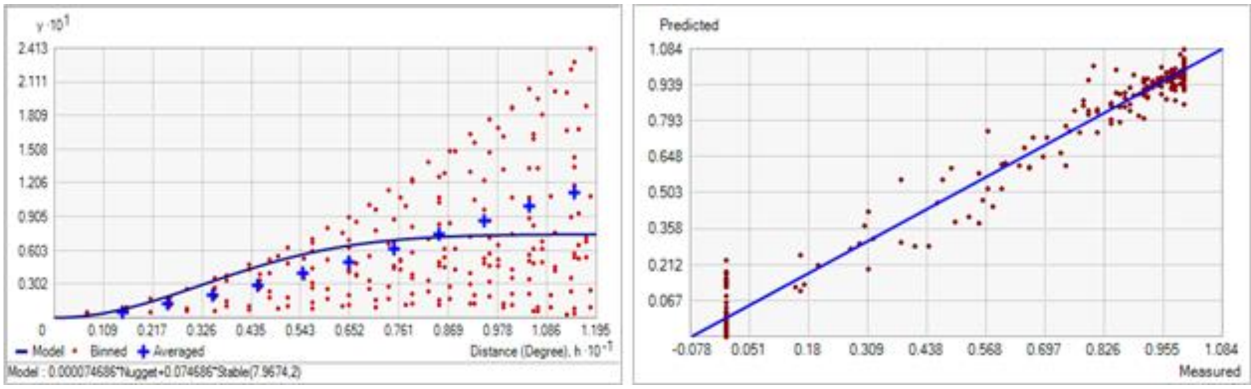

Figure 508. Left panel: Semivariogram of Fall Ice Cover Range. Binned values are shown as red dots; average points are shown as blue crosses; the model fit to the averaged values is shown as a blue line. Lag size: 0.996 degrees; number of lags: 12; Parameter: 2; Range: 7.967 degrees; Partial Sill: 0.075. Right panel: Scatterplot of predicted values versus observed values for the model of Fall Ice Cover Range.

Table 204. Results of cross-validation of the kriged model for Fall Ice Cover Range.

| **Prediction Error** | **Value** |
|---|---|
| Number of Observations | 526 |
| Overall Mean Error | $1.485 \times 10^{-3}$ |
| Root Mean Square Prediction Error | 0.042 |
| Standardized Mean | 0.057 |
| Standardized Root Mean Square Prediction Error | 3.480 |
| Average Standard Error | 0.013 |

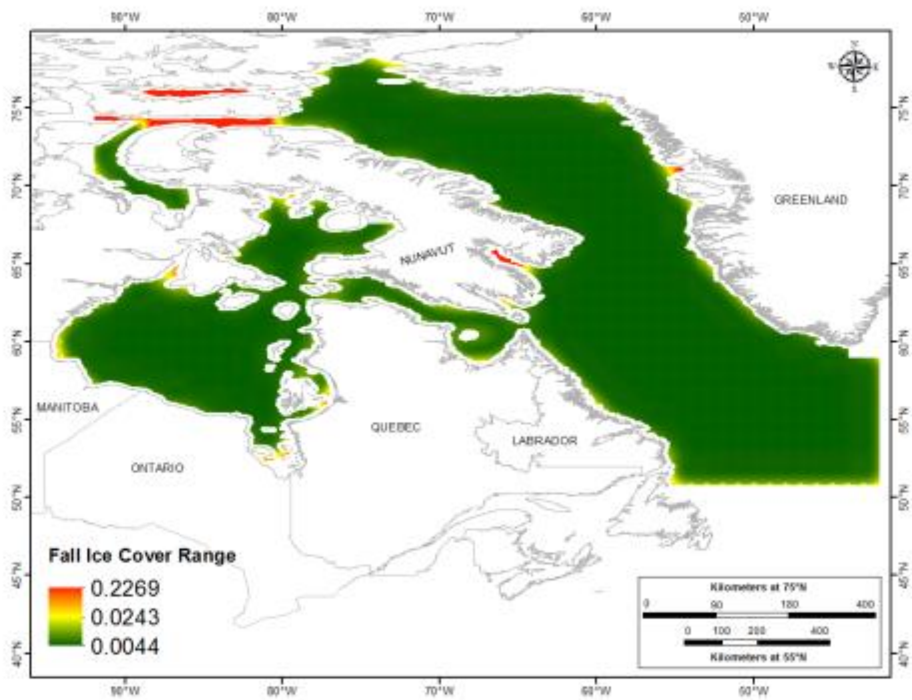


Figure 509. Prediction standard error surface of Fall Ice Cover Range.

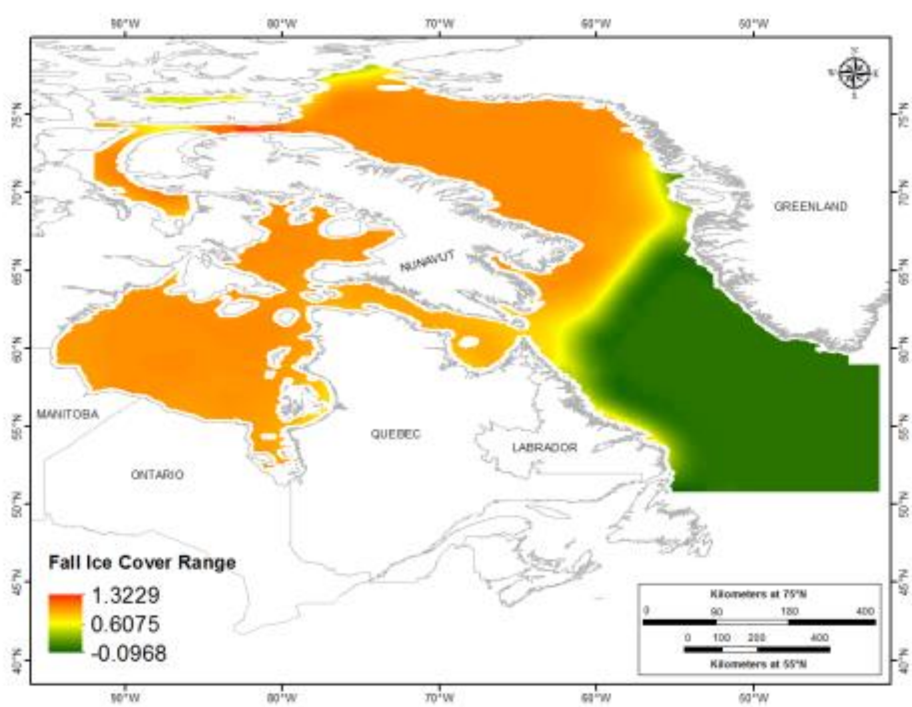


Figure 510. Interpolated prediction surface of Fall Ice Cover Range.

**Fall Ice Cover Average Minimum**

This variable displayed an extremely right-skewed, leptokurtic distribution prior to interpolation (Table 205, Figure 511). The data were higher than predicted by a normal distribution at both tails, while mid-values were lower than the reference line (Figure 512). These areas of under- and over-prediction showed a strong spatial pattern over the region (Figure 512).

The semivariogram showed autocorrelation present in the data (Figure 513). The kriged model showed good fit between measured and predicted values (Figure 513). Good performance of the model was indicated by the cross-validation results (Table 206). The error map showed lower error across the study extent, with high error in Lancaster Sound and other coastal areas (Figure 514).The kriged surface is presented in Figure 515.

Table 205. Distributional properties of Fall Ice Cover Average Minimum.

| **Property** | **Value** |
|---|---:|
| Number of Observations | 526 |
| Minimum | 0.000 |
| Maximum | 0.773 |
| Mean | 0.039 |
| Median | 0.000 |
| Standard Deviation | 0.117 |
| Skewness | 3.980 |
| Kurtosis | 18.914 |

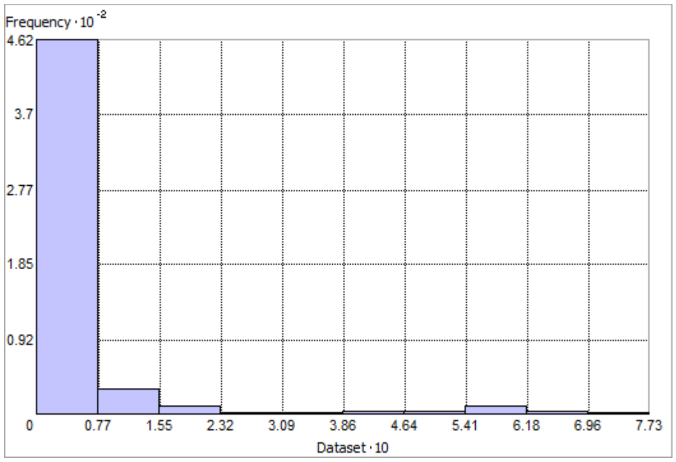

Figure 511. Distribution of Fall Ice Cover Average Minimum. Histogram was illustrated using 10 bins. X axis is shown at 10; Y axis is shown at $10^{-2}$.

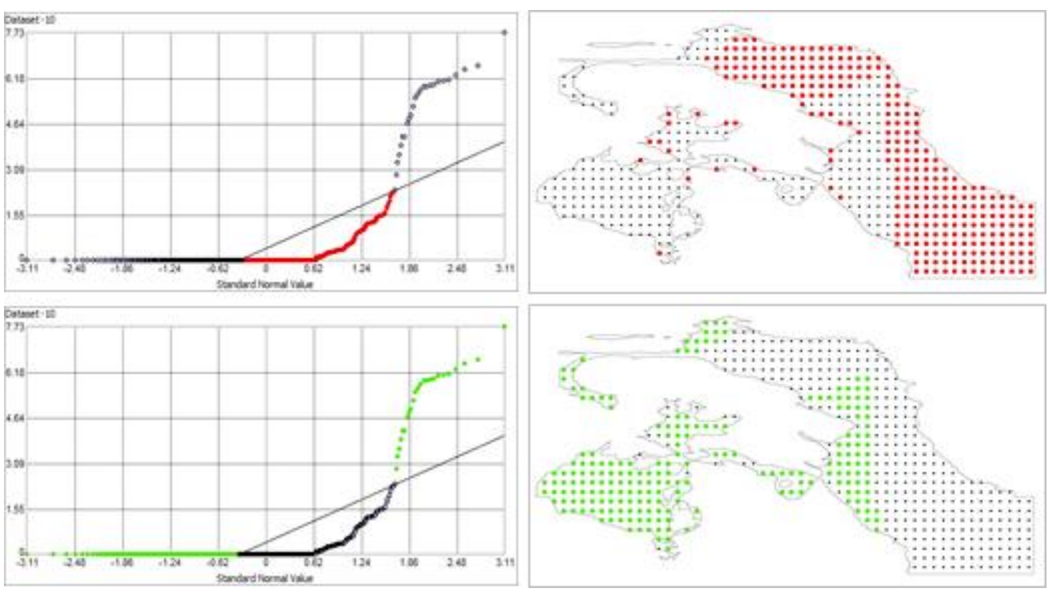
Figure 512. Normal Q-Q plot for data values of Fall Ice Cover Average Minimum. Points falling under (top right panel) and over (bottom right panel) the reference line are mapped.

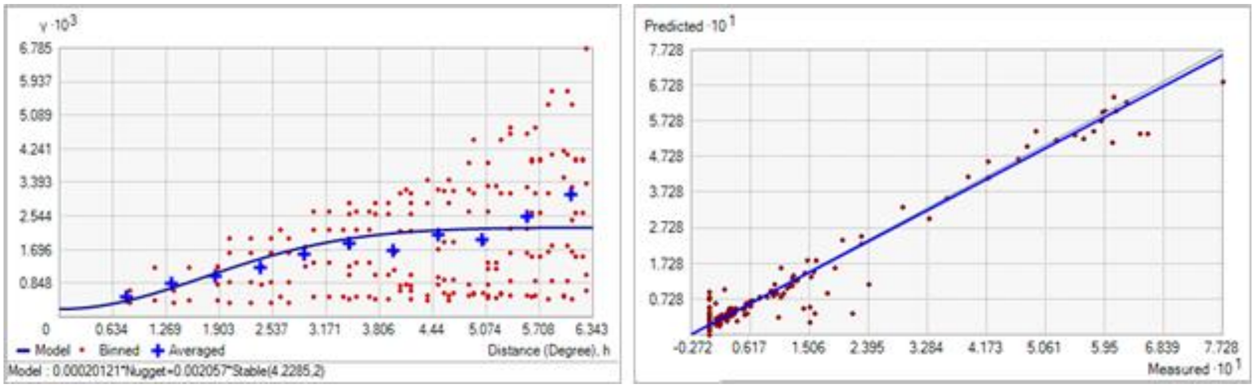


Figure 513. Left panel: Semivariogram of Fall Ice Cover Average Minimum. Binned values are shown as red dots; average points are shown as blue crosses; the model fit to the averaged values is shown as a blue line. Lag size: 0.529 degrees; number of lags: 12; Parameter: 2; Range: 4.228 degrees; Partial Sill: 2.057 x $10^{-3}$. Right panel: Scatterplot of predicted values versus observed values for the model of Fall Ice Cover Average Minimum.

Table 206. Results of cross-validation of the kriged model for Fall Ice Cover Average Minimum.

| **Prediction Error** | **Value** |
|---|---:|
| Number of Observations | 526 |
| Overall Mean Error | -4.291 x $10^{-4}$ |
| Root Mean Square Prediction Error | 0.022 |
| Standardized Mean | -0.010 |
| Standardized Root Mean Square Prediction Error | 1.052 |
| Average Standard Error | 0.018 |

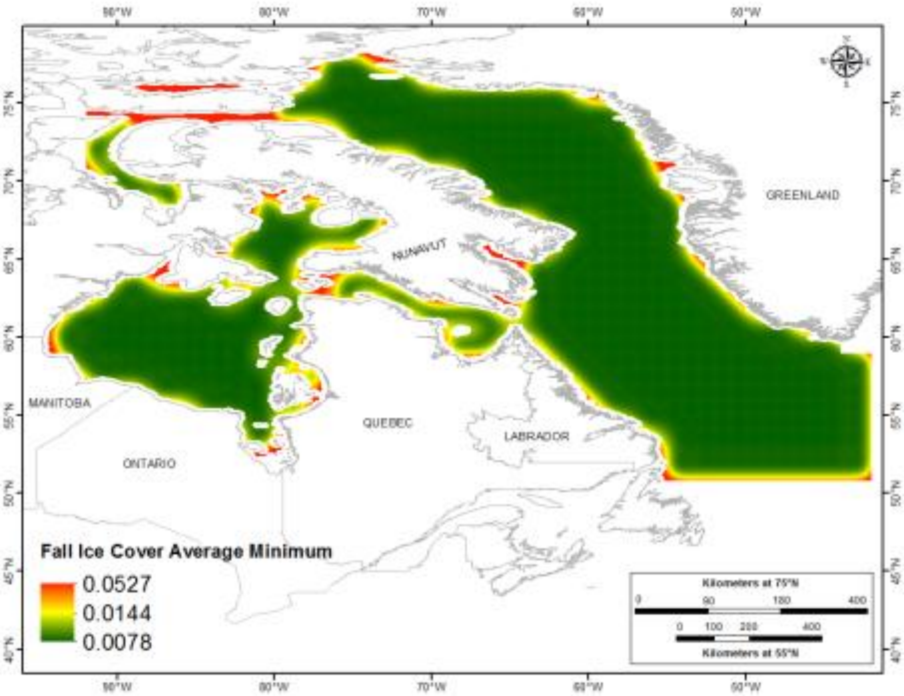


Figure 514. Prediction standard error surface of Fall Ice Cover Average Minimum.

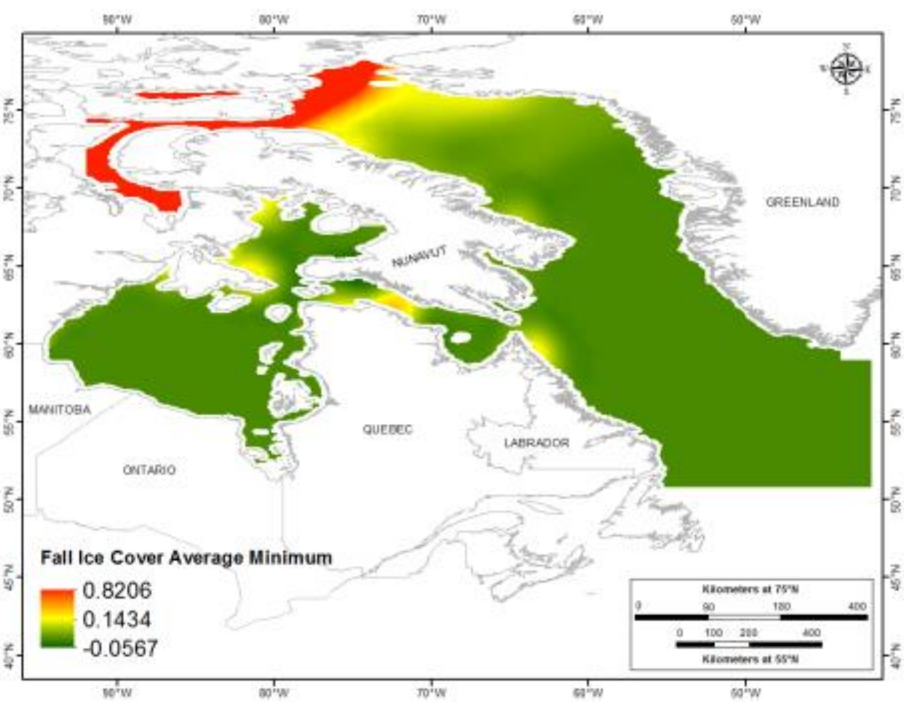


Figure 515. Interpolated prediction surface of Fall Ice Cover Average Minimum.

**Fall Ice Cover Average Maximum**

This variable displayed a bimodal, platykurtic distribution prior to interpolation (Table 207, Figure 516). The data were greater than predicted by a normal distribution at the lowest and upper mid-range values, and lower than predicted at the highest and lower mid-range values (Figure 517). These areas of under- and over-prediction showed spatial pattern over the region.

The semivariogram showed autocorrelation present in the data (Figure 518). The kriged model showed good fit between measured and predicted values (Figure 518). Fair to poor performance of the model was indicated by the cross-validation results (Table 208), with a Standardized Root-Mean-Square Error higher than 1, indicating that variability in the predictions was underestimated. The error map showed lower error across the study extent, with high error in Lancaster Sound and other coastal areas (Figure 519). The kriged surface is presented in Figure 520.

Table 207. Distributional properties of Fall Ice Cover Average Maximum.

| **Property** | **Value** |
|---|---:|
| Number of Observations | 526 |
| Minimum | 0.000 |
| Maximum | 0.997 |
| Mean | 0.500 |
| Median | 0.639 |
| Standard Deviation | 0.430 |
| Skewness | -0.141 |
| Kurtosis | 1.190 |

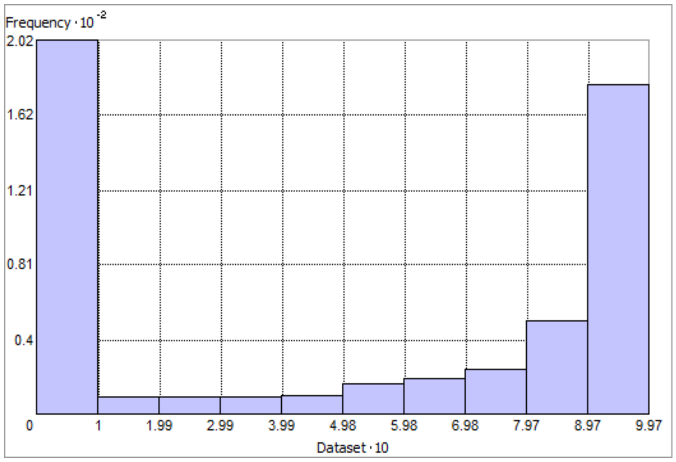


Figure 516. Distribution of Fall Ice Cover Average Maximum. Histogram was illustrated using 10 bins. X axis is shown at 10; Y axis is shown at $10^{-2}$.

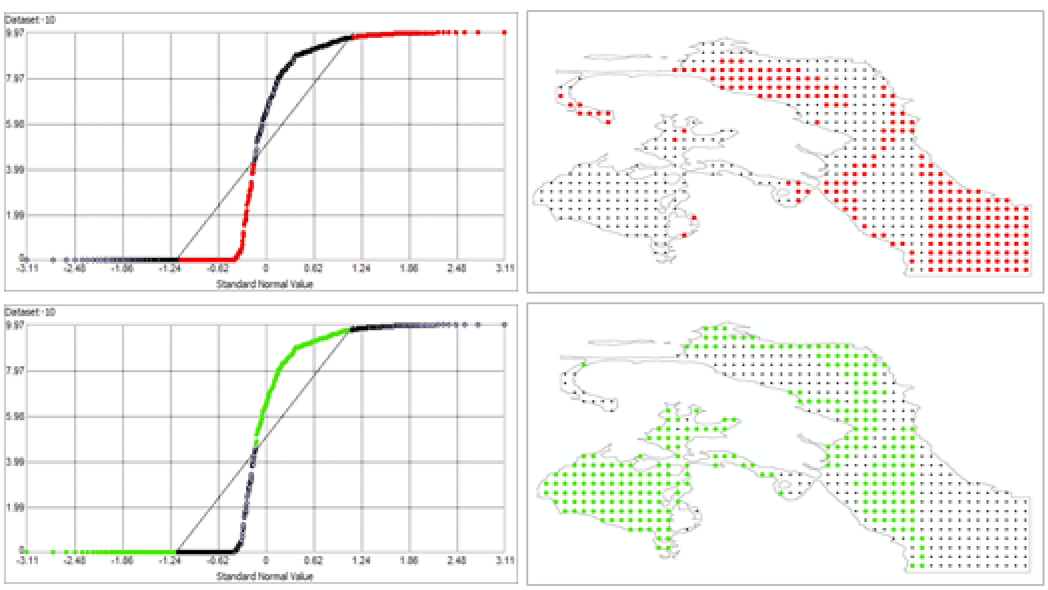

Figure 517. Normal Q-Q plot for data values of Fall Ice Cover Average Maximum. Points falling under (top right panel) and over (bottom right panel) the reference line are mapped.

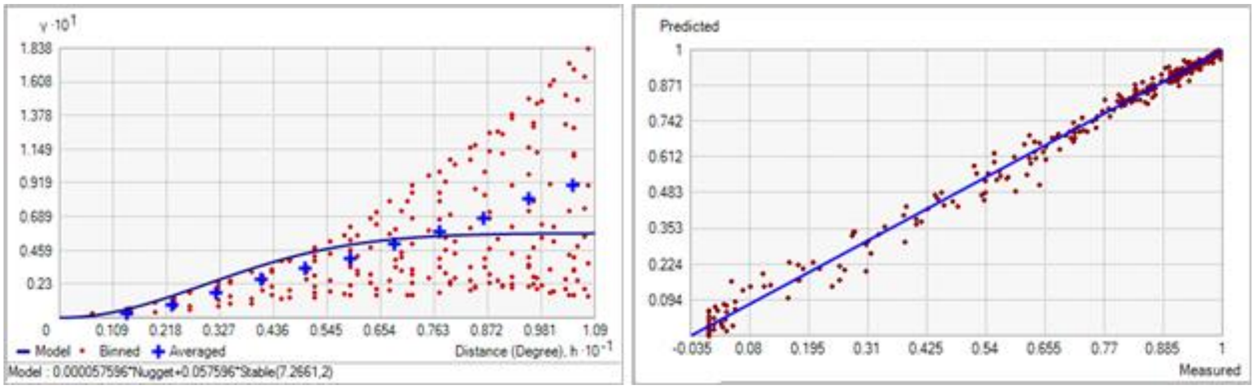

Figure 518. Left panel: Semivariogram of Fall Ice Cover Average Maximum. Binned values are shown as red dots; average points are shown as blue crosses; the model fit to the averaged values is shown as a blue line. Lag size: 0.908 degrees; number of lags: 12; Parameter: 2; Range: 7.266 degrees; Partial Sill: 0.058. Right panel: Scatterplot of predicted values versus observed values for the model of Fall Ice Cover Average Maximum.

Table 208. Results of cross-validation of the kriged model for Fall Ice Cover Average Maximum.

| **Prediction Error** | **Value** |
|---|---|
| Number of Observations | 526 |
| Overall Mean Error | $-2.995 \times 10^{-4}$ |
| Root Mean Square Prediction Error | 0.023 |
| Standardized Mean | $2.621 \times 10^{-3}$ |
| Standardized Root Mean Square Prediction Error | 1.970 |
| Average Standard Error | 0.012 |

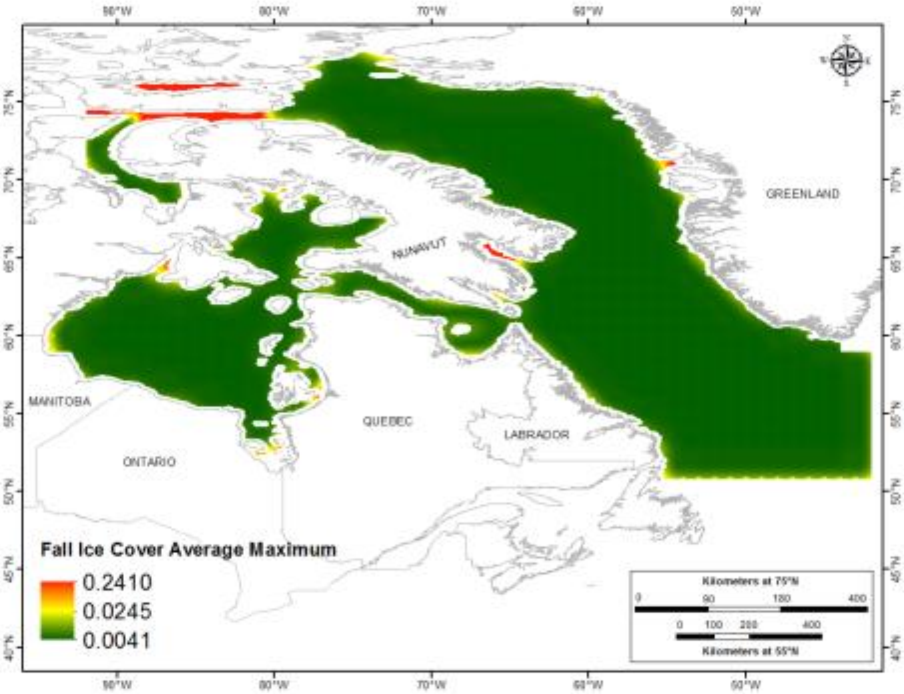


Figure 519. Prediction standard error surface of Fall Ice Cover Average Maximum.

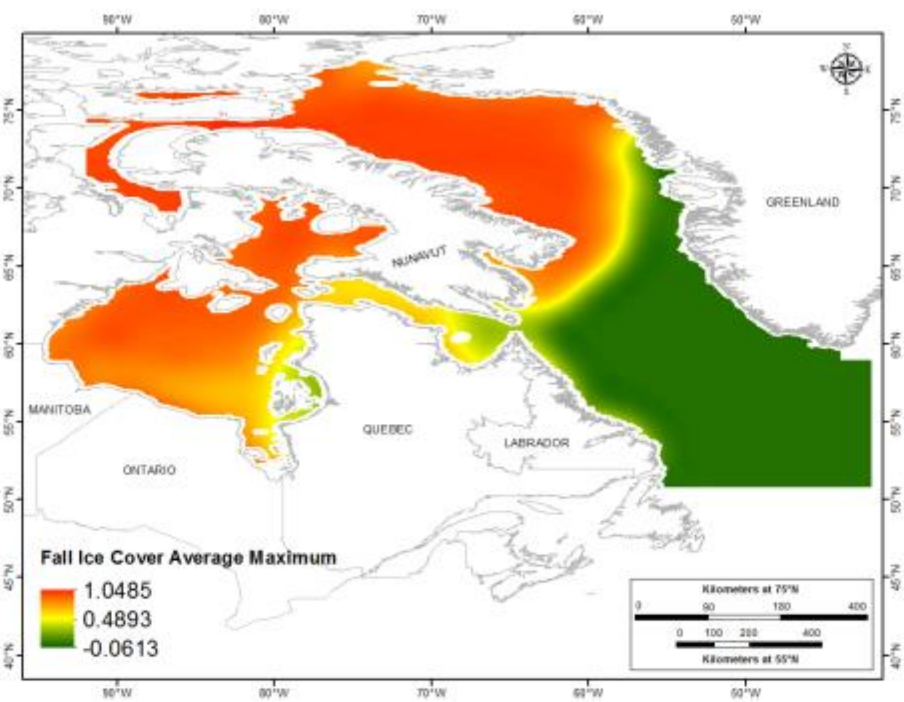


Figure 520. Interpolated prediction surface of Fall Ice Cover Average Maximum.

**Fall Ice Cover Average Range**

This variable displayed a bimodal, platykurtic distribution prior to interpolation (Table 209, Figure 521). The data were greater than predicted by a normal distribution at the lowest and upper mid-range values, and lower than predicted at the highest and lower mid-range values (Figure 522). These areas of under- and over-prediction showed spatial pattern over the region.

The semivariogram showed autocorrelation present in the data (Figure 523). The kriged model showed good fit between measured and predicted values (Figure 523). Poor performance of the model was indicated by the cross-validation results (Table 210), with a Standardized Root-Mean-Square Error higher than 1, indicating that variability in the predictions was underestimated. The error map showed lower error across the study extent, with high error in Lancaster Sound and other coastal areas (Figure 524). The kriged surface is presented in Figure 525.

Table 209. Distributional properties of Fall Ice Cover Average Range.

| **Property** | **Value** |
|---|---:|
| Number of Observations | 526 |
| Minimum | 0.000 |
| Maximum | 0.983 |
| Mean | 0.461 |
| Median | 0.521 |
| Standard Deviation | 0.406 |
| Skewness | -0.044 |
| Kurtosis | 1.223 |

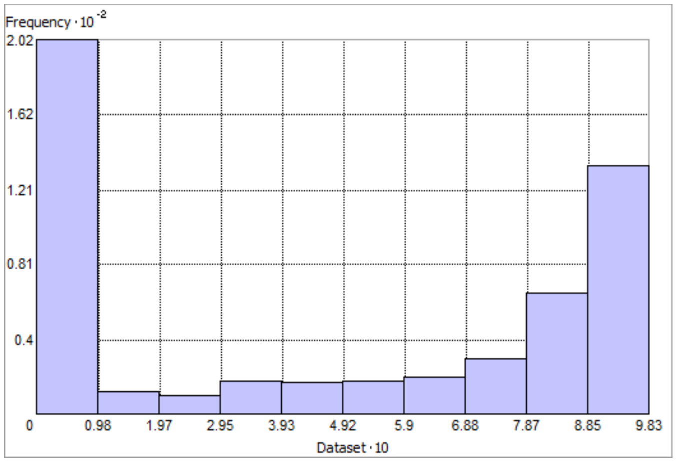

Figure 521. Distribution of Fall Ice Cover Average Range. Histogram was illustrated using 10 bins. X axis is shown at 10; Y axis is shown at $10^{-2}$.

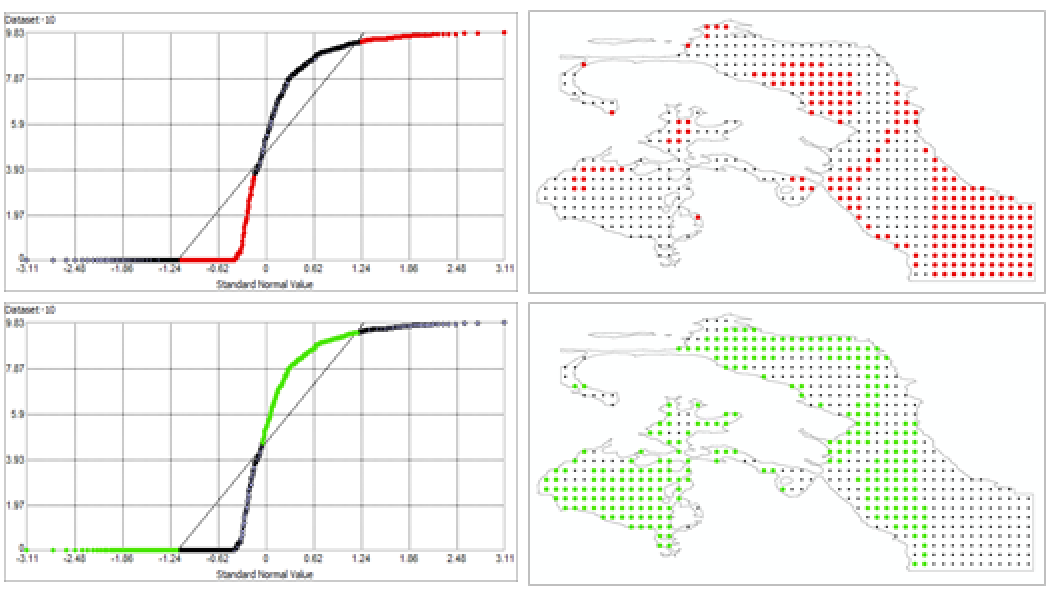
Figure 522. Normal Q-Q plot for data values of Fall Ice Cover Average Range. Points falling under (top right panel) and over (bottom right panel) the reference line are mapped.

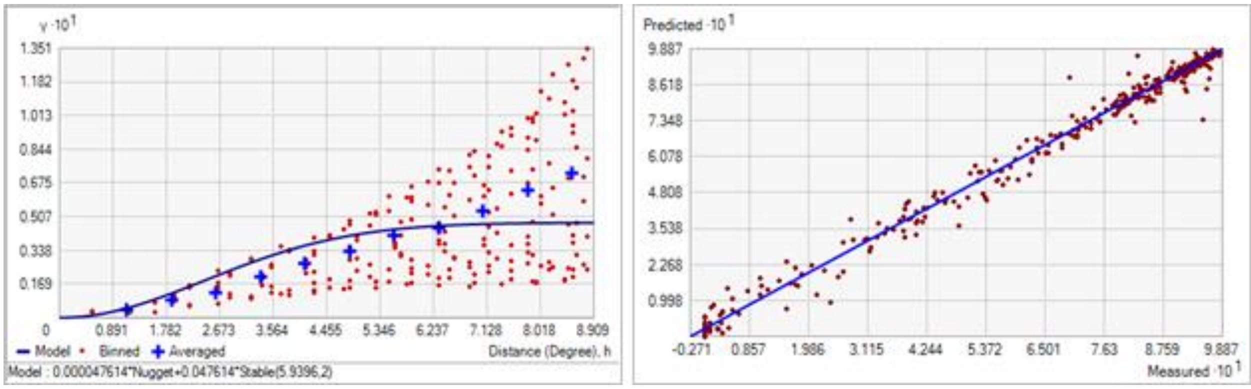


Figure 523. Left panel: Semivariogram of Fall Ice Cover Average Range. Binned values are shown as red dots; average points are shown as blue crosses; the model fit to the averaged values is shown as a blue line. Lag size: 0.742 degrees; number of lags: 12; Parameter: 2; Range: 5.940 degrees; Partial Sill: 0.048. Right panel: Scatterplot of predicted values versus observed values for the model of Fall Ice Cover Average Range.

Table 210. Results of cross-validation of the kriged model for Fall Ice Cover Average Range.

| **Prediction Error** | **Value** |
|---|---|
| Number of Observations | 526 |
| Overall Mean Error | $-7.255 \times 10^{-4}$ |
| Root Mean Square Prediction Error | 0.029 |
| Standardized Mean | -0.011 |
| Standardized Root Mean Square Prediction Error | 2.252 |
| Average Standard Error | 0.014 |

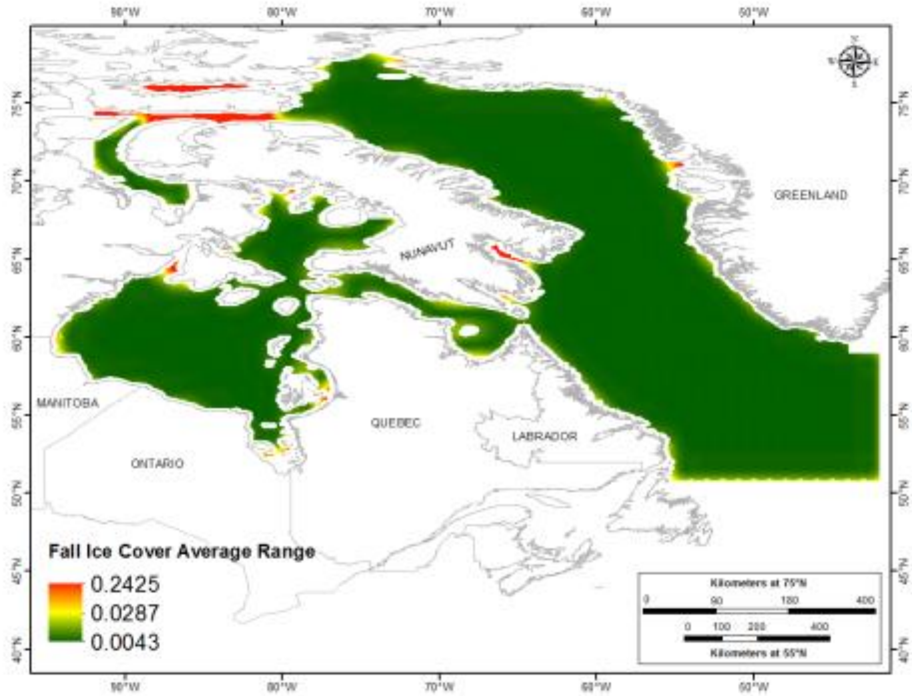


Figure 524. Prediction standard error surface of Fall Ice Cover Average Range.

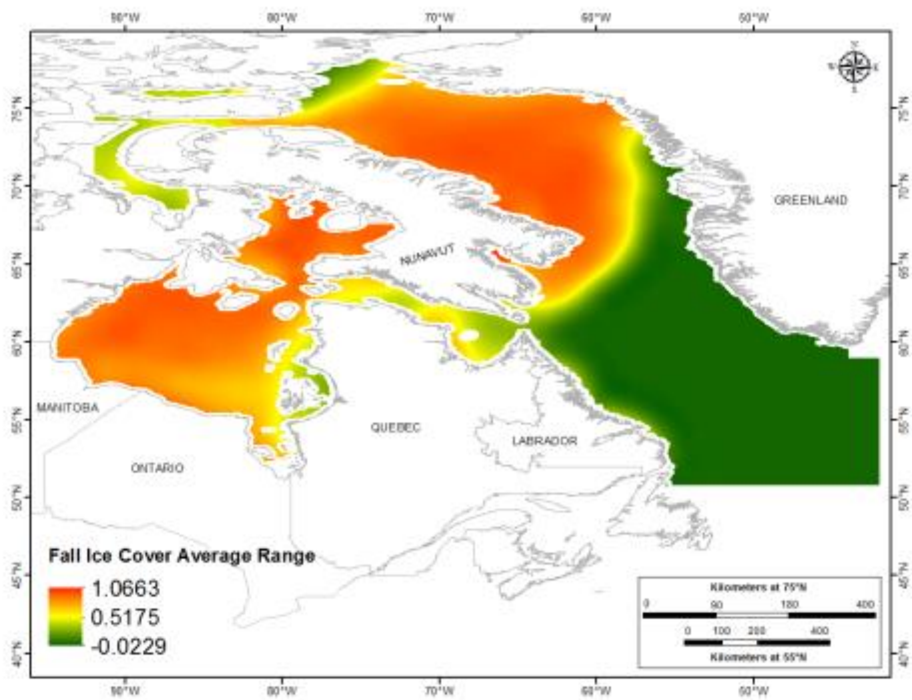


Figure 525. Interpolated prediction surface of Fall Ice Cover Average Range.

**Winter Ice Cover Mean**

This variable displayed a bimodal, platykurtic distribution prior to interpolation (Table 211, Figure 526). The data were greater than predicted by a normal distribution at the lowest and upper mid-range values, and lower than predicted at the highest and lower mid-range values (Figure 527). These areas of under- and over-prediction showed spatial pattern over the region.

The semivariogram showed moderate autocorrelation present in the data (Figure 528). The kriged model showed good fit between measured and predicted values (Figure 528). Good performance of the model was indicated by the cross-validation results (Table 212). The error map showed lower error across the study extent, with high error in Lancaster Sound and other coastal areas (Figure 529). The kriged surface is presented in Figure 530.

Table 211. Distributional properties of Winter Ice Cover Mean.

| **Property** | **Value** |
|---|---:|
| Number of Observations | 526 |
| Minimum | 0.000 |
| Maximum | 1.000 |
| Mean | 0.642 |
| Median | 0.939 |
| Standard Deviation | 0.429 |
| Skewness | -0.648 |
| Kurtosis | 1.553 |

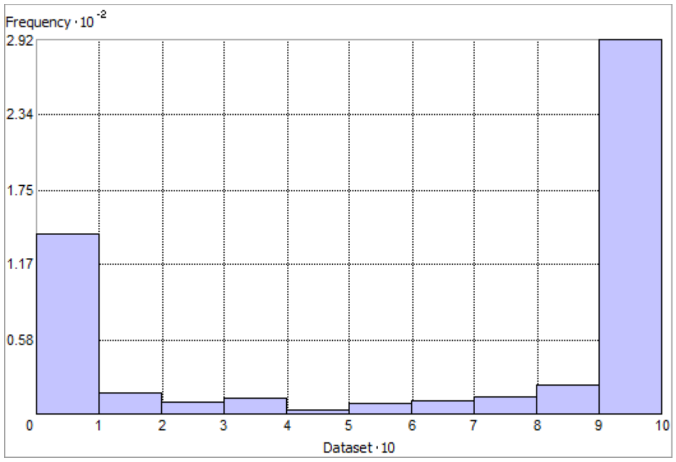


Figure 526. Distribution of Winter Ice Cover Mean. Histogram was illustrated using 10 bins. X axis is shown at 10; Y axis is shown at $10^{-2}$.

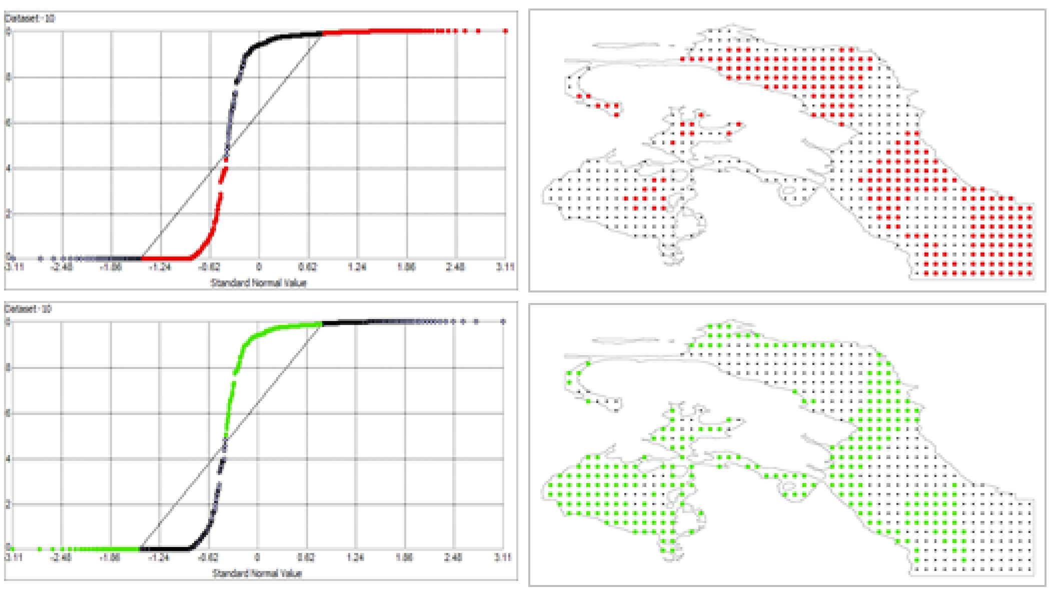


Figure 527. Normal Q-Q plot for data values of Winter Ice Cover Mean. Points falling under (top right panel) and over (bottom right panel) the reference line are mapped.

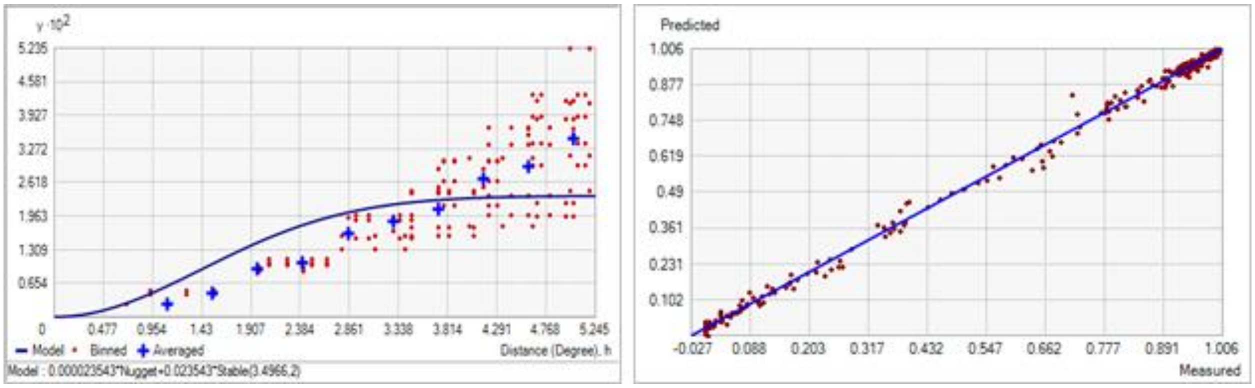


Figure 528. Left panel: Semivariogram of Winter Ice Cover Mean. Binned values are shown as red dots; average points are shown as blue crosses; the model fit to the averaged values is shown as a blue line. Lag size: 0.437 degrees; number of lags: 12; Parameter: 2; Range: 3.497 degrees; Partial Sill: 0.024. Right panel: Scatterplot of predicted values versus observed values for the model of Winter Ice Cover Mean.

Table 212. Results of cross-validation of the kriged model for Winter Ice Cover Mean.

| Prediction Error | Value |
|---|---:|
| Number of Observations | 526 |
| Overall Mean Error | $1.553 \times 10^{-4}$ |
| Root Mean Square Prediction Error | 0.014 |
| Standardized Mean | -0.017 |
| Standardized Root Mean Square Prediction Error | 0.944 |
| Average Standard Error | 0.026 |

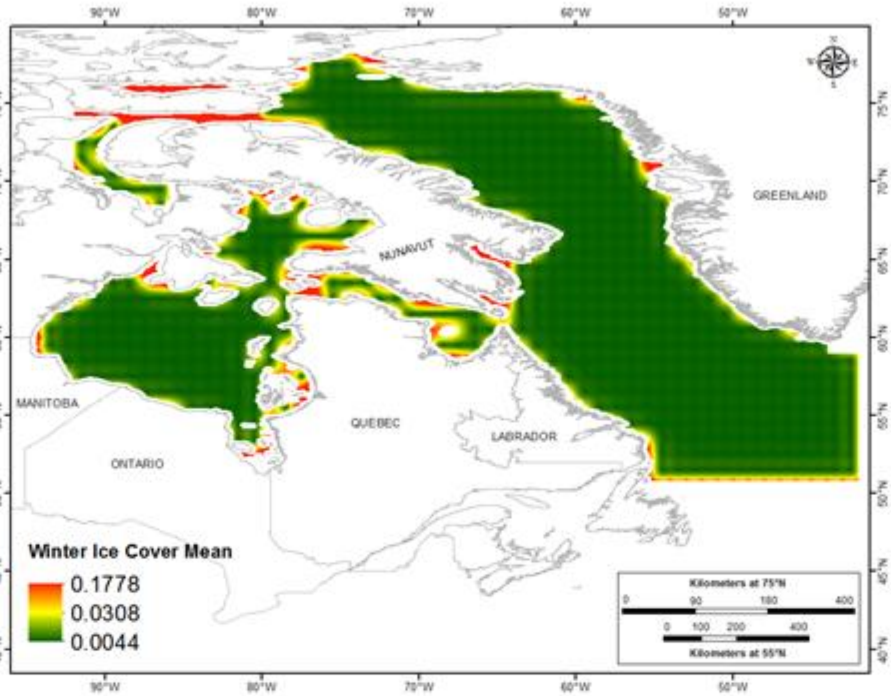


Figure 529. Prediction standard error surface of Winter Ice Cover Mean.

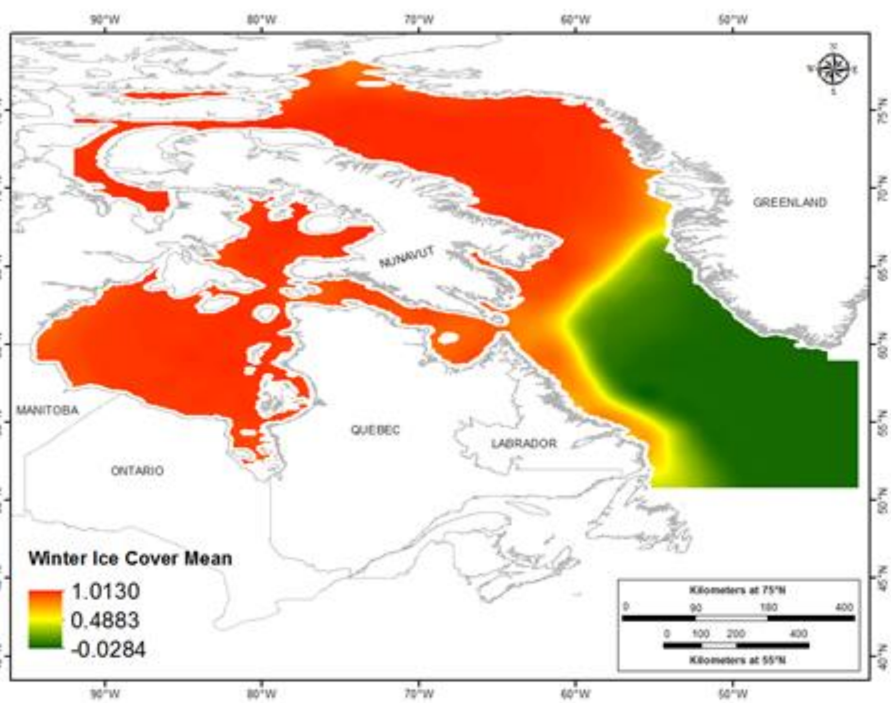


Figure 530. Interpolated prediction surface of Winter Ice Cover Mean.

### Winter Ice Cover Minimum

This variable displayed a bimodal, platykurtic distribution prior to interpolation (Table 213, Figure 531). The data were greater than predicted by a normal distribution at the lowest and upper mid-range values, and lower than predicted at the highest and lower mid-range values (Figure 532). These areas of under- and over-prediction showed spatial pattern over the region.

The semivariogram showed moderate autocorrelation present in the data (Figure 533). The kriged model showed good fit between measured and predicted values (Figure 533). Good performance of the model was indicated by the cross-validation results (Table 214). The error map showed a "bullseye" pattern with error increasing slightly with distance away from data points (Figure 534). The kriged surface is presented in Figure 535.

Table 213. Distributional properties of Winter Ice Cover Minimum.

| **Property** | **Value** |
|---|---:|
| Number of Observations | 526 |
| Minimum | 0.000 |
| Maximum | 0.990 |
| Mean | 0.417 |
| Median | 0.290 |
| Standard Deviation | 0.415 |
| Skewness | 0.255 |
| Kurtosis | 1.304 |

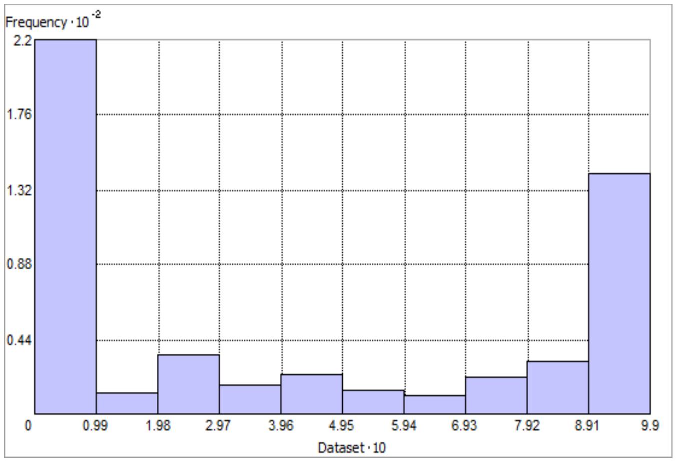


Figure 531. Distribution of Winter Ice Cover Minimum. Histogram was illustrated using 10 bins. X axis is shown at 10; Y axis is shown at $10^{-2}$.

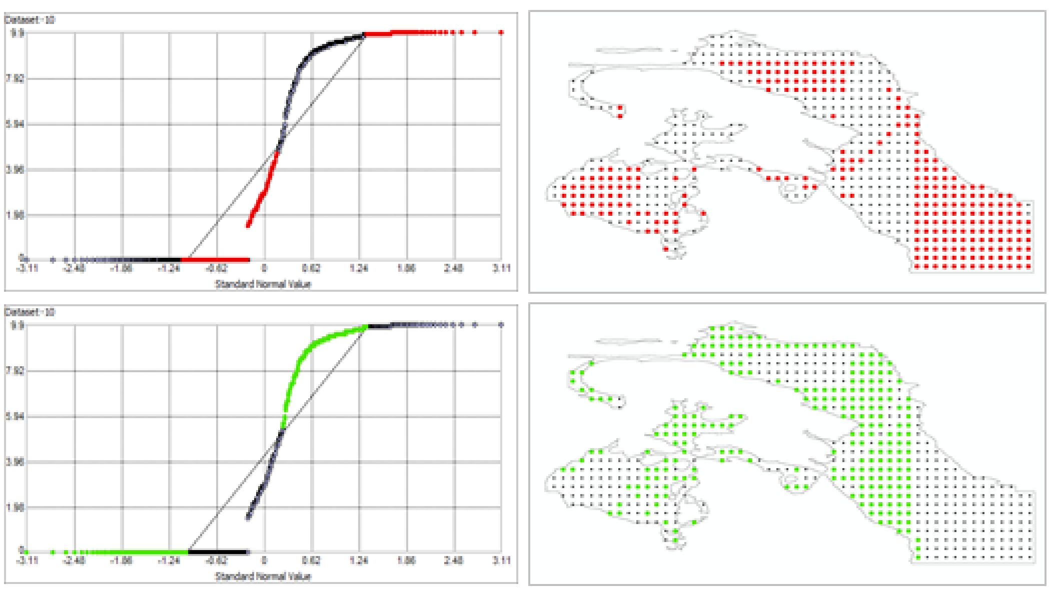


Figure 532. Normal Q-Q plot for data values of Winter Ice Cover Minimum. Points falling under (top right panel) and over (bottom right panel) the reference line are mapped.

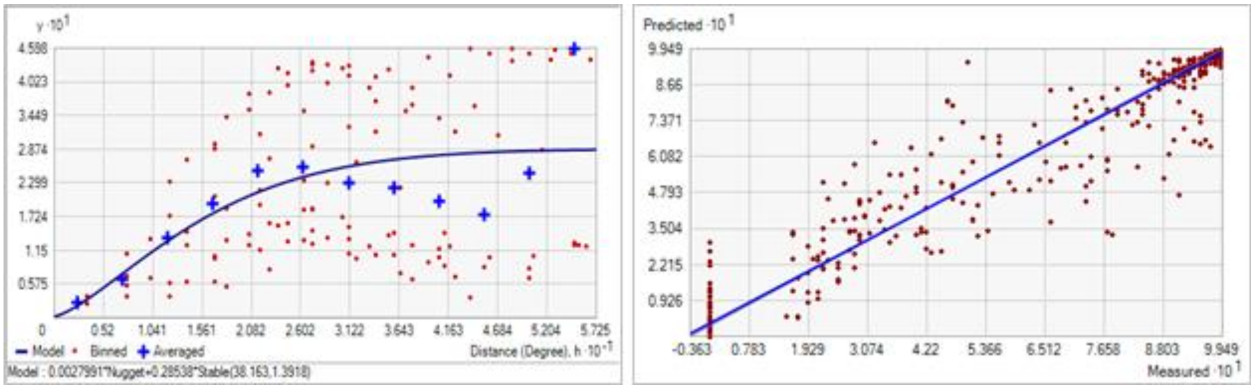


Figure 533. Left panel: Semivariogram of Winter Ice Cover Minimum. Binned values are shown as red dots; average points are shown as blue crosses; the model fit to the averaged values is shown as a blue line. Lag size: 4.770 degrees; number of lags: 12; Parameter: 1.392; Range: 38.163 degrees; Partial Sill: 0.285. Right panel: Scatterplot of predicted values versus observed values for the model of Winter Ice Cover Minimum.

Table 214. Results of cross-validation of the kriged model for Winter Ice Cover Minimum.

| **Prediction Error** | **Value** |
|---|---:|
| Number of Observations | 526 |
| Overall Mean Error | $1.139 \times 10^{-4}$ |
| Root Mean Square Prediction Error | 0.093 |
| Standardized Mean | $9.730 \times 10^{-4}$ |
| Standardized Root Mean Square Prediction Error | 1.135 |
| Average Standard Error | 0.026 |

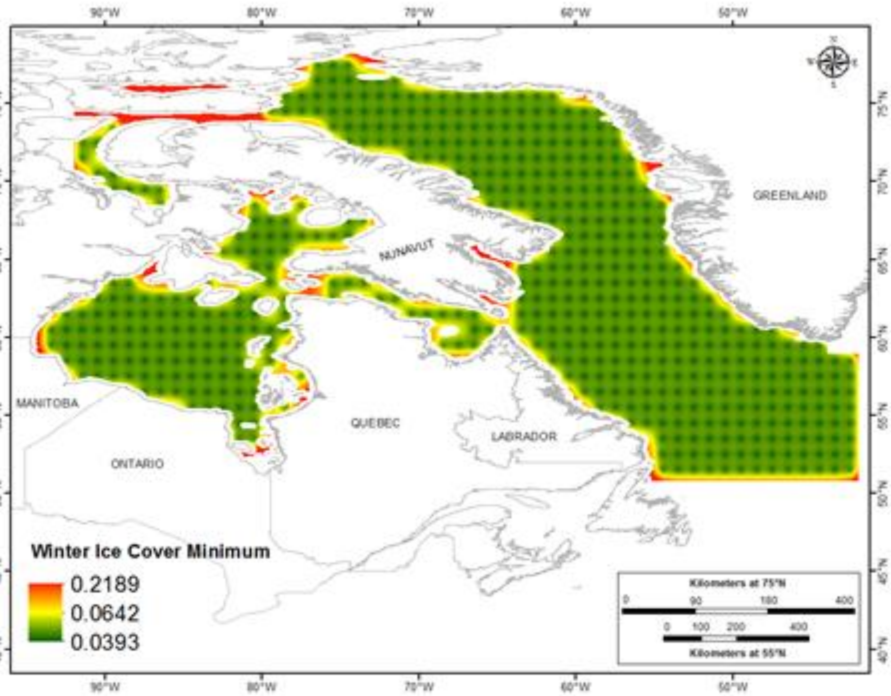


Figure 534. Prediction standard error surface of Winter Ice Cover Minimum.

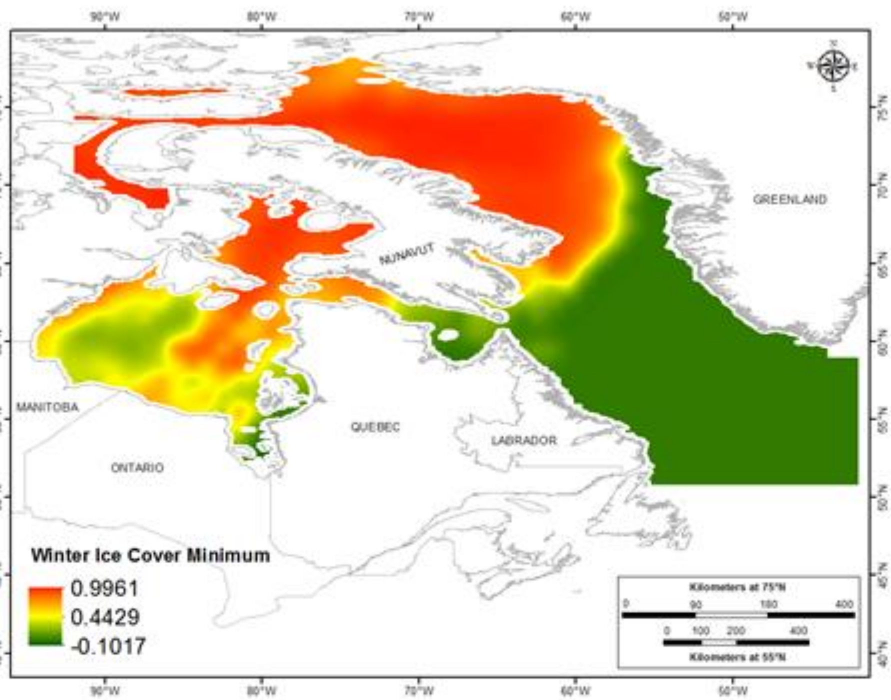


Figure 535. Interpolated prediction surface of Winter Ice Cover Minimum.

**Winter Ice Cover Maximum**

This variable displayed a bimodal and discontinuous distribution and prior to interpolation (Table 215, Figure 536). The data were greater than predicted by a normal distribution at the lowest and upper mid-range values, and lower than predicted at the highest and lower mid-range values (Figure 537). These areas of under- and over-prediction showed spatial pattern over the region.

The semivariogram showed moderate autocorrelation present in the data (Figure 538). The kriged model showed good fit between measured and predicted values (Figure 538). Fair performance of the model was indicated by the cross-validation results (Table 216). The error map showed lower error across the study extent, with high error in Lancaster Sound and other coastal areas (Figure 539). The kriged surface is presented in Figure 540.

Table 215. Distributional properties of Winter Ice Cover Maximum.

| **Property** | **Value** |
|---|---:|
| Number of Observations | 526 |
| Minimum | 0.000 |
| Maximum | 1.000 |
| Mean | 0.764 |
| Median | 0.764 |
| Standard Deviation | 0.393 |
| Skewness | -1.322 |
| Kurtosis | 2.900 |

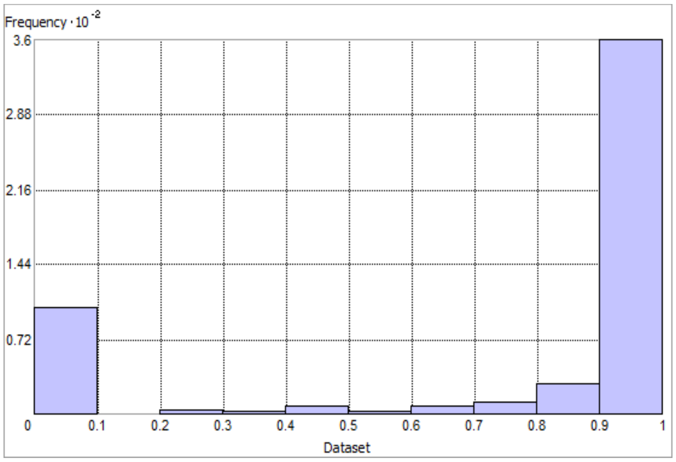


Figure 536. Distribution of Winter Ice Cover Maximum. Histogram was illustrated using 10 bins. Y axis is shown at $10^{-2}$.

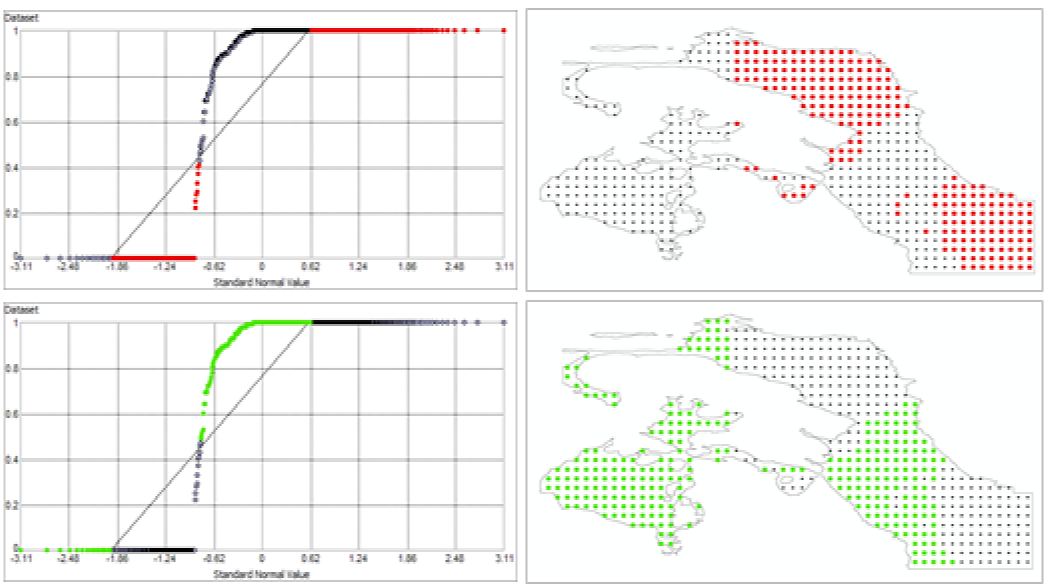

Figure 537. Normal Q-Q plot for data values of Winter Ice Cover Maximum. Points falling under (top right panel) and over (bottom right panel) the reference line are mapped.

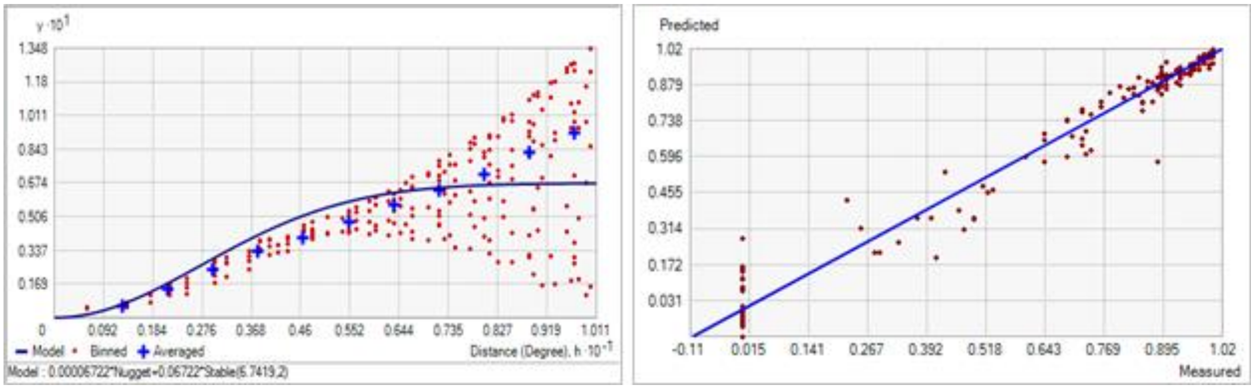

Figure 538. Left panel: Semivariogram of Winter Ice Cover Maximum. Binned values are shown as red dots; average points are shown as blue crosses; the model fit to the averaged values is shown as a blue line. Lag size: 0.843 degrees; number of lags: 12; Parameter: 2; Range: 6.742 degrees; Partial Sill: 0.067. Right panel: Scatterplot of predicted values versus observed values for the model of Winter Ice Cover Maximum.

Table 216. Results of cross-validation of the kriged model for Winter Ice Cover Maximum.

| **Prediction Error** | **Value** |
|---|---:|
| Number of Observations | 526 |
| Overall Mean Error | $-1.314 \times 10^{-4}$ |
| Root Mean Square Prediction Error | 0.038 |
| Standardized Mean | $-1.422 \times 10^{-4}$ |
| Standardized Root Mean Square Prediction Error | 3.646 |
| Average Standard Error | 0.014 |

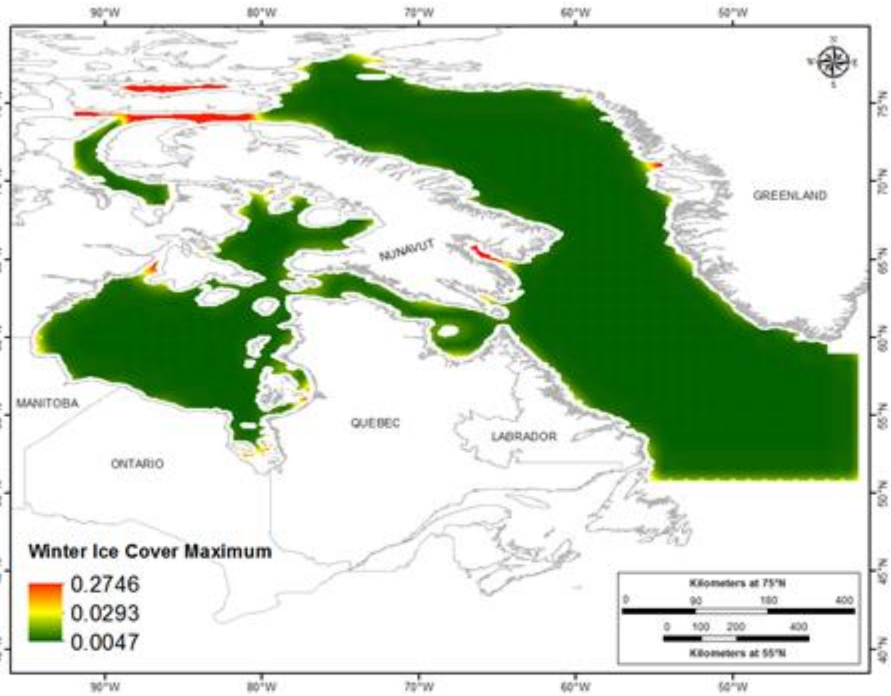


Figure 539. Prediction standard error surface of Winter Ice Cover Maximum.

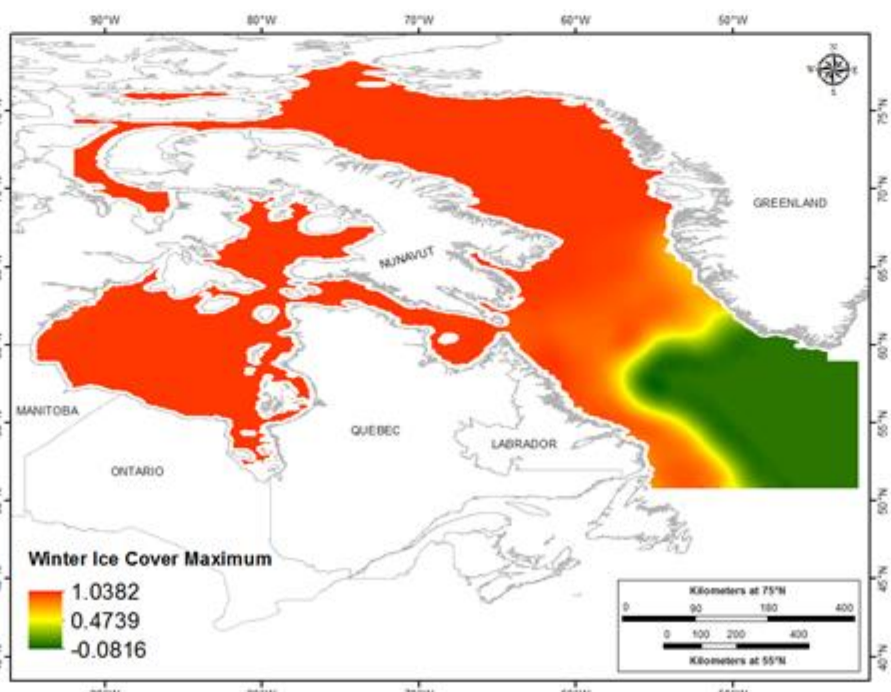


Figure 540. Interpolated prediction surface of Winter Ice Cover Maximum.

**Winter Ice Cover Range**

This variable displayed a right-skewed, platykurtic distribution prior to interpolation (Table 217, Figure 541). The data were greater than predicted by a normal distribution at the lowest and upper mid-range values, and lower than predicted at the highest and lower mid-range values (Figure 542). These areas of under- and over-prediction showed spatial pattern over the region.

The semivariogram showed autocorrelation present in the data (Figure 543). The kriged model showed good fit between measured and predicted values (Figure 543). Good performance of the model was indicated by the cross-validation results (Table 218). The error map showed a "bullseye" pattern with error increasing with distance from data points (Figure 544). The kriged surface is presented in Figure 545.

Table 217. Distributional properties of Winter Ice Cover Range.

| **Property** | **Value** |
|---|---:|
| Number of Observations | 526 |
| Minimum | 0.000 |
| Maximum | 1.000 |
| Mean | 0.347 |
| Median | 0.155 |
| Standard Deviation | 0.360 |
| Skewness | 0.517 |
| Kurtosis | 1.612 |

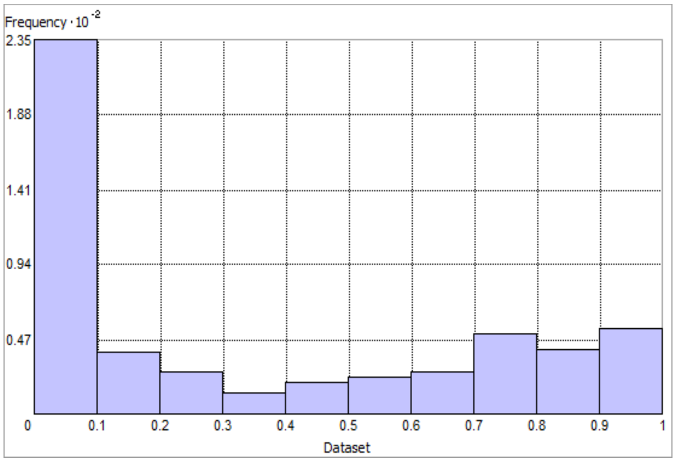


Figure 541. Distribution of Winter Ice Cover Range. Histogram was illustrated using 10 bins. Y axis is shown at $10^{-2}$.

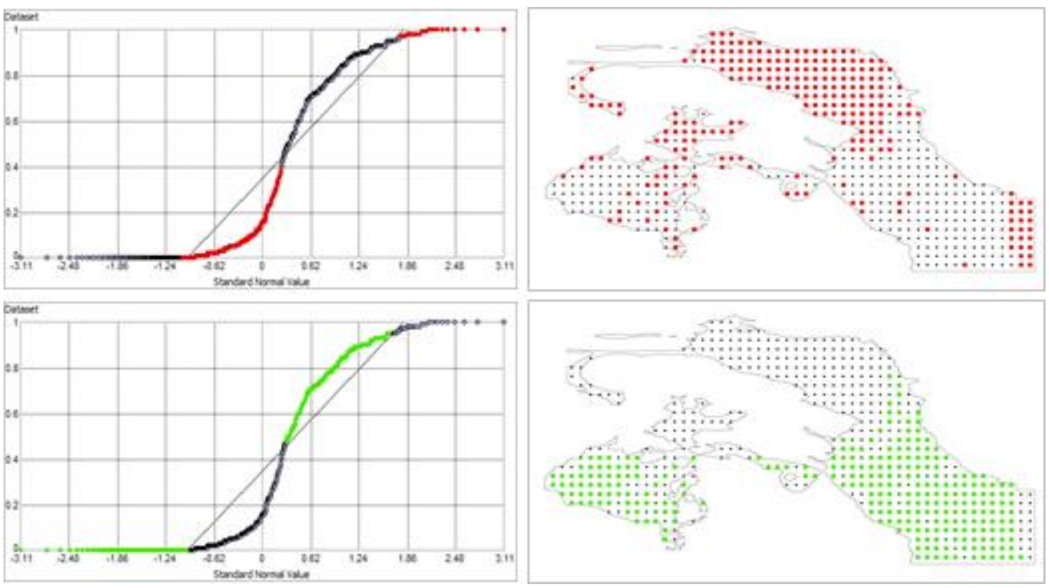

Figure 542. Normal Q-Q plot for data values of Winter Ice Cover Range. Points falling under (top right panel) and over (bottom right panel) the reference line are mapped.

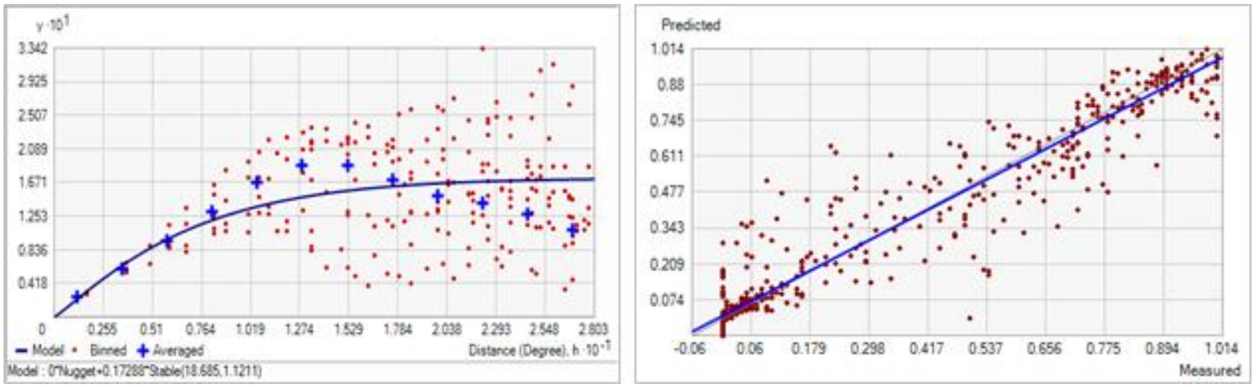


Figure 543. Left panel: Semivariogram of Winter Ice Cover Range. Binned values are shown as red dots; average points are shown as blue crosses; the model fit to the averaged values is shown as a blue line. Lag size: 2.336 degrees; number of lags: 12; Parameter: 1.121; Range: 18.685 degrees; Partial Sill: 0.173. Right panel: Scatterplot of predicted values versus observed values for the model of Winter Ice Cover Range.

Table 218. Results of cross-validation of the kriged model for Winter Ice Cover Range.

| **Prediction Error** | **Value** |
|---|---:|
| Number of Observations | 526 |
| Overall Mean Error | $-4.711 \times 10^{-4}$ |
| Root Mean Square Prediction Error | 0.101 |
| Standardized Mean | $-2.893 \times 10^{-3}$ |
| Standardized Root Mean Square Prediction Error | 0.825 |
| Average Standard Error | 0.124 |

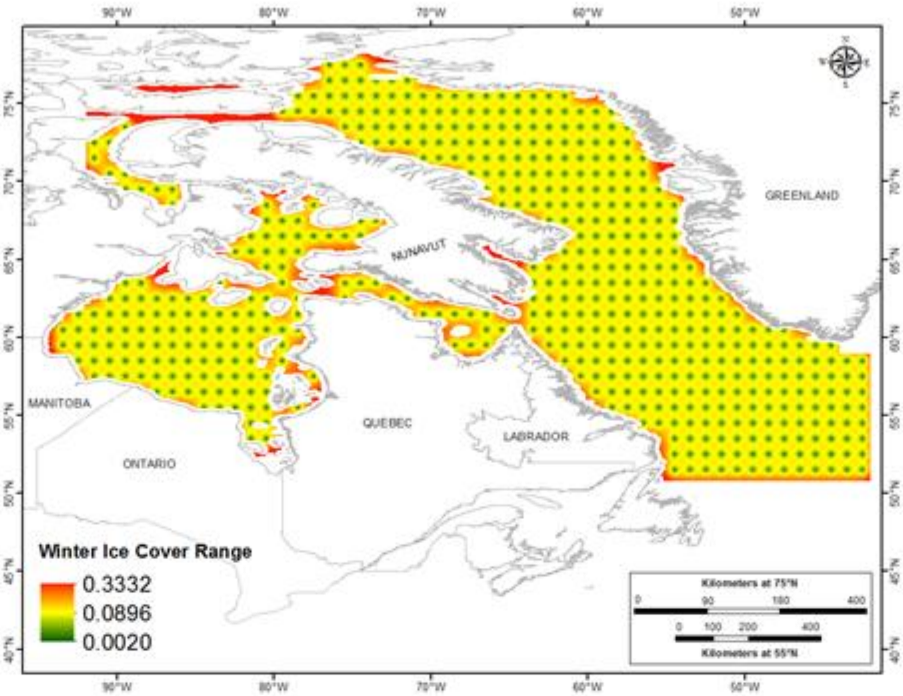


Figure 544. Prediction standard error surface of Winter Ice Cover Range.

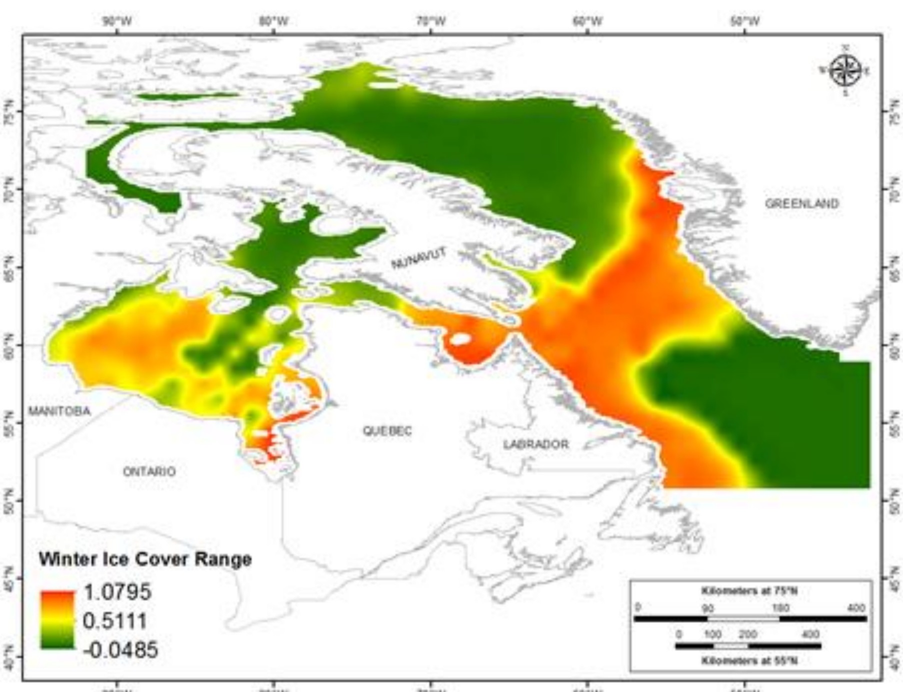


Figure 545. Interpolated prediction surface of Winter Ice Cover Range.

**Winter Ice Cover Average Minimum**

This variable displayed a bimodal, platykurtic distribution prior to interpolation (Table 219, Figure 546). The data were greater than predicted by a normal distribution at the lowest and upper mid-range values, and lower than predicted at the highest and lower mid-range values (Figure 547). These areas of under- and over-prediction showed spatial pattern over the region.

The semivariogram showed autocorrelation present in the data (Figure 548). The kriged model showed good fit between measured and predicted values (Figure 548). Good performance of the model was indicated by the cross-validation results (Table 220). The error map showed lower error across the study extent, with high error in Lancaster Sound and other coastal areas (Figure 549). The kriged surface is presented in Figure 550.

Table 219. Distributional properties of Winter Ice Cover Average Minimum.

| **Property** | **Value** |
|---|---:|
| Number of Observations | 526 |
| Minimum | 0.000 |
| Maximum | 0.999 |
| Mean | 0.602 |
| Median | 0.898 |
| Standard Deviation | 0.433 |
| Skewness | -0.518 |
| Kurtosis | 1.391 |

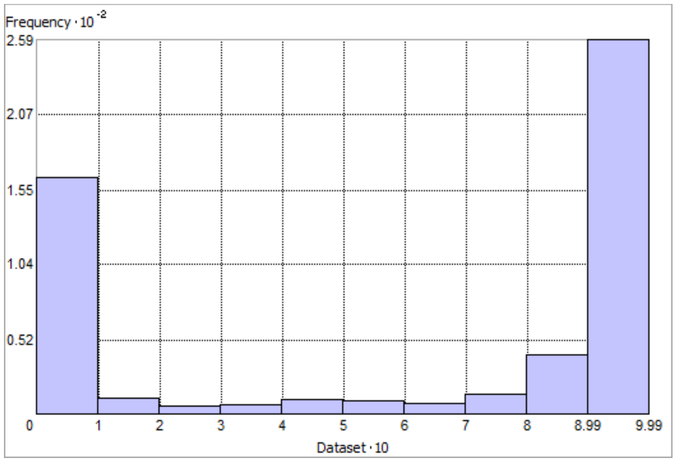

Figure 546. Distribution of Winter Ice Cover Average Minimum. Histogram was illustrated using 10 bins. X axis is shown at 10; Y axis is shown at $10^{-2}$.

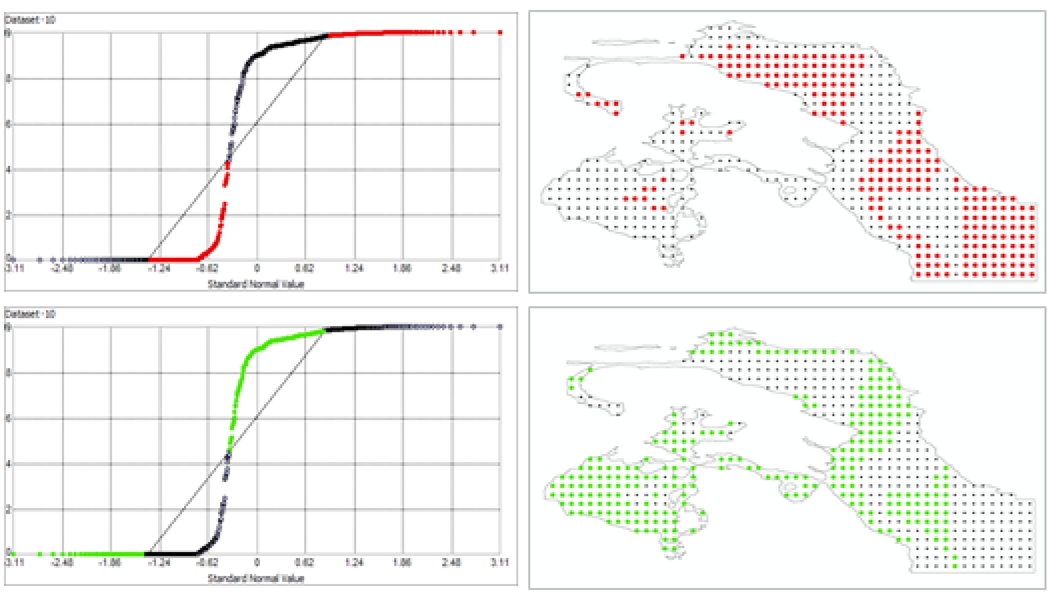
Figure 547. Normal Q-Q plot for data values of Winter Ice Cover Average Minimum. Points falling under (top right panel) and over (bottom right panel) the reference line are mapped.

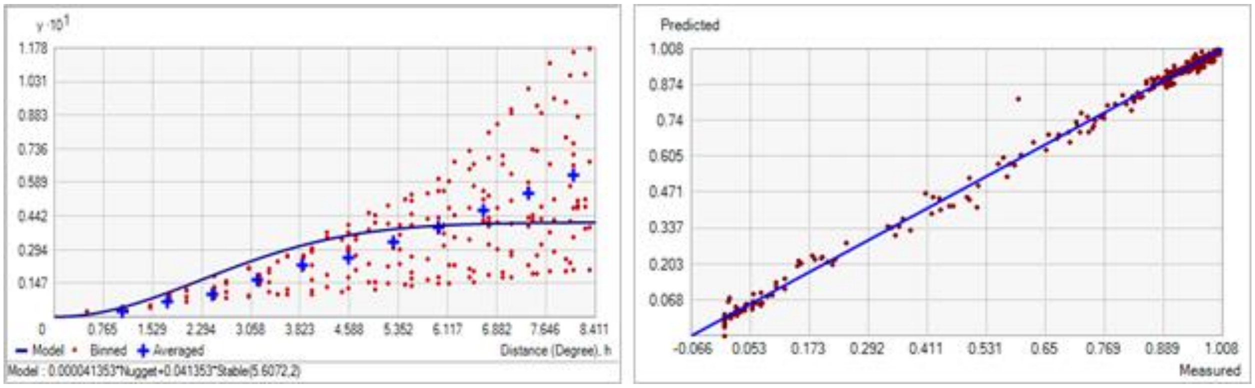


Figure 548. Left panel: Semivariogram of Winter Ice Cover Average Minimum. Binned values are shown as red dots; average points are shown as blue crosses; the model fit to the averaged values is shown as a blue line. Lag size: 0.701 degrees; number of lags: 12; Parameter: 2; Range: 5.607 degrees; Partial Sill: 0.041. Right panel: Scatterplot of predicted values versus observed values for the model of Winter Ice Cover Average Minimum.

Table 220. Results of cross-validation of the kriged model for Winter Ice Cover Average Minimum.

| **Prediction Error** | **Value** |
|---|---:|
| Number of Observations | 526 |
| Overall Mean Error | $7.448 \times 10^{-4}$ |
| Root Mean Square Prediction Error | 0.019 |
| Standardized Mean | 0.017 |
| Standardized Root Mean Square Prediction Error | 1.629 |
| Average Standard Error | 0.015 |

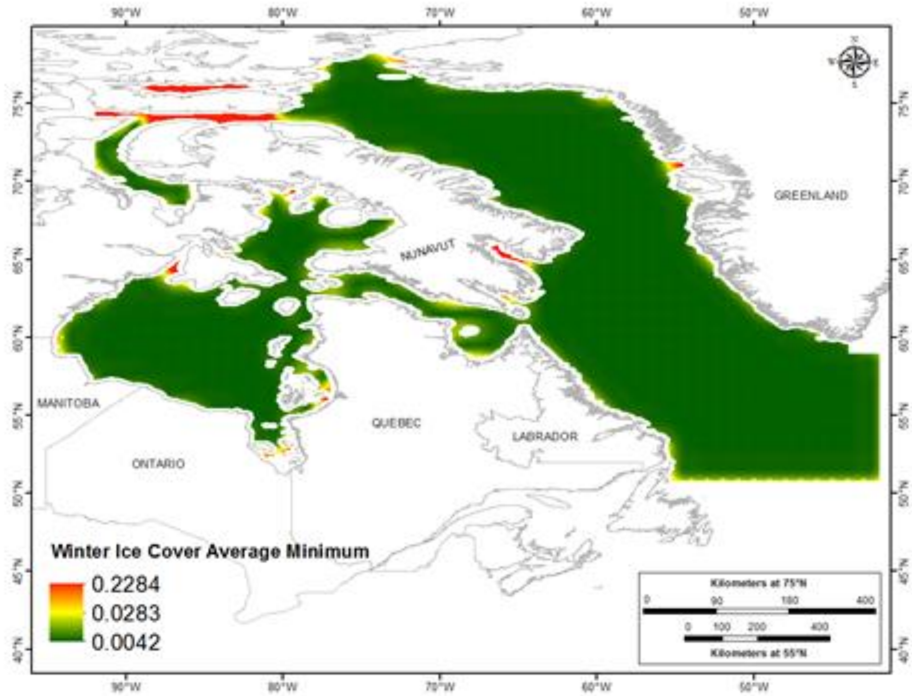


Figure 549. Prediction standard error surface of Winter Ice Cover Average Minimum.

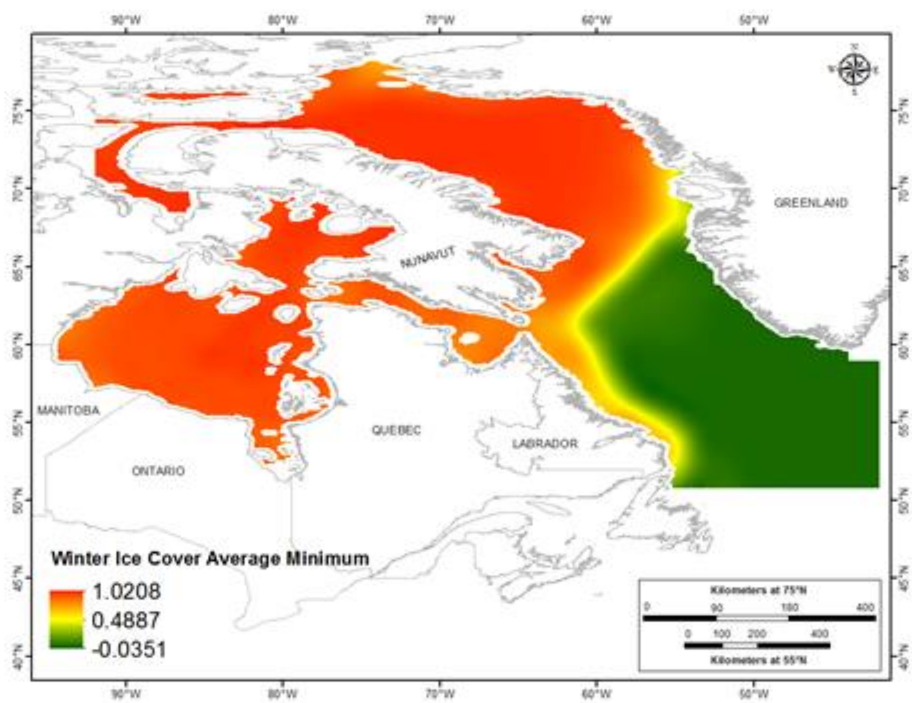


Figure 550. Interpolated prediction surface of Winter Ice Cover Average Minimum.

## Winter Ice Cover Average Maximum

This variable displayed a bimodal, platykurtic distribution prior to interpolation (Table 221, Figure 551). The data were greater than predicted by a normal distribution at the lowest and upper mid-range values, and lower than predicted at the highest and lower mid-range values (Figure 552). These areas of under- and over-prediction showed spatial pattern over the region.

The semivariogram showed moderate autocorrelation present in the data (Figure 553). The kriged model showed good fit between measured and predicted values (Figure 553). Good performance of the model was indicated by the cross-validation results (Table 222). The error map showed low error across the study extent, with high error in Lancaster Sound and other coastal areas (Figure 554).The kriged surface is presented in Figure 555.

Table 221. Distributional properties of Winter Ice Cover Average Maximum.

| **Property** | **Value** |
|---|---:|
| Number of Observations | 526 |
| Minimum | 0.000 |
| Maximum | 1.000 |
| Mean | 0.674 |
| Median | 0.972 |
| Standard Deviation | 0.427 |
| Skewness | -0.769 |
| Kurtosis | 1.722 |

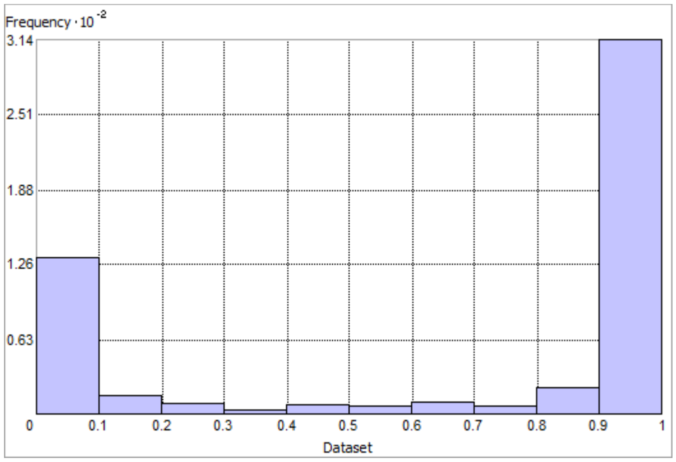


Figure 551. Distribution of Winter Ice Cover Average Maximum. Histogram was illustrated using 10 bins. Y axis is shown at $10^{-2}$.

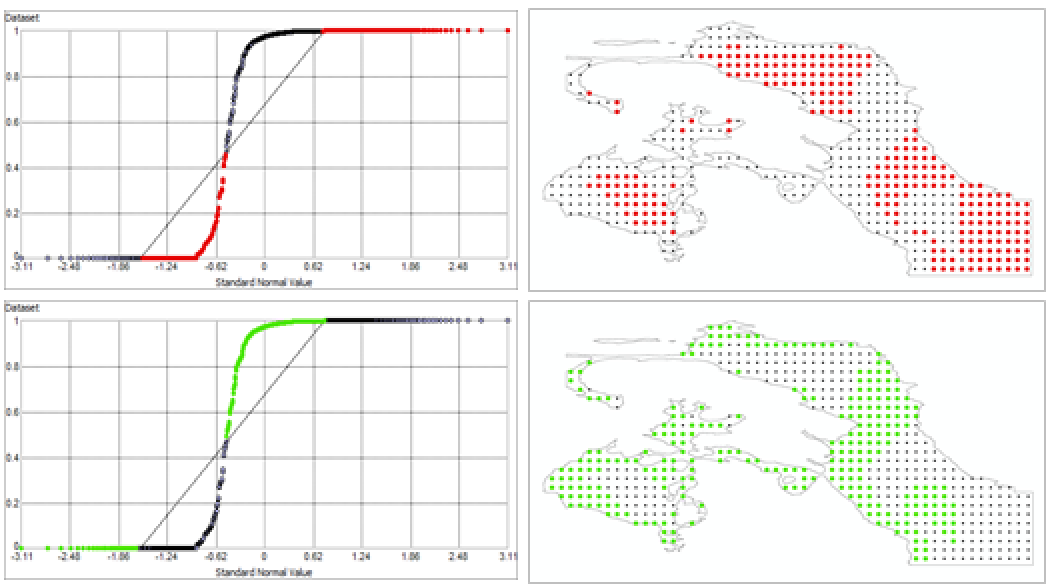

Figure 552. Normal Q-Q plot for data values of Winter Ice Cover Average Maximum. Points falling under (top right panel) and over (bottom right panel) the reference line are mapped.

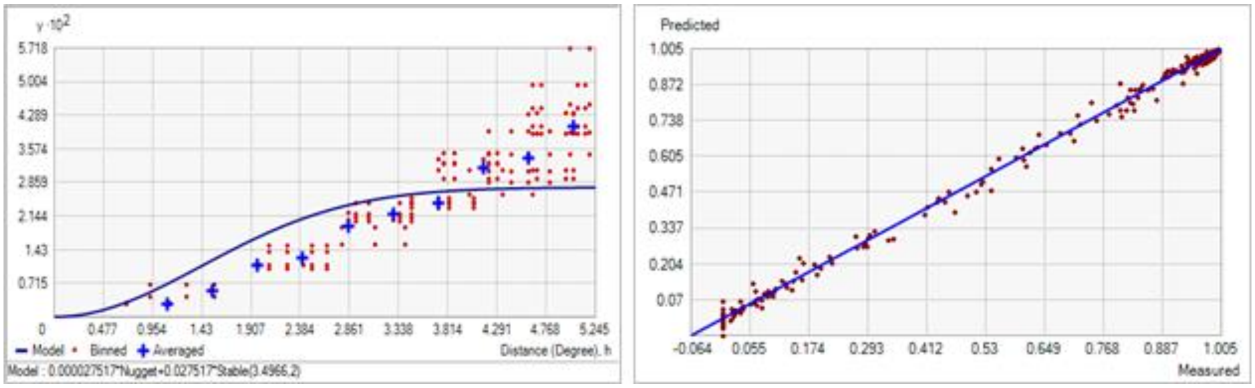


Figure 553. Left panel: Semivariogram of Winter Ice Cover Average Maximum. Binned values are shown as red dots; average points are shown as blue crosses; the model fit to the averaged values is shown as a blue line. Lag size: 0.437 degrees; number of lags: 12; Parameter: 2; Range: 3.497 degrees; Partial Sill: 0.028. Right panel: Scatterplot of predicted values versus observed values for the model of Winter Ice Cover Average Maximum.

Table 222. Results of cross-validation of the kriged model for Winter Ice Cover Average Maximum.

| **Prediction Error** | **Value** |
|---|---:|
| Number of Observations | 526 |
| Overall Mean Error | $1.819 \times 10^{-4}$ |
| Root Mean Square Prediction Error | 0.015 |
| Standardized Mean | $-7.081 \times 10^{-3}$ |
| Standardized Root Mean Square Prediction Error | 0.948 |
| Average Standard Error | 0.029 |

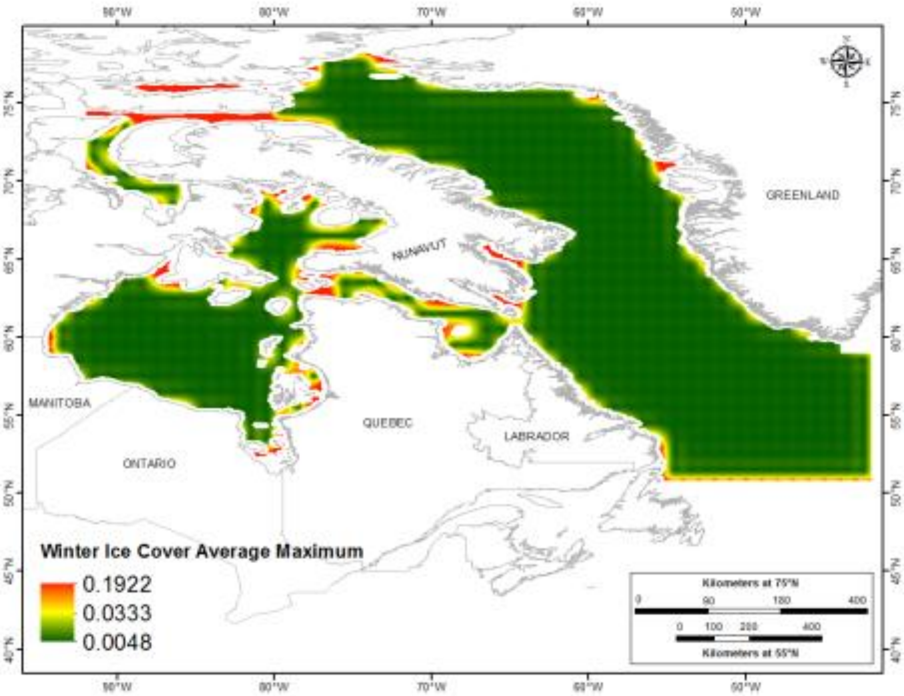


Figure 554. Prediction standard error surface of Winter Ice Cover Average Maximum.

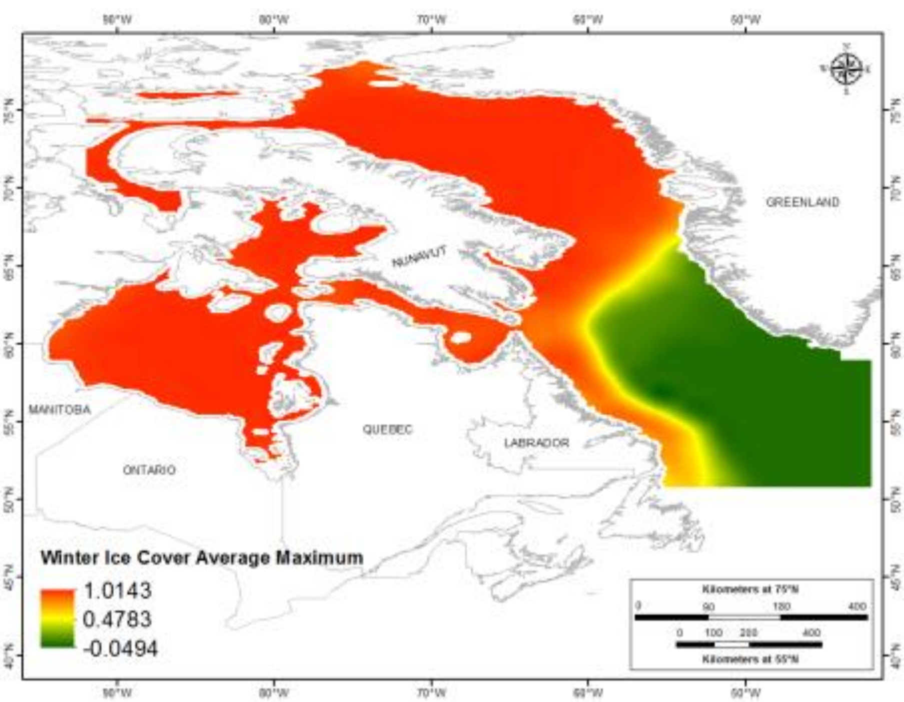


Figure 555. Interpolated prediction surface of Winter Ice Cover Average Maximum.

**Winter Ice Cover Average Range**

This variable displayed a right-skewed, leptokurtic distribution prior to interpolation (Table 223, Figure 556). The data were higher than predicted by a normal distribution at both tails, while mid-values were lower than the reference line (Figure 557). These areas of under- and over-prediction showed spatial pattern over the region (Figure 557).

The semivariogram showed autocorrelation present in the data (Figure 558). The kriged model showed good fit between measured and predicted values (Figure 558). Fair performance of the model was indicated by the cross-validation results (Table 224). The Standardized Root Mean Square Error is large than 1, indicating that variability in the predictions was underestimated. The error map showed low error across the study extent, with high error in Lancaster Sound and other coastal areas (Figure 559).The kriged surface is presented in Figure 560.

Table 223. Distributional properties of Winter Ice Cover Average Range.

| **Property** | **Value** |
|---|---:|
| Number of Observations | 526 |
| Minimum | 0.000 |
| Maximum | 0.553 |
| Mean | 0.072 |
| Median | 0.033 |
| Standard Deviation | 0.107 |
| Skewness | 2.108 |
| Kurtosis | 6.836 |

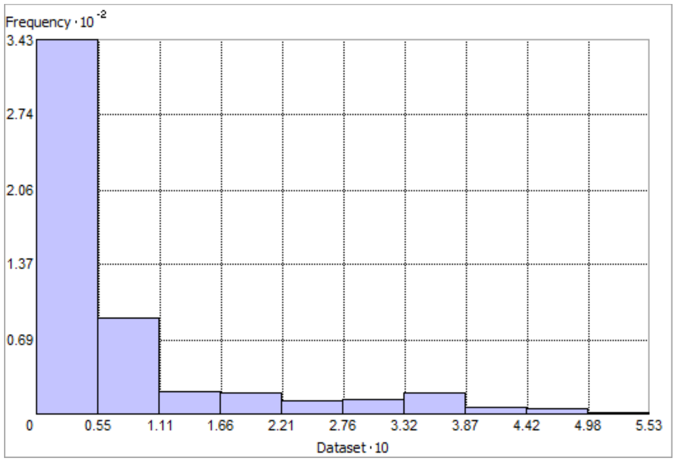

Figure 556. Distribution of Winter Ice Cover Average Range. Histogram was illustrated using 10 bins. X axis is shown at 10; Y axis is shown at $10^{-2}$.

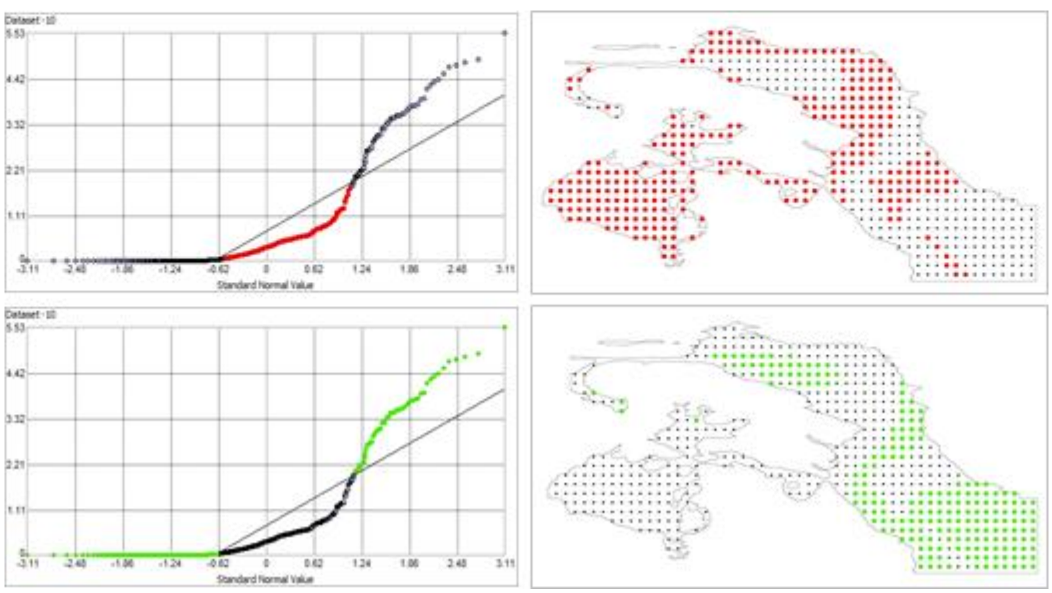
Figure 557. Normal Q-Q plot for data values of Winter Ice Cover Average Range. Points falling under (top right panel) and over (bottom right panel) the reference line are mapped.

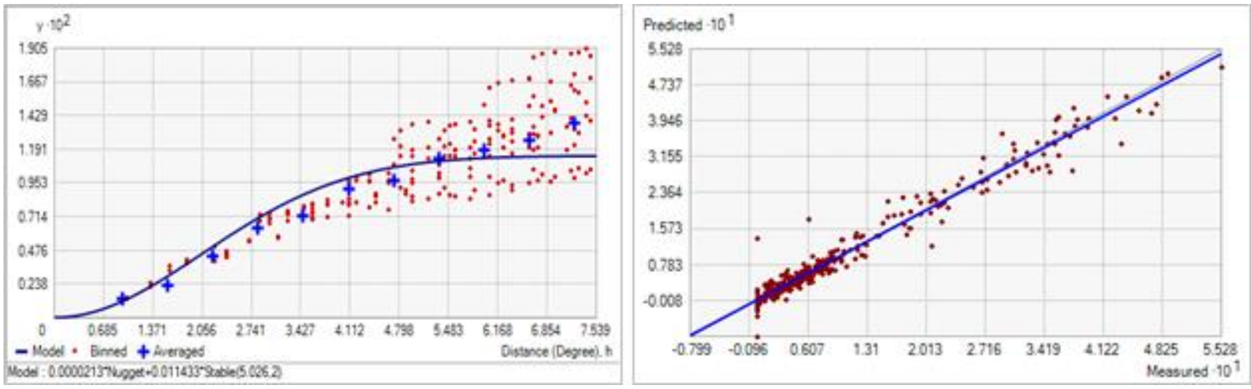

Figure 558. Left panel: Semivariogram of Winter Ice Cover Average Range. Binned values are shown as red dots; average points are shown as blue crosses; the model fit to the averaged values is shown as a blue line. Lag size: 0.628 degrees; number of lags: 12; Parameter: 2; Range: 5.026 degrees; Partial Sill: 0.011. Right panel: Scatterplot of predicted values versus observed values for the model of Winter Ice Cover Average Range.

Table 224. Results of cross-validation of the kriged model for Winter Ice Cover Average Range.

| **Prediction Error** | **Value** |
|---|---:|
| Number of Observations | 526 |
| Overall Mean Error | $-1.696 \times 10^{-4}$ |
| Root Mean Square Prediction Error | 0.018 |
| Standardized Mean | $3.608 \times 10^{-3}$ |
| Standardized Root Mean Square Prediction Error | 2.544 |
| Average Standard Error | 0.010 |

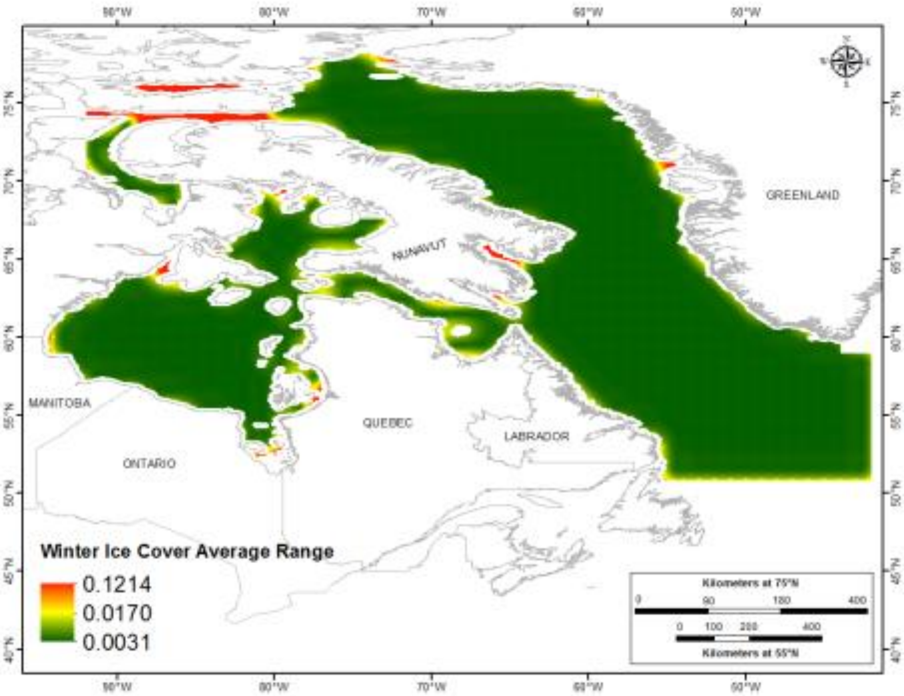


Figure 559. Prediction standard error surface of Winter Ice Cover Average Range.

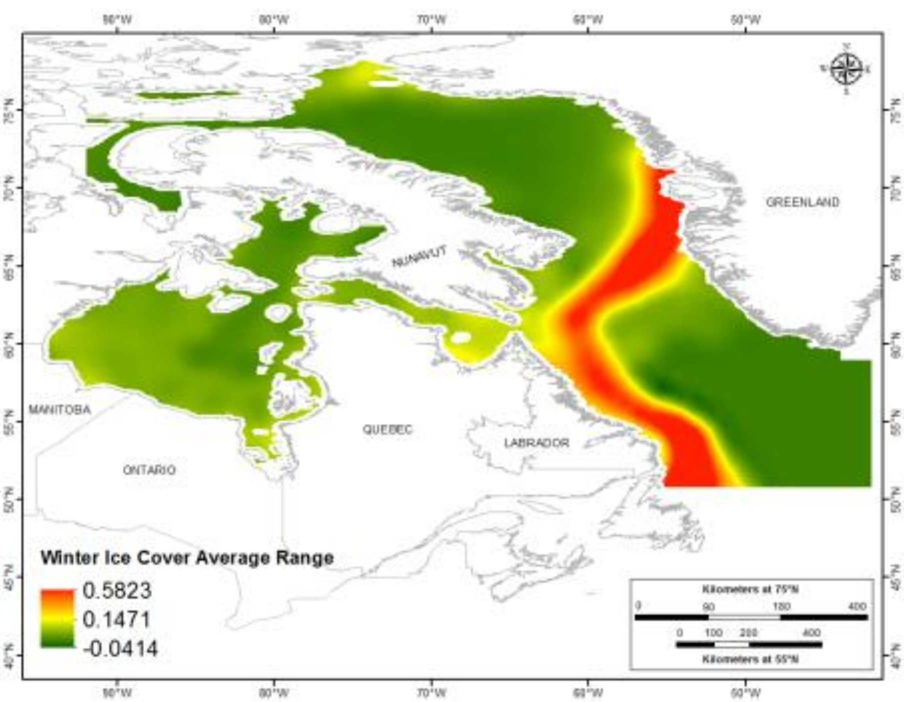


Figure 560. Interpolated prediction surface of Winter Ice Cover Average Range.

## Recommendation on Variable Use for Species Distribution Modelling

This report provides detailed information on 111 environmental data layers for the Eastern Canadian Arctic and Sub-Arctic that were extracted from various sources and with different native spatial resolutions. These data layers were spatially interpolated using ordinary kriging in ArcGIS to provide continuous data surfaces to be used in various modelling applications.

Upon examination of the interpolated surfaces, we noted poor interpolation of those variables with sparse coverage of the raw data. For instance, interpolation of the various metrics of Spring Primary Production provided poor results north of Davis Strait due to sparse coverage of the raw data. Therefore, we do not recommend their use in those areas.

Below we provide a recommendation on our suggested use of these environmental variables in species distribution modelling applications (Table 225). Those variables with restrictions or limitations to their use due to poor interpolation are highlighted in bold. All other variables are considered good predictors of the environmental conditions of the region, with the exception of the extreme temperature values located in Hudson Bay (see methodology). Caution should therefore be taken when applying these data layers from that region.

Variables labelled 'average' (see methodology) are considered more representative of long-term average climate, as the quantities were obtained by taking an average of the minima, maxima, and range values at each point location across years. In contrast, the 'absolute' variables were created by taking the absolute minima, maxima, and range at each point location across all years and are therefore more reflective of extreme or anomalous events. Previous applications of these variables in modelling processes (see Beazley et al., 2016b; Murillo et al., in prep.) used the 'average' variables over the 'absolute', as average climate was considered more relevant to the distribution of long-lived benthic marine fauna than extreme events.

Table 225. Recommended use of each environmental variable in species distribution modelling applications.

| Variable | Recommendation on Use |
|---|---|
| **Temperature** | |
| Bottom Temperature Mean | Recommended for applications requiring data on long-term average climate. |
| Bottom Temperature Minimum | Recommended for applications requiring data on extreme climate. Note erroneously low temperature values in Hudson Bay. |
| Bottom Temperature Maximum | Recommended for applications requiring data on extreme climate. |
| Bottom Temperature Range | Recommended for applications requiring data on extreme climate. |

| | |
|---|---|
| Bottom Temperature Average Minimum | Recommended for applications requiring data on long-term average climate. |
| Bottom Temperature Average Maximum | Recommended for applications requiring data on long-term average climate. |
| Bottom Temperature Average Range | Recommended for applications requiring data on long-term average climate. |
| Surface Temperature Mean | Recommended for applications requiring data on long-term average climate. |
| Surface Temperature Minimum | Recommended for applications requiring data on extreme climate. |
| Surface Temperature Maximum | Recommended for applications requiring data on extreme climate. |
| Surface Temperature Range | Recommended for applications requiring data on extreme climate. |
| Surface Temperature Average Minimum | Recommended for applications requiring data on long-term average climate. |
| Surface Temperature Average Maximum | Recommended for applications requiring data on long-term average climate. |
| Surface Temperature Average Range | Recommended for applications requiring data on long-term average climate. |
| **Salinity** | |
| Bottom Salinity Mean | Recommended for applications requiring data on long-term average climate. |
| Bottom Salinity Minimum | Recommended for applications requiring data on extreme climate. |
| Bottom Salinity Maximum | Recommended for applications requiring data on extreme climate. |
| Bottom Salinity Range | Recommended for applications requiring data on extreme climate. |
| Bottom Salinity Average Minimum | Recommended for applications requiring data on long-term average climate. |
| Bottom Salinity Average Maximum | Recommended for applications requiring data on long-term average climate. |
| Bottom Salinity Average Range | Recommended for applications requiring data on long-term average climate. |
| Surface Salinity Mean | Recommended for applications requiring data on long-term average climate. |
| Surface Salinity Minimum | Recommended for applications requiring data on extreme climate. |
| Surface Salinity Maximum | Recommended for applications requiring data on extreme climate. |
| Surface Salinity Range | Recommended for applications requiring data on extreme climate. |
| Surface Salinity Average Minimum | Recommended for applications requiring data on long-term average climate. |
| Surface Salinity Average Maximum | Recommended for applications requiring data |

| | |
|---|---|
| | on long-term average climate. |
| Surface Salinity Average Range | Recommended for applications requiring data on long-term average climate. |
| **Current Speed** | |
| Bottom Current Mean | Recommended for applications requiring data on long-term average climate. |
| Bottom Current Minimum | Recommended for applications requiring data on extreme climate. |
| Bottom Current Maximum | Recommended for applications requiring data on extreme climate. |
| Bottom Current Range | Recommended for applications requiring data on extreme climate. |
| Bottom Current Average Minimum | Recommended for applications requiring data on long-term average climate. |
| Bottom Current Average Maximum | Recommended for applications requiring data on long-term average climate. |
| Bottom Current Average Range | Recommended for applications requiring data on long-term average climate. |
| Surface Current Mean | Recommended for applications requiring data on long-term average climate. |
| Surface Current Minimum | Recommended for applications requiring data on extreme climate. |
| Surface Current Maximum | Recommended for applications requiring data on extreme climate. |
| Surface Current Range | Recommended for applications requiring data on extreme climate. |
| Surface Current Average Minimum | Recommended for applications requiring data on long-term average climate. |
| Surface Current Average Maximum | Recommended for applications requiring data on long-term average climate. |
| Surface Current Average Range | Recommended for applications requiring data on long-term average climate. |
| **Maximum Seasonal Mixed Layer Depth** | |
| Maximum Spring Mixed Layer Depth | Recommended for applications requiring data on extreme climate. |
| Maximum Summer Mixed Layer Depth | Recommended for applications requiring data on extreme climate. |
| Maximum Fall Mixed Layer Depth | Recommended for applications requiring data on extreme climate. |
| Maximum Winter Mixed Layer Depth | Recommended for applications requiring data on extreme climate. |
| Maximum Average Spring Mixed Layer Depth | Recommended for applications requiring data on long-term average climate. |
| Maximum Average Summer Mixed Layer Depth | Recommended for applications requiring data on long-term average climate. |

| | |
|---|---|
| Maximum Average Fall Mixed Layer Depth | Recommended for applications requiring data on long-term average climate. |
| Maximum Average Winter Mixed Layer Depth | Recommended for applications requiring data on long-term average climate. |
| **Bottom Shear** | |
| Bottom Shear Mean | Recommended for applications requiring data on long-term average climate. |
| Bottom Shear Minimum | Recommended for applications requiring data on extreme climate. |
| Bottom Shear Maximum | Recommended for applications requiring data on extreme climate. |
| Bottom Shear Range | Recommended for applications requiring data on extreme climate. |
| Bottom Shear Average Minimum | Recommended for applications requiring data on long-term average climate. |
| Bottom Shear Average Maximum | Recommended for applications requiring data on long-term average climate. |
| Bottom Shear Average Range | Recommended for applications requiring data on long-term average climate. |
| **Sea Surface Chlorophyll *a*** | |
| Spring Chlorophyll *a* Mean | Recommended for applications requiring data on long-term average climate. |
| Spring Chlorophyll *a* Minimum | Recommended for applications requiring data on long-term average climate. |
| Spring Chlorophyll *a* Maximum | Recommended for applications requiring data on long-term average climate. |
| Spring Chlorophyll *a* Range | Recommended for applications requiring data on long-term average climate. |
| Summer Chlorophyll *a* Mean | Recommended for applications requiring data on long-term average climate. |
| Summer Chlorophyll *a* Minimum | Recommended for applications requiring data on long-term average climate. |
| Summer Chlorophyll *a* Maximum | Recommended for applications requiring data on long-term average climate. |
| Summer Chlorophyll *a* Range | Recommended for applications requiring data on long-term average climate. |
| Annual Chlorophyll *a* Mean | Recommended for applications requiring data on long-term average climate. |
| Annual Chlorophyll *a* Minimum | Recommended for applications requiring data on long-term average climate. |
| Annual Chlorophyll *a* Maximum | Recommended for applications requiring data on long-term average climate. |
| Annual Chlorophyll *a* Range | Recommended for applications requiring data on long-term average climate. |
| **Primary Production** | |

| | |
|---|---|
| Spring Primary Production Mean | **North of Davis Strait not recommended for use; poor coverage of raw data.** |
| Spring Primary Production Minimum | **North of Davis Strait not recommended for use; poor coverage of raw data.** |
| Spring Primary Production Maximum | **North of Davis Strait not recommended for use; poor coverage of raw data.** |
| Spring Primary Production Range | **North of Davis Strait not recommended for use; poor coverage of raw data.** |
| Spring Primary Production Average Minimum | **North of Davis Strait not recommended for use; poor coverage of raw data.** |
| Spring Primary Production Average Maximum | **North of Davis Strait not recommended for use; poor coverage of raw data.** |
| Spring Primary Production Average Range | **North of Davis Strait not recommended for use; poor coverage of raw data.** |
| Summer Primary Production Mean | Recommended for applications requiring data on long-term average climate. |
| Summer Primary Production Minimum | Recommended for applications requiring data on extreme climate. |
| Summer Primary Production Maximum | Recommended for applications requiring data on extreme climate. |
| Summer Primary Production Range | Recommended for applications requiring data on extreme climate. |
| Summer Primary Production Average Minimum | Recommended for applications requiring data on long-term average climate. |
| Summer Primary Production Average Maximum | Recommended for applications requiring data on long-term average climate. |
| Summer Primary Production Average Range | Recommended for applications requiring data on long-term average climate. |
| Annual Primary Production Mean | Recommended for applications requiring data on long-term average climate. |
| Annual Primary Production Minimum | Recommended for applications requiring data on extreme climate. |
| Annual Primary Production Maximum | Recommended for applications requiring data on extreme climate. |
| Annual Primary Production Range | Recommended for applications requiring data on extreme climate. |
| Annual Primary Production Average Minimum | Recommended for applications requiring data on long-term average climate. |
| Annual Primary Production Average Maximum | Recommended for applications requiring data on long-term average climate. |
| Annual Primary Production Average Range | Recommended for applications requiring data on long-term average climate. |
| **Sea Ice Cover** | |
| Spring Ice Cover Mean | Recommended for applications requiring data on long-term average climate. |

| | |
|---|---|
| Spring Ice Cover Minimum | Recommended for applications requiring data on extreme climate. |
| Spring Ice Cover Maximum | Recommended for applications requiring data on extreme climate. |
| Spring Ice Cover Range | Recommended for applications requiring data on extreme climate. |
| Spring Ice Cover Average Minimum | Recommended for applications requiring data on long-term average climate. |
| Spring Ice Cover Average Maximum | Recommended for applications requiring data on long-term average climate. |
| Spring Ice Cover Average Range | Recommended for applications requiring data on long-term average climate. |
| Fall Ice Cover Mean | Recommended for applications requiring data on long-term average climate. |
| Fall Ice Cover Minimum | Recommended for applications requiring data on extreme climate. |
| Fall Ice Cover Maximum | Recommended for applications requiring data on extreme climate. |
| Fall Ice Cover Range | Recommended for applications requiring data on extreme climate. |
| Fall Ice Cover Average Minimum | Recommended for applications requiring data on long-term average climate. |
| Fall Ice Cover Average Maximum | Recommended for applications requiring data on long-term average climate. |
| Fall Ice Cover Average Range | Recommended for applications requiring data on long-term average climate. |
| Winter Ice Cover Mean | Recommended for applications requiring data on long-term average climate. |
| Winter Ice Cover Minimum | Recommended for applications requiring data on extreme climate. |
| Winter Ice Cover Maximum | Recommended for applications requiring data on extreme climate. |
| Winter Ice Cover Range | Recommended for applications requiring data on extreme climate. |
| Winter Ice Cover Average Minimum | Recommended for applications requiring data on long-term average climate. |
| Winter Ice Cover Average Maximum | Recommended for applications requiring data on long-term average climate. |
| Winter Ice Cover Average Range | Recommended for applications requiring data on long-term average climate. |

## ACKNOWLEDGMENTS

This project was funded in part by a one year project under DFO's Strategic Program for Ecosystem-Based Research and Advice (SPERA) and an International Governance Strategy (IGS) project to EK. We thank G. White (DFO-MAR) for providing the primary production data.

## REFERENCES

Arantes, R. C. M., Castro, C. B., Pires, D. O., and Seoane, J. C. S. 2009. Depth and water mass zonation and species associations of coldwater octocoral and stony coral communities in the southwestern Atlantic. Mar. Ecol. Progr. Ser. 397: 71–79.

Barthel, D. 1986. On the ecophysiology of the sponge *Halichondria panicea* in Kiel Bight. I. Substrate specificity, growth and reproduction. Mar. Ecol. Progr. Ser. 32: 291–298.

Beazley, L.I., Kenchington, E.L., Murillo, F.J., and Sacau, M. 2013. Deep-sea sponge grounds enhance diversity and abundance of epibenthic megafauna in the Northwest Atlantic. ICES J. Mar. Sci. 70: 1471–1490.

Beazley, L., Lirette, C., Sabaniel, J., Wang, Z., Knudby, A., and Kenchington, E. 2016a. Characteristics of Environmental Data Layers for Use in Species Distribution Modelling in the Gulf of St. Lawrence. Can. Tech. Rep. Fish. Aquat. Sci. 3154: viii + 357p.

Beazley, L., Murillo, F.J., Kenchington, E., Guijarro, J., Lirette, C., Siferd, T., Treble, M., Wareham, V., Baker, E., Bouchard Marmen, M., and Tompkins MacDonald, G. 2016b. Species Distribution Modelling of Corals and Sponges in the Eastern Arctic for Use in the Identification of Significant Benthic Areas. Can. Tech. Rep. Fish. Aquat. Sci. 3175: vii + 210p.

Beazley, L., Guijarro, J., Lirette, C., Wang, Z., and Kenchington, E. 2017. Characteristics of Environmental Data Layers for Use in Species Distribution Modelling in the Maritimes Region. Can. Tech. Rep. Fish. Aquat. Sci. 3212: vii + 327p.

Berger, V.J., and Kharazova, A.D. 1997. Mechanisms of salinity adaptations in marine molluscs. Hydrobiologia 355: 115-126.

Bender, M., Grande, K., and Johnson, K. 1987. A comparison of four methods for determining planktonic community production. Limnol. Oceanogr. 32: 1085-1098.

Boé, J., Hall, A., and Qu, X. 2009. September sea-ice cover in the Arctic Ocean projected to vanish by 2100. Nat. Geosci. 2: 341-343.

Carney, R.S. 2005. Zonation of deep-sea biota on continental margins. Oceanogr. Mar. Biol. Annu. Rev. 43: 211–279.

Carstensen, J., Conley, D.J., Lophaven, S., Danielsson, A., Rahm, L., and Toompuu, A. 2002. Statistical Analysis and Modelling of Phytoplankton Dynamics: Exploitation of Data in the Nordic and Baltic Monitoring Programs, Nordic Council of Ministers.

Cheng, R.T., Ling, C-H, and Gartner, J.W. 1999. Estimates of bottom roughness length and bottom shear stress in South San Francisco Bay, California. J. Geophys. Res. 104: 7715-7728.

Clark, G.F., Marzinelli, E.M., Fogwill, C.J., Turney, C.S.M., and Johnston, E.L. 2015. Effects of sea-ice cover on marine benthic communities: a natural experiment in Commonwealth Bay, East Antarctica. Polar Biol. 38: 1213-1222.

Clark, G.F., Stark, J.S., Johnston, E.L., Runcie, J.W., Goldsworthy, P.M., Raymond, B., and Riddle, M.J. 2013. Light-driven tippings points in polar ecosystems. Glob. Change Biol. 19: 3749-3761.

de Boyer Montégut, C., Madec, G., Fischer, A.S., Lazar, A., and Iudicone, D. 2004. Mixed layer depth over the global ocean: An examination of profile data and a profile-based climatology. J Geophys Res 109, C12003, doi:10.1029/2004JC002378.

DeCarlo, L.T. On the meaning and use of kurtosis. Psychol. Methods, 2(3): 292-307.

Deutsch, C.V. 1996. Correcting for negative weights in ordinary kriging. Comput. Geosci. 22: 765-773.

DFO. 2009. Development of a Framework and Principles for the Biogeographic Classification of Canadian Marine Areas. DFO Can. Sci. Advis. Sec. Sci. Advis. Rep. 2009/056.

DFO. 2017. Delineation of Significant Areas of Coldwater Corals and Sponge-Dominated Communities in Canada's Atlantic and Eastern Arctic Marine Waters and their Overlap with Fishing Activity. DFO Can. Sci. Advis. Sec. Sci. Advis. Rep. 2017/007.

ESRI, 2011. ArcGIS Desktop: Release 10. Environmental Systems Research Institute, Redlands, CA.

Ettinger-Epstein, P., Whalan, S.W., Battershill, C.N., Nys, R. 2007. Temperature cues gametogenesis and larval release in a tropical sponge. Mar. Biol. 153: 171-178.

Feldman, G.C., and McClain, C.R. 2012. Ocean Color Web, SeaWiFS Reprocessing 2010.0, NASA Goddard Space Flight Centre. Eds. Kuring, N. and Bailey, S.W. June, 2012. http://oceancolor.gsfc.nasa.gov/

Flach, E., Lavaleye, M., deStigter, H., and Thomsen, L. 1998. Feeding types of the benthic community and particle transport across the slope of a NW European continental margin (Goban Spur). Prog. Oceanogr. 42: 209–231.

Fritsen, C.H., Memmott, J.C., Ross, R.M., Quetin, L.B., Vernet, M., and Wirthlin, E.D. 2011. The timing of sea ice formation and exposure to photosynthetically active radiation along the Western Antarctic Peninsula. Polar Biol., 34: 683-692.

Genin, A., Dayton, P.K., Lonsdale, P.F., and Spiess, F.N. 1986. Corals on seamount peaks provide evidence of current acceleration over deep-sea topography. Nature 322: 59-61.

Ginn, B., Logan, A., and Thomas, M. 2000. Sponge ecology on sublittoral hard substrates in a high current velocity area. Estuar. Coast. Shelf Sci. 50: 403-414.

Gogina, M., Glockzin, M., and Zettler, M.L. 2010. Distribution of benthic macrofaunal communities in the western Baltic Sea with regard to near-bottom environmental parameters. 2. Modelling and prediction. J. Mar. Syst. 80: 57-70.

Gogina, M., and Zettler, M.L. 2010. Diversity and distribution of benthic macrofauna in the Baltic Sea: Data inventory and its use for species distribution modelling and prediction. J. Sea. Res. 64: 313-321.

Goovaerts, P. 1997. Geostatistics for Natural Resources Evaluation. Oxford University Press. 483 pp.

Goovaerts, P. 2000. Geostatistical approaches for incorporating elevation into the spatial interpolation of rainfall. J. Hydrol. 228: 113–129.

Guijarro, J., Beazley, L., Lirette, C., Wang, Z., and Kenchington, E. 2016. Characteristics of Environmental Data Layers for Use in Species Distribution Modelling in the Newfoundland and Labrador Region. Can. Tech. Rep. Fish. Aquat. Sci. 3187: viii + 325p.

Howell, K. L., Billett, D. S. M., and Tyler, P. A. 2002. Depth-related distribution and abundance of seastars (Echinodermata: Asteroidea) in the Porcupine Seabight and Porcupine Abyssal Plain, N.E. Atlantic. Deep Sea Res. I 49: 1901–1920.

Johnston, K., Ver Hoef, J.M., Krivoruchko, K., and Lucas, N. 2001. Using ArcGIS Geostatistical Analyst. ArcGIS User manual, ESRI. California, Redlands. 1-300 pp.

Kenchington, E., L. Beazley, C. Lirette, F.J. Murillo, J. Guijarro, V. Wareham, K. Gilkinson, M. Koen Alonso, H. Benoît, H. Bourdages, B. Sainte-Marie, M. Treble, and T. Siferd. 2016. Delineation of Coral and Sponge Significant Benthic Areas in Eastern Canada Using Kernel Density Analyses and Species Distribution Models. DFO Can. Sci. Advis. Sec. Res. Doc. 2016/093. vi + 178 p.

Klitgaard, A.B., Tendal, O.S. and Westerberg, H. 1997. Mass occurrences of large-sized sponges (Porifera) in Faroe Island (NE-Atlantic) shelf and slope areas: characteristics, distribution and possible causes. Pp. 129-142. - In L.E. Hawkins and S. Hutchinson, with A.C. Jensen, M. Sheader and J.A. Williams (eds): The Responses of Marine Organisms to their Environments. Proceedings of the 30th European Marine Biology Symposium, University of Southampton. 362 pp.

Knudby, A., Kenchington, E., and Murillo, F.J. 2013. Modeling the distribution of *Geodia* sponges and sponge grounds in the northwest Atlantic Ocean. PLoS ONE 8(12): e82306. doi:10.1371/journal.pone.0082306.

Kravchenko, A., and Bullock, D.G. 1999. A comparative study of interpolation methods for mapping soil properties. Agron. J. 91: 393–400.

Krivoruchko, K. 2011. Spatial Statistical Data Analysis for GIS Users. ESRI Press, Redlands, CA. 928 pp.

Leys, S.P., Yahel, G., Reidenbach, M.A., Tunnicliffe, V., Shavit, U., Reiswig, H.M. 2011. The sponge pump: the role of current induced flow in the design of the sponge body plan. PLoS ONE 6(12): e27787. doi:10.1371/journal.pone.0027787

Levin, L.A., Etter, R. J., Rex, M.A., Gooday, A.J., Smith, C. R., Pineda, J., Stuart, C. T., et al. 2001. Environmental influences on regional deep-sea species diversity. Annu. Rev. Ecol. Syst. 32: 51–93.

Li, J. and Heap, A.D. 2008. A Review of Spatial Interpolation Methods for Environmental Scientists. Geoscience Australia, Record 2008/23, 137 pp.

Lutz, M.J., Caldeira, K., Dunbar, R.B., and Behrenfeld, M.J. 2007. Seasonal rhythms of net primary production and particulate organic carbon flux to depth describe the efficiency of biological pump in the global ocean. J Geophys Res-Oceans 112: C10011.

Ly, S., Charles, C., and Degré, A. 2011. Geostatistical interpolation of daily rainfall at catchment scale: the use of several variogram models in the Ourthe and Ambleve catchments, Belgium. Hydrol. Earth Syst. Sci. 15: 2259-2274.

MacDonald, I. R., Bluhm, B. A., Iken, K., Gavaev, S., and Strong, S. 2010. Benthic macrofauna and megafauna assemblages in the Arctic Deep-Sea Canada Basin. Deep Sea Res. II 57: 136–152.

Mercier, A., Hamel, J-F. 2011. Contrasting reproductive strategies in three deep- sea octocorals from eastern Canada: *Primnoa resedaeformis*, *Keratoisis ornata*, and *Anthomastus grandiflorus*. Coral Reefs 30: 337–350.

Papiol, V., Cartes, J. E., Fanelli, E., and Maynou, F. 2012. Influence of environmental variables on the spatio-temporal dynamics of the bentho-pelagic assemblages in the middle slope of the Balearic Basin (NW Mediterranean). Deep Sea Res. I, 61: 84–99.

Peck, L.S., Webb, K.E., and Bailey, D.M. 2004. Extreme sensitivity of biological function to temperature in Antarctic marine species. Funct. Ecol. 18: 625-630.

Peterson, I. K., and R. Pettipas. 2013. Trends in air temperature and sea ice in the Atlantic Large Aquatic Basin and adjoining areas, Can. Tech. Rep. Hydrogr. Ocean Sci. 290: v + 59 p.

Platt, T., Sathyendranath, S., Forget, M-H., White III, G.N., Caverhill, C., Bouman, H., Devred, E., and Son, S. 2008. Operational estimation of primary production at large geographical scales. Remote Sens. Environ., 112: 3437-3448.

Polovina, J.J., Mitchum, G.T., and Evans, G.T. 1995. Decadal and basin-scale variation in mixed layer depth and the impact on biological production in the Central and North Pacific, 1960-88. Deep-Sea Res. 42: 1701-1716.

Riigård, H.U., Thomassen, S., Jakobsen, H., Weeks, J.M., Larsen, P.S. 1993. Suspension feeding in marine sponges *Halichondria panacea* and *Haliclona urceolus*: effects of temperature on filtration rate and energy cost of pumping. Mar. Ecol. Progr. Ser. 96: 177-188.

Roberts, J.J., Best, B.D., Dunn, D.C., Treml, E.A., and Halpin, P.N. 2010. Marine Geospatial Ecology Tools: An integrated framework for ecological geoprocessing with ArcGIS, Python, R, MATLAB, and C++. Environ. Modell. Softw. 25: 1197-1207.

Robinson, T.P., and Metternicht, G. 2006. Testing the performance of spatial techniques for mapping soil properties. Comput. Electron. Agric. 50: 97-108.

Soltwedel, T., Jaeckisch, N., Ritter, N., Hasemann, C., Bergmann, M., and Klages, M. 2009. Bathymetric patterns of megafaunal assemblages from the arctic deep-sea observatory HAUSGARTEN. Deep Sea Res. I 56: 1856–1872.

Spetland, F., Rapp, H.T., Hoffmann, F., and Tendal, O.S. 2007. Sexual reproduction of *Geodia barretti* Bowerbank 1858 (Porifera, Astrophorida) in two Scandinavian fjords. In: Custódio, M.R., Lôbo-Hajdu, G., Hajdu, E., and Muricy, G (eds). Porifera Research: Biodiversity, Innovation and Sustainability. Rio de Janeiro, Brazil: Museu. Nacional: 613-620.

Sun, Z., Hamel,J.-F., Edinger, E., Mercier, A. 2010a. Reproductive biology of the deep-sea octocoral *Drifa glomerata* in the Northwest Atlantic. Mar. Biol. 157: 863–873.

Sun, Z., Hamel, J.-F., Mercier, A. 2010b. Planulation periodicity, settlement preferences and growth of two deep-sea octocorals from the Northwest Atlantic. Mar. Ecol. Prog. Ser. 410: 71–87.

Sun, Z., Hamel, J.-F., Mercier, A. 2011. Planulation, larval biology, and early growth of the deep-sea soft corals *Gersemia fruticosa* and *Duva florida* (Octocorallia: Alcyonacea). Invert. Biol. 130: 91–99.

Wassmann, P., Duarte, C.M., Agusti, S., and Sejr, M.K. 2011. Footprints of climate change in the Arctic marine ecosystem. Glob. Chang. Biol. 17: 1235-1249.

Yamamoto, J.K. 2007. On unbiased backtransform of lognormal kriging estimates. Comput. Geosci. 11: 219-234.

## APPENDIX I - Summary of Variables with Negative Values in the Interpolated Prediction Surface Resulting from Ordinary Kriging

Appendix 1 shows a map of each of the thirteen variables with negative values resulting in the prediction surfaces after spatial interpolation using ordinary kriging. The location of the negative values is highlighted in blue. The data distribution prior to modeling and the numbers of cells with negative values for each variable is presented in Table A1. For the sea ice cover variables, Table A2 shows the data distribution and cells that had both negative values and values greater than one resulting from the ordinary kriging process. Maps showing the location of those cells are also shown.

Table A1. Summary of environmental variables with negative prediction values resulting from ordinary kriging.

| Variable | Negative Values in Input | Data Distribution | Total Number of Cells | Cells with Negative Values | Range of Negative Values |
|---|---|---|---|---|---|
| Bottom Salinity Average Range | No | Right-skewed | 1197966 | 477 | $-9.52 \times 10^{-2}$ to $-8.70 \times 10^{-7}$ |
| Bottom Current Minimum | No | Right-skewed, Single large outlier | 1197966 | 557 | $-2.78 \times 10^{-4}$ to- $2.00 \times 10^{-8}$ |
| Bottom Current Average Minimum | No | Right-skewed, Single large outlier | 1197966 | 90 | $-4.19 \times 10^{-4}$to- $2.41 \times 10^{-6}$ |
| Surface Current Minimum | No | Right-skewed, single large outlier | 1197966 | 1992 | $-8.53 \times 10^{-3}$ to $-6.50 \times 10^{-7}$ |
| Surface Current Average Minimum | No | Right-skewed | 1197966 | 9 | $-2.07 \times 10^{-3}$ to $-4.03 \times 10^{-5}$ |
| Maximum Spring Mixed Layer Depth | No | Right-skewed | 1197966 | 60 | -73.02 to -1.02 |
| Maximum Winter Mixed Layer Depth | No | Right-skewed | 1197966 | 444 | -204.85 to -0.55 |
| Maximum Average Winter Mixed Layer Depth | No | Right-skewed | 1197966 | 320 | -124.67 to $-9.70 \times 10^{-2}$ |
| Bottom Shear Minimum | No | Right-skewed, large outlier | 1197966 | 204 | $-2.39 \times 10^{-4}$ to - $9.00 \times 10^{-8}$ |
| Spring Chlorophyll *a* Minimum | No | Right-skewed, double large outlier | 1197966 | 8 | -0.19 to $-5.68 \times 10^{-4}$ |
| Summer Chlorophyll *a* Mean | No | Right-skewed, single large outlier | 1197966 | 59 | -0.40 to $-3.25 \times 10^{-3}$ |
| Summer Chlorophyll *a* Maximum | No | Right-skewed, single large outlier | 1197966 | 4418 | -10.39 to $-9.40 \times 10^{-5}$ |
| Summer Chlorophyll *a* Range | No | Right-skewed, single large outlier | 1197966 | 7847 | -10.63 to $-2.70 \times 10^{-5}$ |

Table A2. Summary of sea ice cover variables with both negative prediction values and values greater than 1 resulting from ordinary kriging.

| Variable | Negative Values in Input | Data Distribution | Total Number of Cells | Cells with Negative Values | Range of Negative Values | Cells with Values Greater than 1 | Range of Values Greater than 1 |
|---|---|---|---|---|---|---|---|
| Spring Ice Cover Mean | No | Left-skewed | 1197966 | 67417 | -0.017 to -1.00 x $10^{-6}$ | 1476 | 1.009 to 1.00001 |
| Spring Ice Cover Minimum | No | Right-skewed | 1197966 | 158214 | -0.048 to -1.00 x $10^{-6}$ | NA | NA |
| Spring Ice Cover Maximum | No | Left-skewed | 1197966 | 67046 | -0.088 to -1.00 x $10^{-6}$ | 153170 | 1.031 to 1.000001 |
| Spring Ice Cover Range | No | Left-skewed | 1197966 | 79258 | -0.057 to -1.00 x $10^{-6}$ | 96499 | 1.056 to 1.000001 |
| Spring Ice Cover Average Minimum | No | Right-skewed | 1197966 | 56653 | -0.023 to -1.00 x $10^{-6}$ | 1053 | 1.020 to 1.000015 |
| Spring Ice Cover Average Maximum | No | Left-skewed | 1197966 | 52485 | -0.033 to -1.00 x $10^{-6}$ | 14193 | 1.007 to 1.000001 |
| Spring Ice Cover Average Range | No | Right-skewed | 1197966 | 56535 | -0.033 to -1.00 x $10^{-6}$ | NA | NA |
| Fall Ice Cover Mean | No | Right-skewed | 1197966 | 91692 | -0.015 to -0.004 | NA | NA |
| Fall Ice Cover Minimum | No | Right-skewed | 1197966 | 5029 | -0.006 to -1..00 x $10^{-6}$ | NA | NA |
| Fall Ice Cover Maximum | No | Left-skewed | 1197966 | 97403 | -0.061 to -1.00 x $10^{-6}$ | 7636 | 1.048 to 1.000001 |
| Fall Ice Cover Range | No | Left-skewed | 1197966 | 72991 | -0.097 to -1.00 x $10^{-6}$ | 143596 | 1.003 to 1.000001 |
| Fall Ice Cover Average Minimum | No | Right-skewed | 1197966 | 141896 | -0.057 to -0.006 | NA | NA |
| Fall Ice Cover Average Maximum | No | Left-skewed | 1197966 | 97403 | -0.061 to -1.00 x $10^{-6}$ | 7366 | 1.048 to 1.000001 |
| Fall Ice Cover Average Range | No | Left-skewed | 1197966 | 85306 | -0.023 to -1.00 x $10^{-6}$ | 316 | 1.066 to 1.000048 |
| Winter Ice Cover Mean | No | Left-skewed | 1197966 | 37643 | -0.028 to -1.00 x $10^{-6}$ | 20153 | 1.013 to 1.000001 |
| Winter Ice Cover Minimum | No | Right-skewed | 1197966 | 53846 | -0.102 to -1.00 x $10^{-6}$ | NA | NA |
| Winter Ice Cover Maximum | No | Left-skewed | 1197966 | 51960 | -0.082 to -1.00 x $10^{-6}$ | 140041 | 1.038 to 1.000001 |
| Winter Ice Cover Range | No | Right-skewed | 1197966 | 71367 | -0.049 to -1.00 x $10^{-6}$ | 6326 | 1.080 to 1.000001 |
| Winter Ice Cover Average Minimum | No | Left-skewed | 1197966 | 64385 | -0.035 to -1.00 x $10^{-6}$ | 29600 | 1.021 to 1.000001 |
| Winter Ice Cover Average Maximum | No | Left-skewed | 1197966 | 38811 | -0.049 to -1.00 x $10^{-6}$ | 57040 | 1.014 to 1.000001 |

| | | | | | | | |
|---|---|---|---|---|---|---|---|
| Winter Ice Cover Average Range | No | right-skewed | 1197966 | 71407 | -0.041 to $-1.00 \times 10^{-6}$ | NA | NA |

**Bottom Salinity Average Range**

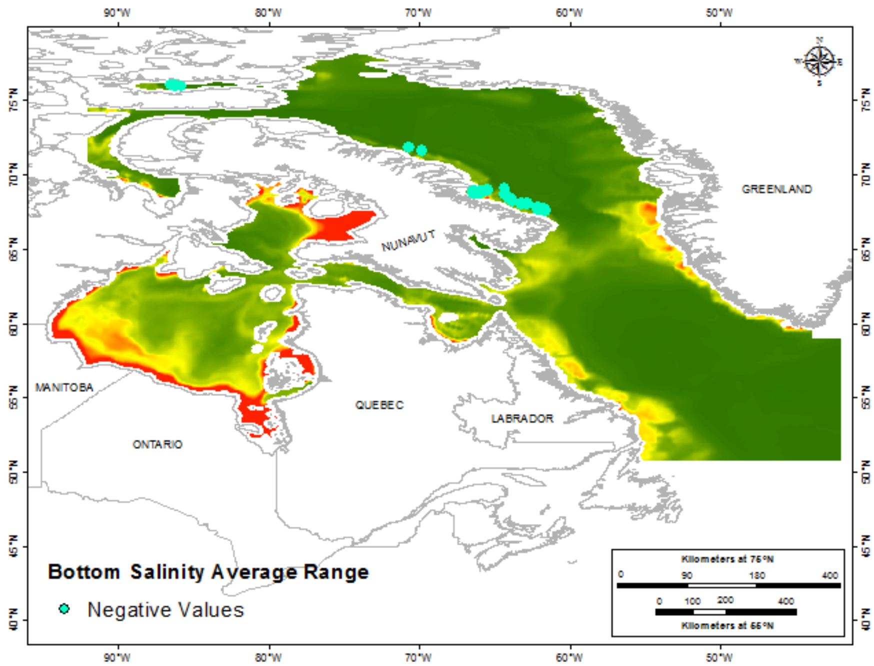


Figure A1. Negative values generated in the interpolated prediction surface of Bottom Salinity Average Range.

**Bottom Current Minimum**

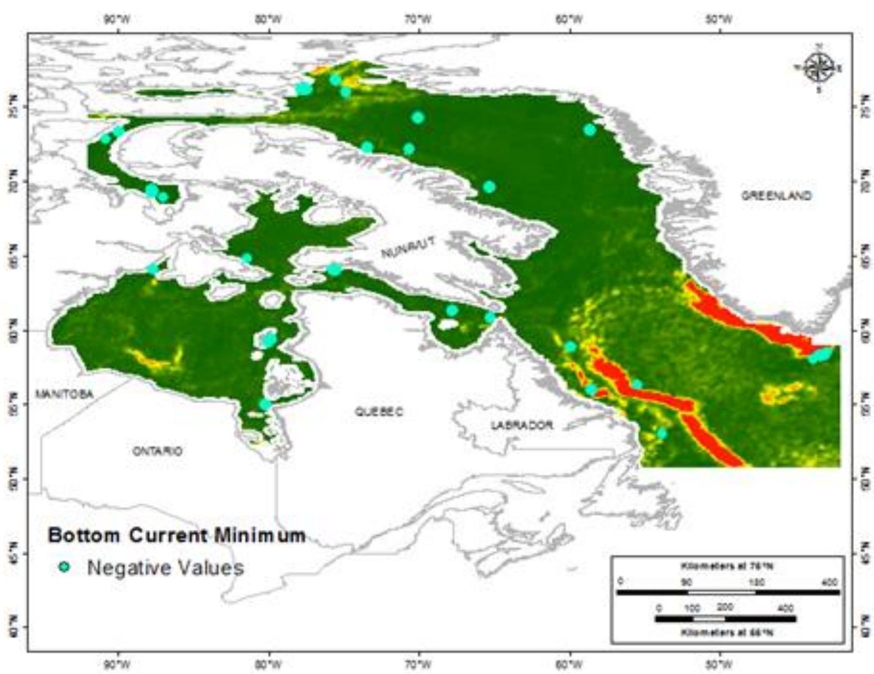


Figure A2. Negative values generated in the interpolated prediction surface of Bottom Current Minimum.

**Bottom Current Average Minimum**

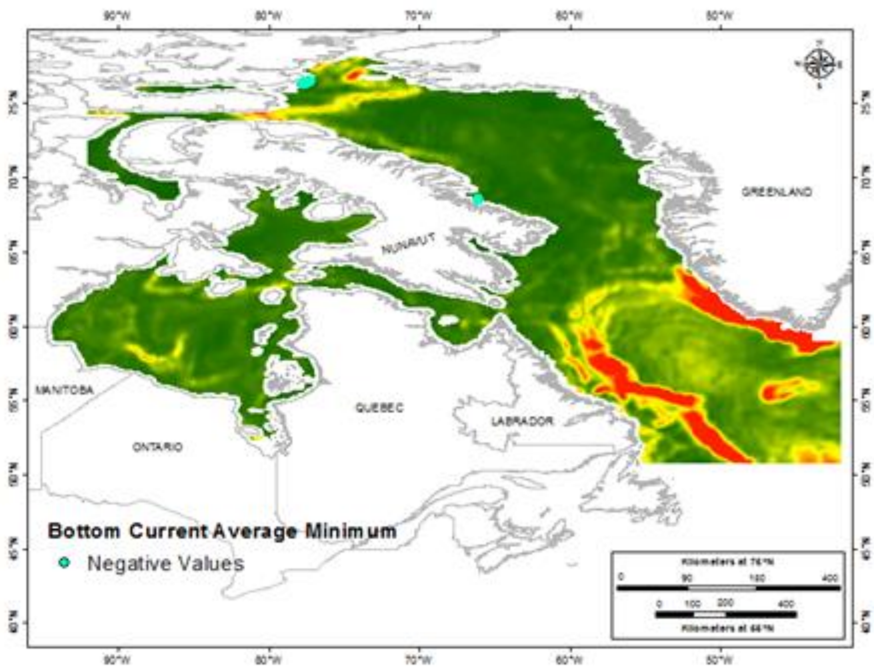


Figure A3. Negative values generated in the interpolated prediction surface of Bottom Current Average Minimum.

**Surface Current Minimum**

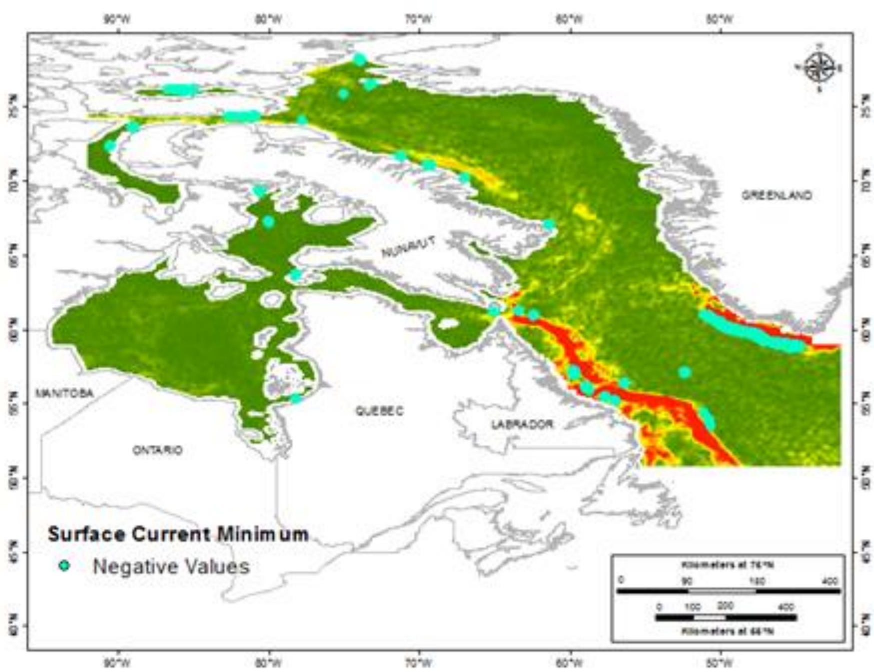


Figure A4. Negative values generated in the interpolated prediction surface of Surface Current Minimum.

**Surface Current Average Minimum**

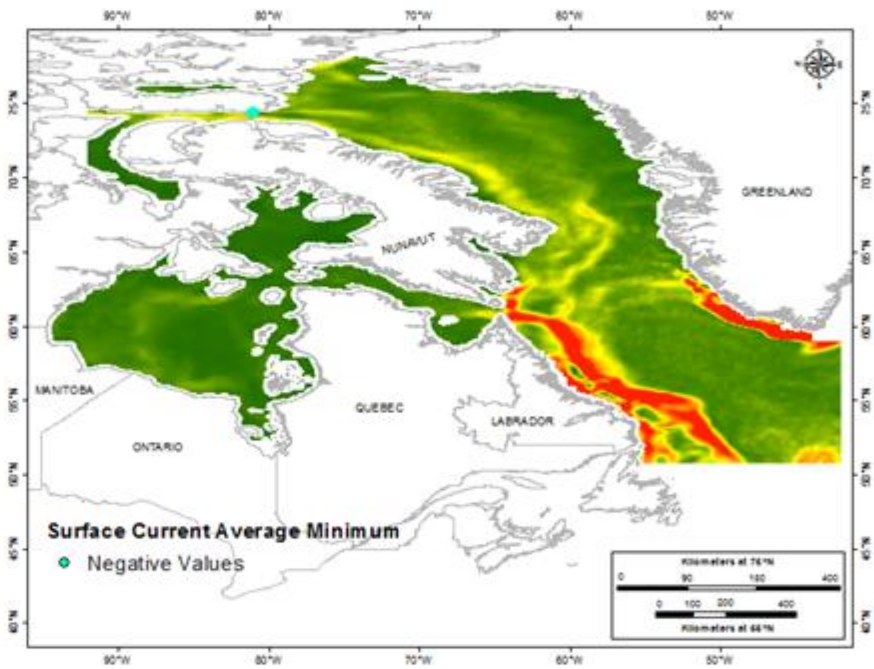


Figure A5. Negative values generated in the interpolated prediction surface of Surface Current Average Minimum.

**Maximum Spring Mixed Layer Depth**

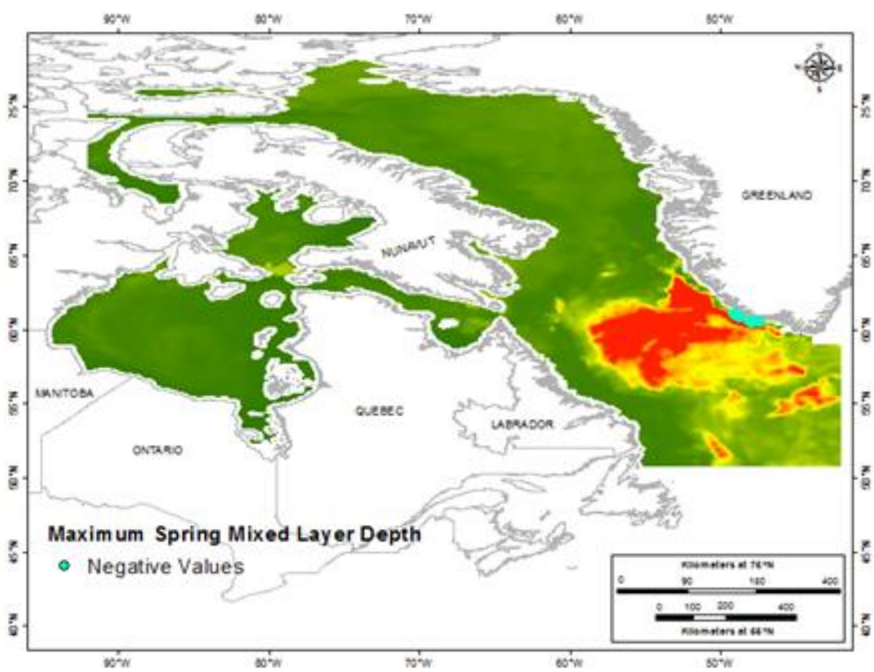


Figure A6. Negative values generated in the interpolated prediction surface of Maximum Spring Mixed Layer Depth.

**Maximum Winter Mixed Layer Depth**

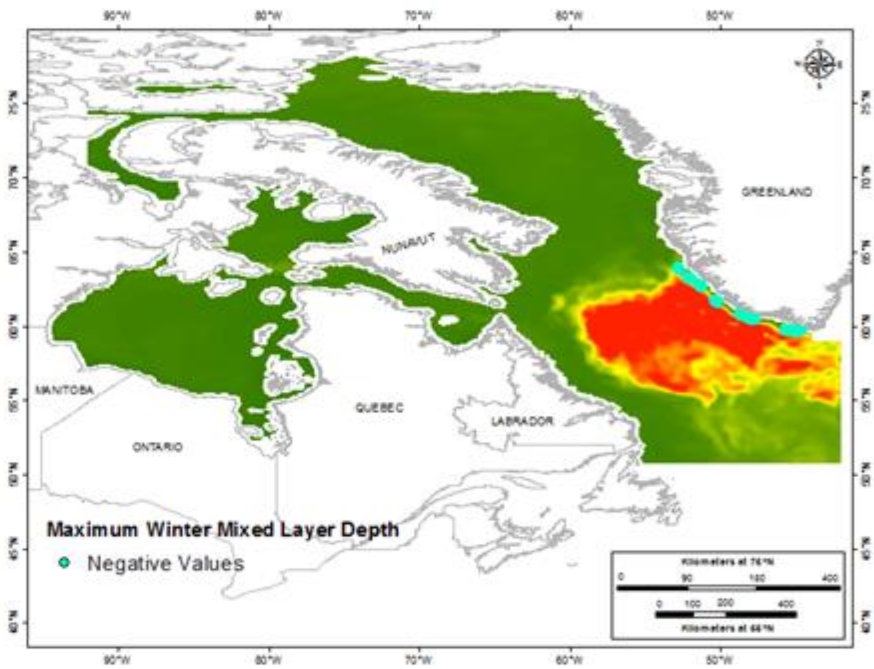


Figure A7. Negative values generated in the interpolated prediction surface of Maximum Winter Mixed Layer Depth.

**Maximum Average Winter Mixed Layer Depth**

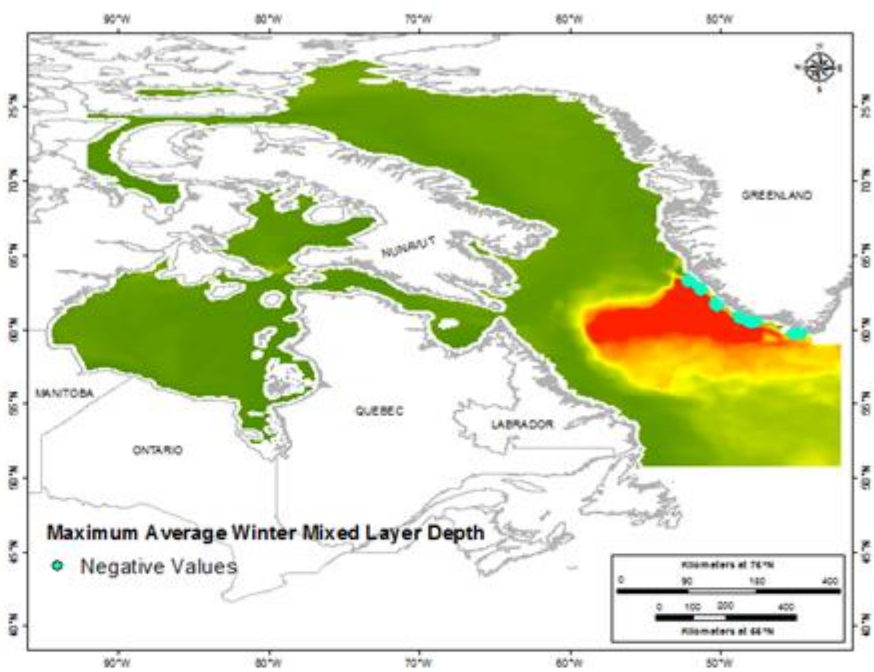


Figure A8. Negative values generated in the interpolated prediction surface of Maximum Average Winter Mixed Layer Depth.

**Bottom Shear Minimum**


Figure A9. Negative values generated in the interpolated prediction surface of Bottom Shear Minimum.

**Spring Chlorophyll *a* Minimum**

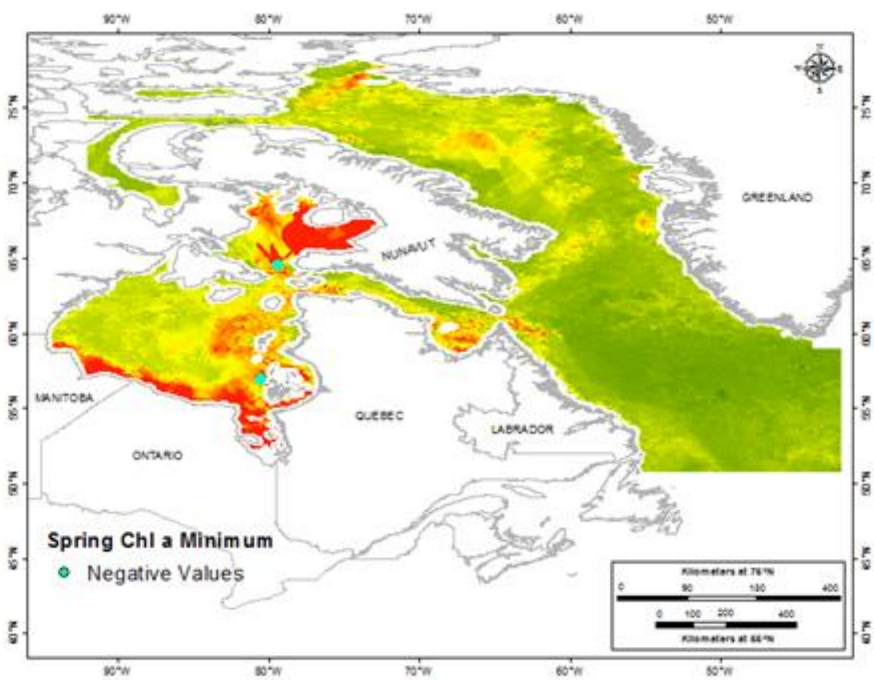


Figure A10. Negative values generated in the interpolated prediction surface of Spring Chlorophyll *a* Minimum

**Summer Chlorophyll *a* Mean**

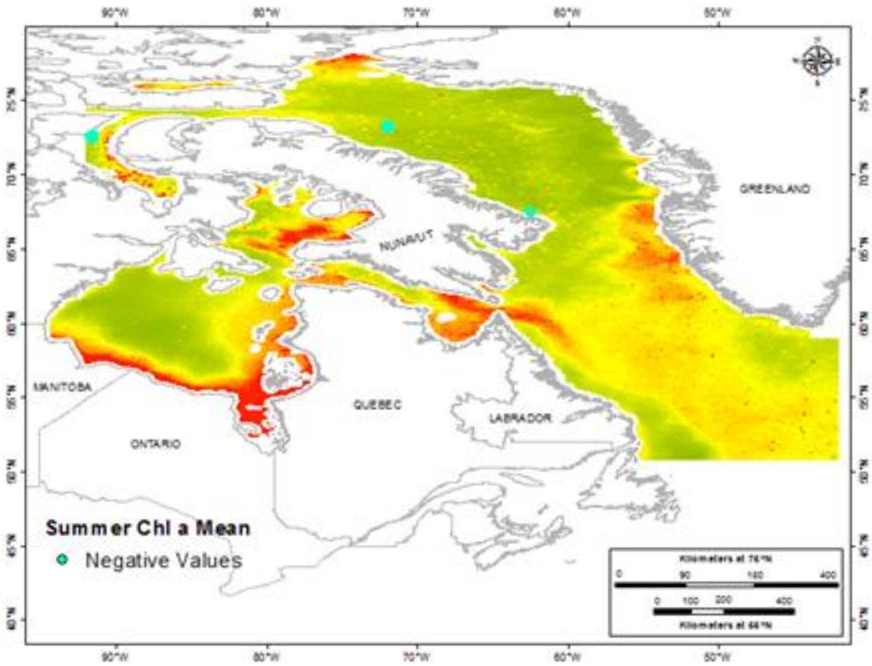


Figure A11. Negative values generated in the interpolated prediction surface of Summer Chlorophyll *a* Mean.

**Summer Chlorophyll *a* Maximum**

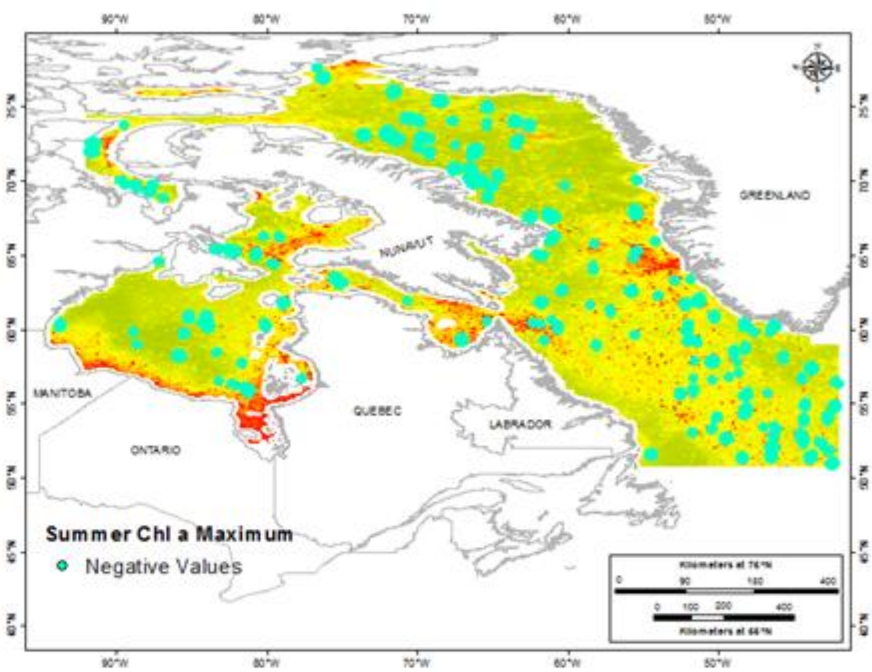


Figure A12. Negative values generated in the interpolated prediction surface of Summer Chlorophyll *a* Maximum.

**Summer Chlorophyll *a* Range**

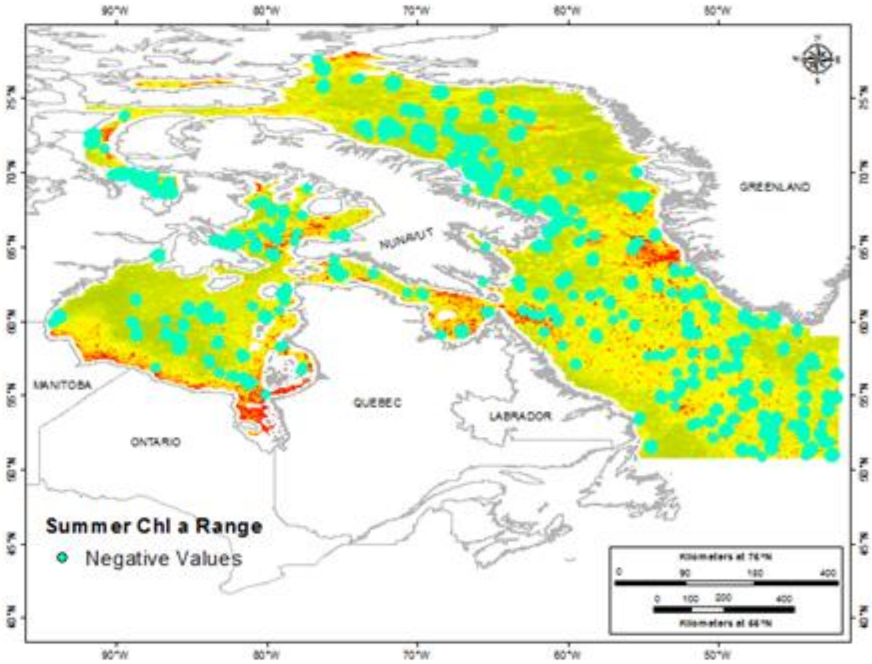


Figure A13. Negative values generated in the interpolated prediction surface of Summer Chlorophyll *a* Range.

**Spring Ice Cover Mean**

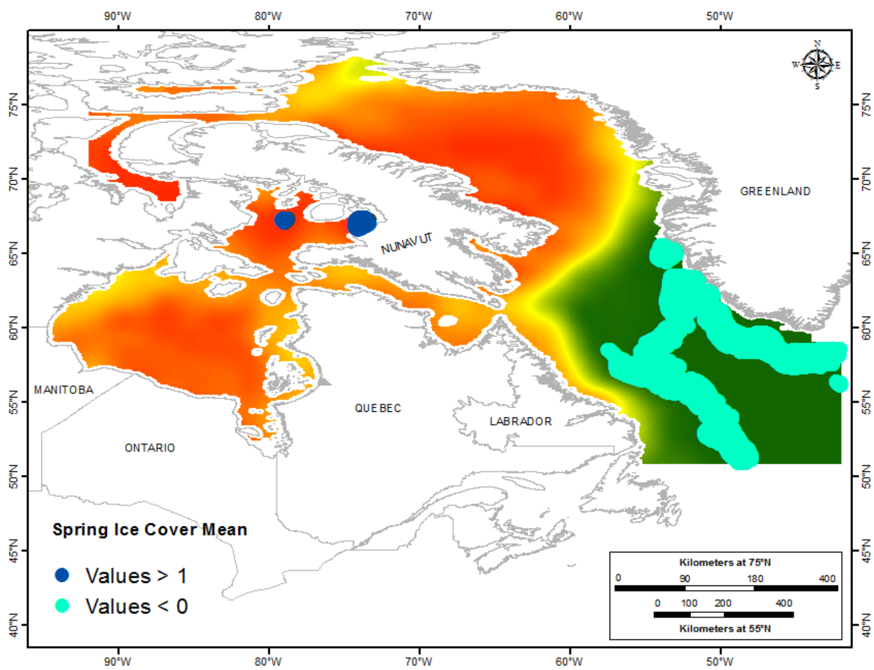


Figure A14. Values greater than 1 and less than zero generated in the interpolated prediction surface of Spring Ice Cover Mean.

**Spring Ice Cover Minimum**

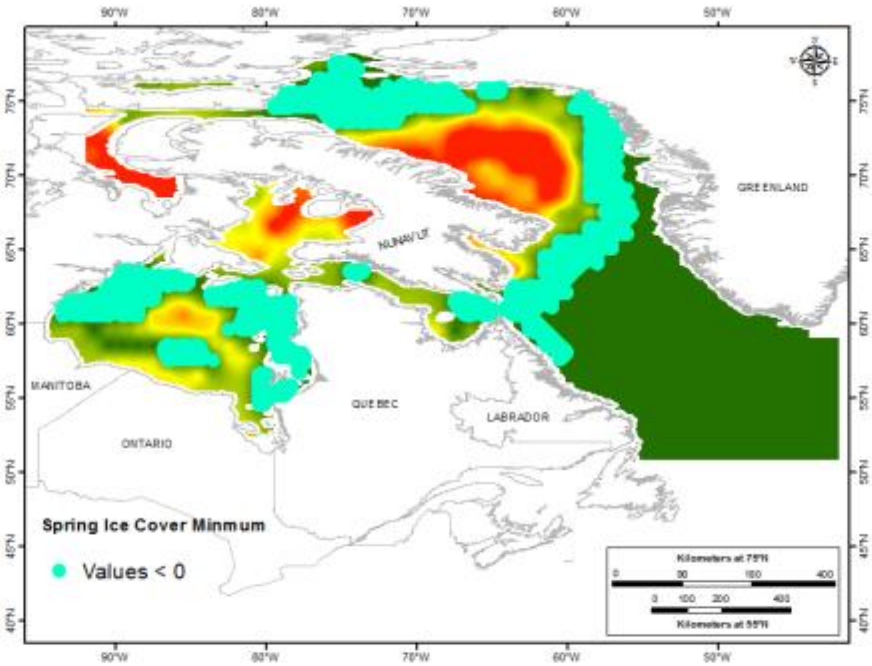


Figure A15. Values less than zero generated in the interpolated prediction surface of Spring Ice Cover Minimum.

**Spring Ice Cover Maximum**

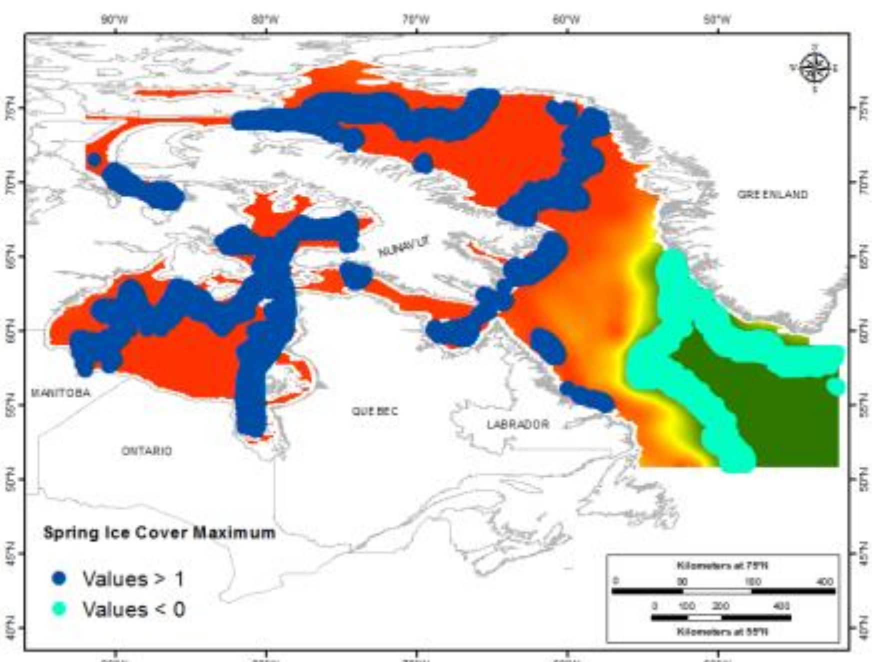


Figure A16. Values greater than 1 and less than zero generated in the interpolated prediction surface of Spring Ice Cover Maximum

## Spring Ice Cover Range

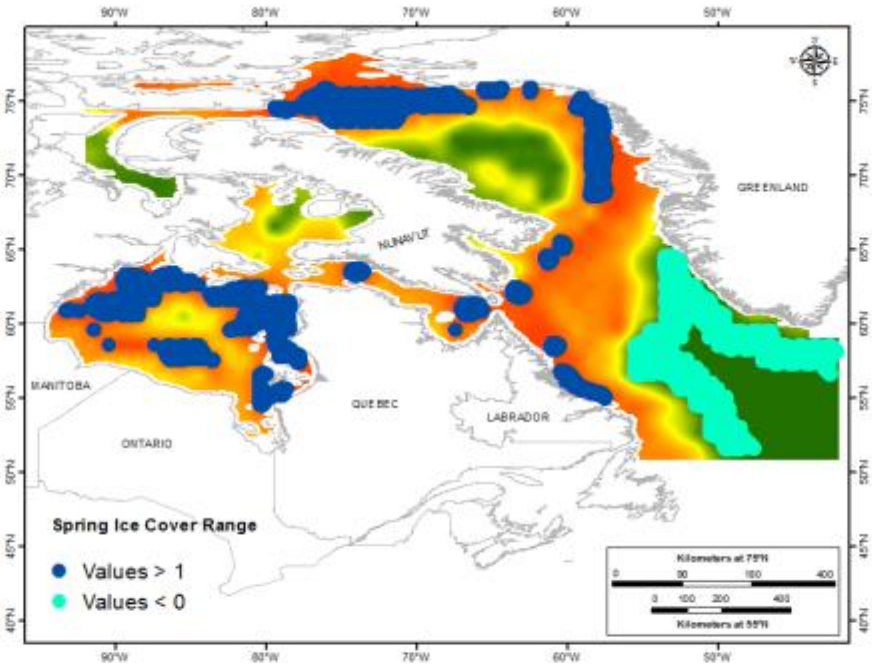


Figure A17. Values greater than 1 and less than zero generated in the interpolated prediction surface of Spring Ice Cover Range.

## Spring Ice Cover Average Minimum

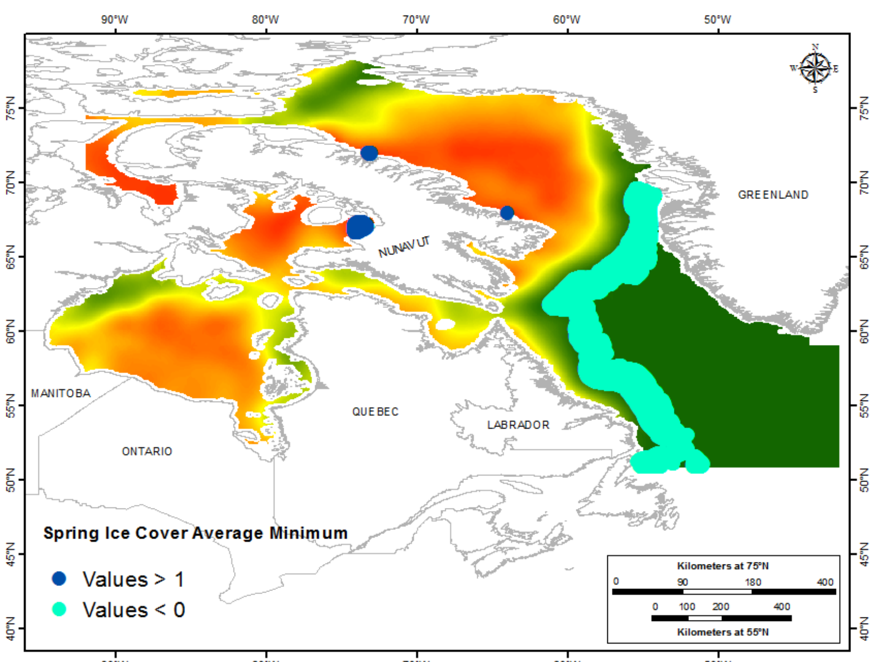


Figure A18. Values greater than 1 and less than zero generated in the interpolated prediction surface of Spring Ice Cover Average Minimum.

**Spring Ice Cover Average Maximum**

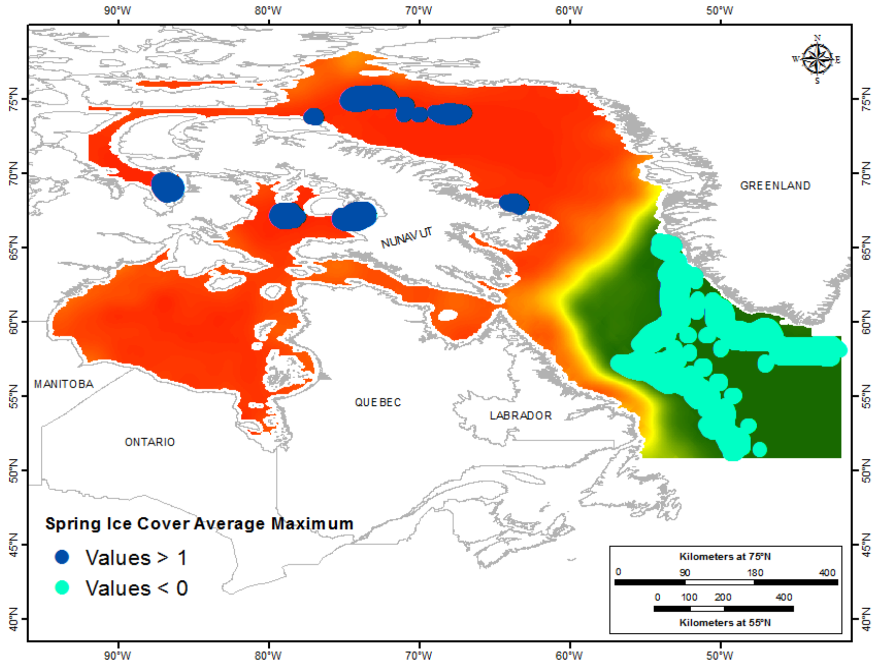


Figure A19. Values greater than 1 and less than zero generated in the interpolated prediction surface of Spring Ice Cover Average Maximum.

**Spring Ice Cover Average Range**

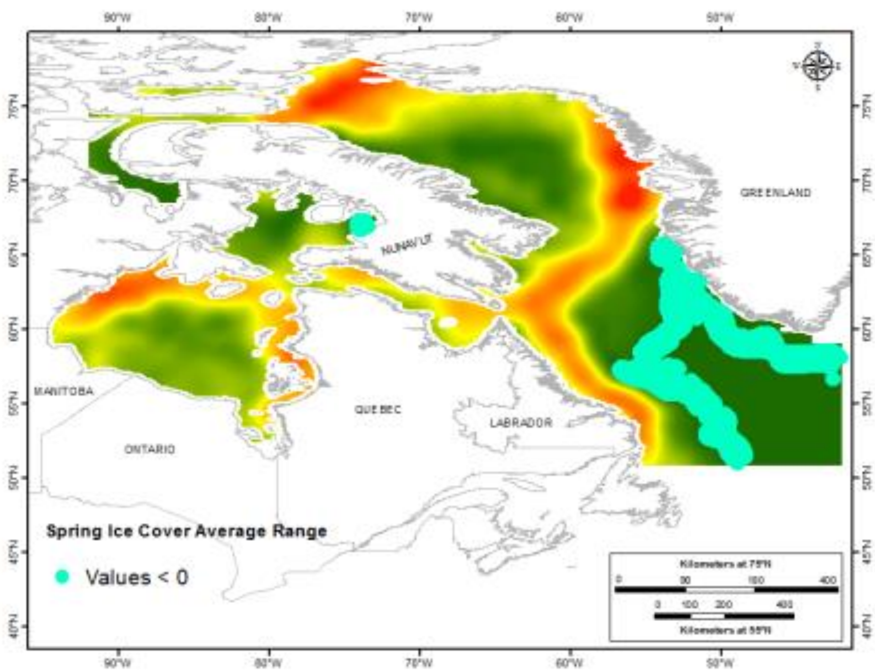


Figure A20. Values less than zero generated in the interpolated prediction surface of Spring Ice Cover Average Range.

**Fall Ice Cover Mean**

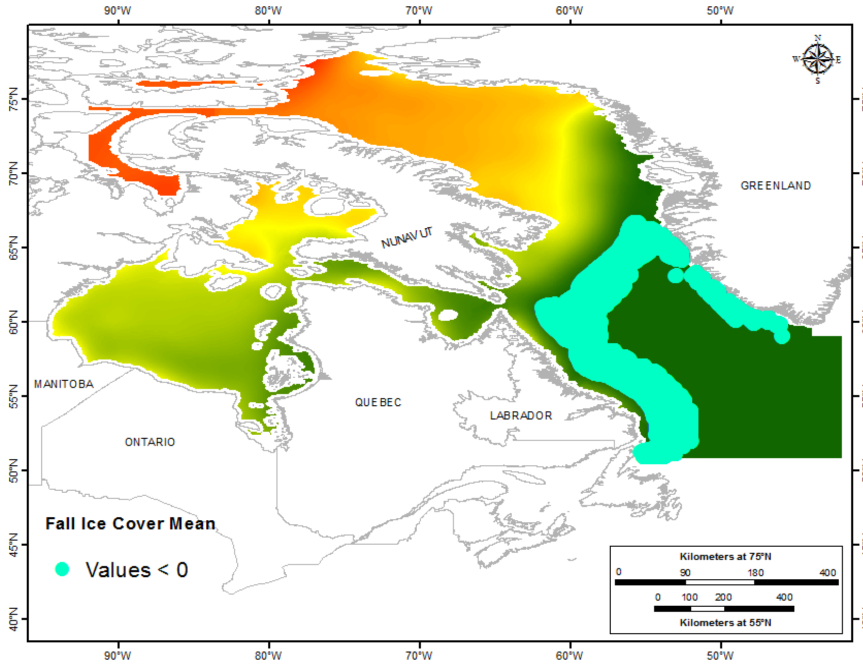


Figure A21. Values less than zero generated in the interpolated prediction surface of Fall Ice Cover Mean.

**Fall Ice Cover Minimum**

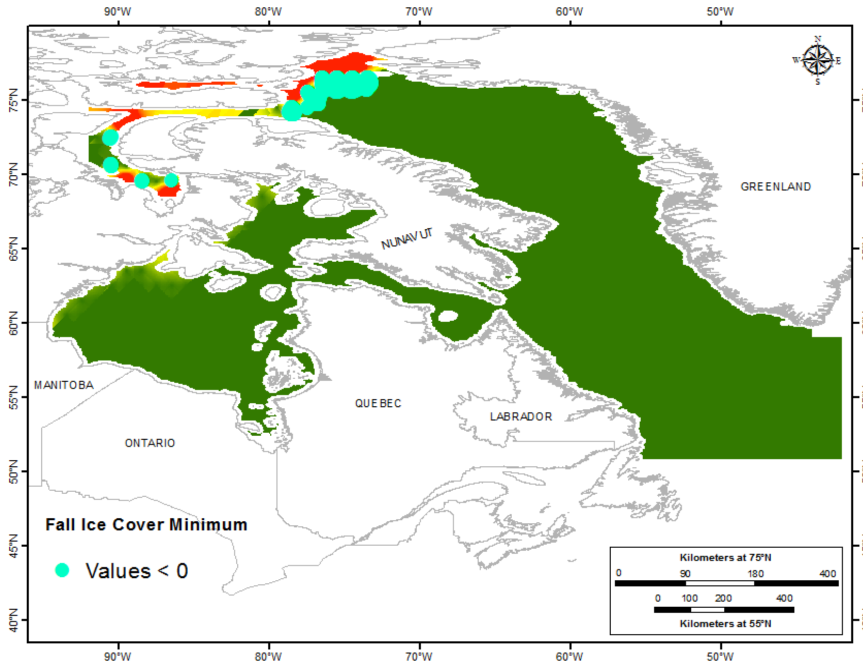


Figure A22. Values less than zero generated in the interpolated prediction surface of Fall Ice Cover Minimum.

## Fall Ice Cover Maximum

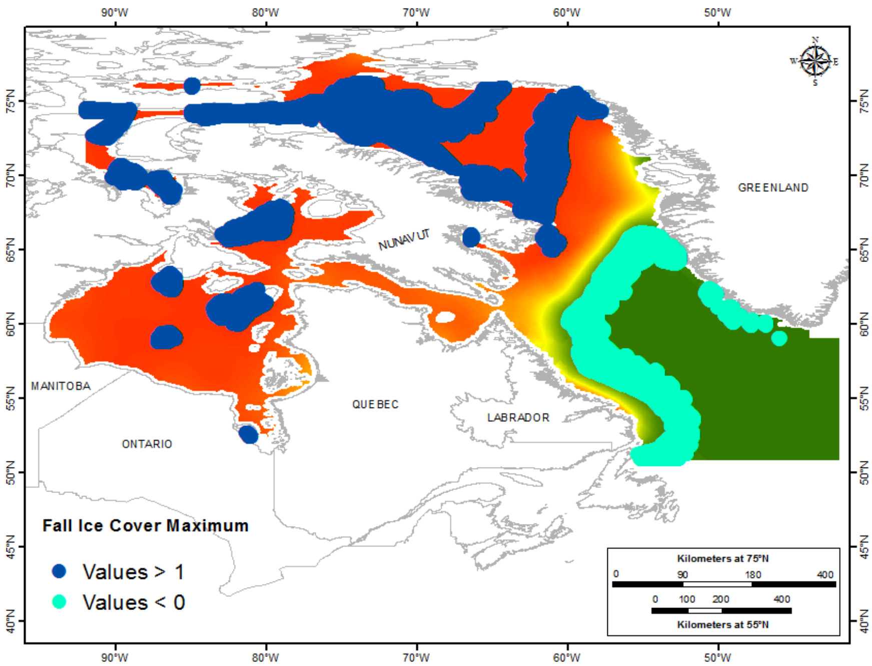


Figure A22. Values greater than 1 and less than zero generated in the interpolated prediction surface of Fall Ice Cover Maximum.

## Fall Ice Cover Range

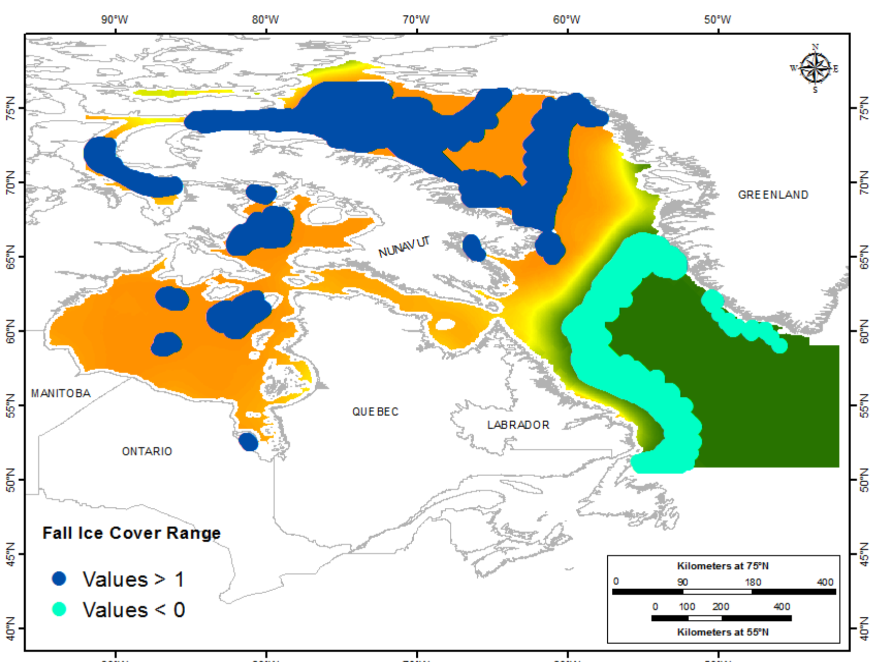


Figure A23. Values greater than 1 and less than zero generated in the interpolated prediction surface of Fall Ice Cover Range.

**Fall Ice Cover Average Minimum**

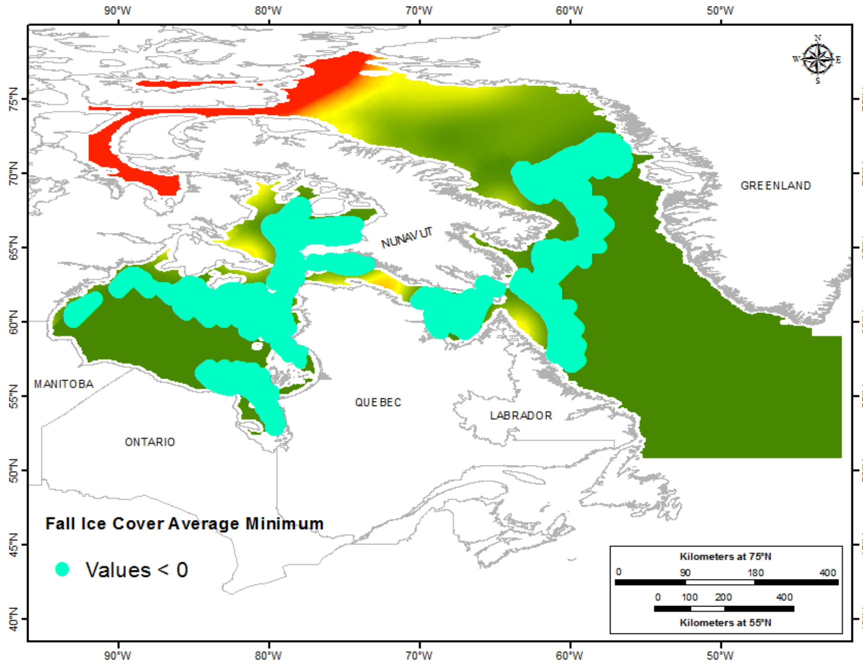


Figure A24. Values greater than 1 and less than zero generated in the interpolated prediction surface of Fall Ice Cover Average Minimum.

**Fall Ice Cover Average Maximum**

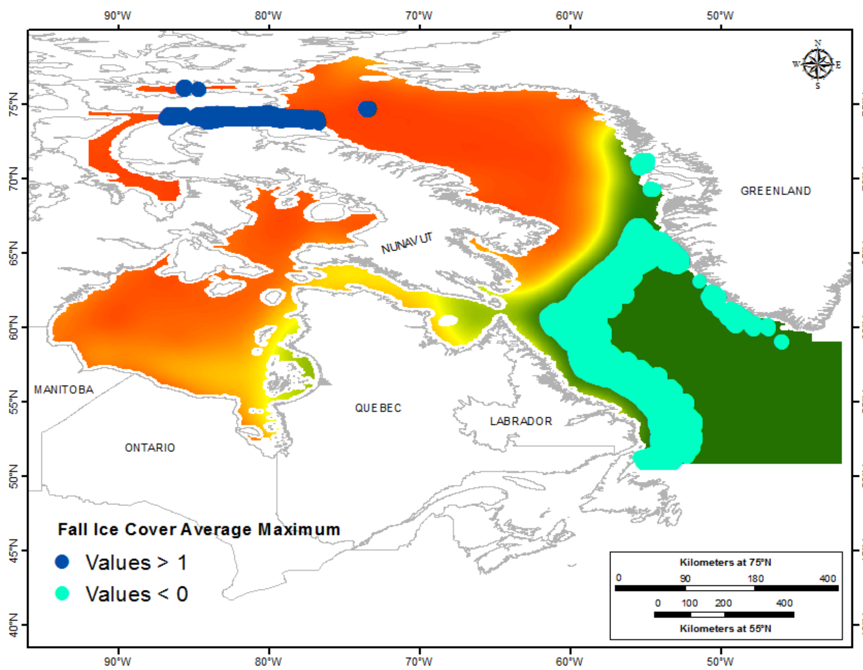


Figure A25. Values greater than 1 and less than zero generated in the interpolated prediction surface of Fall Ice Cover Average Maximum.

**Fall Ice Cover Average Range**

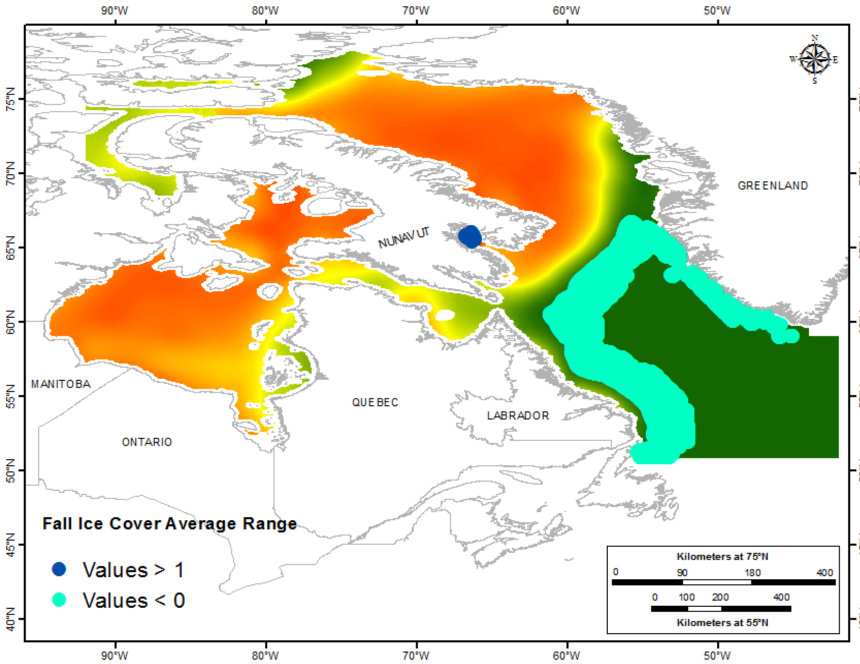


Figure A26. Values greater than 1 and less than zero generated in the interpolated prediction surface of Fall Ice Cover Average Range.

**Winter Ice Cover Mean**

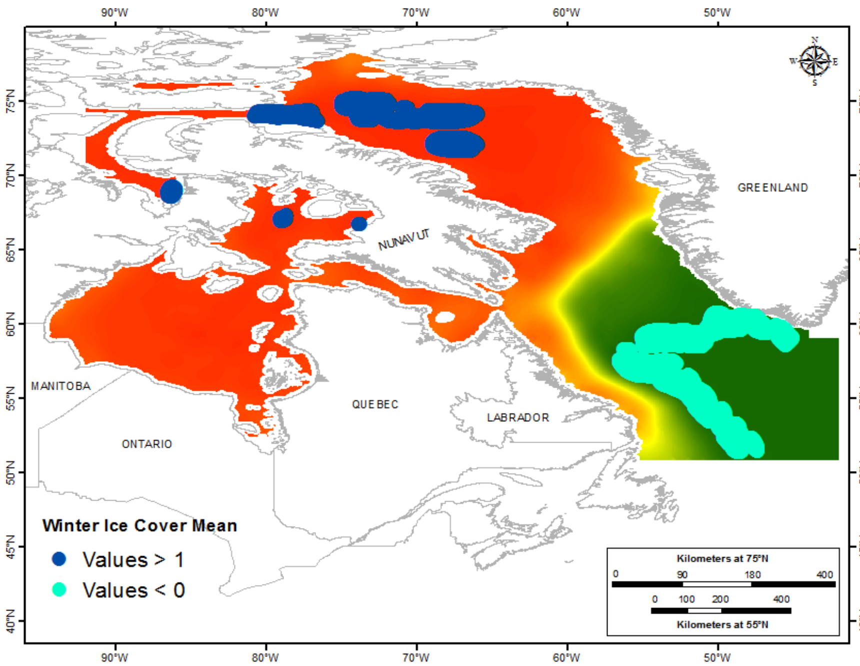


Figure A27. Values greater than 1 and less than zero generated in the interpolated prediction surface of Winter Ice Cover Mean.

**Winter Ice Cover Minimum**

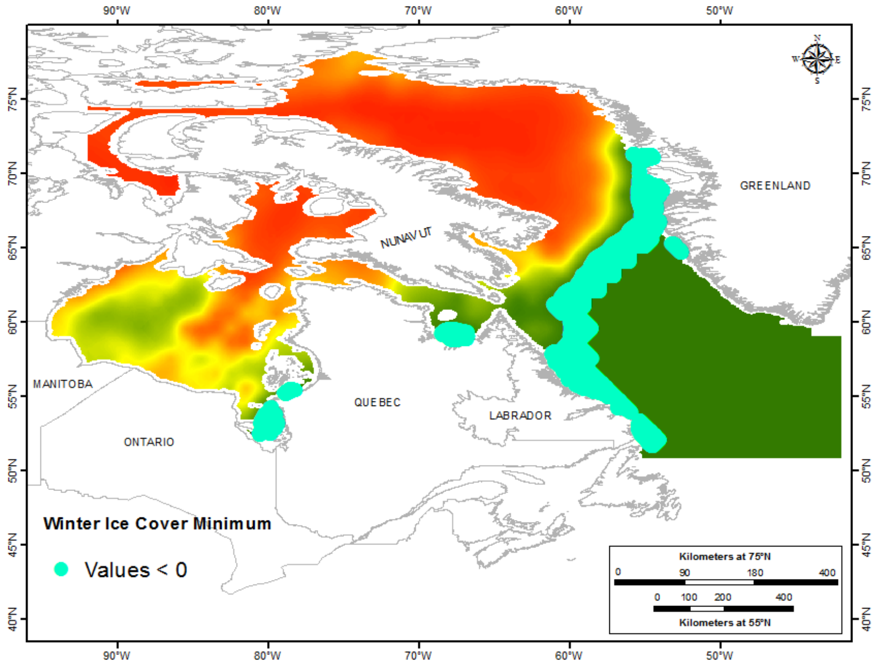


Figure A28. Values less than zero generated in the interpolated prediction surface of Winter Ice Cover Minimum.

**Winter Ice Cover Maximum**

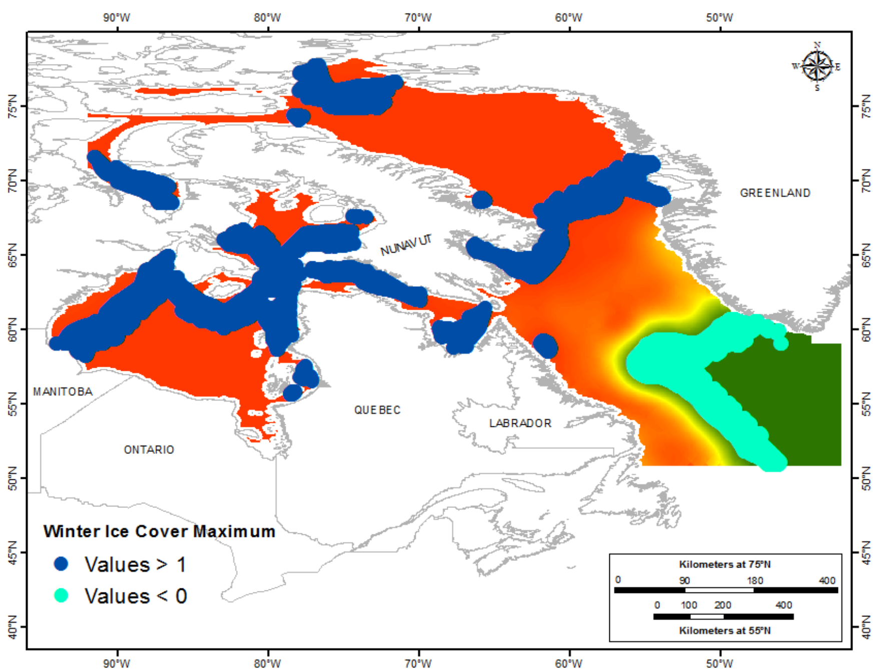


Figure A29. Values greater than 1 and less than zero generated in the interpolated prediction surface of Winter Ice Cover Maximum.

**Winter Ice Cover Range**

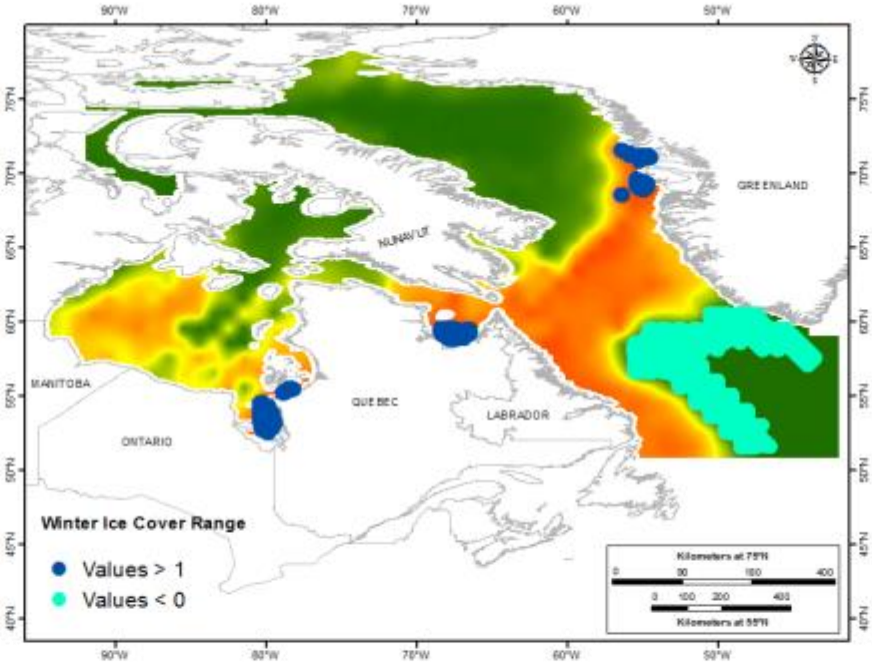


Figure A30. Values greater than 1 and less than zero generated in the interpolated prediction surface of Winter Ice Cover Range.

**Winter Ice Cover Average Minimum**

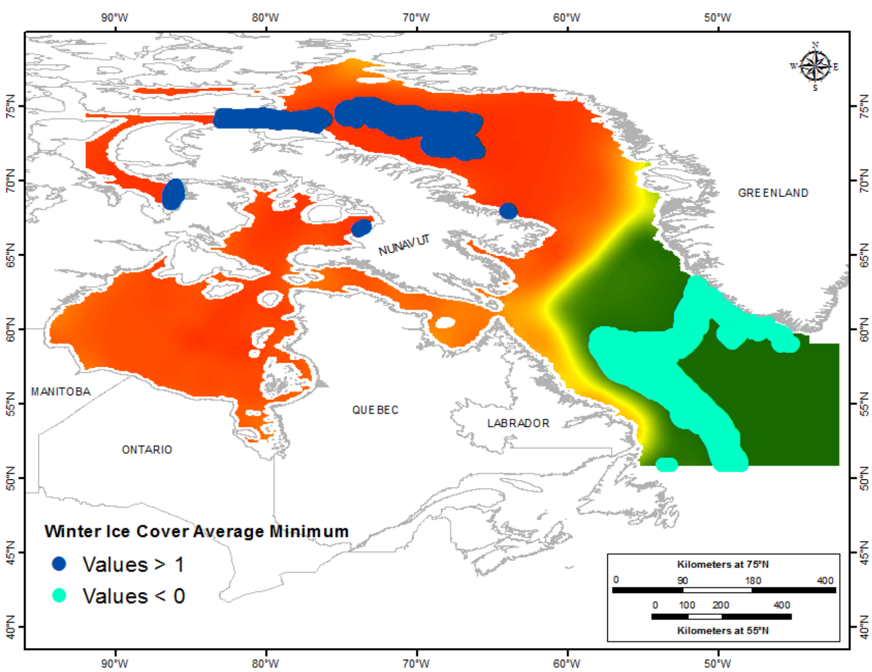


Figure A31. Values greater than 1 and less than zero generated in the interpolated prediction surface of Winter Ice Cover Average Minimum.

**Winter Ice Cover Average Maximum**

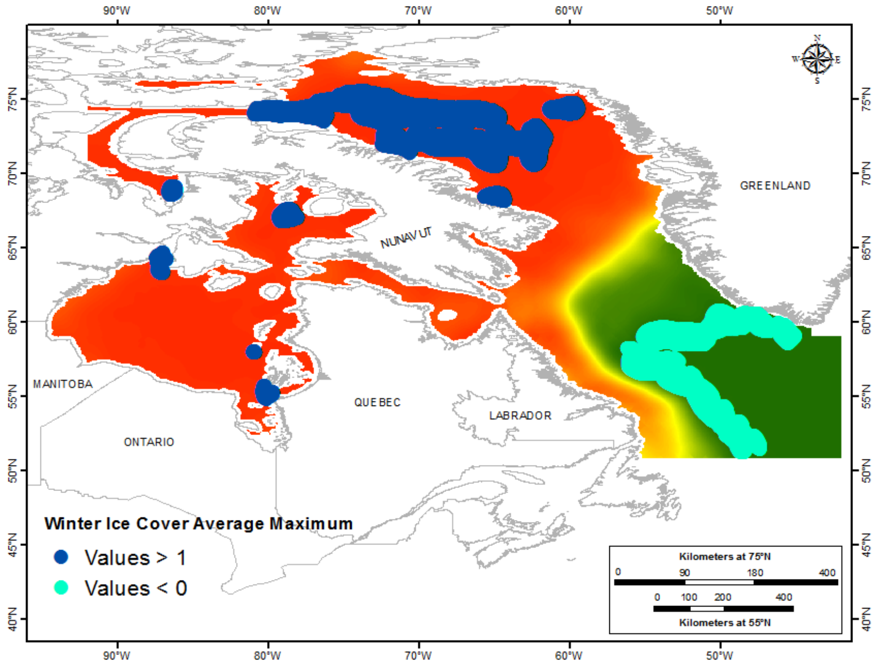


Figure A32. Values greater than 1 and less than zero generated in the interpolated prediction surface of Winter Ice Cover Average Maximum.

**Winter Ice Cover Average Range**

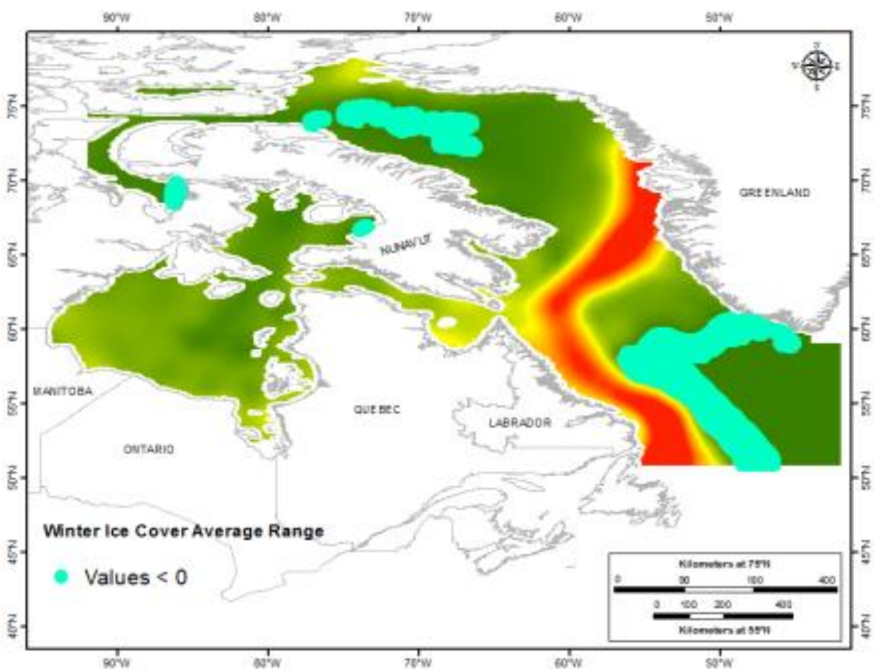


Figure A33. Values less than zero generated in the interpolated prediction surface of Winter Ice Cover Average Range.